NASA Reference Publication 1027

Viking '75 Spacecraft Design and Test Summary

Volume II - Orbiter Design

Neil A. Holmberg, Robert P. Faust,
and H. Milton Holt

NOVEMBER 1980

NASA

NASA Reference Publication 1027

Viking '75 Spacecraft Design and Test Summary

Volume II - Orbiter Design

Neil A. Holmberg, Robert P. Faust,
and H. Milton Holt
Langley Research Center
Hampton, Virginia

National Aeronautics
and Space Administration

**Scientific and Technical
Information Branch**

1980

PREFACE

This publication, in three volumes, discusses the design of the Viking lander and orbiter as well as the engineering test program developed to achieve confidence that the design was adequate to survive the expected mission environments and to accomplish the mission objective. Volume I includes a summary of the Viking Mission and the design of the Viking lander. Volume II consists of the design of the Viking orbiter and Volume III comprises the engineering test program for the lander and the orbiter.

The material contained in this report was assembled from documentation produced by the Martin Marietta Corporation (now Martin Marietta Aerospace) and the Jet Propulsion Laboratory during the Viking spacecraft design and test program. Viking Project personnel contributing to the preparation of this publication and their area of contribution are as follows:

Lander science design and test	Joseph C. Moorman
Lander guidance and control design and test	Anthony Fontana
Lander propulsion design and test	Anthony Fontana
Lander thermal design and test	T. W. Edmund Hankinson
Viking orbiter detailed design information:	
Command and sequencing	Carl R. Pearson
Computer command subsystem	Carl R. Pearson
Flight data subsystem	Carl R. Pearson
Data storage subsystem	Carl R. Pearson
Visual imaging subsystem	Carl R. Pearson
Infrared thermal mapper subsystem	Carl R. Pearson
Mars atmospheric water detector subsystem	Carl R. Pearson
Temperature control	William A. Carmines
Structure subsystem	William A. Carmines
Pyrotechnic subsystem	William A. Carmines
Cabling subsystem	William A. Carmines
Propulsion subsystem	William A. Carmines
Mechanical devices subsystem	William A. Carmines
Test data and information	William A. Carmines

CONTENTS

INTRODUCTION

The Viking Project was initiated in 1968 and was climaxed with the launching of two Viking spacecraft in 1975. The first landing on Mars was July 20, 1976, and the second landing was September 3, 1976. Each spacecraft contained an orbiter and a lander. The objective of the Viking Mission was to increase significantly man's knowledge of the planet Mars through orbital observations by the orbiter as well as by direct measurements made by the lander during Martian atmospheric entry, descent, and landing. Particular emphasis was placed on obtaining biological, chemical, and environmental data relevent to the existence of life on the planet at the present time, at some time in the past, or the possibility of life existing at a future date. Orbiter observations consisted of radio-science, imaging, thermal, and water-vapor measurements used to assist landing-site selection and the study of the dynamic and physical characteristics of Mars and its atmosphere. Lander direct measurements consisted of radio science; atmospheric structure and composition; landing-site imaging; atmospheric pressure, temperature, and wind velocity; identification of the elemental composition of the surface material; physical properties of the surface material; the search for evidence of living organisms and organic materials; and determination of seismological characteristics of the planet. The Viking scientific return was further expanded by the capability of simultaneous Martian observations from orbit and the surface.

This document, divided into three volumes, summarizes the design of the Viking lander and orbiter as well as the engineering test program developed to achieve confidence that the design was adequate to survive the expected mission environments and accomplish the mission objective. The engineering test program covered those aspects of testing prior to delivery of the Viking landers and orbiters to the John F. Kennedy Space Center. Most of the material contained in this document was taken from documentation prepared by Martin Marietta Corporation (now Martin Marietta Aerospace) and the Jet Propulsion Laboratory during the Viking spacecraft design and test program. The detailed reports for the Viking orbiter were JPL internal documents not intended for public release. These documents are in microfilm storage at JPL and are not readily available because of the reproduction cost. This volume contains a detailed description of the Viking orbiter design. All abbreviations and symbols used in this volume are defined in an appendix.

Use of trade names in this report does not constitute an official endorsement of such products or manufacturers, either expressed or implied, by the National Aeronautics and Space Administration.

VIKING ORBITER FUNCTIONAL DESIGN

The Viking orbiter (fig. 1) was a three-axis stabilized spacecraft that was attitude stabilized with the Sun and Canopus as references. The VO had two-way rf communication equipment to transmit all data, including VO monitoring

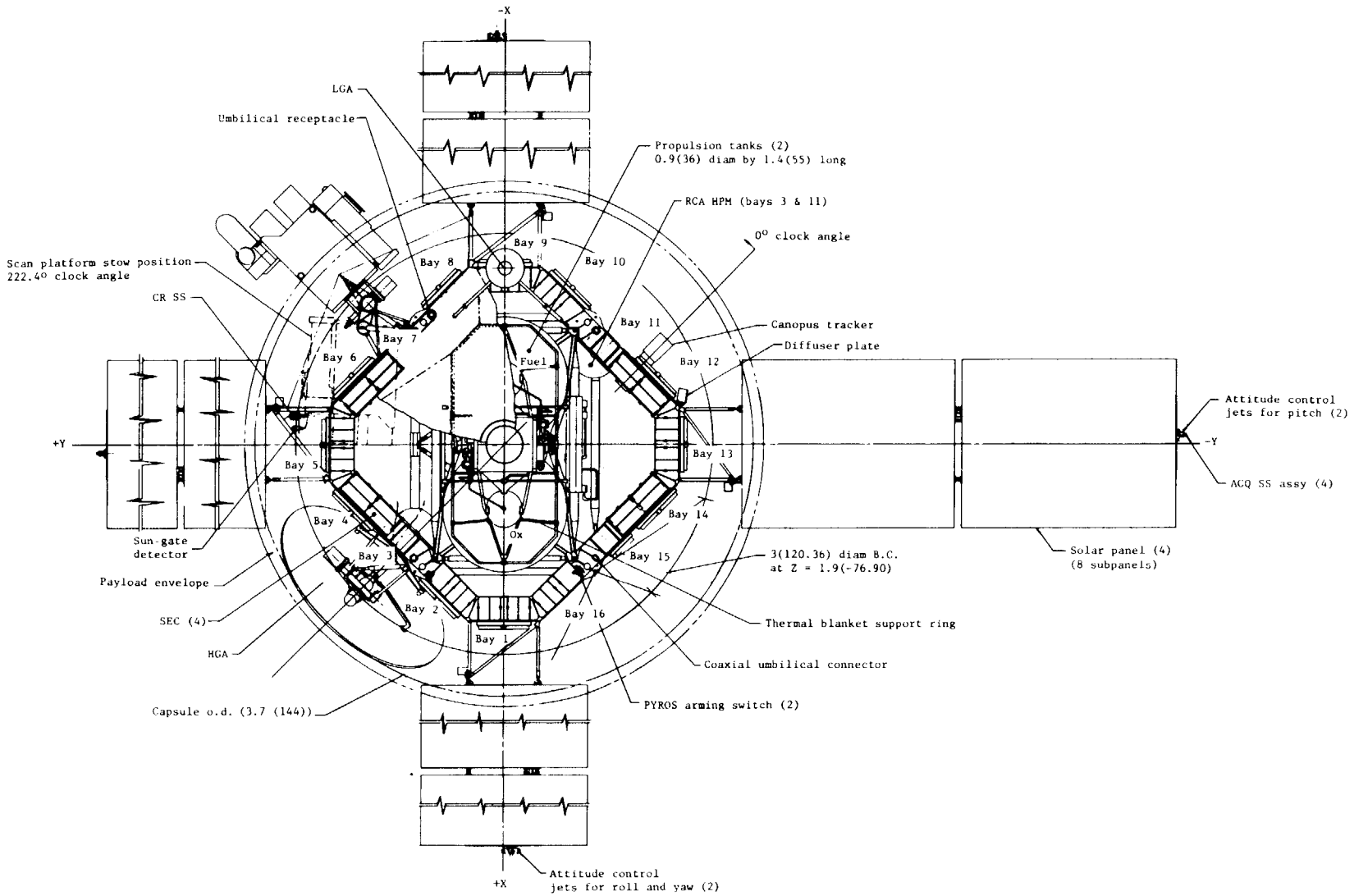

Figure 1.- Mechanical configuration of VO. Linear dimensions are in m (in.).

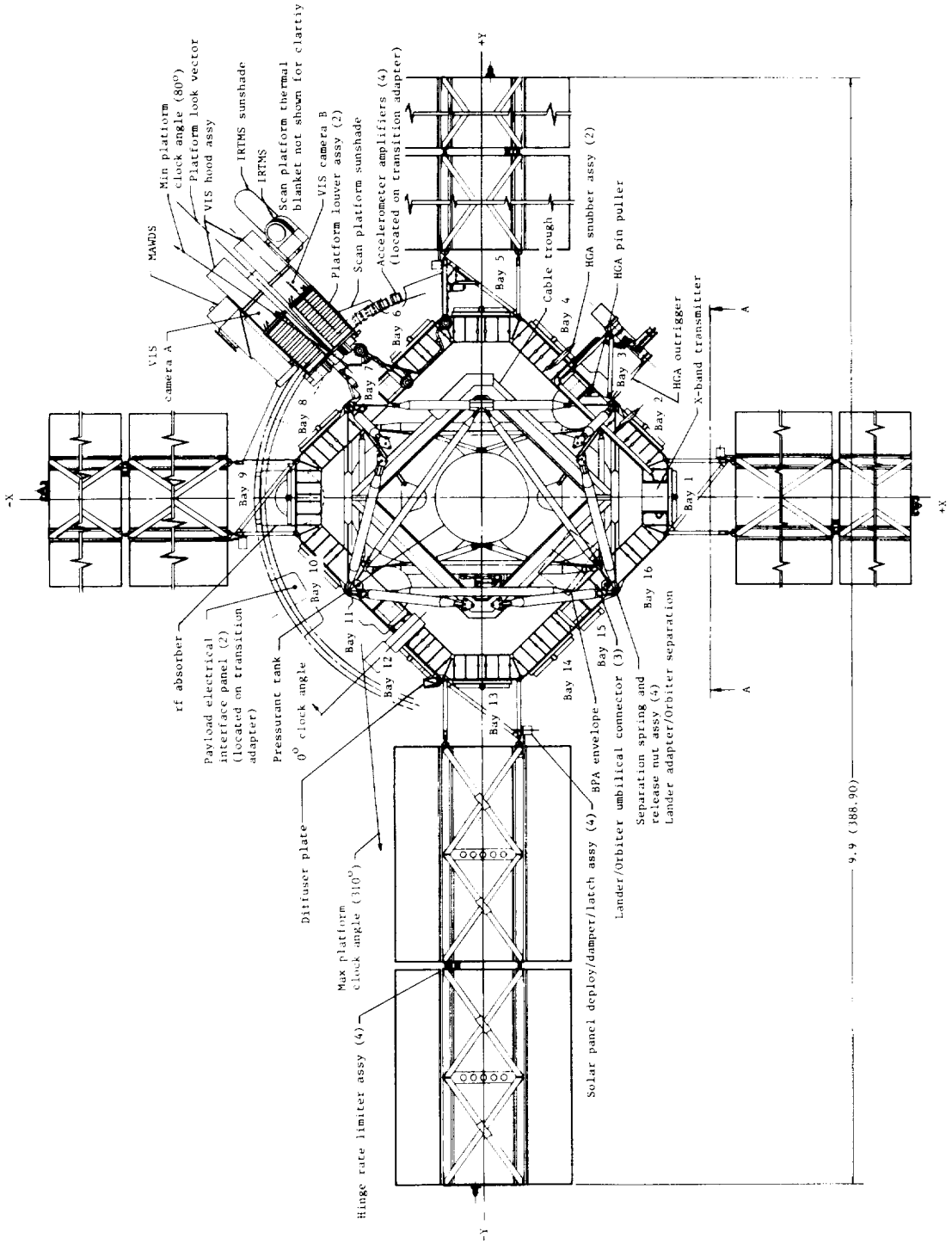

Figure 1.- Continued.

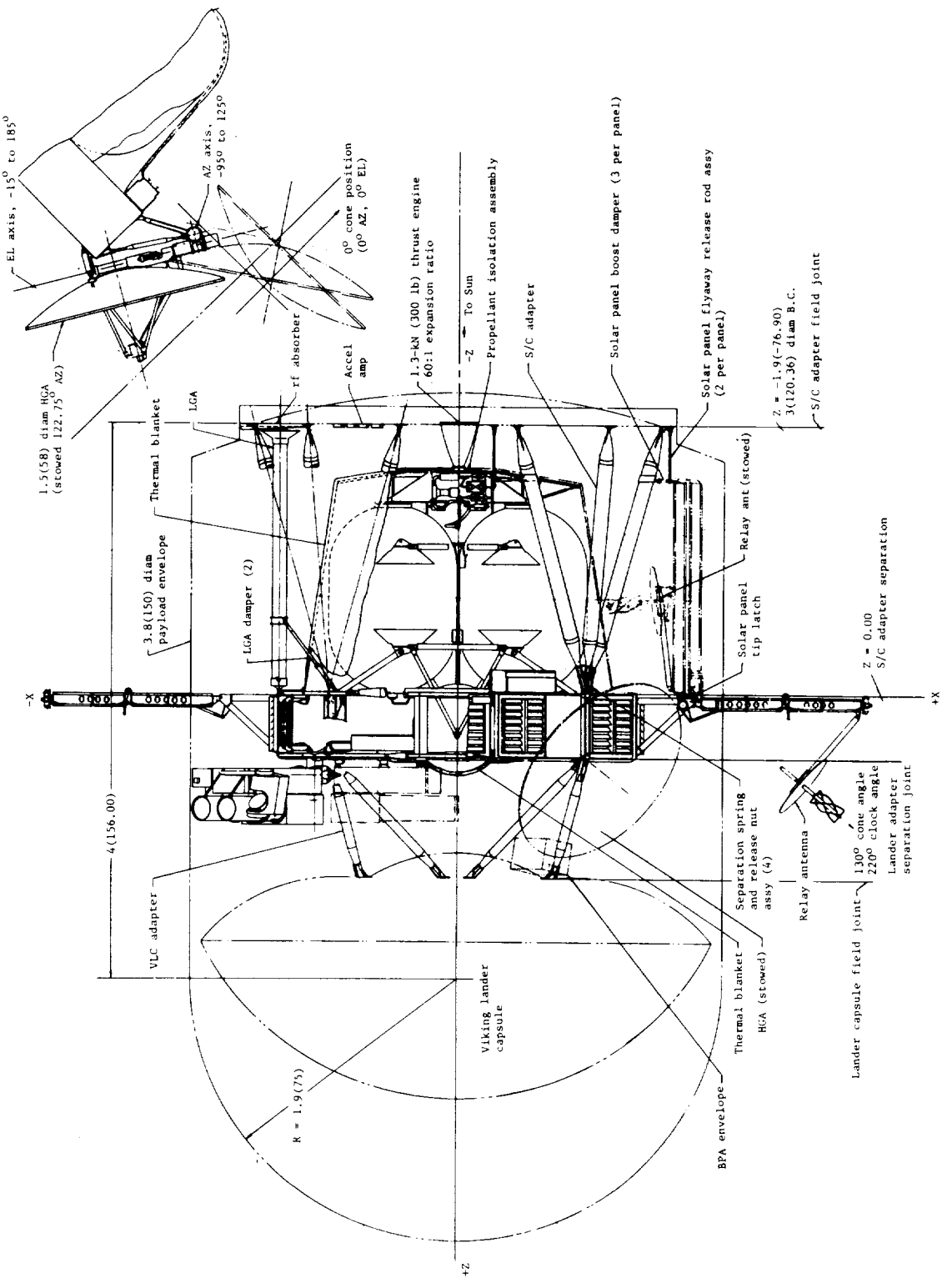

Figure 1.- Concluded.

telemetry and lander relayed data, to Earth; to receive the commands transmitted to the VO; and to receive the angular position and Doppler velocity from range tracking transmissions from the DSN which were needed for orbit determination and navigation. It also had one-way rf communication (receive) with the VL which was used to relay the lander data to Earth. The VO had a completely redundant command and sequencing system to provide complete control and routines to insure safety throughout the Viking Missions.

The scientific instruments of the orbiter allowed experiments to be performed in the vicinity of Mars. The scientific experiments and the corresponding instruments are given as follows:

Experiment	Instrument
Visual imaging	Television cameras (2)
Thermal mapping	Infrared radiometer
Water vapor mapping	Infrared spectrometer
Radio science	X-band transmitter, in conjunction with existing orbiter communication equipment

SYSTEM FUNCTIONAL REQUIREMENTS

The VOS consisted of the VO, the V S/C A, the VLCA, plus all the associated SE, software test facilities, and simulators required for fabrication, handling, testing, and launching. The VLC was mated to the VO by means of the VLCA to form the V S/C. The V S/C was then encapsulated within the Centaur standard shroud and mated to the Titan III E/Centaur launch vehicle by means of the S/C adapter.

During the 10- to 12-mo Earth-Mars interplanetary flight, the VO maintained three-axis attitude stabilization and provided two-way telecommunication links with the DSN tracking stations. The VLC remained almost dormant during this period and depended on the VO for thermal control, power requirements, and relaying of engineering monitoring telemetry. VO midcourse trajectory maneuvers were restricted to a near-Earth period during the first 6 to 30 days after launch and a near-Mars period between 30 and 10 days before encounter. During the interplanetary cruise period, the VO instruments were checked out and calibrated to improve their pointing accuracy. Video images of Mars and star fields were obtained prior to each approach midcourse maneuver to support optical navigation. Beginning about 5 days before arrival at Mars, the VO provided video images of the planet and optical navigation images of the satellite Deimos in preparation for the MOI maneuver. When the S/C arrived at Mars, the VO propulsion system was fired for about 40 min to insert the V S/C into orbit around the planet. Once in orbit, the VO executed orbit trim maneuvers to achieve the initial synchronous orbit geometry required for VLC separation and VL landing.

The nominal synchronous orbit had a period of 24.6 hr, a periapsis altitude of 1500 km, and an apoapsis altitude of about 32 600 km. Before the landing, the VO performed reconnaissance of primary and secondary landing sites with its science instruments mounted on the scan platform.

The VO supported preseparation checkout and separation of the VLC by providing a two-way communication link, special VLC power requirements, sequence initiation, and a celestial orientation for VLC attitude reference. During VLC descent and landing until a few minutes after touchdown, the VO maintained a relay link to receive and record VL data for retransmission to the DSN. The descent relay data were also fed through the VO for real-time transmission to the DSN until touchdown when the data rate was switched from its low to its high rate. Shortly after VL touchdown, the VO passed over the horizon, but the relay link was reestablished on succeeding orbital passes over the VL. The VLCA was separated during the orbit following VL touchdown to permit increased VO scan platform capability. The VO provided support for the VL and conducted independent investigations. Once the direct link between the VL and Earth was established, the relay link continued to be used, but the VO was occasionally released from VL support for periods of time to proceed with Mars observations from nonsynchronous orbit. Typically, about 15 orbit trim maneuvers were performed by the VO while in orbit; these maneuvers included initial trim maneuvers, station-keeping maneuvers to maintain VL support, and period trims for conducting Mars observations. To support and supplement VL investigations, the VO repeatedly used its instruments mounted on the scan platform to acquire data on the landing site and its surroundings during the 2- to 3-mo landed mission. In addition to VL surveillance, the VO used its science instruments to survey other areas of Mars to study the physical and dynamic characteristics of the planet's surface and atmosphere.

The VO instruments were operated at different points in orbit to provide both high- and low-altitude coverage. The scan platform was used to point the instruments to permit the VO to remain on celestial lock whenever possible; however, when the scan platform pointing range was insufficient (as it was for north polar observations), VO turns could be executed to achieve the required pointing, or the VO used a star other than Canopus for its cone-axis reference. (Note that the planetary approach observations were made with the S/C on celestial lock in order that these observations did not interfere with the critical navigation.) For low-altitude observations, single or multiple swaths of contiguous imaging photopairs were acquired by using VO ground track motion to produce area coverage with any one swath and by using the scan platform to slew between each photopair to increase the coverage. The instruments mounted on the scan platform were boresighted so that each one provided coverage of approximately the same 1° by 2° field of view.

The VO received uplink and transmitted downlink communications over either the low-gain or high-gain antennas. Use of the uplink or downlink with the VO transponder provided two-way Doppler, ranging, and DRVID tracking data. Doppler and ranging data were also obtained with the VO X-band transmitter which was coherent with the uplink or downlink S-band signal. Real-time transmission of VO engineering data was required when in the burn attitude for the first midcourse maneuver and the MOI maneuver.

Power was primarily derived from photovoltaic solar cells after launch and following Sun acquisition, except during off-Sun maneuvers and solar occultations when battery power was used. Depending on the geometry of the orbit selected, Sun and Earth occultations could occur during the mission. Mission 1 had Sun occultations which occurred near the end of its primary mission and obtained peak durations of up to 2 1/2 hr. Mission 2 had no Sun occultations in the nominal mission but had occultations of up to 1 hr in early 1977. Orbital operations were restricted to orbits with Sun occultations in order to avoid excessive battery depth of discharge. Battery power was also required during peak system power demand periods (for example, preseparation checkout of the VL) when demand exceeded the capability of the solar cells. The solar cells were used to keep the batteries fully charged at all times.

SYSTEM CONFIGURATION AND ASSEMBLY

Major elements of the VO were the bus structure to which all the other elements attach, the VLCA structure, the truss adapter which attached the V S/C to the Centaur LV, and VO appendages such as the four two-piece solar panels, the scan platform with the VO science instruments, the HGA, the LGA, and the bolt-on propulsion module. A schematic diagram showing the mechanical configuration is shown in figure 1. The major subsystems, along with the abbreviations and locations on VO, are given in table 1. The electronic packaging arrangement

TABLE 1.- MAJOR SUBSYSTEMS

Name	Abbreviation	Location
Structure subsystem	STRUS	
Radio frequency subsystem	RFS	Bays 1 and 16
Modulation/demodulation subsystem	MDS	Bay 1
Power subsystem	PWRS	
Source electronics		Bay 10
Processing and distribution		Bay 12
Batteries (2)		Bays 9 and 13
Computer command subsystem	CCS	Bay 2
Flight data subsystem	FDS	Bay 6
Attitude control subsystem	ACS	
Electronics		Bay 5
High-pressure modules	HPM	Bays 3 and 11
Canopus tracker	CT	+Z from bay 12
Pyrotechnic subsystem	PYROS	Bay 15
Cabling subsystem	CABLS	Central section
Propulsion subsystem	PROPS	Central section
Mechanical devices subsystem	DEVS	
Articulation control subsystem	ARTCS	Bay 5
Data storage subsystem	DSS	Bays 4 and 14
S/X band antenna subsystem	SXAS	
High-gain antenna	HGA	Outbd bay 3
Low-gain antenna	LGA	-Z from bay 9
Visual imaging subsystem	VIS	
Electronics		Bay 8
Cameras (2)		Scan plat
Infrared thermal mapper subsystem	IRTMS	Scan plat
Mars atmospheric water detector subsystem	MAWDS	
Electronics		Bay 8
Detector		Scan plat
X-band transmitter subsystem	XTXS	+Z from bay 1
Relay radio subsystem	RRS	Bay 15
Relay telemetry subsystem	RTS	Bay 15
Relay antenna subsystem	RAS	+X SP

of bay configurations and locations are presented in figure 2; bays are also identified in figure 1.

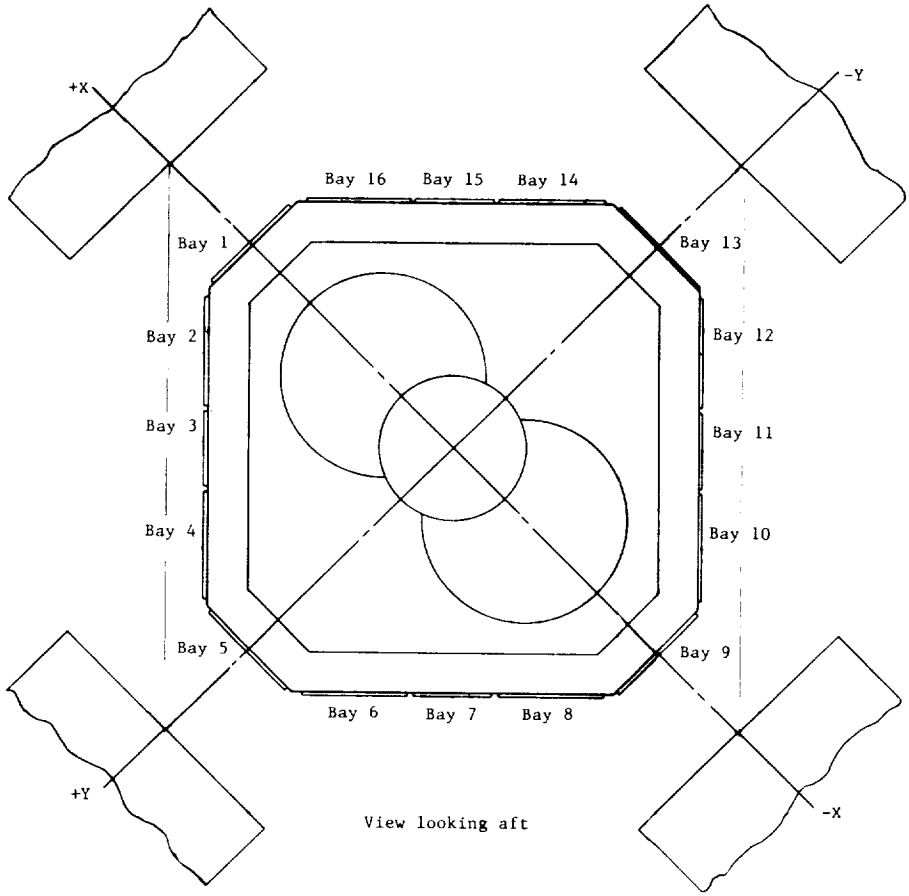

Figure 2.- Electronic packaging arrangement.

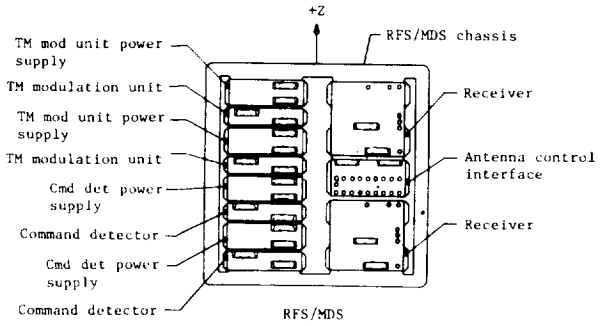

Bay 1

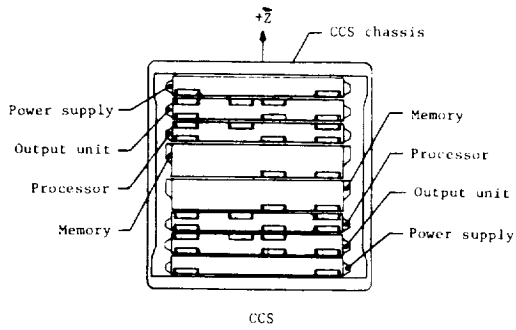

Bay 2

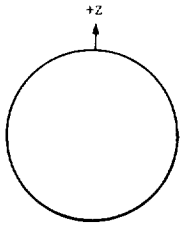

Bay 3

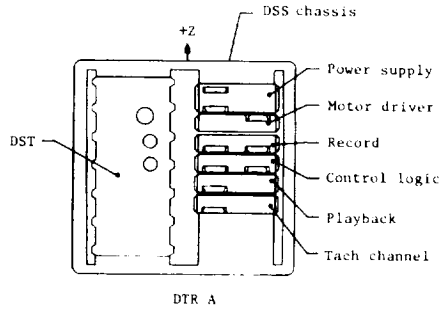

Bay 4

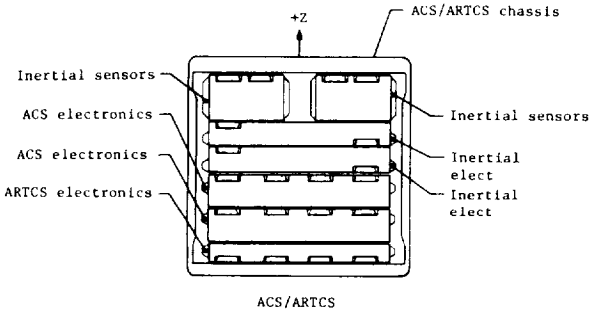

Bay 5

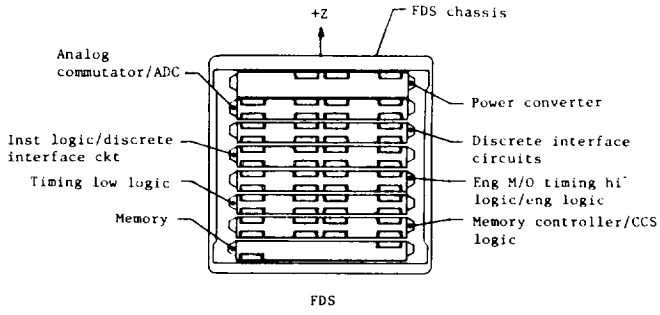

Bay 6

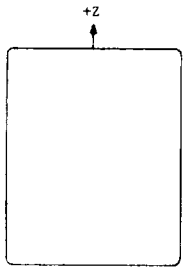

Bay 7

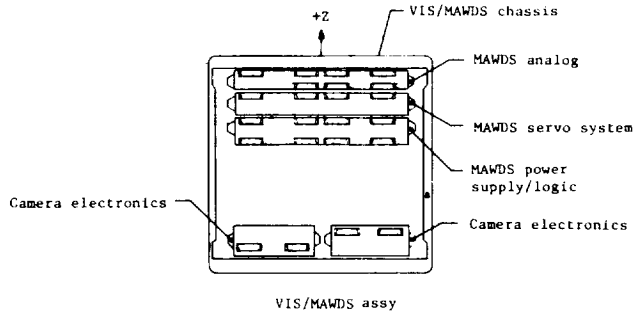

Bay 8

Figure 2.- Continued.

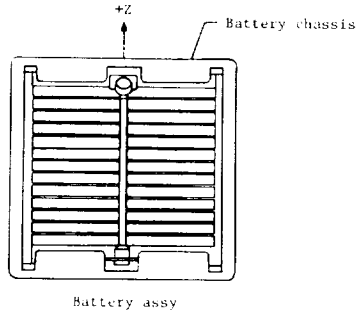

Bay 9

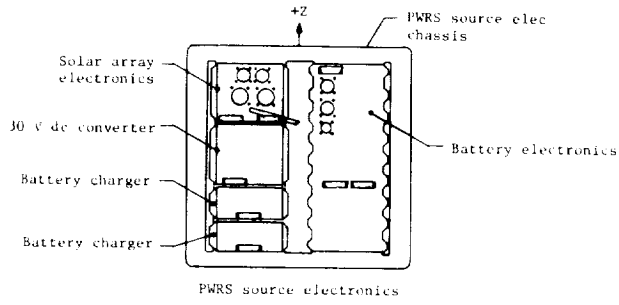

Bay 10

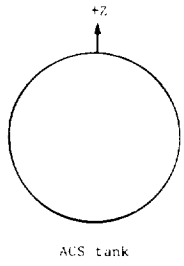

Bay 11

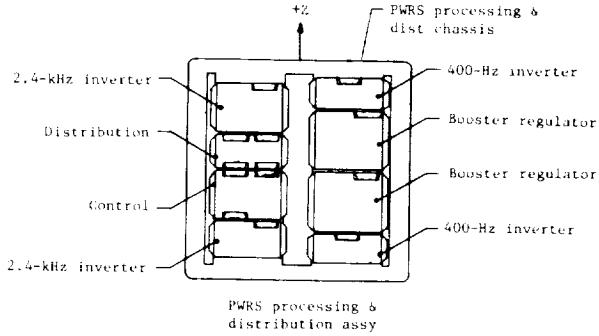

Bay 12

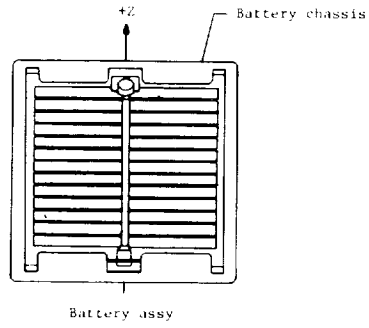

Bay 13

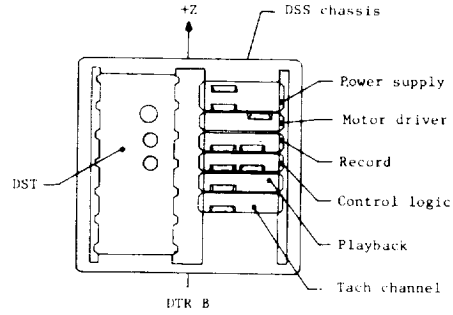

Bay 14

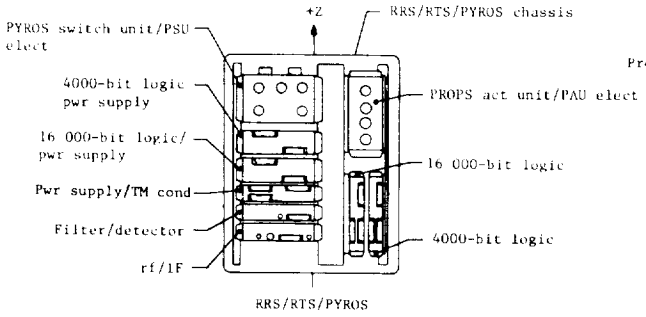

Bay 15

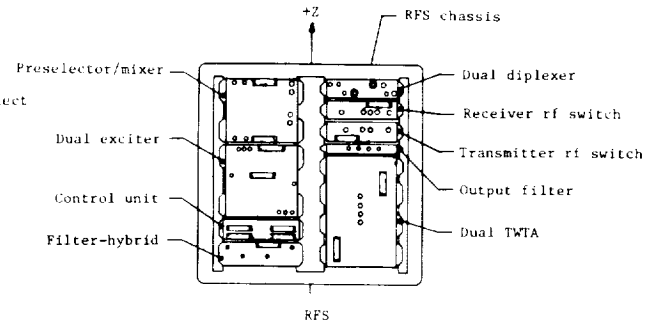

Bay 16

Figure 2.- Concluded.

GUIDANCE AND CONTROL REQUIREMENTS

The VO guidance and control subsystem reduced the initial rates after S/C separation from the launch vehicle and acquired the celestial references (Sun and Canopus), maintained the correct S/C attitude during all mission phases following initial acquisition of the celestial references, automatically reacquired (in conjunction with the CCS) celestial references if they were lost, performed commanded turns of the S/C to any desired orientation relative to the celestial references, controlled the S/C attitude and thrust vector orientation during propulsive maneuvers, and provided control with respect to celestial references for VLC initialization and inertial control during VLC separation.

TELECOMMUNICATION REQUIREMENTS

The primary telecommunications group of subsystems performed three basic important functions for the VO:

(1) Downlink telemetry: Two downlink channels (subcarriers) were provided and called low-rate and high-rate channels or data rates. The low-rate channel, which was always present, carried engineering (performance monitoring) data or the CCS memory data. The high-rate channel (present when required) carried real-time or playback science and/or engineering data.

(2) Uplink commands: Earth to S/C commands were transmitted to the S/C by modulating the S-band uplink with the command information.

(3) Navigation or S/C position monitoring: This was accomplished by two-way coherent Doppler tracking which was the Doppler measurement of the motion of the VO with respect to Earth by coherent retransmission of the uplink rf carrier from the VO to Earth. Ranging was also provided by instantaneous distance measurements (range points) obtained when the S-band uplink was modulated with the ranging code, and the RFS demodulated the received signal and remodulated the same information on the downlink to Earth.

These functions were accomplished with the S-band S/S's on the VO (shown in fig. 3) in conjunction with the elements of the DSN and the MCCC on the ground

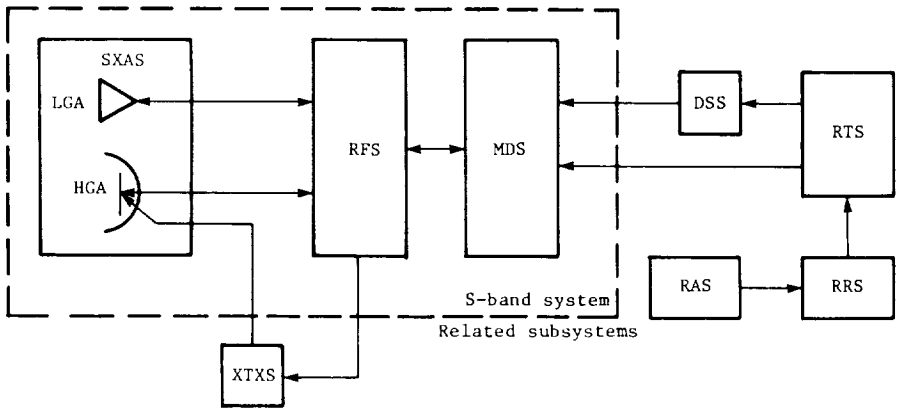

Figure 3.- Functional block diagram of S-band telecommunications subsystems.

(shown in fig. 4). The UHF relay equipment was an important group of telecommunications subsystems provided to support the VL relay links, the primary source of getting data from the surface of Mars to Earth. These S/S's performed in a receive-only mode and consisted of the RAS, RRS, and RTS as shown in figure 3. The UHF S/S's on both VO's could receive the data from either VL for recording on the VO tape recorder for transmission to Earth at the optimum opportunity (real time or delayed).

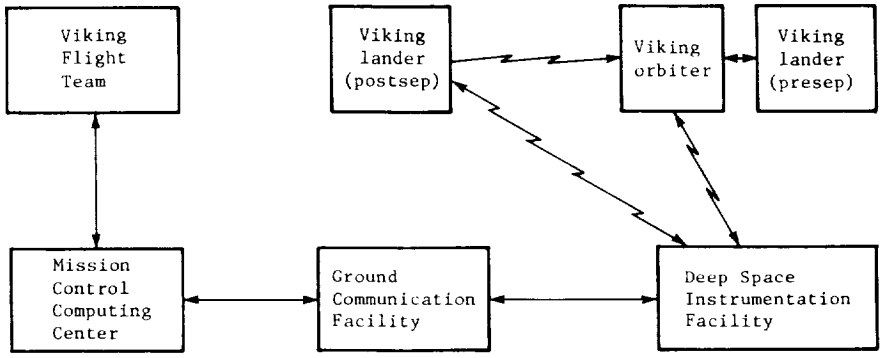

Figure 4.- Overall block diagram of VO telecommunications subsystems.

DATA HANDLING

The VO contained data handling equipment to gather information about the performance and status of engineering S/S's and on-board scientific instruments, about the results of experiments using these instruments, and about the cruise status of the VLC. These data were sent to the on-board telecommunications equipment for transmission to Earth. In addition, the VO stored and/or transmitted VL data acquired via the VL-VO relay link. All data handling and processing was accomplished by the FDS and the MDS.

COMMAND AND SEQUENCING

Ground commands were required to modify VO flight sequences, to initiate VLC sequences when the VLC was attached to the VO, and to counter unexpected VO events. On-board commands could be issued in a predetermined timing sequence via on-board program control or directly as received from the ground. Commands were received from Earth via the SXAS (both the LGA and the HGA) and the RFS, demodulated by the MDS, and decoded by the CCS. Elements of the SXAS, RFS, MDS, and CCS comprised the command system. Figure 5 shows the functional organization of these elements, whose individual roles were as follows:

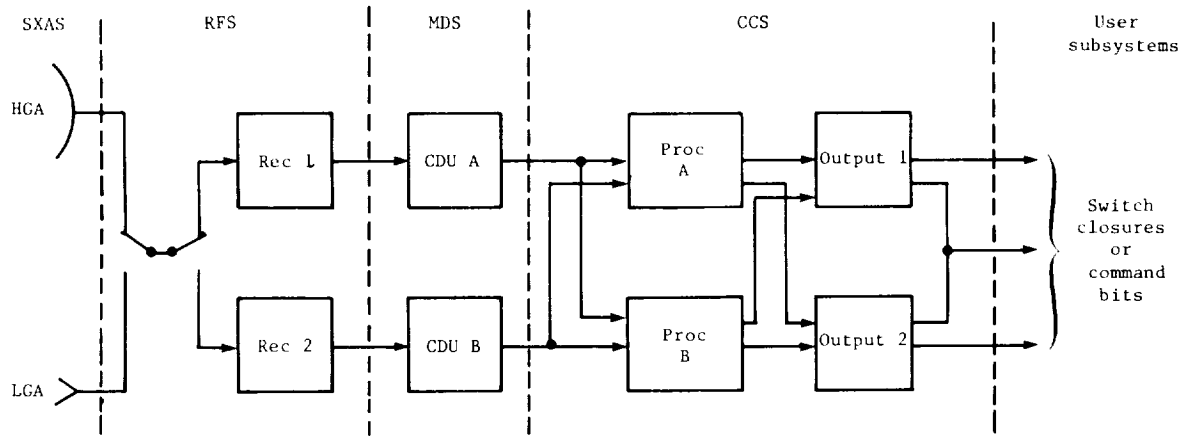

Figure 5.- Simplified block diagram of command systems.

SXAS: To receive the uplink S-band carrier frequency containing the command modulation with either the LGA or the HGA and route it to the RFS via coaxial cables

RFS: To demodulate the command subcarrier from the uplink S-band carrier and send it to an MDS CDU; only one RFS receiver section and CDU were operational at a time

MDS: To establish an in-lock condition for the command detector, detect the command data bits in the command subcarrier and send them to both CCS processors; the CDU had to be in an in-lock condition before command data bits were sent to the CCS for processing

CCS: To decode the data bits to detect valid commands, which were expected 10 bit-times after receipt if the CDU remained in an in-lock condition and to store and execute on-board sequences

Except in emergencies, all VO flight operational sequences were implemented by using validated VO blocks and single commands. A VO block was defined as a group of VO commands and/or events, with a well-defined time interrelationship, that performed a single system level function. VO blocks were developed to implement all anticipated VO flight sequences and were validated in system tests prior to launch. New or modified sequences were tested, if test hardware existed, and validated prior to use in flight. Constraints for using the blocks required initial and final conditions, and options available with each block were included in a block dictionary.

PROPULSION MANEUVERS

The Viking Mission typically required two or three midcourse maneuvers, an MOI maneuver, and approximately 7 to 15 orbit trims. These propulsive maneuvers were accomplished with the 1.3-kN (300-lb) thrust bipropellant rocket engine

described in detail later in the section "Propulsion Subsystem." The total change in velocity capability of the VO with full tanks (1405 kg (3097 lb) of usable propellant) was 1443 m/sec. This capability assumed that the spacecraft mass was 3493 kg (7700 lb) (VLC bioshield cap separated and VLC on-board). For launches with more than 1348 kg (2972 lb) of usable propellant, the VO was capable of performing at least two midcourse maneuvers between approximately TMI + 13 days and TMI + 30 days. When launched with 1348 kg (2972 lb) of usable propellant, or less, the VO was capable of performing at least two midcourse maneuvers between approximately TMI + 6 days and TMI + 20 days. The propellant tanks pressurization at launch was approximately 0.69 MPa (100 psi) at 10° C (50° F). The propellant temperature was raised to approximately 18° C (65° F) prior to raising the tank pressure to an operative level of 1.7 MPa (250 psi). The first available midcourse firing day was dependent on the propellant load and how fast the propellants could be warmed up by the VO SEC's. Each midcourse firing could be conducted as soon as 5 days after the preceding firing, and orbit-trim firings could be conducted about 32 hr apart. These periods were dependent on the abilities of the navigation and performance analysis teams to establish trajectory parameters and determine system performance and on the required engine cool-down periods. Total maneuver times varied depending on the required initial thrust vector control and accelerometer-bias checkouts required, the use of the HGA for real-time maneuver coverage (planned for first midcourse, MOI, and mission B plane-change maneuvers), the size of the attitude maneuvers, and the length of the propulsive engine burn. The minimum engine burn duration capability was about 1.0 sec and the longest engine firing (MOI) was approximately 37 to 42 min. Maneuver accuracies are summarized later and grouped with the guidance and control accuracies.

POWER CAPABILITIES AND REQUIREMENTS

The VO had 2.4-kHz single-phase, 400-Hz three-phase, regulated dc (30 V and 56 V) and unregulated dc (25 V to 50 V) power sources. Unregulated dc power was also provided for the VLC. Arrays of photovoltaic cells arranged on four double-section, folding solar panels furnished primary power for all Sun-oriented operations. Two identical nickel-cadmium batteries were used as a secondary source of power for off-Sun operations and to share the load when power demand exceeded the solar array capability. Redundant power conditioning and distribution functions were provided with two battery chargers, two booster regulators, two 2.4-kHz inverters, two 400-Hz three-phase inverters, two 30-V dc converters, and associated power source logic and control and switching functions. (See the simplified block diagram in fig. 6.) The hardware, operating modes, and performance are described in detail in the section "Power Subsystem."

The VO unregulated (raw) power bus was supplied by solar panels and batteries. These two power sources formed a dynamic system characterized by three stable in-flight operating modes, and a fourth short-term operating mode as follows:

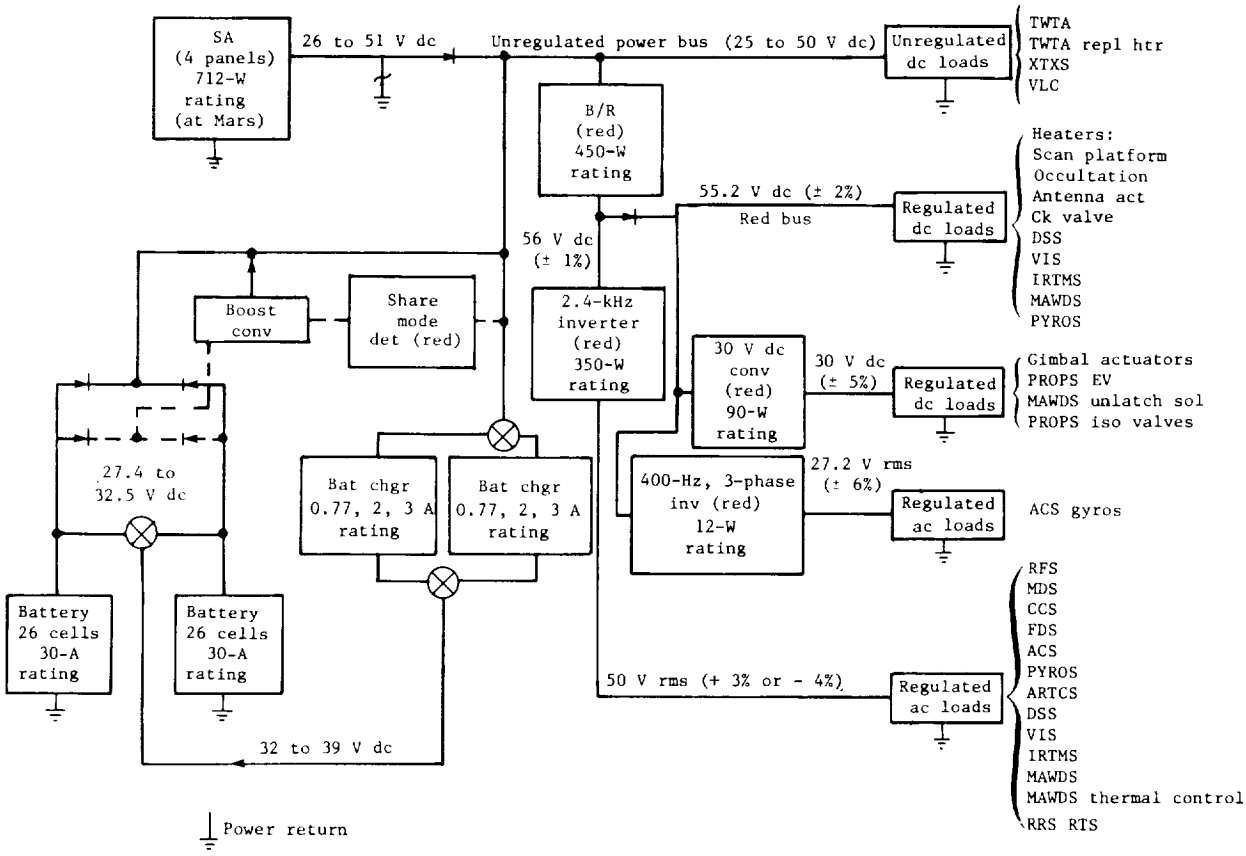

Figure 6.- Simplified block diagram of PWRS.

Solar panel mode: When the VO solar panels were illuminated, raw dc power was supplied by the panels. The VO was considered to be in a solar panel mode when the total VO power load demand was within the output power capability of the panels.

Share mode: A battery/solar panel share mode existed when the fully or partially illuminated solar panel output power was insufficient to support the VO power demand. While in this mode, the solar panel output voltage dropped to approximately the battery voltage and entered a high-current operating mode where the solar panel output power was reduced below the nominal output capability. The remainder of the VO power load was supplied by the batteries. An undesirable share mode existed if power demand fell within the solar panel output capability, but the operating point was at the battery voltage. The boost mode was designed to terminate this mode.

Battery mode: Whenever the solar panels were without illumination the total VO load was supplied by the batteries.

Boost mode: Whenever the VO was in a battery/solar panel share mode and the VO power demand fell to within the fully illuminated solar panel output power capability at its highest voltage, the raw bus could be boosted (after a Sun gate indication) to that higher voltage by the boost converter; thus, the undesirable share mode was exited and a solar panel only mode was entered.

The modes identified as VO power modes and the power profiles for these modes were developed as worst-case situations (launch time, maneuver time, peak power loads, conservative power conversion efficiencies, etc.) to identify power deficiencies or sequence limitations. Even with the conservative assumptions, the VO power capacity was found to be adequate for all anticipated nominal mission sequences and events. In flight, the power requirement and available power were analyzed for the specific power loads and event times to establish what power mode the system operated in and the overall feasibility of the sequence in terms of power usage.

TEMPERATURE CONTROL

The VO was designed and configured to maintain all of its elements within safe temperature limits for conditions which the spacecraft would experience during the mission. Temperatures were monitored within all the VO subsystems. The temperature control design is described in detail in the section "Detailed Design Information."

There was no temperature control subsystem internal to the VO. Temperature requirements of all elements of the spacecraft were established. Passive and active elements were then incorporated into the design to satisfy these requirements (together with the VO subsystem they are a part of) are as follows:

Passive elements:

- Material coatings or finishes (applicable to each subsystem, as required)
- Multilayer blankets (STRUS)

Active elements:

- Bimetallic actuated louvers (DEVS)
- Solar energy controllers (DEVS; controlled by ARTCS)
- Controllable electrical heaters (applicable to each subsystem, as required)

Except for the longer engine firings (primarily MOI), off-Sun line maneuvers, and occultations, the spacecraft was maintained at an acceptable equilibrium temperature with energy being transferred through conduction and radiation. For the transient off-Sun periods, the large thermal capacitance of the VO could maintain the elements within acceptable temperature ranges for approximately

4 hr. Heaters were required in bays 1, 4, 8, and 14. (See fig. 1.) The heaters were automatically turned on when the equipment in these bays was turned off.

The SEC's were used to control the temperature of the propulsion module. Shortly after launch, the SEC's were fully opened to warm the propellants from the air-conditioned on-pad temperature of 7° to 10° C (45° to 50° F) up to 16° to 18° C (60° to 65° F). This warm-up period (which was required prior to pressurizing the propellant tanks) took about 5 days for an off-loaded mission and about 13 days for a mission with the propellant tanks fully loaded. The SEC's were actuated as required during the remainder of the mission to maintain the propellant temperatures at about 18° C (65° F).

The scan platform had a commandable heater located on the structure as well as a thermal replacement heater on each of the instruments. The MAWDS had a servocontrolled heater which was used to maintain the optics and detector at a constant temperature. During normal operations, the instrument replacement heaters were turned on when the instruments were turned off. Should Sun occultation periods exceed 2.3 hr, power management considerations dictated that the replacement heaters be left off. When the science instruments had been turned off, either with or without replacement heaters on, a wait time was required to obtain the required temperature and temperature distribution in the science instruments.

SYSTEM MASS PROPERTIES

The VO system mass properties were controlled by the Viking S/C mass properties control plan. Launch mass properties for each VO were defined by orbiter constraints and idiosyncrasies. The mass and/or inertia properties of the V S/C varied in flight because of expulsion of propulsion and attitude control propellants; the location of the scan platform and HGA; and the onboard/separated status of the VLC bioshield cap, the VLC, and the VLC bioshield base/adapter. Status logs of S/C mass properties throughout the mission were maintained by the OPAG and the LPAG.

DESCRIPTION OF MAJOR SUBSYSTEMS

A simplified functional block diagram of the VO is presented in figure 7. The S/S's are briefly described as follows in the order given in table 1.

Structure subsystem: STRUS provided mechanical support and alignment for all flight equipment, passive thermal control, and micrometeoroid protection. In addition, the structure provided means for handling the assembled VO for flight qualification testing, transporting, and mating operations with the VLC and the LV. STRUS included a basic bus structure of irregular octagonal shape about 2.4 m (8 ft) maximum across the flats; substructures for the PROPS, the solar panels and outriggers, the scan platform, the electronic assembly chassis, the high- and low-gain antennas (except feed assemblies), and the V S/C A and VLCA; and the micrometeoroid and thermal blankets. (See fig. 1.)

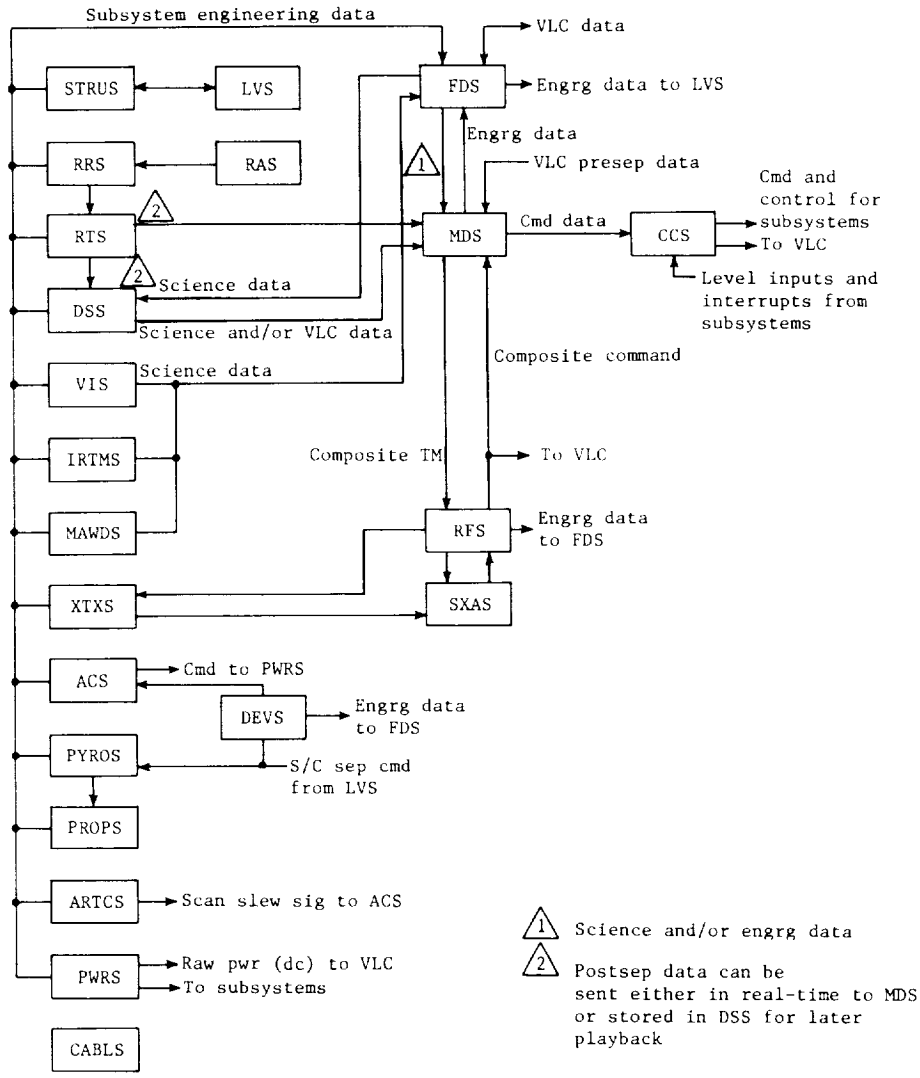

Figure 7.- Simplified functional block diagram of VO.

Radio frequency subsystem: The RFS provided means for simultaneously receiving the DSN uplink S-band signal and extracting from it the composite command signal for routing to the VO MDS or the VLC, accommodating coherent two-way precision Doppler and turnaround ranging, and modulating the S-band downlink with the composite telemetry signal. The RFS included dual S-band receivers, dual TWTA's and dual exciters for transmitting, and attendant control units, power supplies, rf couplers, switches, filters, power splitters, and coaxial cabling. Only one receiver, TWTA, and exciter was powered at any one time, and the redundant units were held in passive standby. RFS control provided for switching to the redundant receiver, TWTA, and exciter upon ground command via the CCS or, automatically, upon on-board malfunction detection logic. Based on CCS commands, RFS control also provided for switching between the high- and low-gain antennas, switching between high- and low-rf power modes, and switching ranging on or off.

Modulation demodulation subsystem: For the DSN to VO uplink, the MDS performed the function of detecting the information data bits of the composite command signal from the RFS, and supplying the command bits, timing, and detector status to the CCS. For the VO to DSN downlink, the MDS performed the functions of modulating one of the two downlink subcarriers with low-rate engineering data from the FDS; block coding the 1000, 2000, 4000, 8000, or 16 000 bps playback data from the DSS or the 2000 bps real-time data from the FDS; and modulating the other downlink subcarrier with either the (block-coded or uncoded) VO data received directly from the DSS or FDS or VLC data received hardline prior to separation or via the RTS after separation. The MDS consisted of two block redundant CDU's and two block redundant TMU's selectable by commands from the CCS.

Power subsystem: PWRS provided the VO with 2.4-kHz single-phase, 400-Hz three-phase, regulated dc (30 V and 56 V), and unregulated dc power. Unregulated dc power was also provided for the VLC prior to separation. PWRS utilized arrays of photovoltaic cells arranged on four double-section, folding solar panels to furnish primary power for all Sun-oriented operations and for providing energy to charge the batteries. Two identical nickel-cadmium batteries were used as a secondary source of power for off-Sun operations to share the load when power demand exceeded the solar-array capability. Redundant power conditioning and distribution functions were provided with two battery chargers; two booster regulators; two 2.4-kHz inverters; two 400-Hz three-phase inverters; two 30 V dc converters; and associated power source logic, control, and switching functions.

Computer command subsystem: The CCS decoded uplink data bits and sent validated commands to VO subsystems and the VLC by sending digital data through isolated switches or by providing discrete 100 ms switch closures. The commands were issued in real time based on direct ground commands or in a sequence according to the programs stored in the CCS memories. The stored sequence could be altered by interrupts initiated on board the VO or by commands initiated on the ground. The CCS included two of each of the following units for redundancy: memories, processors, output units, coded command buffers, discrete command buffers, and power supplies. Each processor can be operated in an individual mode or tandem mode through either or both of the output units. During MOI and for certain other critical operations, both processors could be active in the individual mode, issuing their commands in parallel through their respective output units.

Flight data subsystem: The FDS provided the functions of processing VO or VLC engineering data before separation and VO science data for real-time transmission by the MDS or recording by the DSS and provided control and timing signals for the VIS, MAWDS, and IRTMS, as well as timing for the MDS, PWRS, CCS, and DSS. The desired data mode, data rate, and engineering telemetry format were selected by the CCS sending coded commands to the FDS. The FDS included functional elements for processing engineering data, infrared science and visual imaging data, timing and control units, two memories, and two power converters.

Attitude control subsystem: The ACS provided attitude orientation and control by operating in the following distinct but related modes: the cruise mode, in which three-axis position stabilization was acquired and maintained with the Sun and Canopus as reference objects and three-axis angular rate stabilization was provided by using derived rate feedback; the all-axis inertial mode, in which inertial rate and position error signals were used for the pitch, yaw, and roll channels instead of derived rate and celestial sensor error signals; the inertial roll mode, which was similar to the cruise mode with respect to the pitch and yaw axes except that inertial rate and position error signals were used for the roll channel; the maneuver mode in which the ACS oriented the vehicle to any specified attitude by executing roll and yaw turns in response to coded commands; and the thrust-vector control mode in which the pitch and yaw attitude were controlled during propulsion engine firings by autopilot-controlled gimbal actuation of the engine whereas the roll attitude was controlled by the ACS gas system in the roll channel. In the event of loss of Sun acquisition for any noncatastrophic reason, the ACS automatically sought reacquisition. If Canopus acquisition was lost, internal logic selected the inertial roll mode and awaited further commands from a stored CCS program. The ACS was commanded by the CCS to operate in the all-axis inertial mode prior to initiation of a maneuver mode. The ACS was switched to the inertial roll mode in response to a CCS command prior to expected stray-light events. Roll turns could be commanded by the CCS when operating in the inertial role mode. In the event of Sun occultation, the ACS automatically switched to the all-axis inertial mode in response to signals from the acquisition Sun sensors and Sun gate or preferably the gyros would be warmed up and the transfer would be accomplished by timed command from the CCS. The ACS consisted of two block redundant inertial reference units, a Canopus tracker, Sun sensors, two block redundant attitude control electronics assemblies, a dual reaction control gas system, and engine gimbal actuators.

Pyrotechnic subsystem: PYROS provided for actuation of the VLC adapter release devices, unlatching of the HGA, actuation of the PROPS and scan platform squib valves, and switching of electrical pulses for actuation of propellant-isolation and engine-control valves. PYROS consisted of a redundant pyrotechnic switching unit, a propulsion actuation unit, HGA and solar-panel pinpuller assemblies, and all VO squibs.

Cabling subsystem: CABLS provided the necessary harness for electrical interconnections between VO S/S electronic assemblies and for interface cabling from the VO to the launch vehicle and VLC. The rf coaxial cables were included in the RFS and the SXAS.

Propulsion subsystem: PROPS provided thrust upon command for up to four midcourse maneuvers, the MOI maneuver, and up to 20 orbit-trim maneuvers. Helium pressure was used to feed the storable propellants to the 1.3-kN (300-lb), fixed thrust, two-axis gimballed rocket engine. Sufficient propellant was provided to impart a total velocity change of 1443 m/sec to a separated S/C (3493 kg (7700 lb)) with fully loaded propellant tanks (1405 kg (3097 lb) propellant load)). PROPS consisted of the following equipment (which, when integrated with the propulsion substructure, gimbal actuators, squibs, and cabling, formed a modular assembly capable of being fueled and pressurized prior to installation in the VO): a single pressurant tank, a pressurant control assembly, one cylindrical tank for each propellant, fuel and oxidizer propellant isolation

assemblies, a rocket engine with a film-cooled beryllium chamber and a radiation-cooled nozzle skirt of 60:1 expansion ratio, and interconnecting hardware. Capillary devices were used within the tanks for propellant management. Pyrotechnic valves were used to lock up both the helium pressurant and the propellants during the long cruise periods.

Mechanical devices subsystem: DEVS provided deployment and damping devices and cruise latches for the solar panels, solar energy controllers and louvers for temperature control, release and separation devices for the V S/C A and the VLCA, latch devices for the HGA and RAS antennas and scan platform, and ACS enable and pyrotechnic arming switches.

Articulation control subsystem: ARTCS consisted of the necessary stepping motor actuators, actuator drive links, and block redundant electronics for controlling the pointing of the scan platform, the position of the HGA, and the blade position of the solar energy controllers for PROPS temperature control. Any two articulation functions could be accomplished at one time. The scan platform could be slewed at rates of 0.25 or 1.0 deg/sec in clock and cone angle (simultaneous clock and cone motion, if desired) and could be slewed a minimum step of 0.25 deg in clock or cone angle. Following VLC separation and adapter release, the scan platform can be slewed over a cone angle range of 45° to 175° and clock angle range of 80° to 310°; however, this capability was more restricted prior to VLC separation and, even after separation the full cone angle range was not available over the full clock angle range because of interference of portions of the VO.

Data storage subsystem: DSS recorded VO data from the FDS and VL data from the relay telemetry S/S's. These data were played back through the MDS and RFS to the DSN. The DSS consisted of two identical and completely independent recorders each with a minimum total storage capacity of 5.6×10^8 bits of VO imaging data plus a minimum of 4.0×10^7 bits of FDS high-rate data (VO engineering and infrared science data) or a minimum of 8×10^7 bits of replayed VL data. Each recorder had the capability to record VO visual imaging data on seven tracks simultaneously, record VL data at either 4000 or 16 000 bps on track 8, record FDS high-rate data (VO engineering and infrared science data) at 2000 bps on track 8, and playback recorded data at 1000, 2000, 4000, 8000, or 16 000 bps.

S/X band antenna subsystem: SXAS provided for transmitting and receiving S/X-band signals between the VO and the DSN. The SXAS consisted of the S-band low-gain antenna feed, S/X band HGA feed, and the S- and X-band transmission lines. The LGA provided approximately roll-symmetrical coverage about the VO Z-axis such that the command link could be maintained in any roll attitude throughout the mission while in the Sun-acquired attitude. Both antennas were right-hand circularly polarized, with the LGA designed to operate over the frequency region from 2115 to 2295 MHz and the HGA covering the same frequency region as well as the 8415 MHz frequency with the corresponding much smaller (sharper) beam width and higher gain.

Visual imaging subsystem: The scientific objectives of the VIS were to obtain image information to be used in Viking landing site selection, to obtain repeated coverage of landing sites during the lifetime of the VL on the surface

of Mars, and to obtain image information for the study of the dynamic and physical characteristics of the planet and its atmosphere. The VIS consisted of two identical narrow-angle, electro-optical cameras and their associated electronic subassemblies. The field of view of each camera was 29.52 mrad in the direction parallel to the scan lines and 26.37 mrad in the direction perpendicular to the scan lines. Pixel (picture element) spacing was 25 μrad. Camera A and B boresight axes were offset 24.09 mrad in the direction parallel to the scan lines and 0.0 mrad in the direction perpendicular to the scan lines.

Infrared thermal mapper subsystem: The objectives of the thermal mapping investigation were to aid in the selection of landing sites for the VL's, to monitor the regions surrounding the VL's, and to provide additional information of spatial and temporal distribution of surface temperature and thermal balance to aid in the selection of future landing sites. The IRTMS consisted of four small Cassegrainian telescopes, each with an array of seven thermal detectors in the image plane and associated electronics. The instrument had sensitivity over specific spectral bands within the range of 0.3 to 24 μm. The IRTMS was boresighted with the VIS camera bisector, and the thermal detectors were arranged in a chevron pattern which fell within the combined field of view of the two VIS cameras.

Mars atmospheric water detector subsystem: The objectives of the water mapping investigation were to aid in the selection of landing sites for the VL's and to provide additional information on spatial and temporal distribution of water vapor abundance to contribute to our knowledge of the planet and aid in the selection of future landing sites. The MAWDS consisted of a fixed grating spectrometer, a five-element radiation-cooled PbS detector, and a small input telescope mirror which viewed the surface via a scanning mirror. The instrument had an instantaneous field of view of 16.75 by 2.1 mrad and the scanning mirror stepped through 15 positions to provide a total coverage roughly equal to one-half the combined coverage of the two VIS cameras. The MAWDS was also boresighted with the VIS cameras bisector.

X-band transmitter subsystem: The XTXS provided an X-band downlink signal so that the dispersion between the S- and X-band signals could be used for interplanetary charged particle measurement, Martian atmospheric measurements, and other radio science purposes. The XTXS multiplied the frequency received from the RFS exciter to the X-band frequency, modulated the X-band carrier signal with the detected ranging signal from the RFS, and sent the modulated X-band signal (whose frequency was coherently related to the RFS exciter frequency) to the HGA for transmission to the DSN.

Relay radio subsystem: The RRS supported relay link communications by demodulating the signal received from the VL through the relay antenna S/S, and routing the FSK VL data to the RTS.

Relay telemetry subsystem: The RTS recovered either of two (4000 or 16 000 bps) PCM, split-phase, bit streams from the RRS, restored the data to NRZ-L format, routed either of the restored data streams with bit sync to the DSS for recording, and/or routed the 4000-bps data stream to the MDS for real-time transmission to the DSN.

Relay antenna subsystem: The RAS received the UHF signal transmitted by the VL's to the VO's. The RAS was a right-hand, circularly polarized, low-gain, antenna operating at a frequency of 380.963 MHz. The relay antenna assembly was attached to the back side of a solar panel section and was deployed from its stowed position to the fixed operating position when the solar panels were deployed.

VIKING ORBITER DESIGN APPROACH

DESIGN PHILOSOPHY

The design philosophy adopted for the VO was based upon modifications to the Mariner Mars 1971 design. The design of the VO followed the general guidelines below:

Changes were made

To achieve mission objectives
To accommodate VL requirements
To accommodate Viking launch vehicle requirements
To accommodate parts availability
To meet Viking environmental requirements

Changes were considered which

Reduced cost
Improved reliability
Insured safety

Incorporation of design features to satisfy future requirements of similar missions was permitted only if these requirements were consistent with the Viking Project Office requirements and constraints.

It was a design goal that the VO would be capable of performing operational sequences under control of on-board logic to the maximum extent that was consistent with project constraints. Primary dependence on ground commands would be minimized.

Ground command capability was provided for

Loading computer flight sequences
Initiating/arming certain sequences
Backing-up critical on-board commands
Updating the VL prior to VLC separation

All VO's were identical with respect to electrical and mechanical configuration. The transmitted and received S-band frequencies for each VO were different. The identical nature would not only yield the capability of launching any V S/C initially but would also possess the flexibility for placing either VO in any of the selected orbits. The capability also existed to select or modify the selection of the orbits and time of arrival after launch.

The VO design was based on the environments expected from the time of initial assembly in the JPL SAF through ground test, transportation, launch, cruise, and orbital operations. Flight VO's and their components, however, were not allowed to be subjected to environments beyond flight acceptance levels. Safeguards to prevent overtest levels were provided in the operations and ground facilities but not in the flight hardware.

On-pad tests and operations were limited to the minimum required to turn the VO on, ready it for launch, verify its flight readiness, and functions relative to the VLC. System level checks were performed after the VO had left the final assembly area, and no operation was conducted on the pad, unless that operation had been previously checked out in SAF or at ETR under comparable environments. No provisions were made for component or subsystem testing from the blockhouse. The VO would not be defueled or repaired at the launch pad.

Although it was a requirement that all designs be subjected to type approval and flight acceptance testing, it was a goal that the design approach selected for any element of the system be amendable to verification by analysis.

The requirement for long VO life to achieve mission success was recognized. The VO design lifetime would exceed the defined mission lifetime. No decision was arbitrarily rendered which precluded attainment of VO design lifetimes well in excess of the defined mission lifetime.

The VO design included the capability of terminating and reestablishing rf transmission upon command.

RELIABILITY CRITERIA

The reliability criteria were as follows:

The VO design was governed by the policy that the requirement for reliable operation took precedence over the requirements for additional capability and flexibility beyond that required to achieve the basic mission.

The design took advantage of the experience gained in previous Mariner designs to the maximum feasible extent.

Where there were new designs or modifications to the Mariner Mars '71 designs, care was taken in the choice and control of new fabrication techniques and operational procedures so that the probability of success was enhanced.

Within weight, cost, and schedule constraints, functional or alternate mode redundance was employed such that no single failure mode of any component (electric, mechanical, pyrotechnic, electromechanical, or structural) would cause a catastrophic effect on the mission.

Efforts were taken to reduce the functional interdependence between elements of the VO. Where such dependency must exist, attempts were made to achieve a noncatastrophic performance from the dependent element in the event of a failure in the interface or in the element upon which it depends.

All scientific instruments were designed to be as functionally independent of one another and of the S/C operation as was feasible to increase the assurance that a failure in one instrument or in equipment common to several instruments would have a minimum effect on the total data received.

Particular emphasis was placed upon simple and conservative design along with a complete program of component, subsystem, and system testing.

SCHEDULE CRITERIA

Since the mission objectives involved the 1975 Mars opportunity, all designs, techniques, and components, including all intermediate milestone objectives leading up to the launchings, were required to be compatible with the project development time schedule.

LAUNCH AND LIFETIME CRITERIA

The launch and lifetime criteria for the Viking orbiter were as follows:

The launch weight and dynamic envelope of the supplied flight equipment were maintained compatible with the Viking '75 project specifications. Adequate margins were maintained to avoid conflicts late in the development schedule.

The defined mission lifetime used in the VO design activity was

A maximum of 370 days of interplanetary cruise, plus

50 days of orbital operations with the VLC aboard the VO, plus

90 days of orbital operations after VLC separation

A normally functioning VO would have a minimum lifetime that would meet either VL lifetime requirement

DETAILED DESIGN INFORMATION

COORDINATE SYSTEMS

Several coordinate systems, illustrated in figure 8, were used for the V S/C and its major elements. The VO coordinate system which applied for the

V S/C standard coordinate system

Direction	Axis	Positive rotation	Angle	Symbol
Transverse	X	Y to Z	Pitch	θ
Transverse	Y	Z to X	Yaw	ψ
Longitudinal	Z*	X to Y	Roll	ϕ

*V S/C -Z-axis points toward Sun during flight when on celestial reference.

VLC standard coordinate system

Direction	Axis	Positive rotation	Angle	Symbol
Transverse	Y	Z to X	Pitch	θ
Transverse	Z*	X to Y	Yaw	ψ
Longitudinal	X	Y to Z	Roll	ϕ

*VLC aeroshell apex is in -Z-direction when part of V S/C.

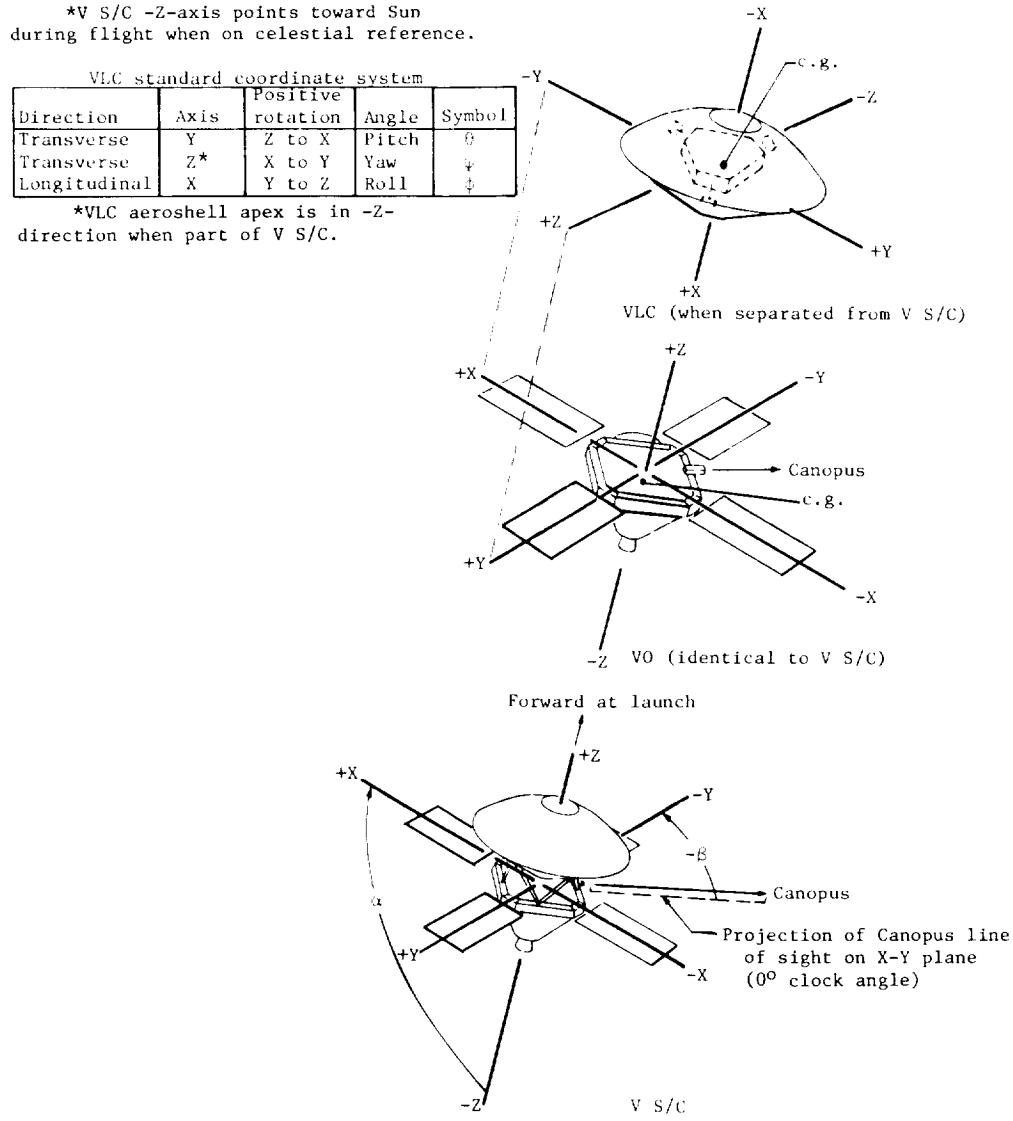

Figure 8.- V S/C, VO, and VLC coordinate axes.

stabilization system is given in figures 9 and 10. An A,B,C celestial reference set of axes are defined as shown in figure 11. The coordinate system for

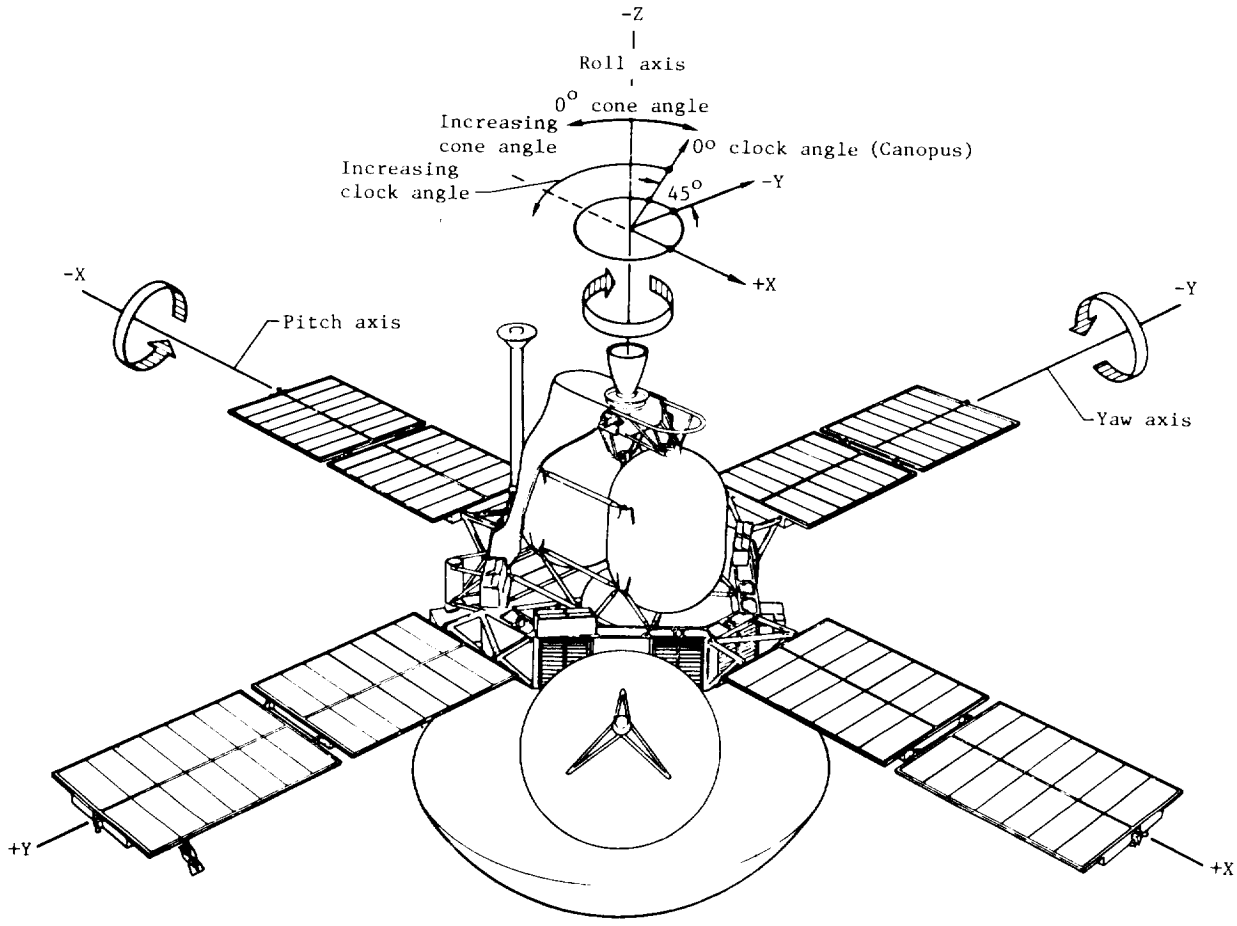

Figure 9.- Orbiter coordinate system.

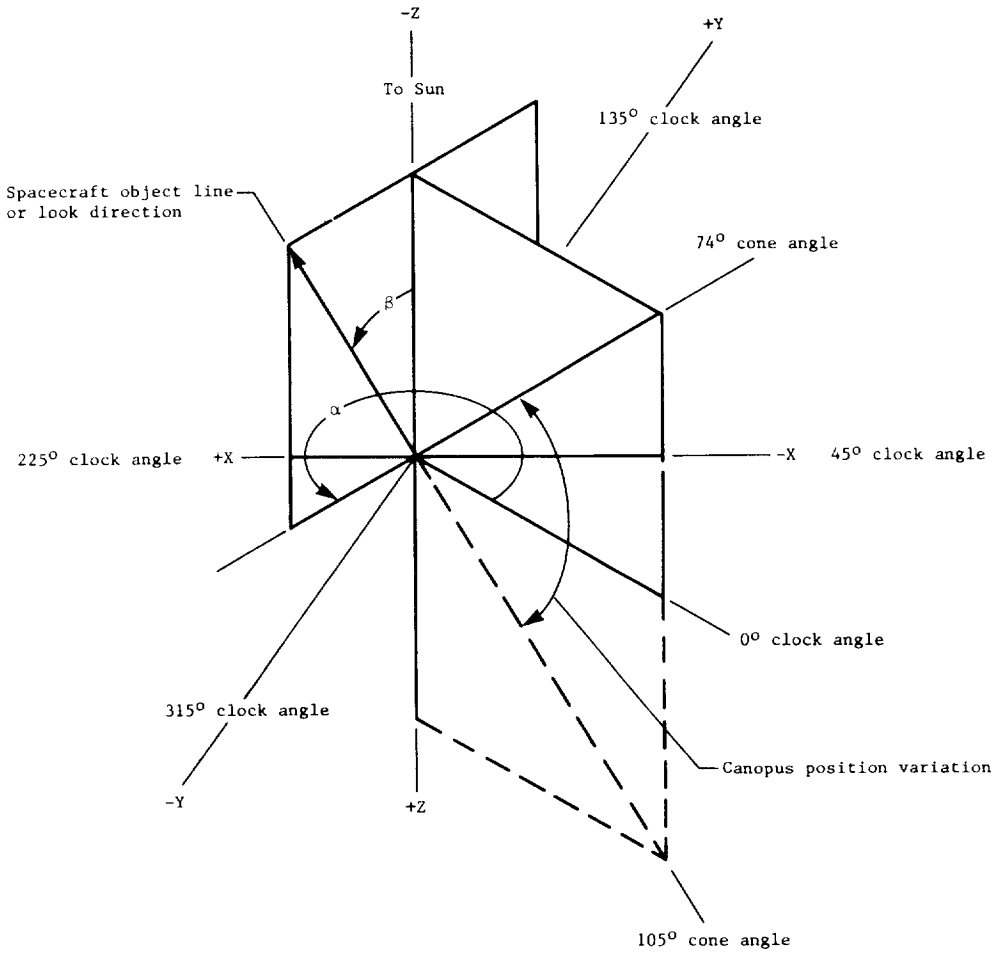

Figure 10.- Coordinate system for cone and clock angles.

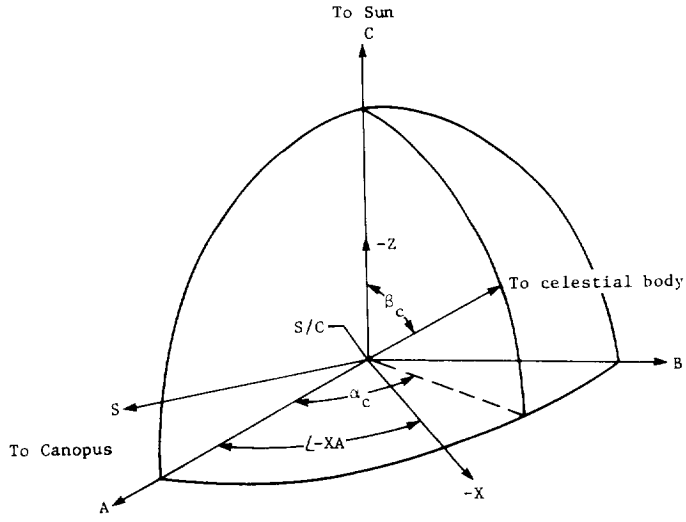

Figure 11.- Celestial reference set.

the scan platform is shown in figures 12 and 13 and the scan platform FOV is shown in figure 14. The two-degree-of-freedom HGA coordinate system is shown in figure 15 and the HGA FOV constraints are shown in figure 16.

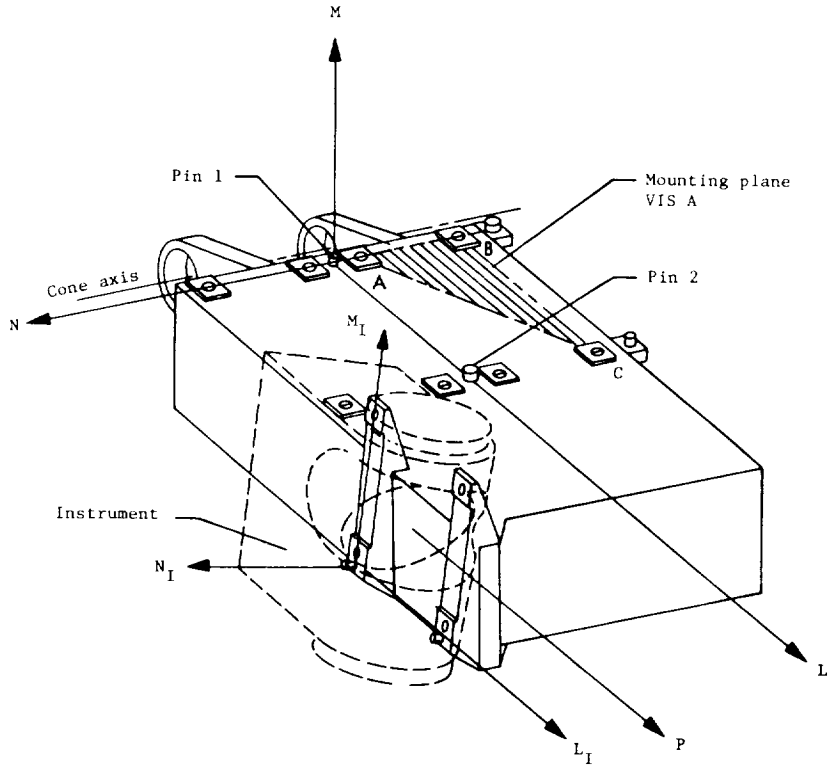

Figure 12.- Scan platform coordinate system.

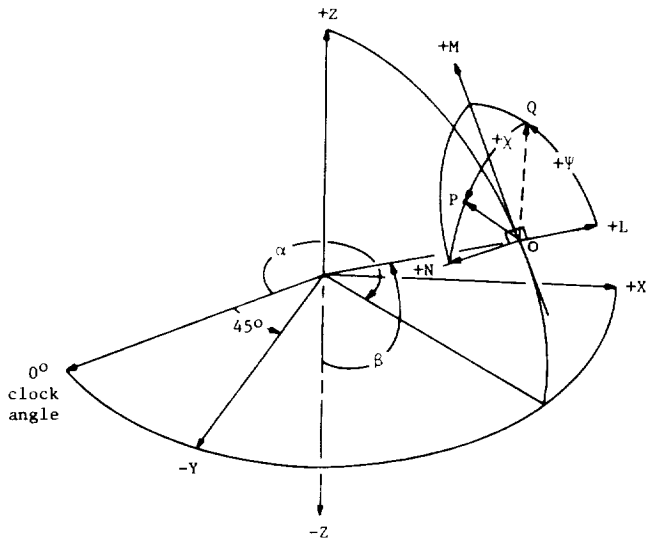

Figure 13.- Orbiter scan platform coordinate system relationship.

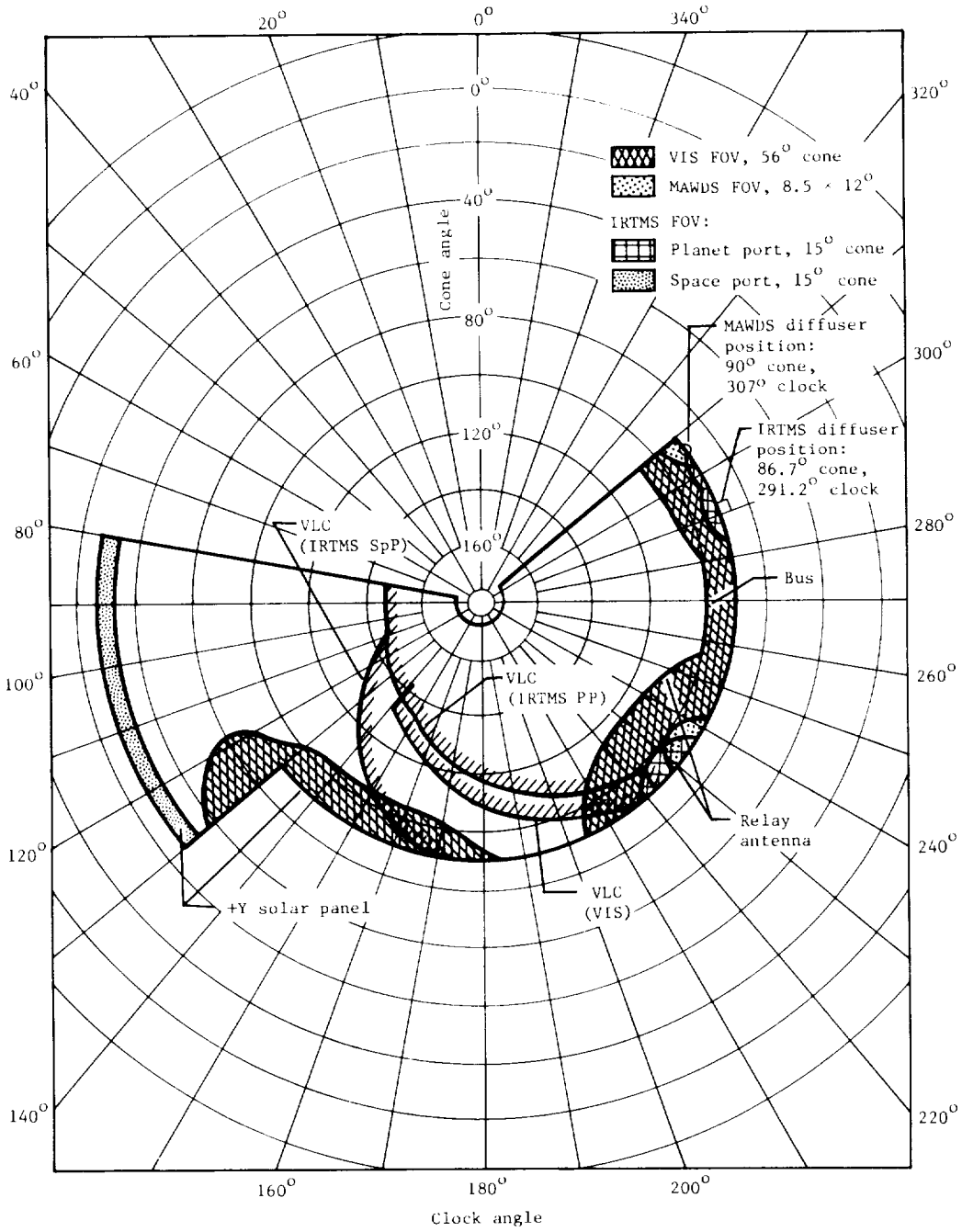

Figure 14.- FOV for platform-mounted science instruments.

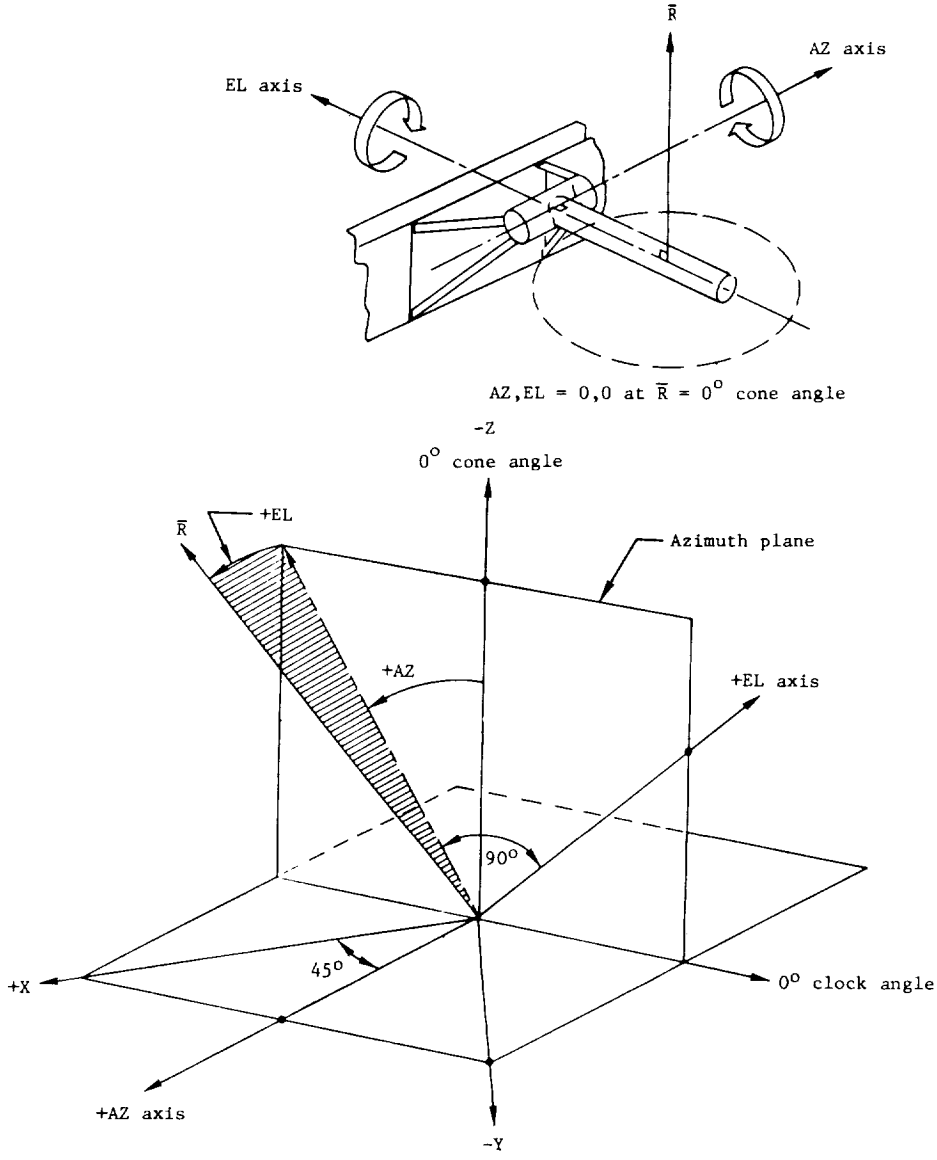

Figure 15.- HGA coordinate system.

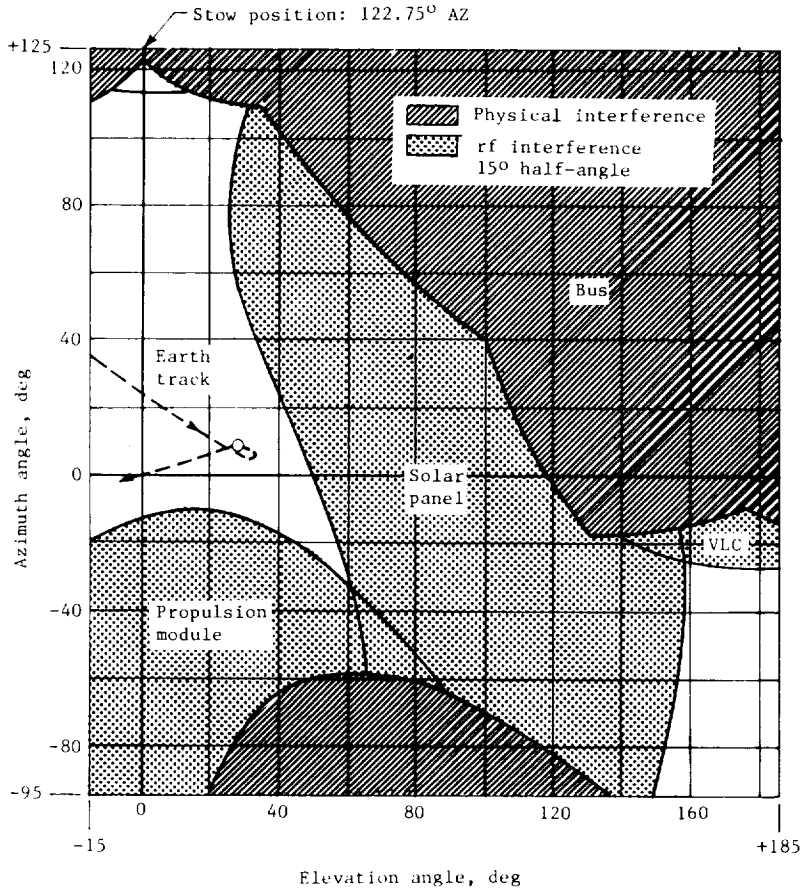

Figure 16.- HGA view constraints for AZ,EL coordinates.

The look directions for the VO equipment were given in VO cone and clock angle coordinates which formed a spherical coordinate system. (See fig. 10.) The VO cone angle was defined as the angle from the VO -Z-axis to the look direction of the equipment and ranged between 0° and 180°. The angle between a plane containing the Z-axis and the look direction of the equipment was defined as the VO clock angle and ranged between 0° and 360°. It was measured from the Z-axis/Canopus-tracker plane and was defined as positive in the clockwise direction when looking along the -Z-axis from the center of the VO. (See figs. 9 and 10.)

The scan platform coordinate system (L,M,N) illustrated in figures 12 and 13 was a right-hand orthogonal coordinate system (where $L = M \times N$) with the origin at the intersection of the center line of pin 1 with the VIS A mounting plane (ABC). The unit vector L, which defined the look direction of the platform and was the nominal bisector of the two VIS camera boresights, was directed from pin 1 toward pin 2, passing through both pin center lines and in the VIS A mounting plane. The unit vector N, which was parallel to the platform cone axis, was in the VIS A mounting plane and normal to L. The unit vector M completed the right-hand orthogonal coordinate system. The L_I, M_I, N_I coordinate

system shown was for a typical instrument. An L_I,M_I,N_I coordinate system was defined with respect to each instrument housing for mounting purposes. The vectors L_{VA},N_{VA} and L_{VB},N_{VB} were parallel to the mounting surfaces of VIS cameras A and B, respectively, whereas L_M,N_M and L_I,M_I were parallel to the mounting surfaces of the MAWDS and IRTMS, respectively. The physical mounting of an instrument was specified by the direction cosines of its coordinate axes L_I,M_I,N_I with respect to the platform coordinates L,M,N. The scan platform coordinates L,M,N were contained in the VO coordinate system as shown in figure 13. The axis N was nominally parallel to the X-Y plane. The L vector of the platform was located in VO clock and cone plane by α_c and β_c, respectively. When the VO is in Sun-Canopus lock, α_c and β_c are also the celestial clock and cone angles of the scan platform L vector.

The HGA boresight direction R was defined relative to VO coordinates in terms of an AZ,EL coordinate system as illustrated in the sketch in figure 15. The AZ-axis was parallel to the VO X-Y plane and was specified in VO cone-clock coordinates as a vector of 270° clock angle and 90° cone angle. Azimuth was measured in the AZ-plane from the -Z-axis to the projection of R on the AZ-plane. Azimuth was defined as positive in the clockwise direction when viewed along the +AZ-axis. Elevation was defined as the angle of inclination of R from the AZ-plane and was measured positive in the direction of the +AZ-axis. The AZ,EL coordinate system, as defined, resulted in two coordinate angle solutions to describe each R orientation; for example, 30° AZ, 20° EL was identical to -150° AZ, 160° EL. This definition was intentionally derived to account for the dual-position antenna pointing capability inherent in the gimbal configuration.

VIKING ORBITER STATES

Each VO subsystem had a definable set of modes of operation; therefore each mode represented a particular state of that S/S. The states to which each S/S was capable of being commanded along with the command numbers and functions are shown in table 2. The command numbers are used throughout this paper in

TABLE 2.- COMMAND LIST

Type	Number	Name	Destination	Function
STRUS				
DC	1A	Aft BS sep	PYROS	Separate aft BS including the VO-VLCA
	1B	Scan plat htr on	PWRS	Switch 56 V dc to scan plat htr if enabled by DC (4N) or (4P)
	1BR	Scan plat htr off	PWRS	Remove 56 V dc from scan plat htr
RFS				
DC	2A	RG on	RFS	Switch 15 V dc in active rec to its video amp
	2AR	RG off	RFS	Remove 15 V dc from video amp
	2B	Exc 1 select	RFS	Switch 2.4-kHz pwr from exc 2 to exc 1
	2BR	Exc 2 select	RFS	Switch 2.4-kHz pwr from exc 1 to exc 2

TABLE 2.- Continued

Type	Number	Name	Destination	Function
			RFS	
DC	2C	TWTA 1 select	RFS	Switch unregulated dc pwr from TWTA 2 to TWTA 1
	2CR	TWTA 2 select	RFS	Switch unregulated dc pwr from TWTA 1 to TWTA 2
	2D	TWT hi pwr	RFS	Select hi-pwr mode for both TWT's
	2DR	TWT lo pwr	RFS	Select lo-pwr mode for both TWT's
	2E	HGA select	RFS	Select HGA for transmitting and receiving
	2ER	LGA select	RFS	Select LGA for transmitting and receiving
	2F	Rec 1 select	RFS	Switch 2.4-kHz pwr from rec 2 to rec 1
	2FR	Rec 2 select	RFS	Switch 2.4-kHz pwr from rec 1 to rec 2
	2K	TWT pwr on	PWRS	Switch unregulated dc voltage to TWT's and turn off repl htr
	2KR	TWT pwr off	PWRS	Remove unregulated dc voltage to TWT's and turn on repl htr
	2X	RFS cmd en	CCS	Enable CCS outputs to RFS
	2XR	RFS cmd inh	CCS	Inhibit CCS outputs to RFS
			MDS	
DC	3A	Cr TM mode	MDS	Select LR engrg data ch only; switch LR ch modulation angle to 41°; and disable HR ch within MDS
	3B	P/B data select	MDS	Enable HR data ch and switch LR ch modulation angle to 11.9°; select BC as input to HR mod and DSS as data source input for BC
	3C	FDS HR data select	MDS	Enable HR ch and switch LR ch modulation angle to 11.9°; select BC as input to HR mod and FDS HR data (2000 bps) as BC input
	3D	Relay TM data select	MDS	Enable HR ch and switch LR ch modulation angle to 11.9°; select 4000 bps data from RTS as input to HR mod
	3E	VLC checkout data select	MDS	Enable HR ch and switch LR ch modulation angle to 11.9°; select hardline (1000 or 2000 bps) data from VLC as input to HR mod
	3F	BC B/P	MDS	Cause HR data to bypass block coder, routing data directly to input of HR mod
	3G	TMU A select	PWRS	Switch 2.4-kHz pwr to TMU A and remove it from TMU B if TMU A had been enabled by (3H)
	3GR	TMU B select (relay 1)	PWRS	Switch 2.4-kHz pwr to TMU B and remove it from TMU A
	3H	TMU A en	PWRS	Enable 2.4-kHz pwr switching to TMU A and remove it from TMU B for TMU A selection by (3G)
	3HR	TMU B select (relay 2)	PWRS	Switch 2.4-kHz pwr to TMU B and remove it from TMU A
	3X	MDS cmd en	CCS	Enable CCS output to MDS
	3XR	MDS cmd inh	CCS	Inhibit CCS output to MDS
			PWRS	
DC	4A	Chgr A on	PWRS	Turn on bat chgr A
	4AR	Chgr A off	PWRS	Turn bat chgr A off
	4B	Chgr A LR	PWRS	Select LR charge mode
	4BR	Chgr A MR/HR	PWRS	Select MR or HR charge mode
	4C	Chgr A MR	PWRS	Select MR mode if in MR/HR mode
	4CR	Chgr A HR	PWRS	Select HR mode if in MR/HR mode
	4D	Chgr B on	PWRS	Turn on bat chgr B
	4DR	Chgr B off	PWRS	Turn bat chgr B off
	4E	Chgr B LR	PWRS	Select LR charge mode
	4ER	Chgr B MR/HR	PWRS	Select MR/HR charge mode
	4F	Chgr B MR	PWRS	Select MR mode if in MR/HR mode
	4FR	Chgr B HR	PWRS	Select HR mode if in MR/HR mode
	4G	Chgr A, bat 1 select	PWRS	Select bat 1 to be charged by chgr A and bat 2 to be charged by chgr B

TABLE 2.- Continued

Type	Number	Name	Destination	Function
			PWRS	
DC	4GR	Chgr A, bat 2 select	PWRS	Select bat 2 to be charged by chgr A and bat 1 to be charged by chgr B
	4H	Boost conv en	PWRS	Enable share-mode booster
	4HR	Boost conv disable	PWRS	Disable share-mode booster
	4J	Bat test load 1 on	PWRS	Connect bat 1 to test load
	4JR	Bat test load 1 off	PWRS	Disconnect bat 1 from test load
	4K	Bat test load 2 on	PWRS	Connect bat 2 to test load
	4KR	Bat test load 2 off	PWRS	Disconnect bat 2 from test load
	4L	Chgr A SO en	PWRS	Enable chgr A to switch to LR charge at predetermined voltage-temp
	4LR	Chgr A SO disable	PWRS	Disable chgr A SO
	4M	Chgr B SO en	PWRS	Enable chgr B to switch to LR charge at predetermined voltage-temp
	4MR	Chgr B SO disable	PWRS	Disable chgr B SO
	4N	Repl htr relay 1 set	PWRS	When repl htr relays 1 and 2 are both set or reset, switch 55 V dc to S/S htr relay and VIS optics, scan clock actuator, PROPS ck valve htr, and 2.4 kHz to MAWDS thermal control
	4NR	Repl htr relay 1 reset	PWRS	See (4N)
	4P	Repl htr relay 2 set	PWRS	See (4N)
	4PR	Repl htr relay 2 reset	PWRS	See (4N)
	4S	Bat 1 connect	PWRS	Connect bat 1 to unregulated dc bus
	4SR	Bat 1 disconnect/ bat 2 connect	PWRS	Disconnect bat 1 from unregulated dc bus unless connected by (4TR); connect bat 2
	4T	Bat 2 connect	PWRS	Connect bat 2 to unregulated dc bus
	4TR	Bat 2 disconnect/ bat 1 connect	PWRS	Disconnect bat 2 from unregulated dc bus unless connected by (4SR); connect bat 1
	4X	PWRS cmd en	CCS	Enable CCS outputs to PWRS
	4XR	PWRS cmd inh	CCS	Inhibit CCS outputs to PWRS
			CCS	
DC	1	Output 1	CCS	Select OU 1
or		Output 2	CCS	Select OU 2
CC		Outputs 1 and 2	CCS	Select both OU 1 and 2
PC	2	Store	CCS	Store single word in CCS memory
	3	Transfer	CCS	Transfer CCS proc control
	4	Internal execute	CCS	
		En proc/output 1	CCS	Enable proc to OU 1
		Inh proc/output 1	CCS	Inhibit proc to OU 1
		En proc/output 2	CCS	Enable proc to OU 2
		Inh proc/output 2	CCS	Inhibit proc to OU 2
		En other proc	CCS	Enable other proc OU
		Inh other proc	CCS	Inhibit other proc OU
	5	FDS memory load	FDS	Load FDS memories
		CCS memory load	CCS	Load CCS memories
		Prog execute	CCS	Transfer program control to first word of loaded data block; after executing instructions, return control to onboard CCS programs
		Conditional prog execute	CCS	Execute instructions only if all preceding memory load blocks are accepted by CCS
	6	Return	CCS	Cause a CCS indirect XFER to location specified by indicated memory address
	7	Store indirect	CCS	Indirectly store accumulator word in location specified by indicated address
	8	Execute	CCS	Execute instruction in location specified by indicated address

TABLE 2.- Continued

Type	Number	Name	Destination	Function
		FDS		
DC	6A1	FDS pwr conv A select	PWRS	Switch 2.4-kHz pwr to FDS pwr conv A
DC	6A1R	FDS pwr conv B select	PWRS	Switch 2.4-kHz pwr from conv A to conv B unless conv B had been disabled by (6A2R).
DC	6A2	FDS pwr conv B en	PWRS	Enable switching of 2.4 kHz to pwr conv B if conv B selected by (6A1R)
DC	6A2R	FDS pwr conv B disable	PWRS	Disable conv B, resulted in FDS pwr off if pwr conv B selected by (6A1R)
CC	6B	FDS data control	FDS	Select engrg data type and data rate
	6B1	Engrg rate	FDS	Provide control of LR engrg data
	6B10	No change	FDS	No change in LR engrg data rate
	6B11	8 1/3 bps	FDS	LR engrg data were at 8 1/3 bps
	6B12	33 1/3 bps	FDS	LR engrg data were at 33 1/3 bps
	6B13	1000 bps/8 1/3 bps	FDS	8 1/3 bps engrg LR data, and 1000 bps engrg data interleaved with 1000 bps IRS data sent to MDS and DSS
	6B2	Data type	FDS	Select data type or format to be used
	6B20	No change	FDS	No change in previous mode
	6B21	Fixed format	FDS	Select fixed engrg format in FDS memory
	6B22	Memory A-I format	FDS	Select A-I format in FDS memory, i.e., launch or orbit II seq
	6B23	Memory B-I format	FDS	Select B-I format which could be set for cruise or VLC descent seq
	6B24	Memory A-II format	FDS	Select A-II format of engrg data which was set up with any programmable maneuver format
	6B25	Memory B-II format	FDS	Select B-II format which could be orbit I format or any other programmable format
	6B26	CCS 1 R/O	FDS/CCS	Select R/O of contents of CCS 1 memory in place of engrg data
	6B27	CCS 2 R/O	FDS/CCS	Select R/O of contents of CCS 2 memory in place of engrg data
CC	6C	P/B rate/FDS redundancy/ Memory fail override	FDS	Select various HR P/B rates for use by MDS & DSS; enable memory that was disabled; select red sources for CCS LR data, sync, SE sync sig, A/PW input for MAWDS gain control, and engrg/ IRS sync
	6C1	Memory fail	FDS	Provide control for FDS memories
	6C10	No change	FDS	No change in memory status
	6C11	No override	FDS	
	6C12	Memory A override	FDS	
	6C13	Memory B override	FDS	
	6C14	Memory A and B override	FDS	
	6C2	Redundancy select	FDS	Provide control of some red functions within FDS
	6C20	No change	FDS	No change in redundancy status
	6C21	Redundancy A	FDS	Select special redundancy A functions
	6C22	Redundancy B	FDS	Select special redundancy B functions
	6C3	P/B rate	FDS	Provide control for selecting various HR P/B rates
	6C30	No change	FDS	No change in previous HR selected
	6C31	1000 bps	FDS	Select 1000-bps P/B rate
	6C32	2000 bps	FDS	Select 2000-bps P/B rate
	6C33	4000 bps	FDS	Select 4000-bps P/B rate
	6C34	8000 bps	FDS	Select 8000-bps P/B rate
	6C35	16 000 bps	FDS	Select 16 000-bps P/B rate
CC	6D	FDS memory address select	FDS	Select FDS memory and memory address for loading of word contained in (CC6E) cmd
	6D1	Memory A	FDS	
	6D2	Memory B	FDS	
	0 to 1023	Memory address	FDS	

TABLE 2.- Continued

Type	Number	Name	Destination	Function
			FDS	
CC	6E	FDS memory word load	FDS	Load 8-bit word into FDS memory location selected by (CC6D) command
	6E0 to 255	Memory word	FDS	
CC	6F	IRS calib	FDS	Reset IR timing seq to perform calib
	6F1	Calibrate	FDS	
DC	6X	FDS cmd en	CCS	Enable CCS outputs to FDS
DC	6XR	FDS cmd inh	CCS	Inhibit CCS outputs to FDS
			ACS	
CC	7A	Maneuver state	ACS	Select rate or inertial mode, roll or yaw turn start/stop, and turn polarity
	7A1	Select	ACS	
	7A10	No change	ACS	No change in maneuver mode or status
	7A11	Inertial mode	ACS	Switch ACS to all axes inertial mode regardless of existing operating mode; used for IRU calib; Sun occultations, propulsive and nonpropulsive maneuvers, and during sep
	7A12	Rate mode	ACS	Normal mode of operation; resulted in SS control of pitch and yaw and CT control of roll
	7A2	Roll turn control	ACS	
	7A20	No change	ACS	No change in roll turn status or control
	7A21	Start roll turn	ACS	Apply bias in IRU roll ch to perform roll turn
	7A22	Stop roll turn	ACS	Normal state; stop roll turn after it had been started in (7A21)
	7A3	Yaw turn control	ACS	
	7A30	No change	ACS	No change in yaw turn status or control
	7A31	Start yaw turn	ACS	Apply bias in IRU yaw ch to perform yaw turn; roll and yaw turns executed simultaneously if commanded
	7A32	Stop yaw turn	ACS	Normal state; stop yaw turn after being initiated in (7A31)
	7A4	Turn polarity	ACS	
	7A40	No change	ACS	No change in turn polarity status or control
	7A41	+ Turn	ACS	Set positive polarity for roll and yaw turns; inhibit automatic ACE 1 to ACE 2 CO in event of Sun loss
	7A42	- Turn	ACS	Normal state; commanded upon completion of a positive turn so that SLCO would not be unintentionally inhibited
CC	7B	IRU control	ACS	Control operating configuration of IRU 1 and 2
	7B1	IRU 1 pwr	ACS	Control pwr to IRU 1
	7B10	No change	ACS	No change in IRU 1 pwr
	7B11	IRU 1 on	ACS	Turn on IRU 1 pwr; in celestial cr mode, when IRU 1 pwr on and IRU 1 en were commanded, the ACS switched to celestial cr - gyros on mode
	7B12	IRU 1 off	ACS	Normal state; turn pwr off if other logic conditions were satisfied; also in logic, enable both IRU's during launch mode
	7B2	IRU 2 pwr	ACS	Control pwr to IRU 2
	7B20	No change	ACS	No change in IRU 2 pwr
	7B21	IRU 2 on	ACS	Turn IRU 2 pwr on for warm-up; same as IRU 1 in all respects
	7B22	IRU 2 off	ACS	Normal state; same as IRU 1

TABLE 2.- Continued

Type	Number	Name	Destination	Function
			ACS	
CC	7B3	IRU en	ACS	
	7B30	No change	ACS	No change in IRU en status
	7B31	IRU 1 en	ACS	Normal state; work with IRU 1 pwr on in (7B11) and determine unit turned on in auto operation
	7B32	IRU 2 en	ACS	Inhibit IRU 1 outputs and enable IRU 2 outputs
	7B4	IRU auto control	ACS	
	7B40	No change	ACS	No change in status
	7B41	Inh	ACS	Inhibit auto IRU pwr turn on/off mode
	7B42	En	ACS	Enable the auto IRU pwr turn on/off mode; normal state
CC	7C	TVC	ACS	Determine operational state of TVC, select roll inertial or rate mode and select pitch and yaw gyro or SS rate input
	7C1	Pitch and yaw rate input	ACS	
	7C10	No change	ACS	No change in pitch and yaw rate inputs
	7C11	SS	ACS	Permit use of R/E signals in pitch and yaw with roll axis on inertial control; use only in event of CT malfunction
	7C12	Gyro	ACS	Normal state; pitch and yaw axes use gyro rate control
	7C2	TVC gain select	ACS	Provide satisfactory dynamic performance
	7C20	No change	ACS	No change in status
	7C21	TVC gain low	ACS	Use after VL sep; two gain values required because of the 5:1 range in pitch and yaw inertias
	7C22	TVC gain high	ACS	Normal state; use during cr to Mars prior to VL sep
	7C3	TVC en	ACS	Use for TVC checkout and during enq burns
	7C30	No change	ACS	No change in status
	7C31	TVC en	ACS	Use only to enter TVC mode for checkout or for enq burns
	7C32	TVC inh	ACS	Normal state; inhibit TVC en
	7C4	RI	ACS	Provide capability to put the roll axis in roll inertial or roll rate control
	7C40	No change	ACS	No change in previous status
	7C41	RI	ACS	Put the roll axis on inertial control regardless of existing operating mode; use for IRU calib, control through star occultations and stray-light violations, propulsive or nonpropulsive maneuvers, and after ACE CO
	7C42	Roll rate	ACS	Normal state; put roll axis on rate control using CT output; if Canopus lost while on roll inertial control, command would result in roll reacq FB&S in attempt to reacquire Canopus
CC	7D	Launch mode/sensor control	ACS	Control launch mode, CT pwr, SG B/U, and auto Sun occultation; launch mode en effective only when +X inbd S/P not deployed
	7D1	Launch mode	ACS	
	7D10	No change	ACS	No change in status
	7D11	Disable	ACS	Provide B/U to ACS en signal, after SP depl, in event SP depl sw did not open at depl, or if ACS en sw or associated logic malfunctioned
	7D12	En	ACS	Normal state; require prior to SP depl to permit ACS en to keep ACS in launch mode

TABLE 2.- Continued

Type	Number	Name	Destination	Function
			ACS	
CC	7D2	CT pwr control	ACS	CT pwr not applied until predetermined time after launch to allow for depressurization of CT to avoid arc-over and corona in hi-voltage sections of CT
	7D20	No change	ACS	No change in status
	7D21	CT on	ACS	Normal state approximately 2 1/2 hr after launch; roll search initiated when CT turned on and after initial Sun acq
	7D22	CT off	ACS	Normal state from launch to 2 1/2 hr after launch; use after star acquired to put ACS in RI mode
	7D3	SG B/U	ACS	Normally not used; use if Earth albedo effects were sufficient to bias roll axis off Sunline and SG was not obtained; should be used in conjunction with acq SS (7J2)
	7D30	No change	ACS	No change in status
	7D31	SG B/U	ACS	Use only as in (7D3) and only if one ACE failed and SG associated with other ACE also failed
	7D32	SG B/U reset	ACS	Normal state; if preceding cmd must be used, this cmd must be used to restore normal state of logic after settling on CR SS and SG is obtained
	7D4	ASOC/TVC path guidance en	ACS	Enable/inhibit ASOC; enable/disable path guidance
	7D40	No change	ACS	No change in status
	7D41	Inh	ACS	Normally use only for TVC checkout to disable path guidance and to disable ASOC for booster sep in Earth shadow, prevent ACS from going into AAI mode
	7D42	En	ACS	Normal state; required to restore to normal state of logic after using preceding cmd
CC	7E	Roll override control	ACS	Control CT FB, roll override, roll reacq logic; first 3 updates resulted in FB&S; roll search occurred if Canopus was not acquired after third try
	7E1	FB&S	ACS	Pulse used to initiate CT FB&S in an attempt to reacquire a star
	7E10	No change	ACS	No change in status
	7E11	FB&S	ACS	Use in exiting from the roll inertial mode; also use prior to commanding (7C42) roll rate or (7A12) rate mode following a maneuver
	7E2	Roll override	ACS	Pulse used to initiate roll search to find a different star if already locked-on incorrect star or following unsuccessful star acq with FB&S's in RI mode
	7E20	No change	ACS	No change in status
	7E21	Set roll override	ACS	Normally use only when in celestial cruise - gyros on or RI modes
	7E3	Roll reacq update	ACS	Pulse used when in RI mode (as a result of RSIN sig to generate FB&S and count number to initiate roll search after 3rd cmd
	7E30	No change	ACS	No change in status
	7E31	Update	ACS	Provide pulse and start reacq seq to lock-on to Canopus
	7E4	Roll reacq en	ACS	Enable/inhibit auto reacq of star by ACS upon losing Canopus
	7E40	No change	ACS	No change in status

TABLE 2.- Continued

Type	Number	Name	Destination	Function
		ACS		
CC	7E41	Inh	ACS	Not normally used; would inhibit RSIN sig and roll reacq FB sig and make (7E3) completely ineffective
	7E42	En	ACS	Normal state; provide reacq capabilities in event of Canopus loss.
CC	7F	Preaim pitch pos	ACS	7-bit word to preposition rocket eng nozzle about pitch axis
	7F0 to 7F127	Pos data	ACS	Position rocket eng nozzle in pitch axis prior to burn
CC	7G	Preaim yaw pos	ACS	7-bit word to preposition rocket eng nozzle about yaw axis
	7G0 to 7G127	Pos data	ACS	Position rocket eng nozzle in yaw axis prior to burn
CC	7H	CT control	ACS	Coded cmd to select CT cone angle and intensity gates
	7H1	CT cone angle	ACS	Select desired CT cone angle throughout the mission
	7H11	Cone angle 1	ACS	Position IFOV of CT at cone angle 1 (103° cone)
	7H12	Cone angle 2	ACS	Position IFOV at cone angle 2 (98° cone)
	7H13	Cone angle 3	ACS	Position IFOV at cone angle 3 (90° cone)
	7H14	Cone angle 4	ACS	Position IFOV at cone angle 4 (82° cone)
	7H15	Cone angle 5	ACS	Position IFOV at cone angle 5 (77° cone)
	7H2	Canopus intensity	ACS	Determine preselected star intensity sig levels to be used to discriminate between stars meeting preselected brightness criteria
	7H21	Intensity gate 1	ACS	Select intensity gate 1 (×0.7)
	7H22	Intensity gate 2	ACS	Select intensity gate 2 (×0.35)
	7H23	Intensity gate 3	ACS	Select intensity gate 3 (×0.15)
	7H24	Intensity gate 4	ACS	Select intensity gate 4 (×0.05)
	7H3	High gate control	ACS	Provide high gate limit to minimize dust particles and other sources from causing erroneous tracking
	7H31	On	ACS	Normal state; provide high gate limit (×4.0) to accomplish (7H3)
	7H32	Off	ACS	Not normally used; eliminate high gate
CC	7J	SS and RCA control	ACS	Set roll reacq inh, control the ACQ SS, and control RCA half-gas systems
	7J1	Roll reacquire	ACS	Control counting of (7E3) cmds by inhibiting only, not resetting
	7J10	No change	ACS	No change in status
	7J11	Roll reacquire inh	ACS	Delay auto initiation of roll search w/o discontinuing hourly FB&S produced by (7E3)
	7J12	Roll reacquire en	ACS	Normal state; when enabled after inhibiting (7J11), count resumed and initiated roll search after count reached 3
	7J2	Acq SS select	ACS	Provide capability to use ACQ SS for control as B/U for CR SS with degraded accuracy
	7J20	No change	ACS	No change in status
	7J21	ACQ SS en	ACS	Provide B/U for CR SS as primary control
	7J22	ACQ SS inh	ACS	Normal state; use CR SS for control
	7J3	RCA 1 control	ACS	Control status of RCA 1
	7J30	No change	ACS	No change in status
	7J31	RCA 1 disable	ACS	Disable RCA 1; use only if failure occurs in RCA 1 and during eng burns with (7C3)
	7J32	RCA 1 en	ACS	Normal state except during TVC as noted

TABLE 2.- Continued

Type	Number	Name	Destination	Function
			ACS	
CC	7J4	RCA 2 control	ACS	Control status of RCA 2
	7J40	No change	ACS	No change in status
	7J41	RCA 2 disable	ACS	Disable RCA 2; use only if failure occurs in RCA 2 and during eng burns with (7C3)
	7J42	RCA 2 en	ACS	Normal state except during TVC as noted
CC	7K	DR and scan slew control	ACS	Switch derived rate ckt in and out of control loop and inhibit scan plat slew signal from ARTCS to ACS
	7K1	DR control	ACS	Switch derived rate ckt in and out of control loop
	7K10	No change	ACS	No change in status
	7K11	En	ACS	Normal state; used during quiescent modes of operation, improved limit cycle perf in presence of noise
	7K12	Disable	ACS	Use during Sun acq, roll search, commanded turns, and TVC operations; failure to use resulted in degraded transient response
	7K2	Scan slew sig	ACS	Avoid unnecessary jet valve actuations and gas usage which resulted from rates induced on the S/C from scan plat slewing; (Rates imparted to S/C at start of slew would be removed at end of slew.) Jet valve actuation unnecessary unless pos deadband was exceeded.
	7K20	No change	ACS	No change in status
	7K21	Inh	ACS	Inhibit scan plat slew sig from ARTCS; use only if a failure in ARTCS input circuitry
	7K22	En	ACS	Normal state; enable scan slew sig from ARTCS and aid in conservation of RCA gas supply
DC	7M	ACE 1 select	PWRS	Switch 2.4-kHz pwr to ACE 1 and remove 2.4-kHz pwr from ACE 2, if ACE 1 has been enabled by (7N)
DC	7MR	ACE 2 select	PWRS	Switch 2.4-kHz pwr to ACE 2 and remove 2.4-kHz pwr from ACE 1
DC	7N	ACE 1 en	PWRS	Enable switching of 2.4-kHz pwr to ACE 1 and remove 2.4-kHz pwr from ACE 2 for ACE 1 selection by (7M)
DC	7NR	ACE 2 select	PWRS	Switch 2.4-kHz pwr to ACE 2 and remove 2.4-kHz pwr from ACE 1
DC	7P	30-V conv on	PWRS	Turn on PWRS 30 V dc conv
DC	7PR	30-V conv off	PWRS	Turn off PWRS 30 V dc conv if turned on with (7P) and if (7QR) in effect
DC	7Q	30-V conv on	PWRS	B/U to (7P)
DC	7QR	30-V conv off	PWRS	Turn off PWRS 30 V dc conv if turned on with (7Q) and if (7PR) in effect
DC	7S	HPM +X/+Y gas share open	PYROS	Open ACS nitrogen tank pyro valve for XFER of gas from PROPS
DC	7T	HPM -X/-Y gas share open	PYROS	Open ACS nitrogen tank pyro valve for XFER of gas from PROPS
DC	7X	ACS cmd en	CCS	Enable CCS outputs to ACS
DC	7XR	ACS cmd inh	CCS	Inhibit CCS outputs to ACS
			PYROS	
DC	8A1	PYROS 30 V en	PWRS	Enable PAU sol iso valve and MAWDS unlatch ckts
DC	8A1R	PYROS 30 V inh	PWRS	Disable PAU sol iso valve ckts if enabled by (8A1)
DC	8A2	PYROS 30 V en	PWRS	B/U to (8A1)

TABLE 2.- Continued

Type	Number	Name	Destination	Function
			PYROS	
DC	8A2R	PYROS 30 V inh	PWRS	Disable PAU sol iso valve ckts if enabled by (8A2)
DC	8B	Aft BS sep en A or B	PYROS	Enable and charge aft BS sep cap bank A using CCS 1 or bank B using CCS 2
DC	8BR	Aft BS sep inh	PYROS	Disable and discharge aft BS sep cap banks
DC	8C	Orbiter PYRO en A or B	PYROS	Enable and charge PYROS cap bank A using CCS OU 1 or bank B using CCS OU 2
DC	8CR	Orbiter PYRO inh	PYROS	Disable and discharge PYROS cap banks
DC	8X1	PSU cmd en	CCS	Enable CCS outputs to PSU (PYROS A from OU 1, PYROS B from OU 2)
DC	8X1R	PSU cmd inh	CCS	Inhibit CCS outputs to PSU (PYROS A from OU 1, PYROS B from OU 2)
DC	8X2	PAU cmd en	CCS	Enable CCS outputs to PAU (PYROS A from OU 1, PYROS B from OU 2)
DC	8X2R	PAU cmd inh	CCS	Inhibit CCS outputs to PAU (PYROS A from OU 1, PYROS B from OU 2)
			PROPS	
DC	10A	Pressurant first open P1	PYROS	Open helium pressurant line first time
DC	10B	Pressurant first close P2	PYROS	Close helium pressurant line first time
DC	10C	Pressurant second open P3	PYROS	Open helium pressurant line second time
DC	10D	Pressurant second close P4	PYROS	Close helium pressurant line second time
DC	10E	Pressurant final open P5	PYROS	Open helium pressurant line third time, when this cmd was issued, there was no way to close the pressurant line again
DC	10F	Fuel B/P valve open FBV	PYROS	Open squib-actuated B/P valve in fuel supply line; use only if sol iso valve fails closed
DC	10G	Ox B/P valve open OxBV	PYROS	Open squib-actuated B/P valve in Ox supply line; use only if sol iso valve fails closed
DC	10H	Ox sol iso valve open OxV	PYROS	Open latching sol valve in Ox supply line if 30-V pwr supplied to PYROS
DC	10HR	Ox sol iso valve close OxV	PYROS	Close latching sol valve in Ox supply line if 30-V pwr supplied to PYROS
DC	10J	Fuel sol iso valve open FV	PYROS	Open latching sol valve in fuel supply lines if 30-V pwr supplied to PYROS
DC	10JR	Fuel sol iso valve close FV	PYROS	Close latching sol valve in fuel supply lines if 30-V pwr supplied to PYROS
DC	10K	EV open A or B	PYROS	Open biprop EV for motor burn when 30-V pwr on; CCS OU 1 closed two series contacts A of quad config; CCS OU 2 closed series B set
DC	10KR	EV close A or B	PYROS	Close biprop EV; CCS OU 1 opened two parallel contacts of quad config; CCS OU 2 opened other parallel set
DC	10L	Occultation htrs on	PWRS	Switch regulated dc to PROPS thrust plate and RCA jet-valve htrs
DC	10LR	Occultation htrs off	PWRS	Remove regulated dc from htrs in (10L)
DC	10M	PYROS iso valves open	PYROS	Open squib-actuated iso valves in both Ox and fuel lines
DC	10N	PROPS ck valve htr on	PWRS	Switch regulated dc to pressurant line ck valve htrs
DC	10NR	PROPS ck valve htr off	PWRS	Remove regulated dc from htrs in (10N)
DC	10P	PROPS gas share open	PYROS	Open helium tank pyro valve for gas XFER to either or both ACS half-gas assy
			ARTCS	
DC	15A	ARTCS 1 on	PWRS	Switch 2.4-kHz pwr to ARTCS 1 elect
DC	15AR	ARTCS 1 off	PWRS	Remove 2.4-kHz pwr

TABLE 2.- Continued

Type	Number	Name	Destination	Function
			ARTCS	
DC	15B	ARTCS 2 on	PWRS	Switch 2.4-kHz pwr to ARTC 2 elect
DC	15BR	ARTCS 2 off	PWRS	Remove 2.4-kHz pwr
DC	15C	Plat unlatch	PYROS	Release press from scan plat latch
DC	15D	HGA unlatch	PYROS	Unlatch HGA
CC	15E	Scan clock pos	ARTCS	Set scan plat clock angle ref in ARTCS 1
CC	15F	Scan clock pos	ARTCS	Set scan plat clock angle ref in ARTCS 2
CC	15G	Scan cone pos	ARTCS	Set scan plat cone angle ref in ARTCS 1
CC	15H	Scan cone pos	ARTCS	Set scan plat cone angle ref in ARTCS 2
CC	15J	HGA AZ pos	ARTCS	Set HGA AZ ref in ARTCS 1
CC	15K	HGA AZ pos	ARTCS	Set HGA AZ ref in ARTCS 2
CC	15L	HGA EL pos	ARTCS	Set HGA EL ref in ARTCS 1
CC	15M	HGA EL pos	ARTCS	Set HGA EL ref in ARTCS 2
CC	15N	SEC 4 pos	ARTCS	Set SEC 4 blade-angle ref in ARTCS 1
CC	15P	SEC 4 pos	ARTCS	Set SEC 4 blade-angle ref in ARTCS 2
CC	15Q	SEC 6 pos	ARTCS	Set SEC 6 blade-angle ref in ARTCS 1
CC	15R	SEC 6 pos	ARTCS	Set SEC 6 blade-angle ref in ARTCS 2
CC	15S	SEC 12 pos	ARTCS	Set SEC 12 blade-angle ref in ARTCS 1
CC	15T	SEC 12 pos	ARTCS	Set SEC 12 blade-angle ref in ARTCS 2
CC	15U	SEC 14 pos	ARTCS	Set SEC 14 blade-angle ref in ARTCS 1
CC	15V	SEC 14 pos	ARTCS	Set SEC 14 blade-angle ref in ARTCS 2
CC	15W	HR slew	ARTCS	Set ARTCS 1 in HR slew mode, which was 1.0 deg/sec for scan plat and HGA and 13.8 deg/sec for SEC
CC	15WR	LR slew	ARTCS	Set ARTCS 1 in LR slew mode, which was 0.25 deg/sec for scan plat and HGA and 3.45 deg/sec for SEC
CC	15Y	HR slew	ARTCS	Set ARTCS 2 in HR slew mode, which was 1.0 deg/sec for scan plat and HGA and 13.8 deg/sec for SEC
CC	15YR	LR slew	ARTCS	Set ARTCS 2 in LR slew mode, which was 0.25 deg/sec for scan plat and HGA and 3.45 deg/sec for SEC
DC	15X1	ARTC 1 cmd en	CCS	Enable CCS outputs to ARTCS 1
DC	15X1R	ARTC 1 cmd inh	CCS	Inhibit CCS outputs to ARTCS 1
DC	15X2	ARTC 2 cmd en	CCS	Enable CCS outputs to ARTCS 2
DC	15X2R	ARTC 2 cmd inh	CCS	Inhibit CCS outputs to ARTCS 2
			DSS	
DC	16A	DTR A on	PWRS	Switch 2.4-kHz pwr to DTR A and turn its repl htr off
DC	16AR	DTR A off	PWRS	Remove 2.4-kHz pwr from DTR A and turn its repl htr on
DC	16B	DTR B on	PWRS	Switch 2.4-kHz pwr to DTR B and turn its repl htr off
DC	16BR	DTR B off	PWRS	Remove 2.4-kHz pwr from DTR B and turn its repl htr on
CC	16C	DTR A state select	DSS	Command to determine DTR A operating state
	16C1	Mode	DSS	Determine operating mode of DTR A
	16C10	No change	DSS	No change in DTR A status
	16C11	Playback	DSS	Play back data from DTR A at 1000, 2000, 4000, 8000, 16 000 bps
	16C12	Slew	DSS	Tape moved at one of six rates with record heads disabled; use to position tape to start a record seq or play back selected portions of stored data
	16C13	Record VIS	DSS	VIS data recorded on tracks 1 to 7 simultaneously
	16C14	Record FDS HR	DSS	FDS HR output (2000 bps) recorded on track 8
	16C15	Record VL 4000 bps	DSS	RTS 4000-bps output recorded on track 8

TABLE 2.- Continued

Type	Number	Name	Destination	Function
			DSS	
CC	16C16	Record VL 16 000 bps	DSS	RTS 16 000-bps output recorded on track 8
	16C17	Ready	DSS	DTR A powered but record heads disabled and tape stopped
	16C2	P/B data rate or slew speed	DSS	Determine desired P/B rate or slew speed
	16C20	No change	DSS	No change in status
	16C21	1000 bps	DSS	DTR A would play back data or slew at 1000 bps
	16C22	2000 bps	DSS	DTR A would play back data or slew at 2000 bps
	16C23	4000 bps	DSS	DTR A would play back data or slew at 4000 bps
	16C24	8000 bps	DSS	DTR A would play back data or slew at 8000 bps
	16C25	16 000 bps	DSS	DTR A would play back data or slew at 16 000 bps
	16C26	VIS record speed	DSS	DTR A set to operate at top speed to record VIS data
	16C3	Direction	DSS	Select direction tape would pass by heads
	16C30	No change	DSS	No change in status
	16C31	Forward	DSS	DTR's recorded or played back in both directions (forward direction was considered norm direction); DTR A selected to run in forward direction with this command
	16C32	Reverse	DSS	DTR A switched to run tape in reverse direction
	16C4	Track	DSS	Select track of DTR A to be used for P/B or recording purposes
	16C40	No change	DSS	No change in status
	16C41	Track 1	DSS	Select DTR A track 1 for P/B or recording
	16C42	Track 2	DSS	Select DTR A track 2 for P/B or recording
	16C43	Track 3	DSS	Select DTR A track 3 for P/B or recording
	16C44	Track 4	DSS	Select DTR A track 4 for P/B or recording
	16C45	Track 5	DSS	Select DTR A track 5 for P/B or recording
	16C46	Track 6	DSS	Select DTR A track 6 for P/B or recording
	16C47	Track 7	DSS	Select DTR A track 7 for P/B or recording
	16C48	Track 8, VL data	DSS	Select DTR A track 8 for VL data, P/B or record
	16C49	Track 8, FDS data	DSS	Select DTR A track 8 for FDS data, P/B or record
CC	16D	DTR B state select	DSS	Cmd to determine DTR B operating state
	16D1	Mode	DSS	Select operating mode of DTR B
	16D10 to 16D17	Same as for (16C)	DSS	Same as for DTR A but control DTR B
	16D2	P/B data rate or slew speed	DSS	Determine desired P/B rate or slew speed for DTR B
	16D20 to 16D26	Same as for (16C)	DSS	Control DTR B in same manner as DTR A
	16D3	Direction	DSS	Select DTR B tape direction
	16D30 to 16D32	Same as for (16C)	DSS	Control DTR B in same manner as DTR A
	16D4	Track	DSS	Select track of DTR B to be used for P/B or recording
	16D40 to 16D49	Same as for (16C)	DSS	Control DTR B in same manner as DTR A
DC	16X1	DTR A cmd en	CCS	Enable CCS outputs to DTR A
DC	16X1R	DTR A cmd inh	CCS	Inhibit CCS outputs to DTR A
DC	16X2	DTR B cmd en	CCS	Enable CCS outputs to DTR B
DC	16X2R	DTR B cmd inh	CCS	Inhibit CCS outputs to DTR B

TABLE 2.- Continued

Type	Number	Name	Destination	Function
		VIS		
DC	36A	VIS A on	PWRS	Switch 2.4-kHz pwr to VIS A and turn its repl htr off
DC	36AR	VIS A off	PWRS	Remove 2.4-kHz pwr from VIS A and turn its repl htr on
DC	36B	VIS B on	PWRS	Switch 2.4-kHz pwr to VIS B and turn its repl htr off
DC	36BR	VIS B off	PWRS	Remove 2.4-kHz pwr from VIS B and turn its repl htr on
CC	36C	FDS memory select	FDS	Select FDS memory from which VIS control words, memory-generated VIS FB data, miscellaneous on and timing sigs, and nom control words were taken; select FDS memory starting address for VIS control parameters
	36C0	No change	FDS	No change in status
	36C1	Memory A	FDS	Select FDS memory A for control
	36C2	Memory B	FDS	Select FDS memory B for control
	0 to 63	Parameter start address	FDS	Provide corresponding FDS memory starting address for VIS control parameters
CC	36D	VIS photo pairs	FDS	Select number of photo pairs and initiate mapping seq; VIS control parameters were taken starting at FDS memory location selected by last (36C)
	36D0 to 36D63	Number of photo pairs	FDS	Indicate number of photo pairs desired (min seq, 2 pictures)
CC	36E	VIS fl wheel step control	FDS	Control VIS nom control word bits 7 to 10 from both FDS memories and 0 bits 2 to 4 and 11
	36E1	GC/LF	FDS	Select VIS B GC setting, and enable/inhibit the LF sw
	36E11	GC norm/LF inh	FDS	Set VIS B GC at norm and inhibit LF
	36E12	GC norm/LF en	FDS	Set VIS B GC at norm and enable LF
	36E13	GC hi/LF inh	FDS	Set VIS B GC on hi and inhibit LF
	36E14	GC hi/LF en	FDS	Set VIS B GC on hi and enable LF
	36E2	Fl step	FDS	Step VIS B fl wheel through one of six different positions at max rate of 1 step/8.96 sec frame
	36E21	No step	FDS	VIS B fl wheel remained stationary
	36E22	Step	FDS	VIS B fl wheel would be set at proper selected pos
	36E3	GC/LF	FDS	Select VIS A GC setting and en/inh LF sw
	36E31	GC norm/LF inh	FDS	Set VIS A same as VIS B
	36E32	GC norm/LF en	FDS	Set VIS A same as VIS B
	36E33	GC hi/LF inh	FDS	Set VIS A same as VIS B
	36E34	GC hi/LF en	FDS	Set VIS A same as VIS B
	36E4	Fl step	FDS	Step VIS A fl wheel in same manner as for VIS B
	36E41	No step	FDS	VIS A fl wheel did not move
	36E42	Step	FDS	VIS A fl wheel commanded in same manner as for VIS B
		IRTMS		
DC	38A	IRTMS on	PWRS	Switch 2.4-kHz pwr to IRTMS and turn its repl htr off
DC	38AR	IRTMS off	PWRS	Remove 2.4-kHz pwr from IRTMS and turn its repl htr on
CC	38B	IRTMS mirror mode	FDS	Select proper IRTMS mirror mode
	38B1	Mirror mode	FDS	Select desired pos of scan mirror
	38B10	No change	FDS	No change in previous status

TABLE 2.- Continued

Type	Number	Name	Destination	Function
		IRTMS		
CC	38B11	Normal	FDS	Scan mirror stepped according to fixed seq generated by FDS; dc restore function initiated when mirror was in space pos; seq included 9 steps or positions and required approximately 287 sec; seq repeated automatically until mode was changed
	38B12	Fixed space	FDS	Scan mirror fixed in space pos and space data collected
	38B13	Fixed planet	FDS	Scan mirror fixed in planet pos to obtain data from planet
	38B14	Fixed ref	FDS	Scan mirror fixed in ref pos to take ref data and alternately collect housekeeping data; this pos was also stow pos at launch
	38B2	Special function modifiers	FDS	Select modified steps for (38B)
	38B21	Reset	FDS	Control F/F in FDS which inhibited the mirror stepping pulses
	38B22	Space inh/initiate dc restore	FDS	Modify norm mode by skipping/inhibiting the second, third, and fourth space calibs
	OR			
	38B21	Reset	FDS	Gains reduced for IR ch 1 to 23 when mirror in ref pos; norm mode
	38B22	Gain change inh	FDS	IR amp gains inhibited from reduction
		MAWDS		
DC	39A	MAWDS on	PWRS	Switch 2.4-kHz pwr to MAWDS and turn its repl htr off
DC	39AR	MAWDS off	PWRS	Remove 2.4-kHz pwr from MAWDS and turn its repl htr on
DC	39B	MAWDS unlatch	MAWDS	Unlatch MAWDS grating (30 V dc had to be on, PYROS enabled, and PAS unlatched)
DC	39C	MAWDS rad htr on	PWRS	Switch regulated dc pwr to MAWDS rad plate htr
DC	39CR	MAWDS rad htr off	PWRS	Remove pwr from MAWDS rad plate htr
CC	39D	MAWDS State select	FDS	Set MAWDS mode and raster direction and control WL calib
	39D1	Auto mode	FDS	
	39D10	No change	FDS	No change in status
	39D11	Integrate det 1	FDS	Use to obtain data from det 1
	39D12	Integrate det 2	FDS	Use to obtain data from det 2
	39D13	Integrate det 3	FDS	Use to obtain data from det 3
	39D14	Integrate det 4	FDS	Use to obtain data from det 4
	39D15	Integrate det 5	FDS	Use to obtain data from det 5
CC	39D2	Manual mode	FDS	
	39D26	Gain state I	FDS	Select highest gain state w/o rastering
	39D27	Gain state II	FDS	Select next to highest gain state w/o rastering
	39D28	Gain state III	FDS	Select next to lowest gain state w/o rastering
	39D29	Gain state IV	FDS	Select lowest gain state w/o rastering
	39D210	Gain state V	FDS	Select highest gain state with rastering
	39D211	Gain state VI	FDS	Select next to highest gain state with rastering
	39D212	Gain state VII	FDS	Select next to lowest gain state with reastering
	39D213	Gain state VIII	FDS	Select lowest gain state with rastering
	39D3	WL calib	FDS	Correct for opt misalignments resulting from thermal gradients on MAWDS
	39D30	No change	FDS	No change in status
	39D31	Calibrate	FDS	Recalibrate MAWDS and maintain accuracy
	39D4	Raster direction	FDS	Control scan mirror pos
	39D40	No change	FDS	No change in status
	39D41	Normal	FDS	Select norm scan mode of mirror which stepped from pos 1 to 15; mirror also positioned to step 8 when in calibrate mode
	39D42	Reverse	FDS	Select reverse scan mode which stepped mirror from pos 15 to 1

TABLE 2.- Concluded

Type	Number	Name	Destination	Function
			XTXS	
DC	42A	XTXS on	PWRS	Switch unregulated dc pwr to XTXS
DC	42AR	XTXS off	PWRS	Remove pwr from XTXS
			RRS	
DC	52A	RRS/RTS on	PWRS	Switch 2.4-kHz pwr to RRS and RTS
DC	52AR	RRS/RTS off	PWRS	Remove 2.4-kHz pwr from RRS and RTS
			VLC	
DC	75A1	BPA reg 1 on	PWRS	Switch VO unregulated dc pwr to BPA reg 1
DC	75A1R	BPA reg 1 off	PWRS	Remove VO unregulated dc pwr from BPA reg 1
DC	75A2	BPA reg 2 on	PWRS	Switch VO unregulated dc pwr to BPA reg 2
DC	75A2R	BPA reg 2 off	PWRS	Remove VO unregulated dc pwr from BPA reg 2
DC	75B	Cr mode	VLC	Switch VLC to cr mode; turn off tape recorder and reset rec XFER
DC	75C	Tape recorder maintenance	VLC	Switch tape recorder on
DC	75D	GCSC A on	VLC	Switch BPA output to GCSC A
DC	75E	Presep checkout	VLC	Transfer VLC to internal pwr and interrupt to GCSC presep checkout
DC	75F	Sep mode	VLC	Interrupt to computer to start sep seq
DC	75G	IRU cover htr off	VLC	Remove pwr from IRU cover htr
DC	75H	Arm BSC	VLC	Arm BS latch cable cutter
DC	75J	Fire BSC sep cut	VLC	Cut BS latch cable
DC	75K	Safe PYROS	VLC	Disable all pyro circuits in pyro assy
DC	75L	Req XFER	VLC	Switch output of req 2 to PCDA equipment bus
DC	75M	VLC update	VLC	Enable GCSC A or B for updating with SC on VO uplink
DC	75N	GCSC B on	VLC	Switch PCDA output to GCSC B
DC	75P	Reset cr loads	VLC	Reset to cr mode
DC	75Q	VLC prelaunch	VLC	Initiate prelaunch test seq
DC	75R	IRU cover htr on	VLC	Switch BPA output to IRU cover htr
DC	75S	Bat float charge	VLC	Initiate C/40 charge rate to all 4 VLC bat simultaneously following bat charge cycle (C/160 rate per bat)
DC	75T	Fire RTG cut/arm BSC nut	VLC	Cut RTG tube and enable release of BSC sep nuts
DC	75U	Fire BSC sep nut	VLC	Release BSC sep nuts
DC	75V	PCDA P/S 1 on	VLC	Switch BPA pwr to PCDA 1
DC	75W	PCDA P/S 2 on	VLC	Switch BPA pwr to PCDA 2
DC	75X1	VLC cmd en 1	CCS	Enable CCS outputs to VLC for ground commanding from either OU
DC	75X1R	VLC cmd inh 1	CCS	Inhibit CCS outputs to VLC for ground commanding
DC	75X2	VLC cmd en 2	CCS	During flight, (75X2) and (75X3) was in effect for VLC cmd; also, (75Y) was sent from one OU simultaneously with desired VLC cmd from other OU (ground cmds required (75X1) only)
DC	75X2R	VLC cmd inh 2	CCS	
DC	75X3	VLC cmd en 3	CCS	
DC	75X3R	VLC cmd inh 3	CCS	
DC	75Y	VLC pulsed en	CCS	
DC	75Z1	BPA chgr B on	VLC	B/U cmd to turn bat chgr B on
DC	75Z2	Spare	VLC	Spare
DC	75Z3	Spare	VLC	Spare
DC	75Z4	Arm RTG cut	VLC	Enable cutting of RTG tube

parentheses without any further identification. The possible VO system states were made up of these S/S states. The VO and its subsystems were designed to operate within the following constraints:

Possible VO states, except "power-off" (PWRS), were attainable by means of at least one of the following types of inputs:

On-board sensing and switching
CCS processor commands
CCS discrete commands
CCS coded commands

The VO power-off state was attainable only by hardline command from the LCE, STCE, or the PSE.

With the exception of switching to the standby power chain, unlatching, and deployment functions, release of stored gas, functions initiated by the V S/C separation event, or propulsion operations, it was not possible to place the VO in a state such that exit from that state was impossible, nor was it possible to cycle the VO through a state in such a manner that no means of returning to that state was possible.

It was possible to condition the VO to the launch state from any other state while on the launch pad, except the power-off state, with the command link only.

The design of the VO was such that no single command could place the VO in a state that resulted in catastrophic loss of the mission. This constraint applied to all nominal phases of the mission, with the exception of maneuvers, where conservative design and operational practices had been used to preclude the execution of inadvertent irreversible events.

At system and subsystem power turn-on, S/S went into a specific pre-determined state. Where this capability existed, it was accomplished by power-on—reset logic or by returning to the last state prior to power turn-off.

A comprehensive set of diagrams which indicated the commands required to achieve a given subsystem state, from any other state, was presented in a specially prepared and updated document for this purpose. These diagrams were very useful and provided a means for understanding the many operating modes and states of the orbiter, a basis for the VO power logic program, and a single location for all VO subsystem switching, logic, state, and block diagrams. Subsystem status was determined by the information contained in telemetry. A command dictionary contained all telemetry indications which described the status of the subsystem, that is, whether a command had been received and properly responded to by the subsystem.

GUIDANCE AND CONTROL

Guidance and control functions were performed primarily by the ACS in conjunction with the CCS and PROPS. (See fig. 17.) The accuracies represented

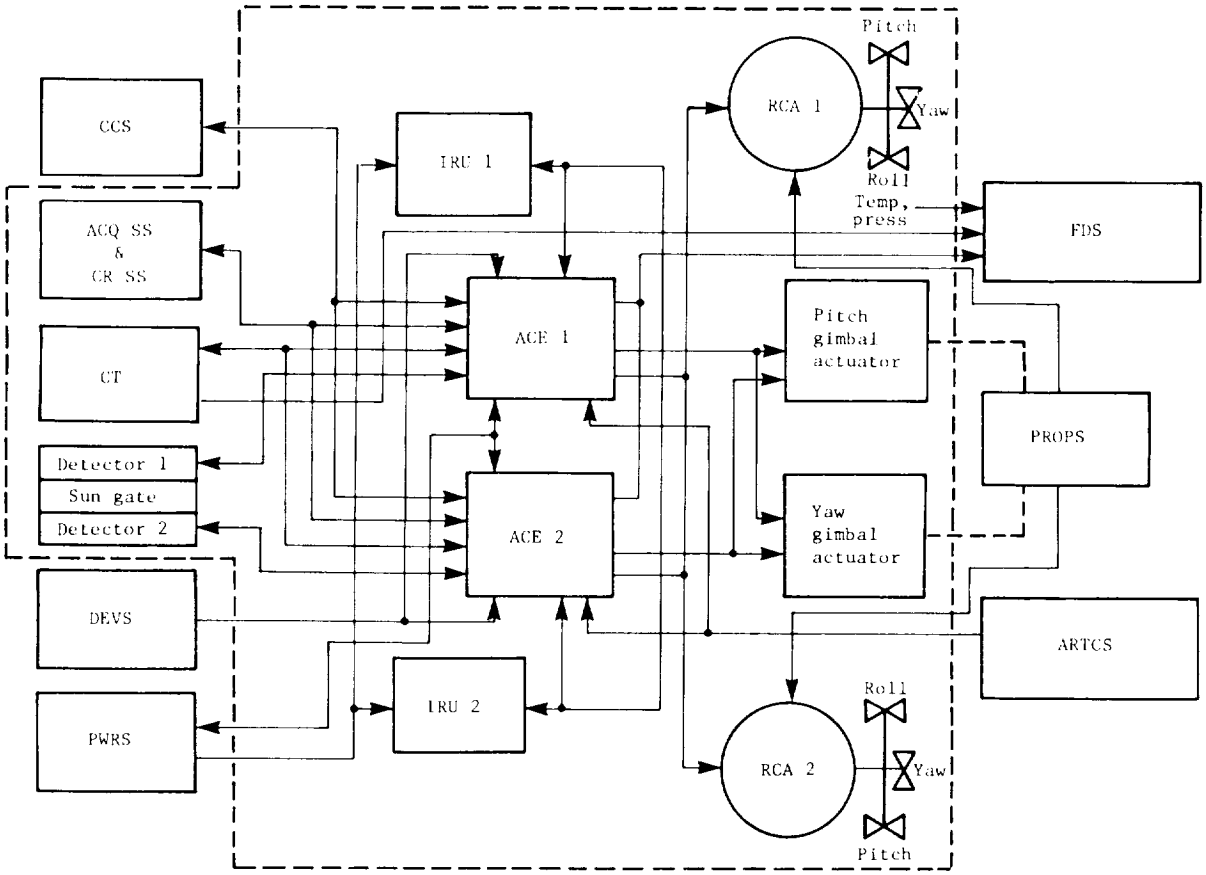

Figure 17.- Simplified block diagram of ACS.

the 99th percentile preflight estimates based on subsystem and system tests and analysis. These G&C functions are given as follows:

Attitude control limit cycle magnitudes: The VO used either celestial reference control or inertial control to maintain S/C attitude. Magnitudes of the limit cycle in these modes are given in the following table:

Parameter	Limit cycle deadband magnitudes, deg	
	Expected nominal	Required
Celestial control:		
Pitch	±0.225	±0.275 max
Yaw	±0.225	±0.275 max
Roll	±0.257	±0.275 max
All-axes inertial:		
Pitch	±0.176	No requirement
Yaw	±0.176	
Roll	±0.088	
Roll inertial control:		
Pitch	±0.225	No requirement
Yaw	±0.225	
Roll	±0.088	

Nonpropulsive maneuvers: The VO was able to perform single turn or multiturn maneuvers to allow pointing of the scan platform instruments or the high-gain antenna at targets not available when in the celestial reference control attitude. The VO, on command, performed roll turns and yaw turns at 0.18 deg/sec.

Propulsive maneuver accuracies: The accuracy of VO propulsive maneuvers depended on the time in the mission the maneuver was conducted, the direction and size of the velocity increment desired, and on the status of in-flight calibration (tracker, gyros, and accelerometers) at the time of the maneuver. Maneuver errors are given in figures 18 and 19.

VLC initialization and preseparation alignment: The VO provided an accurate reference attitude for the VLC deorbit maneuver. Errors in the deorbit maneuver affected landing-point accuracies. VO error sources which affected the reference attitude accuracy are given together with predicted flight accuracies in the following table:

Pitch alignment, deg	0.339 (3σ)
Yaw alignment, deg	0.339 (3σ)
Roll alignment, deg	0.240 (3σ)
Roll inertial accuracy, deg	0.466 (3σ)
Combined reference attitude:	
Pitch, deg	0.584 (3σ)
Yaw, deg	0.584 (3σ)
Roll, deg	0.729 (3σ)

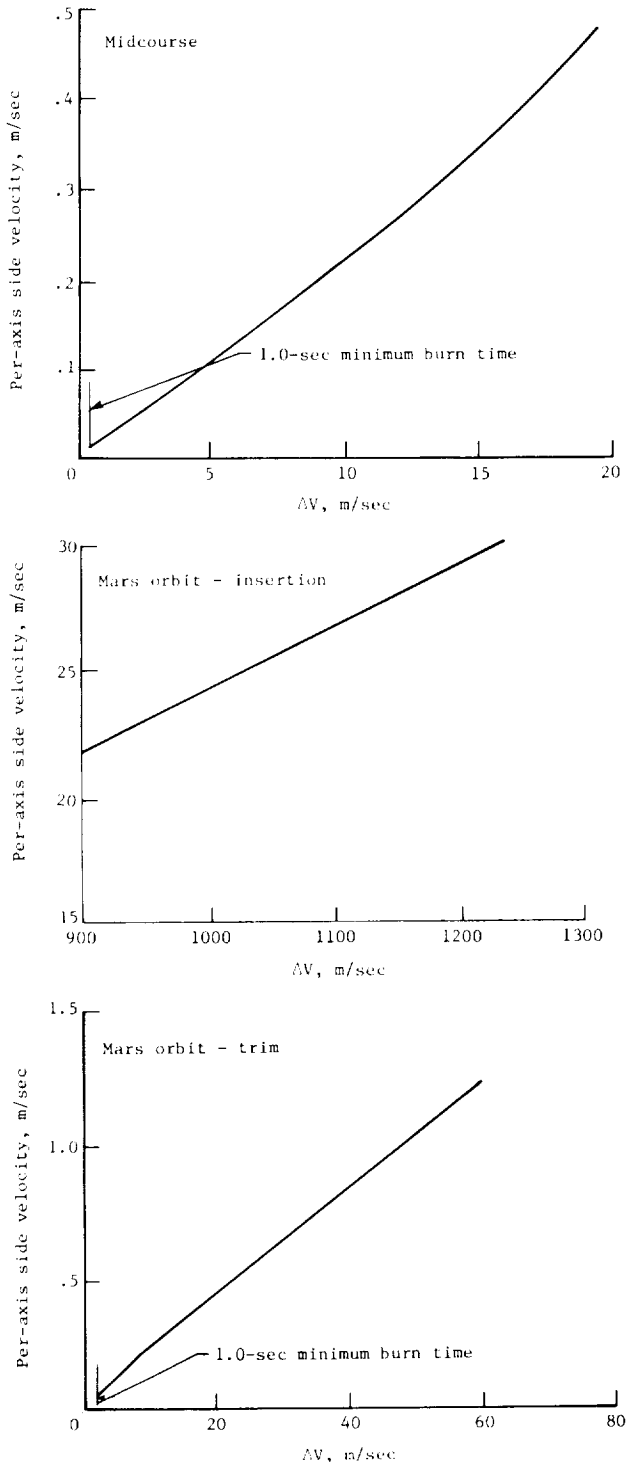

Figure 18.- Propulsive maneuver pointing errors.

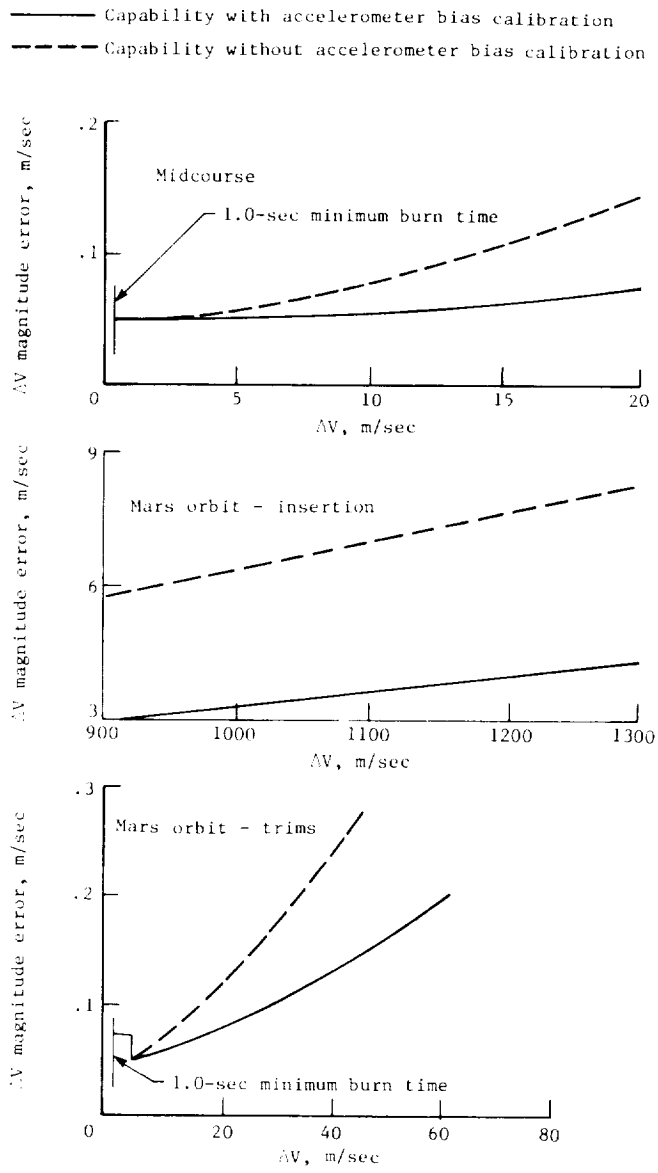

Figure 19.- Propulsive ΔV magnitude errors.

Science scan platform pointing: The VO was capable of pointing the scan platform over the range of S/C clock and cone angles shown in figures 14, 20,

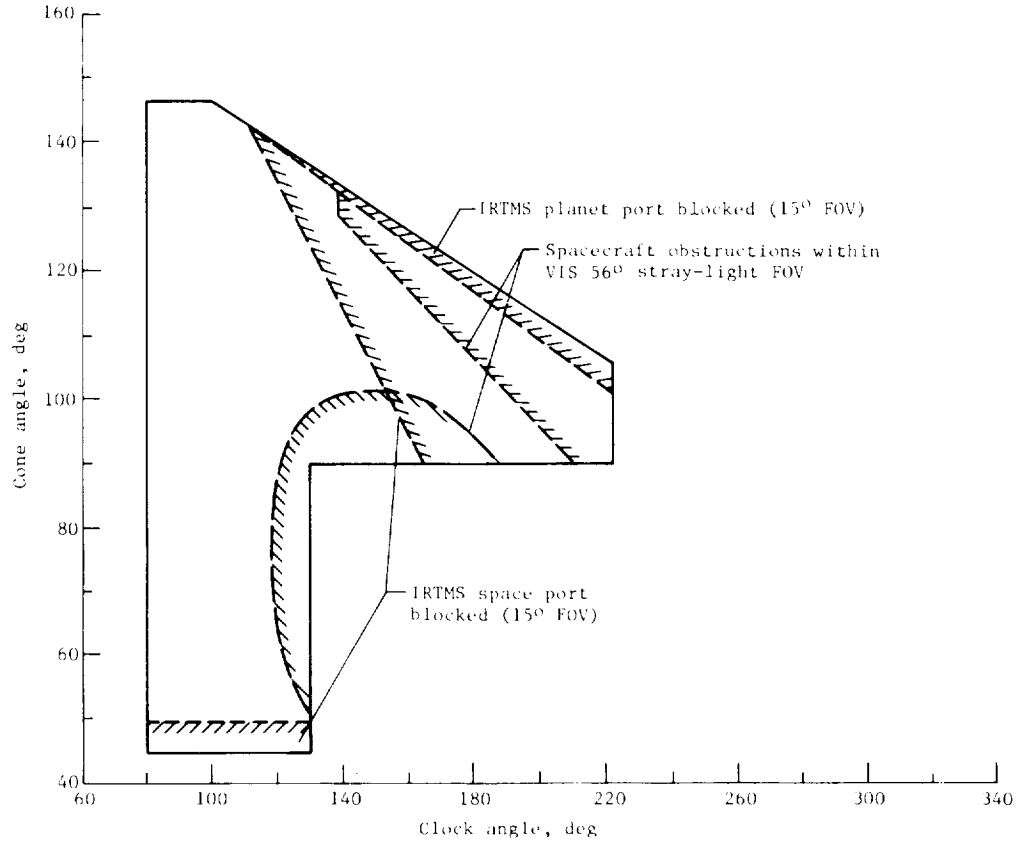

Figure 20.- Science instrument viewing restrictions within scan platform pointing range for prejettison of VLC BS base and adapter.

and 21. Stray-light interference areas are given in these figures. Testing of the VIS showed that, for the expected stray-light intensities, VIS data would not be appreciably degraded within the 56-deg FOV areas; therefore, VIS observations would not be excluded from these areas except when conducting star photography or VIS instrument calibrations. The minimum scan platform slew magnitude which could be commanded was 0.25 deg, and larger slews were commanded to the nearest 0.25 deg of the desired pointing position. The scan platform could

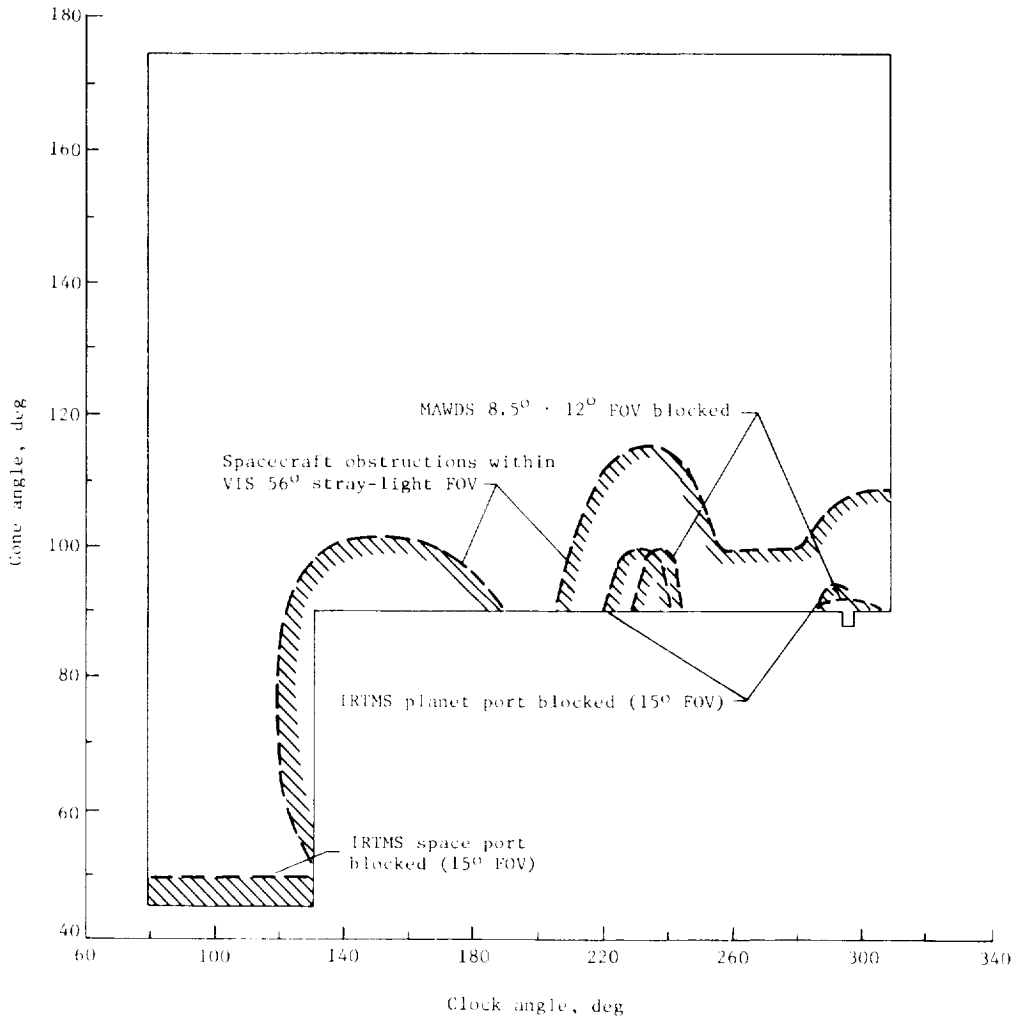

Figure 21.- Science instrument viewing restrictions within scan platform pointing range for postjettison of VLC BS base and adapter.

slew at 1.0 deg/sec. Predicted scan platform pointing accuracies (99th percentile) are shown in table 3. Pointing control referred to the ability to command the scan platform to a desired pointing position; pointing knowledge referred to the knowledge about the actual pointing position after telemetry data (VO limit cycles, scan actuator positions, etc.) are analyzed. Since the accuracies in table 3 are the 99th percentile predictions, expected accuracies should be better. For example, 1σ errors would be about 40 percent of the errors shown. The ability to point to a specific spot on the Mars surface was affected by uncertainties in the Mars pole and radius and in the VO location in orbit (i.e., orbit determination errors), as well as the VO scan platform pointing errors given in table 3. The scan platform was calibrated in-flight in order to meet the pointing accuracy capabilities given in table 3. The scan

TABLE 3.- SCAN PLATFORM POINTING ACCURACY

Attitude control mode	Time	Estimated pointing accuracy, deg (99th percentile)		Operational constraints	
		Control	Knowledge	Control	Knowledge
Celestial		0.50	0.14	(a), (b)	(c), (a)
RI with no turns	Initially		0.17	(d), (a), (b), (e)	(d), (c), (a)
	1 hr after transfer to RI		0.20		
RI after worst turns	Initially	0.64	0.46	(d), (f), (a), (b), (e)	(d), (f), (c), (a)
	1 hr after turn	0.67	0.49		
AAI with no turns	Initially		0.18	(d), (a), (b), (g), (h)	(d), (c), (a), (h)
	1 hr after transfer to AAI		0.29		
AAI after worst turns	Initially	0.90	0.82	(d), (f), (a), (b), (g), (h)	(d), (f), (c), (a), (h)
	1 hr after turn				

[a]Assumed plat was motionless and S/C motion due to slews had settled out.
[b]Assumed selection of commanded scan plat positions were biased to compensate for act control error sources.
[c]Assumed that at least two readings of required pos TM data were available.
[d]Based on gyros being warmed up prior to transfer to inertial.
[e]Assumed that some combination of plat and turn corrections were used to compensate for known roll gyro drift.
[f]Based on worst set of turns; ground selection of optimum set of turns reduced error significantly.
[g]Assumed scan plat positions were compensated for known gyro drifts which accumulated after the last turn.
[h]Assumed that the second roll turn was limited to 90°.

platform (and HGA) pointing accuracies are influenced by other operational considerations such as gyro warm-up periods prior to S/C turns or stray-light periods, and accelerometer bias calibrations and thrust-vector control check-outs prior to propulsive maneuvers.

TELECOMMUNICATION PERFORMANCE

The Viking project telecommunication links are identified in figure 22. The VMCCC generated the commands formulated by the VFT and processed the down-link telemetry from the S/C's for use by the VFT. The DSN provided the means of two-way communication between the VMCCC and the S/C's.

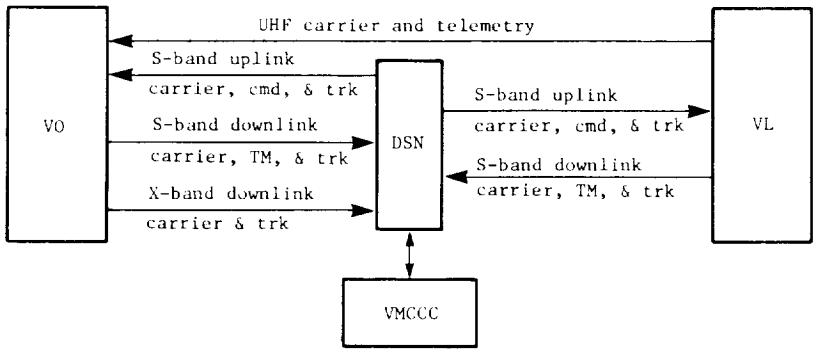

Figure 22.- Telecommunication links.

Design and preflight performance of the links were established and controlled in the system interface requirements. The summarized preflight performance prediction bar charts (figs. 23 to 25) were used as follows. White area indicated that the performance margin was positive based on operation at the sum of the adverse tolerances. A hatched area indicated that the performance margin was positive based on operation at the design point or nominal level, but was negative based on operation at the sum of the adverse tolerances. A solid (black) area indicated that the performance margin was negative even given nominal performance. When the VO LGA was used, the Earth must be within the VO centered cone-clock FOV noted in figure 26. Similarly, if the two-degree-of-freedom HGA was used, the Earth must be within the field of view noted in figure 27.

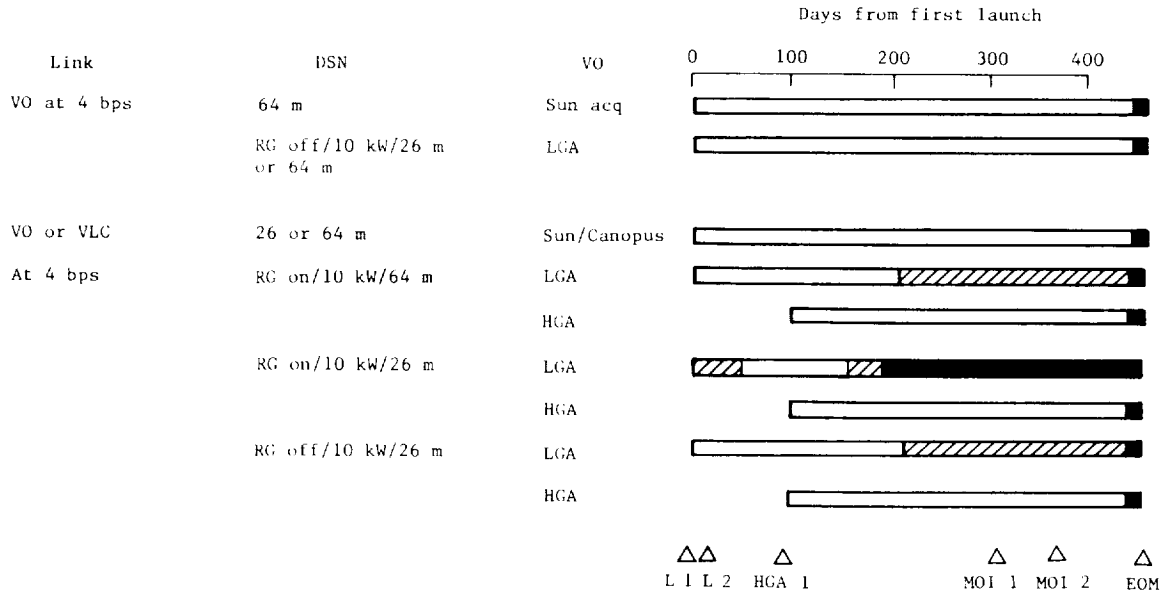

Figure 23.- VO/DSN command performance summary for telecommunications links.

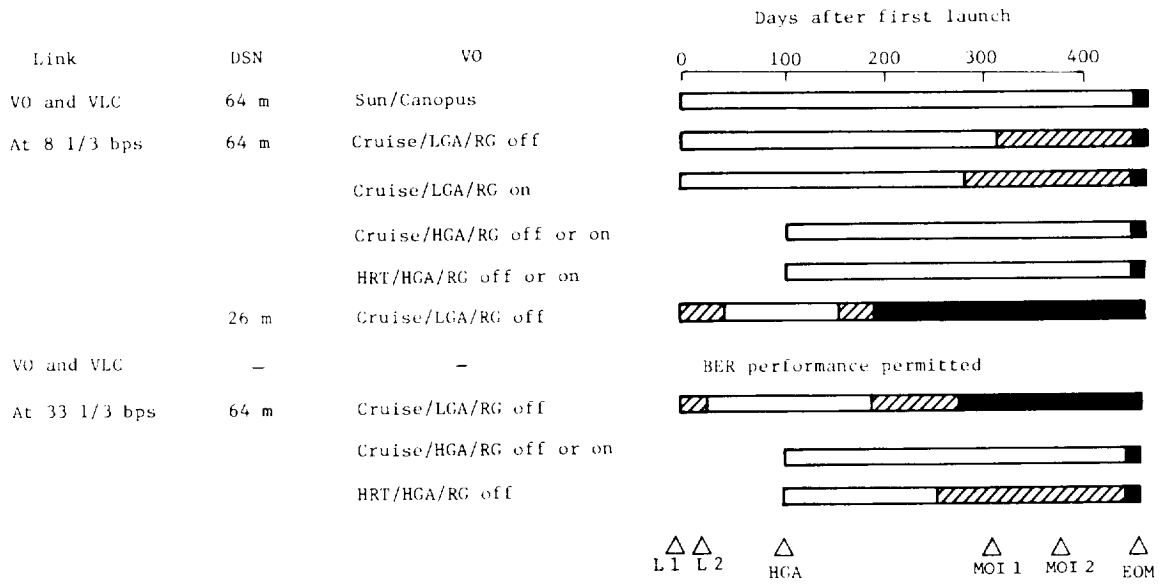

Figure 24.- VO/DSN low-rate telemetry performance summary.

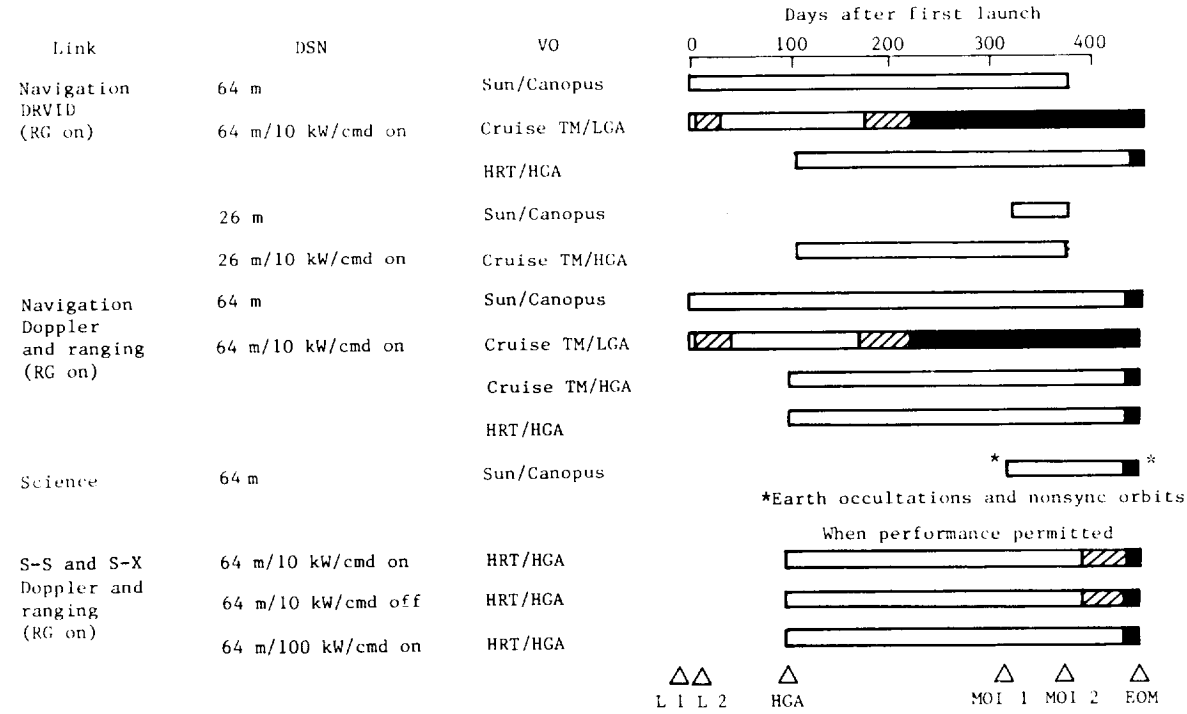

Figure 25.- VO/DSN radio metric data performance summary.

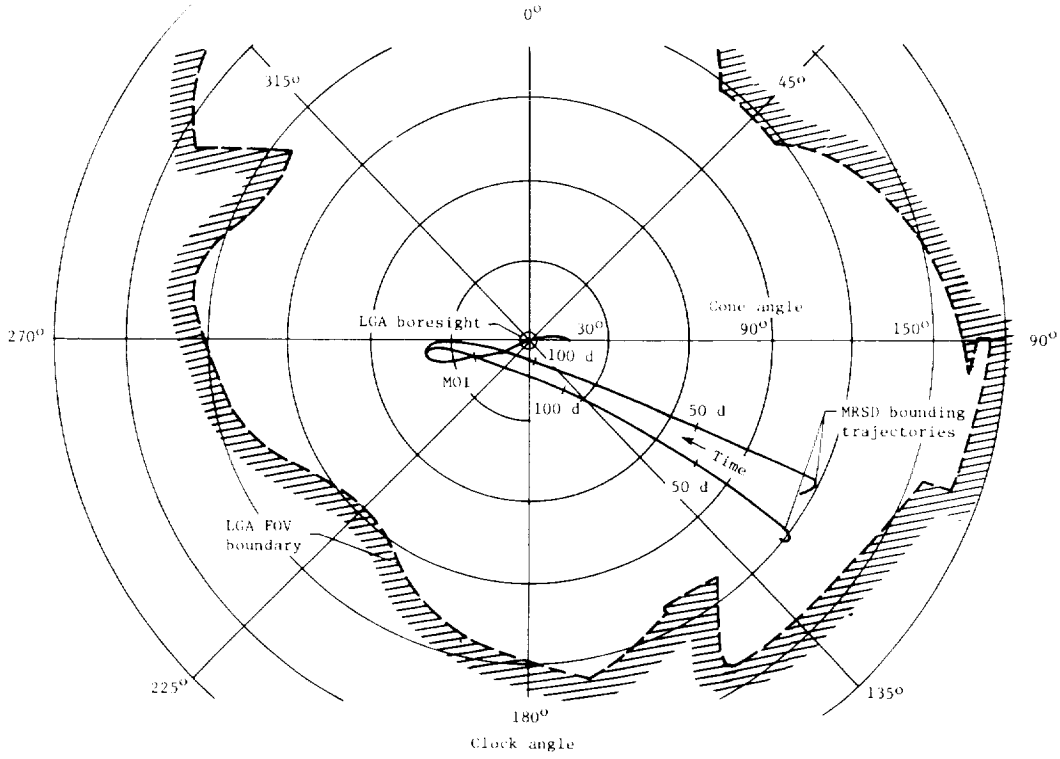

Figure 26.- LGA coverage.

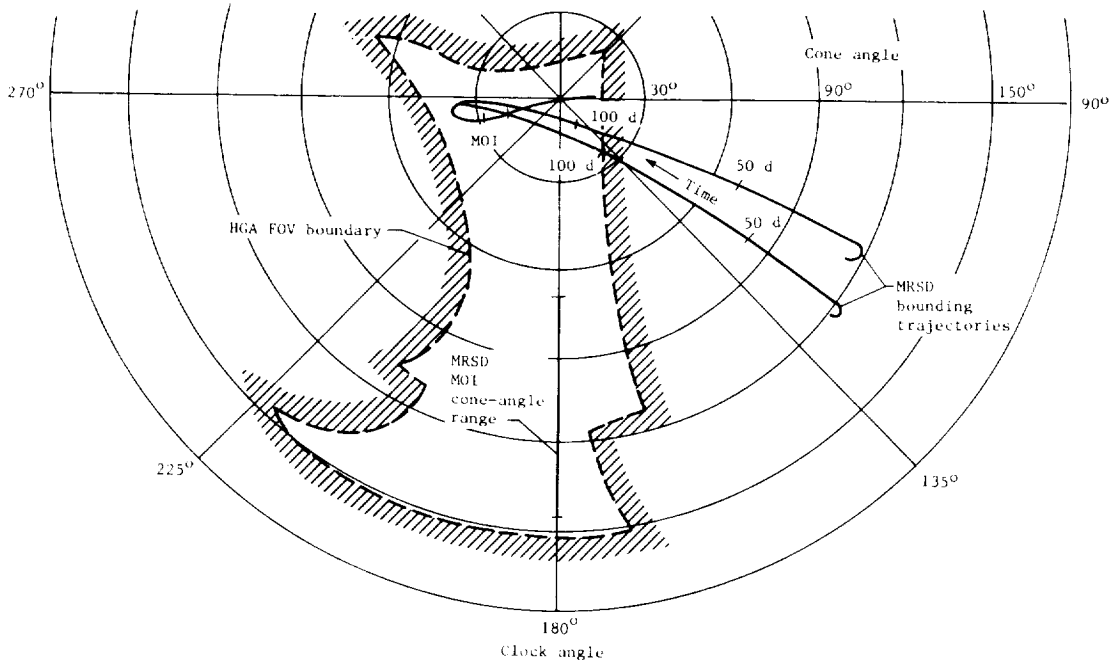

Figure 27.- HGA coverage.

DATA HANDLING

The data handling configuration depicted in figure 28 shows the functional flow of all on-board data. Data were divided into two groups, VO and VLC; each of which is further categorized as follows:

VO data group:

- Engineering data
- Memory data
- IR science data
- VIS data

VLC data group:

- VLC cruise data
- VLC preseparation data
- VLC postseparation (relay) data

All data generated by VO S/S's plus VLC cruise data were routed to the FDS for selection and initial processing. After FDS processing, the data were routed to the MDS and/or the DSS. VLC preseparation data at 1000, 2000, 4000[1], or 16 000[1] bps were routed directly to the MDS. VLC data at 4000 bps (postseparation, descent) from the RTS were routed to both the DSS and the MDS. VL data at 16 000 bps (postseparation, landed) from the RTS were routed to the DSS only. There were two telemetry subcarriers (channels) provided for the transmission of S/C data: a low-rate channel and a high-rate channel. When the high-rate channel was used, it was frequency-division multiplexed with the low-rate channel. The low-rate channel was in operation continuously throughout the mission, and contained either real-time engineering (monitoring/ performance) data or CCS memory readout data. The low-rate channel data were at 8 1/3 or 33 1/3 bps, and were command selectable by the CCS through the FDS. These data were not block coded. The high-rate channel was used whenever necessary and was used for both real-time data or delayed playback data via the FDS memories or the DSS. The data rates available were 1000, 2000, 4000, 8000, and 16 000 bps and were also command selectable by the CCS through the FDS. The FDS was operated in the following modes: (1) FDS high-rate data (2000 bps), consisting of IRS data at 1000 bps bit-interleaved with either data 1's, engineering data, or CCS memory readout data; (2) playback data from the DSS at 2000, 4000, 8000, or 16 000 bps; (3) relay telemetry data

---

[1]These data appeared on the preseparation data interface during portions of the relay radio link checkout. There were no requirements to record or use these data.

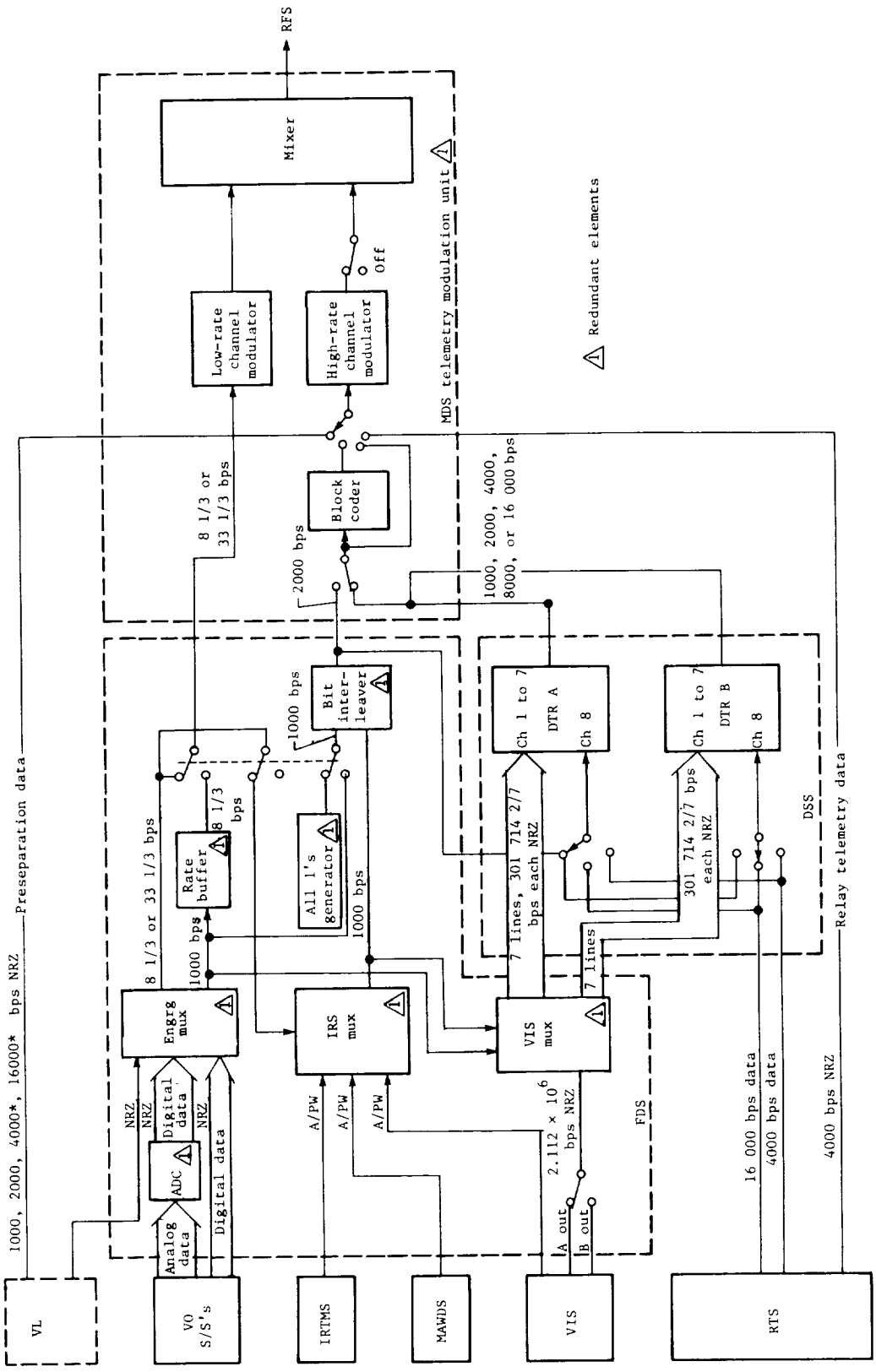

*These data appeared on preseparation data interface during portions of relay radio link checkout. There were no requirements to record or use these data.

Figure 28.- Data handling configuration.

from the VL at either 4000 or 16 000 bps (real time or delayed via the DSS); and (4) VLC preseparation data at 1000, 2000, 4000, or 16 000 bps (as required). Block coding was provided for improved performance for the FDS high-rate and playback modes and was used predominantly throughout the mission.

The FDS memories were required to perform a number of essential tasks and were additionally used to accomplish a variety of FDS housekeeping functions, including reading engineering identifiers for the flexible formats; buffering MAWDS, VIS, and IRTMS (A/PW) science data; storing and updating VO time; storing PN sequences for the VIS and science formats; executing memory-alteration commands from CCS; performing most of the science format multiplexing; and counting TV pictures taken and controlling related FDS logic. Two identical but independent plated-wire memories were used, each comprised of 1024 8-bit words. Each memory had its own controller, which was entirely independent of the other. The FDS hardware is described in more detail later.

Data obtained at various times could be stored on either or both of the two identical independent DTR's. Each DTR was capable of recording any one of the following on command: (1) VIS data at 2.112×10^6 bps; (2) FDS high-rate data at 2000 bps; and (3) VL data from the RTS at 4000 or 16 000 bps. VIS data were presented to each DTR as 7 parallel data streams, each containing one-seventh (301 714 2/7 bps per stream) of the total picture elements (pixels). Complete interchangeability was provided between the VIS's and DTR's; that is, either VIS could be recorded on either DTR and in either direction. Each DTR was capable of storing 5.6×10^8 bits of VIS data. All other data were recorded on track 8 of either DTR at the appropriate data rate selected. The storage capacity on track 8 for each DTR is 8×10^7 bits and/or symbols (FDS high-rate data were recorded on a 2-symbol-per-bit basis, whereas VLC data were recorded on a bit-for-bit basis).

Data stored on each DTR were played back, on command, at 2000, 4000, 8000, or 16 000 bps over the high-rate channel. Playback was accomplished one track at a time and only one DTR could operate in the playback mode at a time.

The following paragraphs describe the types of data generated by VO subsystems:

Engineering data: Engineering data were considered to be that information required to monitor the status and performance of the VO. These data were continuously input to the FDS by the VO S/S's. VLC cruise data were included with the VO engineering data. Where necessary, the FDS performed analog-to-digital conversion.

Engineering data formats: The FDS had seven selectable engineering data formats: fixed, launch, cruise maneuver, Orbit I, Orbit II, and VLC

separation. Any four of these formats plus the fixed hardwire format could be stored in the FDS at the same time, with the FDS selecting and sampling the engineering inputs in accordance with the telemetry structure and channel assignments of the format.

Engineering data rates: There were three selectable data rates for engineering data: 8 1/3, 33 1/3, and 1000 bps. Data at 8 1/3 or 33 1/3 bps were routed over the low-rate channel at all times. Upon CCS command, engineering data at 1000 bps were routed over the high-rate channel to be interleaved with IRS data. Whenever 1000 bps was selected, the low-rate channel operated at 8 1/3 bps and contained data derived from the 1000-bps data. When the high-rate engineering/real-time science telemetry mode was selected, the CCS telemetry in the low-rate channel (8 1/3 bps) was invalid when decoded in the standard manner.

Memory readout data: At various times during the mission it was desirable to read out the contents of the CCS memories. Memory readout was accomplished by replacing engineering data with readout data. The implementation was to place 7-bit bytes of readout data, MSB first, on telemetry deck positions 103 through 137. The nominal data rate for memory readout was 1000 bps although readout at 8 1/3 or 33 1/3 bps was possible. The FDS memory was read out as a part of the IRS format. The CCS readout was accomplished by a routine in the CCS. All or any part of the memory could be read out, with the full single memory readout requiring approximately 1 hr at 33 1/3 bps and 2 min at 1000 bps. The FDS readout was accomplished by utilizing a single word of the IRS format. FDS memories were read out in their entirety on a continuous cyclic basis, such that memory A was read out, then B, then A, etc. Readout of one memory required approximately 10 min.

IRS data: The IRS data consisted of the results of measurements made by the on-board IR instruments (IRTMS and MAWDS), information to monitor the status and performance of these instruments, and the VIS at 1000-bps data rate. The IRS data were interleaved with the 1000-bps engineering data to form a 2000-bps data stream.

VIS data: The VIS data consisted of picture data from either camera, necessary pixel identifiers, and IR science data. Picture data at 2.112×10^6 bps were rate buffered by the FDS and split into two identical sets of 7 data streams each, VIS data 1 through VIS data 14, each at 301 714 2/7 bps. VIS data 1 through VIS data 7 were routed to DTR A, and VIS data 8 through VIS data 14 were routed to DTR B such that both DTR's got identical data streams. Each stream contained one-seventh of the picture elements plus all necessary identifiers and the complete IRS data stream.

A VO telemetry mode was defined as the state of the downlink subcarrier as determined by the source of the data presented to the MDS. A

telemetry mode may, in general, be composed of several submodes such as rates and formats. There were 6 major telemetry modes available as follows: cruise, real-time science, high-rate engineering or real-time science, playback, VLC checkout, and real-time relay. Each mode is summarized in table 4. Each VO telemetry measurement (including both science and engineering measurements), measurement description, measurement characteristic, and a brief description of the impact if the loss of that telemetry measurement or function was experienced were described in a telemetry dictionary. The

TABLE 4.- SUMMARY OF TELEMETRY MODES

Telemetry mode	LR ch data rate, bps	HR ch data rate, bps	Block coding available	HR ch data source	HR ch data content
Cr	8 1/3 or 33 1/3	Off	---	---	---
RT sci	8 1/3 or 33 1/3	2000	Yes	FDS	1000 bps IRS bit-interleaved with 1000-bps data 1's
HR engrg or RT sci	8 1/3 only	2000	Yes	FDS	1000 bps IRS bit-interleaved with one of the following 1000-bps streams: Engrg CCS memory R/O
P/B	8 1/3 or 33 1/3	1000, 2000, 4000, 8000, and 16 000	Yes	DSS (track 1 to 7)	VIS
	8 1/3 or 33 1/3	1000, 2000, 4000, 8000, and 16 000	Yes	DSS (track 8)	VL postsep
	8 1/3 or 33 1/3	1000, 2000, 4000, and 8000	Yes	DSS (track 8)	RT sci or HR engrg/ RT sci
VLC checkout	8 1/3 or 33 1/3	1000, 2000, 4000[a], and 16 000[a]	No	VLC	VLC presep
RT relay	8 1/3 or 33 1/3	4000	No	RTS	VL post sep (used during VL descent to Mars surface only)

[a]These data appeared on the presep data interface during portions of the relay radio link checkout. There were no requirements to record or use these data.

nominal range for each engineering telemetry analog channel, together with calibration curves for converting data numbers to engineering measurement units for all channels in the engineering and science data streams, was included in a telemetry conversion data handbook for each orbiter.

COMMAND AND SEQUENCING

The command and sequencing effort included the planning of desired spacecraft events, the developing of commands necessary to produce those events, the transmitting of the commands to the spacecraft, and the executing of the events by the flight software.

Sequence Generation

The starting point for generating sequences was selecting what group of blocks were required to implement the sequence. A VO block was defined as a group of VO commands and/or events with a well-defined time interrelationship, which performed a single system level function. The sequence of events included in a block was determined by a start time and a specification of a set of time and VO variables. The VO blocks were classified according to the type of function they satisfied. These classes were engineering blocks, maneuver blocks, science blocks, relay blocks, playback blocks, and VLC blocks.

The sequence generation program (SEQGEN) took block requests and merged them with spacecraft engineering sequence requests. Each event was processed to insure that no violations of hardware limits or procedural events had occurred. Each group of events was then translated into a collection of orbiter sequence translator (OSTRAN) macro calls.

OSTRAN converted the macro calls into the assembly language code of the required CCS time/events tables for the events to be issued to the spacecraft. The tables were then assembled and an absolute memory load for both the CCS and FDS memories were produced. OSTRAN also took care of the CCS memory management. Efficient utilization of the allowable CCS memory space dictated that the portion of the memory available for time/event regions be split amorphously into five active areas. They are described as follows:

Even long-term events area contained those time-event tables and/or temporary routines extending over two or more update periods. The area was updated on the even numbered updates.

Odd overlap events area contained the time-event tables and/or temporary routines which extended into or were active during the next odd numbered update period. This area was updated on the even numbered updates.

Current events area contained time-event tables and/or temporary routines covering the period from the most recent update to the next update.

Even overlap events area contained those time-event tables and/or temporary routines which extended into or were active during the next even numbered update period. This area was updated on the odd numbered updates.

Odd long term events area contained those time-event tables and/or temporary routines extending over two or more update periods. This area was updated on the odd numbered updates.

Each of these areas was divided into two subareas of whatever size was required. The first subarea was the master table or absolute hours table which served to initiate regions in the second subarea, the event table regions, at the proper times. OSTRAN produced a Desired Memory Word File (DMWF) which contained a list of the addresses and octal contents of all memory words to be updated.

Orbiter Command Simulator (OCOMSM) is a program that was used to prepare an uplink command file and to make a bit-by-bit detail simulation of the onboard CCS, FDS, and DSS hardware. The primary input to OSOMSM was the DMWF. As the DMWF was processed for conversion to uplink transmission, the information was written on the VO ground command file. This file was then passed to OCTR (Orbiter Command Translator) for entry into the DSN and eventual transmission to the spacecraft. The next to the final step in this process was the manual validation of event traces from the simulation to insure that all events had been correctly processed by all programs to produce the proper onboard actions.

Command Capabilities

Primary command capabilities of the VO system were as follows:

Operated at a rate of 4 bps via either the low-gain or high-gain antenna

Operated with a probability of incorrect single command execution of 10^{-6}

Operated with a probability of no response to a single command of 10^{-3}

Operated with a probability of incorrect execution of a 50-word command block of 5×10^{-5}

Operated with a probability of no response to a 50-word command block of 5×10^{-3}

CCS Flight Software Block Diagram

The CCS software could be subdivided into five main functional units illustrated in figure 29. Generally the flow was from the inputs through

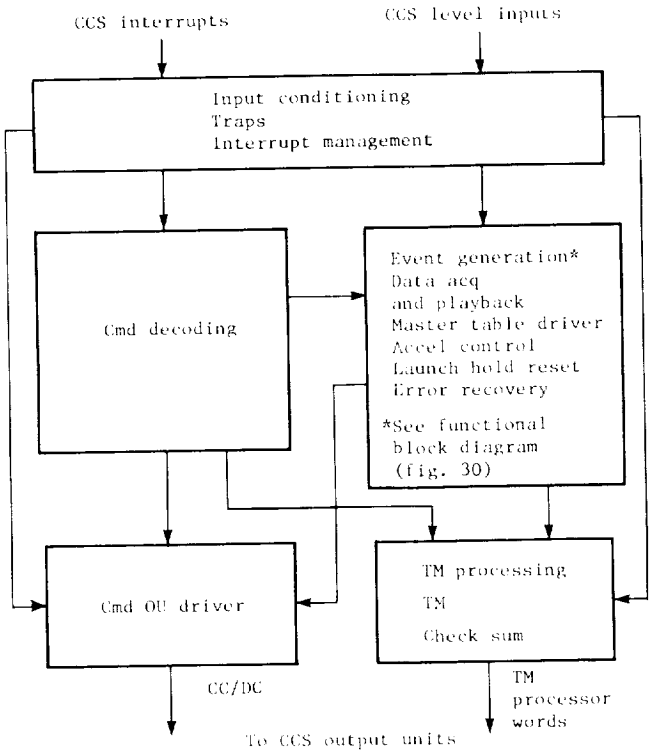

Figure 29.- Functional block diagram of CCS software.

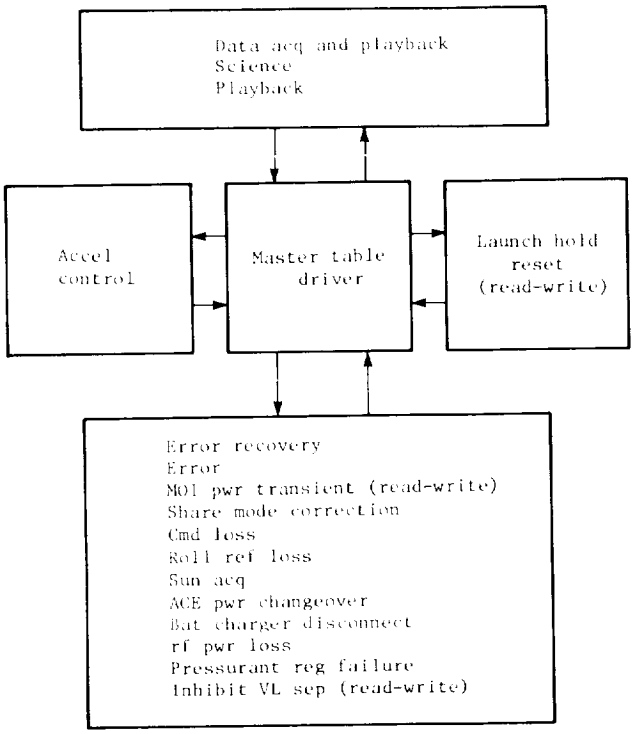

Figure 30.- Functional block diagram of event generation.

intermediate processing to the outputs. The event generation unit could be functionally subdivided into the five subunits illustrated in figure 30. Although not shown in the figure, each subunit had the direct flow of information and control shown in figure 29 for the event generation unit.

The input conditioning unit contained those routines necessary to monitor and direct the CCS interrupts and level inputs. The monitoring consisted of noting the occurrence of an interrupt, counting the number of occurrences of a specific interrupt, or determining which level inputs have changed. The directing of the input consisted of transferring program control to the appropriate routine. The command decoding unit contained the routine CMDPRC (Command Decoding Routine) which was required to decode the base and block command formats. The routine contained a 50-word buffer for the temporary storage of block commands. DC's and CC's which were decoded for execution were passed on to the OU driver unit. The routine was also responsible for the execution of PC's.

The data acquisition and playback subunit of the event generation unit contained those routines tailored for the gathering, storing, and playing back of VO data and the VL relay data. The routines were designed to do all the sequencing necessary for their particular function while being controlled by a minimum number of parameters. This concept minimized the data transmission and storage required for these sequences. The master table driver subunit of the event generation unit contained a routine to keep track of timing interrupts and initiating events and event sequences

at the appropriate times. These events and their associated times were stored in tables which were primarily loaded from the ground. It could also activate routines and, when requested to do so, inform a routine that a specified time interval had passed. The accelerometer control subunit of the event generation unit consisted of the accelerometer control routine. It kept track of accelerometer pulses and initiated an engine shutdown, put out accelerometer related telemetry, and took other appropriate action as it determined necessary. The launch hold reset subunit of the event generation unit contained a routine responsible for the CCS launch-associated operations. This routine included the conditioning of the CCS immediately prior to launch and the initialization of the CCS after spacecraft separation. The error recovery subunit of the event generation unit contained many automatic routines which were responsible for the analysis and correction of specific anomalous spacecraft conditions. The OU driver routine issued commands to the output units on a priority basis. Top priority was the base format CC's and DC's received from the command decoding routine. The lowest priority was the FDS block load CC's also received from the command decoding routine. In between were all other commands temporarily stored in a 20-word buffer on a first-come, first-served basis. The base format CC's and DC's were issued as directed by the command decoding routine. The FDS block load CC's were issued in the individual mode. All other commands were issued in the individual (includes parallel) or tandem mode according to the state of the OU driver routine. The issuance of FDS block load CC's while the OU driver routine was in the tandem mode could cause a tandem error. PC was used to control and program the CCS; CC's were binary coded words used by a subsystem to effect one or more state changes; and DC was an isolated switch closure used by a subsystem to effect a single state change.

TEMPERATURE CONTROL

The VO temperature control design was configured to maintain all parts of the VO within favorable temperature limits for the range of conditions which the VO would experience between launch and an extended stay in Mars orbit.

Temperatures were monitored within all VO subsystems. In addition, heaters, SEC's, and the control of these items required more than a temperature-sensing type interface with the PROPS, ARTCS, PWRS, and CCS. The SEC's and temperature control louvers for the bus and platform were part of the DEVS. Multilayer blankets, shields, and sun shades were part of the STRUS. CABLS provided the required electrical connections. A thermal interface existed with the VLC prior to separation. The energy transferred to the VLC by way of the struts was limited by design and a specular solar reflection was required from the VLC exterior viewed by the VO.

The VO temperature control design utilized both active and passive techniques to create a thermally favorable environment. Bimetallic actuated louvers, the SEC's, and controllable electrical heaters were examples of active control. Paints, coatings, material finishes, thermal capacitance and conductance, multilayer blankets, and sun shades represented the passive techniques employed. Except for the heaters, the active components were characterized by having moving parts whereas the passive techniques relied on a thermal property

of the material, such as its specific heat, thermal conductivity, infrared emittance, and/or solar absorptance. During most of the flight, conduction and radiation were the primary heat-transfer modes. Generally, conduction was utilized to distribute and/or transfer energy to a radiating source. However, convective cooling by propellants was utilized to thermally stabilize the engine during firings of long duration. Also, during the long burns, the flow of the propellants effectively cooled the propellant tank domes near the engine, and the expansion of the propellant pressurant (helium) cooled the components through which it passed and locally helped to lessen the impact of thermal soak back following the long firings. Off-Sun line maneuvers and occultations typify transient conditions experienced by the spacecraft. The thermal capacitance of the spacecraft primarily kept temperatures acceptable during these short time periods of less than 4 hr.

Appendage Items

Thermally, appendage items were those spacecraft elements not included as part of the bus, propulsion module, or scan platform. Generally, these items were passively controlled and thermally decoupled from the bus. As a result, their temperature varied over a large range during the mission. The appendage items are as follows:

High-gain antenna: Figure 31 shows the various elements of the HGA and the location of HGA actuator temperature sensor. There was a continuous heater for each actuator as well as thermal blankets. The antenna dish cross piece structure and the sunlit members of the bus support structure were wrapped with a thermal blanket. The other two bus support members were polished. Other portions of the antenna had been polished or had a finish or coating which was thermally acceptable and protected against corrosion.

Solar panel: Figure 32 shows the solar panel, associated components (deployment damper, rate limiter, etc.), and temperature sensor locations. The back side of the solar panel was painted white. The deployment dampers were blanketed and the portion not covered by the multilayer blanket was polished. The rate limiter, release rod, and latch assembly had a polished finish. Two of the horizontal members (normal to the Sun) of the outriggers had a blanket shade.

Low-gain antenna: Various elements of the LGA are illustrated in figure 33. A polished finish was used on the center post and reflector exterior. The center line of the antenna was parallel to the Sun rays and the reflector interior was painted white. The cover was as-received fiberglass. Blanket wraps covered the coaxial cable and dampers. There were no temperature sensors on the LGA.

Relay antenna: Figure 34 shows the relay antenna. The ground plate had both sides painted black. An alodine coating was employed on the center tube and volute. A polished finish was applied to the deployment mechanism. The hard segment of the cable was goldplated, and white teflon covered the flex segment. There were no temperature sensors on the relay antenna.

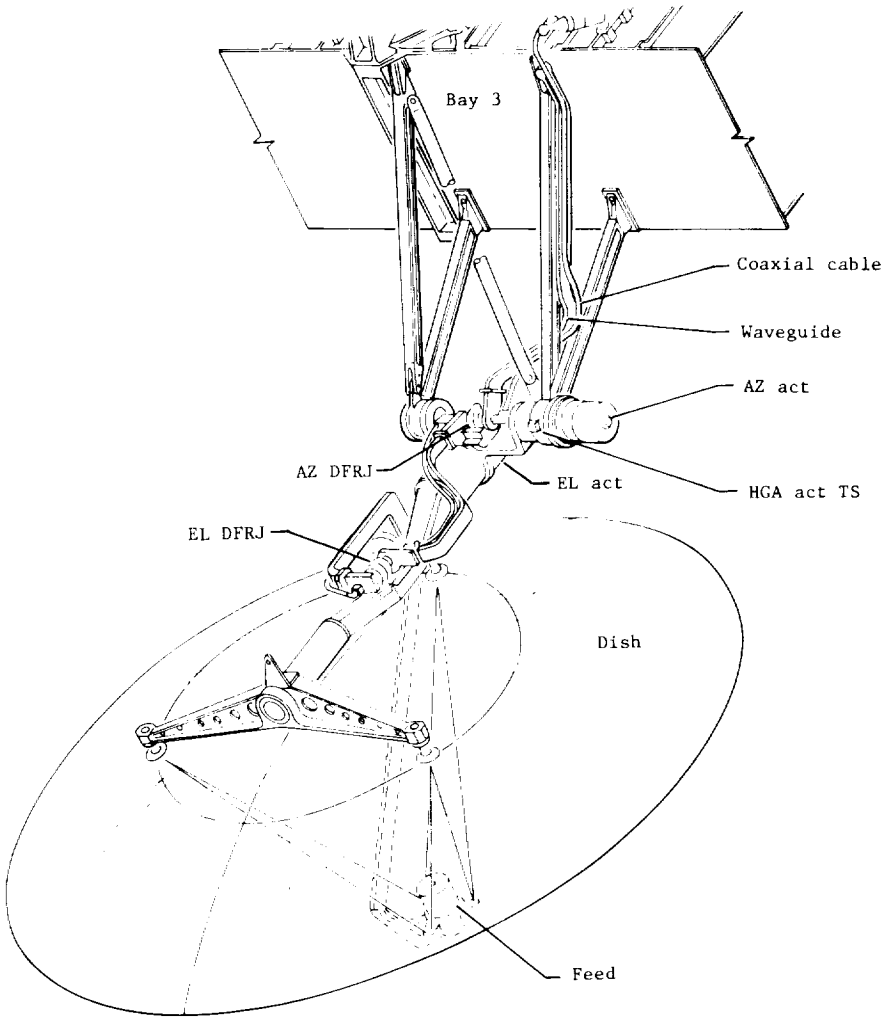

Figure 31.- High-gain antenna.

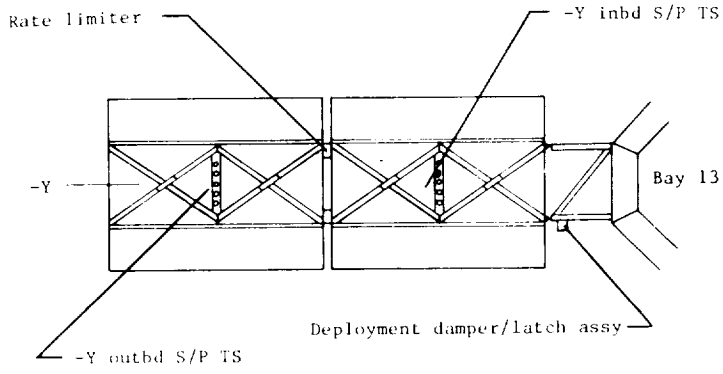

Figure 32.- Solar panel.

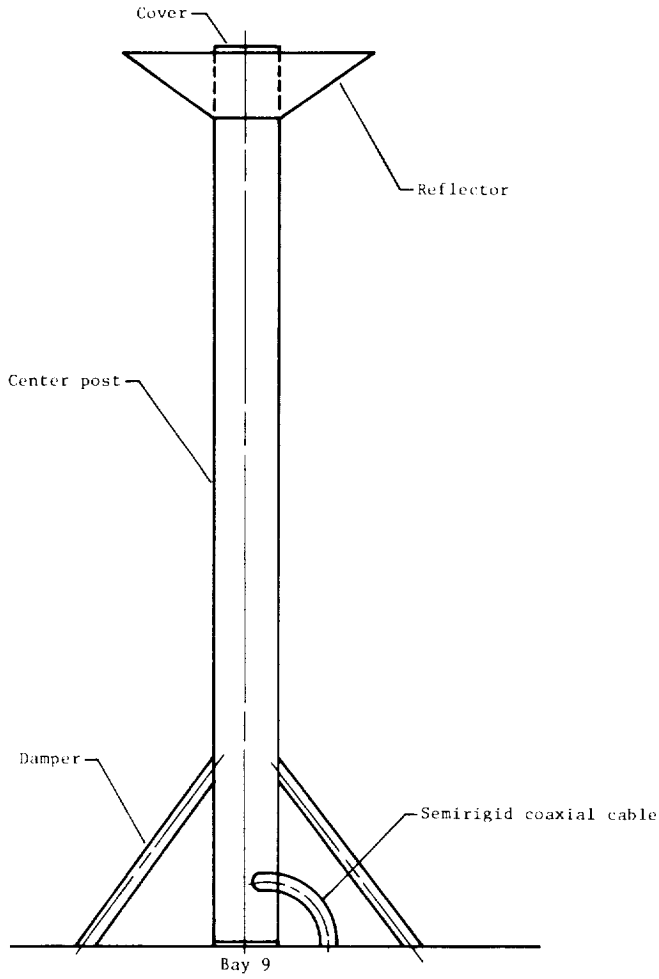

Figure 33.- Low-gain antenna.

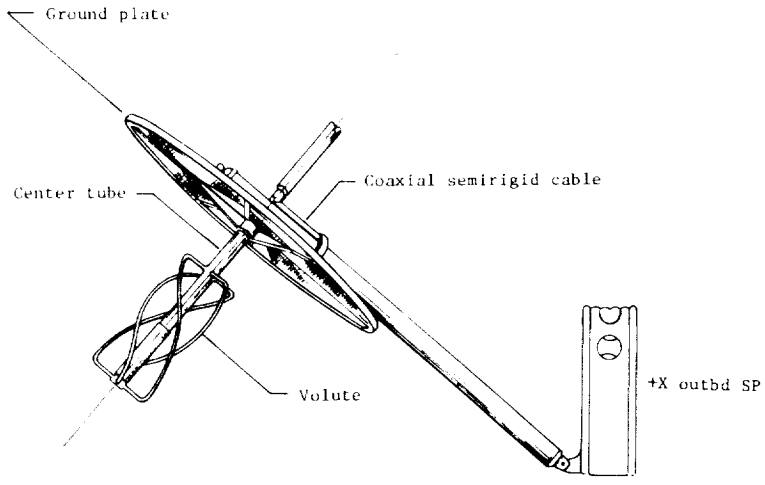

Figure 34.- Relay antenna.

Attitude control jet and acquisition Sun sensor: A pattern of white paint and polish characterized the attitude control jets and accompanying ACQ SS. Fiberglass standoffs were used to isolate the package from the solar panel. Each manifold was heated during occultation. The Sun sensor was coupled to the jets by four polished aluminum standoffs. No temperature sensors were provided for these appendage items.

Sun gate and cruise Sun sensor: The Sun gate and CR SS were mounted together on a bracket between two members of the +Y solar panel outriggers. Except for the view ports, the brackets and sensors were blanketed. The remaining portion of the outrigger had a blanket shade. Location of the temperature sensor is shown in figure 35.

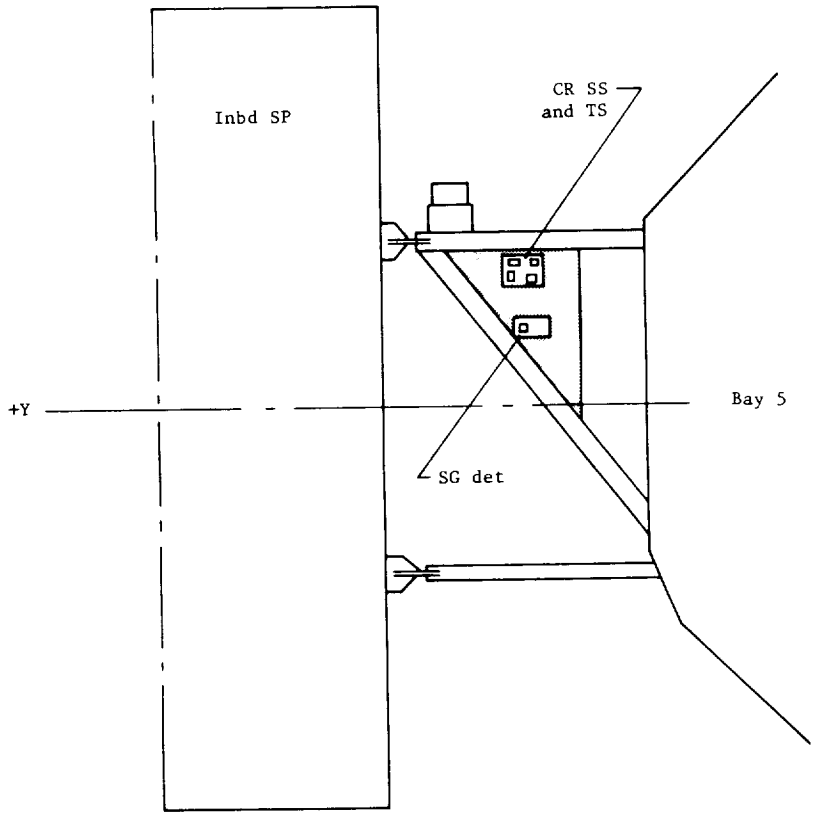

Figure 35.- Sun gate and cruise sensor.

Canopus tracker: The Canopus tracker electronics and baffle box (Sun side only) were blanketed. The electronics were hard-mounted to the bus and were thermally isolated from the baffle box. Figure 36 depicts the tracker and the location of the CT temperature sensor.

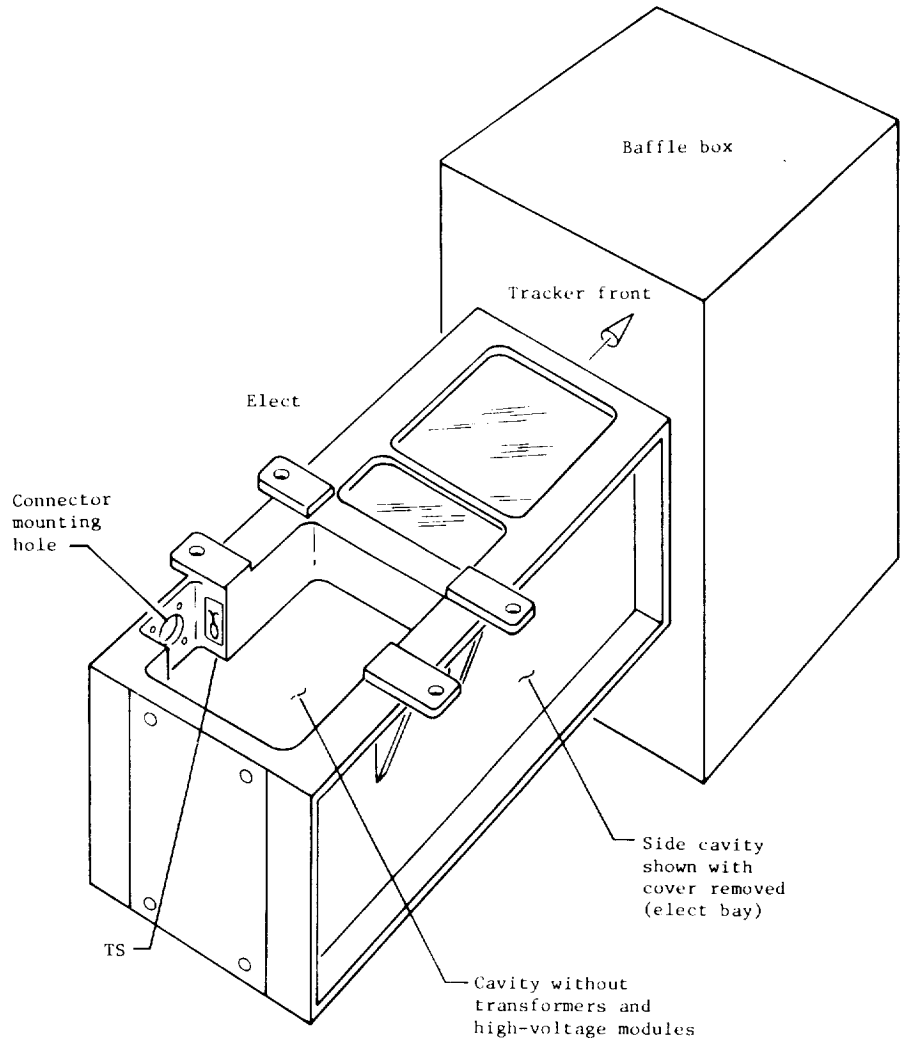

Figure 36.- Canopus tracker.

Separation devices: Like the Canopus tracker, the separation devices were hard-mounted to the bus upper ring (VLC) and lower ring (launch vehicle). Thermal blankets were installed as close as permissible, but temperature stability was provided mainly by the coupling to the bus. No temperature sensors were provided for these devices. Power requirements for the thermal control heaters for the appendages were as follows:

High-gain antenna actuators . . . . . 8 W (4 W per act), continuous
Attitude control jets . . . . . 8 W (2 W per jet assy), switchable

Bus

The bus was divided into 16 bays. (See fig. 37.) Literally, a bay was that volume bounded by the upper and lower rings, the outboard shear plate, and an open inboard face which viewed the propulsion module. Depending upon the desired temperature range and heat generating characteristics of each bay over the mission profile, the white painted shear plate was exposed (large constant energy dissipation), louvered (variable energy dissipation), and blanketed (none or very small energy dissipation). Bays 3 and 11 contain the attitude control nitrogen tanks and the scan platform support structure attaches to bay 7. These three bays had no energy dissipation and were blanketed. Minimum power in bay 16 (RFS) during the mission was approximately 55 W and could be as great as 95 W. As a result, bay 16 had an exposed shear plate. All the other bays had power dissipation that varied from as much as 45 W to 0 W depending upon the flight mode. These bays were louvered and some have replacement heaters. The bus rings were more than 90 percent blanketed. Except for the battery bays, the inboard face of the bus was open to the propulsion module. The inboard face of the bus was open to the propulsion module. The inboard face of the battery bays was blanketed. Polished aluminum shields were used to cover the outboard bus corners and the open areas between adjacent bays. In some instances, some of these shields were cut back to expose more of the white shear plate to further reduce the bay temperature. Significant temperature

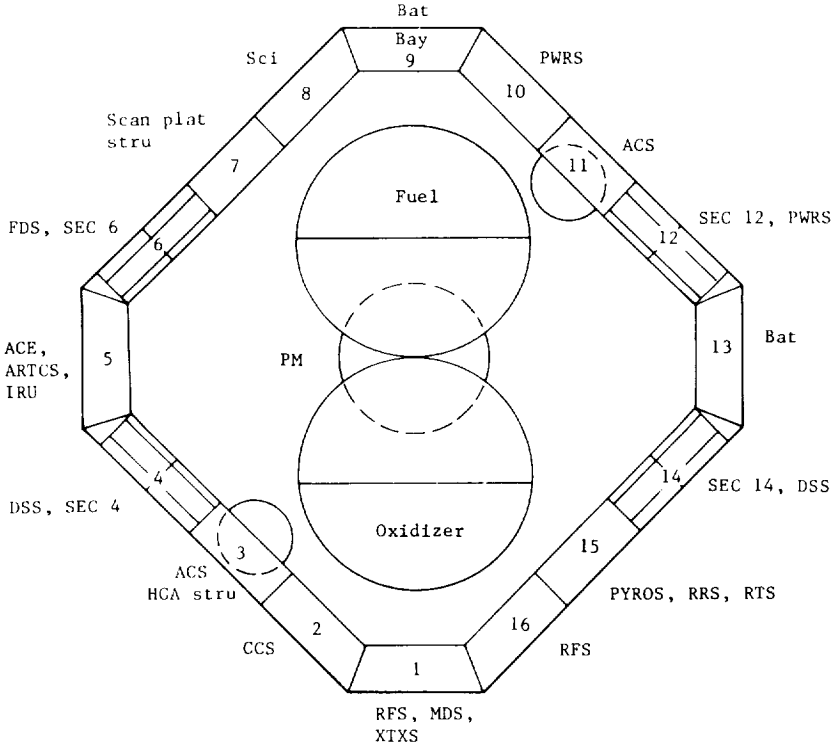

Figure 37.- Orbiter bus.

control features about each bay are shown in table 5. Bay temperature sensors were located in the center interior of the bay on the beam which was conductively coupled to the shear plate. In some instances the bay temperature is the average of four sensors. Power requirements for the temperature control replacement heaters are presented in table 5. The bay 16 heater for RFS provided survival protection after end of mission and if a battery failed during solar occultation. Whenever the tape recorders (DSS and bays 4 and 14) were turned off, the 10-W replacement heaters automatically came on. The 10-W heater in the science bay consisted of 3 W for each VIS and 4 W for MAWDS when the

TABLE 5.- BUS TEMPERATURE CONTROL REQUIREMENTS

Bay	Subsystem	Shear plate side	Propulsion module side	Louver opening temp range		Repl htr pwr, W
				°C	°F	
1	RFS, MDS & XTXS	Louvered	Open	13 to 27	55 to 80	0
2	CCS	Louvered	Open	13 to 27	55 to 80	0
3	ACS	Shielded	Open		N/A	0
4	DSS	Louvered	Open	13 to 27	55 to 80	10
5	ACE & ARTCS	Louvered	Open	18 to 32	65 to 90	0
6	FDS	Louvered	Open	13 to 27	55 to 80	0
7	Scan plat stru	Shielded	Open		N/A	0
8	VIS/MAWDS	Louvered	Open	13 to 27	55 to 80	10
9	PWRS (Bat)	Louvered	Shielded	7 to 21	45 to 70	0
10	PWRS	Louvered	Open	13 to 27	55 to 80	0
11	ACS	Shielded	Open		N/A	0
12	PWRS	Louvered	Open	13 to 27	55 to 80	0
13	PWRS (Bat)	Louvered	Shielded	7 to 21	45 to 70	0
14	DSS	Louvered	Open	13 to 27	55 to 80	10
15	PYROS, RRS & RTS	[1]Louvered	Open	13 to 27	55 to 80	[2]0
16	RFS	Open	Open		N/A	[3]16 or 64

[1]One-half set of louvers; one-half shielded.
[2]4 W cont on htr.
[3]16 W at 25 V; 64 W at 50 V.

instruments were turned off. The switching logic for these heaters is shown in figure 38. (Command numbers from table 2 are included in the figure.) Expected bus temperatures for mode 5 are given in table 6. Also shown in this table are the temperatures following the longest expected, 3.6-hr solar occultation. Significant temperature transients occurred in certain bays due to local power changes. Table 7 presents the expected temperature change for various events.

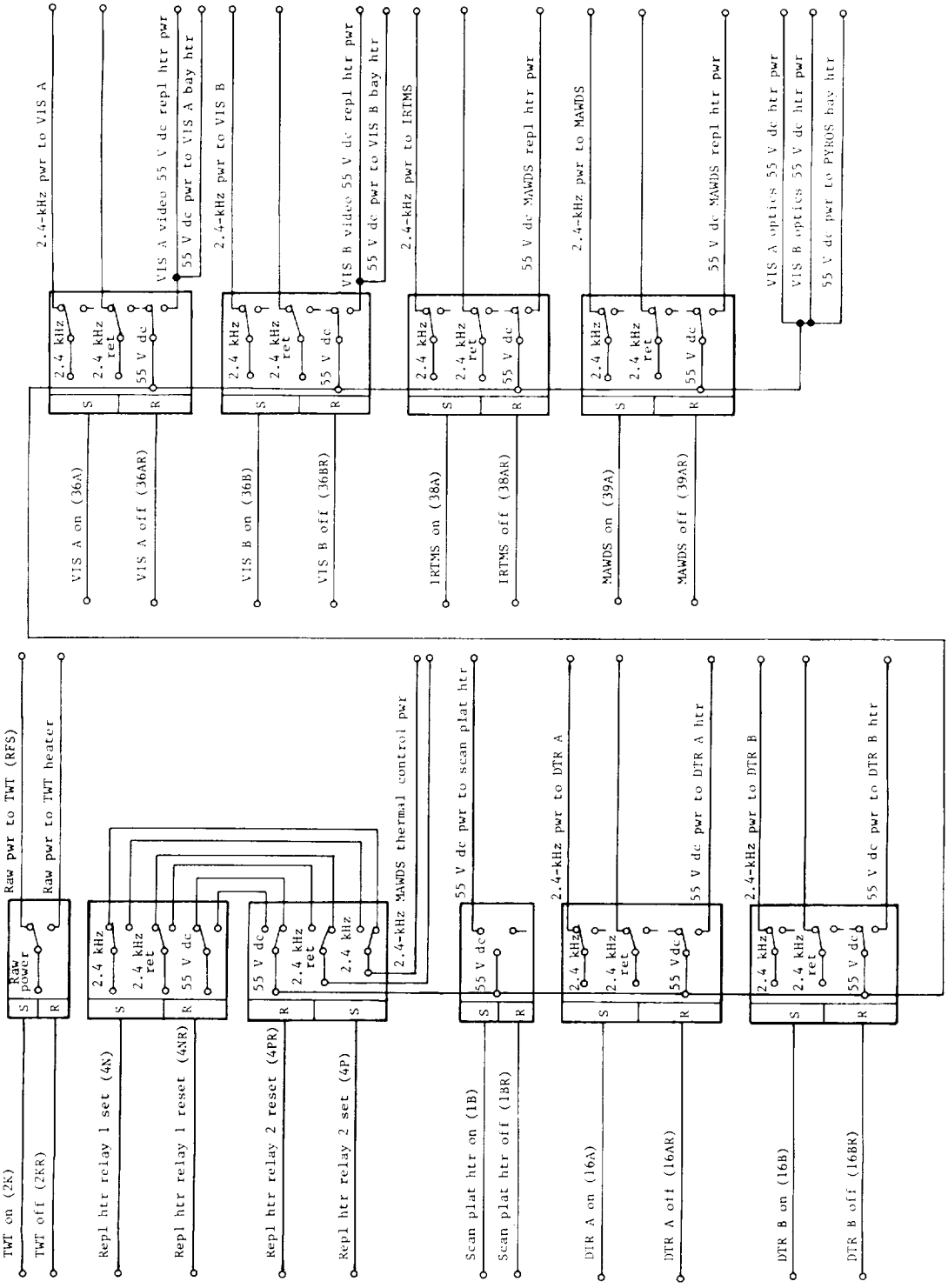

Figure 38.- Functional switching logic for bus replacement heater.

TABLE 6.- EXPECTED BUS TEMPERATURES FOR MODE 5

Item	Expected bus temp, °C (°F) at -				
	Prop warm-up	Earth perihelion	Mars perihelion (sci on)	Mars aphelion	End of 3.6-hr solar occultation
Bay 1	21 (70)	18 (65)	17 (63)	17 (63)	13 (55)
Bay 2	25 (77)	22 (72)	20 (68)	17 (63)	15 (59)
Bay 3	28 (82)	22 (72)	17 (63)	17 (63)	15 (59)
Bay 4	22 (72)	20 (68)	22 (72)	18 (64)	12 (54)
Bay 5	26 (78)	22 (72)	22 (72)	16 (61)	13 (64)
Bay 6	28 (83)	24 (75)	21 (70)	21 (70)	20 (68)
Bay 7	22 (72)	17 (63)	11 (51)	10 (49)	6 (42)
Bay 8	24 (75)	20 (68)	22 (72)	18 (65)	7 (45)
Bay 9	16 (61)	14 (57)	12 (53)	12 (53)	11 (51)
Bay 10	20 (68)	17 (63)	20 (68)	13 (56)	12 (53)
Bay 11	26 (78)	20 (68)	17 (63)	14 (57)	13 (55)
Bay 12	20 (68)	17 (63)	20 (68)	14 (57)	10 (50)
Bay 13	17 (63)	14 (57)	12 (54)	12 (54)	9 (48)
Bay 14	20 (68)	17 (63)	18 (64)	14 (57)	6 (43)
Bay 15	17 (63)	14 (57)	14 (57)	13 (55)	6 (43)
Bay 16	24 (75)	21 (70)	19 (66)	17 (63)	8 (47)
TWT bases	47 (116)	44 (112)	37 (99)	35 (95)	19 (66)
AO	27 (80)	24 (75)	18 (64)	17 (63)	10 (50)
VCO	20 (68)	18 (64)	12 (54)	17 (63)	12 (54)
Accel	28 (82)	24 (75)	22 (72)	13 (56)	20 (68)
Gyros	24 (75)	20 (68)	36 (96)	15 (59)	36 (97)
X-band XMTR	32 (90)	30 (86)	13 (55)	26 (79)	9 (48)
Relay radio rec	19 (66)	16 (60)	14 (57)	13 (55)	7 (45)

TABLE 7.- EXPECTED TEMPERATURE CHANGES

Event	Temp change		Time for change, hr
	°C	°F	
Switch TWT from lo to hi pwr	12	21	12
Turning gyros on	23	41	7
	8	15	6
Switch DTR from ready to VIS record	6	10	7
Turning sci on	4	7	12
Turning XTXS on	18	32	8
HR portion of bat charging	-4	-8	3

Propulsion Module

The PM temperature control design employed both passive and active techniques. An insulated enclosure (fig. 39) was created by the multilayer PM

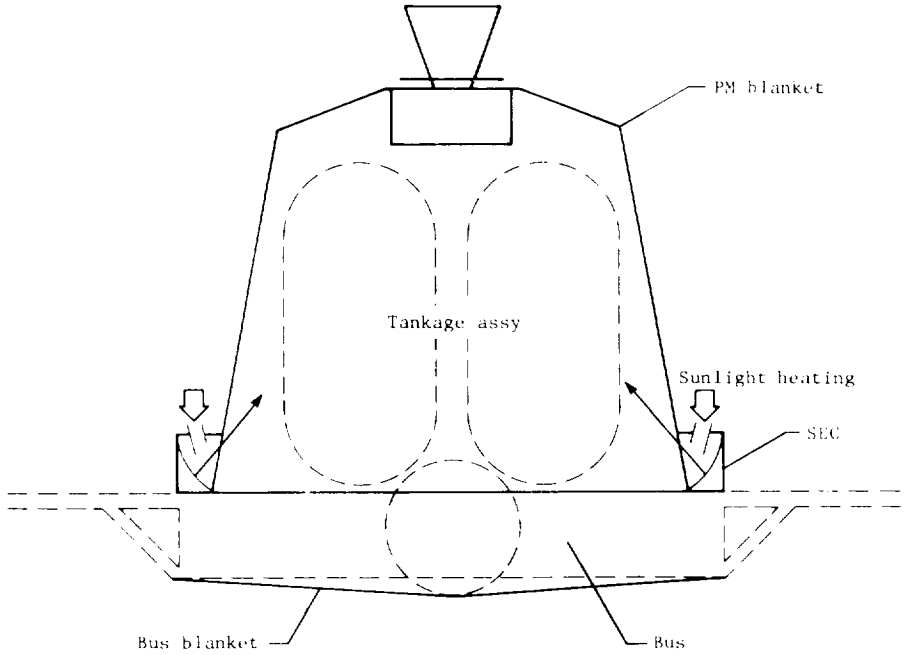

Figure 39.- Propulsion module temperature control.

blanket, bus blanket, and bus. Gradients and temperatures within this enclosure were controlled by introducing solar energy through four commandable solar energy controllers. There was also one commandable electrical heater circuit for the pressurant check valves. Energy from the SEC's was initially reflected off the white painted portion of the tankage assembly and the PCA and re-reflected throughout the enclosure. The thrust plate and propellant isolation assemblies were painted white to help diffuse the solar energy. The outboard portion of the PCA had a multilayer blanket to prevent overheating near Earth when the SEC's were open for propellant warm-up and propellant line lockup. Except for the convective cooling during engine burns, the engine assembly was passively temperature controlled. Flight sensor locations are identified in figures 40 to 43. Only two electrical commandable heaters were employed in the PM. A total of 0.5 W (0.25 W/valve) was applied to the pressurant check valves to keep liquid propellants away from the teflon valve seat. A flight temperature sensor was located at the oxidizer valve outlet. (See fig. 41.) The heater was utilized to maintain the check valve temperature slightly greater than the local bulk propellant temperature as indicated by flight sensors on top of the oxidizer tank and the fuel tank (fig. 40). Both of the tank sensors were located on the bus end domes and during cruise were representative of the

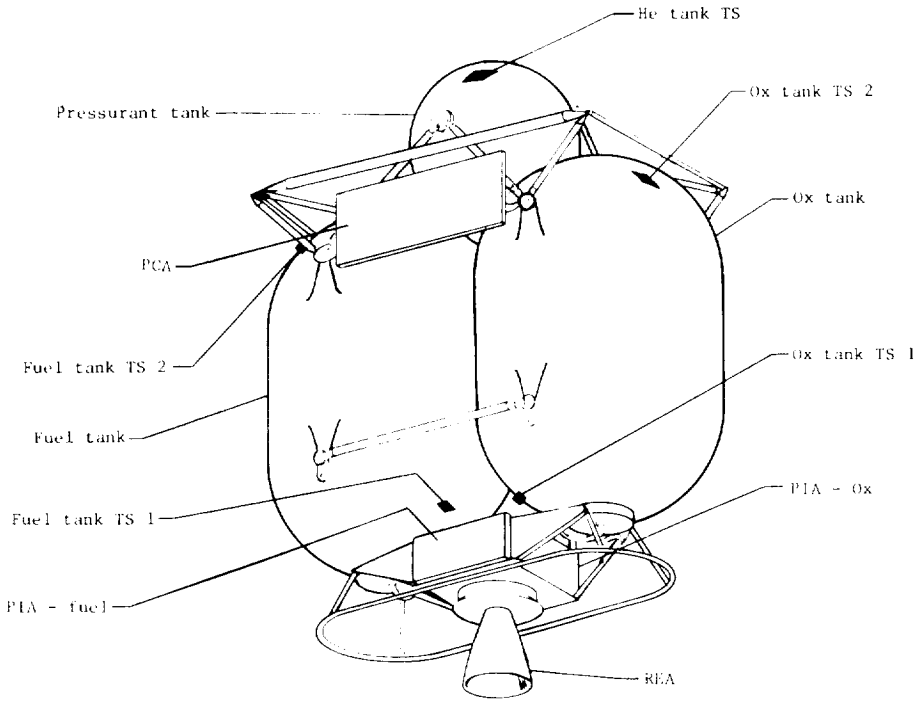

Figure 40.- Flight temperature sensor locations for tank assembly.

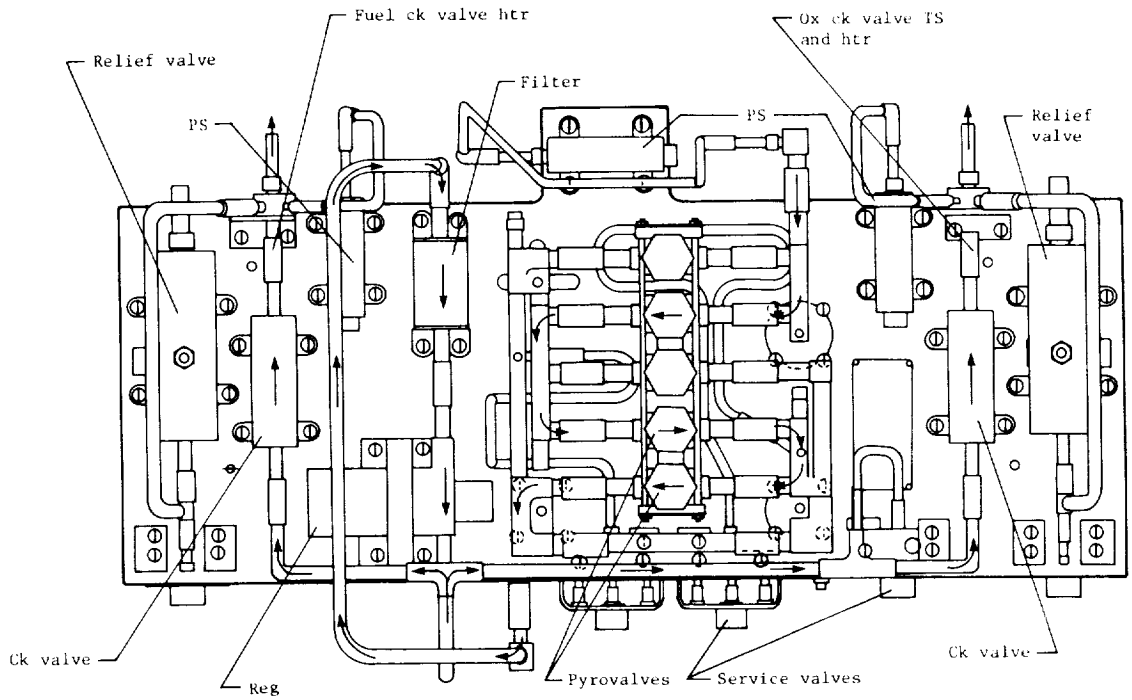

Figure 41.- Flight temperature sensor and heater location for pressurant control assembly.

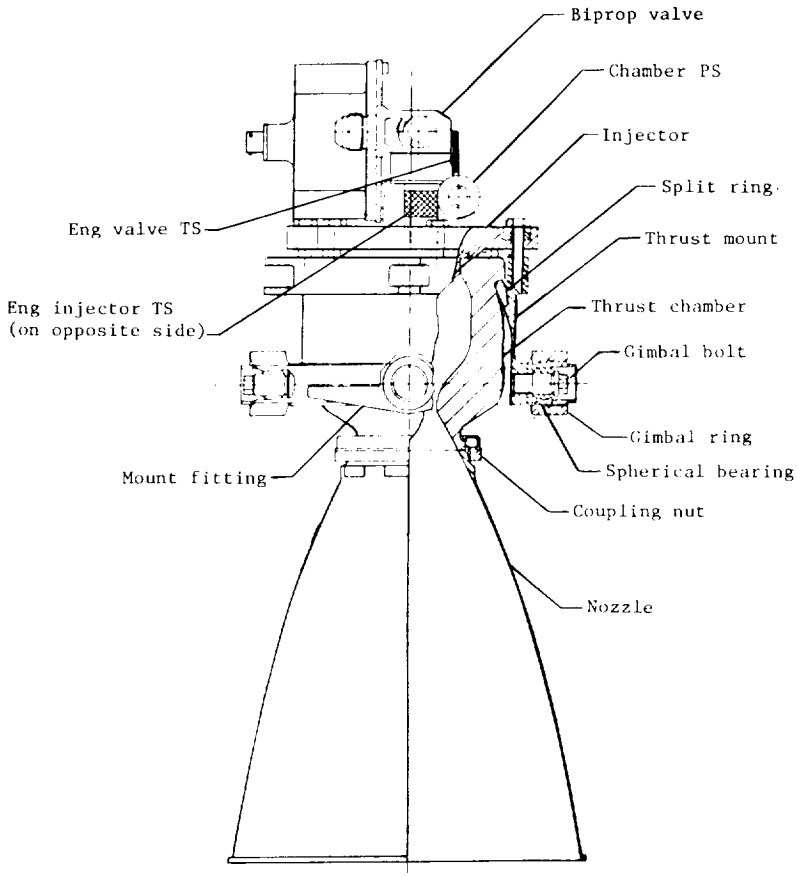

Figure 42.- Flight temperature sensor locations for engine assembly.

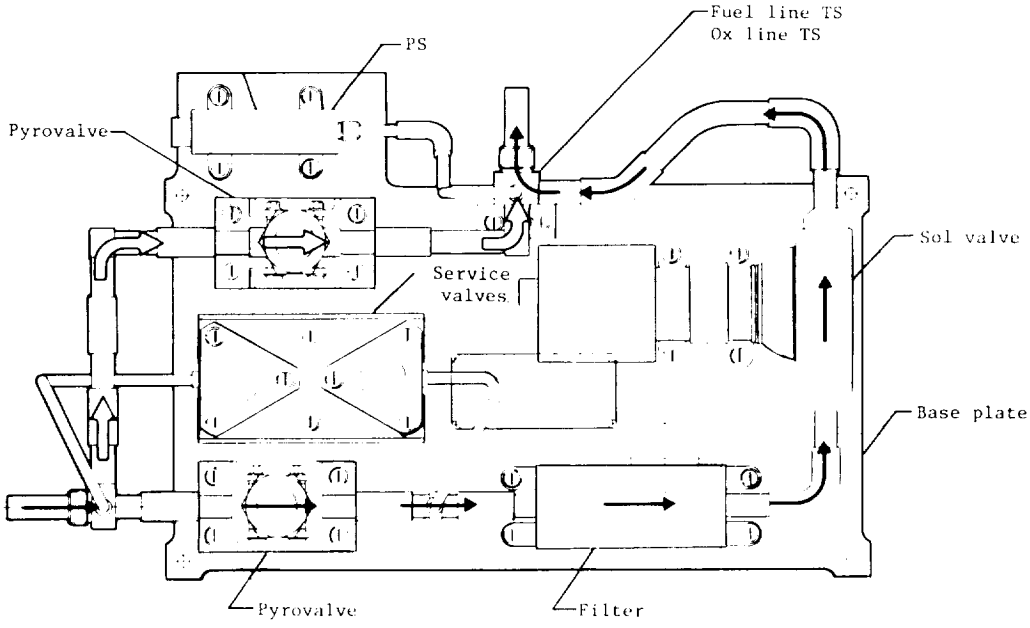

Figure 43.- Flight temperature sensor locations, propellant isolation assembly.

internal liquid temperature. Heating of the PM is primarily by the four SEC's. The net energy captured (useful energy) per SEC is shown in figure 44 for several solar intensities which the V S/C experienced during the mission. The predicted temperature for the propellant bulk and propellant line (between the propellant isolation assembly and the bi-propellant valve) is shown in figure 45 as a function of time. Also indicated in this figure are the following thermally significant events for the PM: propellant warm-up, propellant line lockup, perihelion, and MOI. Expected temperatures for each of these events and various PM items are shown in table 8.

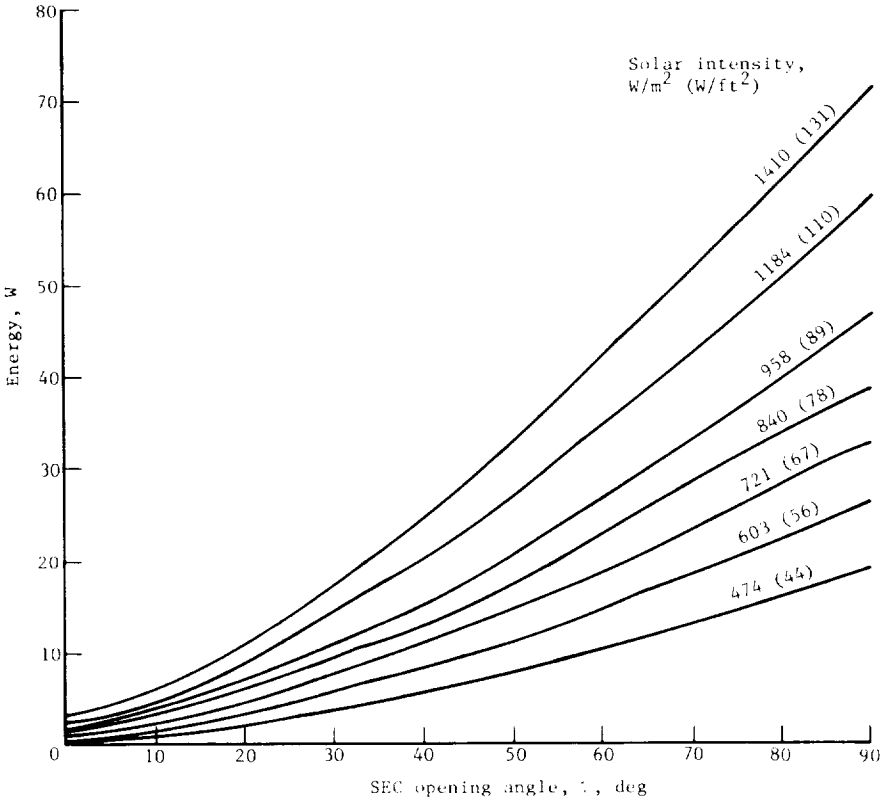

Figure 44.- Solar energy controller net energy captured.

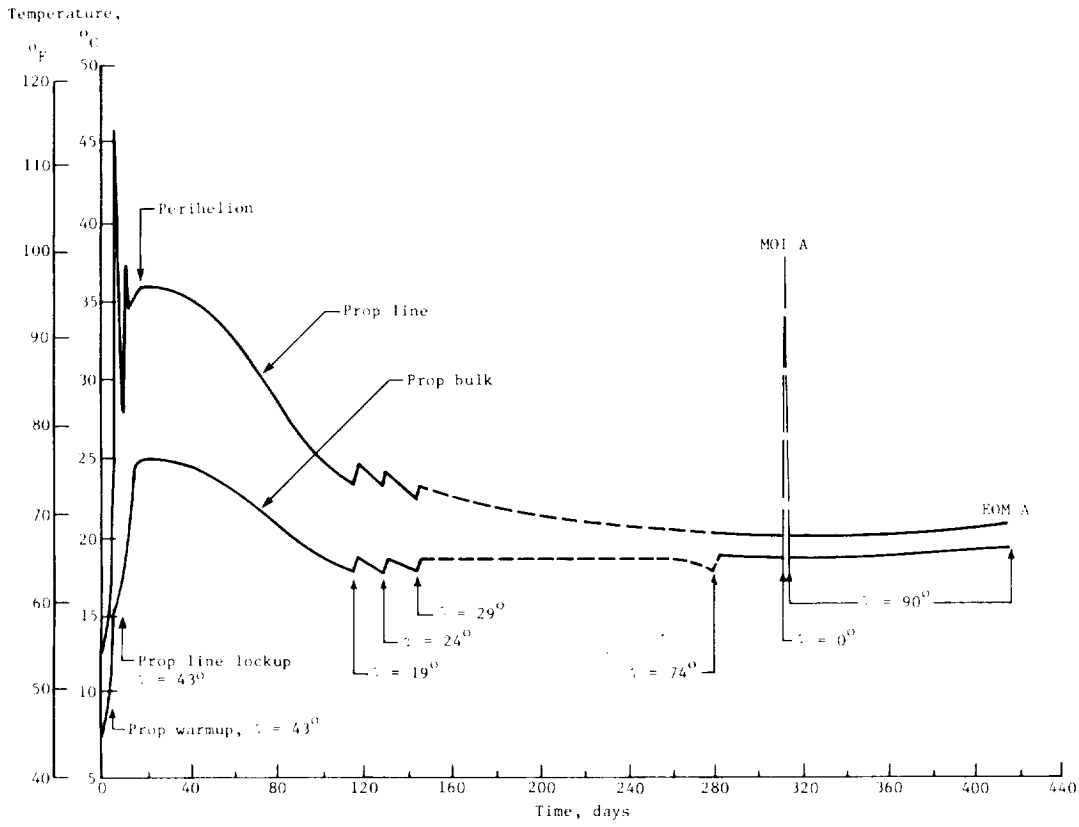

Figure 45.- Predicted propellant bulk and propellant line average temperature.

TABLE 8.- EXPECTED TEMPERATURES OF PROPULSION MODULE

Item	Expected temperature, °C (°F), at -					
	Prop warm-up	Earth perihelion	Mars perihelion	Mars aphelion	Pk during MOI soakback	End of 3.6-hr solar occultation
GA	46 (115)	32 (90)	24 (75)	19 (66)	68 (155)	15 (59)
Prop tank assy						
Aft tank shell	38 (100)	25 (77)	21 (70)	18 (64)	38 (100)	13 (55)
Forward tank shell	31 (88)	21 (70)	19 (66)	16 (61)	19 (66)	12 (54)
Prop iso assy	40 (104)	26 (79)	22 (72)	18 (64)	54 (129)	14 (57)
Pressurant tank	30 (86)	20 (68)	17 (63)	15 (60)	18 (64)	13 (55)
Pressurant control assy ck valve	31 (88)	22 (72)	23 (74)	18 (64)	21 (70)	16 (61)
REA						
Biprop valve	59 (138)	50 (122)	29 (84)	19 (66)	145 (292)	8 (46)
Injector	62 (144)	54 (129)	30 (86)	19 (66)	175 (350)	6 (43)
Gimbal bearing	55 (131)	47 (117)	28 (83)	16 (61)	110 (230)	6 (43)
Act attachment clevis	55 (131)	47 (117)	29 (84)	18 (64)	120 (247)	8 (46)
SEC act	46 (115)	32 (90)	28 (82)	22 (72)	30 (86)	3 (37)

Scan Platform

The MAWDS, the IRTMS, and the VIS are thermally coupled together by the scan platform structure as illustrated in figure 46. Also illustrated in the figure are the VIS electronics flight temperature sensor and scan platform

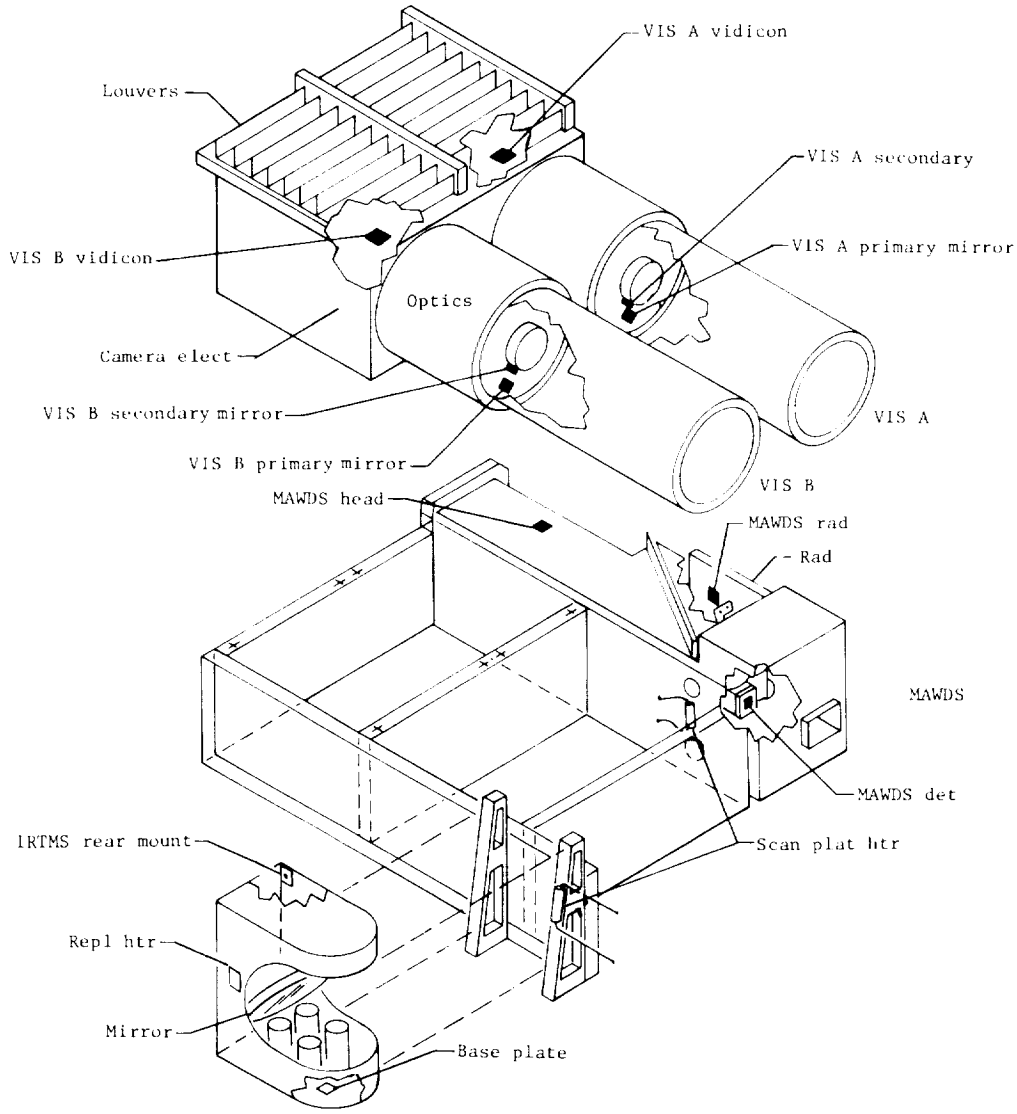

Figure 46.- Scan platform temperature sensor and relay heater locations.

heater locations. Not shown is the multilayer blanket which encompasses all but the louvers, view ports, and MAWDS radiator. The scan platform heaters were commandable and were only required after the VLC separated and when the scan platform was maneuvered into positions previously prevented by the VLC's presence. In addition to the scan platform heater, each instrument contained

a replacement heater which automatically came on when the instrument was commanded off. The scan platform actuators and release mechanisms (fig. 47) are thermally considered a part of the scan platform. Temperatures of these items were acceptable under all normal VO environments. There were no constraints imposed on these passive controlled items. MAWDS had two servocontrolled (automatically on or off, dependent upon the temperature being sensed) heaters. One maintained the optics at a constant temperature. The other, in combination with the radiator, maintained the detector at a constant temperature. The radiator painted white had a commandable heater which prevented condensing of outgassing contaminants.

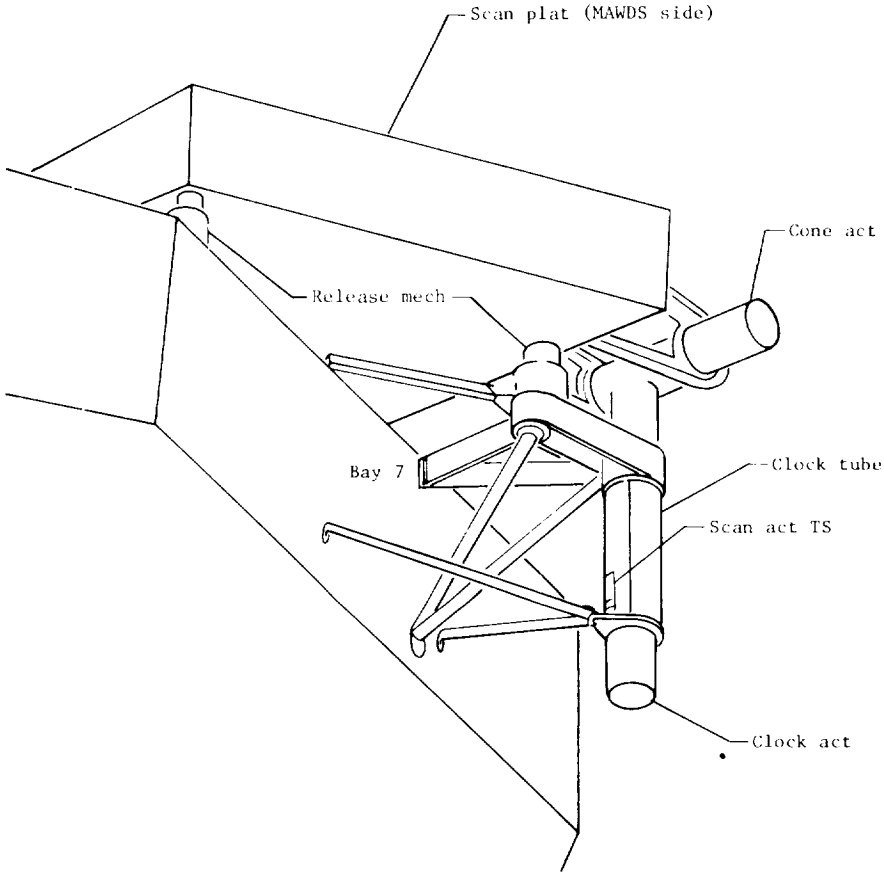

Figure 47.- Scan platform activators and release mechanism.

Replacement heater power for each of the instruments was as follows:

MAWDS	1.0 W
IRTMS	5.9 W
VIS A	14.1 W
VIS B	14.1 W

In addition to these heaters, camera optics temperatures were maintained with a heater power of 3.5 W (1.75 W each, applied continuously), and the scan platform heater when commanded on supplied 9.0 W to the scan platform structure. During normal occultations of less than 2.3 hr, all the heaters could be on for a total of 47.6 W. The power could be reduced to 38.6 W by commanding the scan platform heater off. Power management probably dictated turning all the scan platform heaters off during occultations which exceeded 2.3 hr. Heater and instrument switching logic for the scan platform are shown in figure 48. When commanded

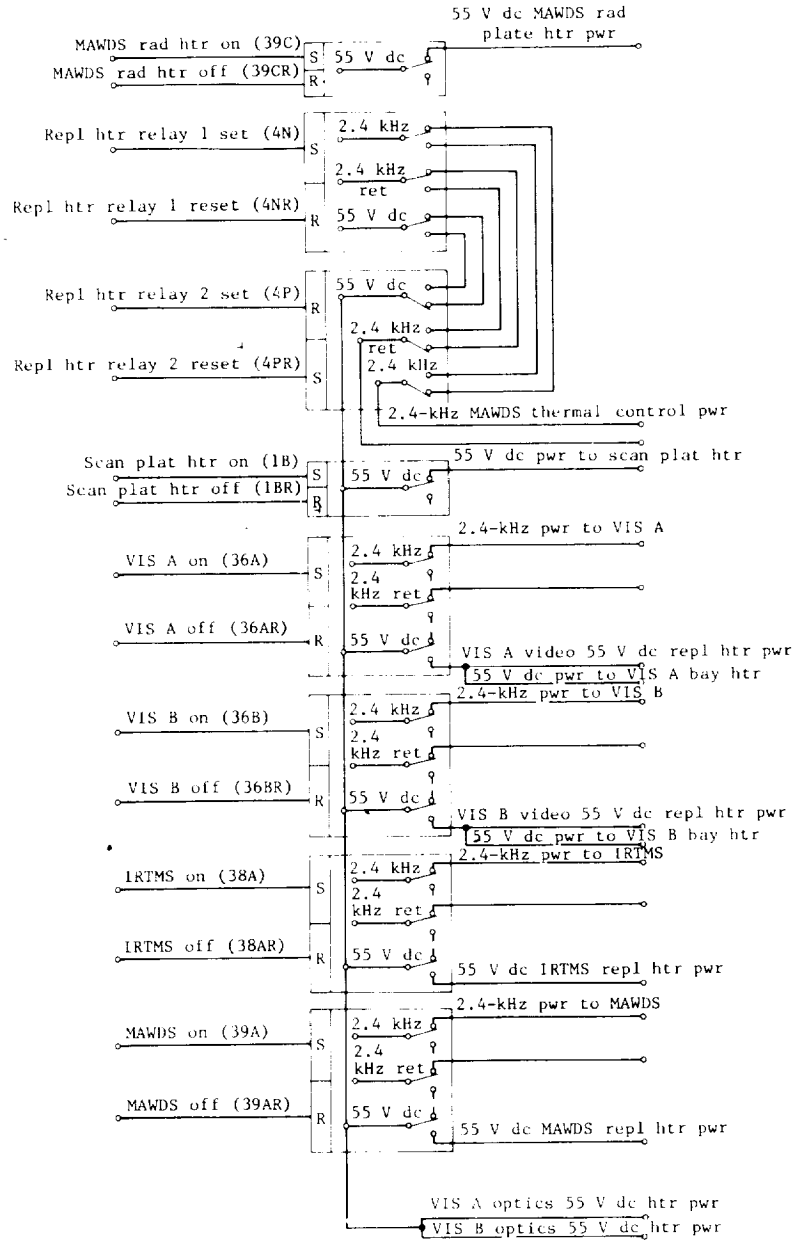

Figure 48.- Scan platform functional switching logic.

on, 10 W was supplied to the MAWDS radiator. The MAWDS detector and optics heaters delivered 2.7 and 6.8 W, respectively, when on. No energy was applied in the off position. Under the coldest conditions the MAWDS servo heaters were on approximately 75 percent of the time.

General operations and constraints of the scan platform were specified. Operating and nonoperating allowable temperature limits for the scan platform are presented in table 9. Generally speaking, there were no significant differences between the operating and nonoperating limits for the instruments. The IRTMS performed nominally only if the temperatures were stabilized to $\pm 10^{\circ}$ C/hr. Expected temperatures of the scan platform are presented in table 10.

TABLE 9.- TEMPERATURE REQUIREMENTS FOR SCAN PLATFORM

S/S & assy	Operating temp range, °C (°F), for -			Nonoperating temp range, °C (°F), for -			Ground operation max tran temp pk, °C (°F)
	Cr	Short-term tran limits (<4 hr)	Preferred cr	Cr	Short-term tran limits (<4 hr)	Preferred cr	
VIS							
Elect	10 to 27 (50 to 80)	-4 to 32 (25 to 90)	16 to 24 (60 to 75)	10 to 30 (50 to 85)	-4 to 32 (25 to 90)	16 to 24 (60 to 75)	32 (90)
Optics[1]	4 to 27 (40 to 80)	-7 to 32 (20 to 90)	10 to 24 (50 to 75)	4 to 30 (40 to 85)	-7 to 32 (20 to 90)	10 to 24 (50 to 75)	32 (90)
MAWDS							
Elect	10 to 32 (50 to 90)	10 to 32 (50 to 90)	10 to 32 (50 to 90)	4 to 38 (40 to 100)	[2] -9 to 41 (15 to 105)	10 to 32 (50 to 90)	41 (105)
Optics[3]	11 to 31 (52 to 88)	10 to 32 (50 to 90)	17 to 26 (61 to 79)	11 to 31 (52 to 88)	[2] -9 to 38 (15 to 100)	16 to 26 (61 to 79)	41 (105)
Det	-80 to -60 (-112 to -76)	-80 to -60 (-112 to -76)	-70 (-94)	[4] -80 to -60 (-112 to -76)	[5] -107 to -29 (-160 to -20)	-70 (-94)	[6] 35 (95)
Rad	-101 to -71 (-150 to -96)	-101 to -71 (-150 to -96)	-86 (-122)	[4] -101 to -71 (-150 to -96)	[7] -118 to -40 (-180 to -40)	-86 (-122)	[8] 35 (95)
IRTMS							
Elect/det	-18 to 16 (0 to 60)	-26 to 16 (-14 to 60)	-14 to -1 (7 to 30)	-18 to 32 (0 to 90)	-26 to 32 (-14 to 90)	-18 to 32 (0 to 90)	32 (90)
Motor	-23 to 10 (-10 to 50)	-34 to 10 (-30 to 50)	-23 to 10 (-10 to 50)	-23 to 16 (-10 to 60)	-34 to 21 (-30 to 70)	-23 to 16 (-10 to 60)	32 (90)
Mirror	-40 to -4 (-40 to 25)	-51 to 10 (-60 to 50)	-40 to -4 (-40 to 25)	-40 to -4 (-40 to 25)	-51 to 10 (-60 to 50)	-40 to -4 (-40 to 25)	32 (90)
Scan act	-10 to 50 (14 to 122)	-10 to 50 (14 to 122)	-10 to 50 (14 to 122)	-10 to 50 (14 to 122)	-10 to 50 (14 to 122)	-10 to 50 (14 to 122)	50 (122)
Plat related	-16 to 75 (4 to 167)	-16 to 75 (4 to 167)	5 to 50 (41 to 122)	-16 to 75 (4 to 167)	-16 to 75 (4 to 167)	5 to 50 (41 to 122)	75 (167)

[1]Axial gradients measured between front aperture corrector and primary mirror were $\leq -9^{\circ}$ C (15° F). Radial gradients measured from center to edge of front aperture corrector were $\leq -15^{\circ}$ C (5° F).
[2]Min temp during orbital nonoperating periods was $<4^{\circ}$ C (40° F).
[3]Max temp difference between any two locations on opt head was less than -13° C (9° F).
[4]Max temp when rad htr was on was less than 35° C (95° F).
[5]Max temp when rad htr was on was less than 47° C (116° F).
[6]Max temp under shrould was less than 45° C (113° F).
[7]Max temp when rad htr was on was less than 39° C (113° F).
[8]Max temp under shrould was less than 51° C (123° F).

TABLE 10.- EXPECTED TEMPERATURES FOR SCAN PLATFORM

Item	Expected temperature, °C (°F), at -			
	Earth perihelion sci off	Mars sci off	Mars sci on	End of 3.6-hr solar occultation
VIS A				
Elect	22 (72)	18 (64)	19 (66)	8 (46)
Optics	21 (70)	16 (61)	17 (63)	8 (46)
	18 (64)	14 (57)	15 (59)	8 (46)
VIS B				
Elect	22 (72)	18 (64)	18 (64)	8 (46)
Optics	20 (68)	17 (63)	17 (63)	7 (44)
	18 (64)	14 (57)	14 (57)	6 (43)
MAWDS				
Elect	18 (64)	20 (68)	20 (68)	6 (43)
Rad [1]	23 (74)	-87 (-126)	-87 (-126)	-101 (-150)
Det [2]	-40 (-40)	-72 (-98)	-72 (-98)	-99 (-146)
IRTMS				
Det	15 (59)	8 (46)	8 (46)	-4 (25)
Repl htr	14 (57)	1 (34)	1 (34)	-12 (10)
Rear mount	16 (61)	8 (46)	8 (46)	-5 (23)
Motor	10 (50)	0 (32)	5 (41)	-8 (18)
Mirror	-10 (14)	-20 (-4)	-12 (10)	-20 (-4)
Act				
Clock	15 (58)	2 (36)	5 (41)	-1 (30)
Cone	14 (57)	7 (44)	7 (44)	0 (32)
Release mechanism	15 (59)	3 (38)	7 (44)	1 (34)

[1] MAWDS rad htr on, plat in stowed pos.

[2] Det TS upper limit; actual det temp with rad htr on was 23° C (75° F) (approx same as rad)

MAJOR SUBSYSTEMS

Structure Subsystem

Purpose

The primary function of the STRUS was to integrate the subsystems which comprised a functioning VOS. As such, the structure provided mechanical support and alignment for all flight equipment. In addition, the structure provided a means for handling the assembled orbiter for flight qualification testing, transporting, and mating operations with the VLC and the launch vehicle.

Description

The orbiter structural design was primarily controlled by mission requirements, including launch, but was influenced as required for safe and expeditious ground operations. The mechanical configuration of the VO is shown in figure 1. The bus structure consisted of an eight-sided equipment compartment approximately 45.7 cm (18 in.) high with side dimensions alternately 50.8 cm (20 in.) and 139.7 cm (55 in.) in width. Twelve bays were provided for standard size electronic assemblies, and four smaller compartments, centrally located on each long side, were provided with structural closures and mounting provisions for mechanical equipment. The bus structure also provided structural support and alignment for the VLC and all other elements of the STRUS and the interfacing subsystems. STRUS containing many VO assemblies was divided into four groups.

The first group contained the major structural elements: the bus structure assembly, the VLCA, V S/C A, and the structural parts of the PM. The load path from the VLC to the Centaur VTA went through three major transitions. The VLC support ring attached to the VLCA at a theoretical three-point field joint (actually there were six fittings). The VLCA was a three-point to four-point transition truss. The four points where the VLCA attached to the bus structure were also separation connections. The load path through the bus structure was primarily a 4-to-4 point direct transfer from the upper to the lower ring through the four major longerons. The bus structure might be viewed as a box consisting of an upper and lower rectangular truss work connected by the four major longerons. Shear support was provided by the electronic assembly chassis. The propulsion module also was attached to the lower part of the four major longerons. There were four attachment points on the lower part of the bus structure, which were also the V S/C separation and release connections. The load was transferred from the bus to the VTA by the 4-to-12 point V S/C A structure, which was composed of four symmetrical tripods. Radial stability of both the CTA and the V S/C A was provided by a ring structure which was designated the VTA. The propulsion module was designed to use the two propellant tanks as structural elements. Tabs on these tanks transferred the major fluid loads to connecting truss elements which, as mentioned, were attached to the lower ring of the bus structure at the four major longerons. Secondary structure was added to provide support for the pressurant tank, PCA, PIA, and engine and gimbal actuators. Secondary structure was also added to the bus structure to support the HGA, scan platform, and solar panels.

The second group of STRUS assemblies included the temperature control blankets and shields. The major items in this group were the larger blankets which cover the propulsion module, the bus, and the scan platform. These blankets were multilayered combinations of metallized plastic film, net spacers, and filters. The propulsion blanket also had an outer layer for protection of the propellant tanks from micrometeoroid damage. In addition to these larger blankets, there were about 100 other smaller shields, blankets, and shades in order to achieve the temperature control of the V S/C elements.

The third group of the STRUS assemblies included the EA chassis and shear plates. These items served a combined function of providing shear members in the bus structure, chassis for packaging most of the electronics, and a heat path that provided for proper temperature control for the electronics. The EA chassis served as a thermal radiator and was designed to accept the louver assemblies which automatically regulated the heat radiated to space.

The fourth group of the STRUS assemblies was a miscellaneous collection of smaller items. Included were four flight accelerometers with their associated signal conditioning amplifiers for monitoring the launch and ascent sequences. For purposes of weight accountability, the various small items such as fasteners, washers, cable clamps, ties, and tapes were listed in this group.

Radio Frequency Subsystem

Purpose and Function

The RFS provided the S-band link with the Earth-based DSN stations for commanding the spacecrafts, transmitting the telemetry data to Earth, providing the navigational tracking data, and supporting the radio science experiments. The RFS formed an important part of the VO telecommunications links as shown in figure 49. The RFS was designed to provide the functions of a command receiver, a phase-coherent ranging transponder, and telemetry transmitter as shown by the block diagram in figure 50. The RFS consisted of (1) a redundant double-conversion, phase-coherent receiver; (2) a redundant continuous-wave exciter that was integrally related in both frequency and phase with the receiver; (3) a redundant TWTA; (4) microwave components that provided rf filtering and switching for connecting either transmitter and its corresponding receiver to the HGA or the LGA; and (5) control units that provided the proper switching to select and control the redundant subassemblies and rf switches. The major functional requirements of the RFS were as follows:

To receive the S-band rf signal transmitted from the deep space stations of the DSN to the VO via the HGA or the LGA

To demodulate the received rf signal and to route the composite command signals to the VO MDS and the VL command detectors

To demodulate the ranging signal transmitted to VO from the deep space stations

To coherently translate the frequency of the received rf signal precisely by the ratio 240/221

To transmit to the DSN via either the HGA or the LGA a modulated S-band rf signal that was either phase coherent with the received signal or generated by its own free running, stable, internal oscillator

To modulate the S-band transmitted downlink with the telemetry data and/or the ranging signal detected by the receiver

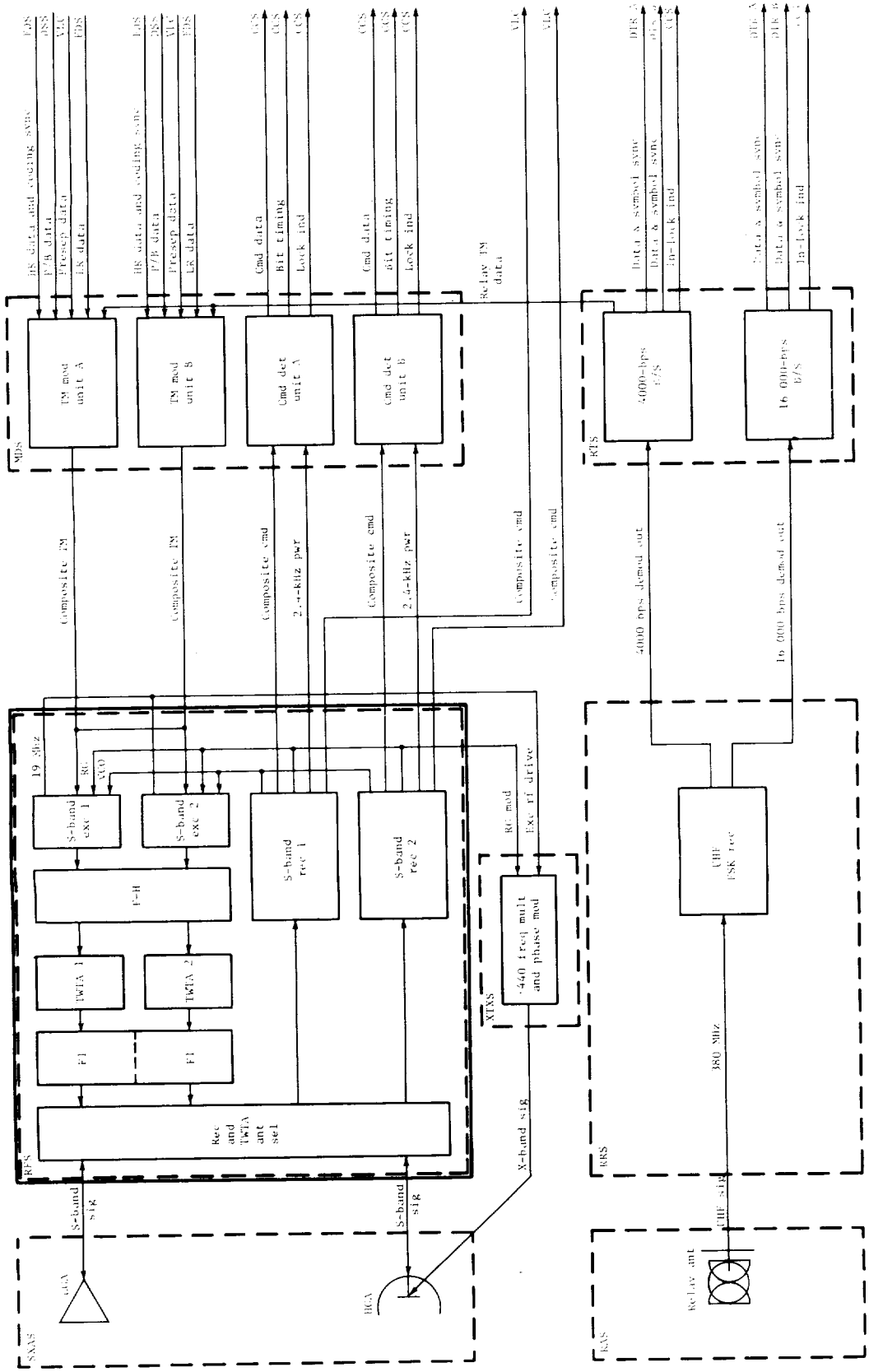

Figure 49.- Functional block diagram of telecommunications showing RFS.

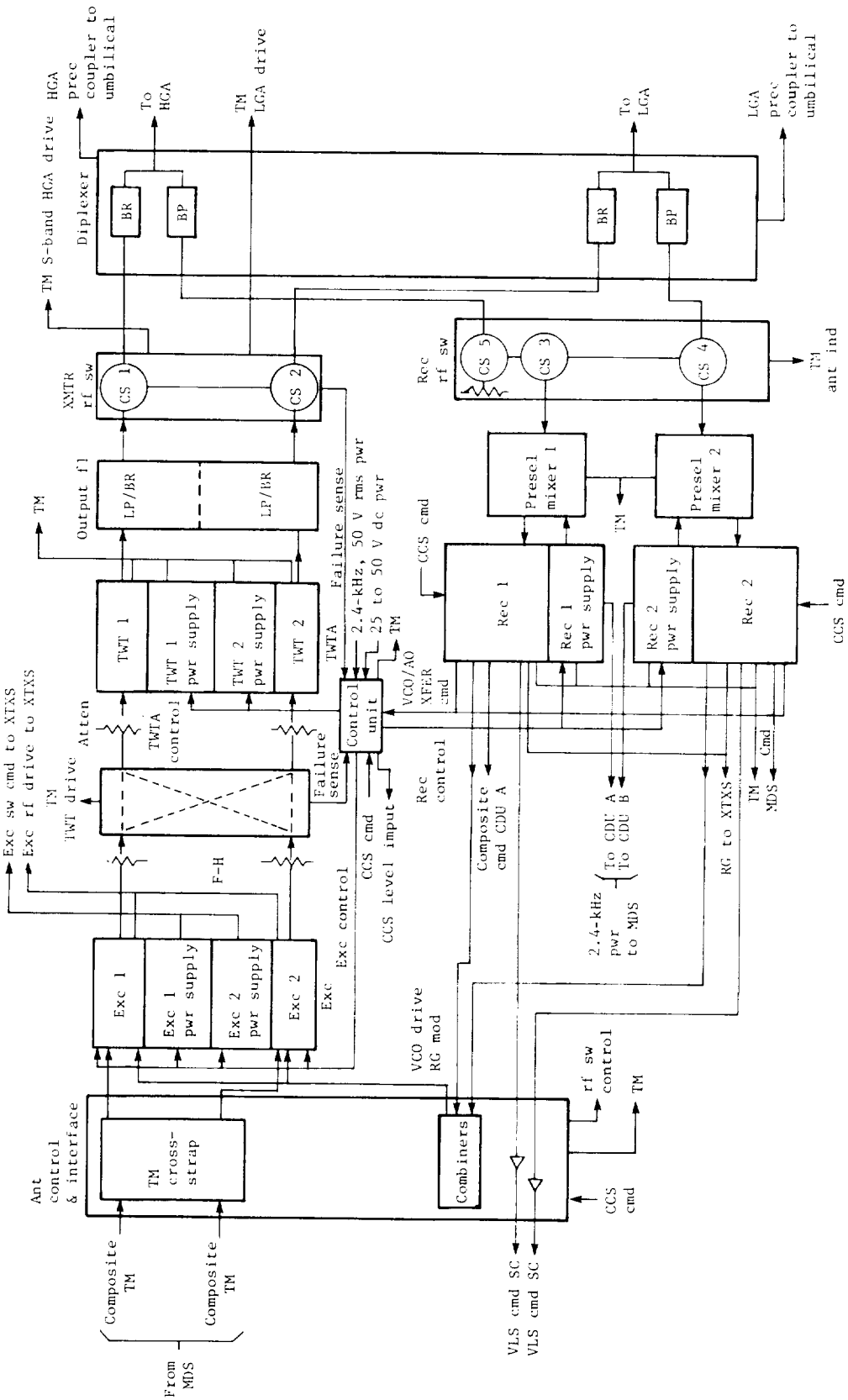

Figure 50.- Block diagram of radio assembly.

To provide the XTXS transmitter with a coherent rf drive from either the VCO (coherent receiver source) or the auxiliary oscillator in two-way or one-way tracking modes, respectively

To provide the same ranging signal detected by the RFS receiver for the XTXS

To provide 50-V, 2.4-kHz prime power to the MDS command detector switched concurrently with the receiver prime power

To provide isolated TM operational and configuration status signals to the FDS

To select either the HGA or the LGA upon command from the CCS

To select either one of the redundant receivers, exciters, and TWTA's and high or low power output upon command from the CCS

Description

The RFS consisted of two receiver subassemblies, one dual preselector/mixer subassembly, one dual exciter subassembly, one dual filter/hybrid subassembly, one dual TWTA assembly, one dual output filter assembly, one receiver rf switch, one transmitter rf switch, one dual diplexer, one control unit subassembly, and one antenna control and interface subassembly. The RFS functional block diagram presented in figure 51 provides more detailed information on the operation of the RFS and indicates the important frequencies used within the subsystem. Some of the electrical specifications and typical values of the RFS are given in tables 11 to 13.

For packaging convenience, the first mixer and preselector of each receiver were separate from the balance of the receiver; however, since they were both part of the same unit (receiver), they were treated as such. A functional block diagram of the receiver subassembly with important frequencies and modules is shown in figure 52. Each receiver was a narrow band, double conversion, APC type which operated at a fixed frequency, factory-set at 2115 ± 5 MHz, with the exact frequency given in table 12. When phase-locked to an uplink signal, the receiver controlled the phase and frequency of the transmitted downlink carrier, demodulated the composite command signal if present, and demodulated the ranging signal if present. Only one receiver was powered at any time; the redundant unit was turned off.

Each of the exciters contained a crystal oscillator which provided the frequency source for the downlink signal when the receiver was not phase-locked to an uplink signal. When the receiver was phase-locked to an uplink signal, the receiver VCO was the frequency source for the downlink signal. Each exciter phase modulated the rf signal with the composite telemetry signal provided by the MDS/TMU and the detected ranging signal when the ranging channel was on. The exciters were capable of operating at any fixed frequency factory selected

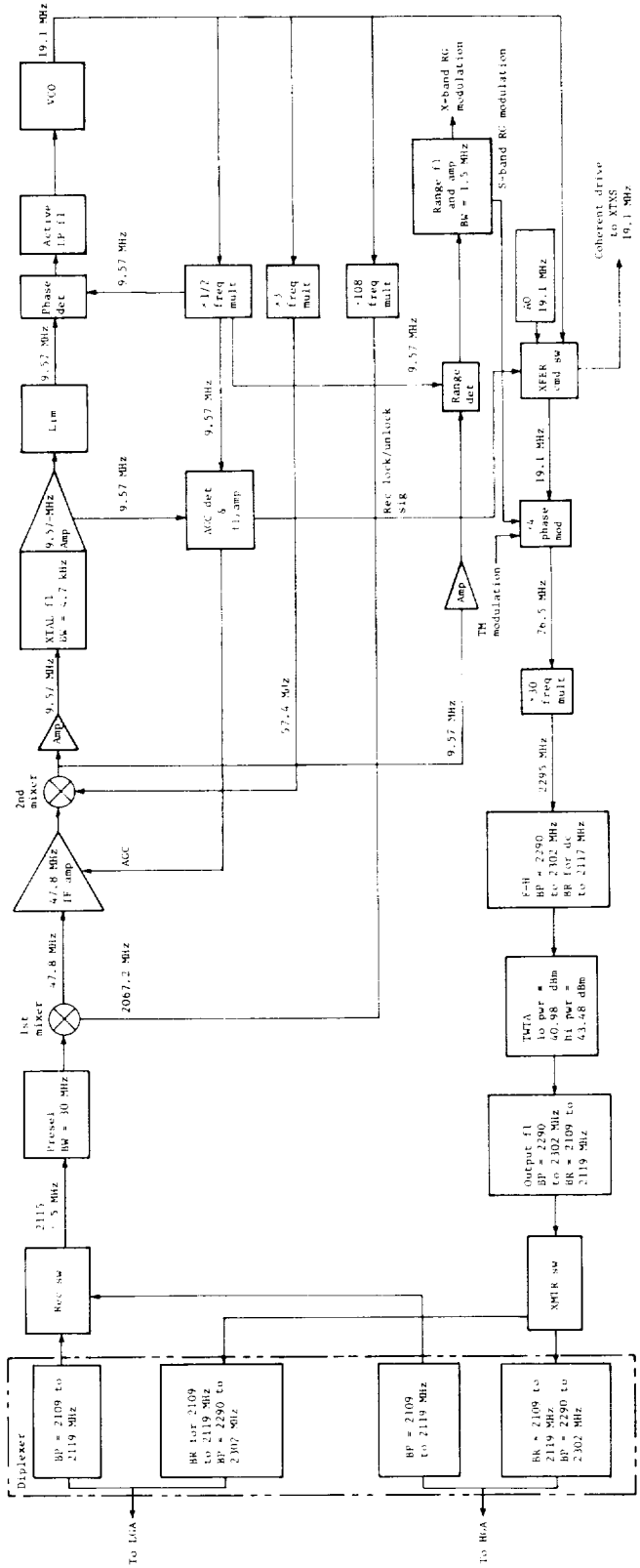

Figure 51.- Functional block diagram of radio frequency subsystem.

TABLE 11.- BASIC RFS CHARACTERISTICS

Parameter	Requirement	Typical value
Received sig freq	2115 ± 5 MHz ($221f_o$)	2111 to 2115 MHz
S-band turnaround ratio	240/221	(1)
XMTR freq	2295 ± 5 MHz ($240f_o$)	2293 to 2297 MHz
First LO freq	$216f_o$	2063 to 2068 MHz
Second LO freq	$6f_o$	≈57 MHz
First IF freq	$5f_o$	≈47 MHz
Second IF freq	f_o	≈9 MHz
VCO and AO freq	$2f_o$	≈19 MHz
VCO freq stability		
(FA temp range)	25 ppm (P-P)	+240 Hz at VCO
Rec threshold sensitivity at -		
LGA input	-151.1 dBm (max)	-151 to -152 dBm
HGA input	-150.9 dBm (max)	
Rec noise fig at -		
LGA input	9.21 dB (max)	7.5 dB
HGA input	9.44 dB (max)	7.7 dB
rf carrier loop noise BW		(1)
Threshold	18 ± 2 Hz	
Strong sig	232 (+ 47.3 or - 40.8) Hz	
Rec input sig range	-70 dBM to threshold	(2)
Lim sig suppression factor	0.0546 (+ 0.0043 or - 0.0042)	(2)
Freq multiplication	110.5	(1)
Phase det sensitivity	0.3 ± 25% V/deg	0.3 V/deg
VCO sensitivity	120 ± 10 Hz/V	120 Hz/V
Loop filter time constant	2690 ± 5% sec	2640 sec
Loop filter time constant	83.3 ± 5% msec	83 msec
Predetection noise BW	4.725 ± 5% kHz	4.6 kHz
Rec rf loop gain		
Strong sig	1.42×10^7 sec^{-1}	(1)
Threshold	7.76×10^5 sec^{-1}	(1)
Damping factor (threshold)	0.707 ± 5%	(1)
Natural resonant freq		
(threshold)	17 rad/sec	(1)
Rec trk range	±66 kHz min	±90
Phase error variation with	<42° for 400 Hz/sec at	
changing freq	sig level of -120 dBm	(1)
AGC loop time constant	23 ± 2 sec	22 sec
AGC loop noise BW	0.5 to 1.5 Hz	(1)
AGC det sensitivity	0.122 ± 20% V/dB	0.122 V/dB
Rec phase jitter	1.9° rms or 5.7° pk	2° pk
Cmd data rate	4 bps	(1)
Cmd SC freq at -		
VLC output	384-Hz sine wave	(2)
MDS output	512-Hz square wave	(2)

[1]Per requirement.
[2]Not applicable.

TABLE 11.- Concluded

Parameter	Requirement	Typical value
MDS cmd output level at ST/N_o = 10.5 dB	82 mV rms ± 20%	82 mV
VLC cmd output level at ST/N_o = 12.5 dB	85 mV rms ± 20%	85 mV
Cmd ch freq response at -70 dBm	$f_{hi\text{-}3dB} \geq$ 1970 Hz $f_{lo\text{-}3dB} \leq$ 46 to 80 Hz	2000 Hz 57 Hz
RG delay	≤1200 nsec	1000 nsec
RG delay stability	±100 nsec	±25 nsec
Differential RG phase delay	45 nsec (over 12-hr period)	<10 nsec
RG ch video noise BW	1.5 ± 0.3 Mhz	(1)
RG code clock freq	500 kHz (nom)	(2)
Downlink RG modulation index	0.45 ± 0.07 rad pk (2 rad/V sensitivity)	0.45
S-band RG output level	0.196 to 0.254 V rms	0.225 mV rms
RG ch freq response	$f_{hi\text{-}3dB} \geq$ 1.08 MHz $f_{lo\text{-}3dB} \leq$ 2000 Hz	1.2 800
XMTR pwr output		
Lo pwr mode	10 W (nom)	9.5 W
Hi pwr mode	20 W (nom)	17 W
XMTR phase jitter	3.6° rms or 10.8° pk (12-Hz loop)	9° (pk)
XMTR downlink TM		
Modulation index	1 rad pk/V pk ± 7%	1.0 rad/V
BW	150 Hz to 2.5 MHz (3 dB)	
XMTR freq ($240f_o$) long term stability (FA temp range)	16 ppm P-P	36.8 kHz P-P at S-band
XMTR short-term stability	2 parts in 10^{10} (1-sec integration time, over a 1-min period)	1.5
X-band XMTR interface (XTXS)		
RG sig level	0.45 ± 0.07 V (pk)	0.45 V (pk)
Coherent drive (VCO/AO)	0 ± 2 dBm ($221f_o/110.5$ (19.1 MHz nom))	0 dBm
rf head losses		
TWTA 1 HGA/LGA	1.43/1.69 dB (max)	0.9 dB
TWTA 2 HGA/LGA	1.68/1.50 dB (max)	1.1 dB
Rec 1 HGA/LGA	1.44/1.42 dB (max)	0.9 dB
Rec 2 HGA/LGA	1.65/1.22 dB (max)	1.1 dB

[1]Per requirement
[2]Not applicable.

TABLE 12.- RECEIVER CHANNEL ASSIGNMENTS

Ch	Radio	Frequency, MHz, of -					
		Rec ($221f_o$)	VCO ($2f_o$)	First LO ($216f_o$)	First IF ($5f_o$)	Second LO ($6f_o$)	Second IF (f_o)
19b	Prototype	2115.017747	19.140432	2067.166667	47.851080	57.421296	9.570216
9b	PTM	2111.607253	19.109568	2063.833333	47.773920	57.328704	9.554784
9b	Flight 1	2111.607253	19.109568	2063.833333	47.773920	57.328704	9.554784
20b	Flight 2	2115.358796	19.143519	2067.500000	47.858796	57.430556	9.571759
16b	Flight 3	2113.994599	19.131173	2066.166667	47.827932	57.393519	9.565586

TABLE 13.- TRANSMITTER CHANNEL ASSIGNMENTS

Ch	Radio	Frequency, MHz, of -	
		VCO/AO ($2f_o$)	XMTR ($240f_o$)
19a	Prototype	19.140432	2296.851852
9a	PTM	19.109568	2293.148148
9a	Flight 1	19.109568	2293.148148
20a	Flight 2	19.143519	2295.222222
16a	Flight 3	19.131173	2295.740741

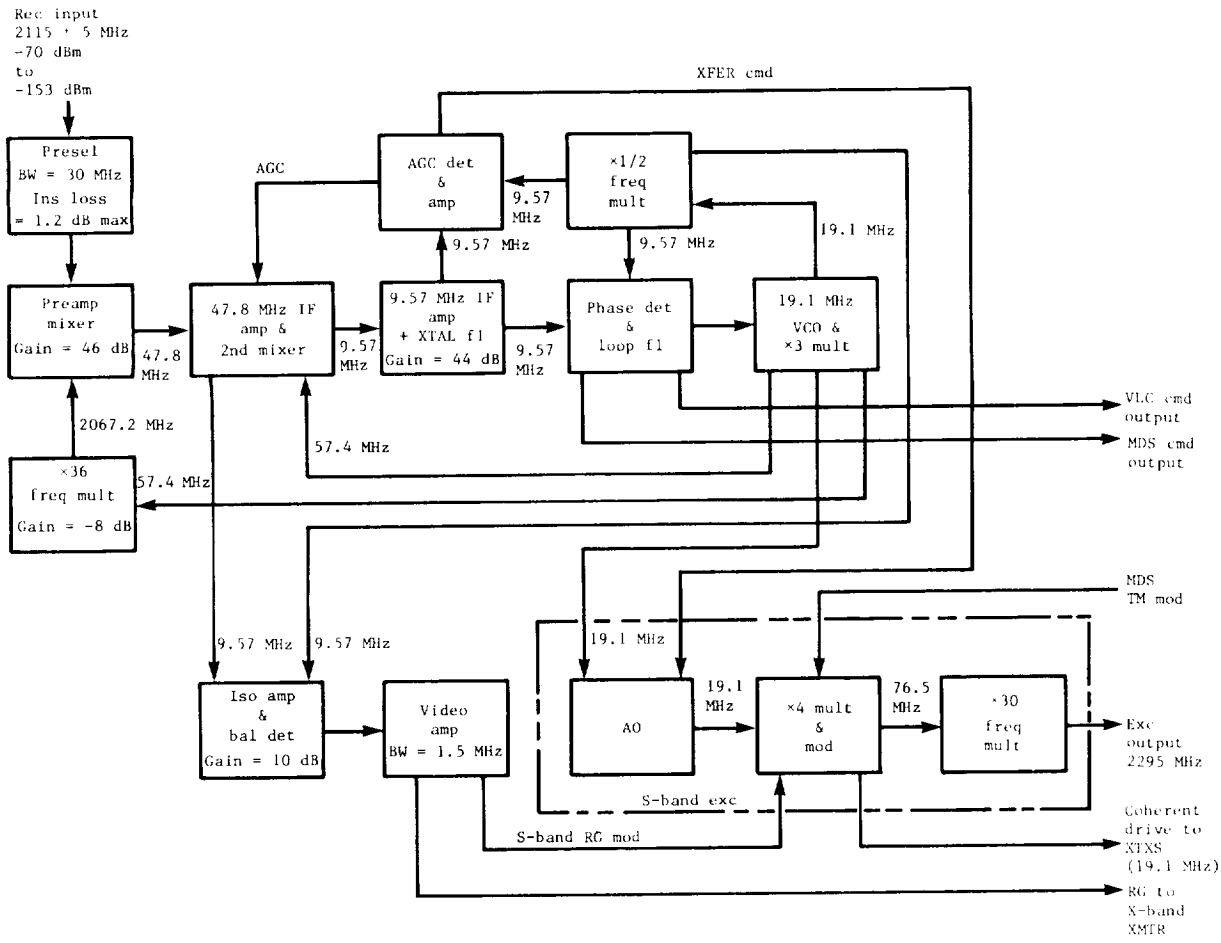

Figure 52.- Simplified functional block diagram of receiver subassembly.

in the 2295 ± 5 MHz band. For the exact frequencies, see table 13. The functional block diagram of the exciters is shown in figure 53 which indicates the module interfaces and the important frequencies and levels. The exciters were powered in the same manner as the receivers; that is, only one of the redundant units was turned on at a time.

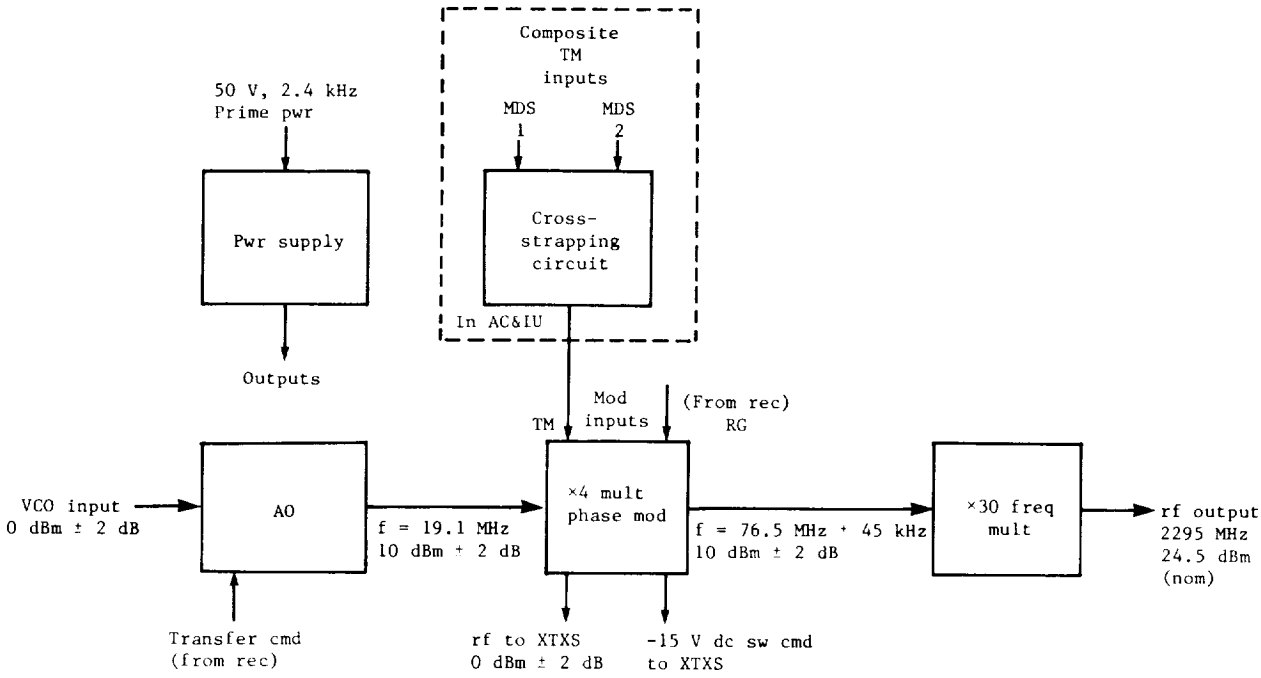

Figure 53.- Block diagram of exciter subassembly.

Redundant TWTA's were used to amplify the exciter output signal. Each TWTA was capable of providing nominal rf output power of either 10 W (low power mode) or 20 W (high power mode) when driven by either exciter. The TWTA configuration is shown in figure 54; only one TWTA provided an output at a time with the other unit being turned off.

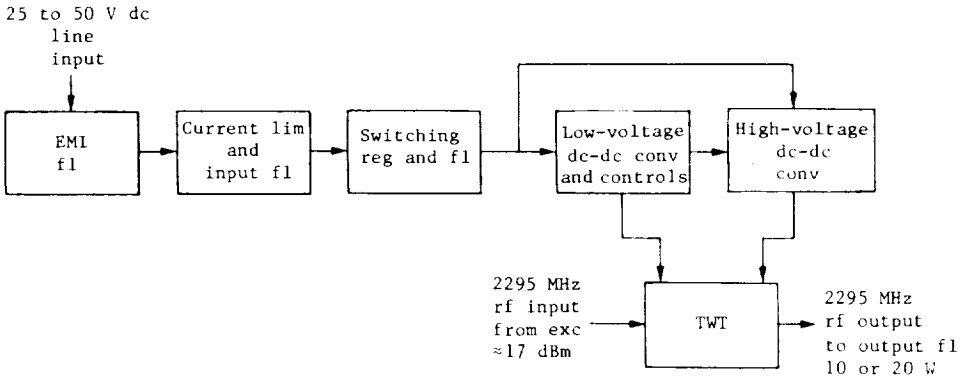

Figure 54.- Block diagram of traveling-wave tube amplifier.

The microwave components consisted of six separate subassemblies variously located in the RFS block diagram. (See fig. 55.) The separate pieces that make up the microwave components are discussed in the following paragraphs. The nominal and maximum rf losses between TWTA and antenna outputs are given in the last portion of table 11. Four fixed attenuator pads were selected to adjust the levels into and out of the filter-hybrid for optimum TWTA drive.

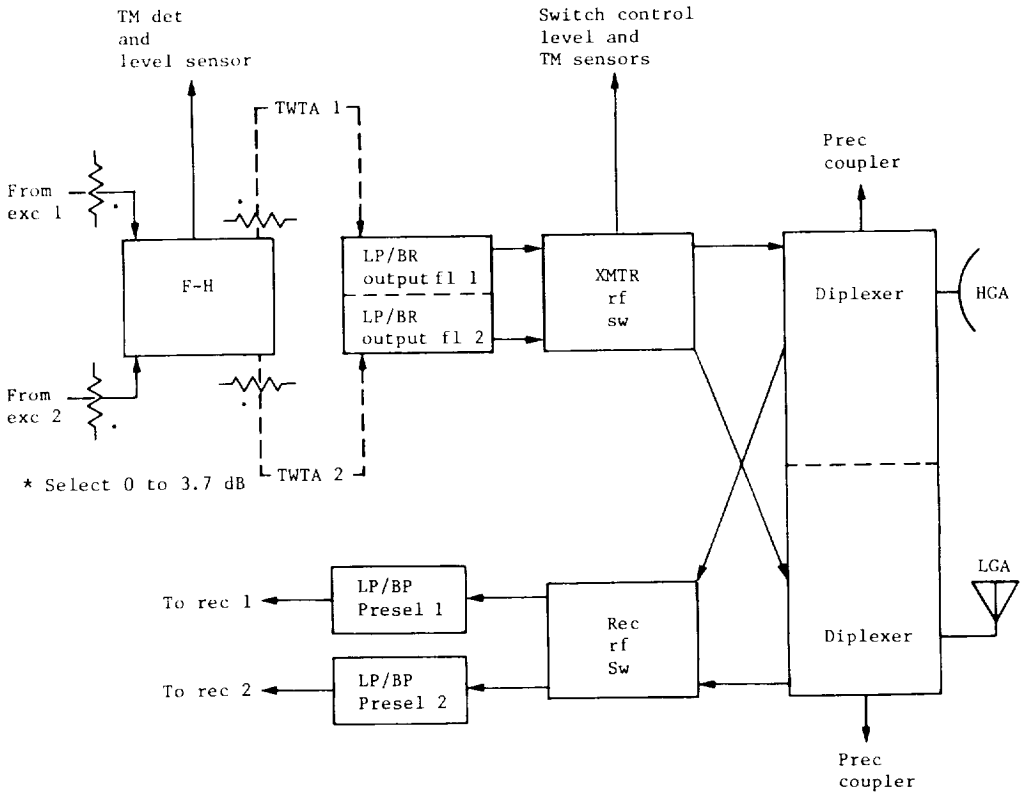

Figure 55.- Block diagram of microwave component.

Filter-hybrid: The purpose of the filter-hybrid was to (1) provide additional filtering of the exciter (2295 MHz) output, (2) split the output from each of the two exciters so that either exciter could drive either TWTA without being switched, and (3) detect the rf level out of each exciter. Since the power from each exciter was split to both TWTA's, the power to each TWTA was down by 3 dB plus the losses. The functional block diagram of the filter-hybrid is shown in figure 56. A summary of the more important characteristics is shown in table 14.

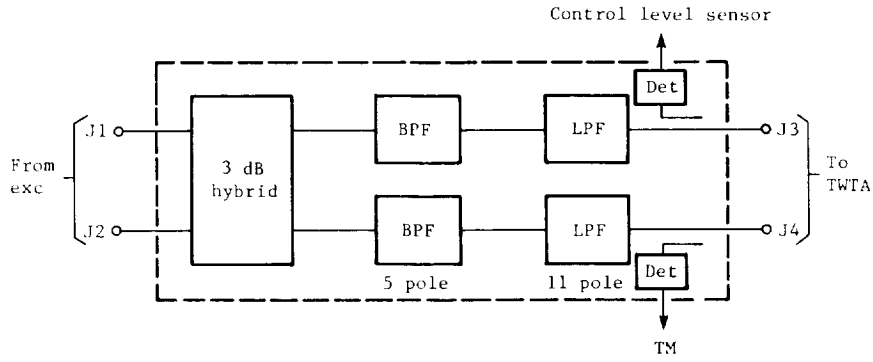

Figure 56.- Block diagram of filter-hybrid subassembly.

TABLE 14.- PERFORMANCE REQUIREMENTS OF FILTER-HYBRID

Freq, MHz	Stop band rejection, J1 to J3 and J2 to J4, dB (min)	BP ret loss, J1, J2, J3, J4, dB	BP ins loss, J1 to J3, J1 to J4, J2 to J3, J2 to J4, dB	Path loss variation between J1 to J3 and J1 to J4 J2 to J3 and J2 to J4 J1 to J3 and J2 to J3 J1 to J4 and J2 to J4. dB	BP iso, J1 to J2 and J3 to J4, dB	Pwr det rf leakage (TM & CLS), 200 mW input to J1, dBm
2290 to 2302	---	19 (min) (VSWR 1.25:1)	4.5 (max); variation across BP 0.2 dB (max)	0.3 (max)	21 (min)	-70 (max)
500 to 2117	100					
2200	75					
2254 and 2337	35					
2392	75					
2477 to 4000	100					
6000 to 10 000	70					

Output filter: Two output (2295 MHz) filters were provided, one at the output of each TWTA. (See fig. 57.) The purpose of the output filter was to remove spurious noise components within the receiver pass band and reduce the TWTA output harmonics. It consisted of two electronically independent, 11-element low-pass filters/four-resonator band-reject filters. A summary of the more important characteristics is shown in table 15.

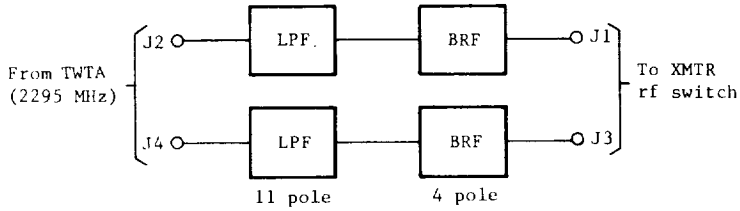

Figure 57.- Output filter.

TABLE 15.- PERFORMANCE REQUIREMENTS OF OUTPUT FILTER

Freq, MHz	Stop band rejection J2 to J1 and J4 to J3, dB (min)	Ret loss, J1, J2, J3, J4, dB	Ins loss, J2 to J1 and J4 to J3, dB
2290 to 2302	---	23 (min) at 25° C 21 (min) at others	0.3 (max) Variation across BP 0.2 (max)
2090	3		
2100	30		
2109 to 2119	60		
2125	30		
2135 and 3200	3		
4580	[a]60		
6000 to 10 000	[a]70		

[a]Ambient (25° C) only, 50-W vacuum test.

Receiver rf switch: The receiver rf switch consisted of three yttrium-iron-garnet circulator junctions, two of which (CS3 and CS4) operated with a common magnetic circuit while the other (CS5) was permanent magnet biased for clockwise circulation and electromagnetically biased for counterclockwise

circulation. The switching coils were fully redundant. The function of this unit was to direct the received input rf power from the LGA to either receiver or from the HGA to either receiver or to an internal energy sink (dummy load) built into the unit (tied to CS5). The block diagram is shown in figure 58 and the important characteristics of the unit, in table 16.

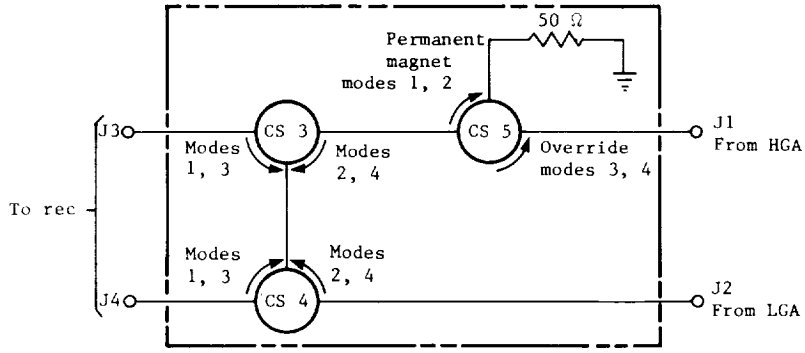

Figure 58.- Block diagram of receiver rf switch.

TABLE 16.- PERFORMANCE REQUIREMENTS OF RECEIVER rf SWITCH

[Frequency range of 2109 to 2119 MHz]

	CS (a)	Temperature range of -		
		15° to 35° C	0° to 55° C	-20° to 75° C
Ins loss, dB	1	0.3 (max)	0.35 (max)	0.4 (max)
	2	.5 (max)	.6 (max)	.7 (max)
	3	.7 (max)	.85 (max)	1.0 (max)
Iso, dB	1	25 (min)	22 (min)	20 (min)
	2	50 (min)	44 (min)	40 (min)
	3	75 (min)	66 (min)	60 (min)

[a]Number of CS in rf path.

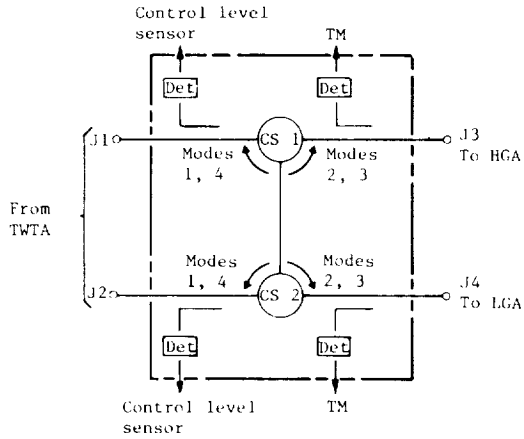

Figure 59.- Block diagram of transmitter rf switch.

Transmitter rf switch: The transmitter rf switch consisted of two YIG circulator junctions operating with a common magnetic circuit and four power detectors packaged as a single unit. The function of this unit was to direct rf power from either TWTA to either the LGA or HGA. All switching coils were redundant. It also monitored incident input power at ports J1 and J2 and exiting output power at ports J3 and J4. The block diagram is shown in figure 59 and major characteristics, in table 17.

TABLE 17.- PERFORMANCE REQUIREMENTS OF TRANSMITTER rf SWITCH

[Frequency range of 2290 to 2302 MHz]

	CS (a)	Temperature range of -		
		15° to 35° C	0° to 55° C	-20° to 75° C
Ins loss, dB	1 2	0.3 (max) .5 (max)	0.35 (max) .6 (max)	0.4 (max) .7 (max)
Iso, dB	1 2	25 (min) 50 (min)	22 (min) 44 (min)	20 (min) 40 (min)
Pwr det rf leakage, dBm (modes 1, 4)		-90 (max)	---	---

[a]Number of CS in rf path.

Diplexer subassembly: The diplexer subassembly consisted of two electrically independent, three-resonator, band-reject filter/three-resonator, band-pass filter combinations, with precision antenna couplers, packaged as a single unit. Its function was to provide diplexing action, permitting simultaneous transmission and reception on a single antenna. The band-reject filter in the transmitter arm rejected receiver pass-band noise generated in the TWTA, whereas the band-pass filter in the receiver arm rejected signals not in the receive band. It also provided output rf power monitoring and an rf link while on the pad via the precision couplers. The block diagram is shown in figure 60 and characteristics, in table 18.

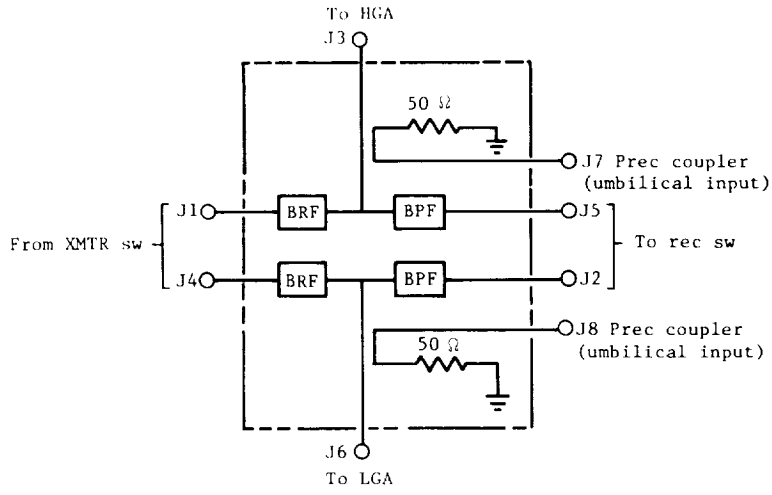

Figure 60.- Block diagram of dual diplexer subassembly.

TABLE 18.- DIPLEXER PERFORMANCE REQUIREMENTS

[50-W vacuum test]

Freq, MHz	Stop band rejection, dB		Ret loss, dB		BP ins loss, dB		Prec coupler, dB	
							Coupling	Directivity
	J3 to J5 J6 to J2	J1 to J5 J4 to J2	J1 J4	J3 J6	J1 to J3 J4 to J6	J3 to J5 J6 to J2	J1 to J7 J4 to J8	J3 to J7 J6 to J8
1927	30 (min)	---	---	---	---	---	---	---
2094	---	3 (min)	---	---	---	---	---	---
2109 to 2119	---	[a]50 (min)	---	21 (min) VSWR 1.2:1	---	0.4 (max)	---	---
2134	---	3 (min)	---	---	---	---	---	---
2290 to 2302	30 (min)	---	21 (min)		0.3 (max)	---	[b]20 ± 2	21 (min)
		BP ins loss variation			0.2 (max)			

[a]FA temp limits only, TA min limit is 45 dB.
[b]Calibrated to an accuracy of ±0.2 dB.

As described earlier, the RFS had three redundant subassemblies, two receivers, two exciters, and two TWTA's; in addition, the two antennas (HGA and LGA) are selectable and other modes of operation are selectable, that is, ranging channel on/off, TWTA output power hi/lo, TWTA power on/off, and command enable/inhibit. The method of selection among the various combinations of these options, including interfaces of the equipment with other subsystems in the VO, was made by certain controls within the RFS. Most of these controls were contained within the two control boxes in the RFS, the CU and the AC&IU. Some of these controls were initiated within the RFS (such as failure sensing), some were ground initiated via the CCS (such as antenna selection) and functions were selected in combinations (such as LGA/RG off). In addition, several interface amplifiers included in the AC&IU were not a part of antenna control, and some isolation amplifiers and other circuitry were included in the CU. Table 19 outlines the control functions of the RFS. The block diagrams of the CU and AC&IU are shown in figures 61 and 62, respectively.

TABLE 19.- CONTROL FUNCTIONS OF RFS

Location	Function	Signal source	Output	Comments
CU	Exc pwr sensor	RFS F-H	Sw closure to CCS	CCS then commanded red exc to turn on if other had failed
CU	Exc control	CCS	2.4-kHz pwr to appropriate exc	Relayed sw contact closure to the RFS; selected exc
CU	Rec control	CCS	2.4-kHz pwr to appropriate rec	Relayed sw contact closure to the RFS, selected exc, selected rec; also simultaneously provided 2.4-kHz pwr to correct MDS-CDU
CU	TWTA 1 level sensor	RFS XMTR rf sw	Sw closure to CCS	CCS then commanded red TWTA to turn on if other had failed
CU	TWTA 2 level sensor	RFS XMTR rf sw	Sw closure to CCS	CCS then commanded red TWTA to turn on if other had failed
CU	TWTA control	CCS	25 to 50 V dc to appropriate TWTA	Relayed sw contact closure to the RFS; selected exc; selected TWTA; also sent status to FDS
CU	TWTA pwr mode	CCS	Appropriate cmd to TWTA P/S	Relayed sw contact closure to the RFS; selected exc; selected 10 or 20 W TWTA output pwr
AC&IU	Ant control	CCS	dc sig to rec and XMTR rf sw	Allowed selection of HGA or LGA; relayed sw contact closure to the RFS; selected exc
CU	Rec and TWTA pwr status	RFS	FDS	
CU	VCO/AO mode	RFS rec 1 and 2	RFS exc 1 and 2	Selected VCO mode when rec was in-lock
CU	Provide combined isolated TM outputs	12 TM sig in RFS	6 TM sig to FDS	Iso amp used dc power supplied by FDS
AC&IU	Ant status	AC&IU	To CU	
CU	Ant status	CU	To FDS	From dc pwr supplied by FDS
AC&IU	Cmd iso	RFS rec 1 and 2 cmd outputs	To VLC	Provided iso without cross-strapping; automatically switched to active cmd output
AC&IU	MDS TMU	TMU 1 and 2	Exc 1 and 2	Provided cross-strapping of either TMU to either exc
AC&IU	VCO to exc	RFS rec 1 and 2 VCO's	Exc 1 or 2	Provided cross-strapping for either VCO to either exc
AC&IU	RG to exc	RFS rec 1 and 2 RG	Exc 1 or 2 and XTXS	Provided cross-strapping of either RG output to either exc

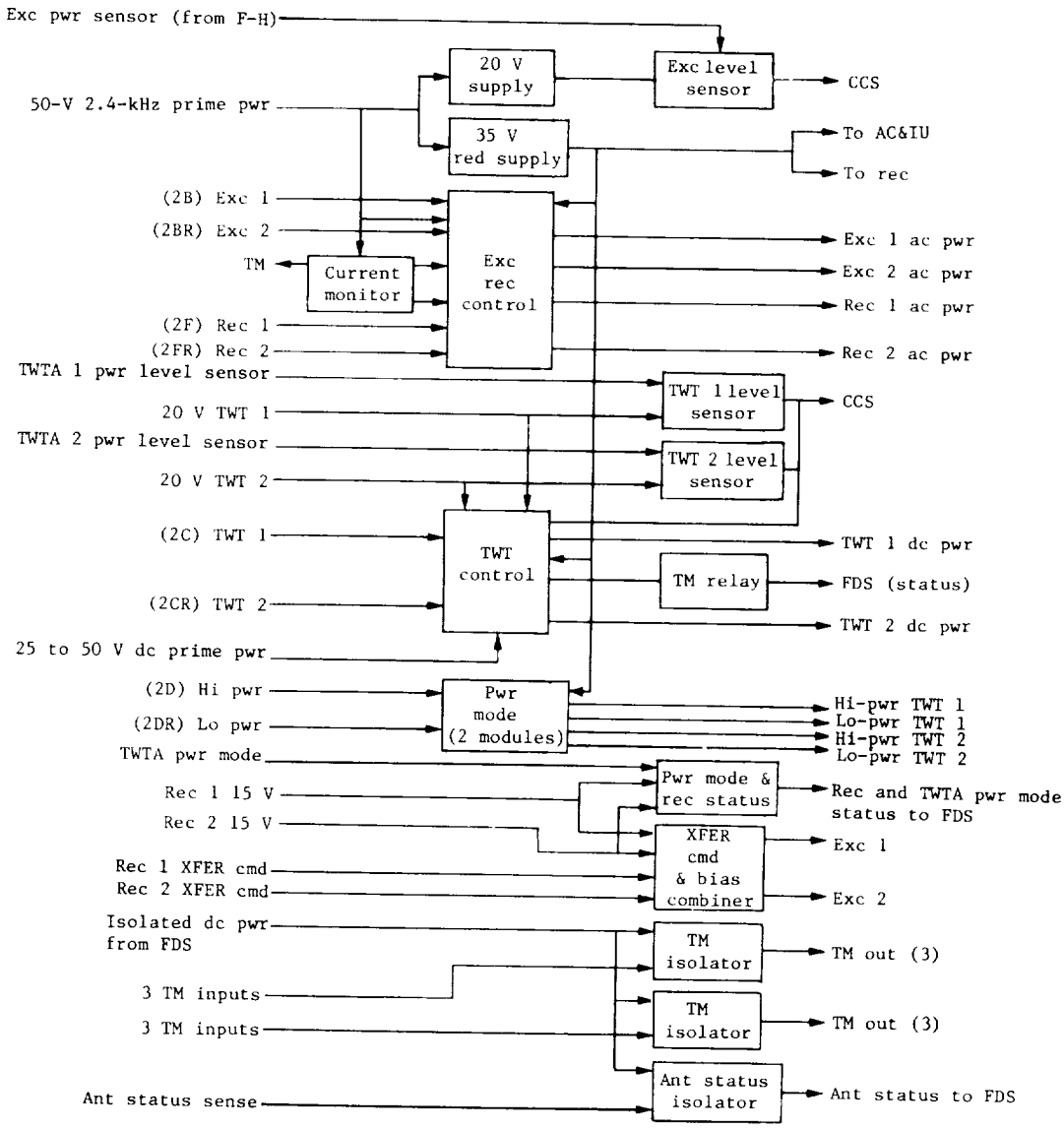

Figure 61.- Block diagram of control unit.

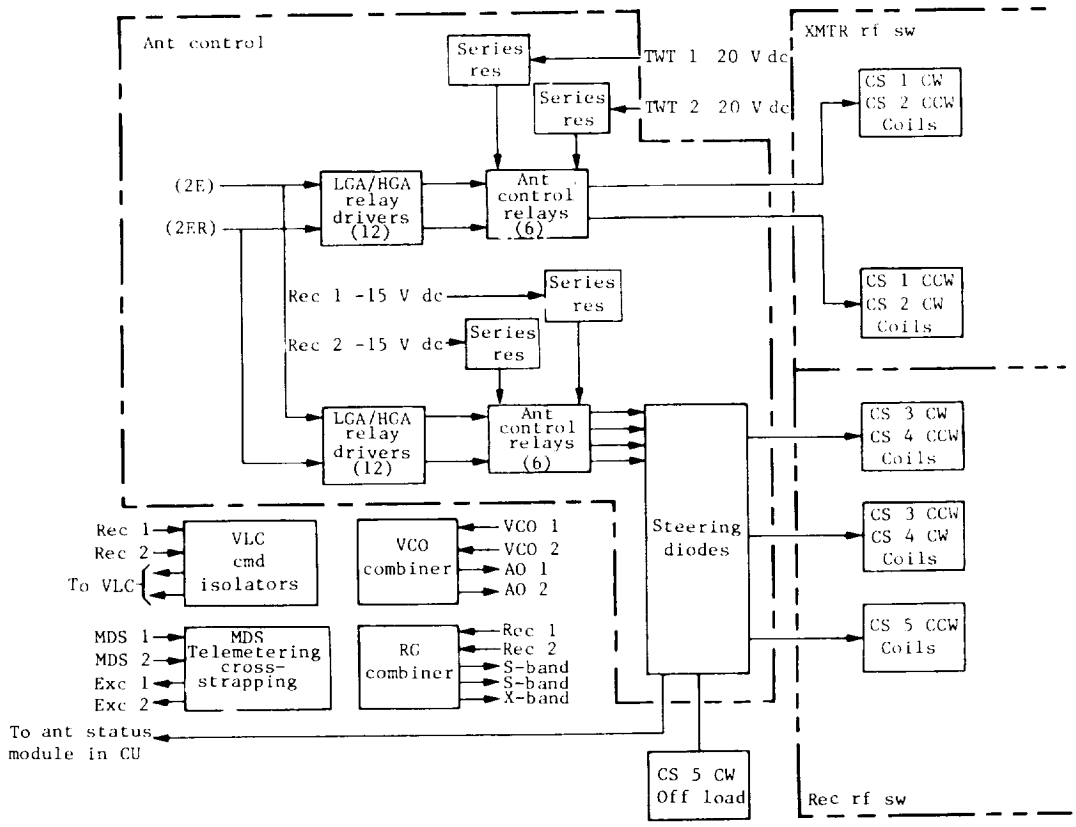

Figure 62.- Block diagram of antenna control and interface unit subassembly.

Operating Modes and Commands

The operating modes that could be commanded from the ground are listed in table 2. In addition, several modes could be selected automatically by the CCS based upon conditions existing on the VO; these modes are listed in table 19. The RFS did not have a desired or mandatory operational sequence. (This does not mean that the ground station, operating with the RFS, did not have desirable or mandatory operational sequences. The sequences were a function of the telecommunications link requirements.) There were no operational constraints for the RFS; however, it was desirable to leave the ranging channel on when it was not required by other mission requirements (i.e., link management constraints) to be off. By leaving the channel on for long periods of time, the receiver became more thermally stable and thus improved the phase and group delay stability of the RFS which in turn improved the navigational accuracy (when making DRVID measurements especially).

Interfaces

All interfaces required for the RFS and the characteristics peculiar to the RFS are as follows.

The RFS supplied composite command signals to the MDS. A single output from each receiver was sent to its associated CDU in the MDS. The command return line was referenced to ground via the RFS circuit reference tree. Each receiver was separately operated with a command detector (i.e., receiver number one with CDU number one). Switching of the CDU's was accomplished by the RFS. The 2.4-kHz power was routed to the MDS CDU's via the RFS, and this power was switched between the redundant CDU's at the same time it was switched between the RFS receivers. The MDS provided its own overload protection, and each CDU required approximately 5 W for operation. With an input signal to the receiver phase modulated with a 512-Hz square wave at 2.46-dB carrier suppression (equivalent to 0.7176 rad (peak)), the RFS receiver output to the CDU was 82 mV rms ± 20 percent when the ratio of the command output signal level multiplied by the time of 1 bit for a rate of 4 bps to noise density was equivalent to 10.5 dB. The maximum signal level output, with a -70-dBm uplink signal level to the RFS, would not exceed 835 mV rms (typical values were 500 to 600 mV rms). The command channel frequency response with a -70-dBm input signal was approximately 80 to 1970 Hz at the 3-dB cutoff points. The source output impedance did not exceed 4000 Ω and the load impedance was a nominal 100 Ω at best lock frequency.

The RFS also supplied composite command signals to the VL prior to separation. The redundant receivers were used in a similar fashion in that each RFS receiver output was connected to a separate DCS receiver input without any cross-strapping. The outputs were isolated from RFS chassis ground and other command or phase detector outputs, so that a short or open circuit at one command output had no effect on the other outputs. Similarly, with an input signal to the RFS receiver phase modulated with a 384-Hz sine wave with 2.5-dB carrier suppression (1.03 rad (peak)), biphase modulated at a rate of 4 symbols/sec, the output to the DCS receiver was 85 mV rms ± 20 percent, when the ratio of the command output signal level multiplied by the time of one symbol-to-noise density was 12.5 dB. The maximum signal output would not exceed 640 mV rms (typically, 400 to 500 mV rms at strong signal level). The frequency response of these channels was similar to the previous channels supplied to the CDU. The receiver command output source impedance was less than 400 Ω with a reactive component less than 400 Ω at 384 Hz.

In the opposite signal path direction between the RFS and the MDS, the TMU supplied an ac coupled composite telemetry signal to the RFS phase modulator. This interface was a coaxial cable with a nominal 50-Ω impedance and grounded at the RFS end of the cable. These inputs were cross-strapped in the RFS, and were either 24-kHz or 24-kHz and 240-kHz square-wave subcarriers, modulated with pulse-code modulation telemetry at a nominal 1 rad (peak)/V (peak) level. The transmitter phase modulation characteristics (phase deviation versus modulating voltage) did not deviate from the best straight line by more than ±2.5 percent from 5 to 300 kHz and by ±5 percent from 500 Hz to 1.5 MHz for peak phase deviations of up to 1.8 rad. The total amplitude modulation would not exceed 2 percent when the transmitter was modulated with a sine-wave signal at frequencies

between 500 Hz and 1.5 MHz at peak phase deviations up to 1.8 rad. The transmitter produced a positive going phase change at the output terminal of the RFS for a positive going voltage change at the TMU input.

The RFS-SXAS interfaces had essentially identical characteristics for both the LGA and the HGA, consisting of 50-Ω impedance systems with source and load VSWR's of 1.4:1 or less. The JPL-designed 4CTC connector was used for both connections between the two S/S's. In addition, two other rf transmitter/receiver paths were provided in the RFS to interface with the umbilical cables and, in turn, the LCE for prelaunch testing only. These interfaces used OSM (Omni Spectra Miniature) connectors and 50-Ω impedance coaxial cables connected to two precision couplers, one in the HGA arm and the other in the LGA arm of the rf diplexer. The coupling factors were -20 ± 2 dB and were calibrated to an accuracy of ±0.2 dB.

The CCS interface with the RFS was used to provide the various commands listed in table 2 to control the different functions of the RFS throughout the duration of the mission. All CCS inputs to the RFS consisted of pulsed switch closures with a minimum duration of 94 msec and a maximum of 117 msec. Maximum open-circuit voltage was 35 V dc and maximum closed-circuit current was 160 mA. This interface was isolated from RFS chassis ground but was referenced to the control unit dc circuit common. The RFS control unit also provided inputs to the CCS which indicated the state of the output power levels from the exciters and the TWTA's, allowing the CCS to choose the redundant unit in the event of power output degradation. These inputs to the CCS were solid-state switch closures, which were closed to signify degradation below a preset threshold.

The interface with the PWRS supplied the RFS with the following prime power:

50 V, 2.4-kHz square wave = 24.9 W nom and 26.3 W max

25 to 50 V dc, lo-pwr TWTA = 54 W nom and 61 W max

25 to 50 V dc, hi-pwr TWTA = 87.6 W nom and 92.5 W max

25 to 50 V dc, replacement heater = 36 W at 37.5 V and 65.5 W at 50 V

This interface was isolated from the RFS chassis ground and all other inputs and outputs, but the control unit circuit common was referenced to the dc power input return.

The FDS interface with the RFS was required to supply the various engineering performance monitoring and state conditions throughout the mission. Analog signal levels were provided between 0 to 100 mV dc and 0 to 3 V dc (clamped at a maximum of ±4 V dc to protect the FDS) and had a source impedance between 100 and 1000 Ω connected to the FDS load impedance greater than 15 MΩ. The status signals were switch closures, isolated from ground, with a closed switch representing a digital 1 state. All measurements were isolated from RFS chassis ground and referenced to the FDS ground only. The FDS supplied a

±12 V dc input to operate several operational amplifiers in the RFS for isolation purposes. Table 20 is a listing of the data transmitted back to Earth for performance monitoring purposes.

TABLE 20.- RFS TELEMETERED PARAMETERS

Function	Parameter measurement range	TM range
[1]AGC (coarse)	-70 dBm to threshold	0 to 3 V dc
[1]AGC (fine)	-105 to -135 dBm	0 to 100 mV dc
[1]SPE (coarse)	Rec ch freq ± 66 kHz	-1.5 to 1.5 V dc
[1]SPE (fine)	Rec ch freq ± 20 kHz	-1.5 to 1.5 V dc
[1]LO drive	-12 to 4 dBm	100 mV dc to 0 V
[1]TWT anode 2 voltage	0 to 145 V dc	0 to 3 V dc
[1]Helix current, TWT	0 to 20 mA	0 to 3 V dc
[1]Lo-gain drive	0 to 25 W	0 to 100 mV dc
[1]Hi-gain drive	0 to 25 W	0 to 100 mV dc
[1]Exc current	180 to 340 mA	0 to 3 V dc
[2]TWTA drive	0 to 100 mW	0 to 100 mV dc
[1]RG on-off		Sw closure
[1]TWTA 1 and 2 pwr mode		Sw closure
[1]VCO 1 and 2 temp	-5° to 66° C (23° to 150° F)	---
[1]AO 1 and 2 temp	-5° to 66° C (23° to 150° F)	---
TWT 1 temp	-9° to 97° C (15° to 206° F)	---
[1]TWT 2 temp	-9° to 97° C (15° to 206° F)	---
[1]Rec current	245 to 455 mA	0 to 3 V dc
[1]Bay 1 temp	-5° to 66° C (23° to 150° F)	---
Bay 16 temp	-5° to 66° C (23° to 150° F)	---
[1]TWT cathode current	0 to 80 mA	0 to 3 V
TWTA 1/TWTA 2		Sw closure
Exc 1/exc 2		Sw closure
Rec 1/rec 2		Sw closure
Ant		Sw closure

[1]1 and 2 share common analog ch.

[2]Exc output drive power defined at monitoring point following combining hybrid.

The XTXS interface was required to provide two isolated rf drive signals to the X-band transmitter, one from each of the redundant RFS exciters. The signals are coherent with the S-band exciters in operation and were approximately 19 MHz at a 1 mW ± 2 dB level. When the active receiver was in-lock to a ground transmitted signal, the drive signal was coherently translated from the received signal. When the receiver was not in-lock, the drive signal was derived from the RFS exciter AO. The RFS also supplied the XTXS with the detected uplink ranging modulation signal from the active receiver. This signal was at a 0.45 ± 0.07 V peak level. All of these signals were fed through standard 50-Ω impedance coaxial cables (two cables for the exciter signals and one cable for the ranging modulation). In addition, two isolated exciter control signals were supplied to the XTXS, one from each RFS exciter power supply. These signals provided the XTXS with the means for internally switching exciter drive concurrently with the RFS exciter switchover. This control output was 0 V when off, and -15 ± 0.5 V dc when on. All of these outputs were referenced to both the RFS and the XTXS chassis grounds.

Modulation/Demodulation Subsystem

Purpose and Function

The MDS had two primary functions:

(1) The generation of a composite telemetry signal for the modulation of the VO downlink to Earth; this function was accomplished by means of the TMU.

(2) The demodulation of the Earth to VO uplink command signal; this function was accomplished by means of the CDU.

Description

The MDS consisted of dual redundant CDU's and TMU's, with one CDU and one TMU only powered at a time and continuously. Figure 63 shows the functional relationship of the MDS in the telecommunications area. Each CDU was connected to one RFS receiver and was switched simultaneously with that receiver, with each CDU receiving the composite command signal from its interfacing RFS receiver only. The CCS was programmed to periodically alternate power to the two RFS receiver/CDU pairs unless inhibited by ground command. Initiation of a switchover to the alternate receiver/CDU pair could also be accomplished by ground command. The TMU's were cross-strapped to the RFS exciters with the desired TMU selectable by CCS command. The low-rate channel operated continuously throughout the entire mission. The high-rate subcarrier was combined with the low-rate subcarrier to form the composite telemetry signal whenever the high-rate channel was required for data.

CDU.- The CDU block diagram is shown in figure 64. The composite command signal consisted of a 512-Hz square-wave subcarrier, biphase modulated with command data bits at 4 bps and B/S at 4 Hz. The CDU acquired the subcarrier, established B/S, detected the command data bits, and provided the data bits, derived bit timing, and lock status to the CCS. Subcarrier and B/S lock status were sent to the FDS. The primary CDU performance parameters are listed in table 21. The CDU established and maintained the demodulation references, detected the command information, and generated the detector status signals. The detector established the subcarrier and B/S references upon receipt of the command acquisition signal, which is shown in figure 65. The detector first established subcarrier sync by comparing the unmodulated subcarrier signal received from the RFS with internally generated, phase-shifted estimates of this signal. The estimate whose phase most closely agreed with that of the input signal was selected as the subcarrier demodulation reference. Subsequently, the detector established B/S by comparing the RFS receiver output, which now had the subcarrier modulated with B/S, with internally generated, phase-shifted estimates of B/S each of which was half-added to the established subcarrier reference. The estimate whose phase most closely agreed with that of the B/S signal received at the detector input was selected as the B/S demodulation reference. The DSN command acquisition sequence, prior to commanding, consisted of idle 1 (subcarrier only) being transmitted for a time interval of at least 65 data bits (16.25 sec), followed by idle 2 (subcarrier modulo 2 B/S) for an interval of at least 25 data bits (6.25 sec).

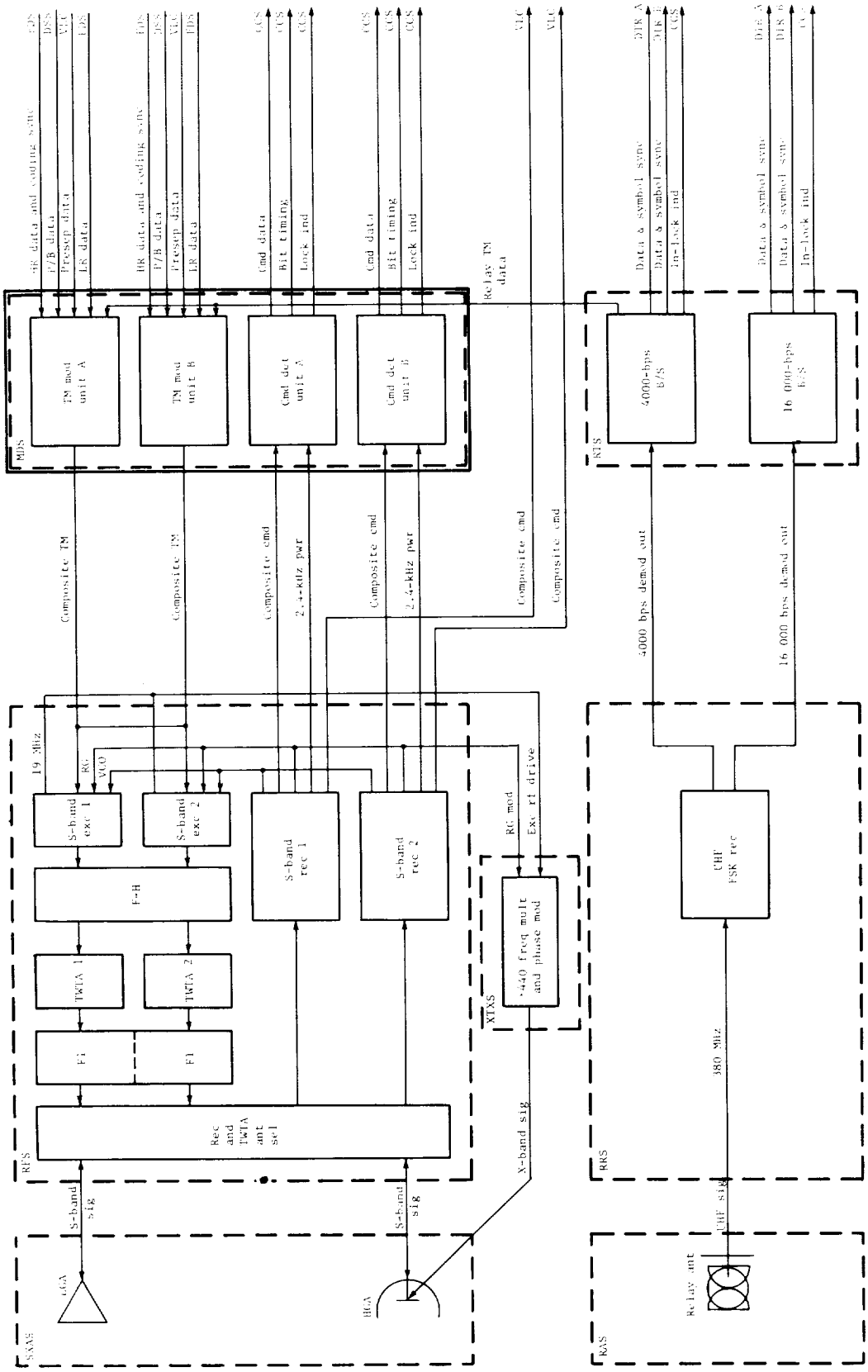

Figure 63.- Functional block diagram of telecommunications showing MDS.

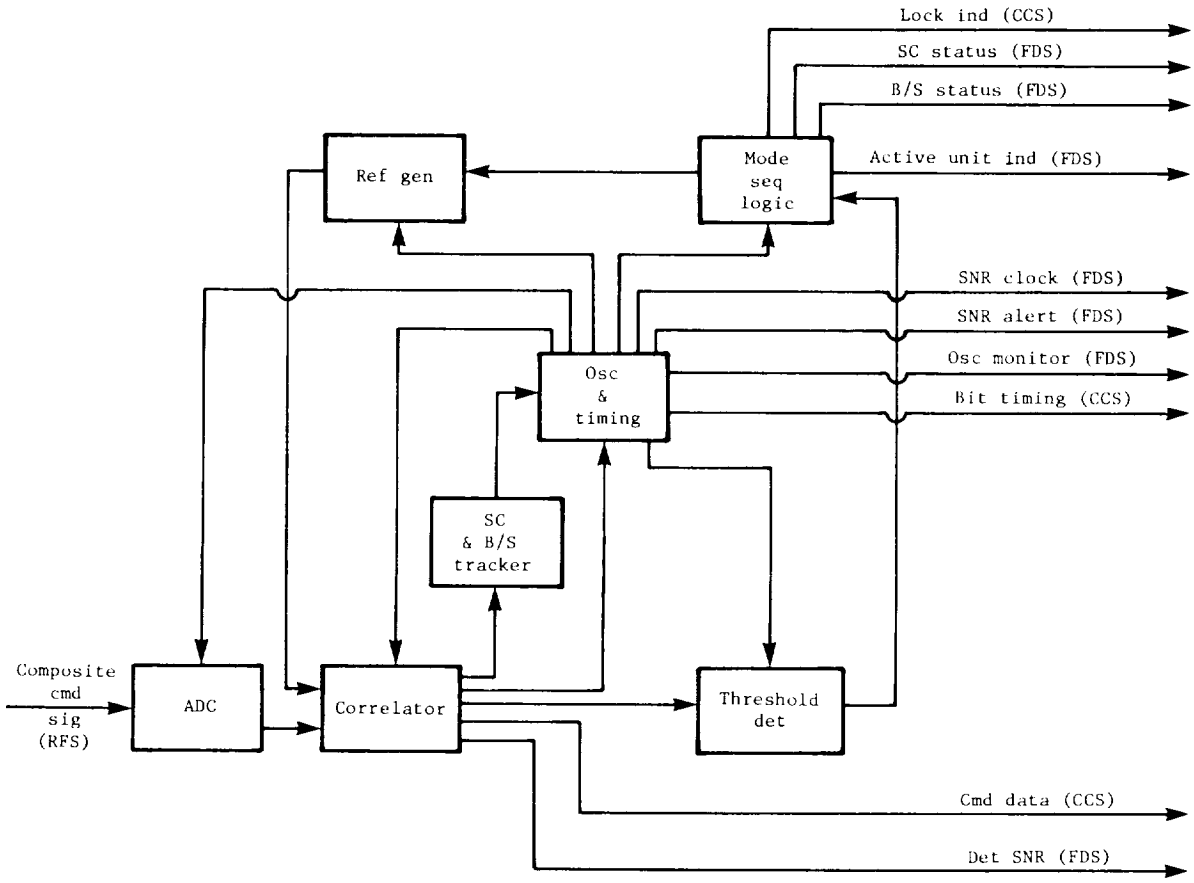

Figure 64.- Functional block diagram of command detector unit.

TABLE 21.- CDU PERFORMANCE PARAMETERS

Parameter	Design value	Tolerance
Cmd sig threshold, ST/N_o	10.5 dB	+1.1 or -0.9 dB
Threshold BER	10^{-5}	
Cmd bit rate	4 bps	±0.01%
Cmd SC freq	512 Hz	±0.01%
Probability of failure to acquire sig and indicate in-lock at threshold	$\leq 10^{-4}$	
Probability of indicating out-of-lock when in-lock	$\leq 10^{-5}$	
Probability of indicating in-lock in presence of noise	$\leq 10^{-8}$	

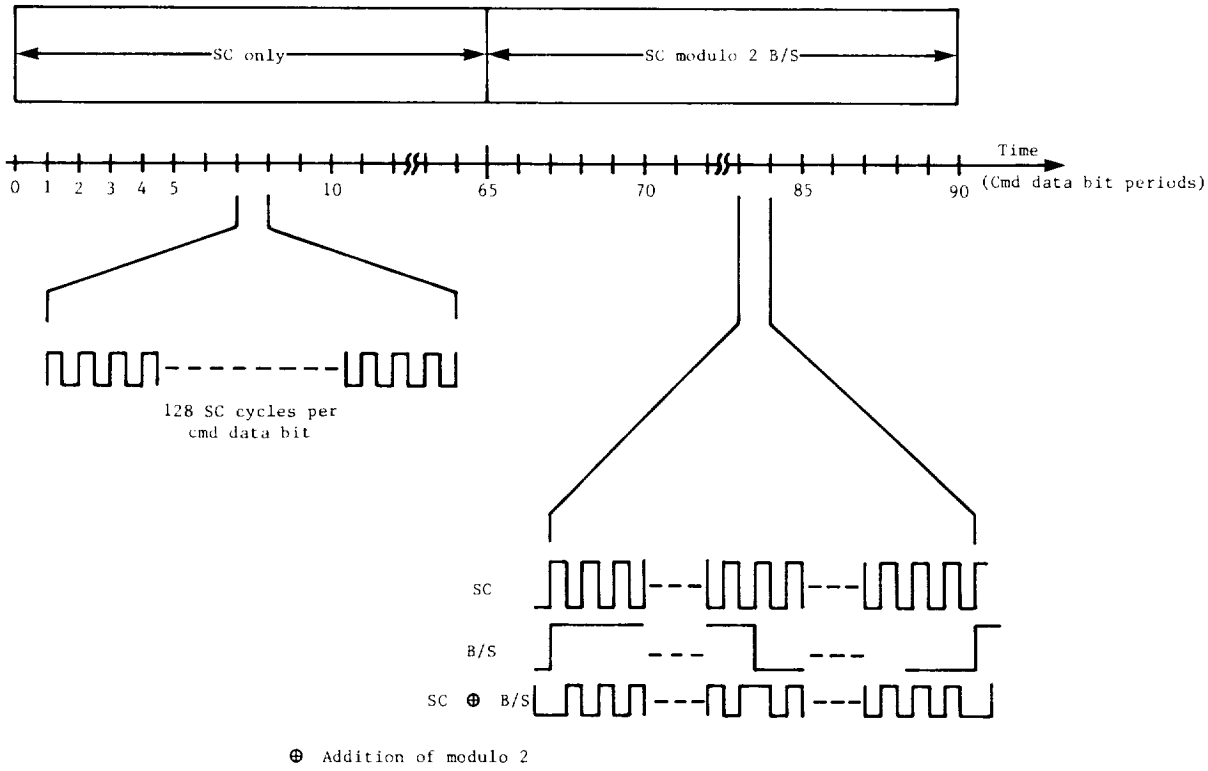

Figure 65.- Command acquisition signal.

After having initially established the subcarrier and B/S references, the detector entered the data mode and was ready to detect command information and provide it to the CCS. In going from its initial state to the data mode, the detector went through 9 of its 10 possible modes of operation. The normal modes of CDU operation, indicated in the MDS status word via telemetry, were out of lock, subcarrier lock, and B/S lock. These operating modes were observed (in real time or recorded by the VO DSS for transmission later) when an Earth to VO uplink existed and the uplink signal consisted of rf carrier only, command subcarrier modulated carrier (idle 1), and command subcarrier modulo 2/bit-sync modulated subcarrier (idle 2), respectively. (See fig. 66.) In addition to these status indications described, the CDU oscillator frequency and the command data signal-to-noise ratio can be checked via telemetry whenever desired. As shown in figure 67, the oscillator frequency was counted down inside the CDU, and the resultant frequency was then counted by the FDS with a seven-stage binary counter for a period of 71.68 sec. The counter overflowed 917 times leaving an average count of 64.51 at the end of the count period. The sensitivity of this measurement was approximately 11.16 Hz (at 1.3 MHz) per DN. The countdown chain in the CDU was affected by the subcarrier tracking process. In order to obtain a valid measurement of the CDU oscillator frequency, the command data bits could not be present on the uplink. In addition, the stability of the timing source in the FDS from which the 71.68-sec gate was derived also influenced the accuracy of the CDU oscillator frequency measurement. To calibrate this effect, a measurement of the CDU oscillator frequency was made when the

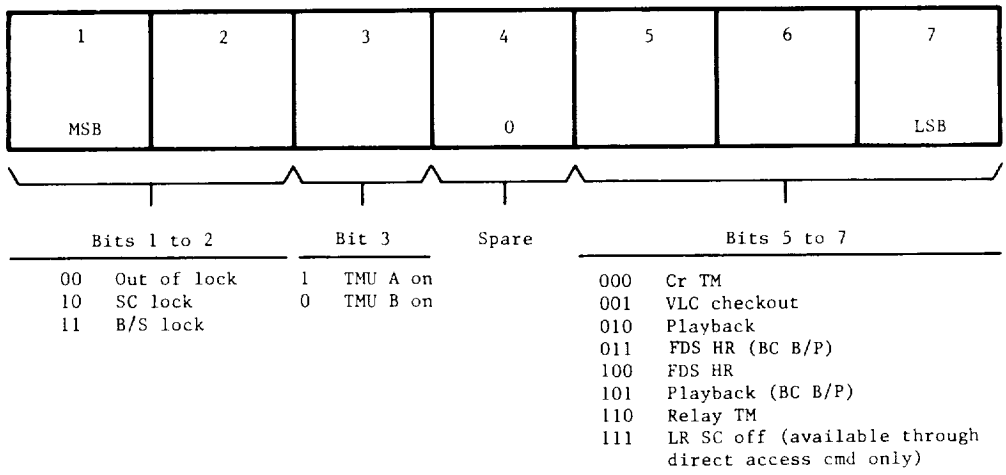

Figure 66.- MDS status word.

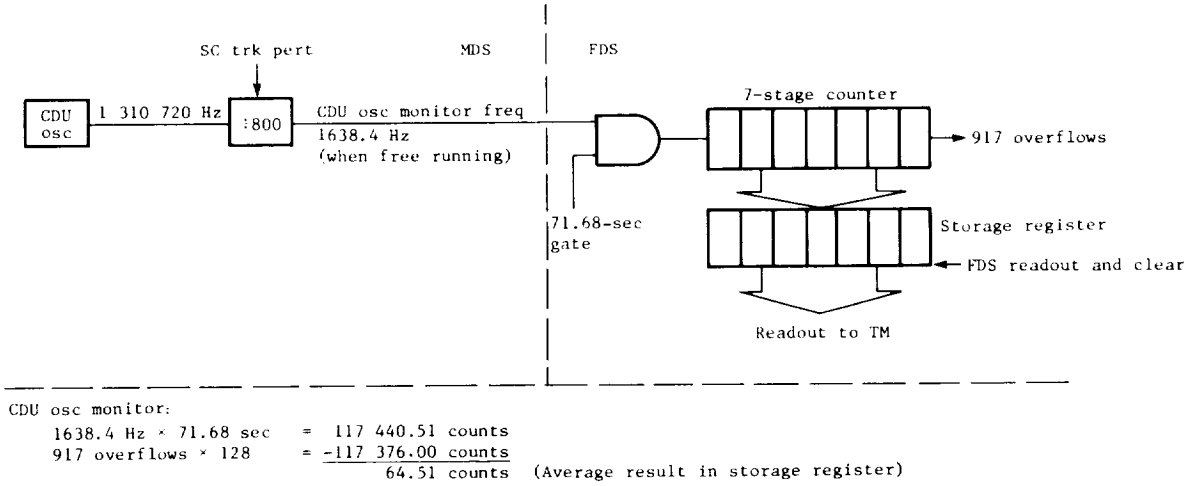

Figure 67.- CDU oscillator monitor implementation.

CDU was locked to an uplink signal. The CDU oscillator frequency was then coherently related to this uplink command subcarrier frequency (plus any Doppler) and any change from the anticipated value was a measure of the FDS oscillator drift.

The CDU SNORE test was the command signal-to-noise-ratio-estimate measurement which was a 20-binary bit result of the integration of the command signal over one command bit period. The 20-bit word was shifted out of the CDU into a 16-bit register in the FDS, dropping the four MSB's as shown in figure 68. The

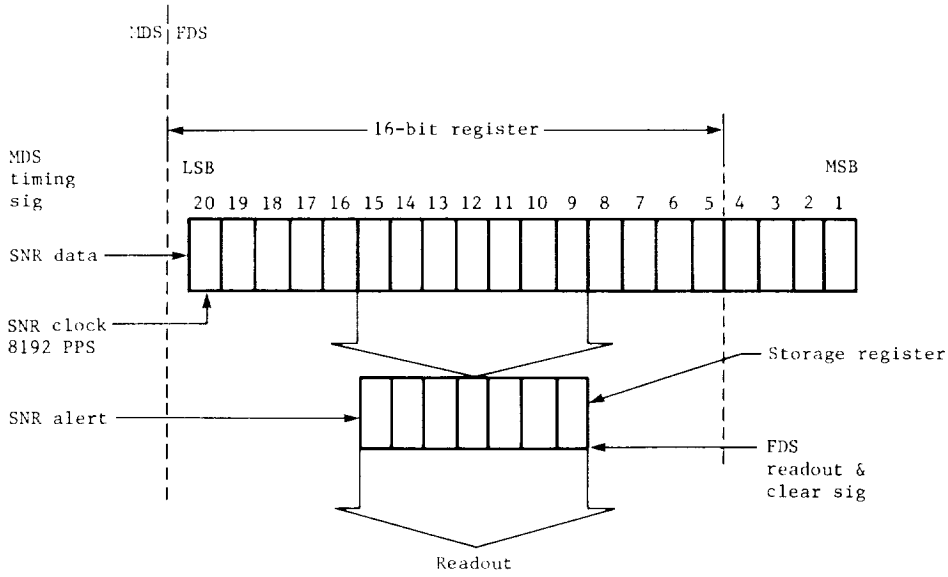

Figure 68.- CDU SNR measurement.

FDS then stored bits 9 through 15 in a register to be read out as the CDU SNR word. The storage register was reset to zero upon readout such that if another readout was called for before the next SNR was shifted in, an SNR word of zero resulted. The CDU being tested would be in B/S lock with no command bits being transmitted, i.e., data zeros would be continuously transmitted during the SNORE measurement. Due to the fact that the CDU input from the RFS could vary over a large dynamic range (approximately 50 to 800 mV rms) with the change in rf input to the RFS, the desired measurement resolution was obtained by breaking the curve up into several segments as shown in figure 69. The curve shown in figure 69 indicates average values of the SNR word. Individual readings varied around the average in proportion to the SNR of the signal. Normally a minimum of 500 samples should be taken to calculate a valid CDU input ST/N_O. Figure 70 shows the relationships between ST/N_O and BER and typical uplink signal levels.

TMU.- A block diagram of the TMU is shown in figure 71. Each TMU generated its own square-wave subcarriers at 24 and 240 kHz, with the low-rate 24-kHz subcarrier biphase modulated (modulo 2 add) with the uncoded low-rate telemetry

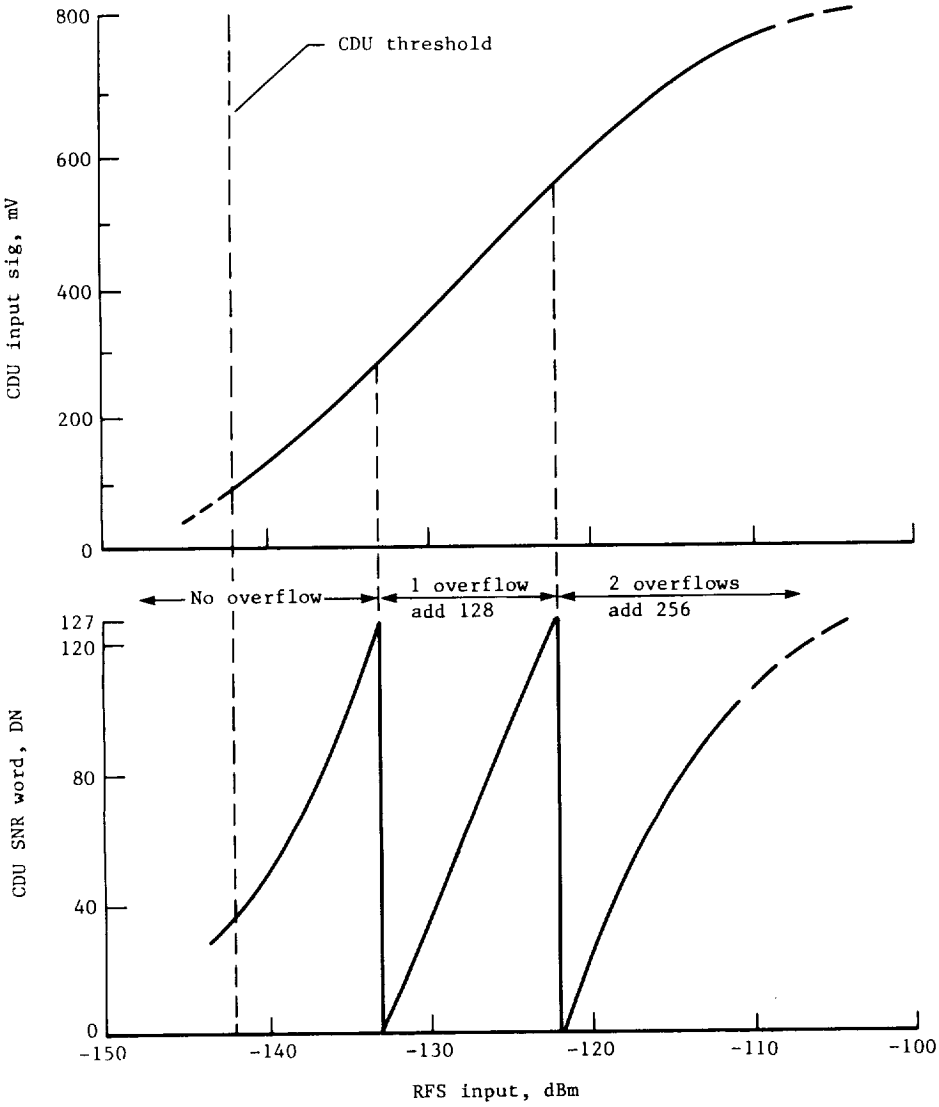

Figure 69.- CDU input signal and SNR word as function of RFS input.

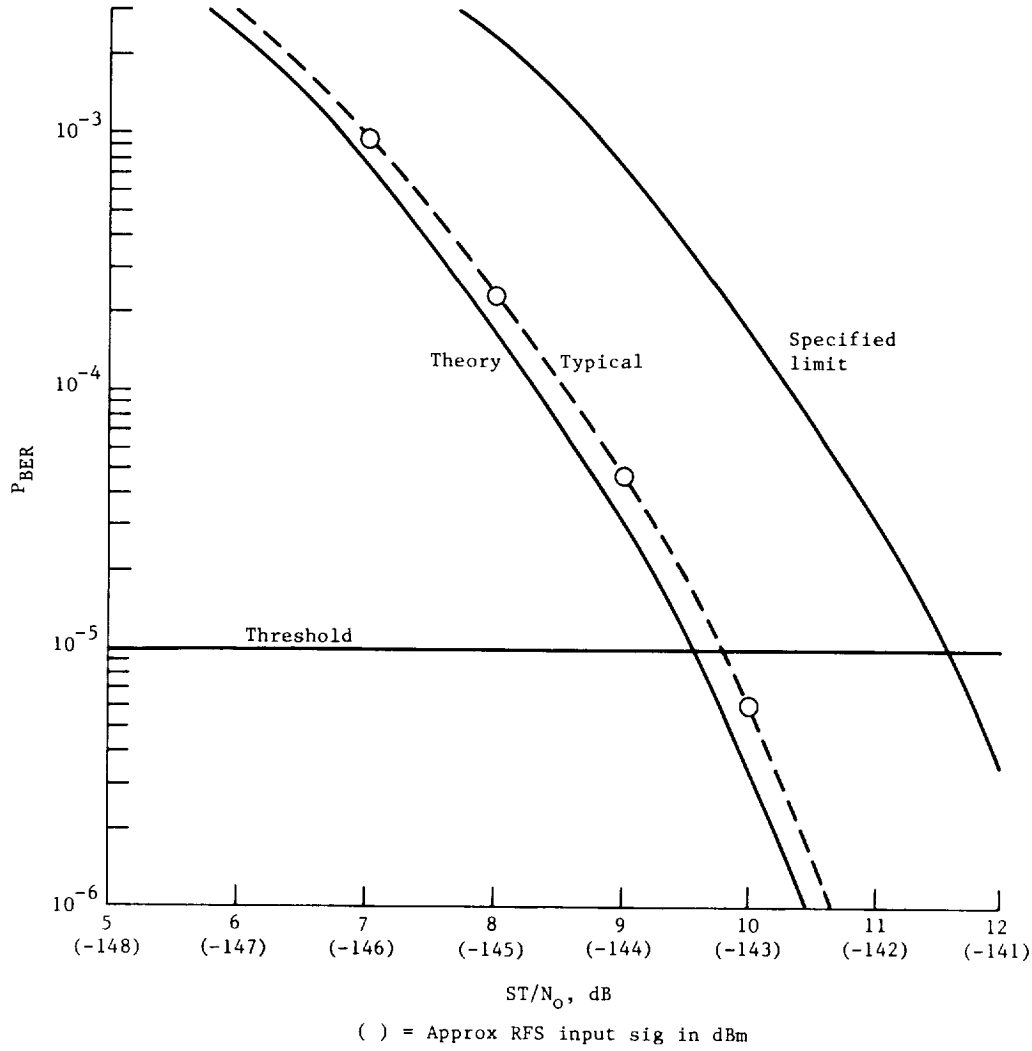

Figure 70.- Probability of bit error.

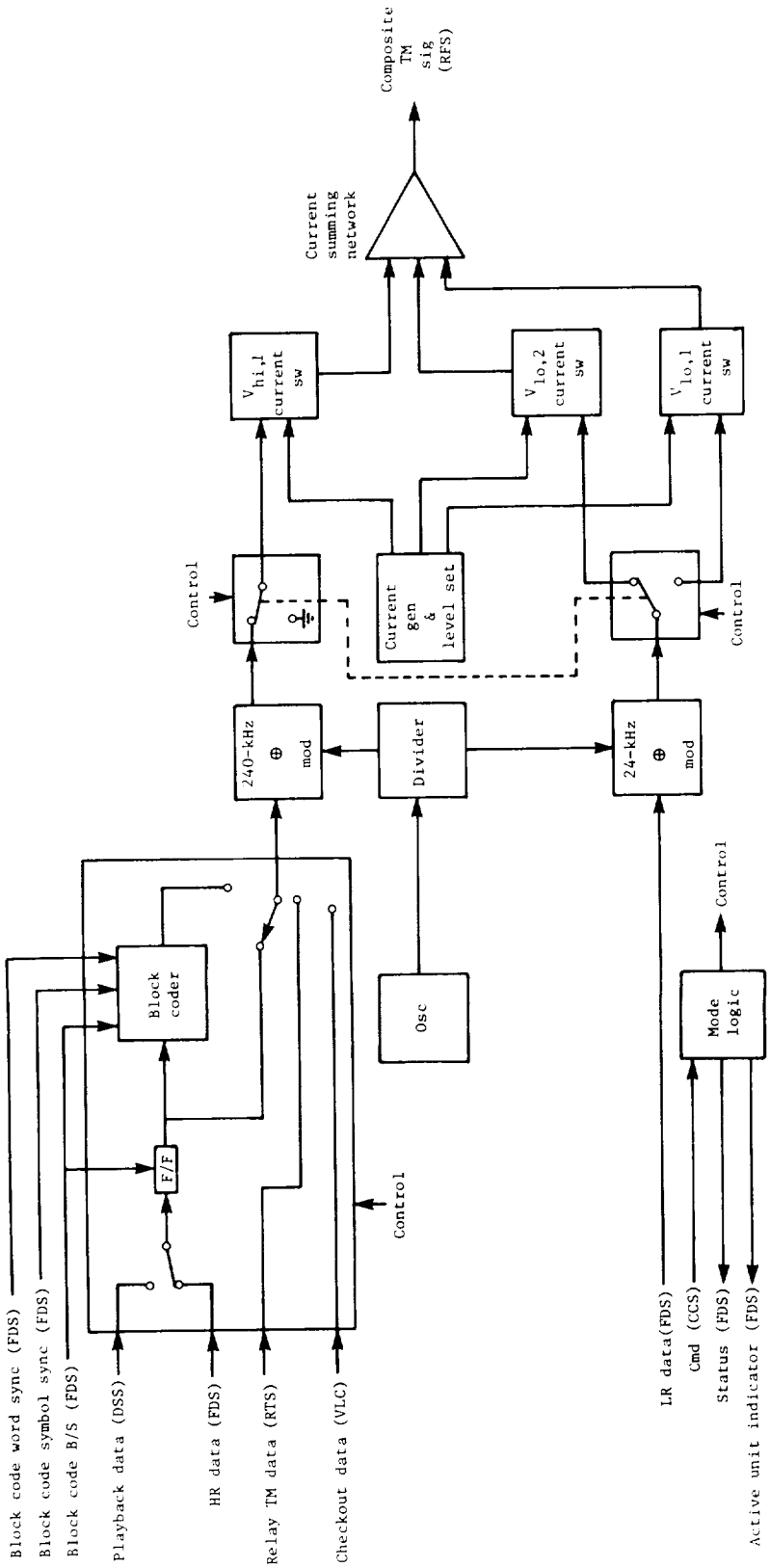

Figure 71.- Functional block diagram of TMU.

data supplied from the FDS at 8 1/3 or 33 1/3 bps. The high-rate 240-kHz subcarrier was biphase modulated with the coded/uncoded high-rate telemetry data supplied from either the FDS at 2000 bps, the DSS at 2000, 4000, 8000, or 16 000 bps, the RTS at 4000 bps, or the VLC at 1000 or 2000 bps. The subcarrier and data streams were not coherent. The TMU's contained a block coder capable of encoding high-rate data supplied from the DSS or FDS. A data switch was controlled by command from the CCS and provided the means to bypass the block coder if desired. The TMU provided a one- or two-channel telemetry system which permitted low-rate data (primarily engineering performance monitoring data) to be continuously transmitted to Earth, either separately or in a weighted sum with selected high-rate data (primarily science data). The normal operating modes were numbered mode 0 through mode 6 depending on the presence and source of high-rate data. These modes are summarized in table 22. The selection of the source of high-rate data was determined by the receipt of a command pulse on one of several interface lines with the CCS. The TMU mode logic assured that the TMU was set to mode 0 upon application of power. Interruptions in the 2.4-kHz power of 100 msec or longer caused the mode logic to reset the TMU to mode 0.

TABLE 22.- TMU OPERATING MODES

Mode	LR ch 24-kHz SC	HR ch 240-kHz SC		
	Modulation voltage, V_{lo}	Modulation voltage, V_{hi}	Data source	Coded or uncoded
0	$\pm V_{lo,1}$ (0.716 V pk)	Off (0.0 V pk)	---	---
1	$\pm V_{lo,2}$ (0.208 V pk)	$\pm V_{hi,1}$ (1.134 V pk)	VLC	Uncoded
2	$\pm V_{lo,2}$ (0.208 V pk)	$\pm V_{hi,1}$ (1.134 V pk)	DSS	Coded
3	$\pm V_{lo,2}$ (0.208 V pk)	$\pm V_{hi,1}$ (1.134 V pk)	FDS	Uncoded
4	$\pm V_{lo,2}$ (0.208 V pk)	$\pm V_{hi,1}$ (1.134 V pk)	FDS	Coded
5	$\pm V_{lo,2}$ (0.208 V pk)	$\pm V_{hi,1}$ (1.134 V pk)	DSS	Uncoded
6	$\pm V_{lo,2}$ (0.208 V pk)	$\pm V_{hi,1}$ (1.134 V pk)	RTS	Uncoded

A block coder was used to encode each 6 bits of high-rate data from the DDS or FDS into 32-symbol biorthogonal code words using the timing signals supplied by the FDS. The biorthogonal, comma-free code was formed from the modulo 2 addition of the biorthogonal code and the comma-free vector,

1000110111010100001001011001111 1
MSB LSB

The resultant biorthogonal, comma-free code word was transmitted to the data switch in a serial stream with MSB first. A functional block diagram of the block coder is shown in figure 72 and the associated timing signals are shown

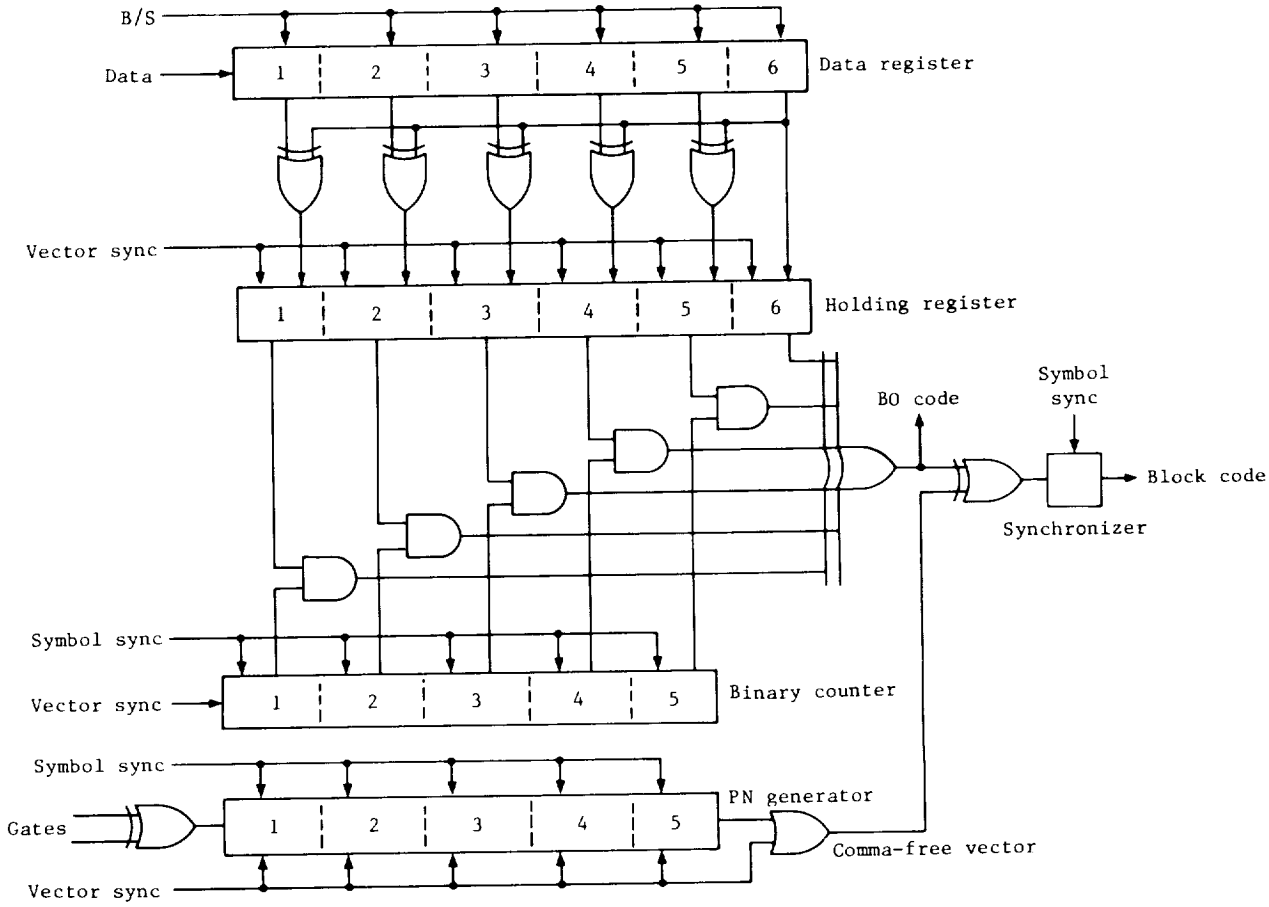

Figure 72.- Functional block diagram of block coder.

in figure 73. The key performance parameters in the TMU involved the frequency and phase stability of the low- and high-rate subcarriers and the amplitude and waveform characteristics of the composite telemetry signal to the RFS. The frequency of the subcarriers could be measured on the ground when the subcarriers are demodulated. The other performance parameters were more difficult to measure after launch since they were interrelated to themselves as well as the RFS performance. The characteristics of the TMU composite telemetry signal are shown in table 23.

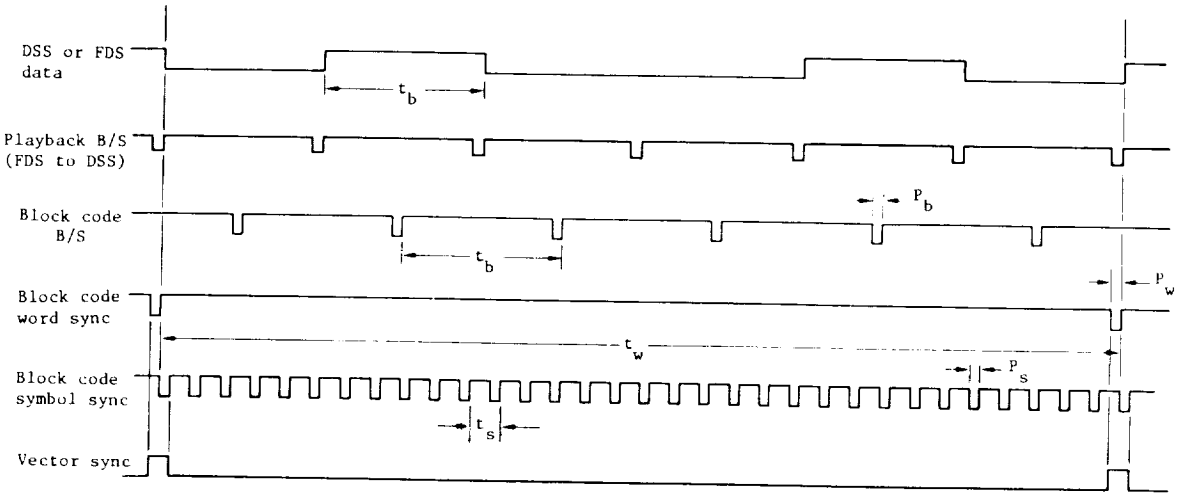

$t_b = 1/f_b$; f_b = 1000 bps, 2000 bps, 4000 bps, 8000 bps, or 16 000 bps

$t_w = 6\ t_b$

$t_s = 1/32\ t_w = 6/32\ t_b$

$P_b = P_s = P_w = t_s/3$ (nom)

$P_b/t_b = 1/16$

$P_s/t_s = 1/3$

$P_w/t_w = 1/96$

Figure 73.- Block coder timing signals.

TABLE 23.- TMU COMPOSITE TELEMETRY SIGNAL PARAMETERS

Parameter	Design value	Tolerance
HR SC:		
Freq	240 kHz	±0.01%
Phase jitter in 4-Hz BW	≦0.02 rad rms	
Initial level setting $V_{hi,1}$	1134 mV pk	±5 mV pk
Level stability $V_{hi,1}$		±1%
LR SC:		
Freq	24 kHz	±0.01%
Phase jitter in 0.85-Hz BW	≦0.02 rad rms	
Initial level setting		
$V_{lo,1}$	716 mV pk	±5 mV pk
$V_{lo,2}$	208 mV pk	±5 mV pk
Level stability		
$V_{lo,1}$		±1%
$V_{lo,2}$		±2%
Composite waveform:		
Rise or fall time (1 SC)	≦50 nsec	
Combined rise or fall time (2 SC)	≦200 nsec	
Asymmetry	≦1.25%	
Overshoot	≦10%	
Settling time (to within 5%)	≦100 nsec	
Ripple	≦1%	
Droop	≦1%	
Spurious freq components (lower than fundamental of lower SC amplitude)	≧30 dB	

Power Subsystem

Purpose

The purpose of PWRS was to generate electrical power for the immediate use of the spacecraft and to store electrical energy for special needs. The subsystem also conditioned electrical power to user requirements and provided the means to distribute power to the various loads. Figures 74 and 75 are simplified block diagrams of PWRS. Power profiles are described for expected VO operational modes.

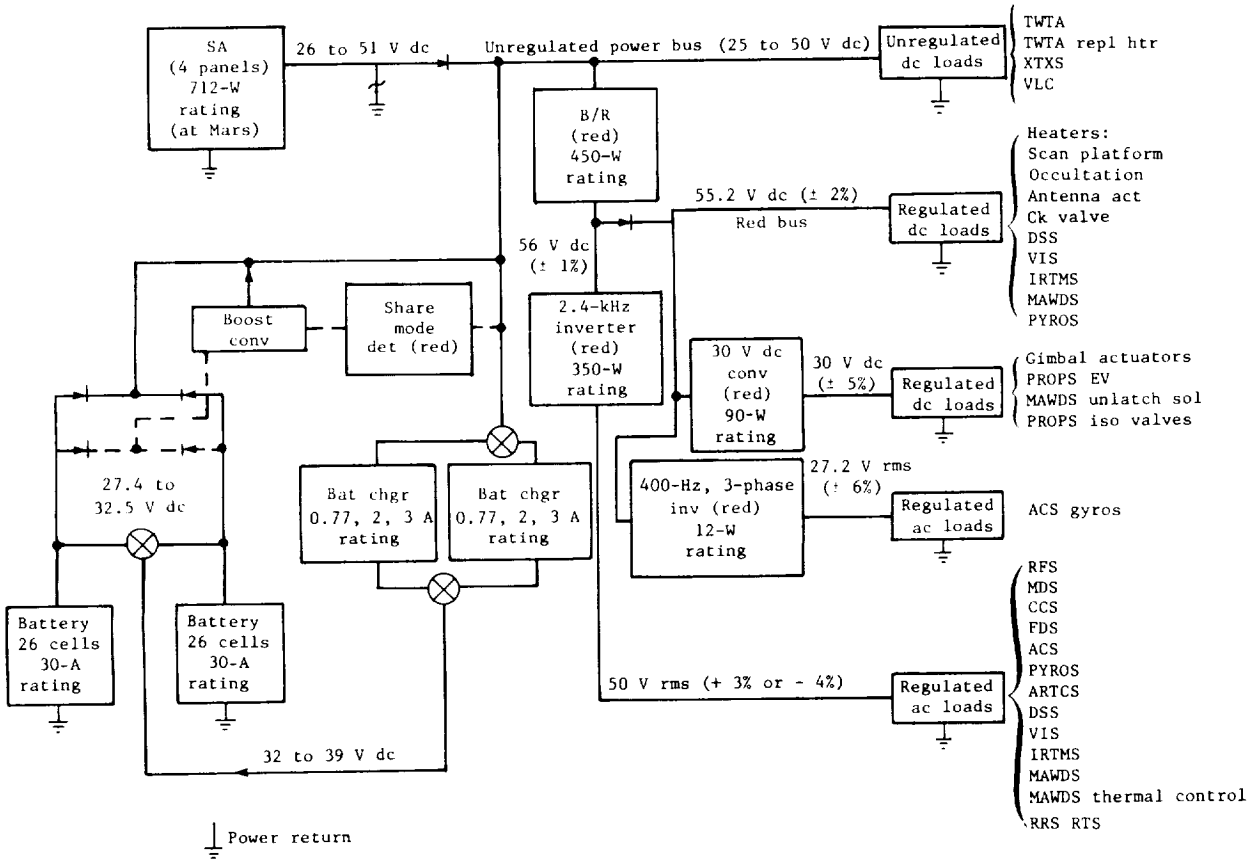

Figure 74.- Simplified block diagram of power subsystem.

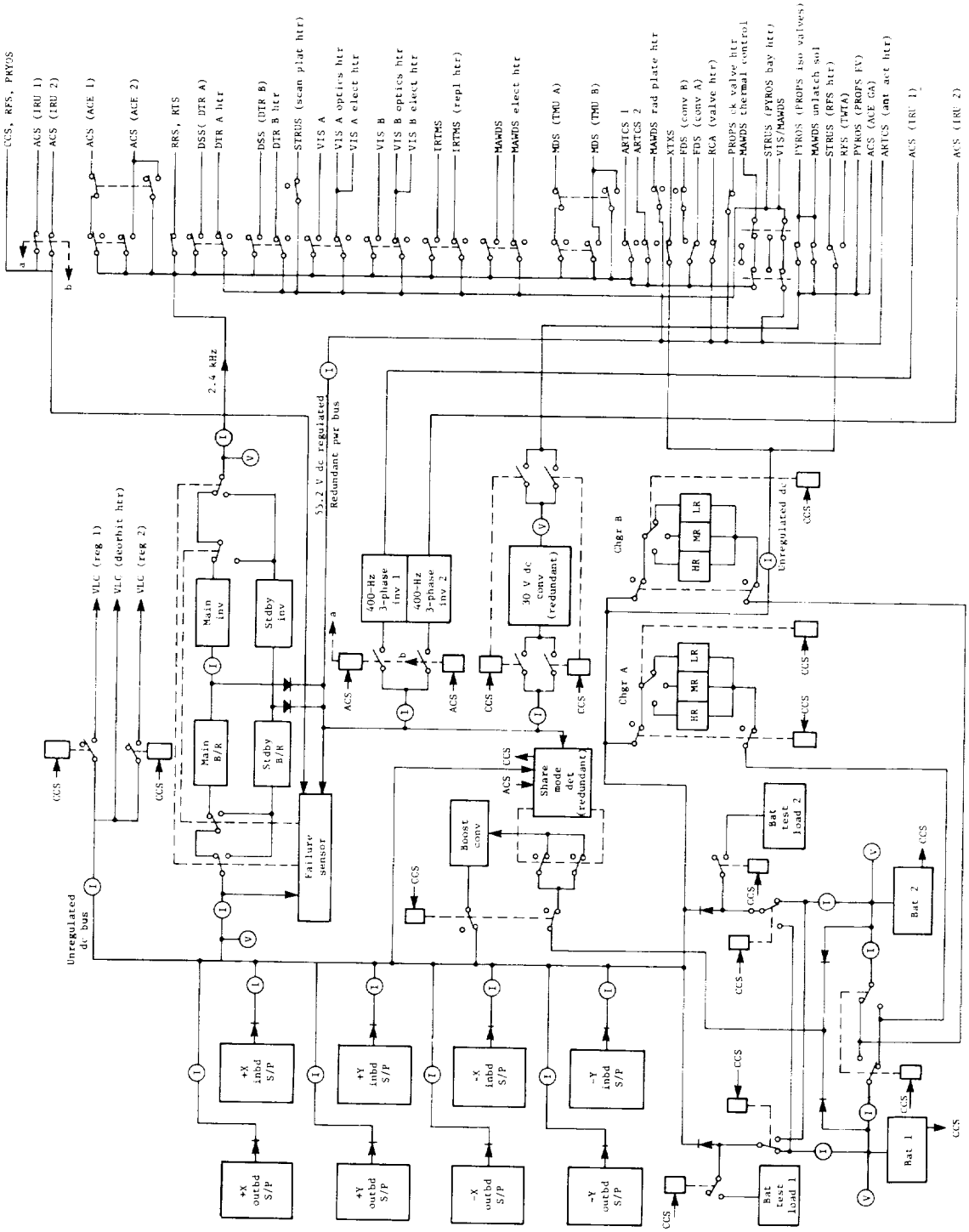

Figure 75.- Simplified functional block diagram of PWRS.

Description

The solar array was the principal electrical power source for the VO and also for the VLC until it separated from the VO near Mars. The array consisted of four solar panels spaced 90° about the bus. Each solar panel had two subpanels. Each subpanel was identical and all were electrically and mechanically interchangeable after initial assembly. Five solar cell module circuits or sections were mounted on each subpanel, and each section was connected in parallel with, and was diode isolated from, the rest. Each section was shunted and voltage limited by six series-connected Zener diodes that were physically mounted on spars on the rear of the subpanels. The eight subpanels were also electrically connected in parallel to form the solar array incorporating a total of 34 760 solar cells mounted on a substrate with a total area of 15.2 m^2 (164 ft^2). Solar panels were folded and stowed parallel to the V S/C Z-axis at launch. When the V S/C was Sun acquired, as it was during most of the mission, its attitude was controlled to maintain the array within 0.25° normal to the Sun to convert solar energy to the electrical energy used by the V S/C.

The two identical rechargeable nickel-cadmium batteries were estimated to have a total of 2100 W-hr at launch. The batteries were a secondary electrical energy source for the VO when the solar array could not support the V S/C electrical requirements. Both or either battery could be used as commanded. After the cruise period, the batteries were estimated to have a total capacity of 1900 W-hr at Mars encounter when discharged to a level of 27.4 V and while operating within a temperature range from -1° to 21° C (30° to 70° F).

Two identical battery chargers charged the batteries, each at one of three different rates: trickle charge rate at 0.77 A, medium rate at 2 A, or high rate at 3 A. The 3-A rate recharged the battery most efficiently and quickly. However, the 2-A charge rate was used when the V S/C load reached levels that prohibited the use of the high charge rate. The trickle charge rate was used to bring the battery to its fully charged state after initial charging at the medium or high rates. It was also used to maintain the battery at full charge.

Unregulated power at a voltage range of 25 to 50 V dc was available from the VO to power the VLC, TWTA, X-band transmitter, battery chargers, and the B/R. Other electrical power used on the spacecraft was conditioned for the users, initially through the B/R module of PWRS.

The B/R boosted the 25 to 50 V unregulated power to 56 V dc. The 2.4-kHz inverter module directly used the B/R output to produce the 50 V rms power used by the V S/C. The balance of the B/R output was routed through fault isolating redundant diodes, after which it was called the power subsystem redundant bus and became the source of regulated dc power for the V S/C at 55.2 V dc. The redundant bus powered the 30 V dc converters, the 400-Hz inverters, the 30 V dc bias supplies, and most of the heaters used on the VO.

All science instruments and most engineering subsystems were powered by the 2.4-kHz inverter. (See fig. 74.) The output of this unit was 50 V rms square wave at a frequency of 2400 Hz with synchronizing pulses provided by the FDS. Besides powering most of the VO subsystems, the frequency of the 2.4-kHz square wave was used to time V S/C events. On-board stored commands were sequenced to

be issued by the CCS with timing pulses generated by its clock. The clock derived its sync pulses from the 2.4-kHz square wave.

The output of the 30-V bias supplies was routed to the CCS. Upon the issuance of a power subsystem related command, the CCS returned the 30-V bias supply power to the power subsystem as two signals over specific lines determined by CCS relay closure. In the power subsystem, the pulses addressed sink-source matrices that directed them to activate a specific power subsystem magnetic latching relay, and the changed state of the relay altered the distribution of spacecraft electrical power as a function of the CCS command.

The 30 V dc converters were designed to support the power requirements of the ACE GA drivers, the MAWDS spectrometer unlatch solenoids, the pyrotechnic isolation valves, and the propulsion engine valve.

The two redundant attitude control inertial reference units were powered by two redundant 400-Hz, three-phase inverters. Each inverter was hardwired to a given IRU. An ACS signal to the PWRS commanded the on/off state of the desired 400-Hz unit, which was a departure from the overall V S/C command design which used the CCS. To reduce the risk of vibration damage to the IRU's, both units were powered at launch and during some pyrotechnic events. One unit at a time functioned during normal operations.

Most of the power conditioning modules in the power subsystem were redundant. The redundant main and standby power chains each consisted of one B/R and one 2.4-kHz inverter. The design featured automatic transfer from the main to the standby chain if a fault occurred in the main chain. The two 30 V dc converters operated in an active parallel redundant configuration, and the 30 V dc bias supplies were quadruply redundant with a redundant pair located in each of the two PWRS bays. The battery chargers were also redundant since switching permitted a given charger to recharge either of the batteries. The B/R, 2.4-kHz inverter, and 30 V dc bias supplies operated continuously during the mission from the time the V S/C was powered at launch. The 400-Hz inverters and 30 V dc converters operated when needed. Table 24 summarizes PWRS design parameters.

Capabilities

The available solar array power as a function of mission time is shown in figure 76. Two fully charged batteries supplied the energy output shown in table 25 when discharged to 27.4 V. The battery degraded during solar occultation periods resulting in reduced energy capability. Single battery operations resulted in higher discharge currents and less total energy capability.

Battery Charging

The mission plan provided for battery charging no later than 24 hr after the VO batteries reached a 20-percent depth of discharge and allowed for continuous charging until the batteries were fully charged. Battery DOD was defined as the percentage of a fully charged battery dissipated by the VO loads.

TABLE 24.- PWRS DESIGN PARAMETERS

SA available pwr:	
Estimated at launch, mW/cm^2, $^{\circ}$C, W	136.5, 64.2, 1575
Estimated at Mars encounter, mW/cm^2, $^{\circ}$C, W	50.6, -10.7, 712
Bat:	
Rated capacity (each), A-hr	30
Estimated capacity (total) at launch, discharge rate 15.0 ± 0.01 A, W-hr	2100
Estimated capacity (total) at Mars encounter, discharge rate 15.0 ± 0.01 A, W-hr	1900
Voltage range, V	27.4 to 39.0
XFER voltage to LR charge, V dc	38.25 ± 0.25
Unregulated pwr bus voltage, V dc	25 to 50
Bat chgr:	
High charge rate, A	3.0 ± 0.15
Medium charge rate, A	2.0 ± 0.10
Low charge rate, A	0.77 ± 0.17
B/R:	
Max pwr rating,[1] W	450
Min pwr rating,[1] W	75
V_{in}, V dc	25 to 50
V_{out}, V dc	56.0 ± 1%
Red bus voltage, V dc	55.2 ± 2%
2.4-kHz inv:	
Max pwr rating, W	350
Min pwr rating, W	75
V_{in}, V dc	56.0 ± 1%
V_{out}, V rms	50 (+ 3% or - 4%)
Output freq, kHz	2.4 ± 0.01%
Free-running freq, kHz	2.4 ± 6%
400-Hz three-phase inv:	
Average load rating, W	12
V_{in}, V dc	55.2 ± 2%
V_{out}, V rms	27.2 ± 6% (line to line)
30 V dc conv:	
Max cont pwr rating,[2] W	90
Pk pwr rating[2] (120 msec), W	162
Min pwr rating, W	5
V_{out}, V dc	30 ± 5%
V_{in}, V dc	55.2 ± 2%
30 V dc bias supplies:	
Max I_{out} (116 msec), mA	110
V_{out}, V dc	32.2 ± 6%
V_{in}, V dc	55.2 ± 2%
Pwr chain XFER to stdby when	
Main B/R V_{out} for 1.5 ± 0.5 sec, V dc	>58.8 ± 0.7
or	
Main 2.4-kHz inv V_{out} for 1.5 ± 0.5 sec, V rms	<46.0 ± 1.0
Share mode det indicates	
Share when unregulated bus voltage and SG sig present, V dc	≤32.6 ± 1.2
Out of share when unregulated bus voltage, V dc	≥34.0
Boost conv parameters:	
Pulse duration, sec	0.5 ± 0.2
Repetition rate, sec	7.5 ± 2.5

V_{in}, V	V_{out}, V	I_{out}, A
27.4	25 ± 1	≧7.5
27.4	≧46.5	≦0.005
32.6	≦62.0	≦0.007

[1] Unit operating without minimum load can be damaged.
[2] Both converters operating.

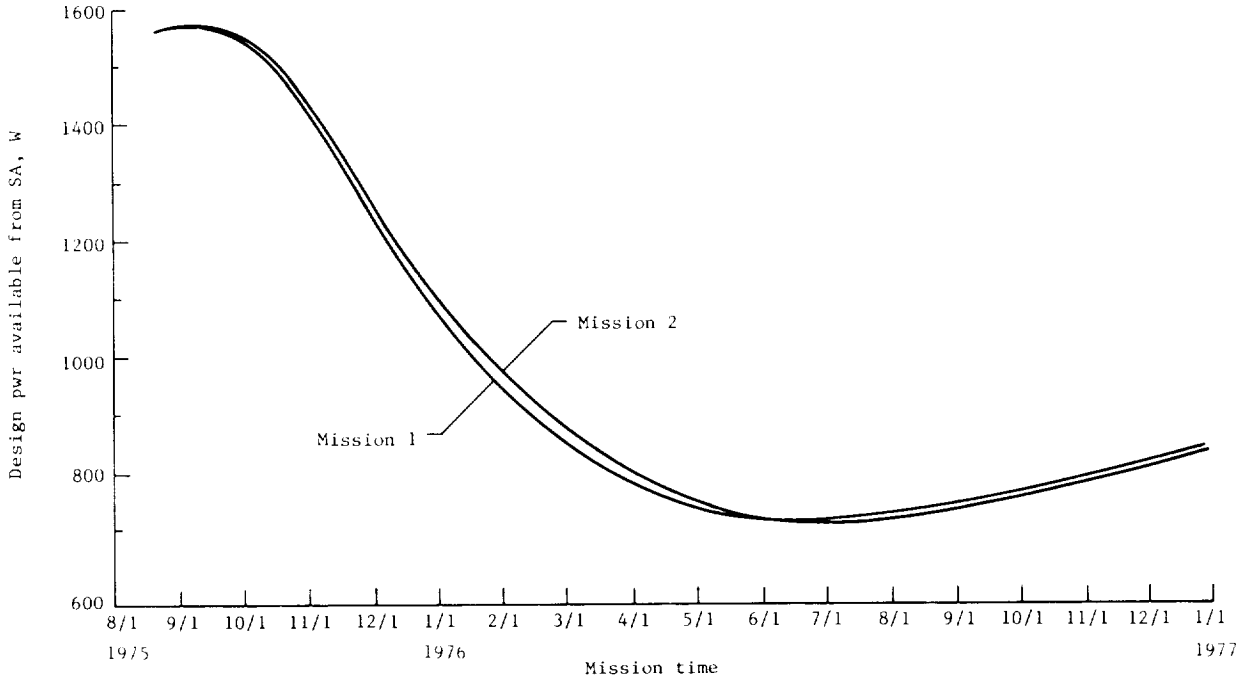

Figure 76.- Solar panel output capability.

TABLE 25.- MAXIMUM ENERGY CAPABILITY OF RECONDITIONED VO BATTERIES FOR VARIOUS MISSION PERIODS

[Battery discharge cutoff voltage of 27.4 V]

Mission period	Bat energy capacity, W-hr	
	Two bat	Single bat
Launch	2100	950
Midcourse	2100	950
MOI	1900	910
VLC sep	1900	910
2.3-hr occultations	1900	865
3.6-hr occultations	1900	---
3.6-hr survival mode	----	865

The batteries, which were charged sequentially or in parallel, must be fully recharged. If charging time allowed, science sequences could be planned after one battery was fully charged. A normal charging sequence included charging at the applicable rate to a 95-percent state of charge, followed by trickle charging. During charging, the charging rate could be switched from the C/10 to the C/15 rate (C = 30 A) to reduce the power load to allow VO science observations. However, about 1 1/2 hr of C/15 charging must be used to replace an hour at the C/10 rate.

The following battery charging rates were used in the mission:

(1) The C/15 charge rate (2 A) was used to recharge the batteries to a full state of charge prior to VLC separation.

(2) The C/10 charge rate (3 A) was used to recharge the batteries to a full state of charge after VLC separation.

(3) Trickle charging (C/40) was used to maintain the batteries at a full state of charge during periods of battery inactivity.

The mission plan included a battery charge sequence during the first day after launch. If the solar array voltage was insufficient to charge the batteries, the spacecraft could be tilted with respect to the Sun in order to lower the solar array temperature and increase the array output voltage. Tilting also was required for battery charging after the near-Earth midcourse maneuvers. The time to charge a single VO battery is shown in figure 77 as a function of battery depth of discharge and charging rate.

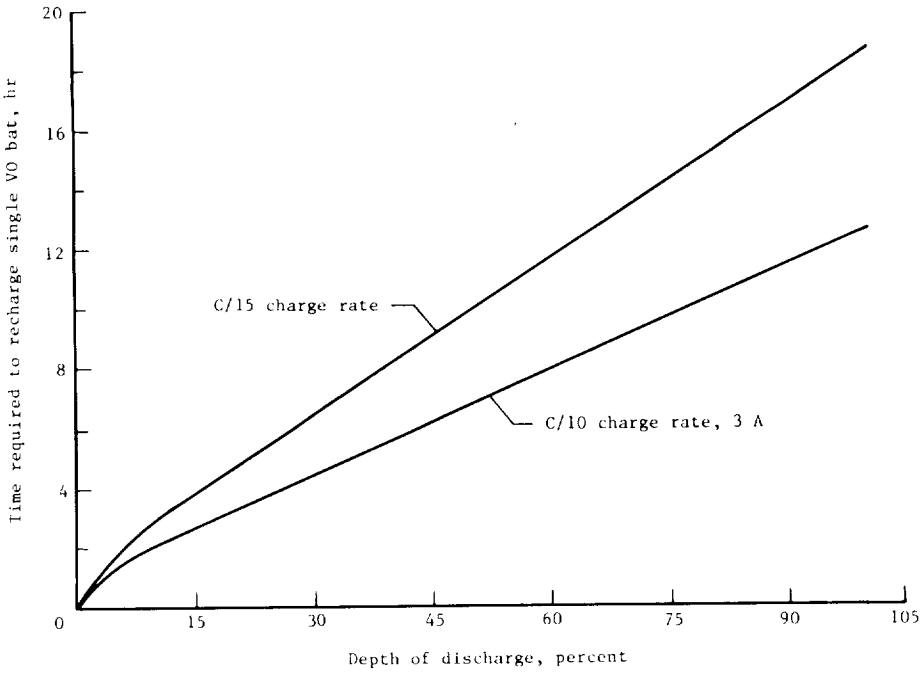

Figure 77.- Orbiter battery charging time.

Power Modes and Power Profiles

The major VO power modes are identified in table 26. Power profiles for these modes are presented in figure 78. As indicated in the profiles, the available solar panel power capability could supply the required power for all the modes shown. Where the battery mode was required (off-Sun maneuvers, etc.), the battery power capability (table 25) exceeded the required power in each case.

TABLE 26.- MAJOR VO POWER MODES

Mode	Operation	Total time	Power, W	Power source
1	Launch through sep with 30-min launch hold	1.33 hr	480.6	Bat
2	Sep through Sun acq	35 min	506.0	Bat
3	Sun acq through Canopus acq	30 min	565.0	SP
4	Near-Earth cr, chgr C/10	20 hr	644.3	SP
5	Near-Earth cr	15 days	522.2	SP
6	Near-Earth cr, VLC maintenance	60 min	499.3	SP
7	Trajectory correction/orbit trim maneuver turns	1.31 hr	498.4	Bat
8	VLC GCMS venting	60 min	694.0	SP
9	VLC bat conditioning charge cycle	5 hr	527.0	SP
10	VLC bat conditioning discharge cycle	21.7 hr	506.6	SP
11	VLC bat conditioning final charge cycle	21.7 hr	572.8	SP
12	VIS geometric/photometric and scan calib	36 min	602.3	SP
13	Approach sci	6 min	612.4	SP
14	Orbit ins maneuver turns	1.31 hr	413.7	Bat
15	Orbit ins maneuver burn	49 min	464.3	Bat
16	Orbit cr with VLC sci	6 min	624.1	SP
17	Orbit cr with VLC sci, P/B	30 min	614.8	SP
18	Orbit cr with VLC, P/B, chgr C/15	20 hr	543.3	SP
19	Canopus stray light with VLC, sci, P/B	30 min	640.6	SP
20	Canopus stray light with VLC, P/B, chgr C/15	12 hr	568.4	SP
21	VLC update	60 min	597.3	SP
22	VLC sep, S-30[1] to S-28.5; S-26.3 to S-25.8; S-23 to S-2.8	26 hr	594.6	SP
23	VLC sep, S-28.5 to S-26.3; S-25.8 to S-23	30 min	547.6	SP
24	VLC sep, S-2.8 to S-1.3	1.5 hr	675.5	SP
25	VLC sep, S-1.3 to S-1	18 min	614.4	SP
26	VLC sep, S-1 to S-0	60 min	497.3	SP
27	VLC entry, relay, P/B, chgr C/15	6 hr	533.4	SP
28	Orbit cr, P/B, chgr C/10	20 hr	531.0	SP
29	Orbit cr, MAWDS, IRTMS, chgr C/15	6 hr	526.3	SP
30	Orbit cr, MAWDS, IRTMS, P/B, chgr C/15	6 hr	542.8	SP
31	Orbit cr, MAWDS, IRTMS, P/B, off-celestial lock	60 min	507.9	Bat
32	Apoapsis pass, sci, P/B	6 min	551.9	SP
33	Periapsis pass, sci	6 min	512.2	SP
34	Periapsis pass, sci, relay	20 min	573.5	SP
35	Plane-change maneuver turns	1.9 hr	364.3	Bat
36	2.3-hr solar occultation	2.3 hr	390.2	Bat
37	3.6-hr solar occultation	3.6 hr	265.9	Bat
38	3.6-hr solar occultation, survival	3.6 hr	206.4	Single bat

[1]Separation time is in hr.

Solar array.- The VO solar array used N on P, 2 by 2 cm, solar cells that were 0.356 mm thick with silver over titanium vacuum deposited electrical contacts that were solder coated. The cell material was phosphorous diffused boron doped silicon with base resistivity at 2 Ω-cm. Array assembly was facilitated with the assembly of solar cells into submodules. Five submodule sections, or submodule circuits, were arranged on each subpanel, sections A to E, with each section divided into two subsections such as A1 and A2 in figure 79. The solar cells occupied more than 91 percent of the available subpanel area. Figure 80 shows the front and rear views of a VO solar subpanel. The output of each subpanel section was diode isolated to prevent a fault in any one section from loading the others. The output of each section was also shunted by six series-connected Zener diodes that limited the output voltage of each section below 51 V. If it were not for this shunt regulation, the array voltage could cause the unregulated bus to exceed its voltage specification when the array operates cold. The electrical configuration of the array isolation diodes and Zener diodes is shown in figure 75. The array Zener diodes were mounted upon spars on the rear of the subpanels that served as heat sinks, and the 30 Zener diodes are seen in figure 80(b).

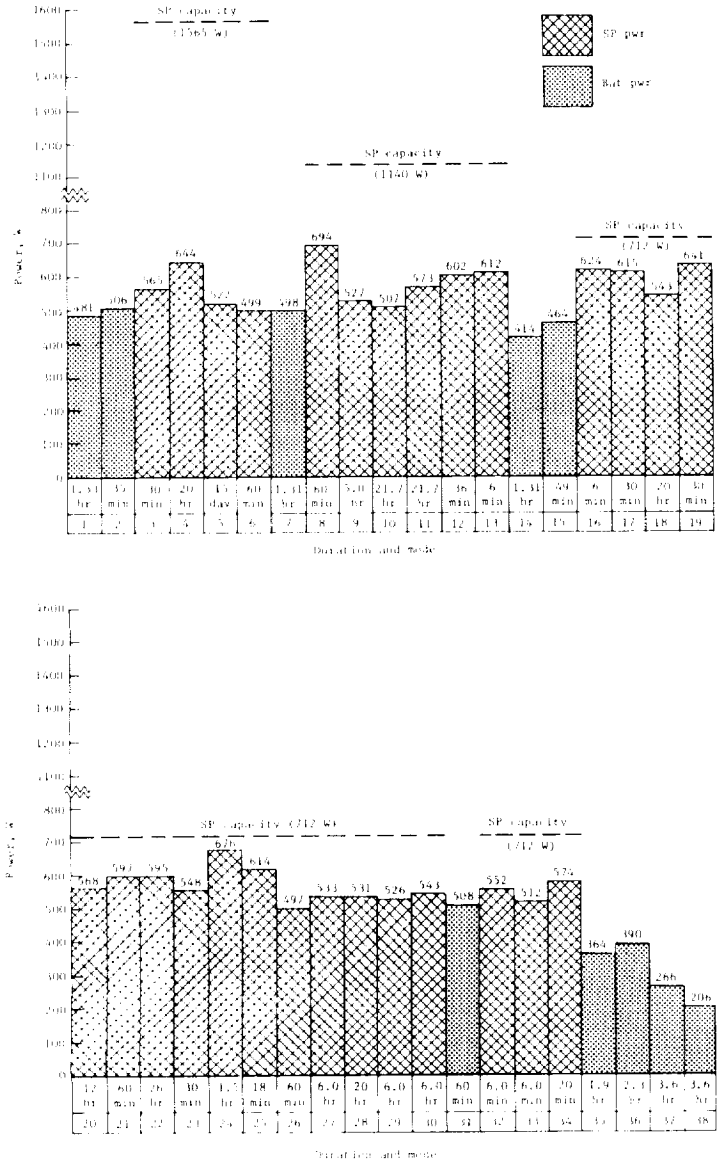

Figure 78.- Power profile.

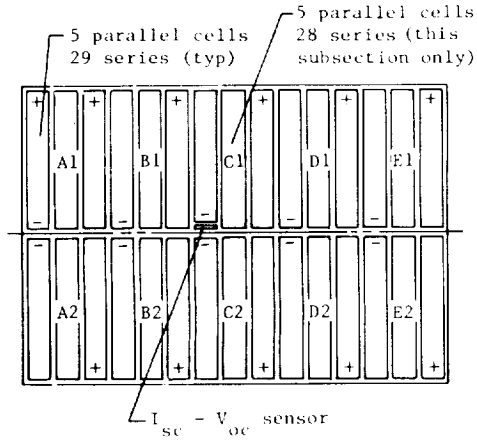

Figure 79.- Schematic diagram of solar subpanel.

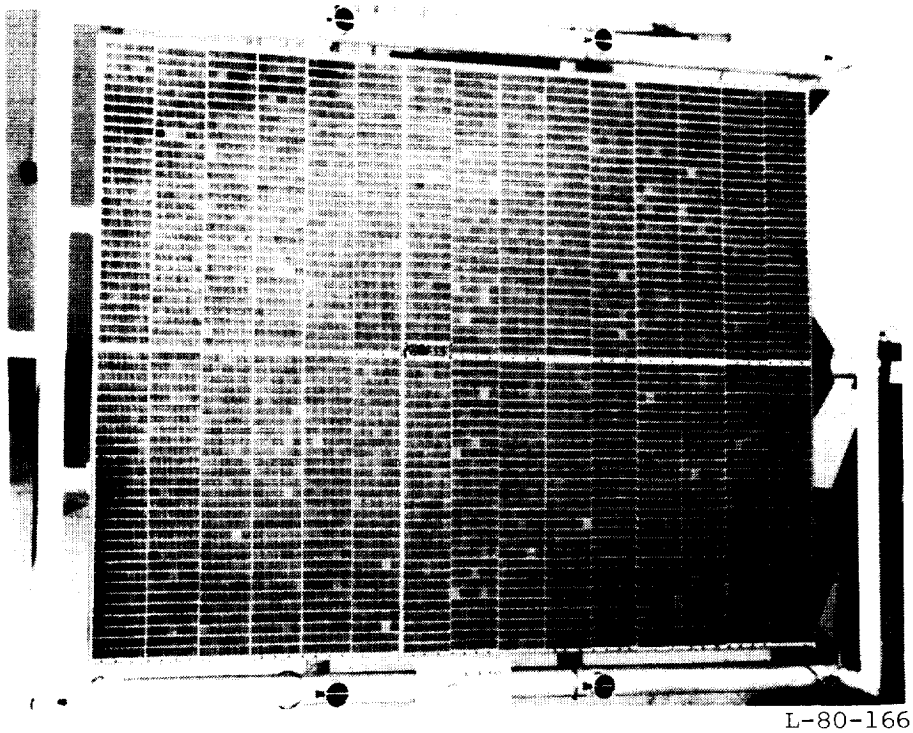

L-80-166

(a) Front view.

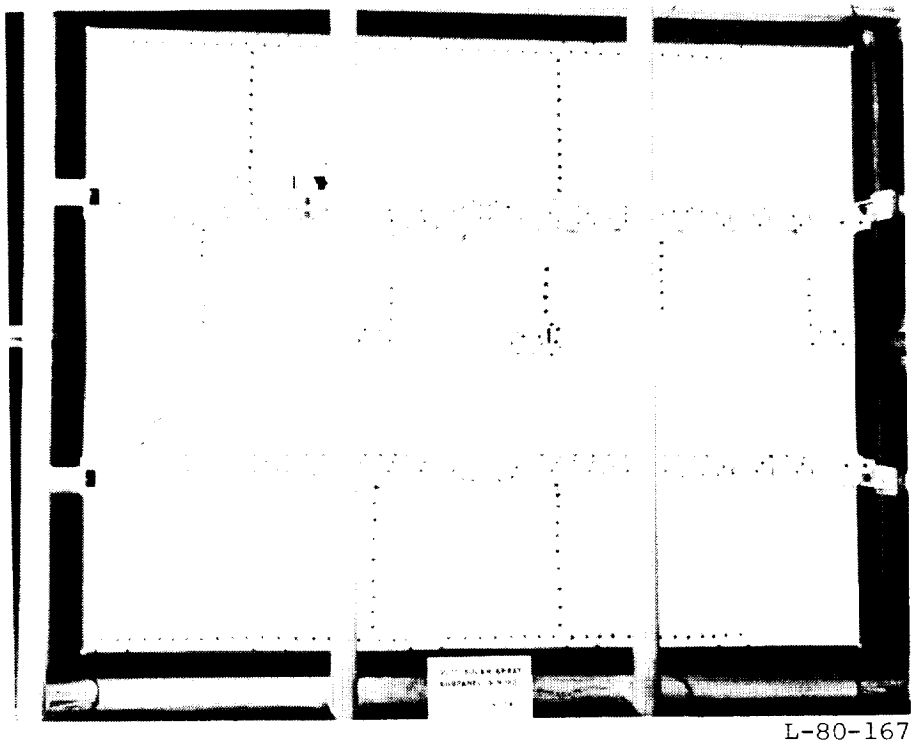

L-80-167

(b) Rear view.

Figure 80.- Solar subpanel.

Array maximum power output was significantly affected by the array temperature, about a 0.28-percent power loss per degree temperature rise. During flight, temperature gradients along a solar panel changed with the distance to the Sun. They were also affected by V S/C structures - particularly the VLC - and the relay antenna attached to the +Z outboard subpanel. Figure 81 shows the best estimate of temperatures along the center line of one of the solar

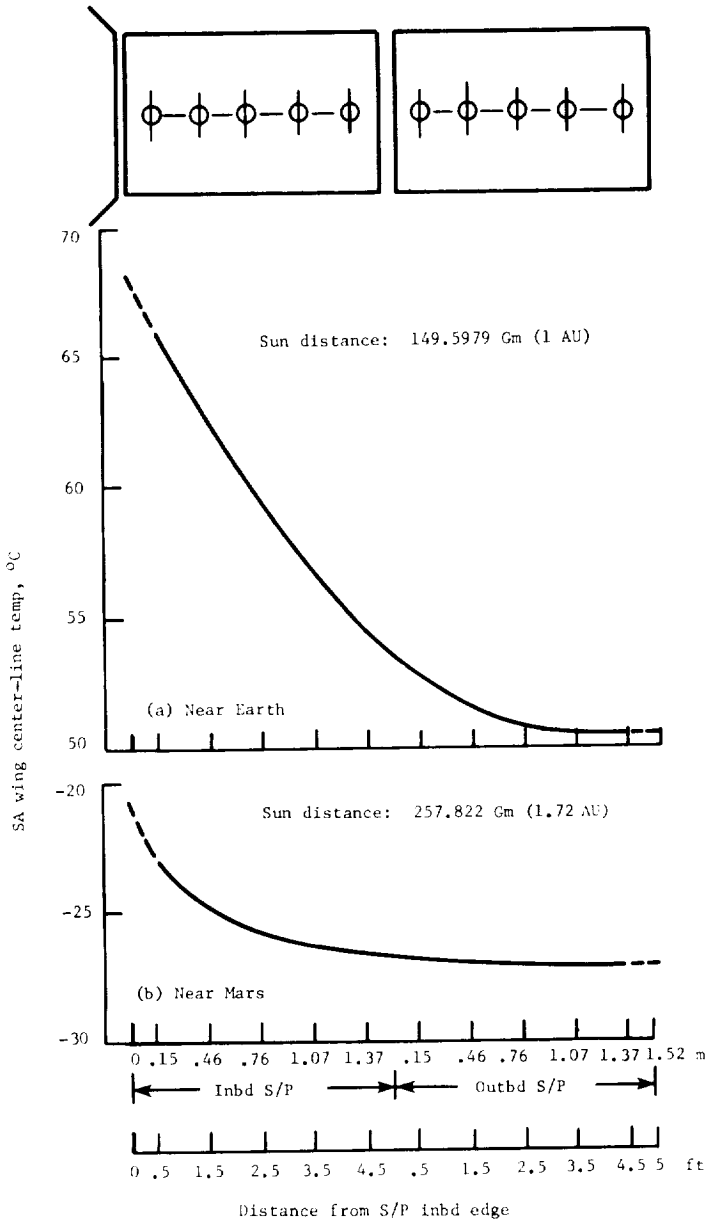

Figure 81.- Temperature profile of solar panel.

panels when the V S/C was near the Sun after launch and again at Mars encounter. The range of subpanel temperature was seen to be about 17° C near Earth and 12° C near Mars. Temperature influence of the V S/C bus was included in this figure; however, the influence of other V S/C structures upon the solar-panel temperature was ignored. Plotted in figure 82 are the estimated temperature,

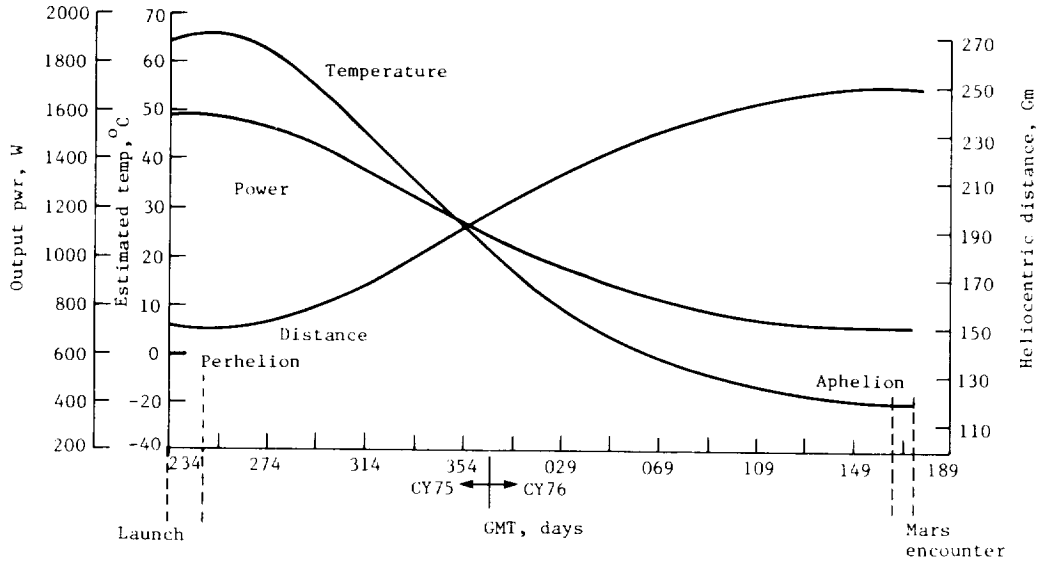

Figure 82.- Estimated solar-array performance during mission A cruise.

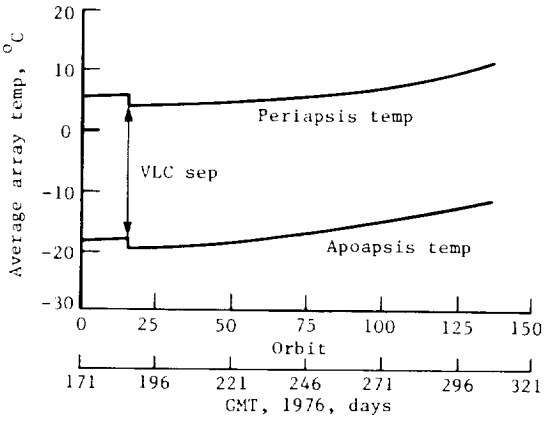

Figure 83.- Average solar-array temperature in mission A orbit.

solar-array output power, and VO heliocentric distance during mission A cruise. The temperature was averaged over the array surface and was the highest worst-case value (the best estimate plus 6° C uncertainty). The effect of Mars proximity upon the average array temperature is shown in figure 83. The planet's influence upon array temperature was greatest near periapsis with the subsolar point nearby. No planetary influence was expected at apoapsis. Also shown is the expected average array temperature decrease after the separation of the VLC. Average array temperatures associated with Sun occultations are shown

in figure 84. The upper curve estimates eclipse conditions near the Sun, the lower describes conditions remote from the Sun.

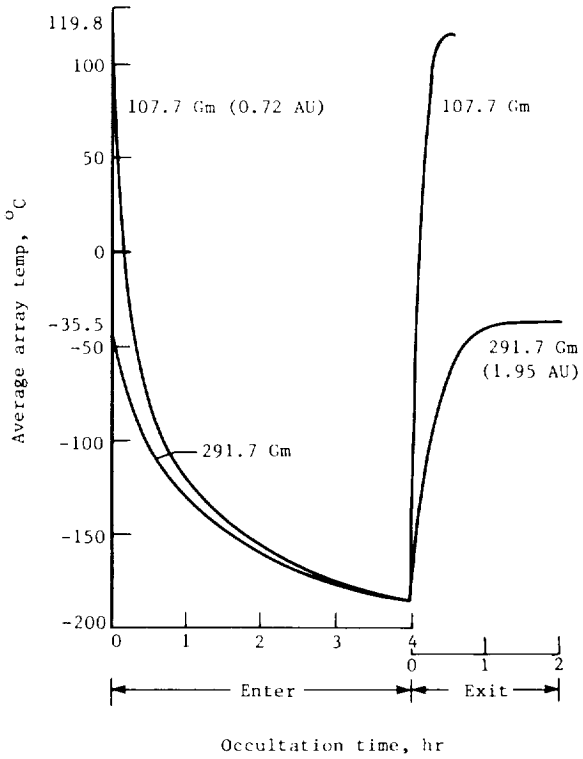

Figure 84.- Average solar-array temperature during Sun occultation.

The solar-array current-voltage sensor data supplemented the performance data obtained directly from the array and those from the solar-array temperature sensors to support status estimates of the solar array. During normal array operations, the array operating point (the I/V coordinates of the array load) moved on just a portion of the array characteristics. It never operated at the extremes of the characteristics. One purpose of the array I_{sc}-V_{oc} sensor was to telemeter data to indicate what the array electrical characteristics were like at its extreme in order to create a larger array data base for array performance evaluation. This purpose was accomplished by telemetering the short-circuit current and open-circuit voltage of individual cells on each -Y subpanel; these cells were typical of those used on the array. The telemetered I_{sc}-V_{oc} cell data, extrapolated to array circuit configuration values, were assumed for the purpose of array analyses to indicate the short-circuit current and open-circuit voltage of the array. A third cell ($I_{sc,r}$) on the I_{sc}-V_{oc} sensor monitored possible array radiation damage. This cell also monitored short-circuit current, but its output had been deliberately degraded about 50 percent by a 1-MeV electron radiative flux at 10^{16} electrons/cm^2 to render the cell less sensitive to further radiation damage. Because the other I_{sc} cell remained more sensitive to radiation damage than the irradiated ($I_{sc,r}$) cell, the output data from both could be compared for evidence of possible radiation damage to the array. Precision resistor loads were selected to measure the short-circuit current of the two cells and the open-circuit voltage of the third cell, and to provide proper input to the VO telemetry system. Figures 79 and 80(a) show the I_{sc}-V_{oc} sensor location on the subpanel. To maintain interchangeability, each subpanel incorporated an I_{sc}-V_{oc} assembly and also a temperature sensor that was mounted on the subpanel rear surface directly beneath the assembly. Once on the V S/C, however, only those sensors that were mounted on the -Y inboard and outboard subpanels are electrically connected into the telemetry system.

A number of environmental sources in space contributed to array degradation during the mission, sources that caused radiation damage and thermal cycling damage. Little array degradation due to thermal cycling was expected during the mission, but possible array radiation damage could be caused by several sources. The dominant source of possible array radiation damage was proton flux generated from solar flares. A summary of array radiation damage in

table 27 shows that the estimated array power was reduced 15 percent over the 18-month mission or was reduced at a rate of 0.83 percent per month.

TABLE 27.- ESTIMATES OF SOLAR-ARRAY RADIATION DEGRADATION

Degradation source	Estimated SA degradation, percent		
	Current	Voltage	Power
Proton Ultraviolet	10.6	5.7	14.0
Neutron	1.0	---	1.0
Total	11.6	5.7	15.0

VO solar-array performance estimates were based upon prelaunch tests of subpanels at Table Mountain, California. Since the Sun's spectra differed in the Earth and space environments, it was reasonable to expect subpanel performance during tests on Earth to differ with their expected performance in space. Special techniques were employed to extrapolate subpanel Table Mountain data to predicted array space performance. The data for the eight VO subpanels were then totaled to obtain the solar-array performance at standard conditions in space, and these data were factored to obtain predicted array performance at any Sun intensity and average array temperature expected during the mission. The array data were further factored during the mission to include array off-Sun operation, array shadowing by V S/C structures, and array degradation. The estimated VO array performance during the mission A cruise period is shown in figure 82 along with the VO heliocentric distance and worst-case estimated array temperature. In addition to the worst-case array temperature, the array performance curve shown in figure 82 also included power losses noted in table 27 and prediction uncertainties associated with array current and voltage.

At launch, the two subpanels of each of the four solar panels were folded at midpoint hinges with the solar cell surfaces of each facing one another and with each pair parallel to the V S/C Z-axis. The inboard subpanel was hinged at its attachment to the bus outriggers. After a time in launch trajectory, pyrotechnic devices released the V S/C from the Centaur and push-off springs separated the two. When the V S/C distance from the Centaur was sufficient to release captive flyaway rods, tip latches released each folded solar panel and damped spring devices on each caused the folded subpanel pair to swing out. At about 57° with the V S/C Z-axis, tip lock cams released the outboard subpanels. The spring-loaded outboard subpanels quickly swung 180° to lock by cam latch with the inboard subpanels, and the locked subpanel pairs continued to deploy until they were 90° with the V S/C Z-axis. At 90°, spring-loaded tapered pins entered receptacles to lock the inboard subpanels at their spacecraft hinge, and the solar cell surfaces of the eight subpanels were then coplanar, locked at right angles to the V S/C Z-axis. The total solar-array deployment sequence took about 65 sec, and the completed solar-array deployment event was telemetered in a launch status word. The first four bits of the word changed from 1 to 0 when each of the four solar panels completely deployed. Each deployment zero signal required an ANDed summation of two signals, one each from a microswitch at the instant the outboard and inboard subpanels of the solar panel locked.

Batteries.- The rechargeable nickel-cadmium battery cell provided electrochemical energy from nickelic hydroxide positive plates and cadmium negative plates. The positive plates were initially impregnated with $Ni(HO_3)_2$ and the negative plates with $Cd(HO3)_2$. Both plates were then electrochemically formed to generate the required electrode surface coating. The battery cell rated capacity was 30 A-hr when discharged to 1.0 V at 24° C.

The VO battery contained 26 storage cells connected in series. Matched cells for each battery assembly were selected on the basis of end-of-charge voltage and A-hr capacity. Two temperature transducers were mounted on the battery. The output of one was monitored by the V S/C telemetry system, and the output of the other was monitored by ground equipment through the umbilical. Two temperature safety devices were also mounted on the battery to automatically limit battery operation if its temperature rose. These devices were thermal switches that were mounted near the expected battery warm spots. One switch closed if the battery temperature rose to $29^{\circ} \pm 1^{\circ}$ C ($85^{\circ} \pm 3^{\circ}$ F) and the closure generated a signal to its charger to transfer to the low charge rate from operation at its medium or high charge rate. A signal, produced when the second thermal switch closed at 38° C (100° F), caused the CCS to switch off the appropriate charger. A signal was also produced when the battery voltage reached 38.25 ± 0.25 V, as the battery approached full charge and ORed with the signal from the first thermal switch to cause charger transfer to low rate. The sensors provided automatic guards to prevent battery overcharge in the medium or high charge rates that would cause excessively high battery temperature and possible irreversible damage. When the V S/C electrical power demand required battery energy, it was supplied automatically to the unregulated dc bus when their isolation diodes were forward biased. No command was required. The fault isolation quad connected diodes in the battery discharge paths prevented either battery from becoming a load on the other. The diodes also prevented uncontrolled charging of the batteries when the V S/C was powered by the solar array in flight or by the solar-array simulators during ground tests. The two batteries were identical, with one of the units located in bay 9 and the other in bay 13. Typical charge and discharge characteristics are shown in figure 85.

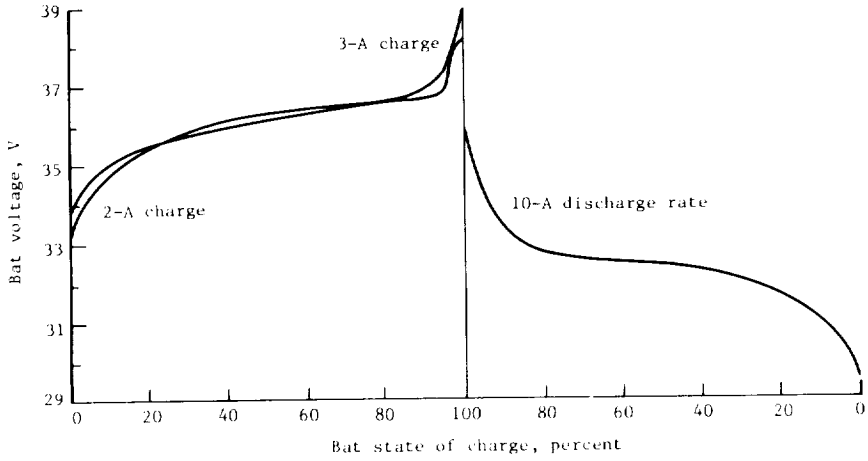

Figure 85.- Typical charge-discharge performance characteristics of battery. Bat temp = 10° C (50° F).

PCE.- The prime function of the PCE was to condition to various forms for VO users the electrical energy converted from Sunlight by the solar array or that converted from electrochemical energy stored in the batteries. The PCE had other functions that relate to power management and power performance monitoring. It housed the relays that by command switched on or off the electrical power to the various VO subsystems. The PCE also housed the sensors that provided signals for the power subsystem telemetry, and it interfaced with power sources external to the VO that supplied its electrical power during test and launch. The PCE was divided between bays 10 and 12 in the VO bus.

The VO design used two identical battery chargers. Normally, one charger served a given battery during the mission, but if a charger failed, the remaining charger could be commanded to charge either battery. Each charger used a pulse width modulated series switching regulator. (See fig. 86 for charger functional block diagram.) Its output was a constant current regulated by a magnetic amplifier with a sensing element at the output. Changes in output current caused the duty cycle of the series regulator to vary to maintain the output current constant. Three charge rates are provided: high rate at 3.0 ± 0.15 A, medium rate at 2.0 ± 0.1 A, and low rate at 0.77 ± 0.17 A. A bias winding in the magnetic amplifier connected to one of three resistors that governed the charge rate. The connection was through charger relays K2 and K3

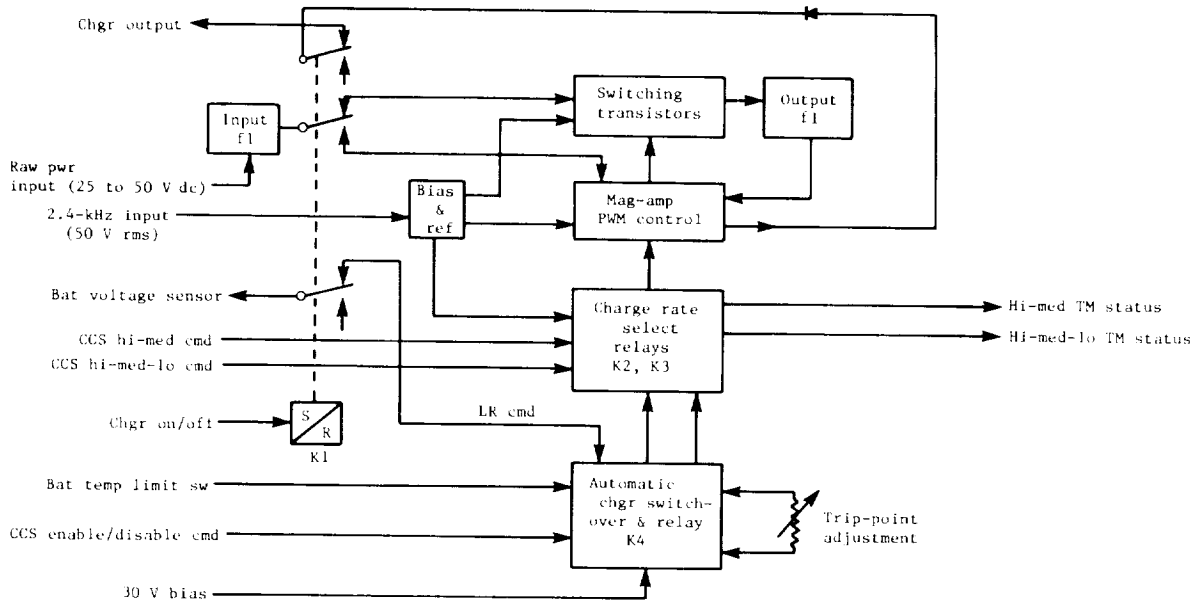

Figure 86.- Functional block diagram of battery charger subassembly.

whose states were selected by on-board or ground commands. (See fig. 87 for typical charger output characteristics.) The charger design featured automatic transfer of charge rate from high or medium rate to low charge rate under the following conditions: Battery voltage reached 38.25 ± 0.25 V, or battery temperature reached 29° ± 1° C (85° ± 2° F). The charger voltage limit sensor circuit caused the transfer to low rate. It used a differential amplifier to compare the battery voltage with a precision reference voltage. When the battery voltage limit was sensed, the amplifier activated a pulse circuit that set the charger K2 relay into the low-rate position. In a like manner, the battery charger transferred to low rate when the voltage limit sensor circuit received a signal from a thermal switch closure that indicated the battery temperature had reached 29° ± 1° C (85° ± 3° F). Another battery thermal switch closed when the battery temperature reached 38° C (100° F). The closure generated a signal to the CCS to switch off the appropriate charger. Note that the automatic charger design features (the transfer to low charge rate and charger turn-off) were charger operations that could also be controlled by command. Turning the charger on or increasing its charge rate could only be achieved by command. High rate was the most desirable recharge mode. The medium charge rate was less efficient, and was used when V S/C electrical loads were too high to permit high-rate charge. The battery voltage trip point at 38.25 ± 0.25 V permitted the battery to recharge to about 90 percent of its capacity at either the medium or high charge rates. After charger transfer to low rate, the battery recharge continued more safely to full battery charge and beyond into overcharge. The low charge rate at 0.77 A was selected to safely overcharge the VO battery for long periods, and it was used to replenish battery capacity lost because of selfdischarge, an inherent characteristic of the nickel-cadmium system. Automatic transfer to low rate could be inhibited by the (4LR) or (4KR) commands that reset the K4 relay of the A and B chargers. This permitted timed recharge sequences at high or medium charge rates under power analyst surveillance when available time prevented battery top-off at the low charge rate. Inhibiting this circuit also isolated some charger failures that prevented the medium- or high-rate charge.

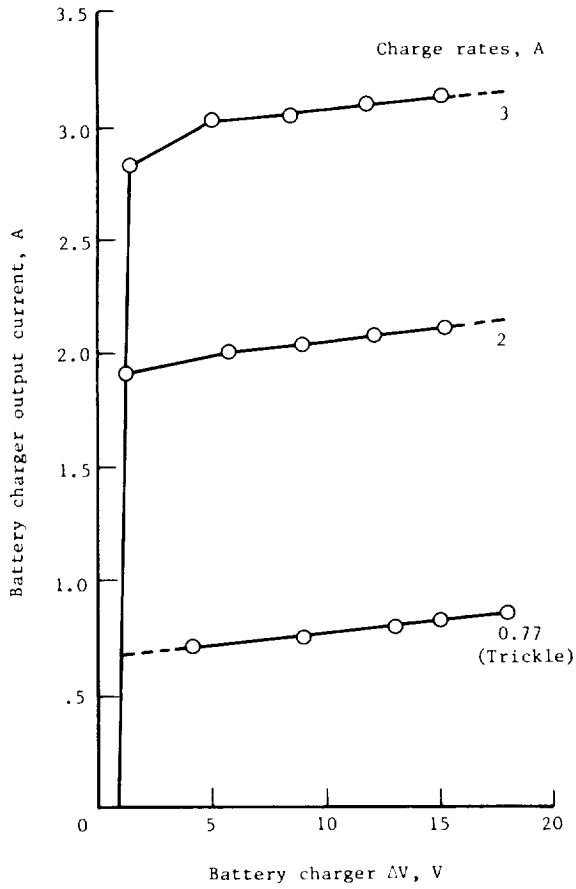

Figure 87.- Typical battery charger performance characteristics. Chgr V_{in} = 41.5 V.

The booster regulator was designed to provide a regulated dc voltage output at 56.0 V ± 2.0 percent from an input of the unregulated dc bus operating at 25 to 50 V dc. In the B/R design, a dc-dc converter added to the unregulated bus input a dc voltage level that automatically adjusted to obtain the desired B/R output voltage level. (See fig. 88 for block diagram.) The output voltage of the converter was controlled by a transistor pulse width modulator which varied the duty cycle of switching transistors. Increasing the duty cycle increased the average regulated voltage. A differential amplifier that compared the 56 V dc output to a Zener diode reference controlled the pulse width modulator. Partial open loop compensation controlled the output voltage during step changes in the input voltage, and an output filter smoothed the varying voltage at the autotransformer output so that the regulated voltage was almost constant. The booster regulator was capable of maintaining an output of 56.0 V dc ± 1.0 percent over an input voltage range of 25 to 50 V dc and to a maximum load of 450 W. Zener diode overvoltage clamp circuit limited the B/R output voltage level to a maximum of 64.0 V dc, a level that could be reached with some power transients or a failure in the regulator feedback loop. The Zener clamp protected the users of 2.4-kHz inverter power since this bus increased in voltage with the B/R. Figure 89 shows booster regulator efficiency as a function of load at different B/R input voltages.

The 2.4-kHz inverter converted the regulated dc output of the booster regulator to square-wave power at 50 V rms (+ 3 or - 4 percent) and at a frequency of 2.4 kHz ± 0.01 percent. This inverter was the prime source of electrical power for the VO and was used for most of the engineering subsystems and all science instruments. (See fig. 75.) Its output frequency served as the timing source of the CCS clock. A frequency signal at 4.8 kHz supplied by the FDS was used to synchronize the unit. (See fig. 90 for block diagram.) The

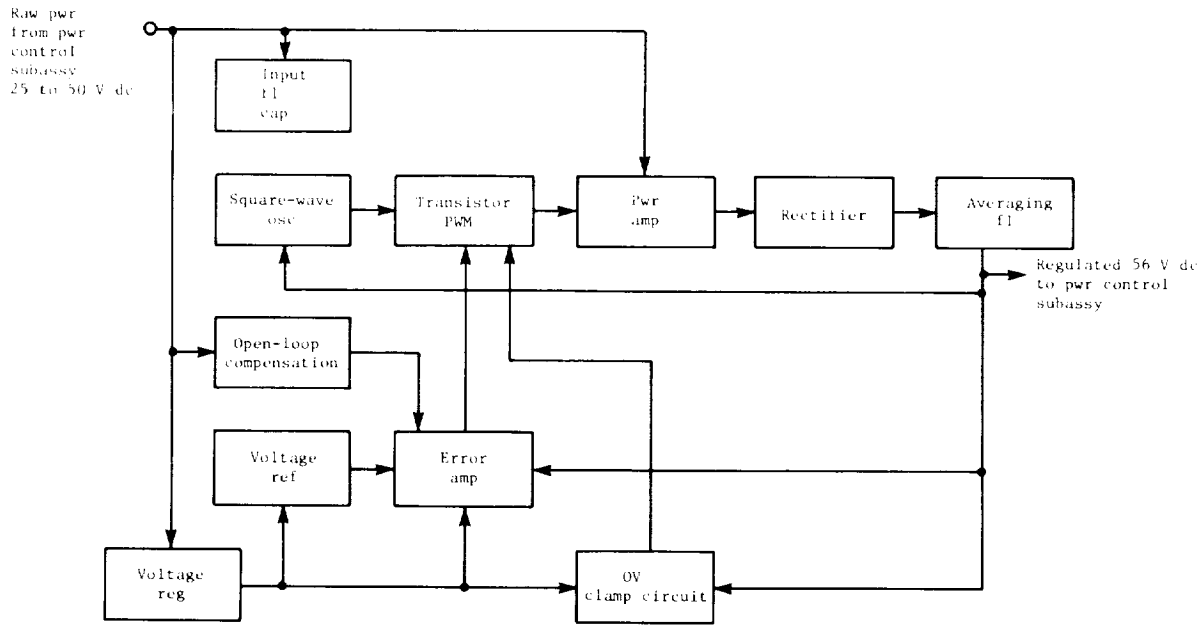

Figure 88.- Functional block diagram of booster regulator.

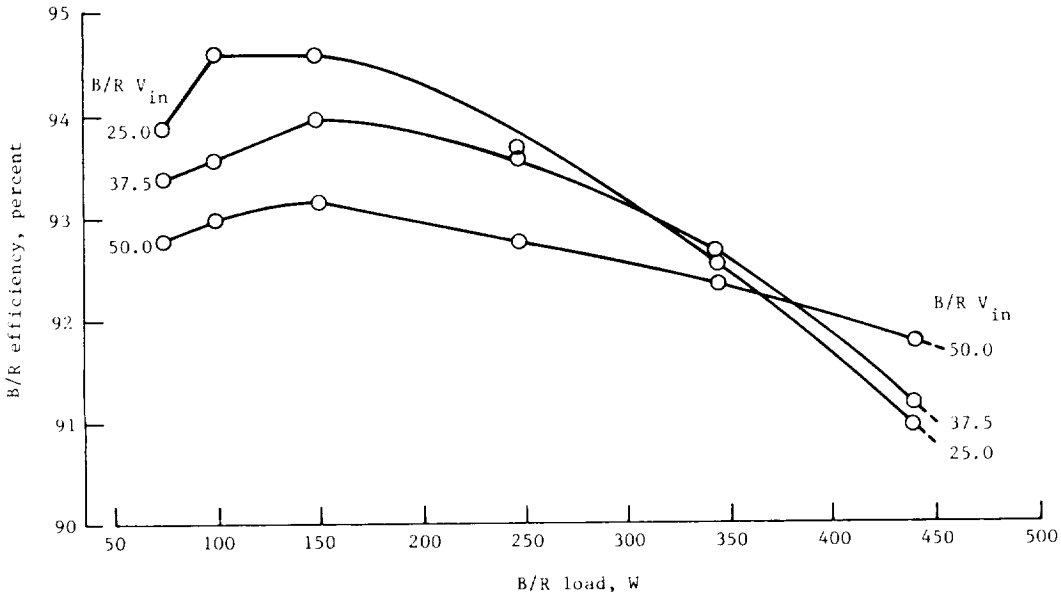

Figure 89.- Typical booster regulator efficiency as a function of load characteristics.

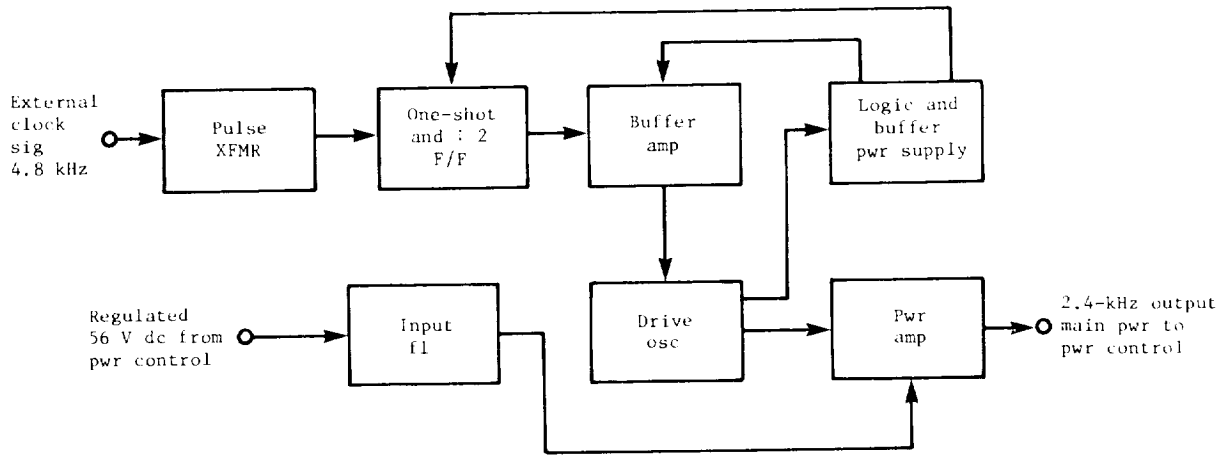

Figure 90.- Functional block diagram of 2.4-kHz inverter.

FDS clock pulse was gated and divided by 2 with a flip-flop circuit. A drive oscillator, fed by the flip-flop, overrode the output of a free-running oscillator frequency drive to force synchronization at 2.4 kHz ± 0.01 percent. If the FDS clock pulse failed or circuitry failed in the 2.4-kHz inverter associated with the clock pulse, the free-running oscillator was not overridden, and while the output frequency of the free-running inverter was still 2.4 kHz, it had a wider tolerance of ±6 percent. The drive oscillator output was to a

driven square-wave inverter circuit and then to a delay circuit that gated the main switching transistors. The output of the main switching transistors form the square-wave output as they turn on alternately for 180° of the wave. The delay circuit prevented both transistors from switching on simultaneously which would cause large current spikes. No closed loop was necessary to regulate the 2.4-kHz inverter output voltage because of the preregulated input voltage. The output of the main switching transistors was routed to an output transformer, and the low loss characteristics of the transformer maintained the output voltage at 50 V rms within the steady-state range between 3 and -4 percent. (See fig. 91 for the typical voltage regulation and efficiency plotted against load of the 2.4-kHz inverter.)

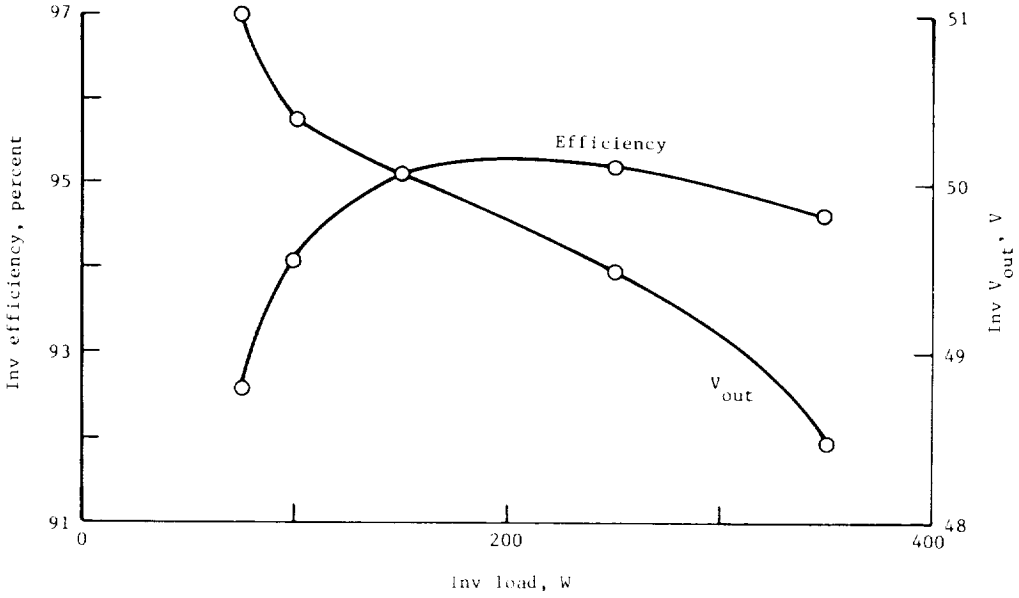

Figure 91.- Typical 2.4-kHz inverter output voltage and efficiency as functions of load.

The 55.2 V dc redundant bus supplied power to the three-phase 400-Hz inverters. Figure 92 shows the block diagram of the 400-Hz inverter. Sync frequency for the unit was derived from the 2.4-kHz power bus that was divided by 6 to obtain 400 Hz. Three driver transformers were each supplied the full 2.4-kHz square wave, but they were phased 120° apart to generate a three-phase square-wave driver system. These driver transformers controlled six output transistors in push-pull pairs that drove each leg of the three-phase output transformer. The output transistors are either 180° conducting or 180° blocking. When conducting, these transistors delivered 55.2 V dc redundant bus power to the primary of the three-phase output transformer that was connected in a delta configuration both at its primary and at its secondary windings. The generated wave shape was time displaced semisquare without third harmonics that circulated at the output of the unit. A 400-Hz inverter was turned on or

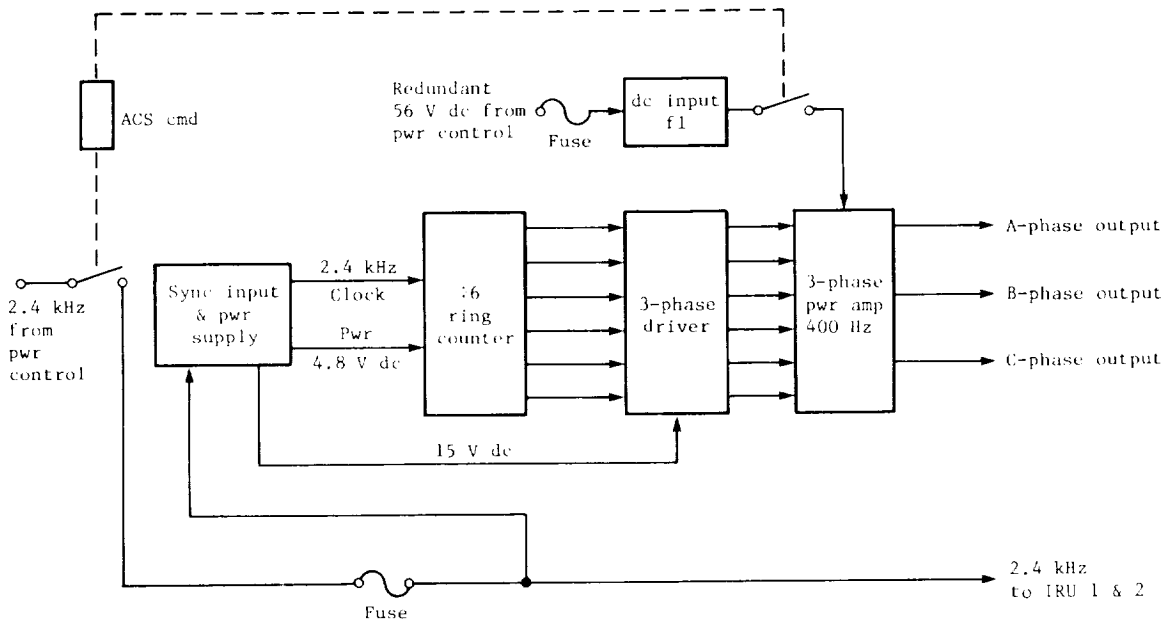

Figure 92.- Block diagram of 400-Hz three-phase inverter.

off by an ACS signal to the power subsystem that actuated a magnetic latching relay. Each inverter output was connected to a given inertial reference unit, the only users of 400-Hz power on the VO. Figure 93 shows typical efficiency-load characteristics of the 400-Hz three-phase inverter.

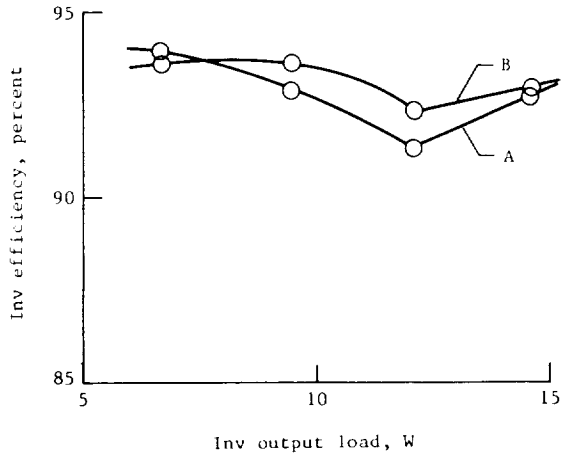

Figure 93.- Typical 400-Hz three-phase inverter efficiency as function of load.

The 30 V dc converter subassembly contained two identical converters that operated in a parallel redundant configuration. (See block diagram in fig. 94.) Both converters were simultaneously switched on or off as needed during the mission via signals from the CCS, and either converter was capable of handling the entire expected load should the other fail. Both the input and output power of the converters were switched by redundant relays that were controlled by the CCS commands. The unit converted to 30 V dc the regulated 55.2 V dc output from the B/R at its redundant bus. The 55.2 V dc was filtered to reduce the introduction of ripple current to the converters. Each converter consisted of a driver and a full-wave switching inverter followed by a transformer-rectifier-filter unit. The inverters were driven by a square-wave signal from the 2.4-kHz power line. In each converter, a balanced output from the input transformer fed the bases of a pair of switching transistors that drove a power transformer.

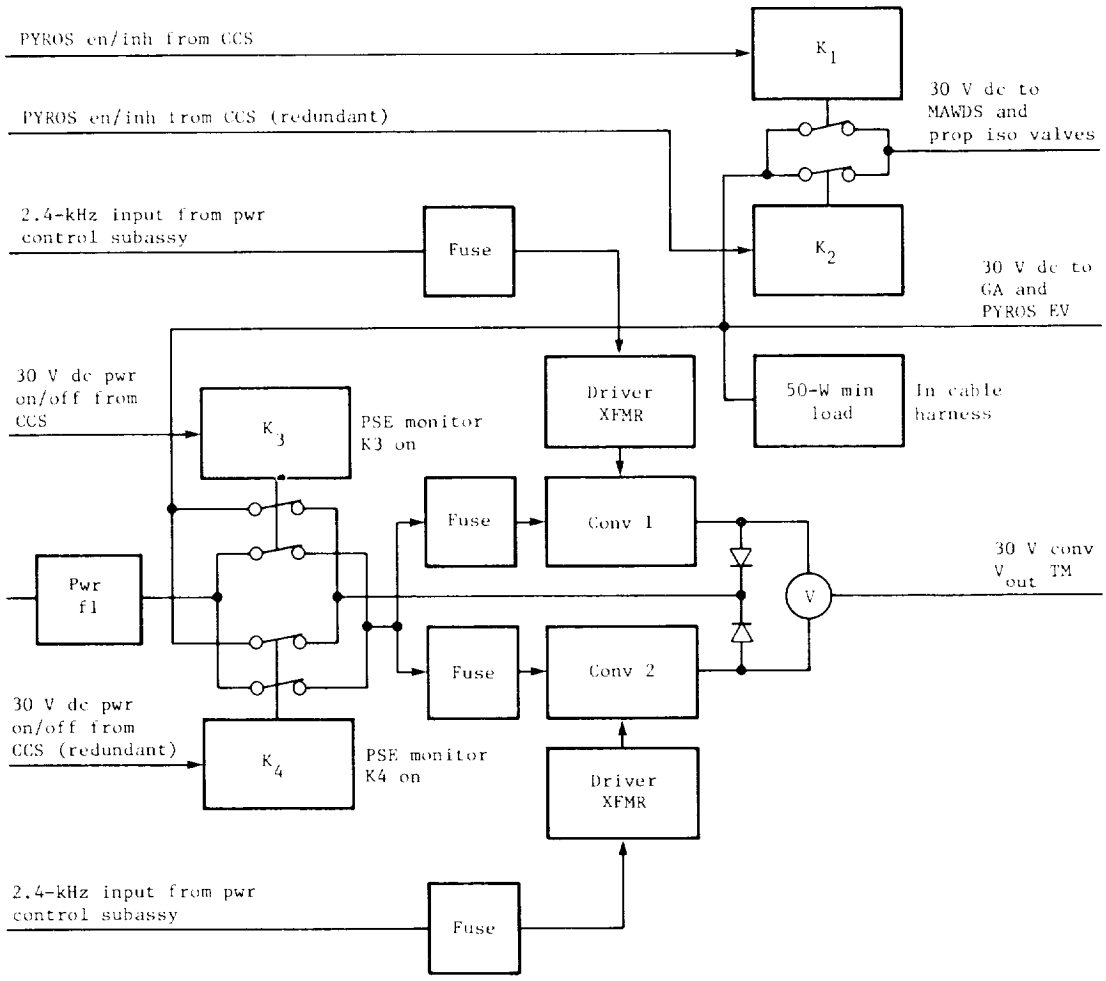

Figure 94.- Functional block diagram of 30 V dc converter.

The main winding of the transformer fed a full-wave rectifier and an LC filter, and the output from the two converters was combined through blocking diodes to provide a single 30 V dc output. The output voltage of the converters was not regulated. Regulation was dependent on the internal impedances of the converter and the regulation of the redundant 55.2 V dc bus. A 5-W resistive load was applied as a minimum load on the 30 V dc output bus. The load was located on the structure in a cable harness. Its purpose was to condition output capacitors in the 30 V dc converters so that the output voltage of the units was at specification for any load additional to the minimum load. The output voltage rose in open-circuit units. Figure 95 shows the variation of the 30 V dc converter output voltage and its efficiency with load.

The next four paragraphs describe PWRS subassemblies whose primary function was not power conditioning but rather housing electronics that perform a variety of functions required for power management and power distribution. They contained failure sensing circuitry and means for activating automatic

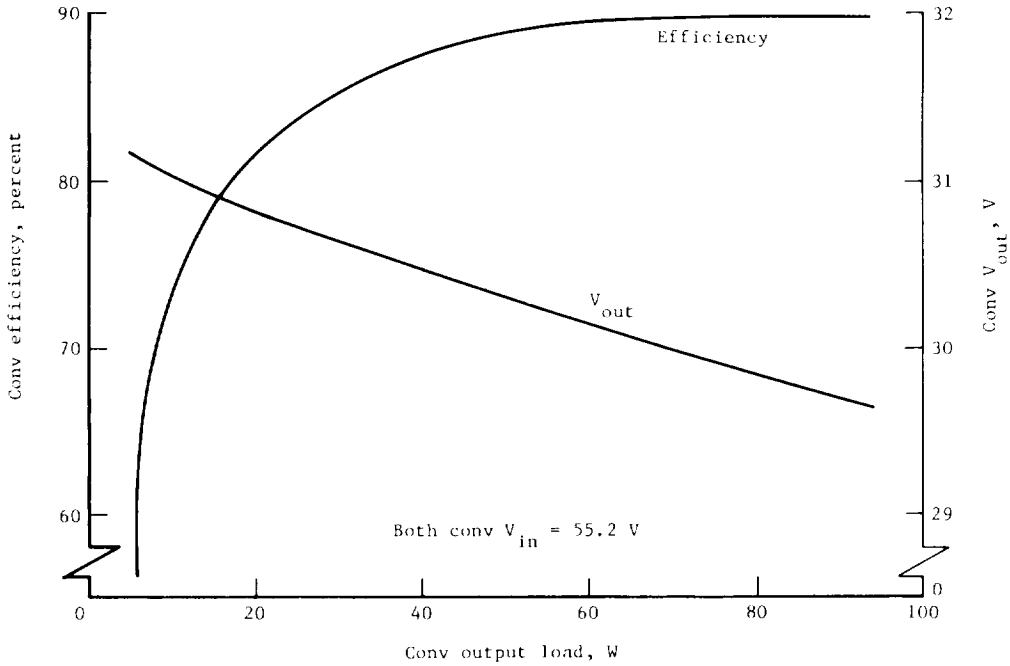

Figure 95.- Typical 30 V dc converter output voltage and efficiency as function of load.

corrective circuitry, contained isolation diodes and fuses, received special status signals, and contained elements that related the PWRS to VO commands, switching, and telemetry.

Most of the contents of the battery electronics subassembly related to battery functions. (See fig. 96.) The one exception was that it contained one of the two redundant 30 V dc bias supplies. The other 30 V dc bias supply was in bay 12 in the power distribution subassembly. The 30 V dc bias supply redundant circuit was one of two in the PWRS, four redundant supplies in all, that converted 55.2 V dc redundant bus power to that at 32.2 V dc ± 6 percent. All the supplies operated continuously and their outputs were connected in parallel. As the command power supply, its regulated output served the CCS as its power source to activate spacecraft relays. The battery chargers also used the 30 V dc bias supply to power relays for the automatic transfer to low rate. The discharge path of each battery was isolated from the unregulated dc bus with quad connected redundant diodes that were located in the battery electronics subassembly. The battery electronics subassembly also contained the following switching functions:

Internal power: A motor-driven switch was used to connect and disconnect the batteries from the spacecraft during ground tests. The switch was activated by ground support equipment through the V S/C umbilical, and the flight command system had no control over its functions. One of the major prelaunch events was to transfer the VO power source from external power to its batteries by means of this switch. This event occurred 7 min before lift-off, and the switch then remained in this position for the balance of the mission.

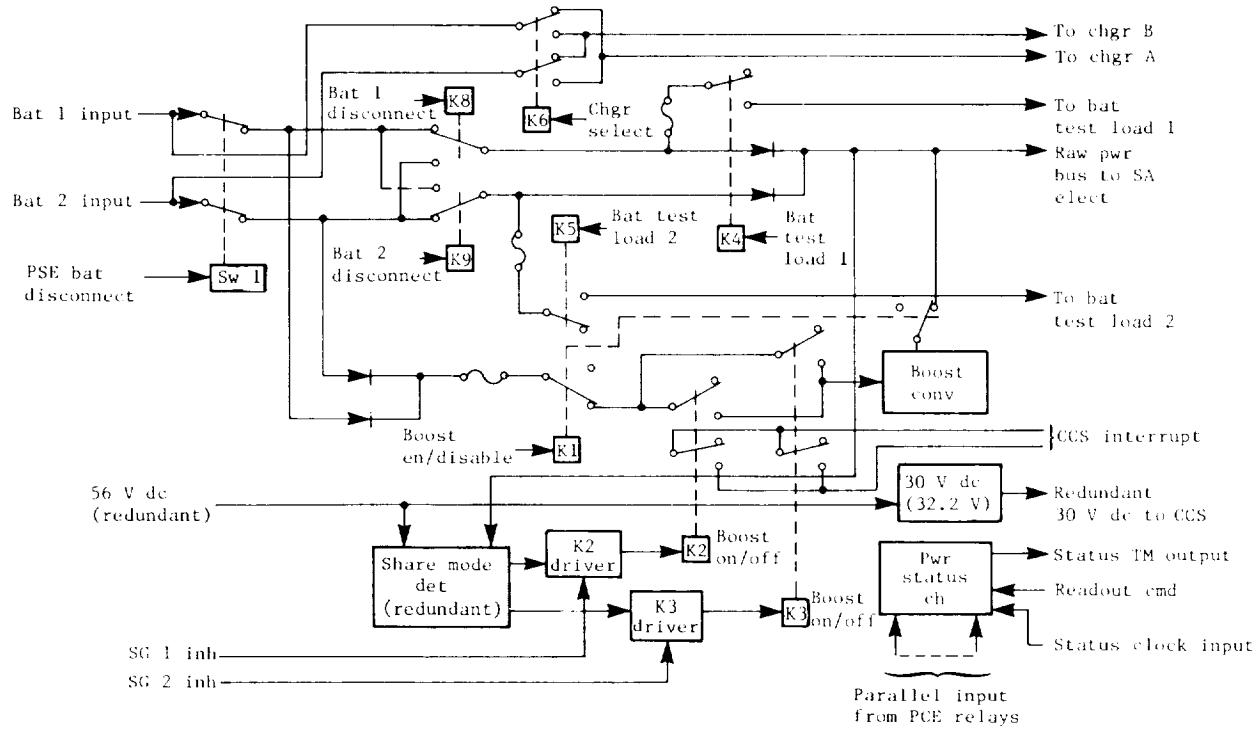

Figure 96.- Functional block diagram of battery electronics subassembly.

Battery charger select switch: Relays K6 and K7 in the battery electronics subassembly could be commanded to select the charger for each battery, although charger A was expected to charge battery 1 and charger B to charge battery 2 for the entire mission. But in the event of a charger failure, the remaining unit was used to sequentially charge one then the other battery.

Battery select switch: Relays K8 and K9 in the battery electronics subassembly could be commanded to connect either or both batteries to the unregulated dc power bus. This design permitted a discharged battery to be recharged isolated from the V S/C and from the possibility of an unscheduled discharge sequence. The discharge path of both batteries could not be simultaneously disconnected from the unregulated bus. VO telemetry indicated the status of the K8 and K9 relays.

Boost mode switches: The battery electronics subassembly also contained relays that controlled boosting, a PWRS feature that automatically selected a more favorable power subsystem operating point. The K1 relay enabled or inhibited the boost mode upon command and simultaneously enabled or inhibited the CCS share mode correction routine. This relay was enabled during the mission. During the boost sequence, the K2 and K3 nonlatching redundant relays in the subassembly were repetitively actuated by the share mode detector.

Battery test loads: The K4 and K5 relays in the battery electronics subassembly connected 30-Ω resistive loads to the batteries for special battery

operations. The loads could be used to safely investigate the condition of a battery or aid in battery reconditioning. The K4 and K5 relays plus the K8 and K9 relays could be commanded in a manner that connected either load to one battery or both loads in parallel (15 Ω) to one battery. The test loads were resistors that were physically located in a cable trough. VO telemetry indicated the status of the K4 and K5 relays.

Much of the solar-array electronics subassembly was concerned with solar-array functions, but it also contained switching controls for the VLC, XTXS, and RFS, telemetry sensors, and fuses. (See fig. 97.) This subassembly contained the 40 isolation diodes used in the circuit of each of the 40 sections in the solar array. The purpose of the isolation diodes was to prevent a faulty subpanel section from loading the others. On separate commands, the K1 relay in this subassembly switched raw power to the VL regulator 1, the relay K2 switched raw power to VL regulator 2, the K3 relay switched raw power to the RFS TWTA power converter, and the K4 relay switched raw power to the XTXS. This subassembly contained the circuit that isolated the unregulated power bus return from chassis ground, 3.01 kΩ in parallel with a 0.01-μF capacitor. The circuit current limited any array or battery short to chassis, and it also shunted to chassis ac noise on the unregulated dc bus. The subassembly provided the tie point for the chassis grounds of this unit, the two battery chargers, the 30 V dc converter, and the bay 10 electronic case chassis.

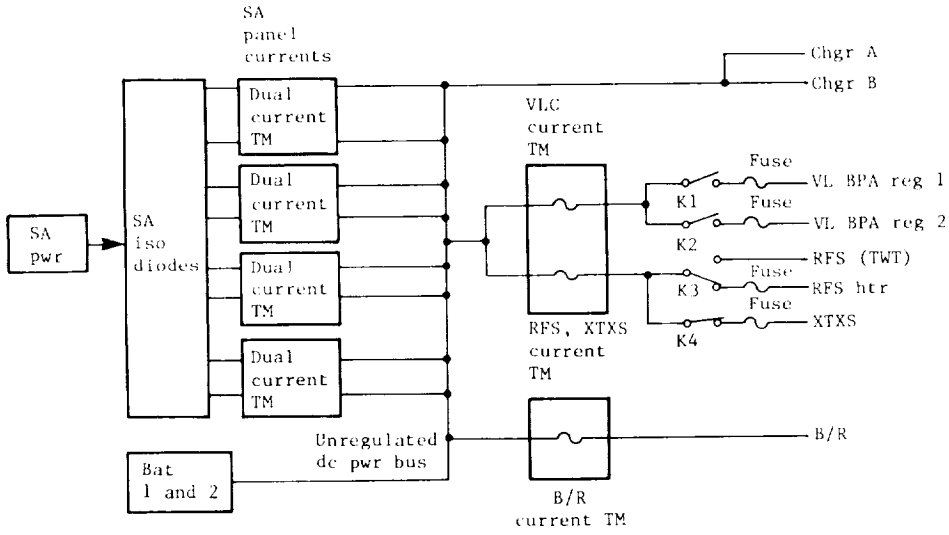

Figure 97.- Functional block diagram of solar-array electronics subassembly.

Figure 98 is the functional block diagram of the power control subassembly. This subassembly contained the redundant fail sensing circuit that monitored the output of the main power chain. Sensing a failure, this circuit activated redundant relays, also in this subassembly, that connected the system to the standby power chain. The other contents of the power control subassembly are as follows:

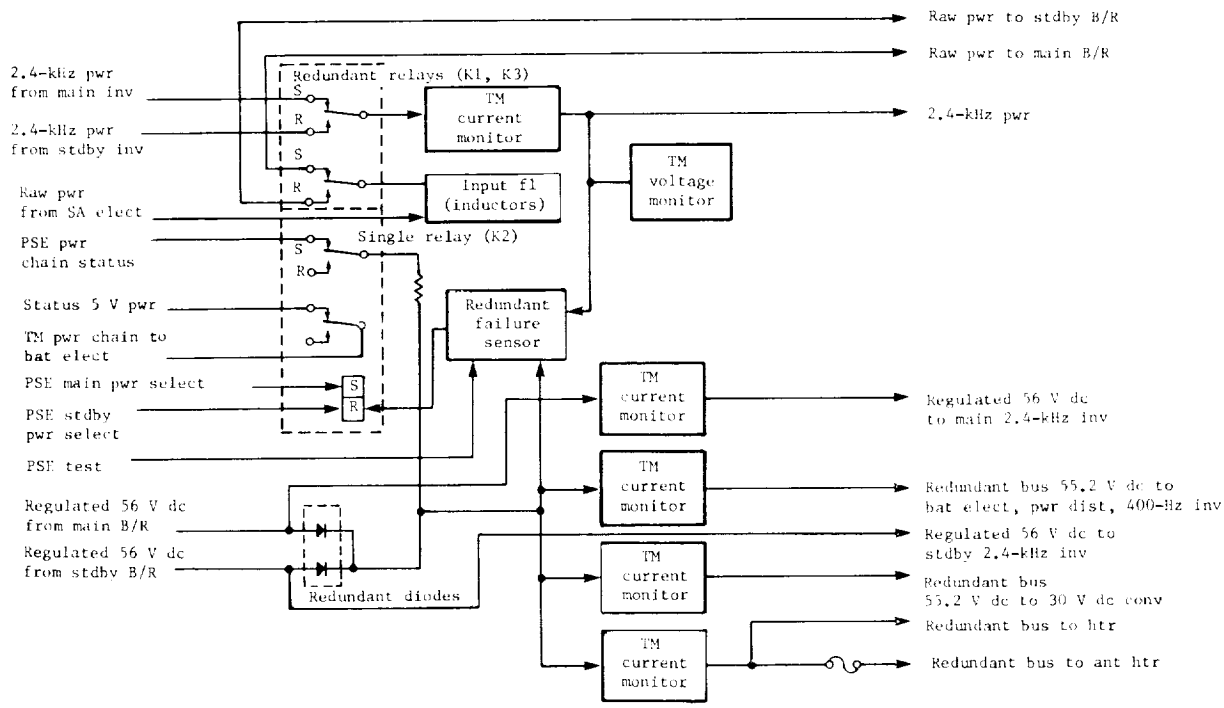

Figure 98.- Functional block diagram of power control subassembly.

Booster regulator voltage limiter: This Zener diode circuit limited the booster regulator output voltage at a maximum of 64 V dc ± 1 percent during transient conditions or certain internal failures.

Filter: This subassembly also contained a physically large inductor that filtered the ripple current present on the unregulated dc bus from the input to the booster regulators.

Switching: The redundant K1 and K3 relays in this subassembly were in the set mode at launch for system operation in the main power chain. If the fail sensing circuit during the mission detected a main power chain failure, the relays were automatically reset to substitute the standby power chain.

Most of the VO power distribution functions were in the power distribution subassembly that contained 21 magnetic latching relays controlled by commands issued to the CCS. The commands caused the CCS to issue signals to the B sink-source power matrix that was designed into the power distribution subassembly. Switchable functions on the 2.4-kHz power bus are as follows:

ACE 1 and 2
ARTCS 1 and 2
DTR A and B
FDS power converter A and B
IRTMS
MAWDS
MAWDS thermal control

RRS and RTS
TMU A and B
VIS A and B

Switchable functions on the regulated 55.2 V dc power bus are as follows:

ACS valve heaters
DTR A and B heaters
IRTMS replacement heater
MAWDS radiator plate heater
MAWDS replacement heater
Propulsion check valve heater
Pyro bay heater
Scan platform heater
VIS A and B optics heaters
VIS A and B vidicon replacement heaters

The 30 V dc bias supply command power bus was the second of the two redundant 30 V dc supplies (32.2 V dc ± 6 percent) in the power subsystem. The other was located in the battery electronics subassembly.

System view.- The dominant redundant feature of the power subsystem was its power chains, each of which contained a booster regulator and a 2.4-kHz inverter subassembly. If one subassembly malfunctioned in the main power chain, the standby power chain that contained a duplicate B/R and 2.4-kHz inverter was automatically substituted. The system of the redundant power chains consisted of the main and standby subassemblies, sensing elements to monitor the performance of the subassemblies, and circuit elements to initiate and perform the power chain transfer. Except for the B/R and 2.4-kHz inverter, all circuitry related to the power chains was located in the power control subassembly. Output frequency of the 2.4-kHz inverter was not sensed. The inverter normally operated in a synchronous mode driven by a 4.8-kHz sync pulse train provided by the FDS that was divided by 2 in the inverter. The 2.4-kHz inverter output frequency was 2.4 kHz ± 0.01 percent in the synchronous mode. However, it did widen to a ±6 percent tolerance if the 2.4-kHz inverter synchronizing circuit failed to cause it to operate in its free-running mode, an event that did not cause power chain transfer. It should be noted that there was a redundant FDS clock on the VO.

The function of the overvoltage processor was to sample the 55.2 V dc B/R redundant bus voltage and compare it with a voltage reference in an operational amplifier. (See fig. 99.) If B/R overvoltage was detected, the OV switch changed to the low state. One line is shown in figure 99, but there were three separate OV sensing lines in the design. The undervoltage processor used a transformer rectifier filter to convert 2.4 kHz ac to a dc signal proportional to the 2.4-kHz bus voltage. Operational amplifiers compared the sample voltage with a reference for possible signs of 2.4-kHz undervoltage, which if detected caused the UV switch to change to its low state. Again, the description and figure 99 note one of three separate UV sensing lines. If a low signal was sensed sufficiently long in the time delay circuit, a capacitor reached a voltage that triggered the fail sense signal amplifier to issue a fail sense signal to a pair of relay driver gates. (See fig. 100.) One of the three lines that

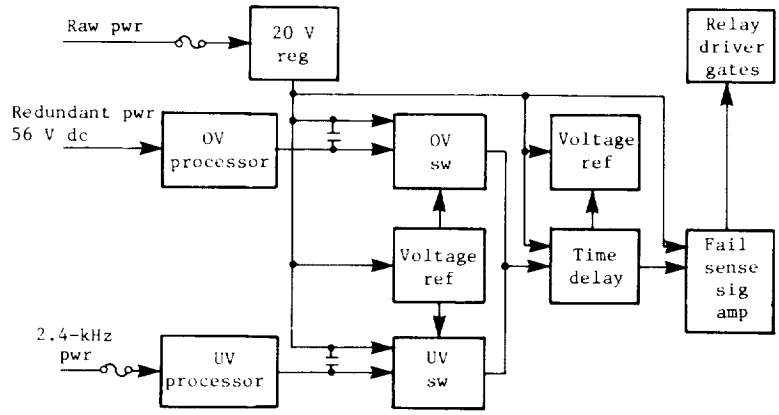

Figure 99.- Fail sensing circuit.

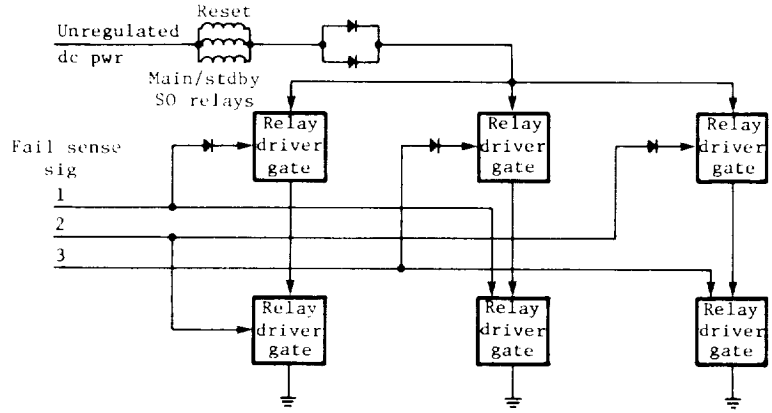

Figure 100.- Majority voting logic for power chain transfer.

monitored the B/R overvoltage and one of the three lines that monitored the 2.4-kHz undervoltage went to one fail sense circuit. There were three fail sense circuits in total that could issue a fail sense signal. The majority voting logic was contained within the relay gate design shown in figure 100. Majority voting guarded against anomalous triggering to the standby power chain by ignoring a signal issued from just one of the three fail sense circuits. Two or more fail sense signals had to be detected to start the chain transfer process that resulted in the reset of the main-to-standby transfer relays; that is, there had to be majority vote of the possible signals. A regulator in the power control subassembly reduced the unregulated dc bus power to 20 V dc that powered the OV and UV switches, the voltage references, time delays, and fail sense amplifiers.

Figure 101 shows the power chain switchover relays. If a majority voted failure was detected in the main power chain for more than about 1.5 sec, the relay driver gate permitted current flow from the unregulated dc power bus to

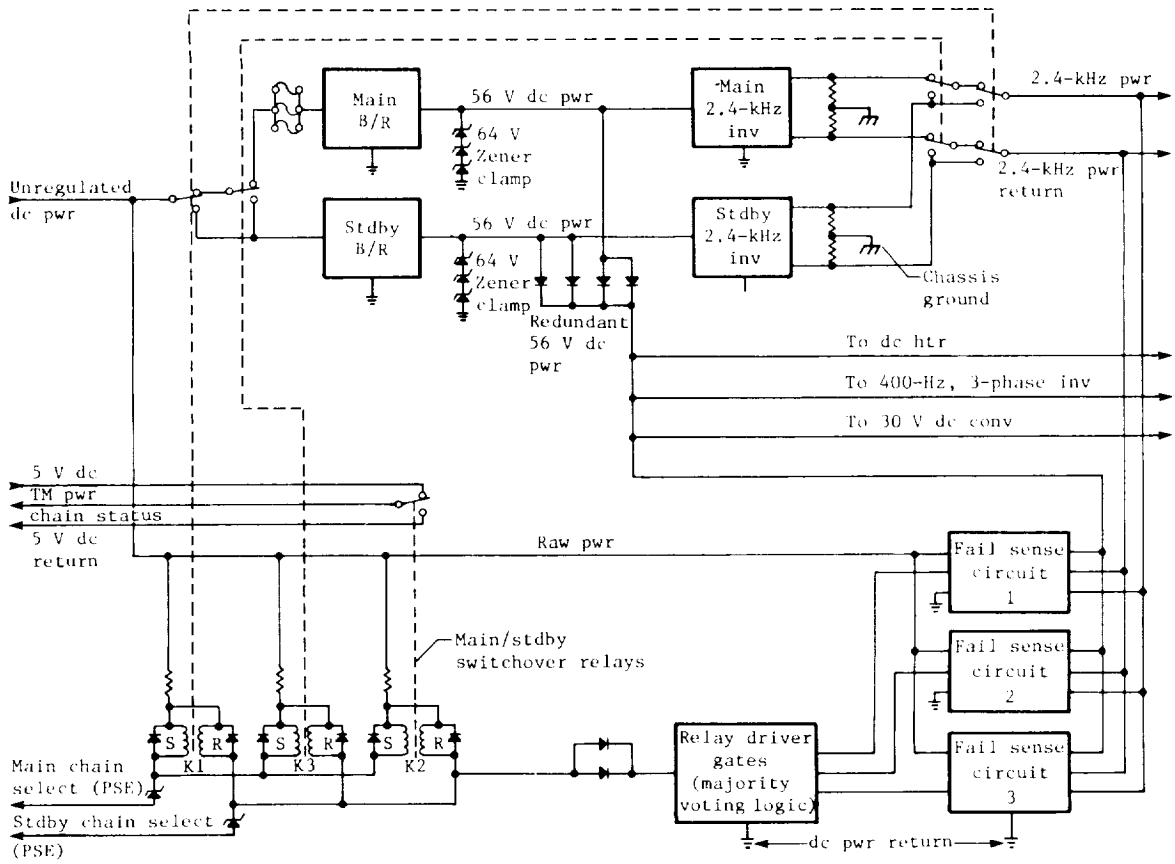

Figure 101.- Power transfer circuit.

the reset coils of the K1 relay in the power control subassembly. When reset, the K1 relay transferred the power subsystem operation from the main to the standby power chain. The relay controlled the input power from the unregulated dc bus to either the main or standby booster regulator, and it also connected the output of either the main or standby 2.4-kHz inverter to the VO electrical system. The state of the K1 relay could be controlled from support equipment during ground tests, but the VO command system had no such control. Accordingly, an automatic chain transfer during mission caused operation in the standby chain for the balance of the mission. The K3 relay in this module was redundant with K1 and both normally operated in unison, but transfer to the standby chain was achieved if only one of the relays changed state. VO telemetry indicated the status of the K1 and K2 relays. A K2 relay in this module also changed state with a power chain transfer to provide a power chain status signal to the FDS for use in the power status channel, and for use on the support equipment. Only a short summary is presented here of other redundant subassemblies in the VO power subsystem. More detailed discussions of redundant design are found in the sections allocated to subassembly descriptions. The two chargers were redundant since one unit could be switched to charge either battery. The two 400-Hz inverters offered some redundance, but each of these units served one IRU and could not be switched to power the other. The outputs of both 30 V dc con-

verters were connected in parallel and turned on and off together. One of the two units supported the VO requirements. One of the four power subsystem 30 V dc bias supplies whose outputs were also connected in parallel served the CCS requirements to actuate VO relays or to power the automatic battery charger transfer to low rate.

The battery could have been unexpectedly called on to share the support of the VO electrical loads along with the array. With a power transient causing the share mode, boosting quickly corrected the unnecessary battery discharge. However, a share mode caused by an unexpected steady-state load increase beyond the solar-array peak power output caused added battery discharge at a time when the batteries had a low state of charge. With the array unable to support the additional load, boosting was ineffectual and served only to further drain the batteries. Decreasing the VO electrical load was required in this situation, and the CCS was programmed to sense the need and to systematically curtail loads. At the start of a boosting sequence, the CCS began a boost pulse count. When the count exceeded six pulses in an 85-sec interval, the CCS turned off a pair of loads. This load decrease may not have been sufficient to achieve successful boost, and if it was not, the pulse count in the next 85-sec interval again exceeded six to cause the CCS to turn off another pair of loads. Loads were turned off in an order of increasing load importance which is shown in the following list of commands (read across):

(3A)	(4AR)	(38AR)	(36AR)
(2AR)	(4BR)	(39AR)	(36BR)
(15AR)	(16AR)	(52AR)	(2DR)
(15BR)	(16BR)	(42AR)	(2DR)
(10NR)	(4NR)	(75A1R)	
(39CR)	(4P)	(75A2R)	

This list was programmed into the CCS memory which was altered during flight. Boost pulses ceased after the VO electrical load decreased sufficiently to permit successful transfer of the operating point. The power subsystem design incorporated a number of protective circuits that are discussed as follows. Zener diodes limited the array voltage and also limited the B/R voltage. Boosting was designed to terminate a share mode that was needlessly discharging the battery. Also, automatic load reduction promoted conditions to achieve successful boost. The battery charger would automatically transfer to the low charge rate from higher charge rates when the battery reached 38.25 ± 0.25 V or $29^{\circ} \pm 1.6^{\circ}$ C ($85^{\circ} \pm 3^{\circ}$ F). The CCS automatically switched off the appropriate charger when the temperature of a battery reached 38° C (100° F). Redundant circuits in the PWRS are summarized here, but they are discussed in detail in subassembly descriptions. The power subsystem fuses, their circuit configurations, and fuse ratings are given in table 28.

TABLE 28.- PWRS FUSES

Circuit	Subassy	Circuit config (a)	Individual fuse rating, A	Quantity
Boost conv input	Bat elect	P	15	3
Bat test load 1 output	Bat elect	P	1	2
Bat test load 2 output	Bat elect	P	1	2
2.4-kHz input to TM sensors	Bat elect	S	.5	5
Lander BPA reg 1	SA elect	PD	15	2
Lander BPA reg 2	SA elect	PD	15	2
Deorbit htr	SA elect	PD	1	2
RFS htr	SA elect	S	1	2
Unregulated dc to XTXS	SA elect	PD	1	2
Dual current TM	SA elect	S	.5	6
DTR A repl htr	Pwr dist	S	1	1
DTR B repl htr	Pwr dist	S	1	1
IRTMS repl htr	Pwr dist	S	1	1
VIS A elect htr	Pwr dist	S	1	1
VIS B elect htr	Pwr dist	S	1	1
MAWDS elect htr	Pwr dist	S	1	1
MAWDS rad htr	Pwr dist	S	1	1
VIS A optics htr	Pwr dist	S	1	1
VIS B optics htr	Pwr dist	S	1	1
PYROS bay htr	Pwr dist	PD	1	2
Scan plat stru htr	Pwr dist	PD	1	2
Propulsion ck valve htr	Pwr dist	P	1	2
HGA act htr	Pwr dist	PD	1	2
RCA - jets and SS htr	Pwr dist	S	1	4
56 V dc input	400-Hz inv	PD	2	2
2.4-kHz bus	400-Hz inv	PD	2	2

[a]S denotes single; P denotes two fuses in parallel; PD denotes two fuses in parallel with diode in one leg.

Operating Modes

The power source during the mission generally was the solar array. Battery operation occurred when the array had no incident solar flux as at launch, when the VO was in the shadow of Earth or Mars, or when the VO was maneuvered sufficiently from the Sun line. The solar array had sufficient Sunlight for the electrical power needs of the VO but when the electrical load required more energy, it was supplied by the batteries. The array-battery share condition occurred automatically as the increased load on the array obtained additional array current that was supplied at reduced voltage, which also reduced the unregulated dc bus voltage. The batteries discharged when the unregulated bus voltage decreased sufficiently to forward bias the battery isolation diodes. Figure 102 shows at point A the power subsystem operating point with the array alone supplying power and at point B the operating point with the battery and the array in share. Both were stable operating points. The operating point could continue to dwell in a share mode after the disappearance of a power transient that caused the share. In this case, the batteries needlessly discharged although the array had sufficient power to supply the requirements of the VO. Boost circuitry was designed to provide sufficient additional power

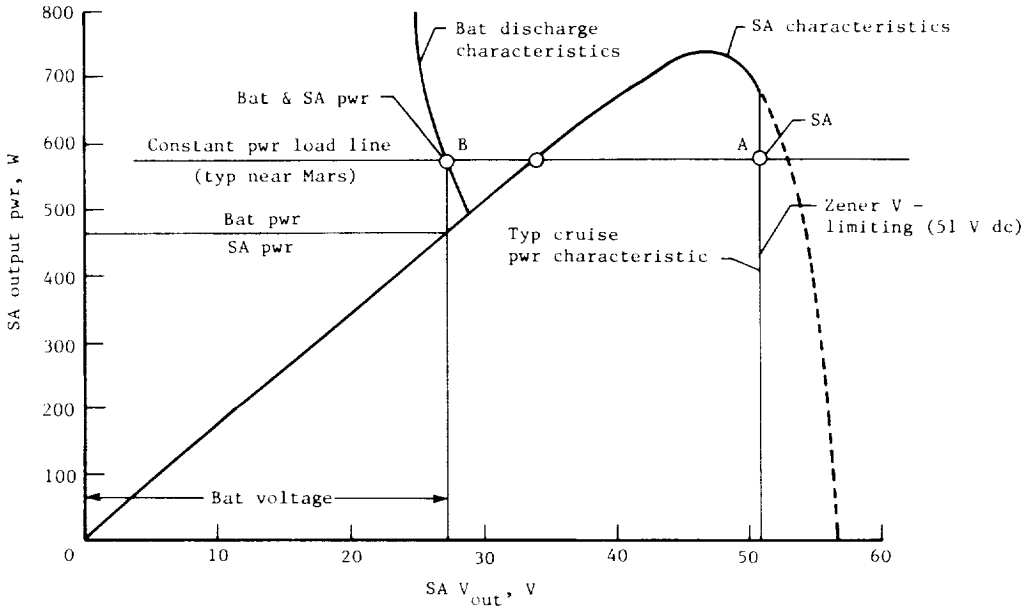

Figure 102.- Solar array and share mode operating points for conditions near Mars.

(table 24) to the unregulated dc power bus to drive its operating point to the higher voltage stable point at point A where the array alone supported the electrical needs of the spacecraft. The circuitry consisted of redundant share mode detectors and a single boost converter that were located in the battery electronics module. The redundant share mode detector circuit sensed the voltage level of the unregulated dc bus. Should it drop to 32.6 ± 1.2 V, the share mode detector actuated nonlatching redundant battery electronic relays K2 and K3, that activated the boost converter. A timing circuit controlled the time of the relay closure to control the width of the pulse output from the boost converter at 0.5 ± 0.2 sec. The timing circuit also limits the relay closure repetition rate to 7.5 ± 2.5 sec. If the boost converter was enabled, the solar array must be Sun acquired in order to boost. The share mode detector ceased to call for boost pulses when the unregulated dc bus voltage became 34 V or higher. The boost converter circuit, powered by the battery, was a self-oscillating dc-dc converter. It provided a high voltage pulse (table 24) to the unregulated dc bus that was designed to shift the operating point at B to A in figure 102. If the VO load was too great to be supported alone by the array, the boost attempts were unsuccessful until the automatic CCS reduction of loads or VO power management by ground command diminished the total VO electrical load to a level that could be accommodated by the array. It was the backup CCS load reduction feature that removed the requirement to design a redundant boost converter circuit. The K1 relay in the battery electronics subassembly was set to enable the boost converter, and VO telemetry indicated the status of this relay. The K2 and K3 relay closures, that were sensed by the timing circuit, were also monitored to be counted by the CCS. When the boost converter was inhibited so was the CCS boost count and load reduction feature. Logic incorporated into the share mode detector circuit automatically inhibited the circuit

when the array was not Sun acquired. If the circuit was enabled by command, it must also have received the Sun-gate signal in order to function. This signal, provided by the ACS Sun sensors, indicated that the solar array was Sun acquired. The share mode detector was automatically inhibited in the absence of the Sun-gate signal. The design eliminated extra VO commanding to inhibit the circuit when boosting would be futile; these would be the occasions when planned maneuvers from the Sun caused expected share with battery discharge and the maximum power output of the array was too diminished by the turn from the Sun to support the VO load. Boosting during these occasions unnecessarily further drained the batteries. If a load decrease permitted successful boosting while off the Sun line, an artificial Sun gate would enable the share mode circuit with the issuance of a (7D) command. Attitude shifts from the Sun caused shadows to be cast upon the solar array by the low-gain antenna, array latches and hinges, and other VO structures. As can be expected, the array power output was diminished by the shadows. However, it was very difficult to accurately analyze the exact decrease of array power after a given maneuver. An adequate estimate of shadows was achieved with a study of shadow patterns cast upon the solar array of a small model of the VO. This investigation was performed in the Celestarium facility at JPL where photographs were taken of the VO model as it was oriented to collimated Sun rays at known yaw and roll angles. Output power estimates of an array that was expected to be shaded as the result of a VO maneuver included factors derived from the photographs. The photographs also yielded the derating factors to be stored as part of the PWRS computer program data base. Although shadowed array sections could generate some electrical power, a worst-case approach was used to simplify the analyses by assuming zero power output for these sections.

Tests showed the nickel-cadmium battery to be capable of reliably sustaining thousands of discharge-charge cycles when the battery was well managed. From the battery point of view, it was well managed when it operated in a cool environment and was maintained in energy balance. Battery energy balance was achieved when VO operations did not excessively drain the battery and operations insured adequate recharge before the battery was again used. A well managed battery system from the mission point of view was to have the batteries fully charged ready for any planned sequence requiring its use or ready for any unscheduled event that suddenly required battery support. It was one of the responsibilities of the power analyst to aid mission sequence design to reconcile both battery management concepts. For most mission activities, the depth of discharge of the VO batteries was limited to 45 percent, although discharge in excess of 45 percent was accommodated during Sun occultation intervals.

Battery charger lockup describes a condition of the charger when it was unable to transfer to the low charge rate mode from either its medium or high charge rate modes. Normally, such transfer was automatic when the battery voltage reached 38.25 ± 0.25 V or the battery temperature reached $29^{\circ} \pm 1^{\circ}$ C ($85^{\circ} \pm 3^{\circ}$ F). But in lockup, the charger could not transfer to its low-rate mode, automatically or by command. The lockup condition was due to an undesired logic state caused by the inability of the differential amplifier circuit in the charger to reset. The circuit had inherent hysteresis. The lockup condition was caused by a procedure that inadvertently permitted the issuance of a medium or high charge rate command to the charger after it had just automatically

transferred to its low-rate mode and before the differential amplifier circuit had been permitted to reset. The charger would then charge at its newly commanded medium or high rates, but it would not automatically transfer to the low rate after the battery reached the prescribed conditions. This mode endangered the battery because of the high temperature generated by the battery overcharging in the medium or high rates. Lockup was avoided after automatic transfer to the low rate because of battery voltage limiting if the battery voltage was permitted to decline to about 36 V before the higher charge rate commands were issued to the charger. The low battery voltage reset the differential amplifier to regain the automatic low-rate transfer feature at the higher battery voltage. If the transfer was caused by high battery temperature ($29^{\circ} \pm 1^{\circ}$ C ($85^{\circ} \pm 3^{\circ}$ F)), the battery had to cool to 24° C ($+ 3^{\circ}$ or $- 1^{\circ}$) (75° F ($+ 5^{\circ}$ or $- 3^{\circ}$)) to achieve the reset. Conditions had to be present to satisfy both the battery voltage and temperature reset requirements for the proper operation of the automatic transfer to low rate. If lockup occurred, the charger was commanded off, and the open-circuit battery would then return to conditions that reset the circuit for automatic low charge rate transfer. The charger was then switched on and the unit operated normally. If the lockup went unnoticed, the battery temperature increased sufficiently to cause the 38° C (100° F) battery thermal switch to close and signal the CCS to turn off the charger.

The 10-month cruise period to Mars caused changes in the battery that resulted in temporarily diminished capacity. Continuing the battery operation in low-rate overcharge for long periods without deep discharges was thought to generate crystalline changes in the battery plates that increased the internal electrochemical impedance of the cell. The result was end-of-charge battery voltage increase and discharge voltage decrease. The impact to mission operations was that in discharge the battery voltage declined more quickly to its lower specification limit (27.4 V) before its anticipated W-hr capacity was realized. This battery condition was reversible with deep discharge and recharge. Whether such battery conditioning was required was determined from ground tests. VO batteries followed on ground the sequences undertaken by the flight batteries, and their battery voltage regulation was studied when simulated Mars orbit insertion sequence loads were applied after the long cruise period. Similar tests studied the battery response to other critical sequences. When the data suggested the need for battery conditioning before the mission event, the VO batteries would be discharged at a high rate for a time using VO loads applied to cause a deliberate share mode. This discharge sequence was followed by another having the batteries discharged with only its test loads at a safer rate until the desired depth of discharge was reached. The batteries were then recharged to complete its conditioning cycle.

Interfaces

Table 29 lists users of the various power busses, both those users that could be switched and those that could not. Note that an IRU could not be switched from its 400-Hz inverter.

The FDS provided a 4.8-kHz clock pulse signal to the power subsystem to synchronize the 2.4-kHz inverter. Magnitudes of current, voltage, and temperature sensed by PWRS sensors were indicated by equivalent voltage output from

TABLE 29.- USERS SUPPLIED FROM ELECTRICAL POWER BUSSES

Unregulated dc

Unswitchable:
- Booster regulators
- Deorbit heaters

Switchable:
- Battery chargers
- TWTA/heater
- XTXS
- VLC
- Boost converter

2.4-kHz inverter

Unswitchable:
- ACS
- CCS
- MDS
- RFS

Switchable:
- 400-Hz inverter A and B
- ACE 1 and 2
- ARTCS 1 and 2
- DTR A and B
- FDS converter A and B
- IRTMS
- MAWDS
- RRS/RTS
- TMU A and B
- VIS A and B

400-Hz inverter A

Unswitchable:
- IRU 1

400-Hz inverter B

Unswitchable:
- IRU 2

Booster regulator

Unswitchable:
- 2.4-kHz inverter
- 30 V dc bias supply
- High-gain antenna heater
- Share mode detectors

Switchable:
- 30 V dc converter
- 400-Hz inverter
- DTR A and B heaters
- IRTMS heater
- MAWDS heaters
- PROPS check valve heater
- PYROS
- RCA jet heaters
- Scan platform heater
- VIS A and B heaters

30 V dc converter

Unswitchable:
- 5-W minimum load

Switchable:
- ACE
- MAWDS solenoids
- PROPS isolation valves
- PYROS engine valves

their circuits. These signals were routed to the FDS to be processed to equivalent DN values that were commutated sequentially and transmitted back in the engineering portion of the VO telemetered data. Some of the sensor signals that described relay status were binary. The rest were voltage levels that lie within specific voltage ranges. (See table 30.)

If the battery temperature exceeded 38^{o} C (100^{o} F), a signal was generated in the battery charger that caused the CCS to turn off the appropriate charger. CCS was involved with all boosting sequences. In share, with proper commands and conditions in effect, the CCS automatically reduced loads until boost was successful. Two matrices were designed into the circuitry of the power subsystem to be accessed by the CCS for VO electrical power switching. One matrix was located in the power distribution subassembly, and the other was designed into the battery electronics, solar-array electronics, battery chargers A and B, and the 30 V dc converter subassemblies. The CCS did not view these as separate matrices but as one having 8 sinks and 12 sources. Each power related command issued by the CCS had a unique sink and source signal. Their intersection on the power subsystem sink-source matrix caused the state change of an appropriate

TABLE 30.- PWRS TELEMETRY FUNCTIONS

Function	Output range	Significance (scale factor)	Measurement range	Resolution per DN
Bay 10 temp	500 to 600 mV	0.7° C (1.27° F)	-31° to 66° C (-23° to 150° F)	0.5° C (1° F)
Bay 12 temp	500 to 600 mV	0.7° C (1.27° F)	-31° to 66° C (-23° to 150° F)	0.5° C (1° F)
Pwr status - ch 1	Digital	N/A	N/A	N/A
Pwr status - ch 2	Digital	N/A	N/A	N/A
+X inbd S/P current	0 to 3 V	1.67 A dc	0 to 5 A	0.03937 A
+Y inbd S/P current	0 to 3 V	1.67 A dc	0 to 5 A	0.03937 A
-X inbd S/P current	0 to 3 V	1.67 A dc	0 to 5 A	0.03937 A
-Y inbd S/P current	0 to 3 V	1.67 A dc	0 to 5 A	0.03937 A
-Y inbd std cell current	0 to 100 mV	0.667 mA	0 to 66.7 mA	0.00053 A
-Y inbd std cell voltage	0 to 100 mV	0.01 V	0 to 1 V dc	0.00787 V dc
-Y inbd radiation cell current	0 to 100 mV	0.667 mA	0 to 66.7 mA	0.00053 A
-Y inbd S/P temp	500 to 600 mV	2.8° C (5.08° F)	-195° to 87° C (-319° to 189° F)	2° C (4° F)
+X outbd S/P current	0 to 3 V	1.67 A dc	0 to 5 A	0.03937 A
+Y outbd S/P current	0 to 3 V	1.67 A dc	0 to 5 A	0.03937 A
-X outbd S/P current	0 to 3 V	1.67 A dc	0 to 5 A	0.03937 A
-Y outbd S/P current	0 to 3 V	1.67 A dc	0 to 5 A	0.03937 A
-Y outbd std cell current	0 to 100 mV	0.667 mA	0 to 66.7 mA	0.00053 A
-Y outbd std cell voltage	0 to 100 mV	0.01 V	0 to 1 V dc	0.00787 V dc
-Y outbd radiation cell current	0 to 100 mV	0.667 mA	0 to 66.7 mA	0.00053 A
-Y outbd S/P temp	500 to 600 mV	2.8° C (5.08° F)	-195° to 87° C (-319° to 189° F)	2° C (4° F)
Bat 1 charge current	0 to 3 V	1.67 A dc	0 to 5 A	0.03937 A
Bat 1 discharge current	0 to 3 V	6.67 A dc	0 to 20 A	0.1575 A
Bat 1 voltage	0 to 3 V	6.67 V dc	22 to 42 V dc	0.1575 V dc
	0 to 3 V	6.67 V dc	22 to 42 V dc	0.1575 V dc
Bat 1 temp	500 to 600 mV	0.7° C (1.27° F)	-20° to 50° C (-4° to 123° F)	0.5° C (1° F)
Bat 2 charge current	0 to 3 V	1.67 A dc	0 to 5 A	0.03937 A
Bat 2 discharge current	0 to 3 V	6.67 A dc	0 to 20 A	0.1575 A
Bat 2 voltage	0 to 3 V	6.67 V dc	22 to 42 V dc	0.1575 V dc
	0 to 3 V	6.67 V dc	22 to 42 V dc	
Bat 2 temp	500 to 600 mV	0.7° C (1.27° F)	-20° to 50° C (-4° to 123° F)	0.5° C (1° F)
B/R current in	0 to 3 V	6.67 A dc	0 to 20 A	0.1575 A
	0 to 3 V	6.67 A dc	0 to 20 A	0.1575 A
Regulated dc htr current	0 to 3 V	1.0 A dc	0 to 3 A	0.02362 A
Unregulated dc current to RFS	0 to 3 V	1.67 A dc	0 to 5 A	0.03937 A
Unregulated dc voltage	0 to 3 V	10.3 V dc	22 to 53 V dc	0.2441 V dc
	0 to 3 V	10.3 V dc	22 to 53 V dc	0.2441 V dc
VLC current	0 to 3 V	5.0 A dc	0 to 15 A	0.1181 A
2.4-kHz main inv current in	0 to 3 V	3.33 A dc	0 to 10 A	0.07874 A
2.4-kHz inv current out	0 to 3 V	3.33 A ac	0 to 10 A	0.07874 A
	0 to 3 V	3.33 A ac	0 to 10 A	0.07874 A
2.4-kHz inv voltage out	0 to 3 V	6.67 V ac	40 to 60 V ac	0.1575 V ac
30 V conv current in	0 to 3 V	1.0 A dc	0 to 3 A	0.02362 A
30 V conv voltage out	0 to 3 V	6.67 V dc	20 to 40 V dc	0.1575 V dc
400-Hz inv current in	0 to 3 V	0.33 A dc	0 to 1 A	0.00787 A
Launch status	Digital	N/A	N/A	N/A
Cr status	Digital	N/A	N/A	N/A
Orbit status	Digital	N/A	N/A	N/A

magnetic latching relay in response to the command, which modified the VO electrical power configuration. Power to cause the state change of the relay was provided by the 30 V dc bias supplies.

The ACS Sun-sensor circuit issued a Sun-gate signal when the array had Sun acquired within its dead band of $5.0^{\circ} \pm 1.5^{\circ}$. This Sun-gate signal was routed to the share mode detector circuit to automatically enable the boosting function. This function enabled with the presence of the Sun-gate signal and disabled in its absence. The operation of the 400-Hz three-phase inverters was not controlled by the CCS but rather by a signal to the appropriate inverter issued by the ACS.

General Operational Data

A summary of VO operational data is contained in this section. The data relate to PWRS telemetry, commands, and logic states. The PWRS telemetry structure is shown in figure 103, and the functional description, measurement range, resolution, and sensor output range are summarized in table 30. PWRS commands that affect the power subsystem are given in table 2.

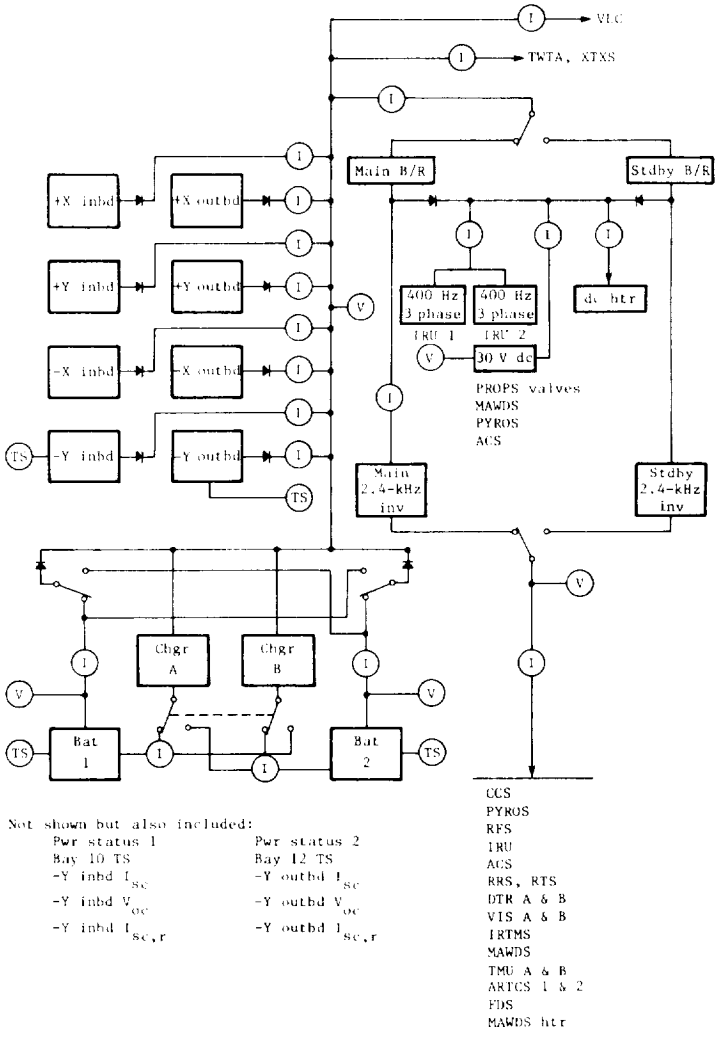

Figure 103.- Telemetry structure of PWRS.

Computer Command Subsystem

Purpose

The computer command subsystem was a special purpose digital computer designed to control the Viking orbiter. The CCS issued VO commands from any one of three sources. Commands were issued upon immediate request from the ground, from timed events loaded into memory, and in response to interrupts received from the spacecraft subsystems. Timed events were issued on hours, seconds, and centisecond resolutions.

Hardware

The CCS was configured as a block redundant computer. Each half of the subsystem was an independent special purpose computer containing a power supply, a processor, a memory, and an output unit. All inputs were applied to both halves of the CCS; either half was capable of providing all mission requirements. The utilization of a dual computer provided both redundancy and extended command capability. The two processors operated asynchronously, and could be programmed to perform different functions simultaneously. When critical command outputs were required, the processor could be operated in a tandem or parallel mode. A functional block diagram of the CCS is shown in figure 104. The VO provided 2.4-kHz power, 2.4-kHz timing, and data in the form of interrupts (pulses) or levels (binary data) to the CCS. The CCS issued CC's and DC's to command the other subsystems. In addition, each output unit provided a FDS telemetry channel with CCS data and status. The processors operated independently; however, their outputs were cross-connected between the two halves of the CCS to allow both processors when enabled to access either output unit. The processors also exchanged data words by using an output unit as the exchange media. A control signal was exchanged by the processors, allowing one processor to disable the other processor's output unit access, to prevent a defective processor from issuing extraneous commands to the spacecraft. The mission was flown with each processor required to pass a hardware and software self-test to remove the clamp in order to gain access to its output unit and issue a command. Once removed the clamp stayed off for two 1-sec pulses.

Processor.- The CCS processor was a binary serial arithmetic processing machine with parallel memory data transfer. The processor was composed of a central processor, an interrupt processor, a clock, and a timing generator. A functional block diagram of the processor is shown in figure 105. The central processor executed the software program by using a repertoire of 64 instructions, controlled the output units, and monitored itself for internal errors. The interrupt processor received the interrupts and level inputs from the VO sub systems and from within the CCS, established their priorities, and made them available to the central processor for execution of the associated software program. The clock derived timekeeping pulses for the CCS from the 2.4-kHz power input via the CCS power supply. The timing generator contained a 4-MHz oscillator and frequency countdown to provide the processor, memory, and output unit

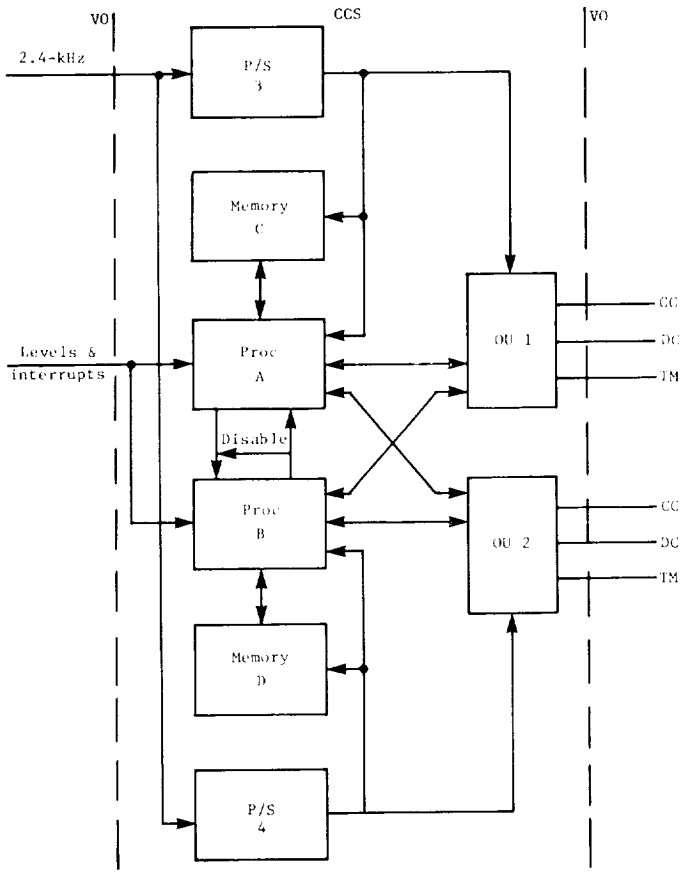

Figure 104.- Functional block diagram of CCS.

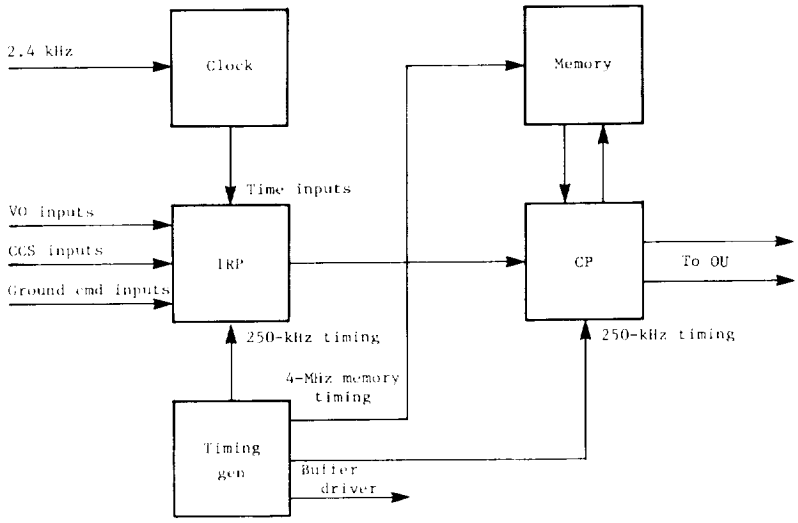

Figure 105.- Functional block diagram of processor.

with the required clocking pulses. The processor clock, in conjunction with software routines, provided a time accounting system with resolution of 100 PPS, 1 PPS, and 1 PPH for the CCS. The timing generator consisted of a 4 ± 1 MHz oscillator and countdown chain. It supplied the clocking pulses required to perform instruction execution and input/output buffer switching. The interrupt processor provided isolation buffers for all external interrupts and level inputs. The level inputs were sampled and provided to the central processor for input by the software program. In addition, they were change monitored and set for internal interrupts to alert the processor when an external level had changed state. The sampled external interrupts and the internal CCS interrupts were scanned once for each central processor instruction cycle. The central processor was alerted to the presence of an interrupt and presented with the memory trap address of the highest priority interrupt that was set. Fifteen external interrupt inputs to the CCS processor were primarily used for counting external events and syncing inputs from external events. (See table 31.) Thirty-two level inputs to the CCS were available; however, only 24 of these inputs were used. These levels, of which 8 were internal level signals were represented by a 4 column by 8 row matrix as shown in table 32. Level inputs were binary data and were constantly available to the central processor for use by the software program. Internal interrupts consisted primarily of error, timing, and machine housekeeping data, and internal levels consisted of error indicators and output unit to processor communication. The interrupt processor provided the central processor with a trap address of the highest priority interrupt present, an alert that an interrupt was present, an alert that a counting interrupt was present, and an error interrupt present signal. The central processor interrupt control used these inputs in determining the processor's response to the interrupt. The central processor executed the instruction set in the sequence specified by the software program. In addition, it provided the input/output interfaces to the output unit, provided internal monitoring (error interrupt), and provided a self test feature. The central processor contained eight registers: accumulator; program counter; link register; condition code register; memory address register; interrupt, mask, and dump register; memory data register; and instruction register. The accumulator was an 18-bit register used as a source of one operand and destination of the result of arithmetic and logical operations. In addition, the accumulator was used as a single-word buffer for data transmission during input/output operations. The program counter held the address of the instruction to be fetched for the program which was running. The link register was used to hold subroutine return addresses. Whenever a successful transfer occurred, the program counter was loaded into the link register; thus, the return address to the program which was transferred was saved. The condition code was a four-bit register which indicated various kinds of status information. The condition code was set by all arithmetic and logical instructions except increment address. The memory address register was used to hold an address when memory was to be accessed. The most significant two bits were used to determine access checking as determined by jumper wires. The interrupt, mask, and dump register was used together to determine the highest priority interrupt awaiting processing. The actual hardware implementation was organized as four groups of eight interrupts. Functionally, however, the interrupts were considered as two groups of sixteen interrupts. The memory data register was used to hold a memory data word which was read from and

TABLE 31.- CCS INTERRUPTS

1*	Internal error
2	Accelerometer pulses
3*	100 PPS
4	Tape index increment DTR A
5	Tape index decrement DTR A
6	Tape index increment DTR B
7	Tape index decrement DTR B
8*	1 PPS
9*	External level 1
10*	Zero reached by interrupts 2-8
11	FDS low-rate frame start
12	FDS low-rate bit sync
13*	OU 1 TM available
14*	OU 2 TM available
15	Command initiate - change in lock (primary)
16	Command sync - bit timing (primary)
17*	Command error (secondary)
18	Command initiate - change in lock (secondary)
19	Command sync - bit timing (secondary)
20*	Reject
21*	Demand read
22*	Initiate read
23*	Output unit available
24	VIS A frame start
25	VIS B frame start
26*	1 PPH
27*	External level 2
28*	External level 3
29*	External level 4
30*	External level 5
31	BOT/EOT DTR A
32	BOT/EOT DTR B

*Internally generated signal.

TABLE 32.- CCS LEVEL INPUTS

Row \ Column	1 (a)	2 (a)	3	4
1	Cmd data (P)	Cmd data (S)	FDS LR data	Spare
2	[b]Cmd error (P)	[b]CCS error	[b]Pwr fail	[b]Other TD tripped
3	Pressurant reg failure	[c]ACE pwr CO	Spare	Spare
4	[c]VO/VL sep	Spare	Lo exc pwr	Lo TWTA pwr
5	Bat 1 hi-temp interrupt	Bat 2 hi-temp interrupt	4000-bps in-lock ind	16 000-bps in-lock ind
6	Canopus acq	SG sig to CCS	Share mode 1	Share mode 2
7	Spare	Spare	Spare	Spare
8	[b]Transfer to OU 1	[b]Transfer to OU 2	[b]OU 1 available	[b]OU 2 available

[a]P denotes primary which is proc A to CDU A or proc B to CDU B; S denotes secondary which is proc A to CDU B or proc B to CDU A.
[b]Internally generated signal.
[c]Complemented signal.

written into the memory in parallel. This register was used as a buffer register between the processor and memory. The instruction register was used to hold the six OP code bits for instruction decoding and two control bits. The OP code was loaded into six bits of the instruction register in parallel at bit time C or bit time E of an execute instruction. The processor instruction repertoire consisted of 64 instructions. There were 16 immediate instructions, 28 direct instructions, 16 indirect instructions, 2 I/O instructions, and the execute and wait instruction.

CCS memory.- The CCS memory consisted of a 0.125-mm (5-mil) plated-wire memory stack with associated read/write electronics to provide storage for 4096 18-bit words. Each quarter of the memory may be separately controlled (by external wiring) to be read only, write protected, or read/write. In the CCS configuration, the lower half of memory was write protected, requiring that a special instruction be executed by the processor prior to any write initiating instructions addressed to this area. The upper half of memory was configured read/write. The memory stack used was a 1024 word by 80-bit 0.127-mm (5-mil) plated-wire memory. There were 4 groups of 32 words per plane and a total of 8 planes per stack. Each word was accessible via a 32 by 32 (x-y) diode matrix. Of the 80 bits per word, 72 were used to obtain 4 groups of 18 bits (processor words). The selection of processor words was accomplished by the sense amplifier/digit drive circuits from the 72 pairs of sense lines provided.

Output unit.- The CCS output unit was a special purpose input-output device for the processors. It served the dual purpose of interprocessor communications and CCS to VO output interface. The interprocessor communication function was used to pass 18-bit data words between processors. The CCS VO output interface was used by the processors to issue discrete and coded commands to the VO. In addition, the output unit provided the telemetry output for the CCS. The output units issued either coded or discrete commands to the rest of the VO. Coded commands were 14-bit data words issued serially to the other subsystems at a rate of 1.2 kHz and synchronous with the VO power frequency. A CC consisted of three signal outputs: one in the CC enable that provided an envelope which surrounded the CC transmission; the second in the actual data stream; and the third output, a stroke, was transmitted after the data to initiate the receiving subsystems response to the command. Discrete commands were pulsed outputs over individual wires to other subsystems. Several of the DC commands were used internal to the output unit to set and reset common relays. External DC's consisted of a relay closure for approximately 106 msec. Downlink telemetry words were sent to the FDS from each CCS output unit at regular intervals determined by the FDS rate mode and commutation format. A 28-bit CCS telemetry word was removed in four samples of 7 bits each. When the 28th bit had been removed, another word was loaded into the telemetry register.

Flight Data Subsystem

Purpose and Function

The FDS provided the VO with the primary source for central timing and controlled, collected, and formatted both science and engineering data. Reference frequencies were supplied to the MDS, DSS, PWRS, and IRTMS. The FDS

controlled and sequenced the science instruments. The FDS also collected both science and engineering data and formatted these data into serial bit streams. The FDS performed analog-to-digital conversion, signal conditioning, and digital data processing as required. The data were sent to the MDS for real-time transmission to Earth or to the DSS for temporary storage.

Figure 106 is a simplified functional block diagram of the FDS. The FDS consisted of six major functional sections: timing and control block, engineering data block, infrared science data block, visual imaging data block, memory block, and power conversion block.

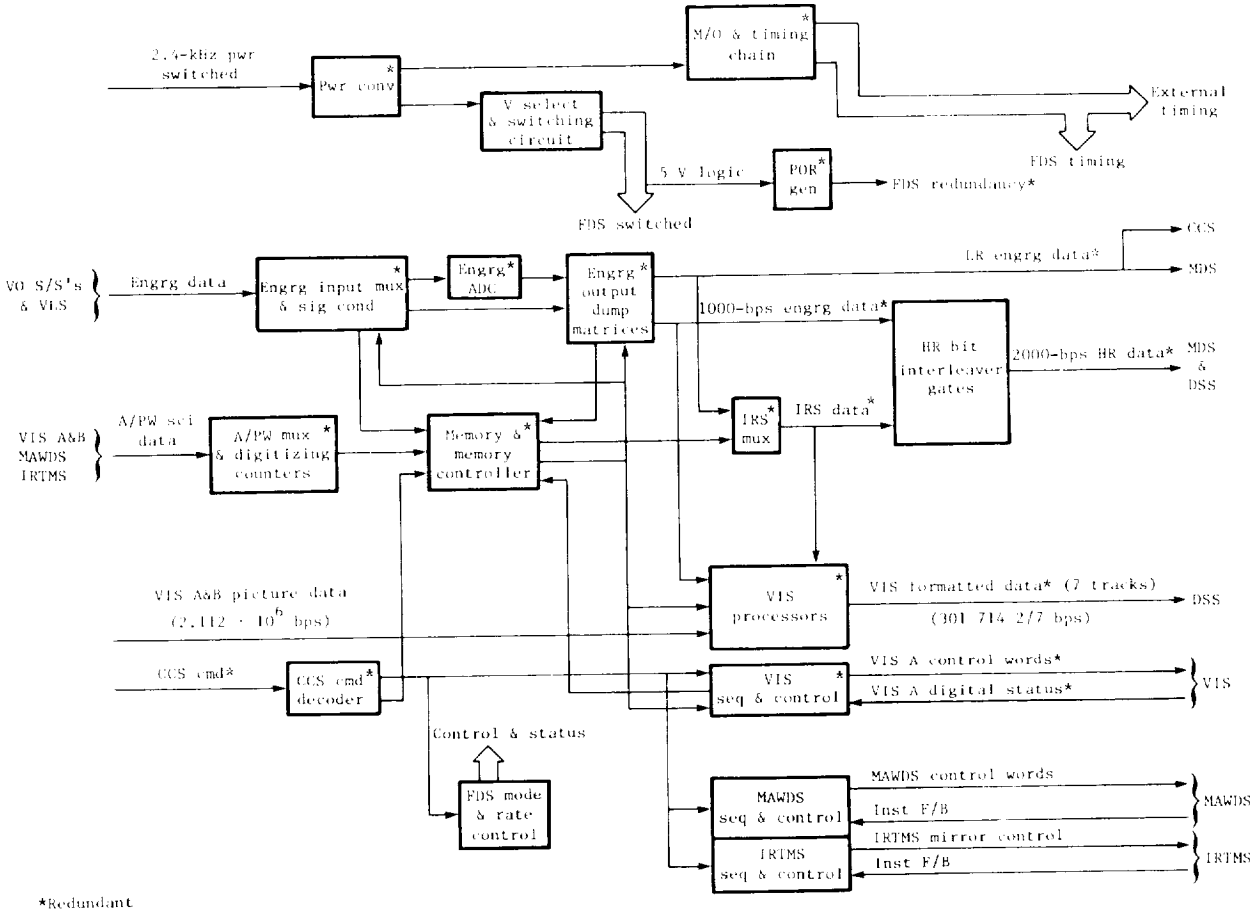

Figure 106.- Simplified functional block diagram of FDS.

Description

Timing and control block.- The timing and control block included the redundant oscillators, timing chains, and coded command decoding logic; the engineering sequencing and control logic; the science sequencing and control logic; and the power-on reset circuitry.

Engineering data block.- The circuits of the engineering data block performed digital and analog measurements that could be made at relatively low rates with no more than 7-bit accuracy. For the most part, the measurements consisted of the following four types:

External shift register: The subsystem being measured contained a register that was shifted out by the FDS.

Bilevel: The subsystem being measured sent a logic voltage level (either a 1 or a 0) that was sampled by the FDS.

Timer: The subsystem being measured sent a pulse that was used by the FDS to gate a signal of a known frequency into a counter.

Counter: The subsystem being measured sent pulses that incremented a counter in the FDS.

Analog engineering measurements consisted of the following four basic types:

Voltage measurements: The subsystem being measured sent a signal to the FDS in one of three voltage ranges: 0 to 100 mV, -1.5 to 1.5 V, and 0 to 3 V.

Strain-gage pressure measurements: The FDS produced signal levels of 12 and -12 V that excited a pressure sensor bridge in the subsystem being measured. The pressure sensors, in turn, sent back to the FDS the signal to be measured. This signal was conditioned-amplified and isolated. The signal level was from 0 to 3 V.

Potentiometric pressure and position measurements: The FDS sent a 3-V reference signal to the subsystem being measured. The 3-V reference appeared across a voltage divider whose ratio was related to pressure or to position. The output of the voltage divider was from 0 to 3 V.

Temperature measurements: The FDS generated a constant current of 1.0 mA that was sent to the temperature sensor in the subsystem to be measured. The temperature sensor produced an output voltage of 500 to 600 mV, which was measured across a sensor resistor divider network.

Accuracies of analog measurements, from the input to the FDS to the output of the ADC, were ±1 percent of full scale for all 0 to 3 V signals, ±1 percent of full scale for all -1.5 to 1.5 V signals, ±3 percent of full scale for 0 to 100 mV signals, and ±3 percent of full scale for all 500 to 600 mV signals (temperature measurements). These accuracies were maintained under all specified environmental conditions encountered in the lifetime of the mission. The accuracy specifications did not include measurement error attributed to the nonzero source impedance of the voltage to be measured by the FDS. Input impedance of the analog measurement circuits of the FDS was greater than 1 MΩ. Since the source impedance was maintained by the subsystem being measured, the associated error was not regulated by the FDS. However, the effect of this error was minimized through measurement calibration during spacecraft assembly. Each engineering analog measurement was converted into a 7-bit digital word for

a range of 0 to 127 DN. Therefore, each word had a maximum resolution of 1/127 (0.787 percent). Zero DN corresponded to the most negative value for each of the 4 voltage ranges. At 0.5 DN equivalent input voltage, the FDS output changed from 0 to 1 DN.

Each of the two analog commutators, A and B, provided a programmable link between the many channels of analog data and the analog-to-digital converters. With the 8-bit commutator register, 256 locations were possible. Of these 256 locations, 32 were used for digital information, leaving 224 analog locations. These analog locations were divided between two identical analog commutators that operated independently for redundancy.

Infrared science data block.- The IRS multiplexers assembled the IRS format. Two identical redundant outputs were generated by separate FDS hardware to be bit-interleaved with 1000 bps engineering data (or all 1's) and transmitted to DSS and MDS and also to be embedded into the VIS ID (TV flyback) data. Most of the IRS format was buffered in FDS memory and was generated, already multiplexed, by reading the memory at appropriate times. The IRS format was produced in 56 5-bit bytes. Forty-five of these bytes were read from memory, where each was a separate memory word: 10 bytes originate in hardware; 1 byte is spare. The A/PW data sources - MAWDS, VIS A and B, and IRTMS - were interlaced in time to enable all four of them to be counted in the same hardware. Two redundant counters were used, one associated with each memory and hence with each multiplexer. VIS and IRTMS A/PW converters processed bipolar data. The counters were implemented to produce sign-and-magnitude outputs. A total of 10 bits was allocated. The sign bit was developed by a polarity latch, and 9 bits of data were taken from the counter proper. A clock rate of 528 kHz was used to scale the data into a 9-bit number. A counter latched at nine 1's to prevent overflow ambiguity for off-scale measurements. MAWDS A/PW handled unipolar data only. All 10 output bits were used for magnitude and came from the counter. A clock rate of 1.056 mHz was used to scale the data into a 10-bit number. The counter latched at ten 1's to prevent overflow ambiguity. It latched at all 0's when the incoming data were zero or negative. The gated A/PW count clock was routed to the MAWDS integrator of the MAWDS sequence and control logic circuits. The low-rate engineering data were embedded into the science format. Engineering data A were embedded in science data A and engineering data B in science data B. Additionally, the required FDS status information to identify the number of new bits was also included. The engineering data (8 1/3 and 33 1/3 bps) resulted in either 2/3 or 9/10 data bits in each IRS minor frame. The engineering data bits were counted in a 1-bit counter, and the resulting parity bit was included as part of the FDS data rate in the FDS status word. FDS, MAWDS, and IRTMS digital words were obtained from various bits originating within the subsystem or the FDS control logic and were multiplexed into the IRS formats. The FDS status word was multiplexed redundantly, A into IRS mux A, and B into IRS mux B. MAWDS and IRTMS digital data were nonredundant, and therefore each status bit was routed to both multiplexers. The high-rate data outputs were controlled by the high-rate gating and control circuitry. The 1000-bps IRS data and the 1000-bps engineering data were bit-interleaved to produce 2000-bps high-rate data. When the engineering data rate was 8 1/3 or 33 1/3 bps, the 1000-bps engineering data consisted of all 1's. The control information for the output of the high-rate multiplexer was

contained in the data rate bits of the coded command of the engineering data control CCS.

Visual imaging data block.- The visual imaging data block received 2.112-mHz data from the VIS ADC. It processed these data from serial format to seven tracks of parallel data suitable for recording on the DTR. The logic circuit that performed this function consisted mainly of steering logic and rate buffering and is referred to herein as the VIS processor. Processed data on the seven tracks to the DSS occurred at a rate of 301 714 2/7 bps (per track). A single VIS line format required 4 8/33 msec to send and contained 1280 bits. Except for track ID, the first 76 bits of the format for a given VIS line were the same for all seven tracks. Bits 77 through 1280 on each track were the binary values for 172 7-bit pixels, MSB first. Each VIS line contained 1204 pixels, one-seventh of which went on each of the seven tracks to each DTR. The two sets of outputs to the two DTR's were identical and redundant. VIS data were received from each camera ADC simultaneously and continuously. Since the cameras were used alternately, only one of these data streams was processed; the other was discarded. Two identical processors handled the VIS data redundantly. Processor A furnished seven tracks of output data for DTR A; processor B served DTR B.

Memory block.- The memory block encompassed two identical plated-wire memories and two associated memory controllers. Each memory provided random access storage and retrieval of 1024 words of digital data, for a total of 2048 words of 8 bits each. The memories were mounted on a common subchassis but were otherwise completely separate and independent. The memories operated in complete synchronism. Each memory included the plated-wire mats and all associated electronics but excluded power conversion and power conditioning. Address bits and data to and from either memory were transferred in parallel. The memories were interrogated without destroying the stored data. Stored data did not change as a result of power interruptions. Normal operation of the memory was inhibited by internal circuitry when any of the supply voltages were outside of predetermined tolerance limits, approximately ±6 to ±8 percent. If this condition occurred during a read or write cycle, the memory completed the cycle properly.

Power conversion block.- The power conversion block included two identical power converters, each of which converted the 2.4-kHz input power to the specific voltages required to operate the FDS circuits, logic, relays, and memories. The power converter function also included relay switching for the outputs of the power converters. The two power converters were used as a redundant set where one was active and the other was standby redundant. Switching of the power input from one converter to the other was controlled by the power subsystem to guarantee that only one power converter was on at any one time and when power was switched off then on again, the power converter last used came back on.

Data Modes, Rates, and Formats

The FDS supplies data to the TMU of the MDS over two pairs of transmission lines. One pair furnished low-rate data, while the other pair supplied high-

rate data. The low-rate data were also supplied to the CCS via a single line to both CCS processors. High-rate data and VIS data were also supplied to the DSS for recording.

Orbiter time.- The fundamental interval in the FDS was the 280-msec period for IRS data minor frame. The count of these 280-msec periods was called VO time. The IRS data format contained a 30-bit VO time word. The length of this word allowed a maximum counting time of 3479.9 days (approximately 116 mo) before repeating. The 30-bit VO time word was contained in both FDS nondestructive memories and could be reprogrammed to any desired count.

Engineering data.- Figure 107 illustrates the basic engineering format structure which was used for all four rates (engineering A at 1000 bps, engineering B at 33 1/3 bps, engineering C at 8 1/3 bps, and engineering D at 8 1/3 bps) and for all five engineering formats (AI (launch), AII (cruise), BI (maneuver), and BII (orbit) programmable formats and a fixed format). Each word in the format was 7 bits long and was read out MSB first. A minor frame (from sync word to sync word) was 32 words long. A major frame was defined as one pass through the 400 deck. At the completion of a major data frame, each 400 deck position had been sampled 1 time; each 300 deck, 2 times; each 200 deck, 16 times; and each 100 deck, 128 times. Because of cummutation limitations, less than the total number of measurements could be commutated at any one time for a given format. Table 33 gives the sampling intervals for each rate.

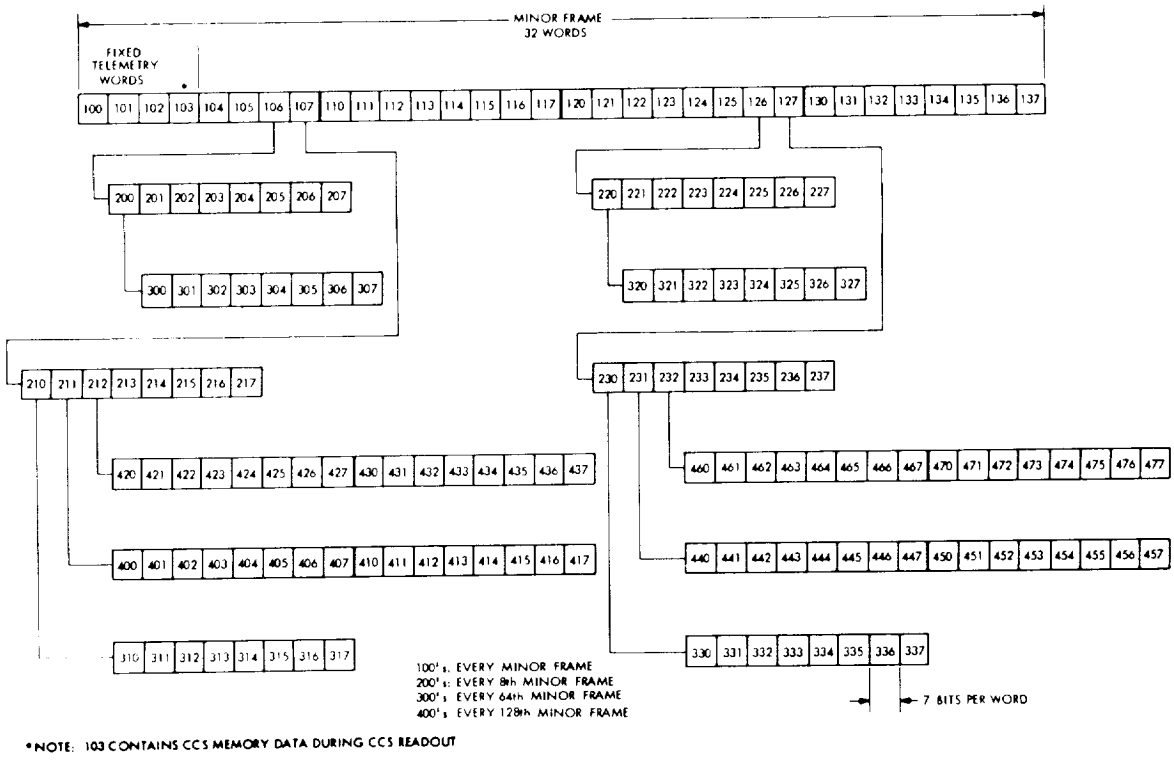

Figure 107.- FDS basic engineering format structure.

TABLE 33.- SAMPLING INTERVALS FOR EACH RATE

Deck	Sampling interval for -			
	Engrg D (8 1/3 bps)	Engrg C (8 1/3 bps)	Engrg B (33 1/3 bps)	Engrg A (1000 bps)
100	26.880 sec	26.880 sec	6.720 sec	0.224 sec
200	215.040 sec (3.6 min)	215.040 sec (3.6 min)	53.760 sec	1.792 sec
300	1720.320 sec (28.7 min)	1720.320 sec (28.7 min)	430.080 sec (7.2 min)	14.336 sec
400	3440.640 sec (57.3 min)	3440.640 sec (57.3 min)	860.160 sec (14.3 min)	28.672 sec

IRS data.- The 1000-bps IRS data were available to the MDS high-rate channel. The data were also routed to track 8 of both digital tape recorders for recording and subsequent playback. Two IRS data sources were formed and supplied to the MDS and DSS. There were 139 measurements allocated for the IRS data. Included were engineering data which were sampled frequently enough to include all measurements for data rates up to 33 1/3 bps, VO time, FDS memory readout, VIS commanded state, VIS actual state, and VIS A/PW data as well as the IRTMS and MAWDS status and A/PW data. Figure 108 is a block diagram of the IRS data format. An IRS minor frame consisted of 280 bits (28 10-bit words); an IRS major frame consisted of 4480 bits (448 10-bit words), which was 16 IRS minor frames. MAWDS engineering measurements were sampled once, IRTMS measurements were sampled 4 times, and MAWDS science measurements were sampled 15 times. VIS digital and VIS A/PW were sampled once out of every two consecutive IR science major frames. Each MAWDS telemetry measurement was represented as a 10-bit word (0 to 1023 DN); therefore, the maximum resolution of 1/1023 (±0.098 percent) was available. IRTMS and VIS engineering telemetry measurements were 9 bits plus the sign, for a maximum resolution of 1/511 (±0.196 percent).

Relationship of IRS data to engineering data.- Since the FDS was a synchronous system, a definite relationship existed between IRS and engineering data outputs. Some of these relationships were as follows:

66 VIS frames equal 1 IRS minor frame

4 IRS minor frames equal 5 engineering minor frames (1000 bps)

24 IRS minor frames equal 1 engineering minor frame (33 1/3 bps)

96 IRS minor frames equal 1 engineering minor frame (8 1/3 bps)

VIS data.- VIS telemetry data were routed to the DSS only. All line-retrace data plus every 7th pixel were routed to each of seven tracks of both TR's. Six status words were assigned as carriers for line-retrace (flyback) data. Additionally, 5 bits were used for IRS data, and this was adequate to

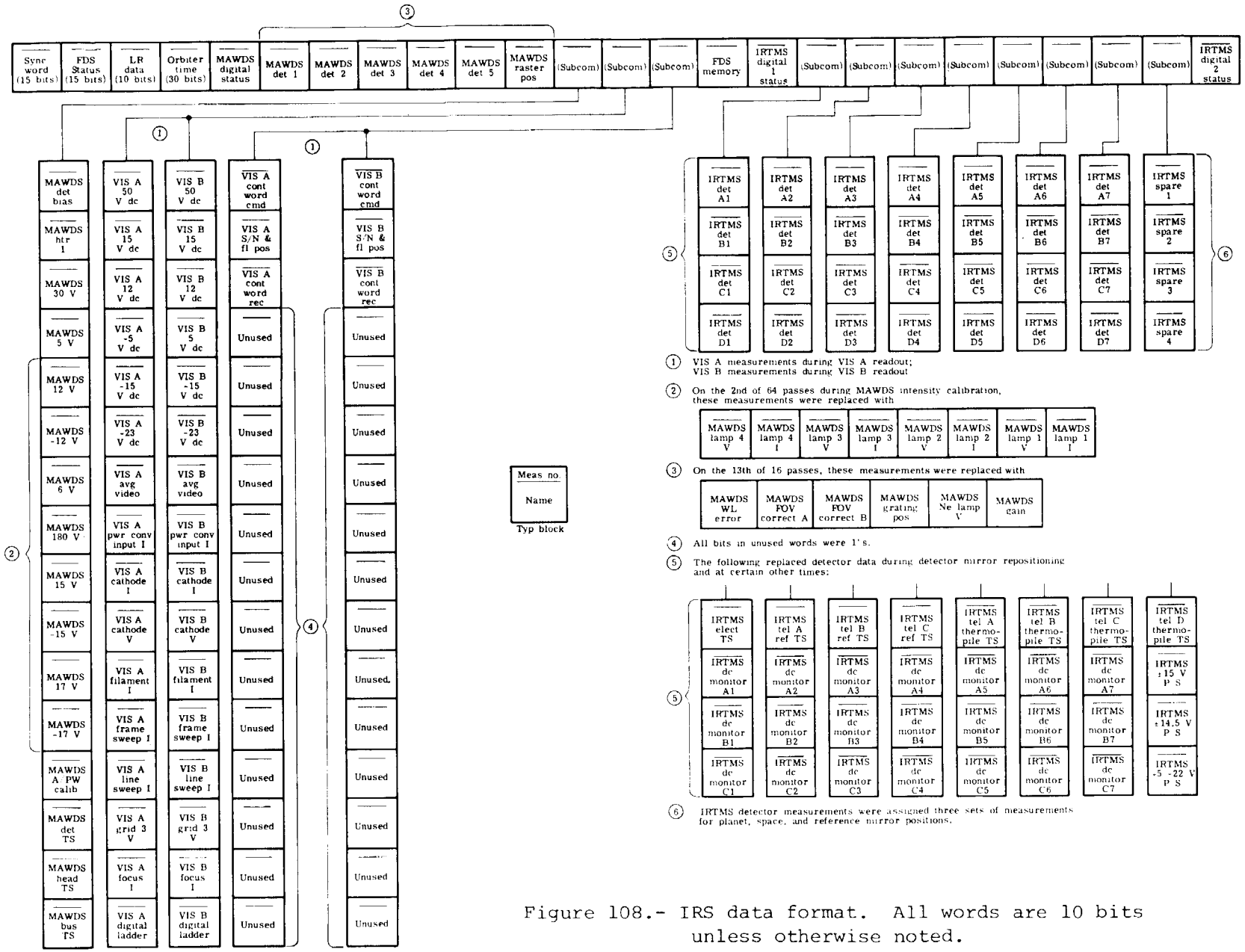

Figure 108.- IRS data format. All words are 10 bits unless otherwise noted.

include all IRS data at 1000 bps. Another 5 bits were used for engineering data, which include all engineering data at 1000 bps. Figure 109 is a block diagram of VIS data. Included is a partial list of 7-bit pixels with a table indicating the routing to DSS for each line. The routing pattern for each subsequent line was identical. This provided the capability to produce a low-resolution picture with the playback of one DTR track. A VIS data frame to DSS consisted of 1280 bits. These bits were allocated as follows: 66 bits for digital data, 5 bits for high-rate engineering, 5 bits for IRS data, and 172 7-bit pixels. Seven VIS data frames (on seven tape recorder tracks) corresponded to one VIS line (1204 pixels). It required 1056 VIS lines to complete a VIS picture frame. The VIS data rate was 2.112×10^6 bps. The bit rate to each DSS track was 301 714 2/7 bps.

Sequence and Control

IRTMS.- Functions to the IRTMS had a basic cycle time of 1.12 sec. During this 1.12-sec period, the FDS measured the 32 IRTMS science channels by means of an A/PW converter within the IRTMS. Control of the analog voltage input to the A/PW converter was provided by multiplexer stepping and multiplexer resetting pulses sent to the IRTMS. At certain fixed times, when the mirror was between the three positions of interest, housekeeping data were substituted in place of the science data; however, this substitution was not controlled directly by the FDS. The IRTMS scan mirror was controlled in one of two possible modes by the FDS. It was fixed in either the reference, space, or planet positions in the fixed mode or it was sequenced in the normal mode. In the normal mode, a desired-position sequence was continuously generated by the FDS. The mode was controlled by information in a coded command sent from CCS to FDS. If the mode position (fixed or sequenced) did not agree with the IRTMS mirror position readout, a series of IRTMS mirror step pulses were sent to the IRTMS. The position readout was compared with the mode position once every 40 msec.

MAWDS.- Functions to the MAWDS had a basic cycle time of 4.48 sec, the time interval between two trailing edges of successive MAWDS raster reset pulses. During the 4.48-sec interval, the FDS measured a 16-sample sequence of MAWDS data, where each sample consisted of a burst of seven measurements. These measurements were performed by means of an A/PW converter within the MAWDS. Control of the analog voltage input to the A/PW converter was provided by multiplexer stepping and multiplexer resetting pulses sent to the MAWDS from the FDS. These signals, as well as the remaining interface signals that were continuous and not controllable by command, are not defined and discussed in detail in this section. They are mentioned only in their relationship to the functions that were controllable by command. These noncommandable signals were as follows:

Raster step
Multiplexer step
Raster reset
MAWDS control
A/PW read

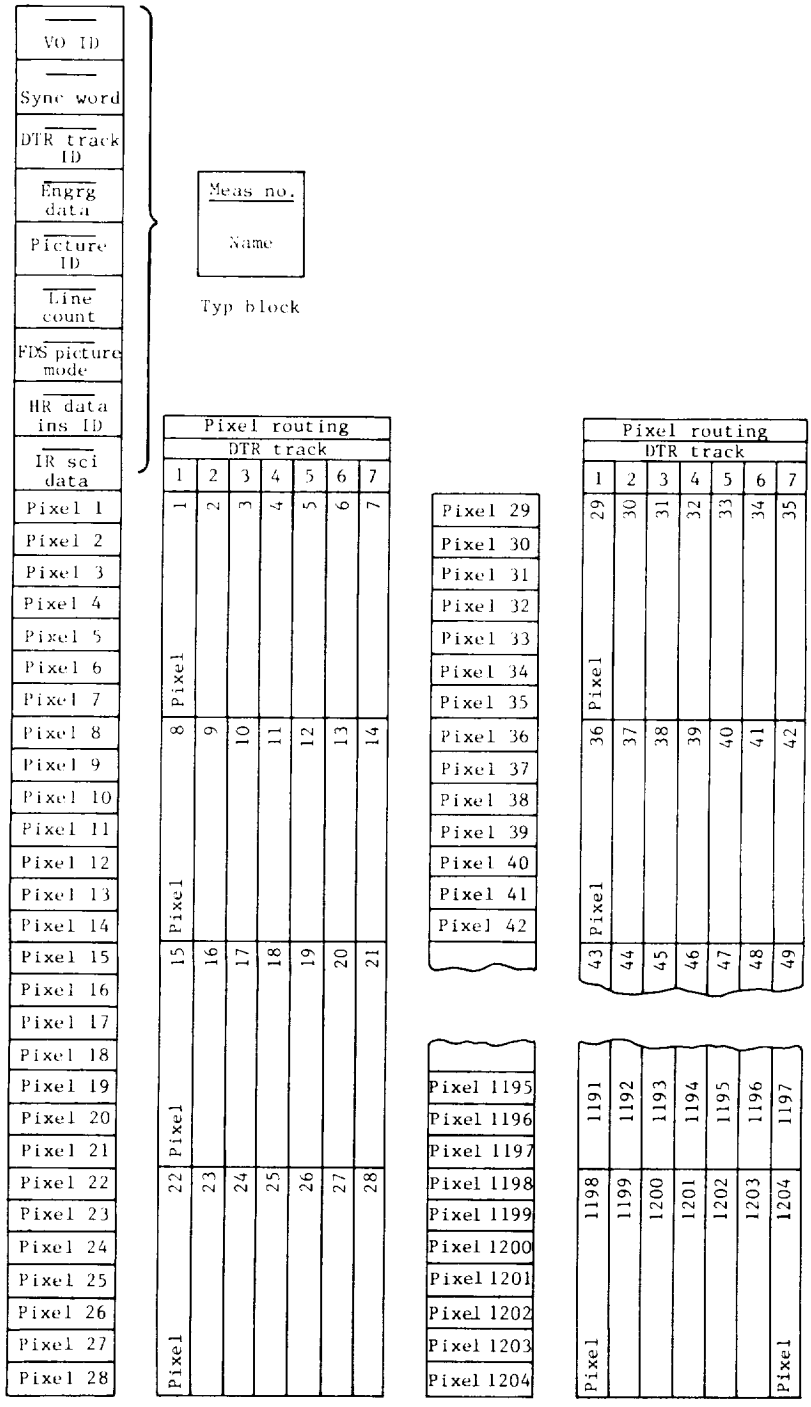

Figure 109.- VIS telemetry format.

The functions that were controllable by command were those that were controlled by information contained in the data of the MAWDS control word, which was serially sent to MAWDS every 4.48 sec. The contents of the MAWDS control word were, in turn, alterable by the contents of the CCS coded MAWDS state select command. A second command, the CCS coded IRS calibrate command, was used to generate a MAWDS intensity calibrate initiate flag in the MAWDS control word. It also reset a counter such that a MAWDS intensity calibrate initiate flag was issued every 66th raster thereafter. The MAWDS intensity calibrate initiate flag was also sent to the IRTMS desired sequence generator for synchronization of the IRTMS desired position sequence with the MAWDS intensity calibrate generation.

VIS.- VIS sequence and control consisted of the VIS state mode control, the parameter buffer, and the memory selector. The VIS state mode control logic controlled the picture-taking sequence of the VIS with respect to the number of pictures taken. The VIS A and B parameter buffers provided rate-buffering of data exchanges between memory controller A and/or B and VIS A and B. Either memory controller could interface with both VIS's. The memory selection logic received and decoded commands involving several functions which ultimately resulted in the appropriate determination of either A or B level selections. The major portion of the control of VIS was provided by two serial digital control words which contained the parameters for the respective VIS cameras. These control words were transmitted to their respective cameras at alternating 4.48-sec intervals. If a picture sequence had not been commanded, the control word consisted of nominal parameters that conditioned the cameras, but normally did not specify the shuttering of a picture. If a picture sequence had been commanded, the control word provided the correct filter position control, engineering electronics control, and shutter time for the upcoming picture sequence.

Attitude Control Subsystem

Purpose and Function

The ACS provided S/C stabilization and orientation from the time of S/C separation from the Titan-Centaur launch vehicle throughout the mission. Specifically, the objectives of ACS were to execute the following functions:

Reduçe the initial rates after S/C separation from the launch vehicle and acquire the celestial references (Sun and Canopus)

Automatically reacquire (in conjunction with the CCS) celestial references if one or the other (but not both simultaneously) was lost

Maintain the correct S/C attitude during all mission phases following initial acquisition of celestial references

Perform commanded turns of the S/C to any desired orientation relative to the celestial references

Control S/C attitude and thrust vector orientation during propulsive maneuvers

Provide control with respect to celestial references for Lander initialization and inertial control during Lander separation

Description

A simplified block diagram of the ACS is shown in figure 110. The ACS is shown within the dashed line. Intrasubsystem and intersubsystem interfaces related to the functioning of the ACS are also shown. The ACS consisted of the following assemblies: ACQ SS's, CR SS's, SG, CT, IRU's, ACE's, RCA's, and GA's. These assemblies are briefly described as follows:

Acquisition Sun sensors: The ACQ SS assembly consisted of four nonredundant identical subassemblies. One subassembly was mounted on each of the four solar panel tips. The ACQ SS provided pitch and yaw control signals. They had a combined unobstructed 4π sr FOV.

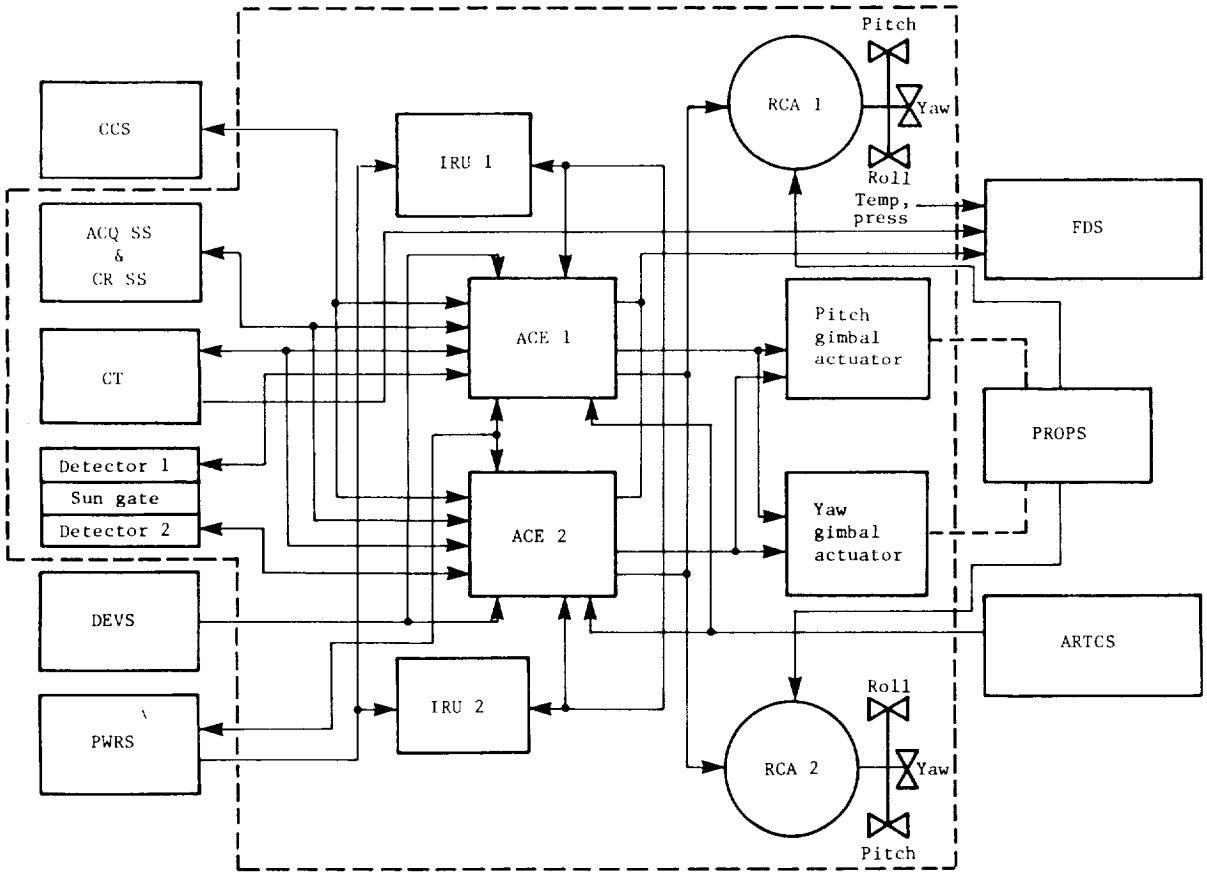

Figure 110.- Simplified block diagram of ACS.

Cruise Sun sensors: The CR SS's were mounted in a single nonredundant assembly on the solar panel outrigger. The CR SS provided pitch and yaw control signals. The CR SS had a FOV which exceeded that of the SG.

Sun gate: The SG was a single assembly with redundant detectors mounted on the solar panel outrigger. One detector was associated with each ACE. The signal generated by the SG was used to identify a Sun-acquired logic state.

Canopus tracker: The CT consisted of a single nonredundant assembly mounted on the VO bus. The CT provided a roll axis control signal and a star intensity signal used for star identification.

Inertial reference unit: The ACS had two identical IRU's. One IRU was required at any given time for control, the other provided standby redundancy. The IRU provided rate and position signals in pitch, yaw, and roll and an acceleration signal in roll. Each IRU consisted of an ISS and an IES. The ISS contained three single-axis rate integrating gyroscopes and one pendulous rebalanced accelerometer. The IES provided gyro and accelerometer control loops for the ISS. Position information was generated in the IES by integrating gyro rate.

Attitude control electronics: The ACS had two identical ACE's. Only one ACE was used at any given time for control, the other provided standby redundancy. The ACE contained the RCA electronics, TVC electronics, and control logic. The RCA electronics controlled the operation of the jet valves and consisted of a celestial sensor buffer amplifier, switching amplifier with dead banc and minimum on-time, rate estimator, derived rate circuitry, position and rate select circuits, and jet valve drivers for each axis. The TVC electronics controlled the operation of the GA's and consisted of a preaim circuit, gimbal servo electronics, compensator, gain selection, and enable controls for the pitch and yaw axes. The ACE received a 14-bit command word input from the CCS. The ACE logic, in conjunction with these commands, internally generated logic functions and the ACS enable and scan slew signals, provided direct control over all ACS operating modes.

Reaction control assembly: The ACS had two identical RCA's. In normal operation, the RCA's provided torque couples about each axis. In case of a failure of either assembly, the other assembly provided single jet, bidirectional torque capability about each axis. Each assembly contained an HPM which contained the nitrogen high-pressure vessel, pressure regulator which drops the pressure for the low-pressure modules, leak-test valve, fill valve, relief valve, filter, and temperature and pressure sensors and two LPM's (one for pitch and one for roll/yaw) each of which contained a filter, tubing with convolutions at the solar panel hinge and fold joints, and jet valves.

Gimbal actuator assembly: The ACS had two identical nonredundant GA's which were mounted along axes parallel to the VO X- and Y-axes and were used to rotate the PROPS rocket engine about the pitch and yaw axes. The geometric thrust axis of the PROPS rocket engine was collinear with the VO Z-axis when the GA's were at their center position. (The coordinate systems and their interrelationships are discussed in the section "Coordinate Systems.") Each GA contained a dc motor, ball screw driven shaft, and a shaft position sensor.

Mechanization

The ACS equipment is described below. The physical location of the equipment on the VO is shown in figure 1.

Sun sensors.- The orientations and sign conventions of the Sun sensors are indicated in figure 111. The Sun sensors were optomechanical devices used to orient the VO with respect to the Sun. They consisted of photoconductors with associated housings and apertures providing the necessary optical configurations to perform their respective functions. The ACQ SS consisted of four identical subassemblies, one of which was mounted on the tip of each solar panel. They provided error voltages to drive the VO roll axis into alignment with the Sun line. The 12 acquisition photodetectors (3 per subassembly) were connected to form a bridge circuit with excitation voltage across each leg. The manner in which the detectors were electrically connected and the transfer function of the ACQ SS are shown in figure 112. Unequal illumination of the bridge circuit legs provided analog voltage output error signals for the pitch and yaw axes. The ACQ SS's were positioned so that, after the solar panels were deployed, the Sun would always be visible to at least one detector. This gave the sensors a 4π sr FOV (complete sphere). An ACQ SS set (one for pitch and one for yaw)

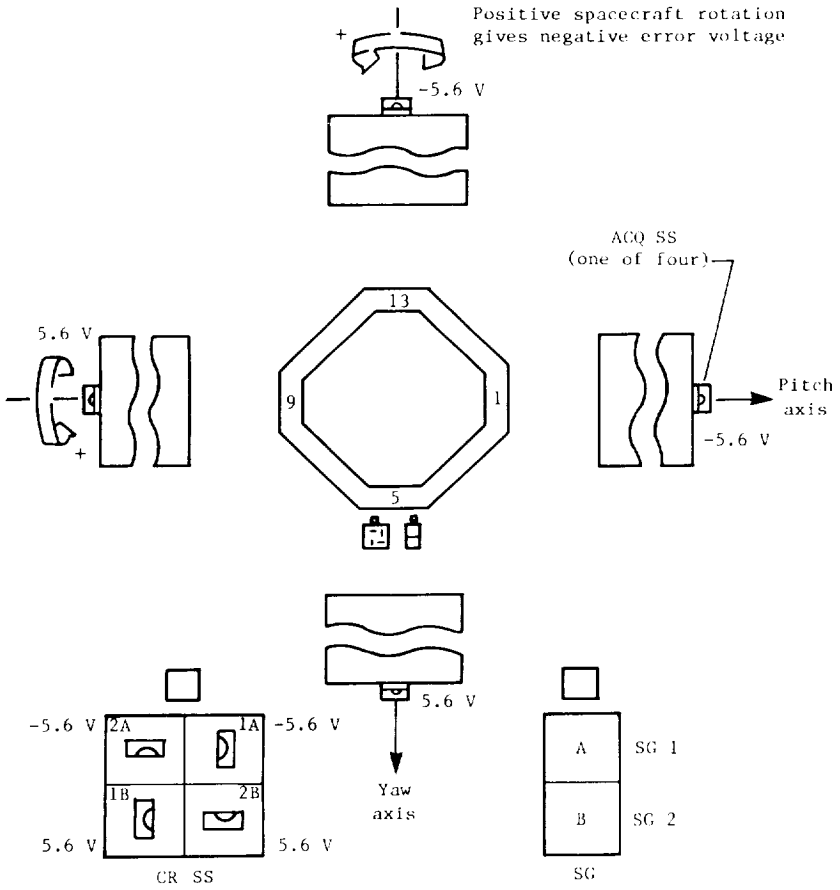

Figure 111.- Orientations and sign conventions of Sun sensors.

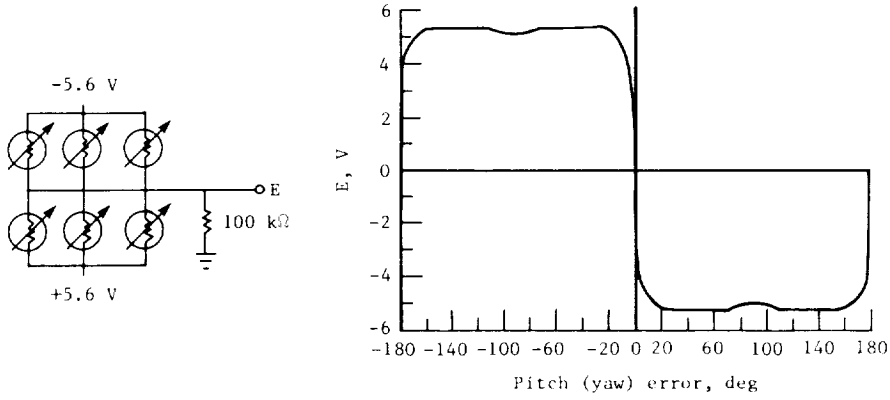

Figure 112.- Transfer function of acquisition Sun sensor.

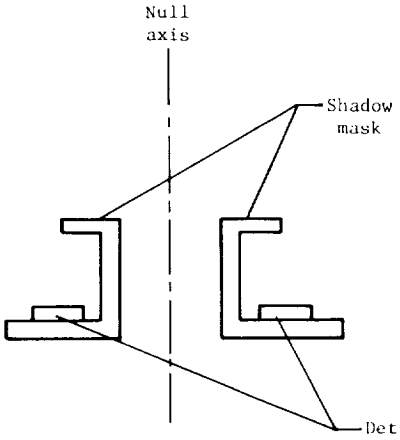

Figure 113.- Sun sensor shadow masks.

consisted of six photoresistors mounted beneath shadow masks. (See fig. 113.) The photoresistors were connected in pairs so that the outputs were proportional to the angular displacement of the sensor null planes from the Sun line. The CR SS consisted of four photodetectors in a single housing on the +Y solar panel outrigger. In a similar manner to the ACQ SS, the photodetectors were connected to form a bridge circuit with excitation voltage across each leg to provide fine pitch and yaw error signals and, because of their configuration, a precise null for VO orientation to the Sun line. The CR SS's were positioned so that their optical axes were parallel to and along the -Z-axis of the VO. A CR SS set consisted of two photoresistors mounted beneath shadow masks. The manner in which the detectors were electrically connected and the transfer function of the CR SS are shown in figure 114. The

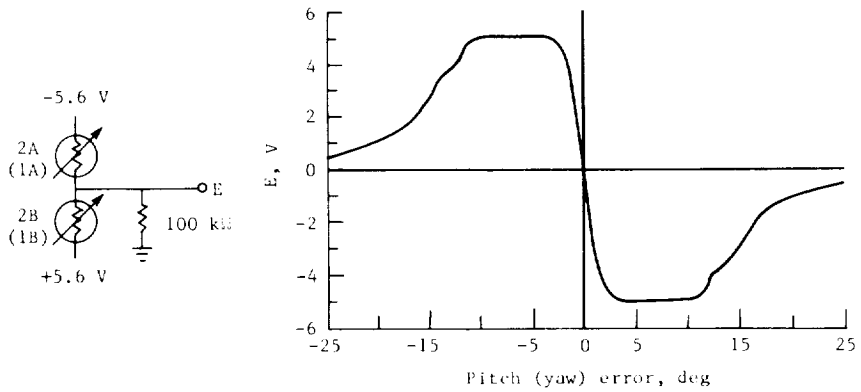

Figure 114.- Transfer function of cruise Sun sensor.

SG was a single assembly with redundant detectors on the +Y solar panel outrigger. One detector was associated with each of the two ACE units. The SG was positioned so that its optical axis was parallel to and along the -Z-axis of the VO. The SG was used to sense the presence of the Sun when the desired VO orientation relative to the Sun had nearly been achieved. Two photodetectors and associated shadow masks are housed in each SG assembly, providing parallel redundancy. Each detector consisted of a photoresistor masked so that it was sensitive to VO cone angle but insensitive to VO clock angle. The SG provided a resistance output varying with angular offset from the Sun line. The resistance of the SG was within the envelope shown in figure 115 for any angle around the optical axis including the effect of solar intensity variations in orbit. The FOV was conical as shown in figure 116. The resistance was less then 149 Ω at 3.5° and greater than 320 kΩ at 6.5°. The SG resistance determined the state of the SGL signal in the ACE. Sun-acquired was nominally indicated by the ACE SGL at 5° half-cone angle. The excitation (±5.6 V dc) for the Sun sensors was supplied by the ACE. Polarities of excitation voltage to the ACQ SS and CR SS were determined by their orientation on the VO as shown in figure 111.

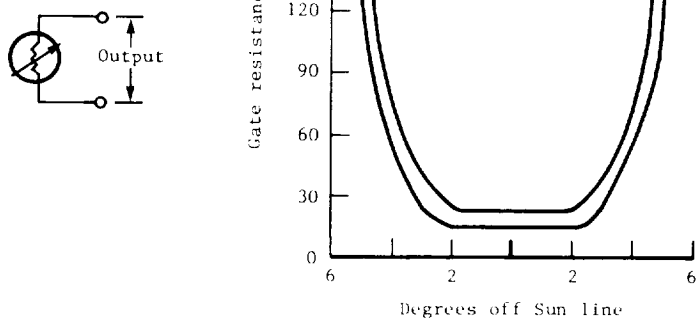

Figure 115.- Resistance of Sun gate.

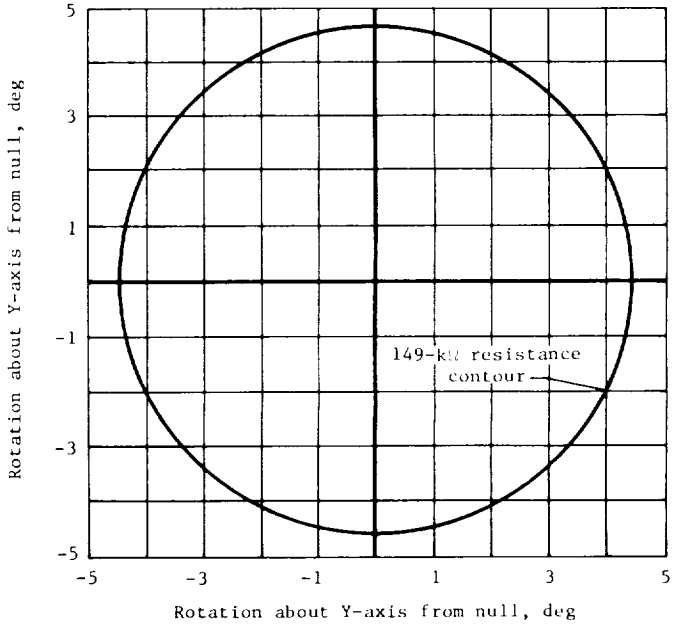

Figure 116.- Sun-gate FOV at 129 klx (12 000 fc).

Canopus tracker.- The CT was an electro-optical device that was designed primarily to provide a single-axis error signal that was proportional to the subtended angle between the line of sight to a star and a reference axis in the mounting plane of the tracker. The images of any objects within the FOV limits were formed by the objective lens on the image dissector tube photocathode. The electron image of the FOV was scanned by the application of a sawtooth voltage to the roll-angle deflection plates in the tube image section. If a

star was within the FOV, this scanning action modulated the resulting electron beam which was then amplified by the dynode multiplier section. Demodulation of this signal, after further amplification, provided a signal whose time-averaged amplitude and polarity were related to the offset of the mean star position from the center of the electron aperture. The current signal was summed in an integrator, amplified, and fed back to the roll-angle deflection plates. This completed a servo loop which nulled the mean star position on the electron aperture plate. The star roll-angle offset was then directly proportional to the offset (tracking) voltage that maintained the null position. This voltage was provided to the ACE as the roll-angle error signal. Star intensity output was obtained directly from the dynode voltage supply through an intensity buffer which regulated slope and amplitude. This signal was provided to the ACE for star discrimination. The cone-angle deflection plates in the image dissector tube were utilized to provide five selectable cone-angle offsets within the total FOV to allow for seasonal variation in cone angle of Canopus. Three coincident level commands sent by the ACE selected the position of the cone angle. A Sun detector, mounted to the baffle assembly, was provided to activate the Sun shutter if the VO became oriented such that the CT FOV approached the Sun line.

CT power (50 V rms, 2.4 kHz, square wave) was supplied from the 2.4-kHz inverter in PWRS through two switches in the ACE. One switch controlled power for Sun shutter operation and the other for the remainder of the CT.

The FOV is described with the aid of figures 117 and 118 as follows:

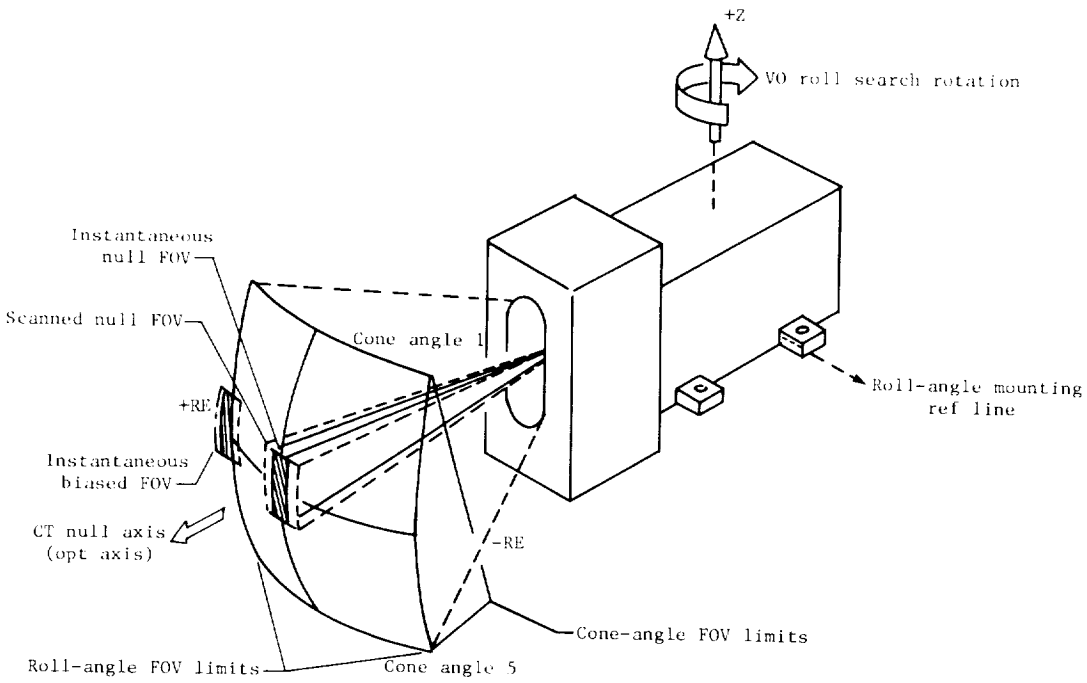

Figure 117.- Canopus tracker FOV geometry.

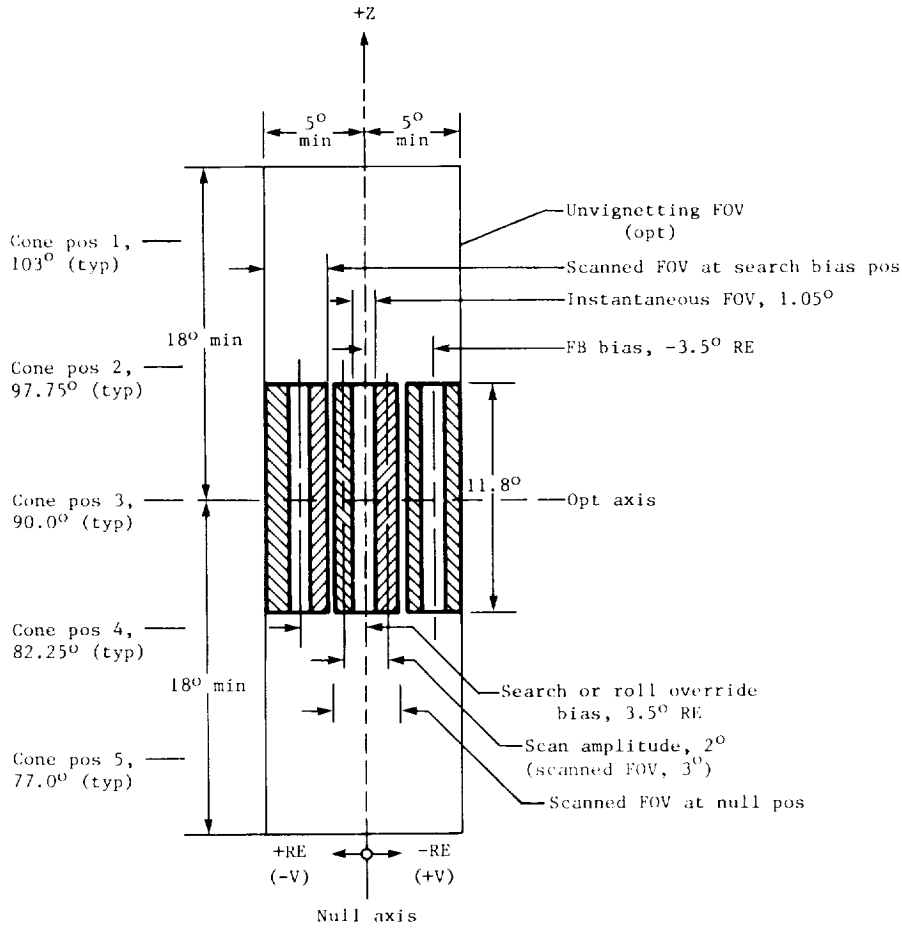

Figure 118.- CT-controlled FOV positions as viewed looking into CT.

Total FOV: The CT had an overall unvignetting FOV of ±18.0° minimum (cone) and ±5.0° minimum (clock).

Instantaneous FOV: The instantaneous FOV was defined by an aperture within the image dissector tube that had an effective FOV of approximately 1.0° (clock) by 11.8° (cone).

Scanned FOV: The instantaneous FOV was scanned over a range of ±1.0° (clock) by means of a sawtoothed waveform. This extended the effective FOV to ±1.5° (clock).

Tracking FOV: The scanned FOV was controlled in clock through a closed internal loop so that it would track a star over the total FOV in clock.

Stray-light FOV: Two stray-light FOV's were defined, one for planetary interference and the other for Mars satellite interference. The planetary stray-light FOV is ±15° (clock) by ±33° (cone). The Mars satellite stray-light FOV is ±6.5° (clock) by ±9° (cone) centered about the applicable cone position.

Field of view control: The CT FOV could be controlled in both clock and cone. The controlled FOV positions are shown in figure 118. The clock angle of the scanned FOV was controlled by three separate fixed biases in addition to the tracking error signal. These biases were input to the roll error integrator. Application of these biases was dependent upon the state of three signals from the ACE. The search bias signal was used for roll search. It caused the integrator output to increase until the scanned instantaneous FOV was positioned at the positive roll error edge of the total FOV (roll search position). During roll search a VO roll rate of approximately 0.26 deg/sec was generated in the negative roll direction. Roll override was initiated by CCS command to the ACE. It was used to disacquire a star. The roll override bias signal caused the integrator output to position the scanned instantaneous FOV to the roll search position (within 20 msec). The flyback bias provided the capability to reacquire the star, if an acceptable one was within the total FOV, without a roll search by sweeping the scanned FOV across the total FOV. The FB bias positioned the scanned FOV at the negative roll error edge of the total FOV within 20 msec. After the FB pulse and if the search bias was applied (as was normally the case), the scanned FOV swept across the total FOV at a rate of between 1 and 2 deg/sec. The cone angle of the instantaneous FOV of the CT was selectable in response to a 3-bit parallel word supplied by the ACE to accommodate seasonal variations in the Canopus cone angle. Five cone angle positions as shown in figure 118 were provided to cover a range of $\pm 17.7^{\circ}$ with a minimum overlap of 3.5° between adjacent cone positions. The commands and cone angle positions are shown in the following table:

Command	Cone position	Cone angle, deg
(7H11)	1	102.95 ± 4.75
(7H12)	2	96.75 ± 4.95
(7H13)	3	90.00 ± 5.3
(7H14)	4	83.25 ± 4.95
(7H15)	5	77.05 ± 4.75

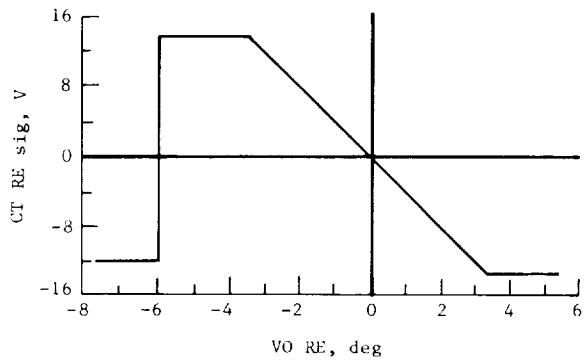

Figure 119.- Transfer function of roll error. Search bias when star beyond CT FOV.

When tracking a star, the CT roll error signal was a measure of the offset of the star image-centered, modulated, instantaneous FOV from the CT null plane. This error signal was provided to the ACE roll channel and had the transfer function shown in figure 119.

The star intensity signal was provided by the CT to the ACE for determining when a star meeting preselected brightness criteria was within the CT FOV. The transfer function of the star intensity signal is shown in figure 120.

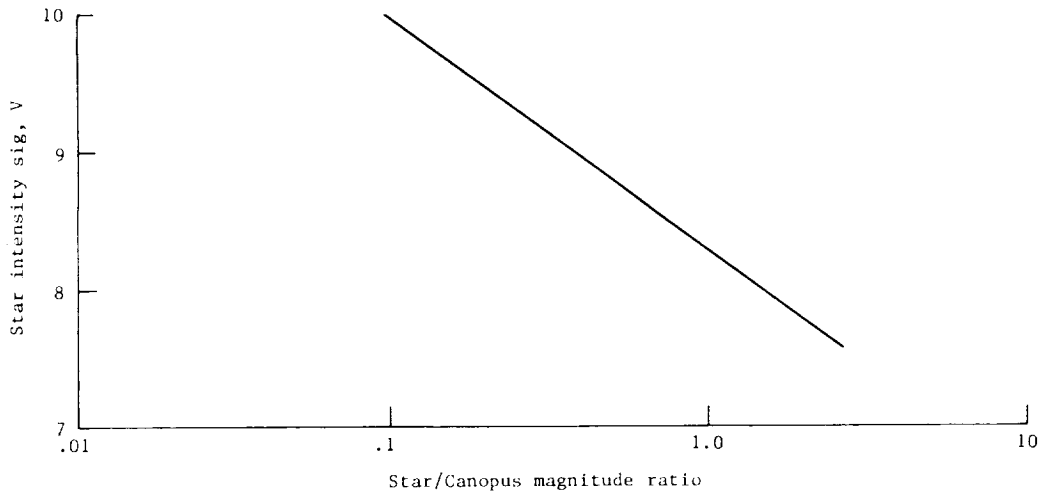

Figure 120.- Transfer function of star intensity signal.

When the CT Sun shutter circuit received the required power from the ACE, an effective solar spectral distribution illumination of 54 to 129 klx (5000 to 12 000 fc), it caused a Sun shutter closure for angles of $\pm 20^{\circ} \pm 4^{\circ}$ in clock angle and $\pm 35^{\circ} \pm 5^{\circ}$ in cone angle as measured from the CT optical axis. The Sun shutter opened again within 10° if the Sun angle was increased beyond the Sun shutter closure envelope.

Interial reference unit.- The IRU was comprised of two subassenblies: an inertial sensor subassembly and an inertial electronics subassembly. The sensors in the IRU consisted of three miniature, single-degree-of-freedom, floated, rate-integrating gyroscopes and one miniature, pulse-captured, linear, single-axis, pendulous accelerometer. Position information was generated by integrating the rate signals. Precision biases of either polarity could be introduced into the roll and yaw integrator inputs in response to bilevel signals from the ACE based upon CCS commands to the ACE to perform commanded turns. The IRU provided three-axis rate signals for damping and a three-axis inertial reference during those times when the VO was not locked onto its celestial references. It also provided a signal from which the linear change in velocity of the VO was derived during PROPS engine burns. Two identical IRU's were provided. Only one IRU was used at any given time, the other provided standby redundancy. Both IRU's were powered during launch and pyrotechnic events to protect the sensors; otherwise, only one IRU was powered. Neither IRU was normally on during cruise. The orientation of the sensing elements is shown in figure 121.

Power was supplied directly to the IRU from PWRS through switches that were controlled by signals from the ACE. The 50 V rms, 2.4-kHz, square-wave power, converted and conditioned as required by the IRU, was used for all functions except powering the gyro spin motors. The 27.2 V rms, 400-Hz, three-phase, stepped square-wave power was supplied from the 400-Hz inverter in PWRS for the spin motors.

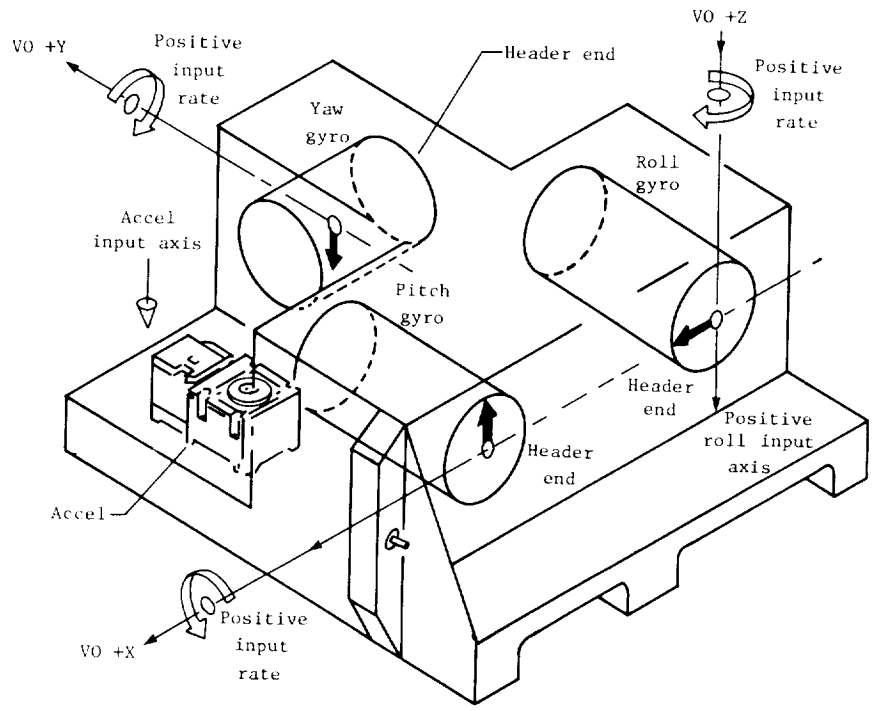

Figure 121.- Inertial sensor orientation.

The IRU had five operating modes as follows:

Rate mode: The IRU provided three-axis rate signals and accelerometer pulses.

All axes inertial mode: The IRU provided three-axis rate signals, three-axis position signals, and accelerometer pulses.

Roll inertial mode: The IRU provided three-axis rate signals, roll position signal, and accelerometer pulses.

Commanded turn mode: A turn bias was input to the rate integrator while in an inertial mode. Yaw turns were performed in the all axes inertial mode. Roll turns were performed in the roll inertial or all axes inertial mode.

Inhibit mode: The IRU was powered, but its rate and position signals and its accelerometer output were inhibited (zero).

The pitch, yaw, and roll rate signals were analog voltages proportional to the rates about the respective axes and had a transfer function as shown in figure 122 for RCA control.

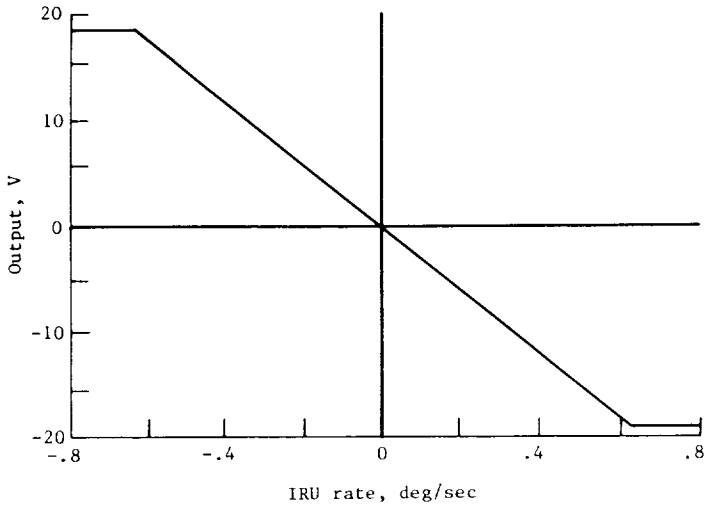

Figure 122.- Transfer function of rate signal for RCA control.

The pitch and yaw rate signals (roll rate was also provided for telemetry) were analog voltages proportional to the rates about the respective axes and had a transfer function as shown in figure 123 for TVC control.

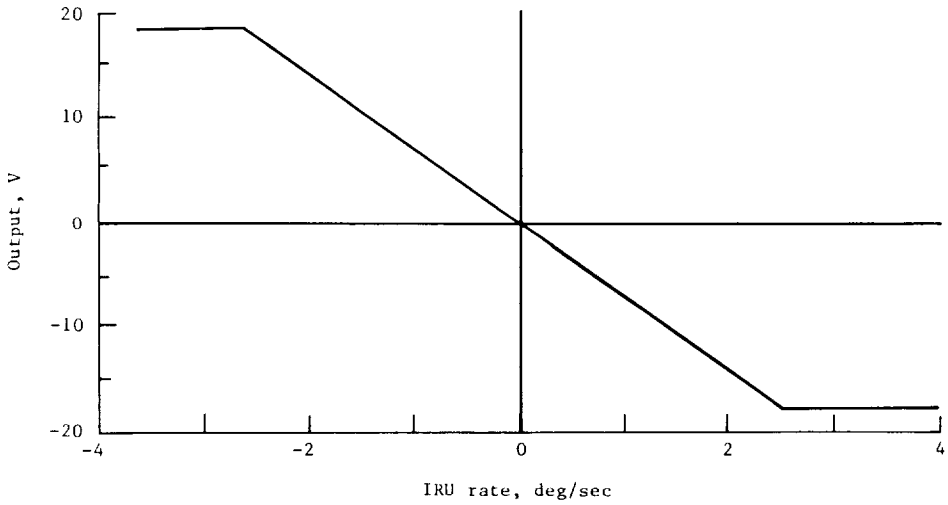

Figure 123.- Transfer function of rate signal for TVC control.

The pitch, yaw, and roll position signals were analog voltages that were the integral of the respective rate signal voltages from the time the inertial mode signal was received by the IRU. The transfer function was as shown in figure 124.

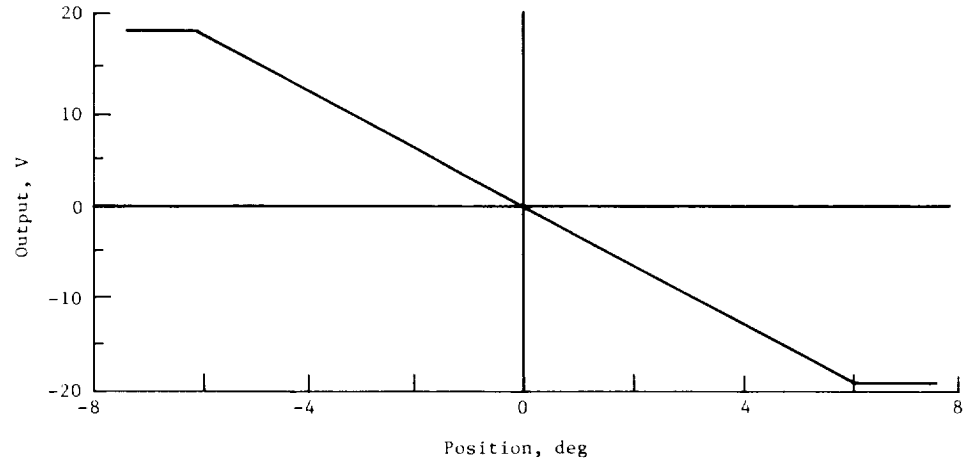

Figure 124.- Transfer function of position signal.

The accelerometer was mounted with its sensitive axis along the Z-axis such that it sensed accelerations in the +Z direction. The output of the measured proof-mass motion was demodulated and compared with a reference voltage in a comparator. When it exceeded the reference, the comparator output was high. As long as the comparator output was high, the slave flip-flop provided pulses at 400 PPS to the proof-mass restoring torquer and to the CCS. The pulses were calibrated so that the CCS measured velocity change by counting pulses. Each pulse represented a velocity change of 0.03 m/sec. The CCS counted pulses until enough had been generated to represent the desired VO velocity change at which time the CCS terminated the engine burn. The accelerometer had a nominal preset bias of 400×10^{-6}g to avoid a deadband and to permit in-flight calibration. An analog loop around the accelerometer provided proof-mass capture during launch. The analog loop provided a capture range for accelerations of up to 18g.

Attitude control electronics.- The ACE provided three basic functions: RCA control, TVC control, and mode control. The RCA electronics controlled the operation of the RCA jet valves in response to sensor signals to provide VO attitude control. The RCA electronics consisted of Sun sensor excitation circuitry, switching for position and rate signal selection, sensor signal buffer amplifiers, jet valve driver enable/disable circuitry and a sensor signal summing amplifier, threshold detector with deadband and minimum on-time, rate estimator derived rate circuit, and jet valve drivers for each axis. The TVC electronics controlled the GA's to orient the PROPS rocket engine in response to preaim commands and IRU signals. The TVC electronics consisted of a preaim circuit, gimbal servo electronics, compensator, and gain selection and enable controls. The preaim circuit received a 7-bit data word from the ACE memory and converted it to an analog signal. The analog signal biased the gimbal position so that at the start of engine burn the thrust vector passed through the predicted VO CM. The gimbal servo electronics consisted of compensation networks, GA drivers, and derived rate feedback. The gimbal servo operated as a closed-loop controller to position the gimbal to the commanded position. Derived rate feedback was utilized for damping. The compensator consisted of

forward loop compensation and feedback compensation (path guidance). Two separate gain settings were utilized to accommodate changes in VO pass properties. The mode control electronics accepted, decoded, and processed the CCS commands in conjunction with control logic to provide the desired mode control switch states. The ACE received a 14-bit command input from the CCS, ACS enable signal from DEVS, and scan slew signal from ARTCS. It also generated internal ACS logic functions and had direct control over all ACS operating modes including CT operation. Two identical ACE assemblies were provided. Power was supplied to one and only one of the two ACE's at all times by command to PWRS from the CCS. An exception was that ±30 V dc was supplied to both ACE's during propulsive maneuvers to power quad redundant circuitry (GA drivers) which was shared by the two ACE's.

The ACE received 50 V rms, 2.4-kHz, square-wave power from PWRS. Power conditioning was provided by the ACE to derive the required internal supply voltages, jet valve drive power, dc excitation for the Sun sensors, and ac excitation voltage for the GA LVDT's. A power dropout detector was provided for proper initialization of the ACE logic at power turnon, after a prolonged (>5 msec) power dropout, and for maintaining the established logic states within the ACE during momentary power dropouts of up to 5 msec. A 2.4-kHz logic clock was derived from the 2.4-kHz input power. Power switching of the 2.4-kHz, square-wave voltage to the CT and CT Sun shutter circuitry was also provided. In addition, when the TVC electronics were to be used, 30 V dc was supplied to both ACE's from PWRS; otherwise, the inactive ACE was unpowered.

The CCS-ACE interface consisted of an enable, data, and strobe line. Signal timing and message structure were as illustrated in figure 125. Each message consisted of 14 bits. The first received bit was always a 0 and did not convey any information for the ACE. The second received bit was a parity bit. Odd parity was employed. Bits dl to d8 were data, and bits al to a4 were address bits defining one of nine blocks. The ACE derived a 1.2-kHz data transfer clock from the 2.4-kHz clock which was generated from the 2.4-kHz input power. Since the 1.2-kHz clock was derived from the VO 2.4-kHz power source, it was in synchronism with the CCS commands which were also timed from the 2.4-kHz power. The data transfer clock was used to enter the 14-bit word

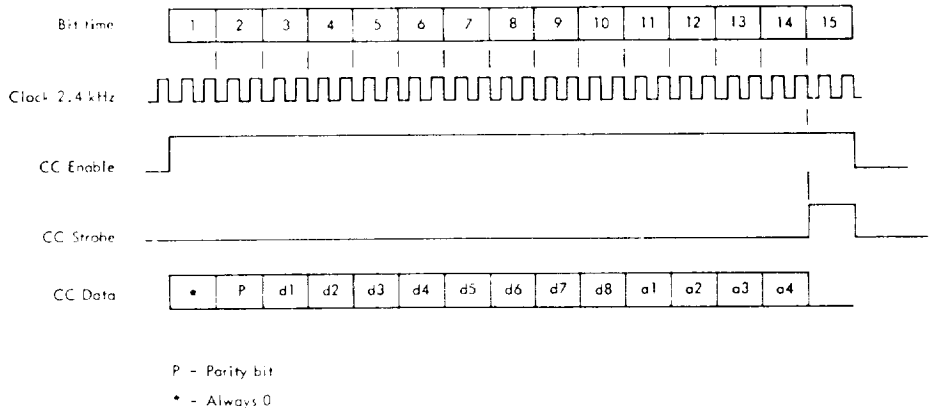

Figure 125.- Command message structure to ACS.

into the command input register within the ACE. This occurred when the function CC enable · CC strobe was true. The ACE generated a transfer pulse clock logically equivalent to the state of CC strobe, when parity checked. When the transfer pulse was true, the command was decoded by the address bits, and the data bits were processed.

The RCA electronics consisted of Sun sensor excitation circuits, sensor signal conditioning circuits, switching amplifiers, rate estimators, derived rate circuits, and jet valve drivers enable/disable circuits. The ACE provided ±5.67 V dc for ACQ SS and CR SS excitation. A pitch (yaw) ACQ SS buffered and amplified the pitch (yaw) Sun sensor inputs. A CT buffer was provided to buffer the CT roll error input. An SG buffer was provided to sense the SG resistance and generate the SGL signal. SGL was false when the SG resistance was greater than 176 kΩ and was true when the resistance was less than 149 kΩ. The switching amplifier algebraically summed the position and rate inputs as selected by the position and rate signal selection logic. When the sum of the signals exceeded a preset threshold, a high output was generated at one of the two outputs of the switching amplifier. At all other times, both outputs were in the low state. Signal processing provided the deadbands required. The output of the switching amplifier changed state within 20 msec after the sum of the input signals exceeded the threshold level of a detector. The output of the switching amplifier remained in the high (jet on) state for a minimum of 20 msec for any transition above the threshold level which included the 1 to 0 transition of the 20 msec toggle. For transitions above the threshold in excess of nominally 30 msec, the jet turned off within 20 msec after the input to the detector went below the threshold level. The pitch (yaw or roll) R/E circuits provided an input signal to the pitch (yaw or roll) switching amplifier for rate damping during the cruise mode. The rate signal to the R/E was derived from the buffered celestial sensor signal and the bilevel feedback signal from the jet valve driver circuit. The net result of the R/E signal processing was differentiation with a second-order lag filter at 0.55 rad/sec for the celestial sensor signals and a single-order lead at 0.75 rad/sec with the same second-order lag filter for the jet valve signals. The response of these dynamics to a step input (jet valve signals) approximated an integration. Saturation resulted after several seconds of jet valve on time. The bilevel feedback signal was 0 V when neither valve was energized and was 6.2 V dc or -6.2 V dc (depending on positive or negative jet valve actuation) when a valve was energized. The derived rate circuit provided additional control loop damping and noise immunity. The derived rate circuit received the RCA electronic jet valve pulses. The derived rate output increased exponentially when the jet valves were on and decays exponentially when the jet valves were off. This output was supplied to the summing junction of the switching amplifier. The derived rate circuit was controlled by command from the CCS and was used during the celestial or inertial cruise modes. The jet valve drivers provided 75 mA into a 90- to 440-Ω load (jet valve resistance over the temperature range) for the jet-on condition. There were two outputs per axis per polarity (12), each output drove one jet valve. The RCA electronics provided the switching required to select the buffered ACQ SS, buffered CR SS, or IRU position signals as the position inputs to the pitch and yaw switching amplifiers. For roll, the buffered CT roll error or the IRU roll position signal was selected as the position input to the roll switching amplifier. Switching was provided for inhibiting the rate signals from entering the switching amplifiers. Six jet valve drivers were provided for each of the

two RCA's. Provisions for selection of the active jet valve drivers were included in the logic.

The TVC electronics controlled the motion of the pitch and yaw GA's and consisted of a preaim circuit, compensator, gimbal servo electronics, gain selection circuits, TVC, and path guidance enable/disable circuits for each of the two axes (pitch and yaw). Each preaim circuit accepted a parallel data word from the ACE memory and converted it to an analog signal. The analog output of the preaim circuit was an input to the gimbal servo electronics where it was summed with the processed GA LVDT signal to provide closed-loop command control of the gimbal position (inner servo loop). The preaim command biased the gimbal so that at the start of engine burn the thrust vector passed through the predicted VO CM. The compensator consisted of the mixing input resistors, forward filter-amplifier, and the positive feedback path guidance loop. The IRU pitch and yaw position and rate signals were summed and amplified in accordance with the mixing resistor matrix values. The path guidance loop amplified and filtered the output of the forward filter-amplifier and fed this signal back to the input of the forward filter-amplifier as positive feedback. Enabling/disabling of the path guidance loop was controlled by CCS command. The gimbal servo electronics consisted of a preamplifier and threshold detectors, an LVDT signal demodulator/feedback compensation path for closing the GA loop, and a GA driver for each axis. The preamplifier summed the input command from the preaim circuit, the output of the forward filter-amplifier, and the LVDT feedback compensation signal to form the inner loop error signal into the threshold detectors. The threshold detectors turned on the appropriate GA driver (+ or -) when the magnitude of the error signal from the preamplifier exceeded the threshold level. The feedback consisted of three paths, one from each of the two threshold detectors and the demodulated and filtered GA LVDT output. These signals were summed, amplified, and filtered by the summing amplifier. The GA driver provided 2.4-kHz, pulse-width modulated, 30 V dc power to the GA motor. Each axis (pitch and yaw) of the TVC electronics included one-half of a quad redundant GA driver. The design was such that when the two halves were operating together between the two ACE's (cross-drive), a full quad redundant GA driver was formed for each axis. When the TVC electronics were used, 30 V dc was supplied to both ACE's from PWRS. The TVC electronics provided the switching required to select TVC high or low gain which altered the gain of both the forward filter-amplifier and the path guidance amplifier. Switching was also provided for enabling/disabling the TVC outer loop (path from the IRU inputs) and for enabling/disabling of the path guidance loop.

The command and control of the ACS at any time was defined by the state of the ACE command memory, certain externally generated logic signal inputs, the level of sensor signals, and the internal logic state of the ACE. The output state of the ACS was defined as the state of the RCA control, TVC control, CT control, IRU control, and external ACS control. The state of RCA control was defined by pitch and yaw position signal selection; roll position signal selection; pitch, yaw, and roll rate signal selection; and RCA 1 and 2 selection. For the pitch and yaw channels, the ACQ SS, CR SS, or IRU position signals were selected to provide the attitude input. For the roll channel, the CT roll error or IRU position signal could be selected to provide the attitude input. Either the IRU rate or the R/E signal could be selected for rate input. The pitch, yaw, and roll valve drivers for the two RCA's were enabled independently. The

state of TVC control was defined by the state of TVC enable, TVC path guidance enable, and TVC gain selection. The TVC enable function enabled or disabled the inputs to the pitch and yaw gimbal servo electronics. The path guidance enable functions enabled or disabled path guidance feedback. The TVC gain selection function was employed to compensate for changes in the VO inertia and CM migration to maintain stable TVC loop operation during engine burns. The state of CT control was defined by the state of CT power, CT FOV bias signals, and CT demodulator inhibit. Power was supplied separately to the main portion of the CT and to the CT Sun shutter circuitry. The CT FOV could be biased in clock with any one of three bias signals. Two of the biases caused the FOV to go to the positive roll error edge (search) position. One bias was used for biasing the FOV during roll search and for sweeps across the total FOV; the second was used to release an acquired star to search for a different star; and the third caused the FOV to go to the negative roll error edge (flyback) position to initiate a sweep of the total FOV. The CT demodulator inhibit function was used to disable the CT tracking loop until a star meeting the intensity gate settings appeared within the CT FOV. The state of IRU control was defined by the state of IRU power, IRU inhibit, and commanded turn signals. IRU power was supplied to neither, one, or both the IRU's by PWRS in response to pulsed on-off commands from the ACE. IRU inhibit signals to the two IRU's were used to inhibit (zero output) or enable the position and rate outputs and the accelerometer output of the IRU. The commanded turn signals provided for introducing bias currents into the IRU integrators for performing roll or yaw, positive or negative commanded turns. Command/logic derived signals were supplied to three other subsystems: PWRS, CCS, and FDS. The state of these signals was defined by the state of the following functions:

Power subsystem: Sun gate signal to PWRS indicated when the Sun was acquired via the state of a mechanical switch controlled by the SGL signal.

Computer command subsystem: Three level signals were provided to the CCS: Sun gate signal to CCS indicated when the Sun was acquired; Canopus acquisition indicated when a star was acquired; and ACE power changeover indicated when power should be switched from ACE 1 to ACE 2 as a function of internal ACE 1 logic states.

Flight data subsystem: Turn timing signal to FDS indicated when a turn (roll or yaw) was being commanded.

Reaction control assembly.- The RCA normally provided the VO with pure torque couples about the control axes for the purpose of controlling the VO attitude. There were two mutually interchangeable RCA's as shown in figure 126, each of which provided one-half of the torque couple. The RCA used compressed nitrogen gas as the propellant. Each of the gas storage vessels held 7 kg (15.5 lb) of gas when fully loaded at 30.3 MPa (4400 psig) and 37.8° C (100° F). The specific impulse is 68 sec at 20° C (68° F) and the jet thrust is 0.133 N (0.03 lb). The effective impulse expended for a 22-msec electrical pulse into a pair of jet valves (minimum impulse bit) was 5.6 mN-sec (0.00126 lb-sec). The distance from the roll axis to the jet valves on the ends of the solar panels was 5 m (16.4 ft). The pitch jet valves were located at the outer edges of the +Y and -Y solar panels and were oriented to produce torque in a plane 0°41' CCW from the YZ-plane, perpendicular to the Z-axis. The yaw jet valves

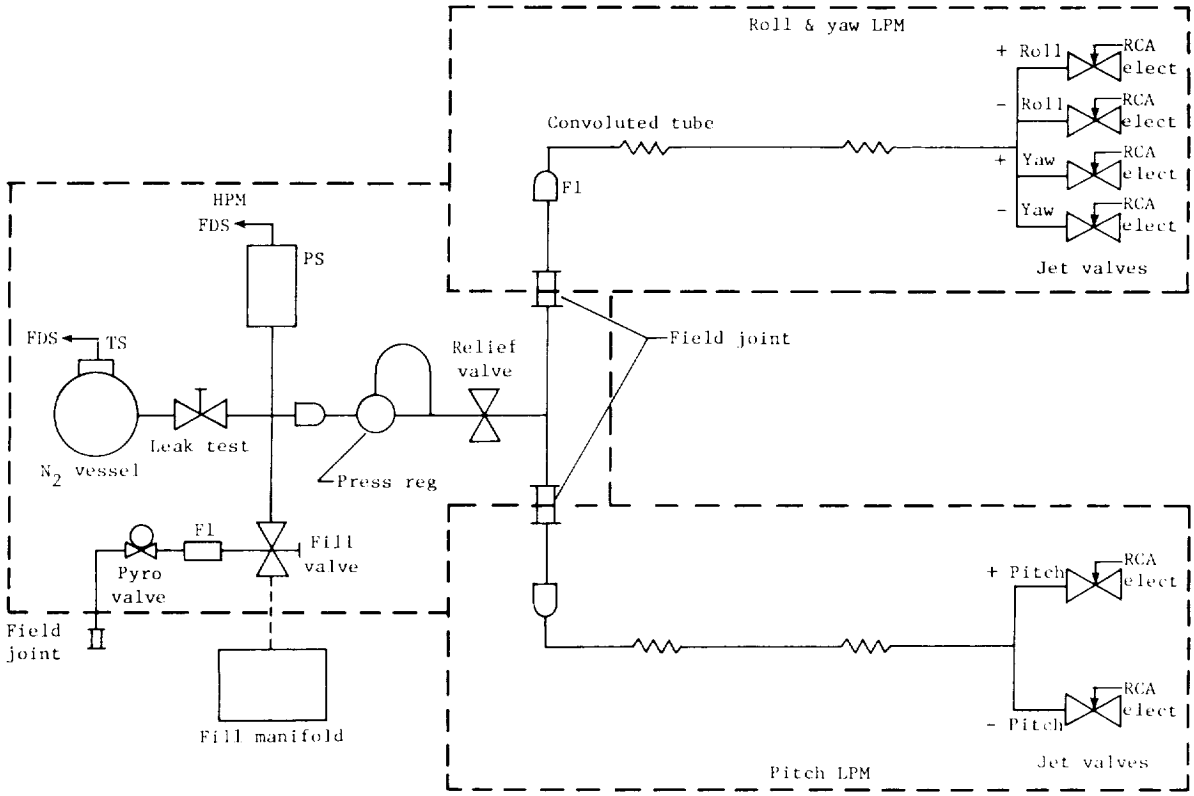

Figure 126.- Schematic diagram of RCA.

were located at the outer edges of the +X and -X solar panels and are oriented to produce torque in a plane $0^{o}41'$ CCW from the XZ-plane, perpendicular to the Z-axis. The roll jet valves were located at the outer edges of the +X and -X solar panels and are oriented to produce torque in the XY-plane, 25^{o} from perpendicular to the X-axis. The 25^{o} angle provided for reduced gas impingement on the solar panels. The relief valve exhaust plume was directed to produce essentially zero net torque. Each RCA consisted of one HPM and two LPM's. The two LPM's were the pitch control module and the roll/yaw control module. The three modules were interconnected through field joints located in the immediate vicinity of the HPM.

Jet valve actuation power was supplied by the ACE. Because of the large range in solenoid coil resistance (440 Ω at 71^{o} C (160^{o} F), 90 Ω at -157^{o} C (-250^{o} F)) constant current valve drivers were provided in the ACE. Heater power was supplied under CCS control directly from the 55 V dc regulated supply in PWRS.

The primary functions of the HPM were to provide propellant high-pressure storage and to provide the propellant at regulated pressure to the RCA low-pressure distribution lines. An ancillary function on the HPM was to provide the FDS with signals proportional to the propellant pressure and temperature. The HPM was a self-contained, all welded subassembly.

The LPM's, self-contained subassemblies, had the function of providing torques about the VO control axes. LPM tubing was routed along the edges of the VO bus to the solar-panel outriggers, along the outriggers to the inner solar-panel hinge joints at the side opposite the solar-panel deployment mechanisms, along the inner solar-panel support structure to the outer solar-panel hinge joints, and along the outer solar-panel support structure to the panel outer edges. The tubing was provided with convoluted (flexible) sections in correspondence to the inner and outer solar-panel hinge joints to allow for panel folding in the launch configuration and for panel deployment after interplanetary orbit injection.

Gimbal actuator.- Two identical nonredundant GA's were used to rotate the rocket engine gimbals about the pitch and yaw axes. A ball screw element converted the rotary torque of a standard dc torquer into a linear force over a total shaft travel of 2 cm (0.785 in.). Position feedback was provided through the output of an LVDT which was coaxial with the ball screw assembly. Output shaft velocity is shown as a function of engine gimbal drive force in figure 127. The GA's were driven with 2.4-kHz, pulse-width-modulated, 30 V dc power from the ACE's. The 30 V dc was supplied to the ACE from the 30 V dc converter in PWRS. The LVDT provided the ACE with gimbal position information for closing the gimbal position loop. Excitation (18 V ac, 2.4 kHz, sine wave) to the LVDT was supplied by ACE.

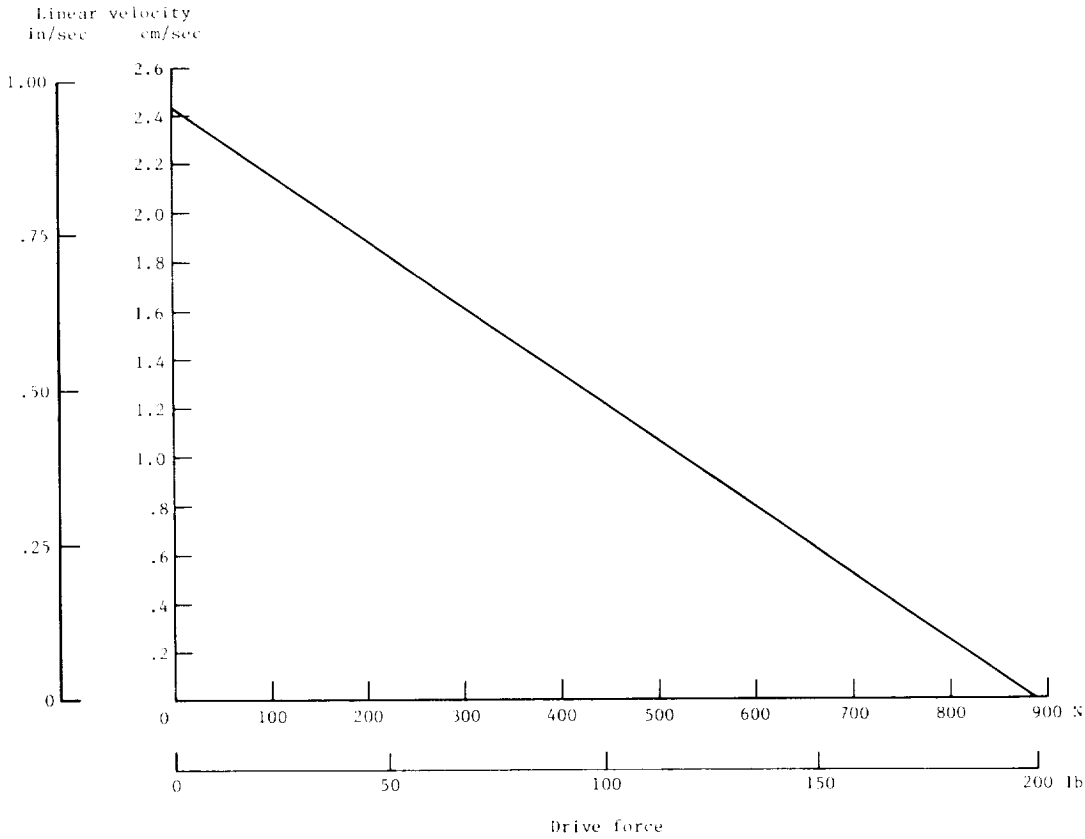

Figure 127.- Gimbal actuator velocity as function of load.

Operating Modes

There were eight primary operating modes: launch, Sun acquisition, Canopus acquisition, celestial cruise, roll inertial, all axes inertial, commanded turn, and thrust vector control. The operating mode was primarily a function of the position and rate sensing being used for control. The control torques were provided by the RCA except for pitch and yaw during thrust vector control. Descriptions of the operating modes are as follows:

Launch mode: The ACS was powered but functionally disabled during launch. Power was supplied to both IRU's to enhance the tolerance of the sensing elements to the launch and separation environments. Power was also supplied to the CT Sun shutter circuit to permit actuation of the Sun shutter if the CT FOV approached the Sun line and the TVC channels were powered to hold the rocket engine in a mechanically clear position. Both IRU's were enabled so that their outputs could be monitored prior to and during launch. During launch the ACS was essentially passive; its primary function was to survive the launch environment.

Sun-acquisition mode: At solar-panel deployment, the ACS enable signal enabled the ACS in the Sun-acquisition mode. In the Sun-acquisition mode the ACQ SS outputs and the IRU rate outputs were used as the controlling signals for the positioning of the pitch and yaw axes. The roll axis control signal was provided by the IRU roll rate output. The position and rate signals were input to the switching amplifiers in the ACE which caused RCA jet valve actuation to achieve and maintain the sum of the inputs within the deadband values. The ACQ SS signals caused the -Z-axis of the S/C to be rotated into Sun alignment. When the Sun line fell within the FOV of the SG (approximately 5° half-cone), the Sun gate logic circuitry issued a signal which identified a Sun-acquired condition. The ACQ SS inputs to the RCA electronics were then disabled, and the CR SS inputs were enabled. Meanwhile the roll control channel, driven by the IRU roll rate signal, reduced the roll rates to within the rate deadband. The deadbands were set as wide as possible consistent with mission accuracy requirements to minimize RCA gas consumption. Furthermore, to provide predictable gas jet operation, the switching amplifiers provided a minimum on time of 20 msec which controlled the magnitude of the nominal limit cycle rate. Upon completion of Sun acquisition, the pitch and yaw axes were controlled by the CR SS and the IRU pitch and yaw rate signals, and the roll axis was controlled by the IRU roll rate signal. In this orientation, the sensitive surface of the solar panels faced the Sun. During Sun occultation, the Sun sensors had no output. For this condition, the ACS reduced the rates about all three axes to within the rate deadbands by using rate information provided by the IRU. Once the VO rates had been reduced below the deadband values, the switching amplifiers turned off the jet valves. The VO then simply drifted within the rate deadband until such time as the VO entered the Sunlight, at which time the Sun sensors generated an output and Sun acquisition began.

Canopus acquisition mode: Two to 4 hr after launch, 2.4-kHz power was supplied to the CT by CCS command through a switch in the ACE. A search bias logic signal was sent to the CT from the ACE to position the scanned FOV to the positive roll error edge of the total FOV. Saturated negative output from the CT was summed with the IRU roll rate signal which caused the negative roll jet

to be actuated to establish the roll search rate. Stars other than Canopus (or other selected star) were discriminated against on the basis of star intensity and cone angle. The ACE via CCS command controlled the CT cone angle and the CT provided a star intensity signal to the ACE. When a star satisfying the intensity gate logic was detected, the CT demodulator was enabled by a logic signal from the ACE and the CT began tracking the star. The CT then provided a signal to the ACE switching amplifier that was proportional to the roll angular error. The ACE switching amplifier caused jet valve actuation to achieve and maintain the sum of the CT roll error and IRU roll rate signals within the deadband value.

Celestial cruise mode: After successful completion of roll search and star acquisition, power was automatically removed from the two IRU's. The IRU's were turned off to enhance the life of the gyros and to avoid possible adverse rate noise effects. Upon IRU power turnoff, the ACS logic automatically switched out the IRU rate inputs and switched in the R/E outputs to the switching amplifiers for damping. The derived rate may be selected during gyros on or R/E on to reduce noise effects. The R/E outputs provided rate information generated from the CR SS and jet actuation signals in pitch and yaw, and generated from the CT and jet actuation signals in roll. Feedback from the jet actuation signals from the R/E and the derived rate caused the jets to be turned off earlier than if only the sensor signals were used. This action increased the limit cycle damping which decreased gas usage. The IRU's were turned on by CCS command during celestial cruise (celestial cruise with gyros on). The IRU rate outputs were substituted for the R/E outputs whenever an IRU was on and its outputs were enabled. The celestial cruise mode was used during the transit from Earth to Mars and during Mars orbit. During Mars orbit there were Sun occultations and star occultations and the lit crescent of Mars entered the CT stray-light FOV with erroneous roll error signals generated. During Sun occultations, the all axes inertial mode was used. During star occultations and stray-light violations, the roll inertial mode was used. Switching between the celestial cruise and all axes inertial modes was normally accomplished by programmed CCS command or it could be performed automatically as a function of the Sun gate and other logic signals. Switching between the celestial cruise and roll inertial modes was automatic upon loss of the star. If the star was lost or if a bright object entered the CT FOV, FB&S was automatically initiated. If the star was not reacquired, an automatic roll reacquisition sequence was initiated. The enabled IRU was turned on automatically, the IRU roll position signal replaced the CT roll error signal as the roll attitude reference, and the IRU rate signals replaced the R/E signals for rate input on all three axes. The CCS roll reference loss routine provided programmed commands which caused FB&S by the CT to attempt to reacquire the star.

Roll inertial mode: In the roll inertial mode, the roll control signals consisted of the IRU roll position and rate outputs. Pitch and yaw axis control signals were provided by the CR SS and the IRU pitch and yaw rate outputs. Roll inertial control was used during star occultations, CT stray-light violations, roll calibration maneuvers, and commanded turn sequences. The roll inertial mode was entered by command or automatically as described in the description of celestial cruise mode.

All axes inertial mode: In the all axes inertial mode, attitude control signals were provided by the position and rate outputs of the IRU in all three axes. All axes inertial control was used during Sun occultations, gyro drift calibrations, commanded turn sequences, and propulsive maneuvers. The all axes inertial mode was entered by CCS command or automatically as described earlier. IRU drift calibrations were performed by observing the CR SS, CT, and IRU position sensing data while in the all axes inertial mode.

Commanded turn mode: Midcourse, MOI, and orbit turn maneuvers required that the PROPS rocket engine thrust be directed in a prescribed inertial direction. The VO was positioned for the engine burns by a combination of roll and yaw turns. Commanded turns were made from either the roll inertial or all axes inertial mode. A roll turn could be made from the roll inertial mode as well as from the all axes inertial mode. A yaw turn was possible only from the all axes inertial mode. The IRU output caused the S/C to rotate at a defined rate about the selected axis during a commanded turn. The IRU was powered for warm-up prior to initiating commanded turns in order to meet required turn angle accuracy requirements. Roll and yaw turns were initiated and terminated by CCS command. The polarity of the turn was also controlled by CCS command. The turn was accomplished by switching a precision voltage, generated within the IRU, into the IRU integrator. The magnitude of the turn was governed by the length of time between the turn start and stop commands. When the voltage was applied to the integrator, the IRU position output caused the switching amplifier to actuate the gas jets until the resulting VO rate produced a gyro rate signal to balance the precision voltage. The VO then continued to turn at this constant rate. After a period of time defined by the stored roll or yaw commands, the precision voltage was switched off. The IRU position output decreased as the null position was reached, and the rate output caused actuation of the gas jets to remove the roll or yaw rate to limit cycle about the new roll or yaw position. Upon completion of the powered flight, reacquisition of the cruise celestial references was accomplished by unwinding the commanded turns. Turns were unwound by repeating the turn sequence in reverse order. After the appropriate turn commands had been completed, CCS commands returned the ACS to the celestial cruise mode.

Thrust vector control mode: Control was the same as during the all axes inertial mode except the pitch and yaw axes were controlled by gimballing the PROPS rocket engine to continually point the thrust vector through the VO CM. The TVC compensator processed IRU rate and position signals and contained the path guidance function. Inner loop feedback consisted of gimbal angle position from the LVDT and outer loop feedback consisted of VO rate and position from the IRU. The accelerometer in the IRU provided velocity pulses to the CCS where they were counted. A signal from the CCS caused engine shutdown when the desired velocity increment had been achieved. To minimize control effort at the beginning of engine burn, the engine was gimballed before ignition so that the thrust vector pointed through the predicted VO CM. This was accomplished by CCS commands in pitch and yaw. The preaim command range was $\pm 4.02^{\circ}$ about each axis. Because of the large range in VO inertias over the life of the mission (6777 to 1356 kg-m^2 (5000 to 1000 slug-ft^2)) and CM migration, provisions were included for selection of high or low TVC loop gain to provide acceptable

dynamic performance. The gain was controlled by CCS command. High gain was used prior to lander separation and low gain after lander separation. Prior to engine ignition, the thrust vector was pointed inertially in the desired direction (through the predicted VO CM) by rotating the VO with commanded turns. (The commanded turns included consideration of the preaim position of the engine.) The difference between the expected and actual CM location and engine misalignments gave rise to an initial transient in VO rotation at engine ignition. As the torque rotated the VO, the IRU sensed the error angles with respect to the reference direction. These IRU signals were filtered and used to drive the gimbal servos. The engine was rotated until the gimbal angles were such as to pass the thrust vector through the actual CM. At this time the thrust vector pointing errors were the VO attitude errors plus the gimbal angle changes from the commanded preaim angles. With path guidance disabled, the VO maintained this attitude during the entire burn. With path guidance enabled, the path guidance amplifier sensed the amplified IRU signals and fed them back to the TVC input through a filter as positive feedback. The positive feedback caused the gimbal angles to increase slowly in magnitude. This increase produced a torque on the VO in the opposite direction from that which occurred at the initiating of the turn. The gains in the path guidance loop were ideally set so that when the IRU error signal exactly cancelled the positive feedback, the attitude of the VO was such that the thrust vector was aligned with the desired reference inertial direction and through the CM (VO angle was equal in magnitude but opposite in direction to the gimbal angle change from the preaim command). Thus, path guidance compensated thrust vector pointing for the initial CM offset from the predicted location and for CM migration effects during engine burn but not for engine misalignments. The CM migration occurred due to the unequal weight flow rates of fuel and oxidizer. In effect, as the CM migrated during the burn, the path guidance held the thrust vector fixed and rotated the VO around the CM. Thrust vector control was enabled by CCS command at essentially the same time as the command to initiate engine burn was given. This command also disabled actuation of the pitch and yaw gas jets to avoid unnecessary use of gas during engine burn. Path guidance may be enabled or disabled by the CCS command. With path guidance enabled, the path guidance loop was not actually closed until TVC was enabled. TVC damping was better without path guidance. In-flight performance determined whether short duration (<3.5 sec) burns with path guidance disabled would be executed. Thrust vector control was disabled by CCS command at essentially the same time as the command to terminate engine burn was given.

Operational Sequence

In-flight operation could be thought of in terms of three phases as follows:

Acquisition and transit cruise phase: Three-axis stable orientation was established by using the celestial sensors (with the Sun and Canopus, or other acceptable star, as reference objects) in conjunction with the RCA gas jets. In this orientation the sensitive surface of the solar panels faced the Sun. Reacquisition of the Sun and/or star, in the event of inadvertent loss of acquisition for any noncatastrophic reason, was automatic.

Powered flight phase: Maneuvers were employed during the three powered-flight phases of the mission. In response to preloaded CCS commands the VO, under IRU control, was oriented so that the thrust vector of the rocket engine was aligned through the VO CM in a predetermined direction in space. VO orientation and stability during engine burn were maintained by TVC positioning of the GA's. After the engine burn period, the cruise orientation and celestial reference control were reestablished.

Orbit cruise phase: The primary scientific data acquisition during the Viking 1975 mission occurred during the 140-day period following MOI. The orbital cruise phase was similar to the transit cruise phase. Three-axis orientation was maintained with the Sun and star as reference objects in conjunction with the RCA gas jets. There were times during orbit cruise when the Sun was occulted, necessitating three-axis inertial control using the IRU. There were also times when the star was occulted or when stray light from the Mars crescent caused erroneous pointing, necessitating roll axis inertial control with the IRU.

Mode Control

The ACS operating modes were defined in terms of the source of the position and rate signals and the source of the control torque. The major operating modes are given in table 34. Some of these modes were transient rather than steady state, for example, roll search. Variations to these modes were possible by command; for example, the R/E could be used for pitch and yaw rate information in the celestial cruise with gyros on mode. Modes 15 and 16 in table 34 were the same as modes 4 and 7 except that the ACQ SS's were used in place of the CR SS. Selection of redundant and/or alternate assemblies and backup modes are a part of mode control. Discussion of the mode sequences, input control variables, and output and internal logic functions is as follows:

TABLE 34.- ACS MODE DEFINITION

Mode	Name	Pos information	Rate information	Control torque
1	Launch	None	IRU	None
2	All axes rate	None	IRU	RCA
3	Sun acquisition	ACQ SS	IRU	RCA
4	Sun acquired - roll drift	CR SS	IRU	RCA
5	Roll search	CR SS	IRU	RCA
6	Canopus acquisition	CR SS, CT	IRU	RCA
7	Celestial cruise	CR SS, CT	R/E	RCA
8	Celestial cruise - gyros on	CR SS, CT	IRU	RCA
9	Roll inertial	CR SS, IRU	IRU	RCA
10	All axes inertial	IRU	IRU	RCA
11	Roll turn - roll inertial	CR SS, IRU	IRU	RCA
12	Roll turn - all axes inertial	IRU	IRU	RCA
13	Yaw turn	IRU	IRU	RCA
14	Thrust vector control	IRU	IRU	Eng, RCA
15	Sun acquired - roll drift (B/U)	ACQ SS	IRU	RCA
16	Celestial cruise (B/U)	ACQ SS, CT	IRU	RCA

Mode sequences: It would not be practical to define all possible operating modes and the paths that could be followed in sequencing between them. Of particular interest was the mode sequencing from launch through all the normal modes, mode sequencing associated with reacquisition of celestial references if they were lost, and mode sequencing following initialization; these mode sequences are discussed as follows:

Normal mode sequencing: Figure 128 is a typical state diagram showing the modes associated with a totally normal mission (first 14 modes listed in table 34). Three commands were required to set the proper TVC preaim positions and CT cone angle and intensity gate level settings following power turn-on. Furthermore, because the S/C was in the Earth's shadow at separation, the command for ASOC inhibit was required in order to enter the all axes rate mode. Otherwise, the ACS would enter the all axes inertial mode. ASOC enable was subsequently commanded so that the ASOC function would be enabled to perform its function if required. The CCS was programmed to ignore the ACE changeover signal until after the separation rates had been removed in order to prevent a changeover due to normal jet actuation for rate removal. After Sun acquisition, if the system settled on ACQ SS rather than CR SS control (due to Earth albedo), SG backup was commanded. This was done before the CCS was programmed (Sun acquisition routine) to execute ACE changeover if it did not get a Sun acquired indication from the ACS. SG backup reset was commanded after settling on the CR SS to return control of the SGL to the SG.

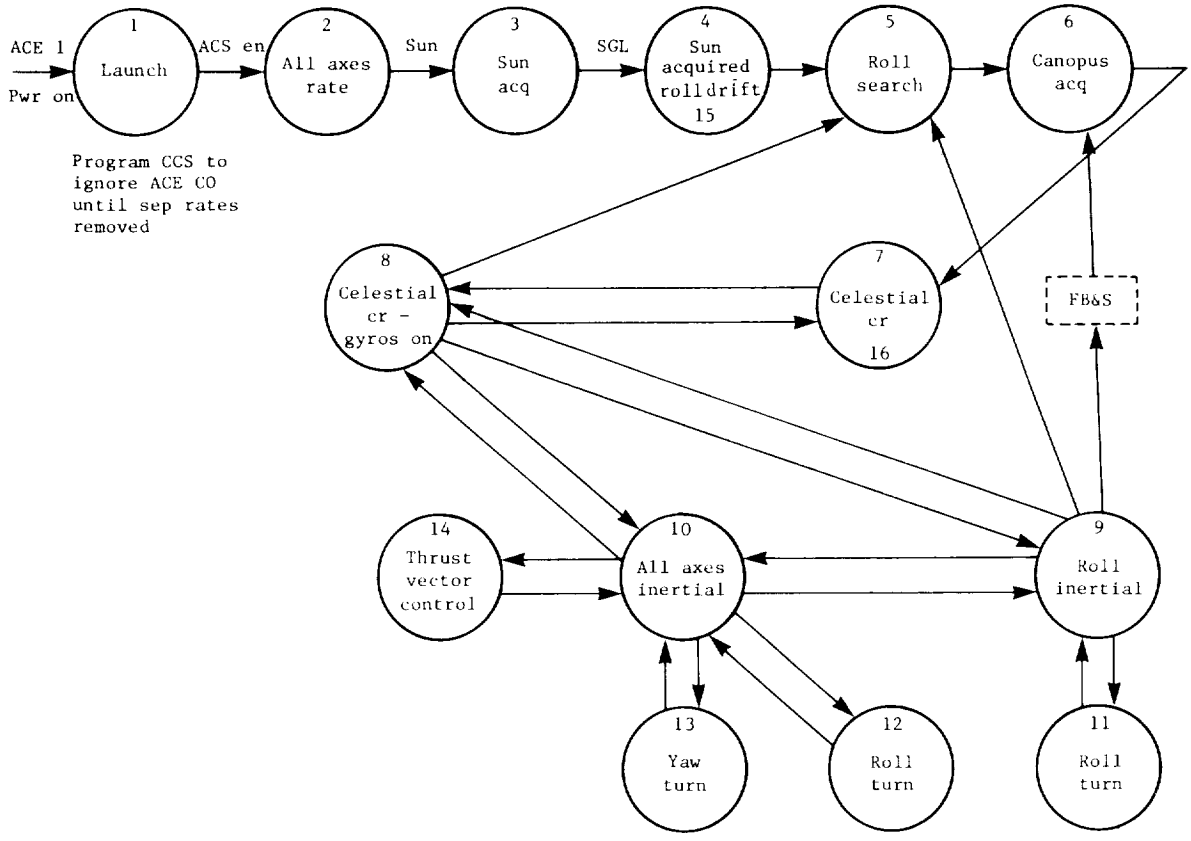

Figure 128.- State diagram of ACS normal mode sequencing.

Automatic mode sequencing for reacquisition of celestial references: The initial assumption was that the system was in the celestial cruise mode. If the Sun was lost, the all axes inertial mode was entered through the ASOC logic. If the star was lost, the roll inertial mode was entered through the roll sequence inertial logic. Depending upon the state of SGL and Canopus acquisition logic, there might be automatic sequencing between the all axes inertial and roll inertial modes. If the roll inertial mode was entered from the all axes inertial mode, FB&S occurred when exiting from the all axes inertial mode provided that Canopus acquisition logic was reset while operating in the roll inertial mode. An FB&S also occurred if roll inertial was entered by commanding (7C41), and Canopus acquisition logic was reset during the roll inertial interval. If the star was lost or if a bright object entered the FOV of the CT, gate satisfied logic (GS) became false. If GS remained false for less than 5.1 sec, the ACS returned to the celestial cruise mode after a period of up to 5.1 sec of open loop (drift) operation. If GS remained false for greater than 5.1 sec, FB&S occurred. If the star was regained or if the bright object was lost and the star was regained, the ACS returned to the celestial cruise mode after a period of 10.2 to 15.3 sec of open loop (drift) operation. If GS did not become true on the FB&S, the ACS went to the roll inertial mode after 10.2 sec. An FB&S occurred at each programmed (7E11) or (7E31) command from the CCS roll reference loss routine. If the star was not acquired on either of the first two (7E3) commands, roll search accompanied by FB&S was initiated on the third (7E3) command.

Mode sequencing following initialization: No initializations occurred after launch. Initialization resulted whenever power was supplied to the ACE either as a result of an automatic ACE changeover (due to a spin-up signal, SLCO, or a power drop-out), a ground commanded ACE power changeover, or a power drop-out with no ACE changeover. (Automatic changeover did not occur when operating on ACE 2 or when operating on ACE 1 with changeover inhibited in the CCS.) The function of initialization was to initiate attitude control from a defined state. The ACS was in the launch mode while initialization was true. The (7F), (7G), and (7H) commands were issued after initialization. This was done as soon as possible for (7H) in order to reestablish the proper CT cone angle and star intensity gate settings for acquisition of the desired star. (This was not done prior to 1.4 sec after the application of power because initialization could still be true.) The CCS commanded roll inertial control as part of the automatic ACE power changeover routine. After initialization, the ACS began Sun acquisition if the Sun was present. If the Sun was occulted, the ACS entered the all axes inertial mode until the VO became Sunlit. Note that the ACS went directly to the roll inertial mode if SGL was true. There were four logic functions, all of which were associated with CT and roll axis control, that were not initialized. Because of the logic functions that were not initialized, alternate mode sequences for getting to the celestial cruise mode, namely, roll search or roll inertial control, were possible if an initialization not associated with automatic ACE changeover occurred. The probability was high that the roll search route would be followed. If an acceptable star was in the CT FOV at initialization and if the star remained within the FOV during Sun acquisition, it was possible to enter the celestial cruise mode directly without first going into roll search or roll inertial mode to the celestial cruise mode.

Input control variables: The ACS logic control variables consisted of commands from CCS, logic signals generated within the ACS, and logic signals provided by other subsystems.

Output and internal logic functions: There were a total of 37 command and logic controlled outputs. All except 5, which were provided to other subsystems, were used to control switches within the ACS for mode control. In addition to these 37 outputs, 13 logic functions, completely internal to the logic, were identified to facilitate the understanding and definition of the logic.

Redundancies and Backup Features

The ACS had many design features to enhance its reliability. These included redundancy as well as ground commands and automatically controlled backup features.

Where block redundancy was provided, there was fault isolation to insure that failures within one assembly would not affect operation of the other. Cross-strapping was used extensively to avoid redundant assembly selection switching. Redundancy was provided in the following areas:

Dual reaction control assemblies: One-half of each torque couple about each axis was provided by one RCA and the other one-half was supplied by the other RCA. If one RCA failed, the remaining RCA was capable of furnishing adequate torque capability and gas capacity to control the VO through at least the first 20 days of Mars orbital operation. Because of the independence of the two RCA's, if one jet valve stuck open and exhausted the N_2 supply of one RCA, there would still be two-thirds of the N_2 supply available in the other RCA. If a jet valve in one RCA developed a leak, the other RCA would be disabled until the gas in the leaking RCA was all used then the other RCA would be reenabled. Both RCA's were used normally; either RCA could be disabled independent of the other by CCS command.

Dual attitude control electronics and Sun gate assemblies: SG 1 was dedicated to ACE 1 and SG 2 was dedicated to ACE 2. In addition, the TVC electronics in each ACE provided one-half of a quad redundant GA driver. The design was such that, when the two halves were connected together between the two ACE assemblies (cross drive), a full quad redundant GA driver was formed. The PWRS supplied 30 V dc (GA driver power) to both ACE assemblies; the inactive ACE was otherwise unpowered. The ACE to be powered was controlled by CCS command from the ground to PWRS. If ACE 1 was already powered, automatic switchover to ACE 2 would occur, depending upon the state of certain logic functions within ACE 1, unless the automatic switchover function had been inhibited in the CCS. Only the ACE power changeover signal from ACE 1 to ACE 2 was input to the CCS.

Dual inertial reference units: In addition to providing block redundant IRU's, the relays in the IRU were redundant as follows:

Inertial control relays: The relays (two) which enabled the integrators opened the near short circuit around the integrator feedback capacitor. These relays were in series around each integrator. If either set of redundant contacts opened (relay energized), the integrator was enabled.

Commanded turn relays: The two relays, in parallel, which enabled commanded turn voltage to each of the integrators (roll and yaw) closed the circuit from the bias voltage source to the integrator. The closing of either set of two series connected contacts (relay energized) of either relay enabled the bias voltage to the integrator. The two relays which selected turn voltage polarity had two sets of contacts (one from each relay) connected in series so that both had to be in the relay deenergized position to command a negative turn. The other two sets of contacts (one from each relay) were connected in parallel so that if either or both were in the relay energized position, a positive turn resulted.

IRU inhibit relays: Power (±20 V dc) to the IRU electronics was routed through two redundant relays. Lack of this power resulted in no rate or position outputs and no accelerometer output.

Either none, one, or two IRU's could be on at any given time as determined by CCS command or automatically if automatic operation had not been inhibited. (Two were on automatically only during launch; only one was enabled at any given time except during launch.)

In addition to the selection of redundant elements, functions or equipment were bypassed, substituted, or altered by ground command. Failure of the ACS enable switch or its interface circuit was overridden by CCS command after solar panel deployment to make the state of the ACS enable logic irrelevant. If the CR SS failed, the ACQ SS was used for cruise control by CCS command. Accuracy was degraded and the IRU was used for rate information. (The R/E was not used with the ACQ SS.) The SG and the associated logic in the ACE generated a Sun-acquired logic signal that was used for performing automatic functions. The Sun-acquired logic state was generated by CCS command. The IRU rate signals were automatically used at any time the IRU was on and its outputs were enabled. The CT star intensity signal was used in the ACE to provide star discrimination on the basis of star brightness relative to that of Canopus. Only if the brightness fell between the low gate and high gate settings was the star considered acceptable for acquisition. To allow for degradation and change in the CT sensitivity with time and the temporary decrease in sensitivity following exposure to high intensity sources (e.g., the Earth), four low gate settings covering the range of 0.7 to 0.05 times Canopus brightness were provided and selectable by CCS command. The high gate restriction could also be removed by CCS command. Most of the time, the CR SS and CT provided the attitude error signals used by the ACS. Functional backup to these sensors was provided by inertial control by using the IRU. However, since the gyros were subject to drift, the attitude of the VO was determined on the ground and the appropriate commands were sent to reposition the VO by using commanded turns. A number of

secondary sources of attitude measurements were available and included TV pictures of stars, solar panel currents (from shading by the HGA), and antenna gain patterns. Earth albedo effect was sufficient to cause the Sun not to fall within the SG FOV as the system settled on Sun sensor control. Therefore, depending upon the pitch and yaw angle profiles during Sun acquisition, the Sun-acquired signal may not be obtained with normal equipment performance. This condition was circumvented by CCS command or by waiting until the Earth albedo effect decreased sufficiently as the distance between the S/C and the Earth increased.

The following automatic backup features were provided:

Reacquisition of Sun: Reacquisition of the Sun, if lost for any non-catastrophic reason, was automatic within the ACS. If the Sun-acquired state was lost for an extended period of time, the CCS Sun acquisition routine commanded ACE changeover.

Reacquisition of star: Following a loss of the star, an FB&S was automatically performed. If a star was not acquired, the ACS switched to the roll inertial mode. Additional FB&S's were performed in response to the CCS commands initiated by this routine.

Automatic IRU control if Sun occulted: Mode switching to account for Sun occultation was normally programmed and controlled by CCS commands to the ACS. However, if a Sun occultation (as determined by the logic) occurred, the ACS automatically switched to the all axes inertial mode.

Automatic IRU control if star occulted: Roll was automatically switched to inertial control if the star was lost.

Automatic ACE switching: The ACE 1 control logic provided a level input to the CCS for automatic switching from ACE 1 to ACE 2 if any of the following events occurred:

ACE 1 detected a power dropout of 5 msec or longer.

ACE 1 detected a S/C spin-up condition. If the jet valves were energized continuously for more than 90 sec with 2 valves on (time was dependent upon how many valves were on), ACE power changeover was indicated to the CCS by ACE 1 (must be operating in ACE 1). This automatic function was inhibited in the CCS during specific programmed events during the mission.

ACE 1 detected loss of the Sun when operating on Sun sensor control when Sun occultation was not indicated.

Automatic IRU switching: If a spin-motor malfunction was detected when operating on ACE 2 or when operating on ACE 1 with ACE changeover inhibited in the CCS, automatic IRU changeover occurred.

Automatic Sun sensor switching: When on CR SS control, control was automatically switched from the CR SS to the ACQ SS if the Sun was lost from the SG FOV as detected by the logic.

Interfaces

The ACS interfaced with eight other subsystems: STRUS, PWRS, CCS, FDS, CABLS, PROPS, DEVS, and ARTCS. The major subsystem interfaces are shown in figure 110. The subsystem interfaces involved with the functioning of the ACS are described in this section.

Power subsystem.- The inputs that the PWRS provided to the ACS were switchable 50 V rms, 2.4-kHz, square-wave power to neither, either, or both IRU's and to either of the two ACE's as commanded; switchable 27.2 V rms, 400-Hz, three-phase, stepped square-wave power to neither, either, or both IRU's as commanded; switchable 30 V dc power to both ACE GA drivers; and switchable, regulated 55 V dc power to the RCA jet valve and ACQ SS heaters. The outputs that the ACS provided to the PWRS were commands for controlling IRU power switching with each ACE supplying four lines to PWRS with a 20-msec IRU 1 on pulse signal, a 20-msec IRU 1 off pulse signal, a 20-msec IRU 2 on pulse signal, and a 20-msec IRU 2 off pulse signal and a switch closure to PWRS when the ACS was not Sun acquired.

Computer command subsystem.- The inputs that the CCS provided to the ACS were enable signal which bracketed data and strobe to indicate the period of activity during which data were to be clocked into the ACE register; data word for a series of levels representing 1's and 0's for 14 bit times; and strobe signal which followed data immediately and indicated that all data had been sent. The outputs that the ACS provided to the CCS were an accelerometer (IRU) output in the form of pulses with each indicating an incremental change of velocity; a switch closure when the SGL indicated that the Sun was acquired; a switch closure when the Canopus acquisition logic indicated that a star was acquired; and a switch opening when the ACE power changeover logic indicated that an ACE changeover should be made. In response to the ACE power changeover signal, the CCS commanded PWRS to switch power from ACE 1 to ACE 2, depending upon the state of other conditions in the CCS. The ACE power changeover signal from ACE 2 was not supplied to the CCS.

Flight data subsystem.- The FDS provided 1-mA constant current to the temperature sensors and ±12 V dc power to the pressure sensors to produce the specified voltage range. The outputs that the ACS provided to the FDS were telemetry signals as required and turn timing signals. The ACS provided a switch closure to the FDS when a roll or yaw turn was being executed.

Mechanical devices subsystem.- The DEVS provided a switch to indicate solar panel deployment to the ACS. The switch was closed during launch and opened upon complete deployment of the inboard panel. Unfolding of the outboard panel began approximately 20 sec before the inboard panel was fully deployed.

Articulation control subsystem.- The ARTCS provided a switch closure to the ACS which indicated when the scan platform was being slewed in either or both axes.

Propulsion subsystem.- The ACS interfaced with the PROPS for the purpose of gas sharing. On command from the CCS the PROPS helium system was tied into the RCA high-pressure vessels. The RCA then operated with helium instead of nitrogen. This interface was not used unless the RCA high-pressure vessels had first been emptied of nitrogen.

Commands

Of the three types of commands - DC, CC, and PC - only DC and CC were used to control the G&C subsystems. PWRS used only DC's; ACS and ARTCS used only CC's. The discrete command was decoded by the CCS and resulted in discrete switch closures within the user subsystem. One DC of the matrix required an OU execution time of 105 ± 5 msec. Two DC's of the pulsed type could be issued at the same time if they met certain requirements; otherwise, they each required an OU execution time of 105 ± 5 msec. The coded command was partially decoded by the CCS and then sent to the user subsystem for further decoding. VO subsystem users receiving coded command data from the CCS did so over three interfaces: data word for a series of levels representing 1's and 0's for 14 bit times; stroke signal which followed data immediately and indicated that all data had been sent; and enable signal which bracketed data and strobe to indicate an activity period.

Telemetry

ACS telemetry data were provided in the five engineering data formats discussed in the section "Flight Data Subsystem." The measurement assignments in the four programmable engineering formats were modified with CCS coded commands by altering the contents of the FDS memory. The assignments for the fixed engineering format were hardwired in the FDS logic and could not be changed. For the five engineering formats, the format structure shown in figure 108 was used. The FDS was capable of handling four different analog voltage signal ranges. Digital signals for telemetry were sent to the FDS as either a serial bit stream or as parallel bilevel signals.

Engineering measurements which were redundant only because of having redundant ACE's were cross-strapped so that these measurements could be read on a single input to the FDS from whichever ACE was powered. The cross-strapping was important in the determination of significance (scale factor) of the signals because of the loading produced by the unpowered ACE.

Performance Characteristics

The following table presents the subsystem level nominal performance characteristics for the ACS (P&Y denotes pitch and yaw; R denotes roll; HG denotes high gain; LG denotes low gain):

Sensor characteristics

ACQ SS

Look direction, deg	0 (cone)
FOV, sr	4π
Scale factor, V dc/deg	-1.4
Saturation, deg	-3.6 to 3.6

CR SS

Look direction, deg	0 (cone)
FOV, deg	-20 to 20
Scale factor, V dc/deg	-2.8
Saturation, deg	-1.8 to 1.8

SG

Look direction, deg	0 (cone)
FOV	
For logic setting, deg	5.0 (cone)
In ACE, deg	0.1 (hysteresis)
Threshold for logic level setting in ACE	
for 0^{o} cone angle	0.02 solar constant

Canopus tracker

Look direction, deg	0 (clock)
Cone position	
1, deg	102.95
2, deg	96.75
3, deg	90.00
4, deg	83.25
5, deg	77.05
FOV	
Total instantaneous, deg	1.05 (clock) by 11.8 (cone)
Total scanned, deg	3.0 (clock) by 11.8 (cone)
Total, deg	5 (clock) by ±18 (cone)
Planetary stray-light interference, deg	±15 (clock) by ±33 (cone)
Satellite stray-light interference, deg	±6.5 (clock) by ±9 (cone)
Sun shutter	
Look direction, deg	0 (clock), 90 (cone)
FOV, deg	±20 (clock), ±35 (cone) (>54 klx (>5000 fc))
Threshold, klx (fc)	22 (2000)
Intensity gate settings in ACE	
High gate	<3.0 × Canopus (not violated) <4.0 × Canopus (violated)
Low gate	
1	>0.70 × Canopus (not violated) <0.40 × Canopus (violated)
2	>0.35 × Canopus (not violated) <0.20 × Canopus (violated)
3	>0.15 × Canopus (not violated) <0.08 × Canopus (violated)
4	>0.05 × Canopus (not violated) <0.025 × Canopus (violated)

Scale factor, V dc/deg . . . . . -4.0
Saturation, deg . . . . . -3.5 to 3.5

Inertial reference unit
Gyro channels
Sensitive axis . . . . . Pitch, yaw, and roll
Position scale factor, V dc/deg . . . . . -2.975
Position saturation, deg 6.05
Rate scale factor for -
RCA, V dc/deg/sec . . . . . -28.25
TVC, V dc/deg/sec . . . . . -7.2
Rate saturation for -
RCA, deg/sec 0.64
TVC, deg/sec 2.50
Accelerometer
Sensitive direction . . . . . +Roll
Velocity increment/pulse, m/sec 0.03
Saturation digital loop, Earth g units 1.2
Capture capability analog loop, Earth g units 18
Acceleration bias, Earth g units 400

Actuator characteristics
Reaction control assembly - N_2
Jet thrust, N (lb) . . . . . 0.133 (30×10^{-3})
Jet torques for -
2 RCA's, N-m (ft-lb) . . . . . 1.33 (0.98) (P&Y)
1.21 (0.89) (R)
1 RCA, N-m (ft-lb) . . . . . 0.66 (0.49) (P&Y)
0.61 (0.45) (R)
Initial gas weight at 30.3 MPa (4400 psig) and
37.8° C (100° F), kg (lb) 7.0 (15.5)
Specific impulse at 20° C, sec 68
Minimum impulse per jet (22 msec electrical on-time), sec 16
Pitch-yaw cross coupling, percent . . . . . 1.2 (P&Y)

Reaction control assembly - He
Jet thrust, N (lb) . . . . . .0.124 (27.8×10^{-3})
Gas weight (equivalent N_2) at -
After MOI, kg (lb) 4.1 (9)
After VL landing, kg (lb) 3.2 (7)
EOM, kg (lb) 1.8 (4)
Specific impulse, sec 158

TVC gimbal actuators
Actuator travel, cm (in.) . . . . . ±0.997 (±0.3925)
Gimbal angular range, deg . . . . . 8.9 to -8.9

RCA control parameters
Acquisition coast rates for -
ACQ SS, deg/sec . . . . . ±0.19 (P&Y)
CR SS, deg/sec . . . . . ±0.21 (P&Y)
CT, deg/sec . . . . . ±0.23 (R)

Position deadbands (no noise) for -

ACQ SS, deg	±0.50 (P&Y)
CR SS, deg	±0.25 (P&Y)
CT, deg	±0.257 (R)
Inertial, deg	±0.176 (P&Y)
	±0.088 (R)
Rate deadband (IRU), deg/sec	±0.026 (P&Y)
	±0.017 (R)

Rate to position gain (IRU) for -

ACQ SS, sec	19.3 (P&Y)
CR SS, sec	8.7 (P&Y)
CT, sec	14.9 (R)
Inertial, sec	6.8 (P&Y)
	5.1 (R)

Rate deadband (R/E) for -

CR SS, deg/sec	0.033 (P&Y)
CT, deg/sec	0.034 (R)

Rate to position gain (R/E) for -

CR SS, sec	6.8 (P&Y)
CT, sec	7.6 (R)
Roll search rate, deg/sec	-0.23 (R)
Commanded turn rate, deg/sec	±0.181
Position error beyond which jets are full on, R/E with zero rate, deg	0.75 (P&Y)
	0.96 (R)
Derived rate time constant, sec	33.7
Position error beyond which jets are full on, DR with zero rate, deg	1.63 (P&Y)
	3.15 (R)

TVC control parameters

Preaim commanded range, deg	±4.023
Gimbal angle/preaim command bit, deg/bit	0.0633

Scale factor:

Path guidance loop open

Gimbal angle change/deg of IRU position output, deg	5.85 (HG)
	1.627 (LG)
Gimbal angle change/deg of error in preaim command, deg	1.0
VO angle change/deg of error in preaim command, deg	0.171 (HG)
	0.615 (LG)

Thrust vector pointing error/deg of error in preaim command, deg . . . . . 1.171 (HG)
1.615 (LG)

Path guidance loop closed
Time for gimbal to slew from 0^{o} to full travel with engine off and 0.336^{o} (1 V) IRU output, sec . . . . . 2.7 (HG)
8.0 (LG)
Rate to position gain, sec 2.09

ACS-related S/C characteristics
Separation rates:
Maximum Centaur residual turning rates, deg/sec <0.5 (P&Y)
>0.5 (R)
Maximum rate imparted to S/C at launch vehicle separation (excluding Centaur residual rates), deg/sec . . . . . <0.5

RCA induced angular rate, deg/sec^2 . . . . . 0.010 (P&Y)
0.020 (R)
Acceleration (2 jets), deg/sec^2 . . . . . <0.056 (P&Y)
<0.033 (R)

Propulsion maneuver linear accelerations for -
Mid-course correction 1, Earth g units 0.04
Orbit trim 2, Earth g units 0.14

Constraints and Operating Procedures

Launch constraints were needed to protect the equipment from the stresses and environments to which it was exposed from launch to celestial reference acquisition. Both IRU's were powered during launch and pyrotechnic events to protect the sensors from the effects of vibration and shock. The GA control loops were energized during launch to avoid possible uncontrolled motion of the rocket engine in the presence of the launch loads and to hold the rocket engine in a mechanically clear orientation.

In-flight constraints were needed to protect the equipment from the effects of the environments and to prolong its life. The equipment design temperatures are listed in table 35. The equipment temperatures were monitored and corrective action taken if possible to maintain the temperatures within these values. Heaters were provided on the RCA jet valve and ACQ SS subassemblies. These heaters were used during Sun occultation periods to avoid extremely low temperatures. Flight operations were conducted to minimize the use of IRU's to enhance gyro life. Both IRU's were powered during pyrotechnic events. ACE 1 to ACE 2 changeover was inhibited in the CCS when performing maneuvers during which the Sun entered the CT FOV because CT Sun shutter power was off for approximately 1 sec when an ACE changeover occurred. Maneuvers of this kind were avoided if possible.

TABLE 35.- ACS EQUIPMENT DESIGN TEMPERATURES

Assembly	Temperature, °C	
	Low	High
ACQ SS	-85	85
CR SS	-75	85
SG	-75	85
CT	-30	62
IRU	0	55
ACE	-20	75
GA	-35	[a]100
HPM	-30	85
LPM:		
Dist assy	-125	90
Thruster assy	-85	85

[a]168° C soakback when GA not operating.

In-flight operational constraints were also needed to avoid adverse operating modes or conditions. In addition, there were operating procedures which prolonged the life of the ACS, for example, reduced RCA gas usage.

CCS programming was the primary method for controlling ACS mode switching to maintain control during Sun and star occultations although the ACS had provisions for automatic mode switching if the mode switching was not performed by the CCS. CCS programming was relied upon for controlling ACS mode switching to maintain the proper attitude during CT stray-light violations. ACE 1 to ACE 2 changeover was inhibited during initial acquisition to avoid possible ACE changeover during rate removal. ACE 1 to ACE 2 changeover was also inhibited whenever power was commanded from ACE 2 to ACE 1; otherwise, the ACE changeover signal generated at ACE 1 power turn-on caused automatic power switching back to ACE 2.

TVC gain was high prior to lander separation and low after lander separation to maintain adequate TVC loop stability margins. TVC enable was initiated concurrently with initiation of rocket engine burn and inhibited concurrently with the end of the burn except as required for TVC checkout. This was particularly important when the path guidance loop was enabled because the GA's could be driven into the stops within a matter of seconds. Improved transient performance with no loss in velocity correction resulted with path guidance disabled for engine burns of less than 3.5 sec. This was determined after noting in-flight performance.

If the Earth albedo effect was sufficient to bias the roll axis off the Sun line so that the SG was not obtained during Sun acquisition, the Sun gate backup was commanded after reaching steady-state control on the ACQ SS prior to the time that the CCS Sun acquisition routine caused ACE power changeover. After settling on the CR SS, Sun gate backup reset was commanded to restore the normal state of the logic. Transient actuation of the RCA jet valves was expected when exiting directly from the celestial cruise mode because of transients in the IRU outputs. If power was commanded to the IRU not enabled, the

ACS remained in the celestial cruise mode while the IRU was warming up. This procedure was used if operation in the celestial cruise mode was preferable during IRU warm-up. This procedure could avoid the transient jet actuations at IRU turn-on and would result in lower gas consumption if gyro noise was significant. A warm-up period of at least 1 hr was required for the IRU to meet commanded turn accuracy requirements. IRU 2 enable was the more desirable normal state of the IRU enable logic signal. If initialization occurred in a mode other than celestial cruise, the IRU that was being used prior to initialization would continue to be used; thus, the large transient was avoided that could occur during gyro run-up if IRU's were switched at initialization. The normal procedure for performing roll override was to command (7E2) after going to the celestial cruise - gyros on mode to avoid the transient that resulted when initiating roll search with the IRU's off. The state of spin-up inhibit logic was checked (via telemetry) prior to entering the celestial cruise - gyros on mode and it was reset if set. If initialization occurred with IRU 2 on, IRU 2 could remain on and not respond to IRU 2 off signal until the logic signal IRU 2 pwr was cycled on then off.

Normal operation was always with ACE 1 so that ACE 2 could serve its redundant role if automatic logic indicated the need for changeover. (Automatic ACE changeover only occurred from ACE 1 to ACE 2 and not from ACE 2 to ACE 1.) Both RCA's were used normally to provide design torques and damping. The use of one RCA provided the potential for reduced gas usage during celestial cruise. The merits of using one or both RCA's were evaluated in flight. Launch mode disable was commanded after solar panel deployment to make ACS operation independent of the state of ACS enable. It was advisable to command launch mode disable prior to critical events such as propulsive maneuvers.

Pyrotechnic Subsystem

Purpose and Function

The pyrotechnic subsystem provided for squib actuation of all VO electroexplosive devices, electrical energy storage and power switching for initiation of the VO electroexplosive devices (except spacecraft release devices), and switching of electrical power for actuation of solenoid valves used in the PROPS. The functions involving the PYROS were to separate spacecraft, to unlatch high-gain antenna and scan platform, to open PROPS propellant isolation pyrotechnic valves, to open and close PROPS pressurant control pyrotechnic valves, to actuate PROPS propellant isolation solenoid valves and engine solenoid valve, to separate aft bioshield/VLC adapter, to open PROPS and ACS HPM gas share pyrotechnic contingency and/or failure correction valves, and to open PROPS propellant bypass pyrotechnic valves.

Description

PYROS hardware items consisted of electrically initiated hot-wire squibs, a PSU used for initiation of squibs, and a PAU used for actuation of the PROPS solenoid valves. The approximate location of the squibs is shown in figure 129. The PSU and PAU were electronic subassemblies located in bay 15 of the VO. A

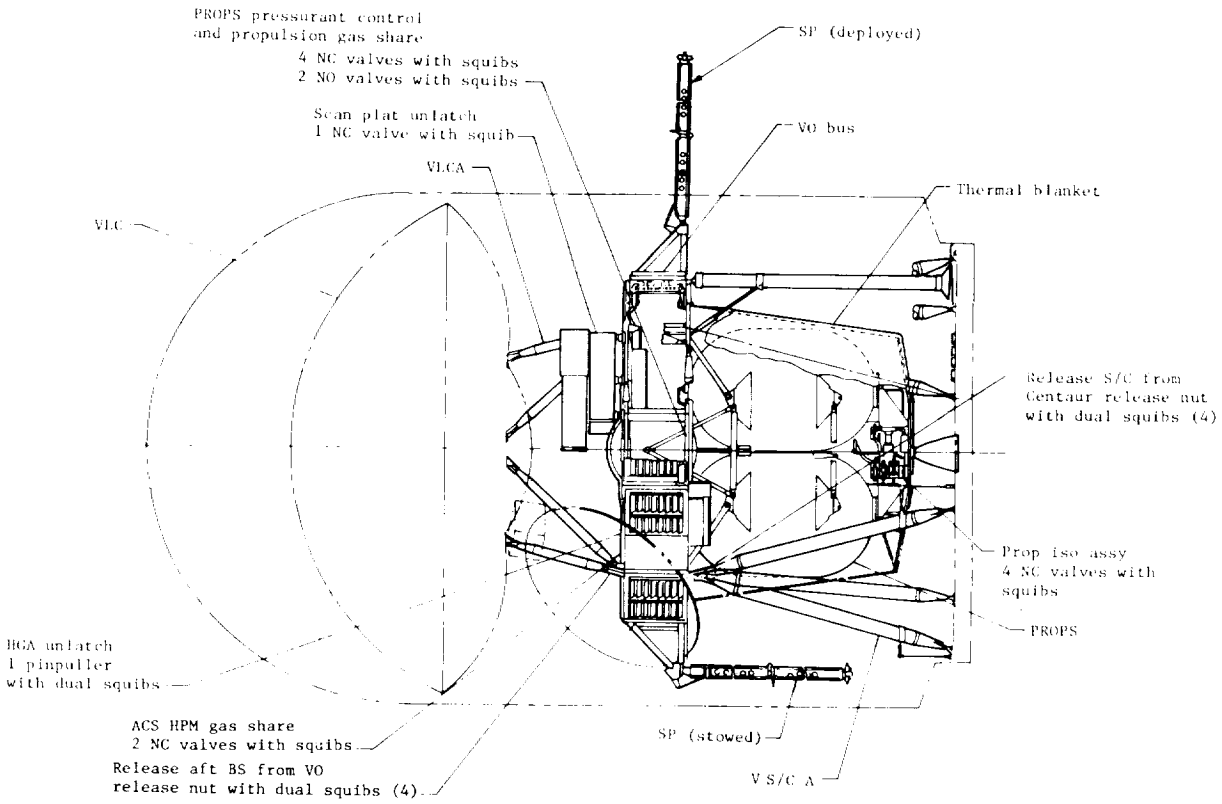

Figure 129.- Location of squibs and electroexplosive devices.

block diagram of PYROS is presented in figure 130. As shown in the figure, the spacecraft separation release device squibs were initiated (fired) by the Centaur pyro control unit in the LV. The other PYROS squibs were fired by the PYROS PSU as commanded by the CCS. The PROPS solenoid valves were actuated with power from the 30 V dc converter, when switched by the PAU, as commanded by the CCS.

Squibs.- A total of 31 squibs of 4 different sizes were used in the PYROS in squib-actuated devices. The four squib configurations had the same basic design, shown in the cross-sectional view in figure 131. Each of the four squib types had a different quantity of explosive output charge, as dictated by the requirements of the device which was to be actuated. Two of the four squib types had a single bridgewire and were used in redundant pairs in a pinpuller and in release devices. The other two squib types had dual bridgewires and were used in explosive valves (one squib per valve). The squib type usage is shown in the block diagram in figure 130.

Pyrotechnic switching unit.- The PSU (fig. 132) was configured in an active parallel redundant manner to discharge firing of hot bridgewire squibs. The PSU also provided for enable/inhibit (charge/discharge) control of the energy storage capacitor banks.

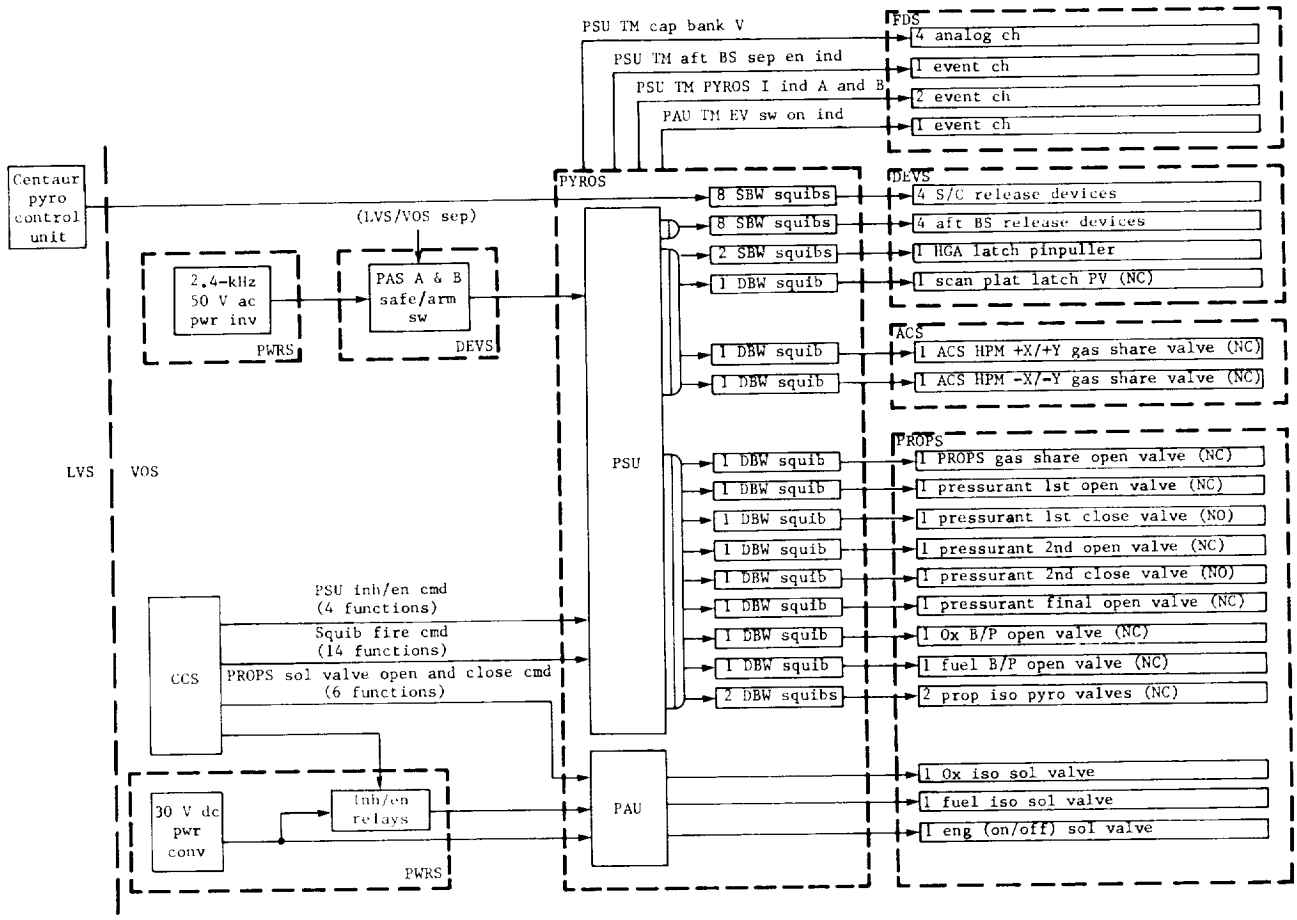

Figure 130.- Functional block diagram of PYROS.

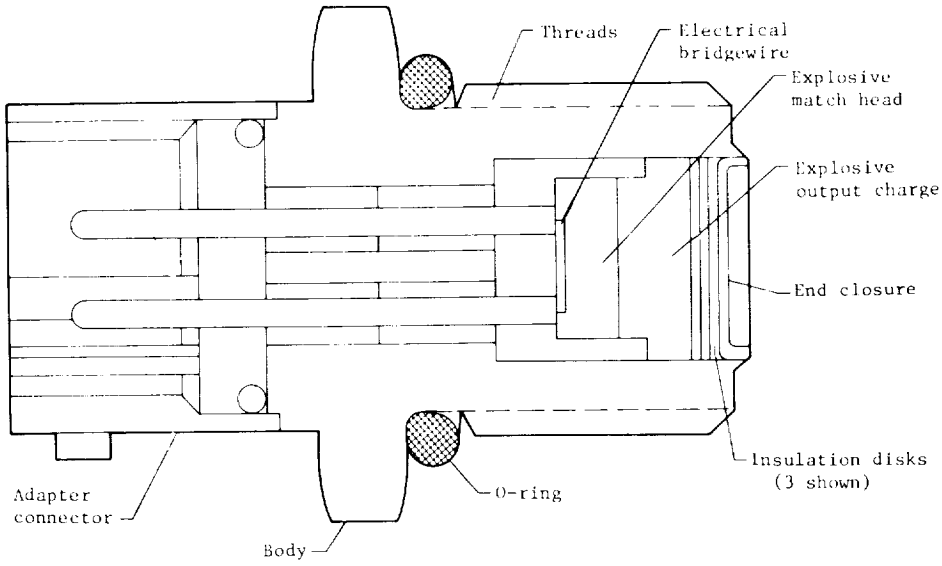

Figure 131.- Cross-sectional view of PYROS squib.

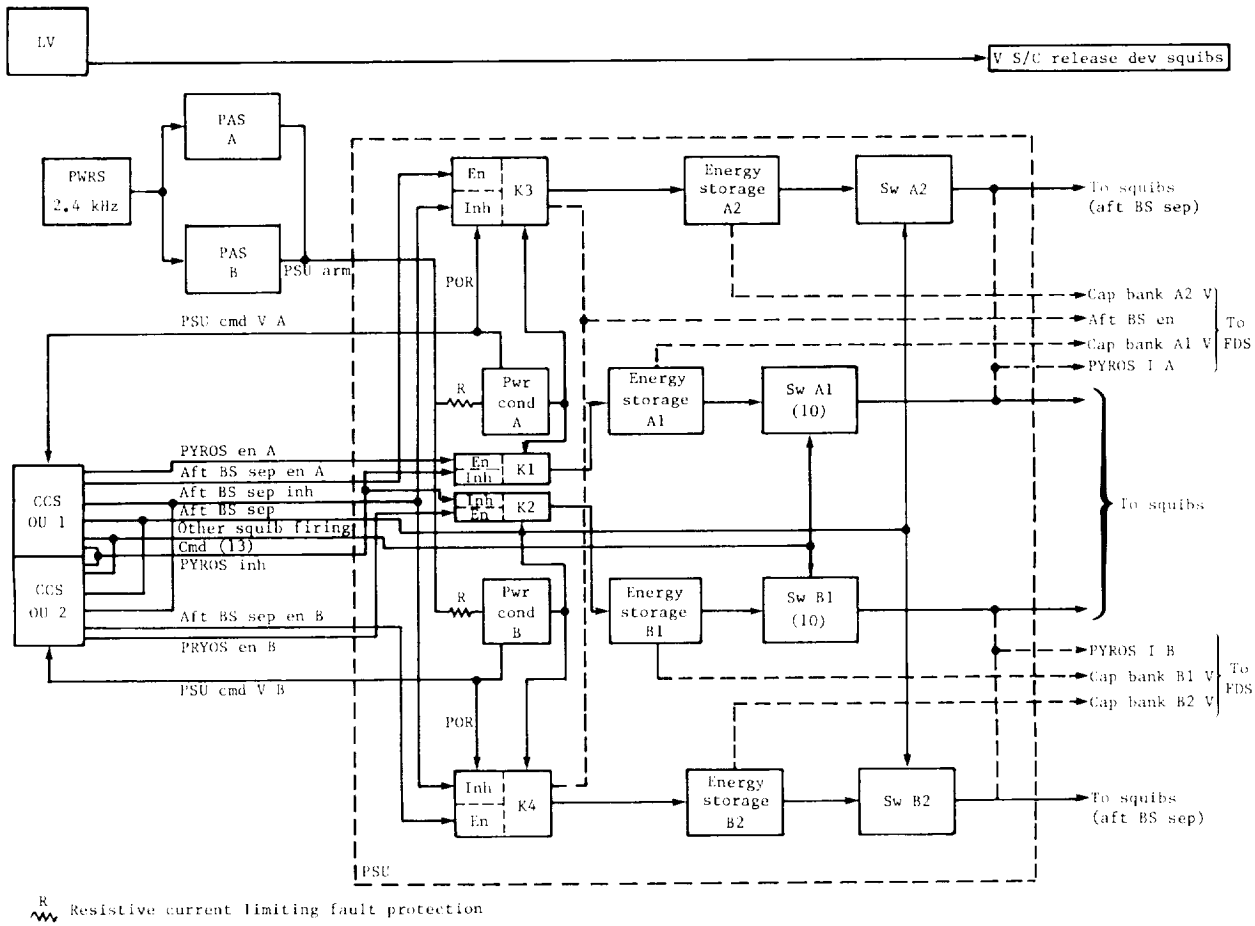

Figure 132.- Block diagram of PSU.

Propulsion actuation unit.- The PAU (fig. 133) received power from the 30 V dc converter within the PWRS. Upon receipt of the appropriate command from the CCS, the PAU switched the 30 V dc power to open or close solenoid valves which were used for propellant isolation and bipropellant engine control within the PROPS.

Cabling Subsystem

Purpose

The cabling subsystem provided the necessary electrical interconnections between all VO equipment through the system cabling harnesses, the subsystem electronic assembly harnesses, and the interface cabling from the VO to the LVS and VLC. There were 34 electrical harnesses in the orbiter plus an additional 7 on the two adapters. The rf cabling and waveguides are part of the RFS or antenna subsystems rather than CABLS.

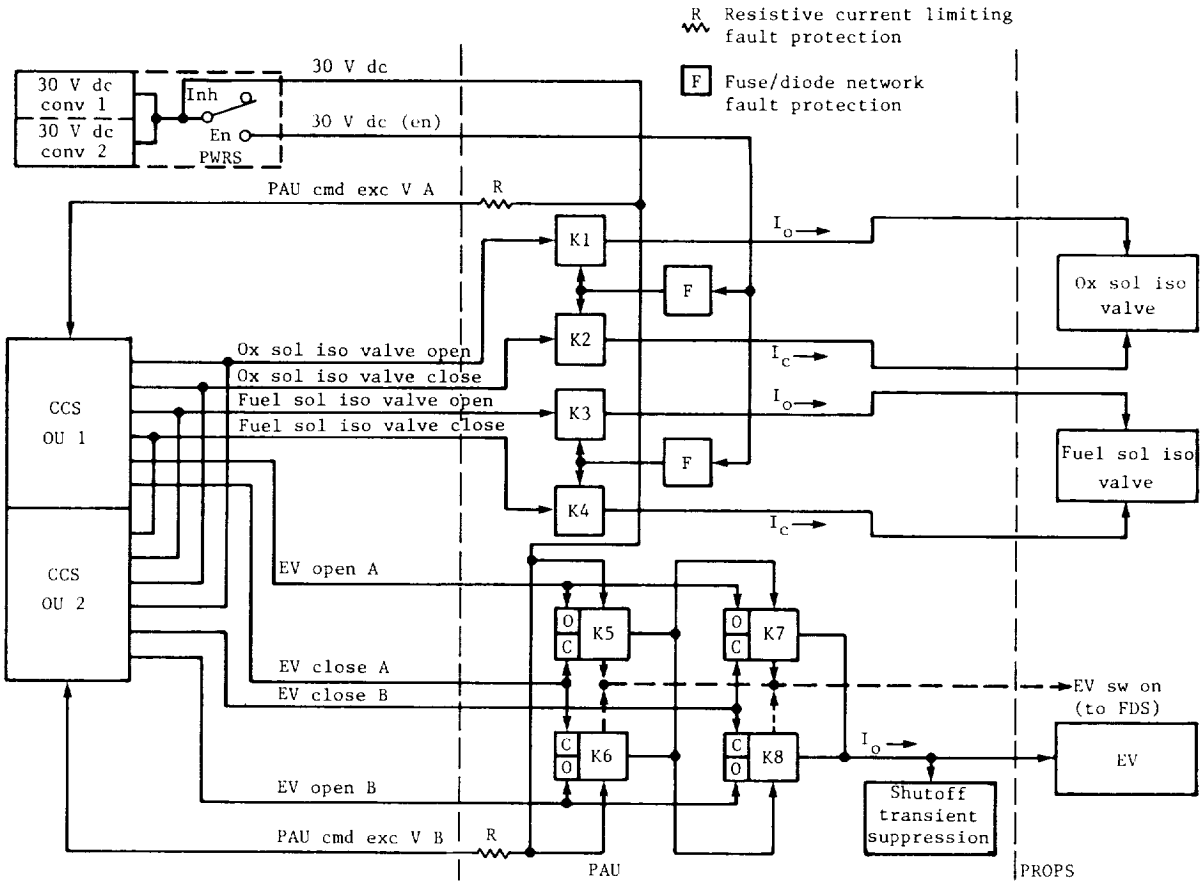

Figure 133.- Block diagram of PAU.

Description

In all harnesses, the connectors were potted, spare connector locations were not wired, redundant wiring did not in general exist, and 22-gage Teflon insulated wire was used and shielded only when necessary. The electrical system ground was attached to the structure via a connection to the cable trough. All pyro functions (fig. 131) for V S/C A separation were on the Centaur side of the in-flight separation interface and all VLCA/aft BS separation pyro functions were on the orbiter side of the interface. This avoided pyro firing currents going through the separation connectors. Performance margins and component derating were applied to wires and connectors to allow for the effects of the thermal and vacuum environments, such as heating by the Sun, cooling in a shadow, and wire bundle flexing during flight. Electrical cross-coupling of cabling circuits was controlled within the limits required for reliable system operation by providing isolation of incompatible circuits, by using physical separation, by twisting, and by shielding. Power was distributed to the VO subsystems and to the VLC during cruise as required. Power cables were designed and fabricated to minimize electrostatic and electromagnetic coupling with other circuits and to minimize power losses. Cabling utilized for electroexplosive device firing circuits excluded undesired electrical energy by the use of

complete and continuous shielding from the pyrotechnic control unit to the device housing, including exclusive use of approved type connectors.

Physical Characteristics and Restraints

Consideration was given to the following physical factors affecting the design: insulation properties; mechanical strength; protection from heat; dissipation of heat; and accessibility during construction, rework, adjustment, and test. The cable harnesses were designed to withstand the environmental stresses encountered on Earth during testing, checkout, and launch, as well as those environments encountered in space. The effects of the space environment upon all components and materials used in the cabling subsystem were evaluated for compliance with design criteria. Wiring across articulated interfaces was given special design consideration to insure reliable operation over the required range of motion under all anticipated environments. Cables were protectively jacketed in regions of possible abrasion or stress concentration. Every effort was made to select connectors sufficiently dissimilar to prevent incorrect coupling to other connectors in the vicinity. Electronic subassembly receptacles, test receptacles, and in-flight separation receptacles of the flight orbiter employed sockets (not pins) which were recessed within the connector insulating insert. Subsystems did not share connectors. Connector shells were conductively mounted to the associated mechanical element (subchassis, bracket, etc.). The connectors at the interfaces between the VO and V S/C A and between the VO and VLCA were capable of separation in flight. The connectors at the interfaces between V S/C A and Centaur and between the VLC and aft bioshield were capable of being connected and disconnected under field conditions. Direct access test circuits between the VO and the support equipment were carried by the orbiter cabling to test receptacles mounted on the lower brackets of electronic assemblies as required to be consistent with orbiter design criteria. Twisted groups of wires utilized adjacent connector contacts. Wires were also grouped within a connector to separate signals and power of differing characteristics as much as possible to minimize cross-coupling. Splicing was kept to a minimum; however, splices were allowed to save weight.

Propulsion Subsystem

Purpose and Function

The propulsion subsystem was a modular element designed to deliver over 3.87 MN-sec (870 000 lb-sec) of propulsive impulse to the V S/C. The basic purpose of the PROPS was to produce, upon command, a directed impulse to accomplish ITC, an MOI maneuver, and up to 20 MOT maneuvers. Proven concepts and hardware were integrated into the basic design to yield the highest possible reliability. The subsystem design requirements were formulated from V S/C physical and operational constraints, LV characteristics, ground and in-flight conditions, and PROPS characteristics. In summary, the PROPS was capable of providing a total velocity change of 1480 m/sec to a 3430-kg (7556 lb) spacecraft with a usable propellant mass of 1387 kg (3055 lb); providing, in a single burn, an MOI velocity increment ranging from 900 to 1325 m/sec; performing up to 4 ITC's, 1 MOI, and 20 MOT's; performing a firing within 32 hr after the

preceding firing; providing a minimum impulse capability of 534 N-sec (120 lb-sec); performing an engine firing within 240 sec after termination of the last attitude orientation maneuver; producing thrust with very small swirl disturbance, that is, less than 45.2 N-cm (4.0 in-lb) of roll torque about the roll axis; and functioning without degradation in performance for 510 days after launch in a vacuum and gravity-free environment within a temperature range of -1° to 32° C (30° to 90° F).

Description

PROPS was a fixed thrust, multistart, pressure-fed, Earth-storable bipropellant system utilizing the propellants nitrogen tetroxide (N_2O_4) and monomethylhydrazine (CH_3NHNH_2) with helium for pressurization. A two-axis, gimballed engine and electromechanical actuators provided thrust vector control in the pitch and yaw directions during engine operation. The subsystem with its structure was a mechanically defined module with eight subassemblies and is depicted in figure 134. These eight subassemblies were functionally and physically independent and extended the modular design concept into the subsystem. These subassemblies are identified in figure 134 as PTA, PCA, PTA's - fuel and oxidizer, PIA's - fuel and oxidizer, REA, and GSA. Two identical propellant tank assemblies and two identical propellant isolation assemblies were integrated into the subsystem to store and control the flow of propellants - oxidizer and fuel. Subassemblies were fabricated and tested prior to integration into a propulsion module. Brazed tubing fittings were utilized in nearly every joint to minimize leakage. Where these fittings could not be used, metallic

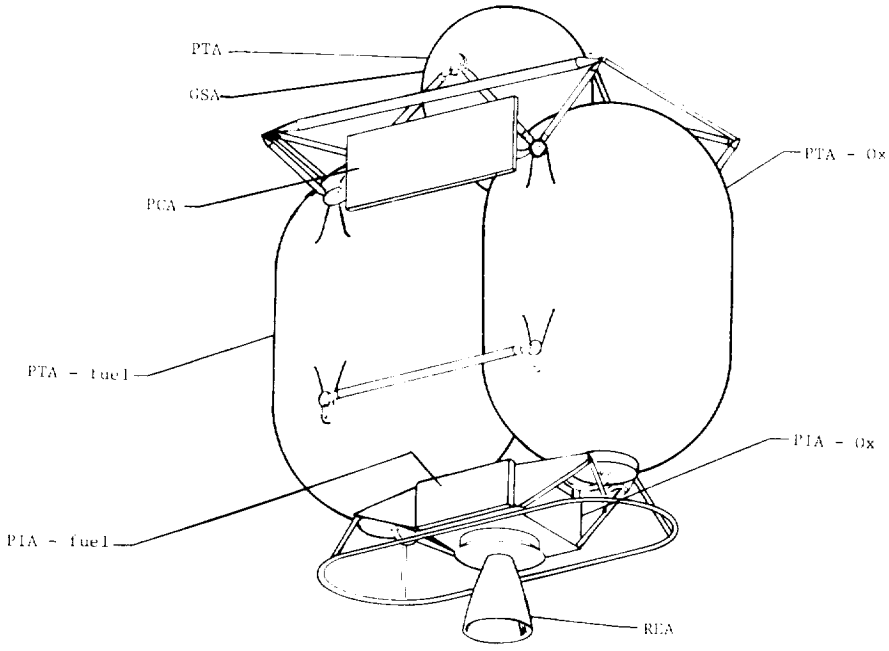

Figure 134.- Propulsion module.

seals were employed. Pyrotechnically actuated valves and redundantly sealed test and service ports were used to minimize external leakage. Flexible steel convoluted propellant lines were used to connect the engine to the PIA's. The basic operation of the subsystem can be described from a propulsion schematic shown in figure 135. Note the eight identified subassemblies. Propellants

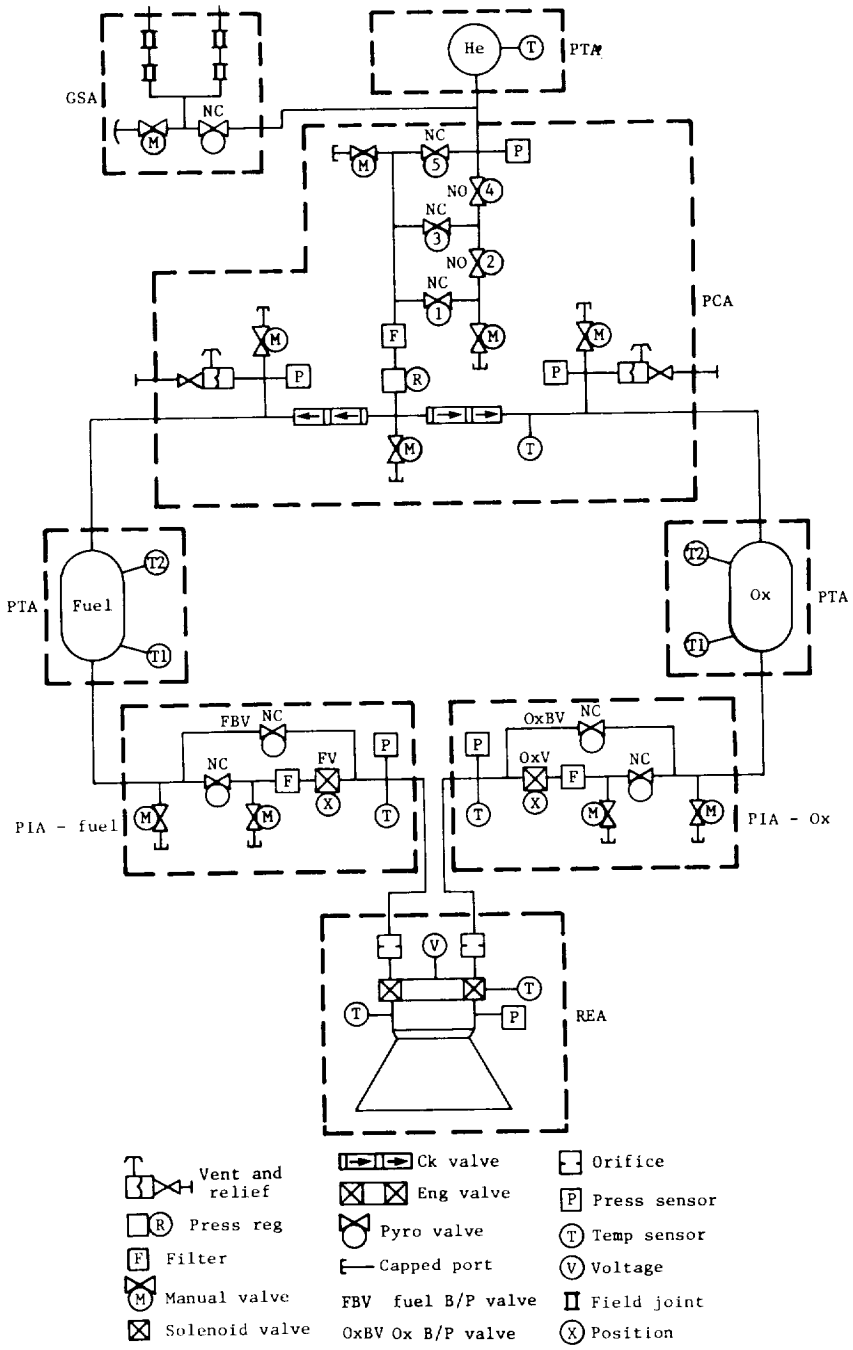

Figure 135.- Schematic diagram of PROPS.

flowed from the propellant tanks, through the propellant isolation assemblies, and into the rocket engine combustion chamber. There they mixed and chemically reacted creating gaseous reaction products which were accelerated through the engine and ejected at high velocity. The combustion chamber nominally operated at a pressure level of 800 kPa (116 psia) while the propellant tanks operated at 172 kPa (250 psia). The pressure level in the propellant tanks was maintained by a regulated pressurant gas (helium) fed through the pressurant control assembly. The pressurant gas was withdrawn from the pressurant tank which varied in pressure from approximately 24 MPa (3500 psia) early in the mission to 6 MPa (900 psia) at end of mission. The pressurant and propellant isolation assemblies provided fluid filtering and positive isolation of the pressurant gas supply and the propellant liquids during long periods of cruise. The gas share assembly was not an integral part of PROPS. Gas share was an add-on feature which provided a capability to transfer propulsion pressurant gas to either of the reaction control assemblies in the RCA. Gas transfer was not a normal function and was used only if a failure developed or if the normal mission was extended. PROPS was prepared for operation by opening the fluid circuits in the pressurant and propellant isolation assemblies. Thrust start and termination was then controlled by commanding the engine valve open and closed. Since the propellants were hypergolic, the subsystem had a potentially unlimited restart capability.

Figure 136 is a cutaway sketch of the rocket engine assembly. The elements of the engine included a torquemotor operated, mechanically linked bipropellant valve; a chamber pressure sensor; a 2219-T6 aluminum unlike-doublet injector; a 6Al-4V titanium split ring; a 6Al-4V titanium thrust mount; a one-piece beryllium thrust chamber; a 7075-T73 aluminum gimbal ring assembly; a René 41 coupling nut; and a radiation-cooled nozzle extension.

The thrust chamber utilized the unique properties of beryllium and controlled injector parameters, with fuel film cooling for internally regenerative

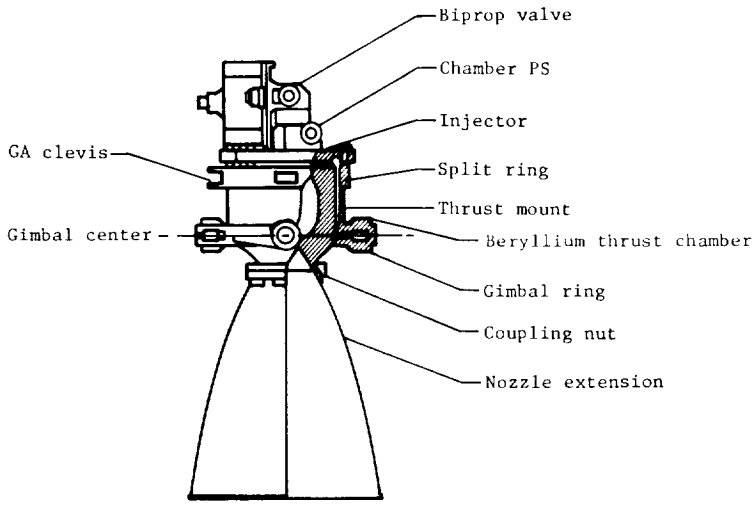

Figure 136.- Rocket engine assembly.

operation. Figure 137 is a simplified schematic illustrating the characteristics of the heat flow paths. The hatched area represents a cutaway of the

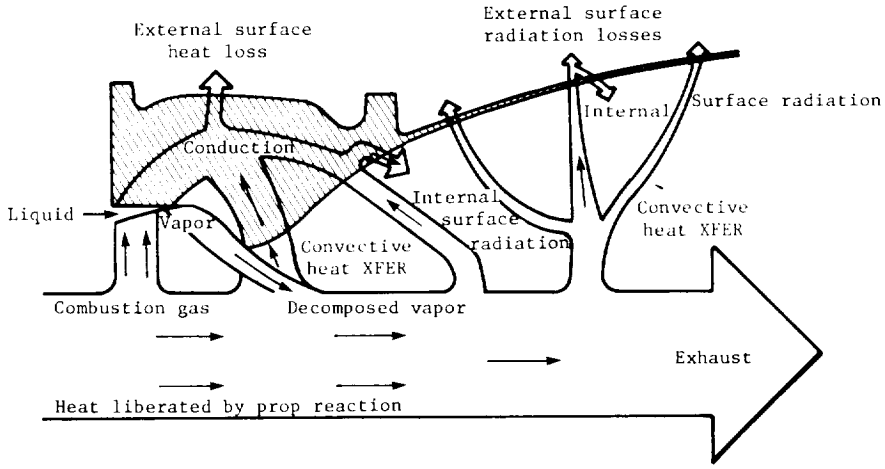

Figure 137.- Schematic diagram of conduction cooling heat flow.

rocket engine, the arrows indicate heat flow direction. The engine bipropellant or "Moog" valve was bolted to the engine injector. The valve contained a single actuator which was mechanically linked to oxidizer and fuel poppets. The valve was magnetically closed and was electrically opened by applying 30 V to the actuator coil. The valve seats in both the oxidizer and fuel side were made of Teflon. The pointing position of the rocket engine was controlled by two gimbal actuators. The engine moved within a gimbal ring (fig. 136), the the gimbal center was located in spacecraft coordinates at Z = -1.6 m (-63.58 in.). The gimbal actuators (in the null position) lay in a plane parallel to the spacecraft X-Y plane at Z = -1.55 m (-61.05 in.). Each engine was accurately calibrated and tested prior to integration into the propulsion subsystem. Calibration was achieved by the installation of hydraulic resistance orifices in the inlets of the Moog valve and performance was established from hot-fire engine testing. A summary of design and nominal performance characteristics is presented in table 36.

The propellant isolation assemblies provided a means for isolating propellants during ground handling and extended flight cruise. Two identical assemblies were required, one for the fuel side and one for the oxidizer side. A sketch of an assembly is shown in figure 138 with the major elements identified. The primary flow path was through the fired isolation pyro valve filter and solenoid valve. A secondary or bypass path could be opened if a solenoid valve opening failed. Then, the flow path bypassed the solenoid and filter elements. The propellant isolation assemblies were installed between the propellant tanks and a flexible line running to the rocket engine. The two pyro valves in each PIA were normally closed and provided absolute propellant

TABLE 36.- ROCKET ENGINE RATED PERFORMANCE SUMMARY

Prop:		
Ox		N_2O_4
Fuel		CH_3NHNH_2
Thrust chamber physical characteristics:		
Combustion chamber		
Diameter, cm (in.)		7.62 (3.0)
Volume, cm^3 (in^3)		274 (16.7)
Characteristic length, cm (in.)		29.5 (11.6)
Contraction ratio		4.9
Nozzle		
Throat diameter, cm (in.)		3.44 (1.3555)
Exit diameter, cm (in.)		26.7 (10.5)
Expansion ratio		60:1
Contour		Modified 80% bell
Throat area, cm^2 (in^2)		9.31 (1.4431)
Exit area, cm^2 (in^2)		558.6 (86.59)
Steady-state performance characteristics:		
Thrust, kN (lb)		1.34 (301.0)
Specific impulse, N-sec/kg (lb-sec/lb)		2858 (291.7)
Chamber press, kPa (psia)		797.7 (115.7)
Mixture ratio		1.51
Prop flow rates		
Ox, kg/sec (lb/sec)		0.282 (0.6208)
Fuel, kg/sec (lb/sec)		0.187 (0.4111)
Characteristic velocity, m/sec (ft/sec)		1587 (5207)
Thrust coefficient		1.802
Press drop at -	Oxidizer	Fuel
Injector, kPa (psid)	353.7 (51.3)	341.98 (49.6)
Mooq valve, kPa (psid)	199.9 (29.0)	199.3 (28.9)
Calib orifice, kPa (psid)	227.5 (33.0)	293 (42.5)

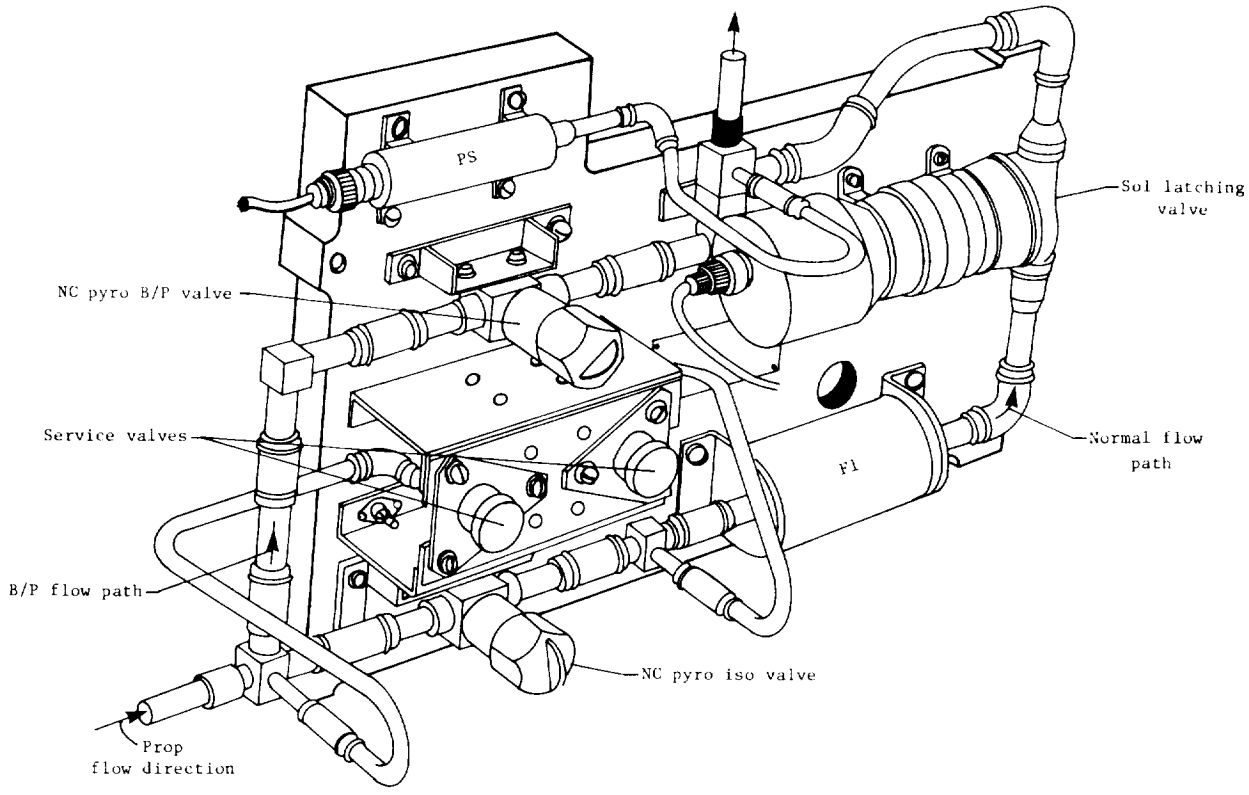

Figure 138.- Propellant isolation assembly.

isolation during ground operations prior to the first propulsive maneuver. Figure 139 illustrates the valve configuration in the open position after actuation.

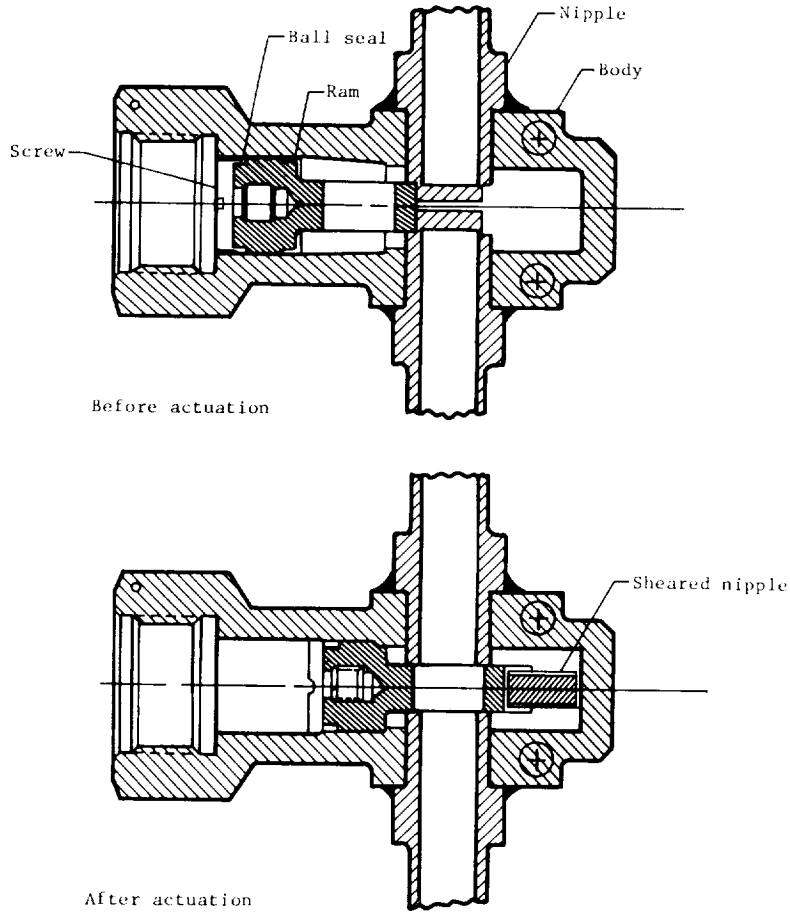

Figure 139.- NC squib actuated pyro valve.

Two identical propellant tank assemblies were utilized. Each assembly consisted of the elements shown in figure 140. The vane assembly and communication channel function was to position the propellant over the outlet port and center the ullage gas bubble around the pressure-vent port in a 0g environment. The propellant feedlines were connected to the outlet port and the pressurant gas supply to the pressure port. The tank's nominal internal volume is 0.717 m^3 (43 769 in^3). The vane assembly and communication channel was referred to as the PMD. The PMD configuration was an integrated surface tension device. The general features included a 12-blade vane assembly and a capillary (communications) channel. The vane assembly centered the ullage bubble in the tank top (pressure port end) in a 0g field and maintained pressurization tube contact with the ullage bubble in a low-g field ($<10^{-5}$g). If liquid condensed on the tank top or separated from the bulk liquid, the communication channel

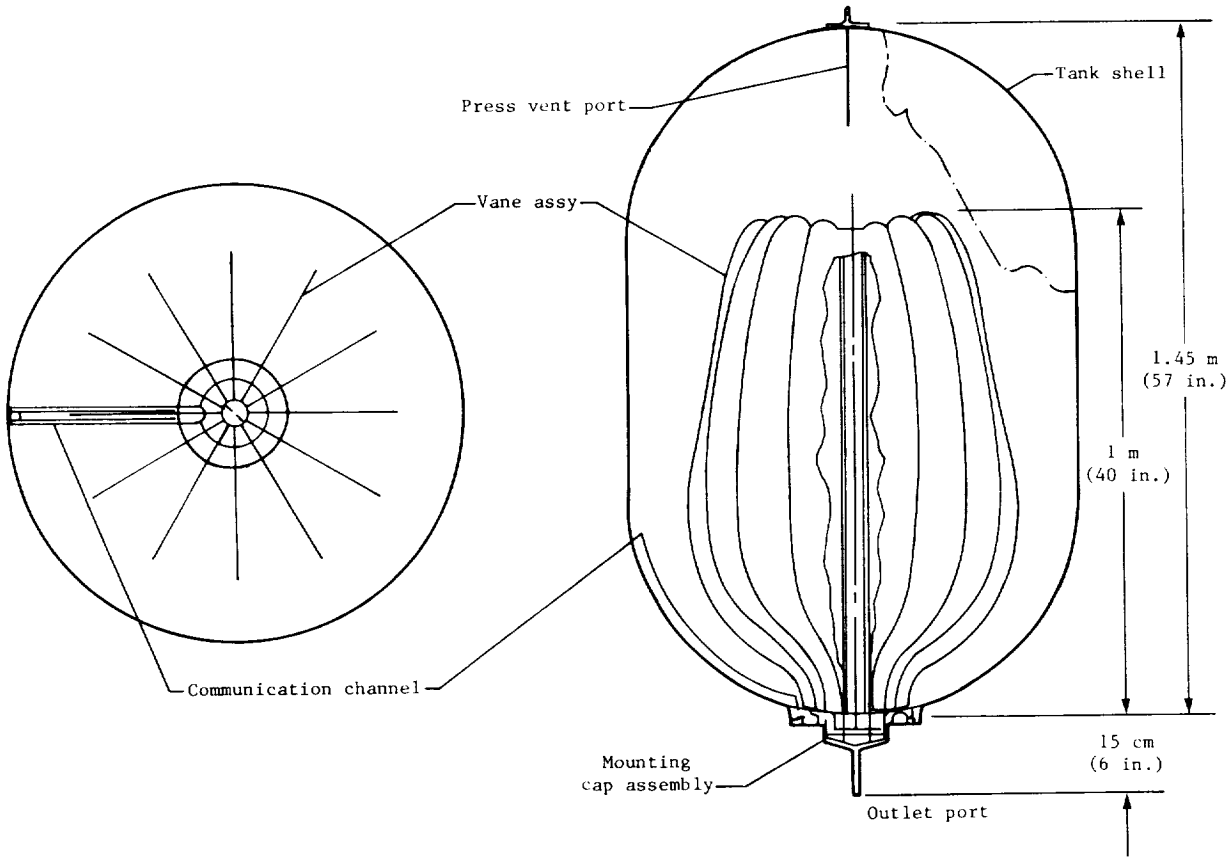

Figure 140.- Propellant management system.

transferred the liquid from the tank top to the liquid bulk. Helium pressurant gas entered the propellant tank through the pressure-vent port. In the event of tank overpressurization, due to an unusual thermal transient or regulator failure, helium also vented from the same port.

Propellant tank pressurization and pressurant gas conservation were achieved by the actions of the pressurant control assembly. High-pressure gas was regulated to a lower pressure (1758 ± 55 kPa (255 ± 8 psia)) and fed to each of the two propellant tanks. Figure 141 is a sketch of the pressurant control assembly. The five pyro valves were located in the middle section, the regulator was located to the left of the pyro valves, and the check valves were near the outer edges. In figure 141 circled numbers have been added to trace the gas flow path. Helium entered at (1) and flowed through various combinations of pyro valves identified by (2). The gas exited the pyro package at (3) and flowed through the filter and regulator before encountering a "T" which split the flow for delivery to the two propellant tanks. After leaving the T, (4), and (4') the gas flowed through the check valves and left the assembly at (5) and (5'). Two relief valve assemblies were tied into the system downstream of the check valves. Each relief valve assembly contained a series of redundant burst

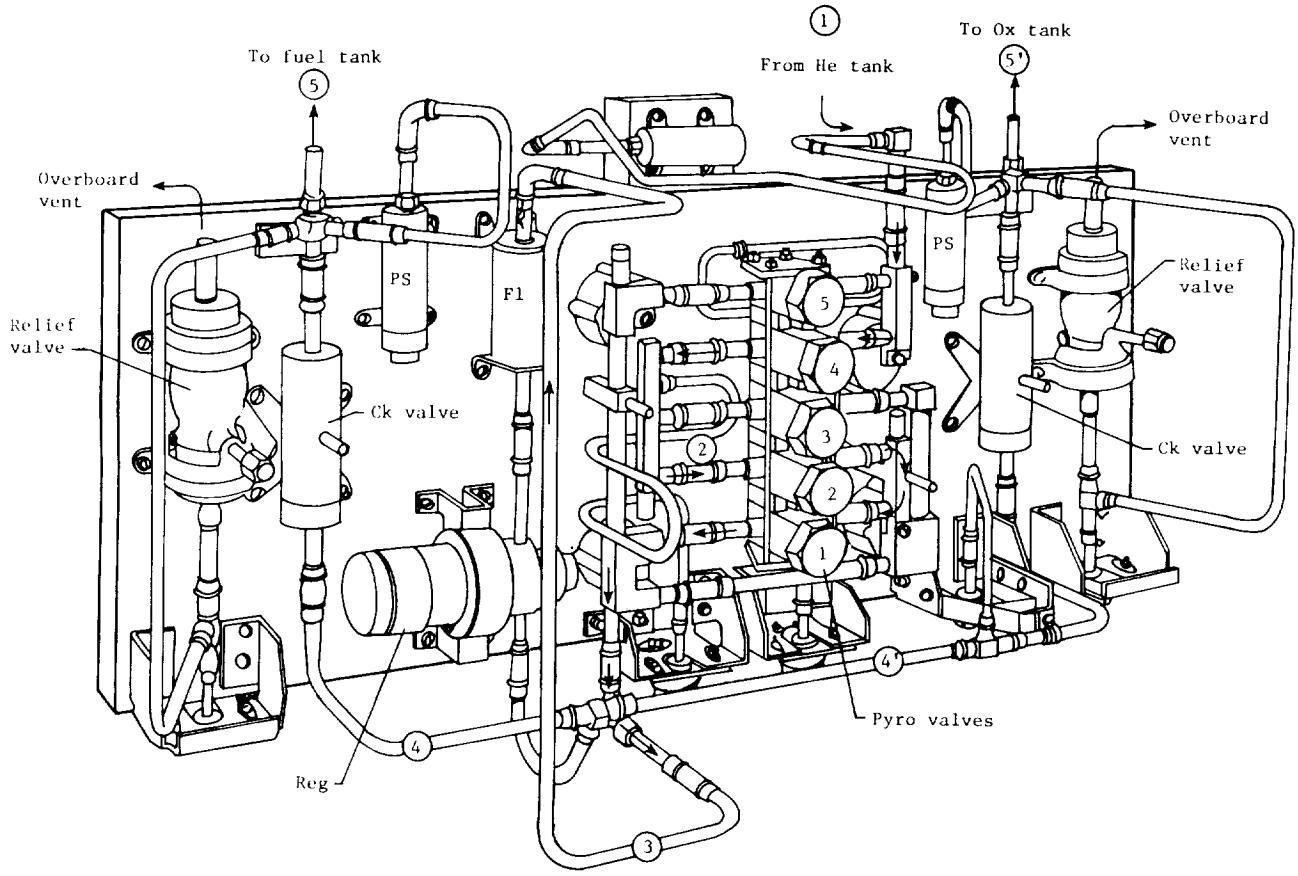

Figure 141.- Pressurant control assembly.

diaphragms and vented pressurant gas overboard if the propellant tank pressures exceeded 2241 ± 35 kPa (325 ± 5 psia) (burst diaphragm rupture point). The pyro package consisted of three normally closed valves and two normally open valves. The normally closed valves were like the propellant isolation valves shown in figure 139. The normally open valves had an open flow path which was blocked by a ram when the squib fired. The arrangement of the valves and interconnecting manifolds provided pressurant gas isolation until pyro valve 1 was actuated open. Then high-pressure gas was supplied to the regulator for propellant tank pressurization. Pyro valve 2 actuation blocked gas flow to pyro valve 1 and reestablished high-pressure gas isolation. In a similar manner, pyro valve 3 opened the system, 4 isolated, and 5 reopened. The pyro valve package provided for launch plus two flight gas isolation intervals and three opening sequences. The end state or firing of all pyro valves produced an open flow path.

The pressurant tank assembly consisted of a 0.63-m-diameter (24.734 in.) spherical tank with mounting tabs and an inlet-outlet port. The tank volume was 0.1298 m^3 (7923 in^3) and its full load capacity was 4.86 kg (10.7 lb) of helium.

The gas share assembly was an add-on system which could be used to transfer propulsion helium gas to one or both high-pressure modules in the reaction control assembly of the attitude control subsystem. The propulsion portion of the gas share assembly consisted of tubing, one NC pyro isolation valve, field joints, and a service valve. The pyro valve isolated the helium gas. All joints upstream of the pyro valve were brazed to assure minimum leakage.

Mechanical Devices Subsystem

Purpose and Function

Various functions of release, deployment, actuation, damping, latching, and in-flight adjustments were performed by the mechanical devices subsystem. These were located on the configuration as shown in figure 142.

The devices can be grouped into six functional groups as follows:

Solar-panel related devices
Temperature control devices
Separation devices
Scan platform release devices
Antenna release and deployment devices
Arming and event indicating devices

Description

The Viking spacecraft (orbiter and lander) was bolted at four places to the spacecraft adapter with a multiphase high-tensile bolt equipped with a built-in strain gauge to control preload at the joint. The bolt was located on the spacecraft side of the separation interface and a pyrotechnically actuated segmented nut was located on the adapter side of the interface. Each nut and bolt pair was torqued to a preload (as read by the strain gauge) of 52 kN (11 600 lb) tension. Upon a command issued by Centaur, the release-nut pyrotechnic devices were fired, the nut released, and the bolt ejected into a bolt catcher. Separation was effected by the four separation springs located adjacent to the release nuts giving a relative velocity between the spacecraft and the Centaur and adapter assembly. Identical release and similar separation springs were used to separate the lander adapter from the orbiter.

During the separation event the two PAS's were actuated by relative motion of about 7.6 mm (0.3 in.) between the orbiter and the spacecraft adapter. Signals were issued to the following areas:

(1) PYROS arming power

(2) MAWDS unlatch enable

(3) Separation indication to FDS

(4) Separation indication to CCS

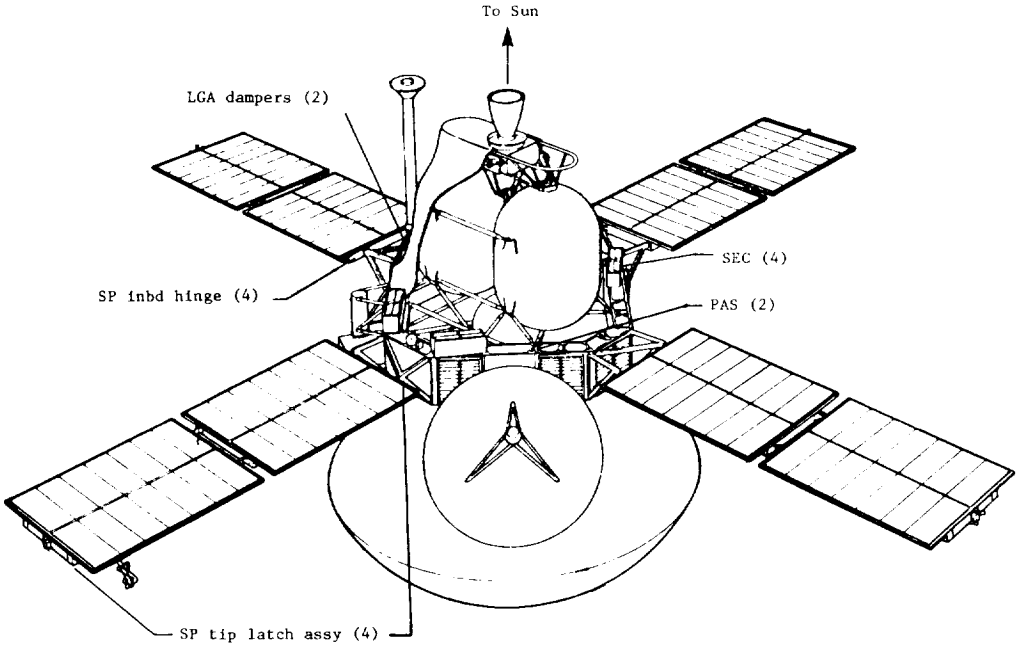

Top view.

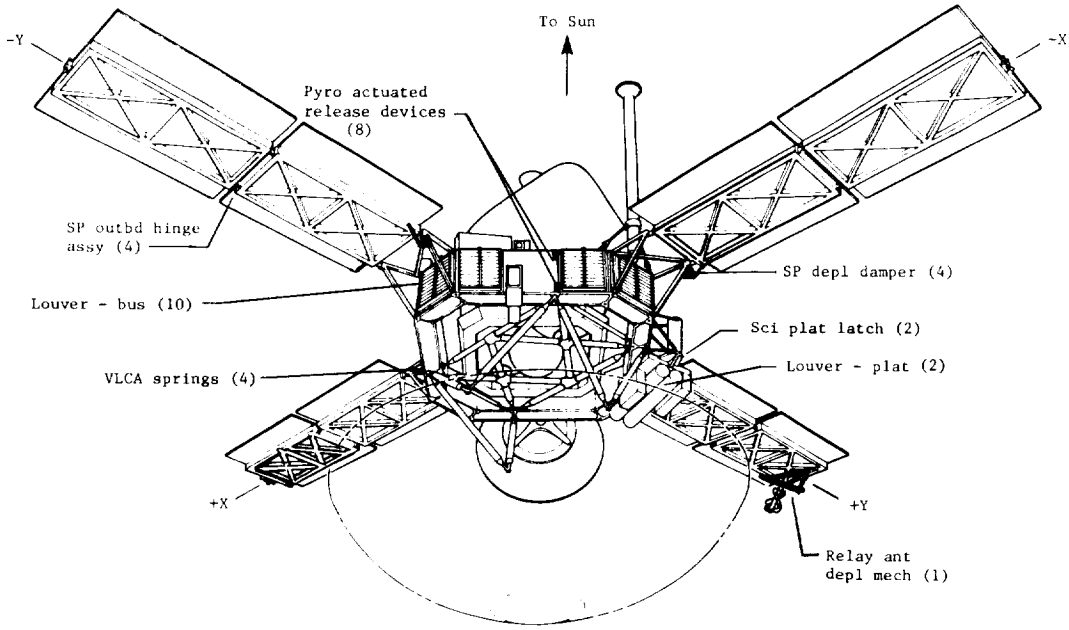

Bottom view.

Figure 142.- VO configuration.

During the launch phase, the low-gain antenna was supported and damped by two low-gain antenna dampers of a modified M71 S/C design located such that their axes were about 90° to each other and attached to the antenna at about a third of the distance from its base. The center line of each damper intercepted the center line of the antenna at about a 45° angle and extended over to the antenna base at the spacecraft separation plane.

The solar-panel assembly was double folded during launch and held in the launch position by the solar-panel flyaway release rod at the outboard hinge and by the tip release latch at the inboard hinge. During launch, the flyaway rod and the panel were allowed to move through lateral motion in two directions and were damped by three boost dampers attached between the flyaway rod and the spacecraft adapter. During separation, after about 3.2 cm (1.25 in.) of relative motion, the solar panel slid off the end of the flyaway release rod and the panels were then free to deploy. Initial deployment rotation was only about the inboard hinge axis. This rotation continued for 55° until the solar-panel tip latch at the inboard hinge disengaged a cam allowing the tip latch pin to disengage the solar-panel tip. When the tip latch pin was disengaged the solar-panel outboard hinge rotation started. The outboard hinge rotation took about 7 sec to complete the 180° of rotation and to latch. The outboard panel was completely unfolded and latched before the inboard hinge motion completed its 90° of motion and latched. When the solar panels were in the deployed position and latched, the device was then in a configuration to damp the solar-panel motions induced by engine firing or scan platform slewing. See figures 143 and 144 for pictures of the solar-panel flyaway release rods.

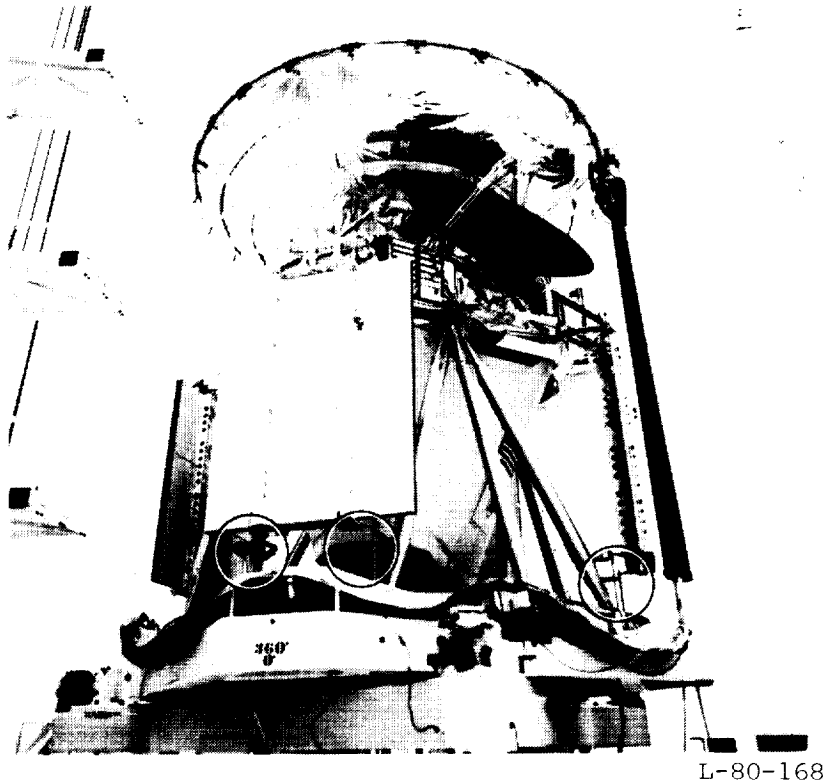

L-80-168

Figure 143.- Location of SP flyaway release rods.

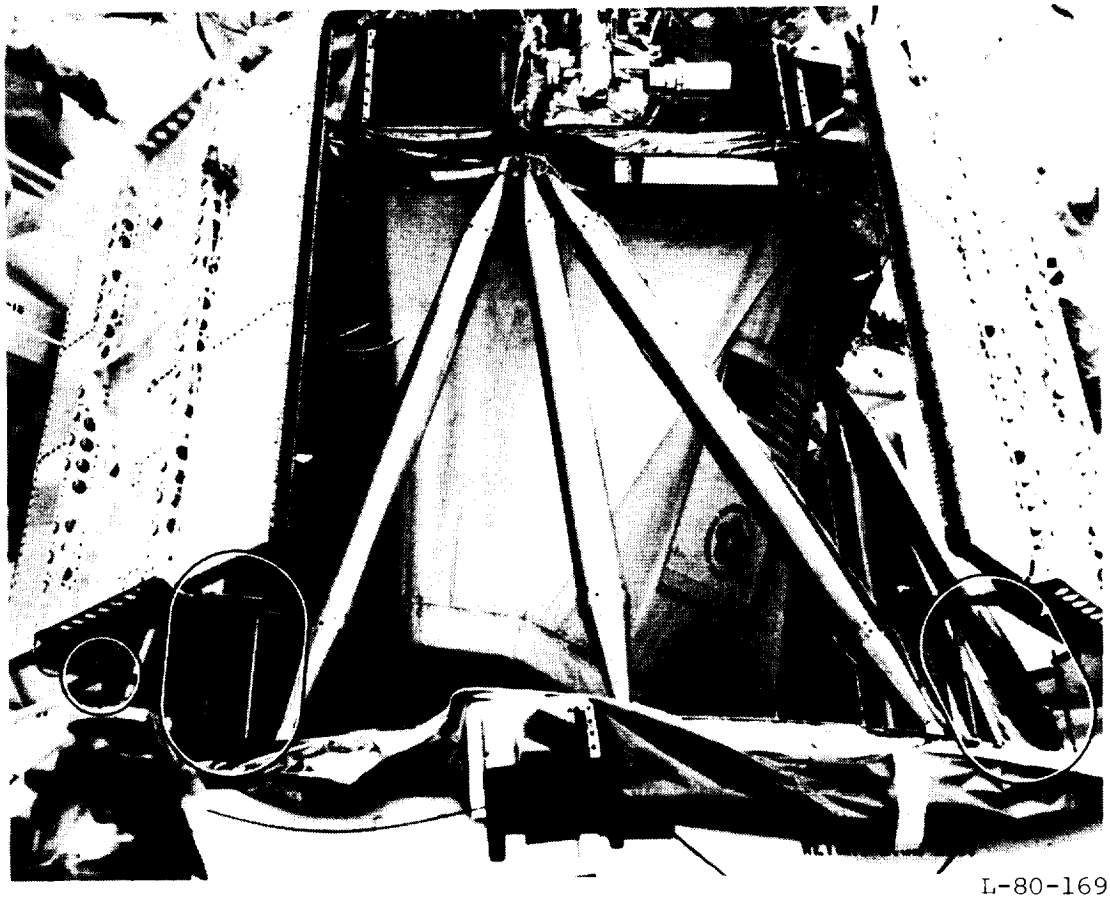

L-80-169

Figure 144.- Close-up of SP flyaway release rods.

The relay antenna was folded next to the back of the outboard +X subpanel during the launch phase. Simultaneous with the panel tip release, the relay antenna was unlatched by relieving the force on a spring-loaded control cable. This control cable pulled a clevis pin and allowed the antenna spring strut to deploy the antenna to its required position.

The high-gain antenna was constrained in the stow position during launch by a pin puller which preloaded the antenna reflector against two snubbers on the bus. Actuation of the pin puller released the antenna so that it could be pointed by the two-axis drive actuators.

During launch, the instrument scan platform structure was preloaded against three structural hard points on the bus by a set of three pneumatic latches. About 5 days after launch, by command, a pyrotechnically actuated valve vented the nitrogen gas in the latches which released the preload and allowed unlatching to take place. Prior to the unlatch command, the pressure in the system was monitored for leaks by data readout in the engineering telemetry stream. See figure 145 for a close-up view of the scan platform latches.

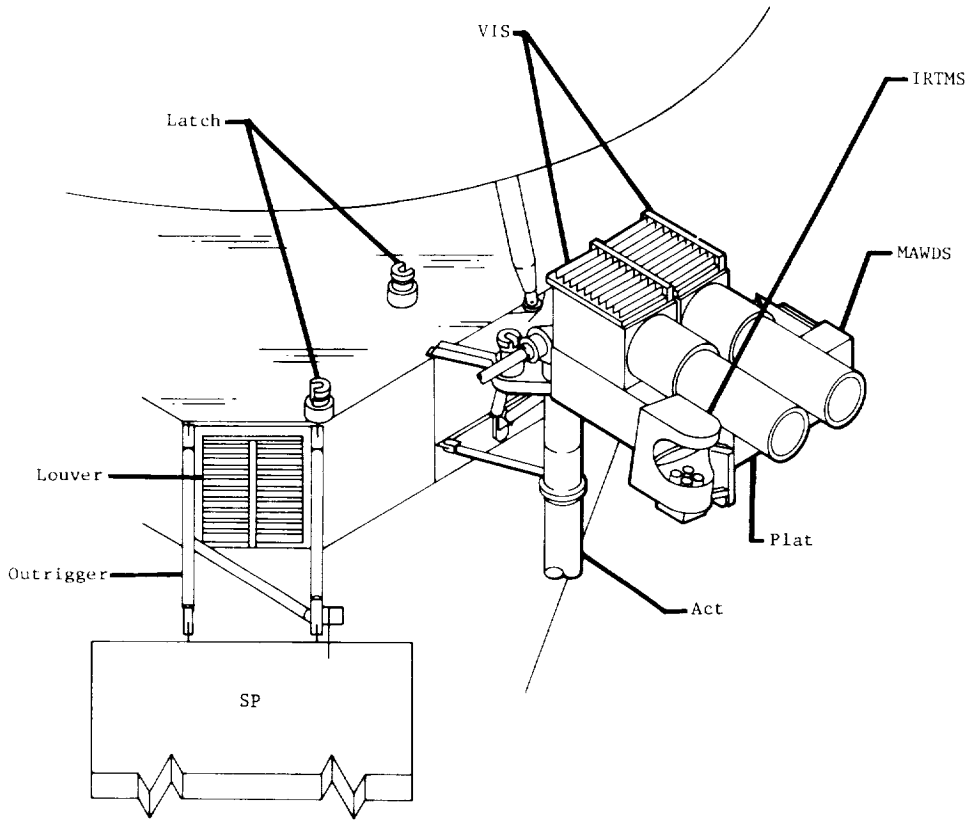

Figure 145.- Mechanical devices scan platform.

During the cruise and orbit portion of the mission, the bus and scan platform temperature control was partly accomplished by the use of louver assemblies which were made of highly polished aluminum frame and blades that were actuated by bimetal actuators. In the open position, a highly emittive surface was exposed to space. In the closed position, the polished blades covered the emittive surface. The opening set point temperature was manually adjustable and was selected and set prior to launch. The Viking louvers were similar to those on the Mariner spacecraft.

The SEC was a temperature control device that allowed Sunlight to enter an opening and reflect the solar energy into the propulsion tank cavity. The SEC opening was variable by virtue of two louver blades that were mechanically linked together and motor actuated by ground command. See figures 146 and 147 for preinstallation close-up photographs of the SEC.

Articulation Control Subsystem

Purpose and Function

The ARTCS provided closed-loop positioning of the articulated elements on the VO - namely, the scan platform, HGA, and SEC blades - in response to command

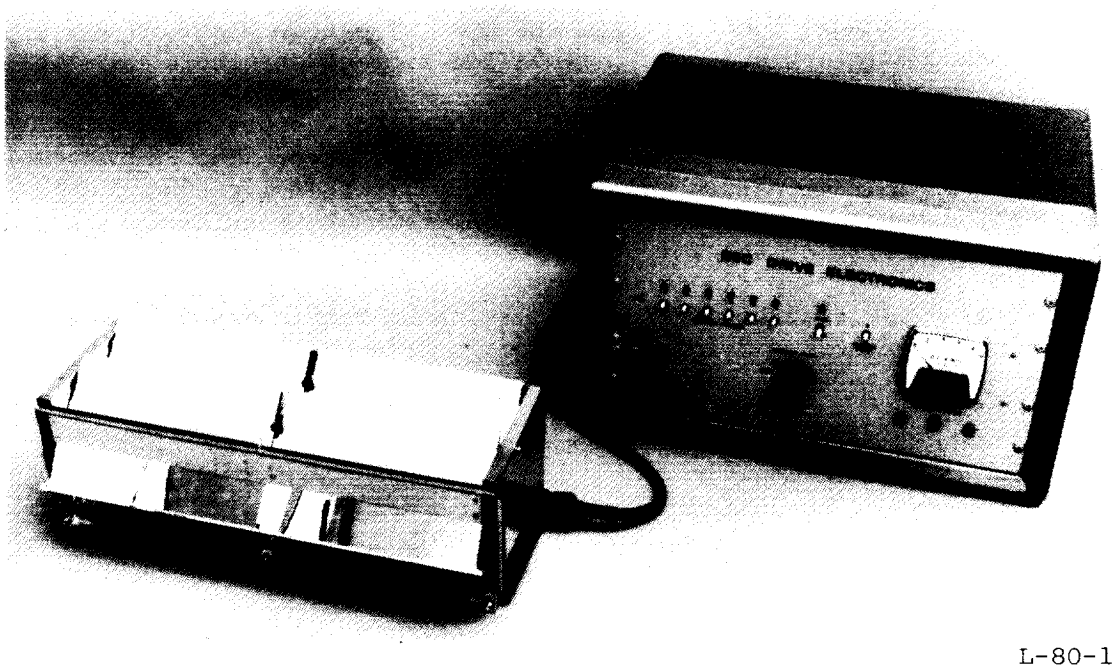

L-80-170

Figure 146.- Typical SEC.

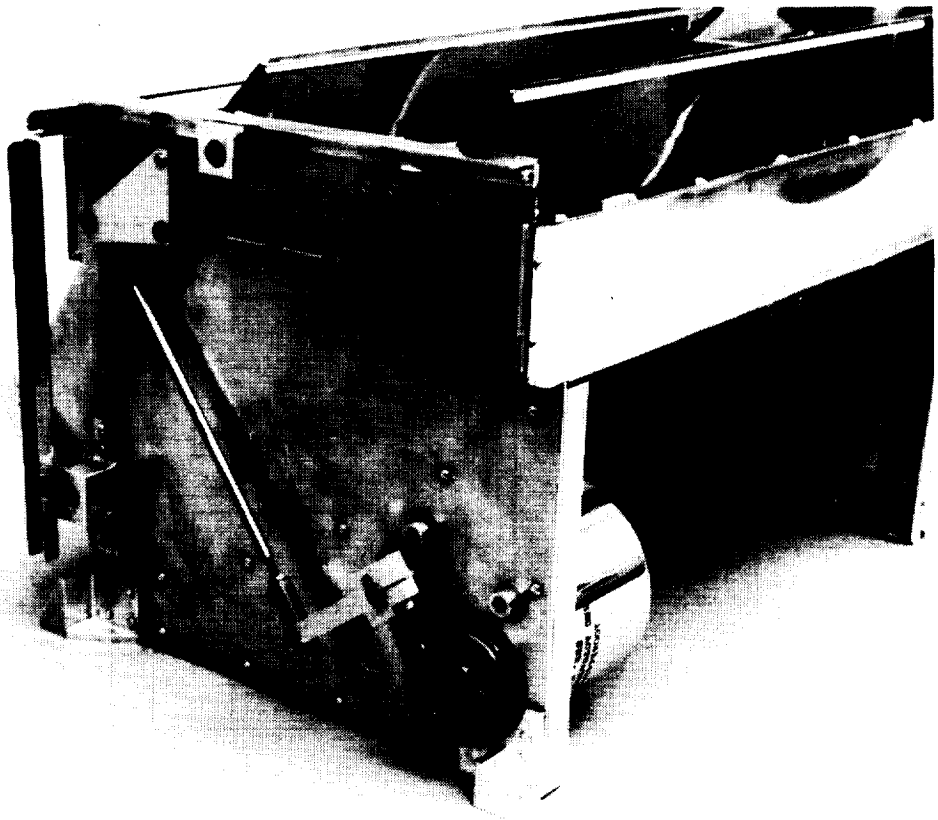

L-80-171

Figure 147.- Close-up of SEC.

angles in the form of coded commands from the CCS. The scan platform was a two-degree-of-freedom (clock and cone), gimballed support structure upon which the science instruments - VIS, IRTMS, and MAWDS - were mounted. The HGA was mounted on a two-degree-of-freedom AZ and EL, gimballed support structure for the purpose of keeping the antenna pointed toward the Earth. The SEC assemblies, of which there were four, consisted of two louvered, reflective blades used for maintaining temperature control of the PROPS fuel tanks by regulating the Sun radiation on the interior of the VO.

A simplified block diagram of the ARTCS is shown within dashed lines in figure 148. Intrasubsystem and intersubsystem interfaces related to the functioning of the ARTCS are also shown. The ARTCS provided the following functions:

Position control of the scan platform (two axes)

Position control of the HGA (two axes)

Position control of the four sets of SEC blades (one axis)

Position telemetry for each axis of the scan platform, HGA, and the SEC blades

Scan slew status signal to ACS

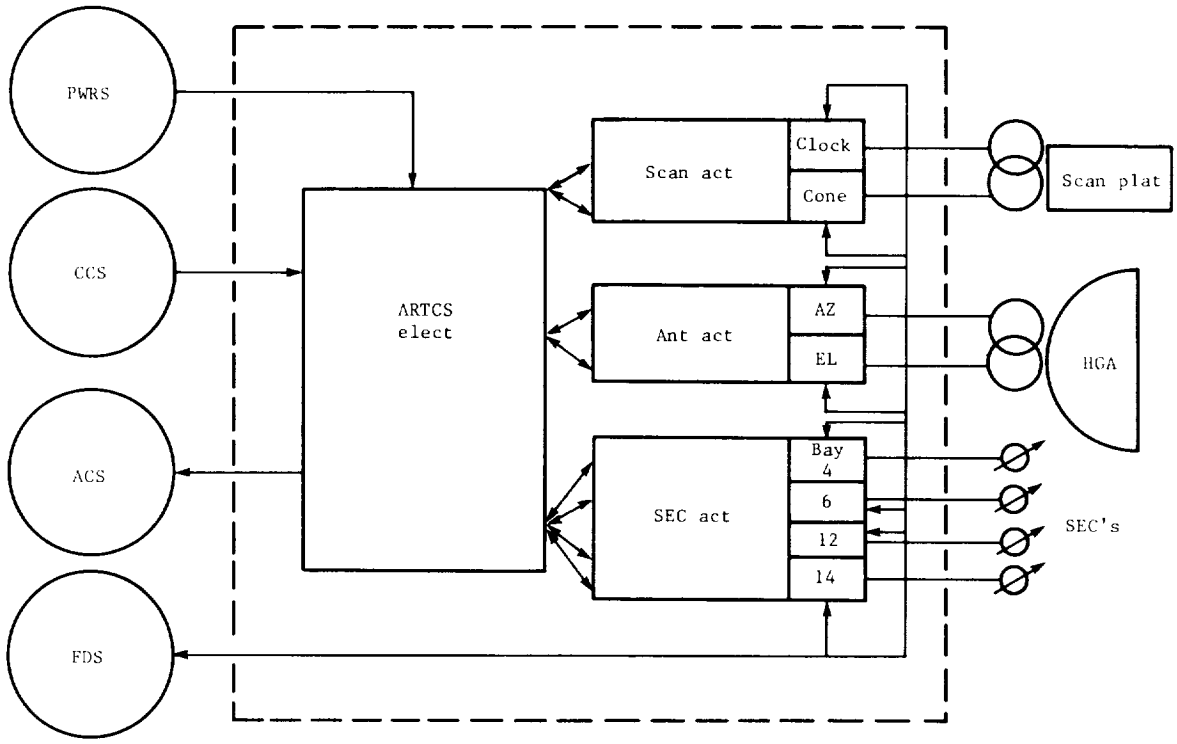

Figure 148.- Simplified block diagram of ARTCS.

Description

The ARTCS consisted of the following assemblies: ARTCS elect, scan platform actuators, antenna actuators, and SEC actuators. A detailed description of each assembly is presented later, but a brief description is as follows:

Articulation control electronics: The ARTCS elect accepted CCS position commands and provided drive signals to the commanded actuator stepping motor to slew the actuator until its position, as indicated by an F/B pot, agreed with the position command. Except for the actuator drivers, the ARTCS elect consisted of two identical control channels to provide redundancy and the ability to slew any two actuators simultaneously. The electronics in each of the two channels were multiplexed to allow the position of any one of the eight actuators to be controlled with a single set of electronics.

Actuators: The scan platform, antenna, and SEC actuators were identical in concept but differed in size, weight, torque, angular range, and slewing speed. All were driven by stepping motors. Stepping motor rotation was fed through a gear train to the actuator shaft. Each actuator had two redundant F/B pot's, one dedicated to each of the two ARTCS elect channels. Each actuator also had a coarse telemetry pot and the scan and antenna actuators have a fine telemetry pot. The three scan actuators were identical and interchangeable, as are the four SEC actuators. One scan actuator and one antenna actuator were used for the HGA.

The VO coordinate systems and their interrelationships are discussed in the section "Coordinate Systems."

Mechanization

A simplified functional block diagram of the ARTCS is shown in figure 149. Since control electronics channels 1 and 2 are identical, only channel 1 is shown for description. For simplicity, 8 motor drivers and 8 actuators were each combined into a single block. The ARTCS equipment is described as follows. The physical location of the equipment on the VO is shown in figure 1.

ARTCS electronics: The electronics consisted of two identical control channels to provide redundancy and the ability to slew any two actuators simultaneously. Each control channel consisted of a power supply, input unit, error detector, slew control, motor drive pulse generator, and multiplexers. In addition, the ARTCS elect contained one driver for each of the eight actuators and a scan slew status output unit.

ARTCS elect power: The ARTCS elect received 50 V rms, 2.4-kHz, square-wave power from PWRS. The 2.4-kHz power was supplied separately to each of the redundant ARTCS elect channels. Power conditioning was provided in the ARTCS elect to derive the required internal supply voltages, actuator drive power, and excitation for the actuator F/B pot's. A power drop-out circuit was provided for initialization of the ARTCS elect logic at power turn-on, after a prolonged power drop-out, and for maintaining the established logic states during momentary power drop-outs of up to several msec. A 2.4-kHz clock was

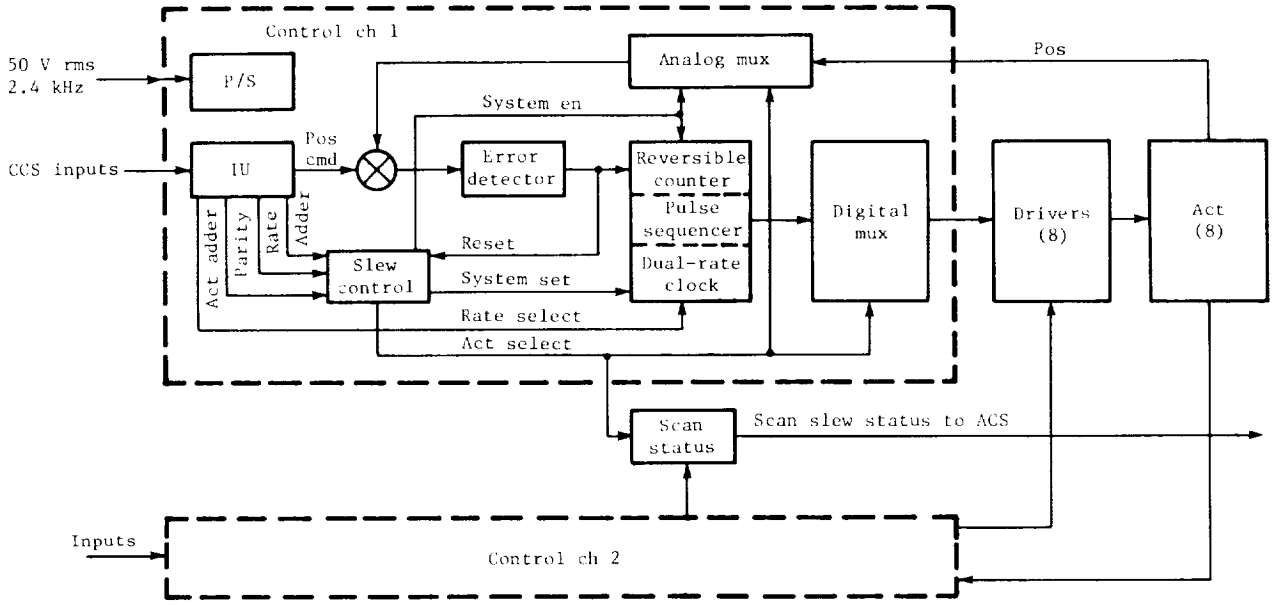

Figure 149.- Simplified functional block diagram of ARTCS.

derived from the 2.4-kHz input power. A 5 V dc delayed supply was derived and used to delay activating the actuator drivers until after the remainder of the electronics had been powered to avoid excessive inrush currents.

Input unit: The input unit received from the CCS an enable signal, a 14-bit digital data word, and a strobe signal as shown in figure 150. The data word contained 3 bits for address, 1 bit for parity, and 10 bits for actuator position information. Upon receipt of the CC enable signal, the data word was clocked into the input register. The address and position information was examined to determine if it was a slew rate command and if so, the dual rate clock was set accordingly. The address information was decoded and sent to the multiplexers to select the commanded actuator. The position information was converted to an analog signal by a DAC for comparison with the actuator position

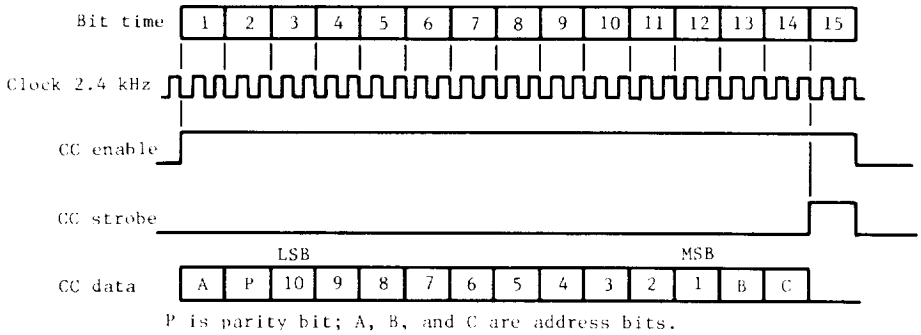

Figure 150.- Command message structure to ARTCS.

F/B voltage. Upon receipt of CC strobe which followed the data word, an odd parity check was performed on the data word. If parity checked, a signal was sent to the slew control unit to initiate slewing of the selected actuator. The input unit consisted of a command receiver, 1.2-kHz clock, 14-bit shift register, DAC, parity F/F, actuator address decode logic, and slew rate decode logic.

Error detector: Feedback pot signals indicating actuator shaft positions were fed back through the analog multiplexer switches for comparison with the commanded position signal from the DAC. The error signal resulting from the difference between the commanded position and the actuator F/B position was sent to the error detector. The error detector generated a logic state at its output that was dependent upon the polarity of the error signal into the error detector. This signal maintained its logic state until the logic circuit was reset when the input error crossed zero. This signal was used to generate the proper counting direction for the reversible counter in the motor pulse generator.

Slew control: The slew control contained the mode control logic. Based on inputs from the input unit, it determined if motor drive pulses should be generated and if so it provided the logic signals necessary for steering the pulses to the selected actuator and for bringing the correct F/B pot signal back through the analog multiplexer. The slew control disabled the system after the slew had been completed as indicated by the error detector output.

Motor drive pulse generator: The motor drive pulse generator provided a delayed train of pulses to the selected actuator driver at the commanded rate and in the count-up or count-down sequence depending upon the polarity of the error as indicated by the error detector. The motor drive pulse generator consisted of a dual-rate clock, reversible counter, delay F/F, and pulse sequencer.

Multiplexers: The multiplexers steered the four motor drive pulses from the pulse sequencer to the selected actuator driver (digital multiplexer) and the selected actuator F/B pot output to the error detector input summing amplifier (analog multiplexer).

Actuator motor drivers: A separate, nonredundant driver was provided for each actuator. Each motor driver consisted of four power switches. The motor drive pulse generator (pulse sequencer) provided four lines, one for each of the power switches, to each actuator driver. All actuators were continuously supplied and 28 V dc power generated in the ARTCS elect power supply. The actuator driver successively grounded the four motor windings causing a 90° motor shaft rotation for each pulse from the motor drive pulse generator. Channel 1 and 2 signals were ORed at the actuator driver input so that either channel could operate the driver. Commanding the same driver simultaneously with channel 1 and channel 2 was prohibited.

Scan platform slew status unit: The scan platform slew status unit provided a scan platform slew logic signal for use by the ACS. The signal was a logic signal which indicated when either the scan platform clock angle or cone angle was selected. The scan slew signal had reached 90 percent of its final output voltage level within 15 msec after a scan platform actuator was selected. The total time delay to reach 90 percent of the final switched value after

removal of the scan actuator select signal was between 0.10 and 1.0 sec. Slewing (motor drive pulses) did not begin for a minimum of 20.42 msec after an actuator was selected.

ARTC actuators: Each actuator was pressurized in order to protect the mechanism from corrosive gasses and to preserve the lubrication in the space vacuum environment. The gas used for pressurization was a mixture of 90 percent nitrogen and 10 percent helium by volume. A resistance heater was mounted in the actuator on the gear structure to prevent damage due to low temperatures that were encountered during the mission. A glass-to-metal, hermetically sealed electrical connector was mounted on the actuator housing in order to provide for electrical inputs and outputs.

Scan platform actuator: Two scan platform actuators were used to point the science platform, one driving the clock axis and the other driving the cone axis. The actuator consisted of a standard size 11, permanent magnet stepping motor; spur gear reduction gearing; three-gang pot; single pot; and clutch.

Antenna actuator: An antenna actuator was used to drive the EL-axis of the HGA. The antenna actuator was similar to the scan platform actuator differing primarily in size, weight, output torque, and shaft angle range. The antenna actuator was driven by a modified, size 8 stepping motor. Both HGA actuators provided holding torque while unpowered in order to maintain HGA pointing during propulsive maneuvers. This requirement necessitated the use of a scan actuator with standard size 11 stepping motor to drive the HGA about its AZ-axis.

Solar energy controller actuator: There were four SEC assemblies on each VO, each requiring one actuator. The SEC was driven with a size 8 stepping motor and was provided with a single three-gang pot (two for feedback and one coarse telemetry output), but it did not contain a fine telemetry pot or a clutch.

Operating Modes

The operating modes of the ARTCS related to the actuator that was being slewed and the rate at which it was being slewed. In addition, there was an idle mode in which the ARTCS was inactive except for passively restraining the articulated elements from moving with friction and motor detent torque. The ARTCS was placed into the idle mode at power turn-on, after completion of each actuator slew, and if a power drop-out occurred.

Control Variables

The ARTCS logic input control variables consisted of commands from CCS and logic signals generated within the ARTCS. There were a total of 15 command and logic controlled outputs and 5 internal logic functions.

The key logic signals associated with generating the motor drive pulse (MDP) sequencing and their timing are shown in figure 151. The sequencing-initiating signal SYS SET (system set) was true for only one-half of a 1.2-kHz clock period during CC strobe. When SYS SET became true, RC F/F 1 (dual rate clock), and M SEQ EN (motor sequence enable) were initialized and SYS EN (system enable) became true and was latched. The reversible counter outputs were such that the pulse sequence out of the pulse sequencer was 1,2,3,4 if count up was true and 4,3,2,1 if count down was true. M SEQ EN, which was an output to the pulse sequencer, inhibited the transmission of what would have been the first two motor drive pulses to the actuator driver. This provided a delay of 20.42 msec for the high slew rate (82.05 msec for low slew rate), after ACT SEL (actuator select) became true, to generate the motor drive pulses. This allowed ample time for the ACS to respond to the scan platform slew signal prior to the

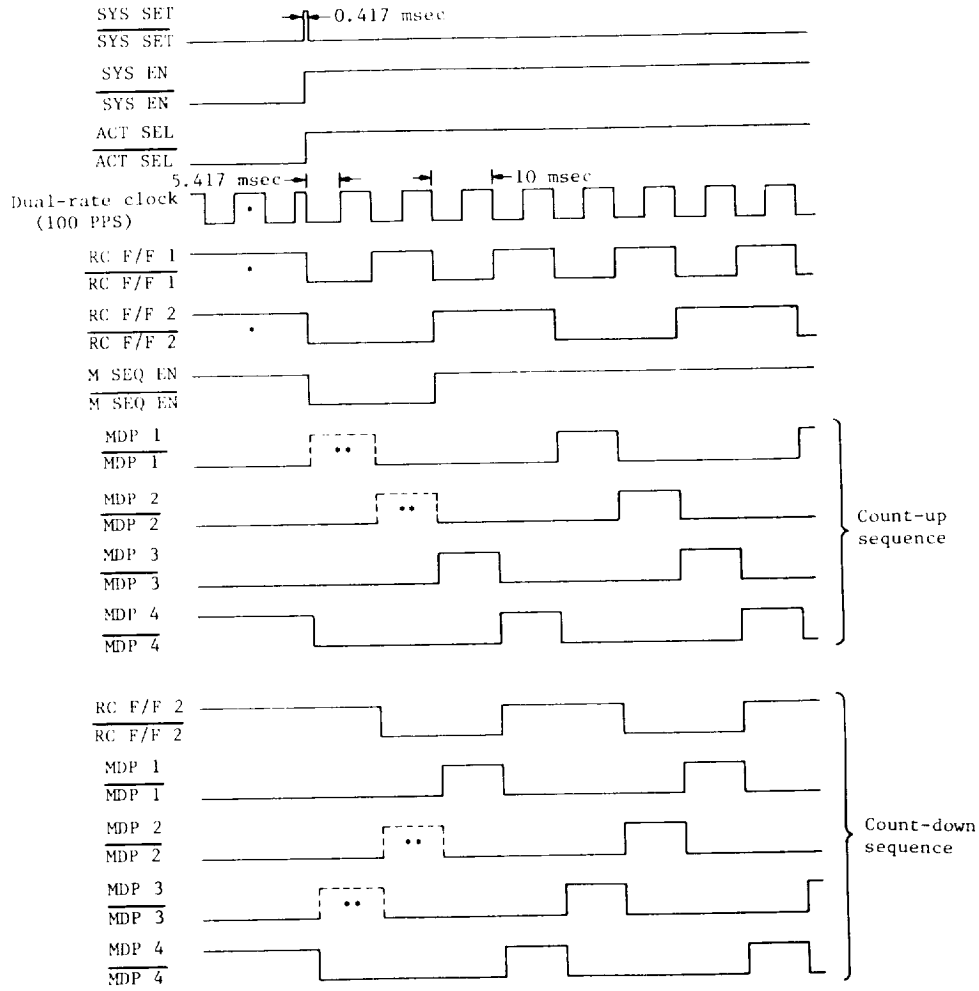

*Either state prior to SYS SET

**These were not transmitted through the pulse sequencer.

Figure 151.- Timing diagram for motor drive pulse generator.

actual scan platform slew start. The initial state of the reversible counter (RC F/F 1 and RC F/F 2) for a slew was the state it had at the conclusion of the previous slew. The initial states of RC F/F 1 and RC F/F 2 are shown as true in figure 151. Regardless of the initial state of RC F/F 1 and RC F/F 2, the first output pulse from the pulse sequencer followed in sequence if it were not inhibited by M SEQ EN; for example, if the previous slew terminated with MDP 2, the first pulse on the succeeding slew would be 3 for count up or 1 for count down. However, because 2 pulses were inhibited by M SEQ EN, the first pulse, if it was to the same actuator, would be 180° from the motor winding energized last on the previous slew. When a different actuator was addressed, the last winding energized on the previous slew was random with respect to the first winding energized on the next slew.

Logic/Mode Initialization

The logic/mode was initialized (not necessarily to the same state) when one of the following occurred:

INIT: When INIT (initialization) was true, the slew rate memory F/F was in the reset (low slew rate) state and SYS EN was false. When SYS EN was false, the slew was terminated because the reversible counter stopped and the digital and analog multiplexers provided open circuits. No further action occurred until a new CCS command was received. SYS EN went false several mseconds after power drop-out; the slew rate was reset (low rate) after SYS EN.

New CCS command other than a slew rate command: Upon completion of the receipt of a new command, other than a slew rate command, SYS SET was true for one 2.4-kHz clock period during which time it initialized the dual-rate clock, F/F 1 of the reversible counter, and a delay F/F (M SEQ EN). In addition, SYS EN was permitted.

Actuator reached its commanded position: When the actuator reached its commanded position, CNT UP EN (count-up enable) and CNT DN EN (count-down enable) was disabled which disabled SYS EN. In addition the 1.2-kHz clock and the parity F/F were initialized by CC enable.

Premature Commands

Of interest were the consequences of issuing a CCS command to an ARTCS channel while it was in the process of executing a previously issued command; these are discussed as follows:

Second command was slew rate command: If the command word was such that the fluctuations in the output of the DAC caused the error detector input to go through zero, the slew was terminated. Note that while the new command was being entered the address bits were also changing and, therefore, the output of different F/B pot's was entering the error detector summing junction. If the error detector input did not go through zero, the actuator that was addressed after the complete data word had been entered was slewed to the new commanded position at the new slew rate. This would be either a SEC 4 or SEC 14 slew.

Therefore, it seemed appropriate to include in any slew rate command the desired position for the particular SEC or to allow sufficient time for the first slew to finish.

Second command was position command to same actuator: If the command word was such that the fluctuations in the output of the DAC caused the error detector input to go through zero, the slew was terminated when the second command word had entered the register, and the sequence for slewing the actuator to the new commanded position commenced. If the error detector input did not go through zero, the slew continued to the new commanded position with an interruption in motor pulsing of 20.42 msec (if on high slew rate) or 82.05 msec (if on low slew rate) and the motor pulse sequence was disrupted when the SYS SET pulse occurred after receipt of the complete command word.

Second command was position command to different actuator: If the command was such that the fluctuations in the output of the DAC caused the error detector input to go to zero, the slew was terminated. When the complete command word had been received, the sequencing for slewing the addressed actuator to the commanded position began. If the error detector input did not go through zero, slewing of the actuator addressed by the second command began when the complete command word had been received and slewing of the previously addressed actuator ceased.

Redundant Channels

Redundant electronic channels were provided in the ARTCS elect except for the actuator drivers and scan platform slew status circuitry. The F/B pot's in the actuators were also redundant with an F/B pot being dedicated to each of the two channels. Simultaneous slewing of two actuators was not possible if one of the channel F/B pot's failed. A failure of an actuator or motor driver resulted in the loss of slewing capability for that actuator.

Interfaces

The ARTCS interfaced with seven other subsystems (as shown in fig. 148): STRU, PWRS, CCS, FDS, ACS, CABLS, and DEVS. The interfaces involved with the functioning of the ARTCS are described as follows:

Structure subsystem.- The science instruments mounted on the scan platform were provided with articulation freedom, approximately as shown in figure 14. The total required ranges were 45° to 175° in cone angle and 80° to 130° in clock angle. The stowed position was 90.0° in cone angle and 222.58° in clock angle. The actuator electrical and mechanical limits were 256.72° and 300°, respectively. The actuators were mechanically attached to the scan platform to provide a range of $90.0^{\circ} \pm 128.36^{\circ}$ in cone angle and $195.0^{\circ} \pm 128.36^{\circ}$ in clock angle. Stops were provided by STRUS to limit clock angles to between 80° and 310°. Stops were also provided by STRUS to limit cone angles from 45° to 175° between clock angles of 80° and 130° and from 90° to 175° between clock angles of 130° to 310°, except that the stops allowed a cone angle of 86.7° in the

region of 291.2° clock. Physical and FOV interference limitations are shown in figure 14. The scan platform was mounted on a single structural frame located outboard of bay 7 on a two-degree-of-freedom gimbal outrigger structure.

The HGA angular ranges were such that the HGA boresight could be pointed at Earth from MOI -80 days until the end of the mission. During this time period, the HGA FOV (defined by a 15° half-cone angle measured from the perimeter of the antenna) was unobstructed within the range shown in figure 16. The total required ranges were -60° to 121° in AZ and -15° to 185° in EL. The stowed position was 122.75° in AZ and 0° in EL. The actuator electrical and mechanical limits were 256.72° and 300°, respectively, for AZ and 204.24° and 210°, respectively, for EL. The actuators were mechanically attached to the HGA to provide a range of 0° ± 128.36° for AZ and 85° ± 100.5° for EL. Stops were provided by STRUS to limit AZ angles from -95° to 125°. The EL angles were limited by the actuator from -15.5° to 185.5°. The HGA was mounted outboard of the bus structure by means of a boom-outrigger support structure which provided two degrees of freedom for antenna pointing. The PYROS provided latch and squib-actuated (upon command) unlatch capability for the HGA.

The SEC angular range required was 0° to 90.0°. The actuator electrical and mechanical limits were 90.24° and 90.25°, respectively. Each actuator was mechanically attached to its SEC to provide a range of 45.0° ± 45.1°. The stops in the SEC actuators were relied upon to limit SEC travel.

Power subsystem.- The PWRS provided the following inputs to ARTCS: switchable 50 V rms, 2.4-kHz, square-wave power to either or both ARTCS channels as commanded and regulated 55 V dc power to the two HGA actuator heaters continuously. The power consumption for various modes of operation is given in table 37.

TABLE 37.- ARTCS POWER CONSUMPTION

Operational mode	Pwr used from 2.4-kHz, 50 V rms bus, W						Pwr used from 55 V dc bus, W
	Per ch			Dual ch			
	Max	Nom	Min	Max	Nom	Min	
Stdby	8.4	6.0	3.8	16.8	12.0	7.6	
Scan plat slew	20.5	15.0	10.0	41.0	30.0	20.0	
HGA slew AZ	20.5	15.0	10.0	36.1	26.0	17.3	
HGA slew EL	15.6	11.0	7.3	36.1	26.0	17.3	
SEC slew	15.6	11.0	7.3	31.2	22.0	14.6	
Ant htr							8.0

Computer command subsystem.- ARTCS related commands are given in the command table. (See table 2.) The CCS provided the following inputs to the ARTCS: enable signal which bracketed data and strobe signals to indicate the period of activity during which data were to be clocked into the ARTCS register; data signal of a series of levels representing 1's and 0's for 14-bit times; strobe signal which followed data immediately and indicated that all data had been sent.

Flight data subsystem.- The FDS provided a 1-mA constant current to the temperature sensors and 3 V dc excitation for the coarse and fine telemetry pot's. The ARTCS provided 16 analog telemetry measurements, 4 of which were redundant, to the FDS. (See table 38.) No digital (status) signals were provided.

TABLE 38.- ARTCS TELEMETRY MEASUREMENTS

Measurement	FDS range, V dc	Significance (scale factor), deg/V dc	Stowed pos DN	Resolution per DN, deg
Scan clock pos, coarse	0 to 3	85.66	78	2.023
[a]Scan clock pos, fine	0 to 3	1.673	34	.0395
Scan cone pos, coarse	0 to 3	85.66	64	2.023
[a]Scan cone pos, fine	0 to 3	1.673	64	.0395
HGA AZ pos, coarse	0 to 3	-85.66	3	2.023
[a]HGA AZ pos, fine	0 to 3	-1.673	70	.0395
HGA EL pos, coarse	0 to 3	68.15	11	1.610
[a]HGA EL pos, fine	0 to 3	2.023	101	.0478
SEC 4 pos	0 to 3	-30.56	98	.722
SEC 6 pos	0 to 3	-30.56	98	.722
SEC 12 pos	0 to 3	-30.56	98	.722
SEC 14 pos	0 to 3	-30.56	98	.722

[a]Redundant measurement also.

Attitude control subsystem.- The ARTCS provided a switch closure to the ACS whenever the scan platform was slewing. The two ARTCS elect channels were ORed for this purpose with a scan slew indication if either or both channels were slewing a scan platform actuator.

Mechanical devices subsystem.- The scan platform latch system provided a three-point linear load path to support the scan platform during the boost phase of the mission. The assembly pneumatically preloaded and restrained the scan platform to the VO bus and released the joint on command via a squib-actuated valve. The gas used to actuate the latch was dumped overboard through a balanced tee as part of the unlatch dump sequence. Continuous readout of the internal pneumatic pressure of the scan latch cylinders was provided to the FDS through the scan latch pressure sensor. The sensor was capable of detecting steady-state pressure (leakage analysis) and monitoring the unlatch cycle.

Performance Characteristics

The following table presents the subsystem level nominal performance characteristics for the ARTCS:

	Scan & HGA AZ	HGA EL	SEC
Actuator characteristics:			
Motor step size, deg	90	96	90
Actuator shaft rotation per motor step, deg	0.00993	0.00991	0.1365
Angular range for mechanical stops, deg	0 ± 150	0 ± 100.5	0 ± 45.12
Output shaft travel for full range of coarse TM pot, deg	0 ± 128.36	0 ± 102.12	0 ± 45.79
Output shaft travel for full range of fine TM pot, deg	5.0185	6.0692	N/A
Output shaft travel for one revolution of fine TM pot, deg	5.1253	6.1983	N/A
Pull-in torque[a], N-cm (in-lb) (Scan)	>169 (>15)	>339 (>30)	>7 (>0.63)
(HGA AZ)	>904 (>80)		
Pull-out torque[a] at motor drive pulse rate of 100 steps/sec (no load), N-cm (in-lb)	>1808 (>160)	>508 (>45)	>50 (>4.4)
Holding (detent) torque[a], N-cm (in-lb)	>2825 (>250)	>874 (>75)	>23 (>2)
Clutch torque[a], N-cm (in-lb)	2828 to 4519 (250 to 400)	904 to 1808 (80 to 160)	N/A
Backlash[a] and windup[b], arc-min	<8.5	<10	<30
Gear train and shaft stiffness, N-m/rad (ft-lb/rad)	8135 (6000)	2712 (2000)	- - - -
Control parameters:			
Command resolution, deg	0.2509	0.1996	1.432
Angular range, deg	0 ± 128.36	0 ± 102.5	44.45 to -45.12
Motor drive pulse rate			
Low rate, PPS	24.5	24.5	24.5
High rate, PPS	100	100	100
Slew rate			
Low rate, deg/sec	0.243	0.243	3.34
High rate, deg/sec	0.993	0.991	13.65

[a]Measured at output shaft.

[b]With 56.5, 17, and 5.7 N-cm (5, 1.5, and 0.5 in-lb) reversing torque, respectively, for scan, antenna, and SEC actuators.

ARTC-related VO characteristics:

Articulation angle for 0^{o} actuator shaft angle and -	
Scan platform clock angle, deg	195
Scan platform cone angle, deg	90
HGA AZ, deg	0
HGA EL, deg	85
SEC, deg	45
Actuator load inertia for -	
Scan platform, kg-m^2 (slug-ft^2)	<27 (<20)
HGA AZ, kg-m^2 (slug-ft^2)	<5.4 (<4)
HGA EL, kg-m^2 (slug-ft^2)	<2.7 (<2)
SEC	Negligible
Actuator load resisting torques	
Friction for -	
Scan platform clock angle, N-cm (in-lb)	56.5 to 169 (5 to 15)
Scan platform cone angle, N-cm (in-lb)	56.5 to 169 (5 to 15)
HGA AZ, N-cm (in-lb)	<203 (<18)
HGA EL, N-cm (in-lb)	<113 (<10)
SEC, N-cm (in-lb)	<7 (<0.62)
Total (including cable torques) for -	
Scan platform clock angle, N-cm (in-lb)	<339 (<30)
Scan platform cone angle, N-cm (in-lb)	<339 (<30)
HGA AZ, N-cm (in-lb)	<452 (<40)
HGA EL, N-cm (in-lb)	<847 (<75)
SEC, N-cm (in-lb)	<7 (<0.62)
Actuator load mass moments for -	
Scan platform clock angle, kg-m^2 (slug-ft^2)	<13.6 (<10)
Scan platform cone angle, kg-m^2 (slug-ft^2)	<13.6 (<10)
HGA AZ, kg-m^2 (slug-ft^2)	<2.4 (<1.8)
HGA EL, kg-m^2 (slug-ft^2)	<0.5 (<0.4)
SEC	Negligible

Constraints and Operating Procedures

The following constraints and operating procedures pertain to the operation of the equipment for the protection of the equipment and to the proper operation of the subsystem in flight.

The need for in-flight constraints arose to protect the equipment from the environment and to enhance its life. The equipment design temperatures are given in the following table:

Assembly	Temperature, ^{o}C	
	Low	High
ARTCS elect	-20	75
Scan act	-40	85
Ant act	-40	85
SEC act	-40	85

The equipment temperatures were monitored and corrective action taken if possible to maintain the temperatures within these values. Heaters were provided in the scan platform and antenna actuators. The heaters in the scan platform actuators were not used. The heaters in the two HGA actuators were on continuously.

The ARTCS control loop was such that the ARTCS elect provided motor drive pulses until the actuator F/B pot signal canceled the CCS command word (DAC output). There were two possible conditions, other than failure modes, under which the F/B pot would never cancel DAC output; namely,

If the actuator was commanded into a mechanical stop either on the actuator or on the device it was driving.

If tolerances were such that the F/B pot output at full electrical travel was less than the maximum DAC output and a DAC output beyond the maximum pot output had been commanded. (This resulted in driving into a mechanical stop.)

If either of these two conditions had existed, the ARTCS elect would continue to provide motor drive pulses until a CCS command had been issued to bring the actuator back into the region where the F/B signal would null the DAC output. Continuing to drive the actuators was not expected to result in damage for several hours, but it would increase the temperature stress on the actuator motor and ARTCS elect actuator driver. These conditions were avoided by limiting the CCS commands as determined by assembly and system test.

There was no constraint within the ARTCS that prevented both ARTCS elect channels from simultaneously providing drive signals to the driver of one actuator if so commanded by the CCS. Programming of the CCS was relied upon to not create this situation. If this situation did occur, the response of the actuator was indeterminate depending upon the timing of the signals into the drivers from the two ARTCS elect channels. One possibility was that the actuator would not move in the direction to satisfy the command and the temperature stress on the actuator motor and the ARTCS elect actuator driver would be increased. The thermal stress would be greater than in the instance described in the previous paragraph.

The need for in-flight operational constraints arose in order to avoid adverse operating conditions or unplanned actuator slewing. The scan platform was in the stowed position (against the STRUS stop) during propulsion maneuvers; otherwise, the acceleration-induced torques on the platform would cause the actuators to be backdriven or the clutch to slip with possible damage due to the rapid encounter of the platform with the STRUS stops.

A CCS command was not supposed to be issued to ARTCS while it was still executing a previously issued command. If a premature slew rate command was issued, slewing of the previously commanded actuator would be terminated and no further slewing would occur or the SEC actuator addressed would be slewed to the angle associated with the second command. The slew rate would be in accordance with the new command. If a premature position command was issued to the same actuator, it would be slewed to the angle associated with the new command. If

a premature position command was issued to a different actuator, slewing of the first actuator would cease and the actuator associated with the new command would be slewed to the angle associated with the new command.

If an invalid command was received while the ARTCS was in the idle state, there would be no ARTCS response. If an invalid command was received while a previously issued valid command was being executed, slewing of the actuator would be terminated if the commanded word was such that the fluctuations in the output of the DAC caused the error detector input to go through zero. If the error detector input did not go through zero as the command was being received, the addressed actuator would be slewed to the commanded angle regardless of the parity of the command word.

Data Storage Subsystem

Purpose and Function

The DSS of the VOS consisted of two identical DTR's and was used in the application of long duration, interplanetary spacecraft data storage. A DTR was comprised of two subassemblies: a DST and an associated DSE. The DTR was an 8-channel multispeed digital tape recorder capable of recording and reproducing a minimum of 6.4×10^8 bits of science engineering and visual imaging data.

The major functions of the DTR were as follows:

To store VIS data received from the FDS

To store high-rate engineering and other science data received from the FDS

To store VL data received from the RTS

To play back the stored (recorded) data via DSE conditioning circuitry through the MDS at selected bit rates consistent with telemetry capabilities and constraints

Description

As shown in figure 152, the DSS consisted of two identical but independent DTR's. Each DTR consisted of a 9-track tape transport (DST) and the electronics (DSE) required to store and play back data. Control inputs to the DTR's to select mode, bit rate, track, and tape direction were via commands from the CCS. Data to be stored were received from the FDS or the RTS. VIS data from FDS were multiplexed on seven parallel lines to either DTR. The data rate for each line was 301 714 2/7 bps. Full resolution pictures were recorded by either recorder in the VIS record mode. Science or engineering data from the FDS at 2000 bps were recorded on track 8. Simultaneous recording of more than one data source or bit rate was not possible on either DTR.

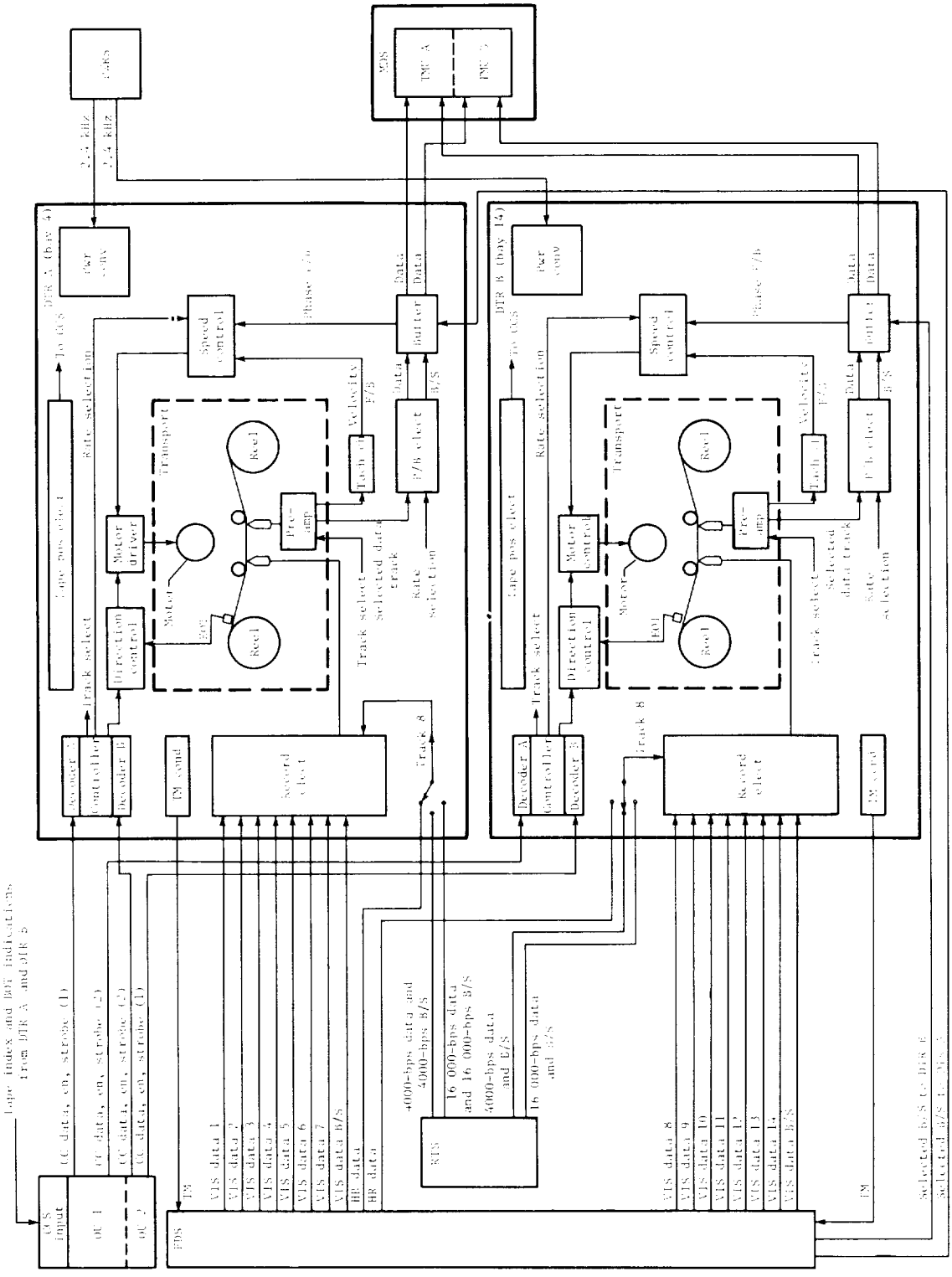

Figure 152.- Block diagram of DSS.

DST.- The DST was essentially the mechanical portion of an electromechanical device. Its functions were strictly controlled by the DSE during normal operation; thus, the DST was not accessed directly. A description of the DST internal mechanisms is included to provide insight into DSS operational characteristics and limitations.

The DST outer shell, a sealed metal case pressurized to 19.3 kPa (2.8 psig), served to protect the actual instrument from gaseous and particulate contaminants. To protect the precision tape shuttling mechanisms from mechanical disturbances, the internal deck plate mounting surface was shock mounted to the case.

The DST internal transport mechanism (figs. 153 and 154) was a coplanar reel-to-reel tape recorder, which used seamless belts to transmit motion from motor to tape and provide speed ratio reduction. This kinematically complex, peripheral belt, capstan differential drive design provided uniform tape tension, bidirectional operation, and smooth tape motion at low speed. The DST was comprised of 13 separate rotating components. High precision bearings were essential to minimize torque disturbance which caused nonuniform tape speed at the magnetic heads (flutter). Many of these components rotated at just 3 rpm during the 1000-bps playback rate. A damper mechanism as shown in figure 153

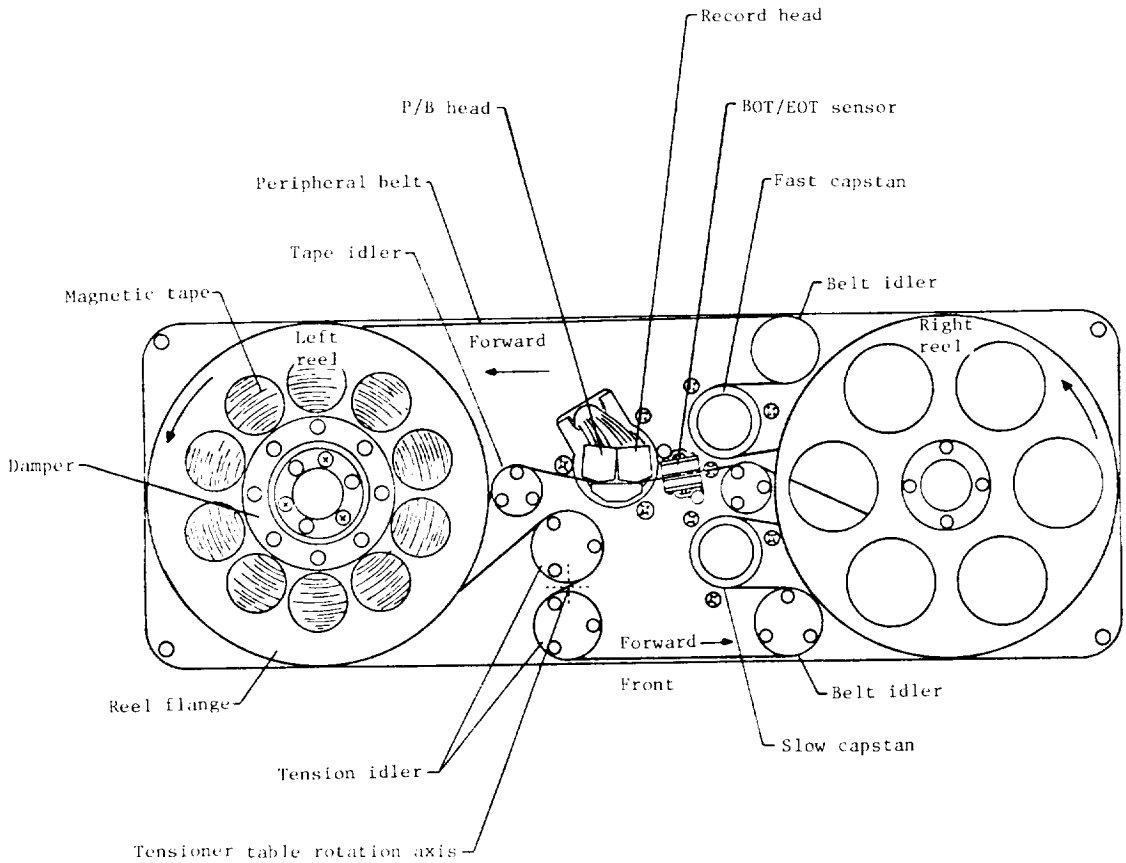

Figure 153.- Top side deck configuration.

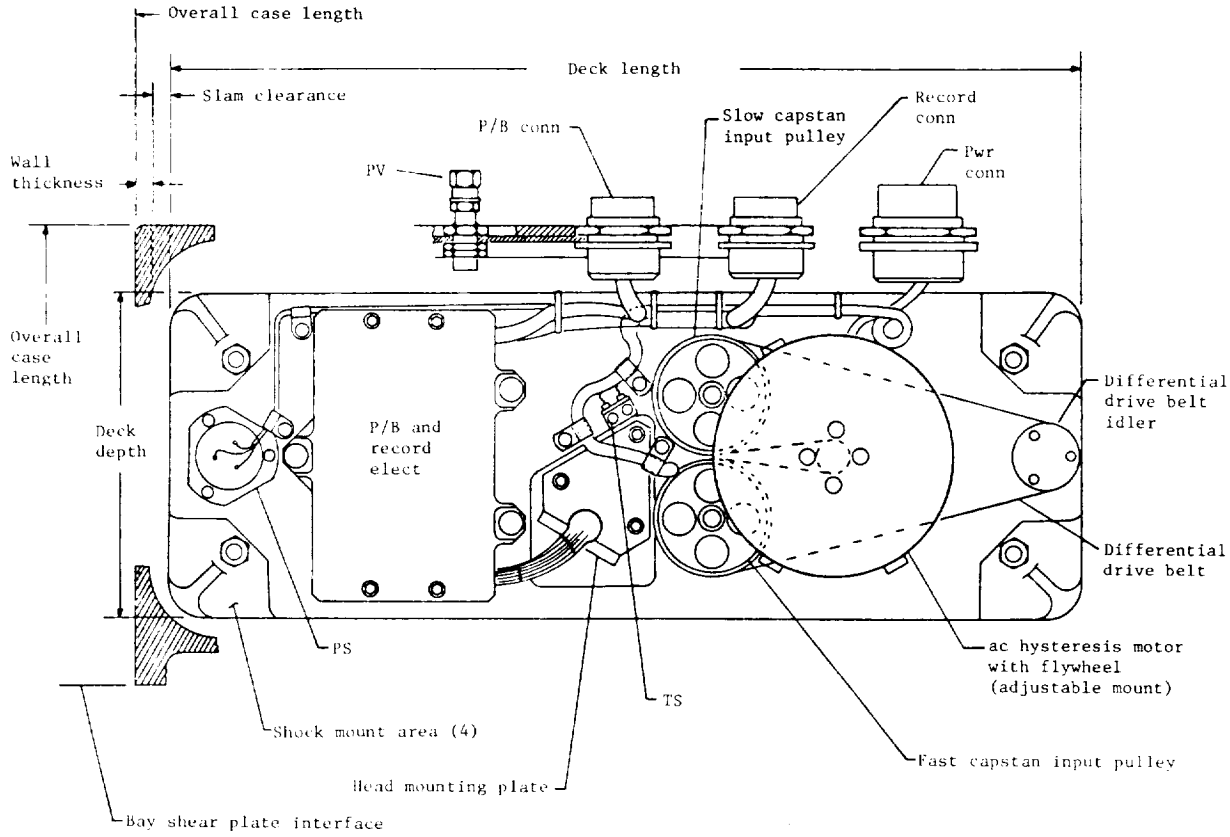

Figure 154.- Bottom-side deck configuration.

was built as part of the left reel assembly of the DST. This damper reduced the transport resonance frequency by the usage of rubber damper material installed in the mechanism. BOT occurred with left reel full. The magnetic tape used in the DST was 1.27 cm (0.5 in.) wide, type 900, manufactured by the 3-M Company. A tape map is shown in figure 155. During operation, the tape shuttled from reel to reel with motor power supplied from the DSE. The end-of-tape (or beginning-of-tape) condition did not correspond to physical tape end; rather, a signal was generated when 27, 18, and 9 m (90, 60, and 30 ft) from the end. Normal logic interlocks prevented movement, other than coast-down distance, beyond the first signal.

DSE.- The purpose of the DSE control logic was to receive and process coded commands from the CCS. Inputs were also received from the BOT and EOT events and from the power-on-reset circuit. The power-on-reset initial condition circuit placed the DTR in the ready mode upon application of power or following a dropout of input power greater than 1 msec. The occurrence of a BOT event while moving in the reverse direction or an EOT event while moving in the forward direction caused the DTR to automatically switch to the ready mode. The coded commands from the CCS were divided into four fields to indicate basic operating mode, tape speed during playback or slew, direction of tape motion, and the selected playback track.

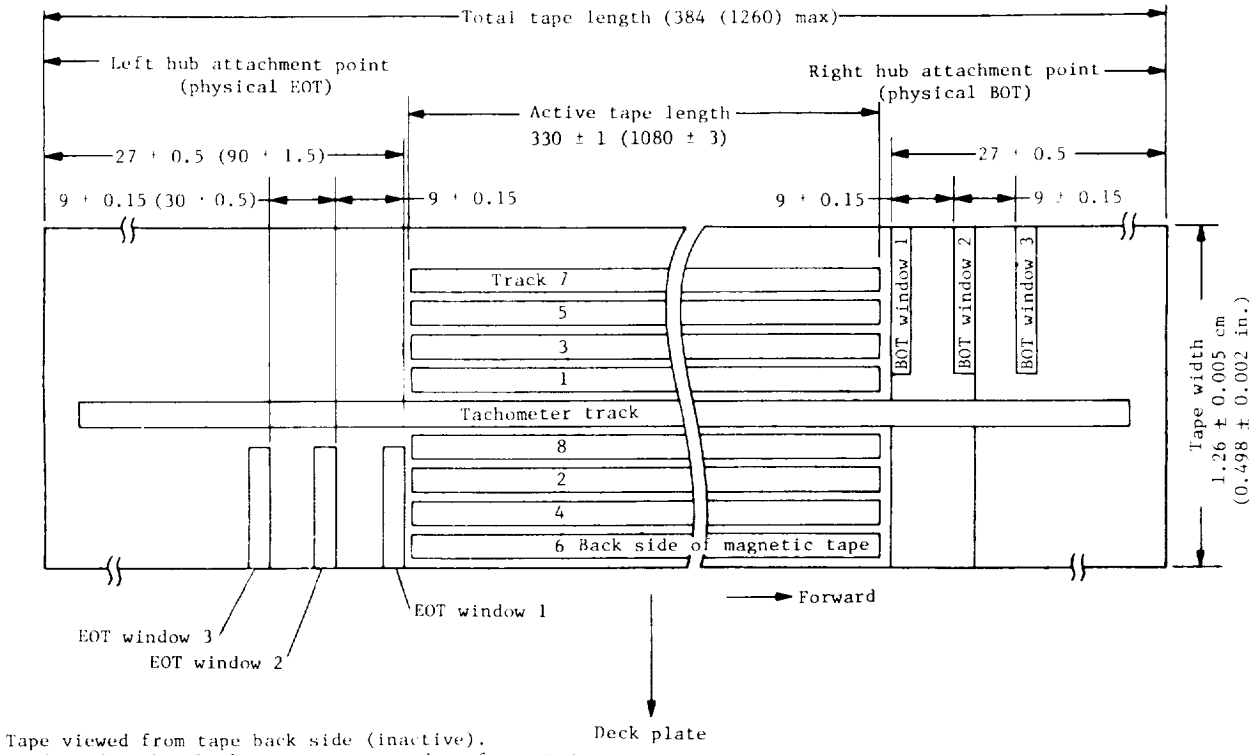

Figure 155.- Magnetic tape map (transport frontal profile). Dimensions except tape width are given in m (ft).

The DSE record electronics selected the proper data source and conditioned the data for transfer to the DST. VIS data from the FDS came to the DTR on seven separate lines and was simultaneously recorded on tracks 1 to 7. The data rate of each line was 301 714 2/7 bps. The VIS bit sync was divided by two and used to convert the data input from NRZ to Manchester code format. Manchester code is formed by the exclusive or combination of the NRZ data and the square-wave clock (at data rate frequency). The seven lines of Manchester data were routed to the TMEM where they were divided by two to form Miller code such that data and B/S information were recorded on each track. VL data were recorded on track 8 while the tape was running at speeds corresponding to either 4000 or 16 000 bps. FDS data were received at a 2000-bps data rate but were symbol encoded to a 4000-bps rate and recorded at the 4000-bps tape speed.

The purpose of the DSE playback electronics was to recover the playback data signal and derive a bit sync clock. The DTR could be operated at any one of five selectable tape speeds during the playback mode. Data were played back one track at a time by turning on one of the eight preamplifiers in the TMEM. The playback data signal from the TMEM was further amplified, filtered, gain compensated, and peak detected. The peak detector sensed both positive and negative peaks such that its output represented the Miller code form of the data previously recorded. The output of the peak detector was sampled by a one-half bit period integrating amplifier. The timing pulses to initialize the integrating amplifier and to store the output level were derived from the bit

synchronizer PLL. The detected data were converted to NRZ format and sent to the data buffer. The bit synchronizer PLL locked to the playback data and generated the B/S timing signals. The PLL allowed the B/S information to be recovered from the playback data in the presence of moderate drop-outs and flutter. The bit synchronizer PLL determined the location of the Miller code data transition and reset the integrating amplifier so that each data transition would be coincident with the reset pulse. After the detected Miller code data had been converted to NRZ format, they were routed through a buffer. The buffer transferred the data from the bit sync clock to a stable external clock from the FDS. This removed the flutter from the data, that was inherent in the system when operating the motor under servo control.

The tape position logic was a counter which divided the tach clock by a count of 10 000. This resulted in either an increment or a decrement pulse to CCS for every 8 cm (3 in.) of tape, depending on whether the tape was moving in the forward or reverse direction. The increment and decrement pulses were used by the CCS to maintain current tape position and identify where each group of data was recorded. With this information it was then possible to command the tape to a known position to play back a particular group of data.

The telemetry coder assembled and transmitted to the FDS two 7-bit digital status words: mode word and playback word. The mode word contained mode, rate, and tape direction information and the playback word contained track, buffer counter position, and PLL lock status.

DSE-DST interfaces.- The DSE-DST interfaces consisted of the record and playback signals, the motor driver voltages, and the BOT/EOT signals. The TMEM, while functionally a part of the DSE, was physically located within the DST. The TMEM provided the DSE to tape head interface circuitry and contained the record head drivers and the playback preamplifiers for the 9 tape tracks. The record circuitry consisted of a Manchester-to-Miller encoder and a record head driver for each of the 8 data tracks. The same circuitry was provided for recording the tachometer signal, but this circuitry was not used during flight. The playback circuitry consisted of a separate preamplifier for each data track and a single common amplifier as the second stage for the playback signal. Only one of the preamplifiers was enabled at any one time. A separate two-stage amplifier was provided for the tachometer signal.

The tape reels were driven by a two-phase motor in the transport. The direction of motor rotation was determined by the relative phase ($\pm 90^{\circ}$) of the signals to the motor windings. The motor speed was controlled by modulating the amplitude of the control phase motor voltage with the servo error signal. A constant voltage was applied to the reference phase winding at all tape speeds.

The DSE supplied current to each light source and monitored the photoconductive transistors within the DST. When BOT or EOT was reached, the light source transmitted through the transparent tape window activated the phototransistor. The signal was conditioned to logic level amplitude with a pulse width dependent on tape speed. The DSE was activated by the trailing edge of the pulse. The signals were routed to the control logic of the DSE and buffered to the CCS.

Operational Performance

The total data storage capacity of the DTR on 8 tracks was a minimum of 6.4×10^8 bits or 8×10^7 bits per track. The bit packing density, on tape, was 2625 ± 20 percent bits/cm (6667 ± 20 percent bits/in.). The magnetic tape transport was designed to operate at six different tape speeds. The highest record speed was accomplished by operating the motor at synchronous speed. Other speeds were accomplished by operating the motor at asynchronous speed with servo control. The mean tape speeds were as follows:

VIS record 301 714 2/7 bps	114.7 cm/sec (45.16 in/sec)
16 000 bps	6.1 cm/sec (2.40 in/sec)
8000 bps	3.0 cm/sec (1.20 in/sec)
4000 bps	1.5 cm/sec (0.60 in/sec)
2000 bps	0.76 cm/sec (0.30 in/sec)
1000 bps	0.38 cm/sec (0.15 in/sec)

The bit error rate for the DST was less than 1×10^{-4} at 16 000, 8000, 4000, and 2000 bps. Run-up time was the time from the instant that motor power was applied until the average VIS record speed was attained. Run-up time did not exceed 8.5 sec. The total start time plus stop time did not exceed 17.5 sec. The DTR mechanical devices, for example, bearings, belts, tape, and magnetic head surfaces, were consumable in that they possessed a limited lifetime before degradation began to appear. The design life requirements after delivery for assembly into the flight VO were

457 km (1.5×10^6 ft) of tape across the heads

6500 tape passages of any given section of tape across the heads

10 000 start/stop cycles. The following were counted as start/stop cycles: any velocity change was equal to 1/2 start/stop cycle, a direction reversed at any speed was equal to 1 start/stop cycle, and a single start or stop was equal to 1/2 start/stop cycle.

S/X Band Antenna Subsystem

Purpose

The SXAS was the means by which the VO transmitted and received the S-band rf signals to and from the Earth and transmitted only X-band rf signals to the Earth. The SXAS consisted of an LGA designed for S-band only and an HGA designed for both S- and X-bands, two DFRJ's, and associated waveguides and cabling. Figure 156 is a drawing illustrating the antennas, rf cabling, and the waveguide plumbing. Figure 31 is a pictorial view of the HGA support structure and shows the DFRJ's and part of the rf cabling and waveguide assemblies.

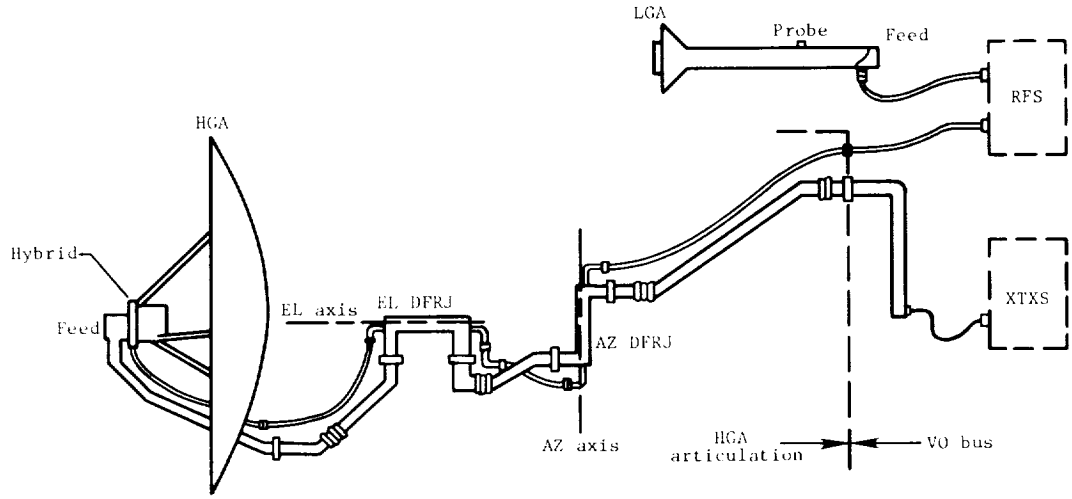

Figure 156.- SXAS.

Description

LGA.- The LGA was used to receive commands and transmit telemetry data during the early phase of the mission when the Viking S/C was near Earth and whenever the HGA could not be used for any reason; that is, maneuvers, whenever the S/C was off Sun or celestial lock and the HGA was unable to point toward the Earth due to mechanical limitations. The LGA was also thought of as the emergency backup antenna in the failure mode routines loaded in the CCS memories because commands could be received and low-rate telemetry data transmitted by the LGA with the S/C in almost any orientation and throughout almost the entire mission. The LGA was designed for right-hand circular polarized radiation, and figure 157 illustrates typical patterns of the LGA. Figure 158 shows the field of view of the LGA and indicates the variations in the antenna patterns caused by the surrounding structures. Table 39 shows the performance characteristics of the LGA.

HGA.- The HGA consisted of a parabolic reflector with a 1.47-m-diameter (58 in.) circular aperture and a feed-to-diameter ratio of 0.3795. The S/X band feed was designed for left-hand circular polarization (to provide right-hand circular polarization from the HGA); connected to semirigid coaxial cable for S-band and waveguide for X-band; supported by a three-point, six member truss configuration; and optimized to receive at 2115 ± 5 MHz (S-band) and to transmit at 2295 ± 5 MHz (S-band) and 8415 ± 20 MHz (X-band). The HGA was in a stowed position at launch and then deployed via command after S/C separation. The HGA was not used for the first 100 days of the mission; however, after that time, whenever the S/C was in the celestial-lock orientation (Sun and Canopus acquired), the HGA boresight could be pointed toward the Earth with commands from the CCS via the ARTCS (orthogonal axes control system) to provide the high data rate capabilities and X-band performance required for the mission.

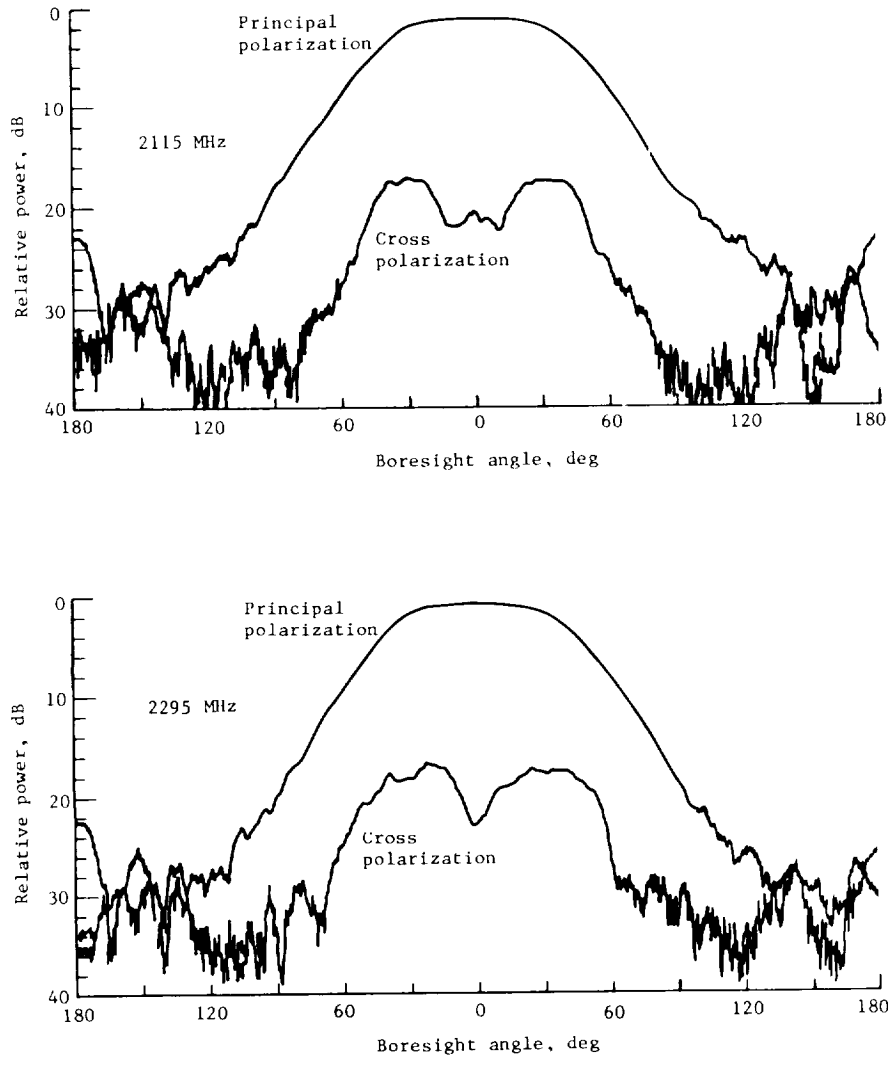

Figure 157.- Typical LGA patterns.

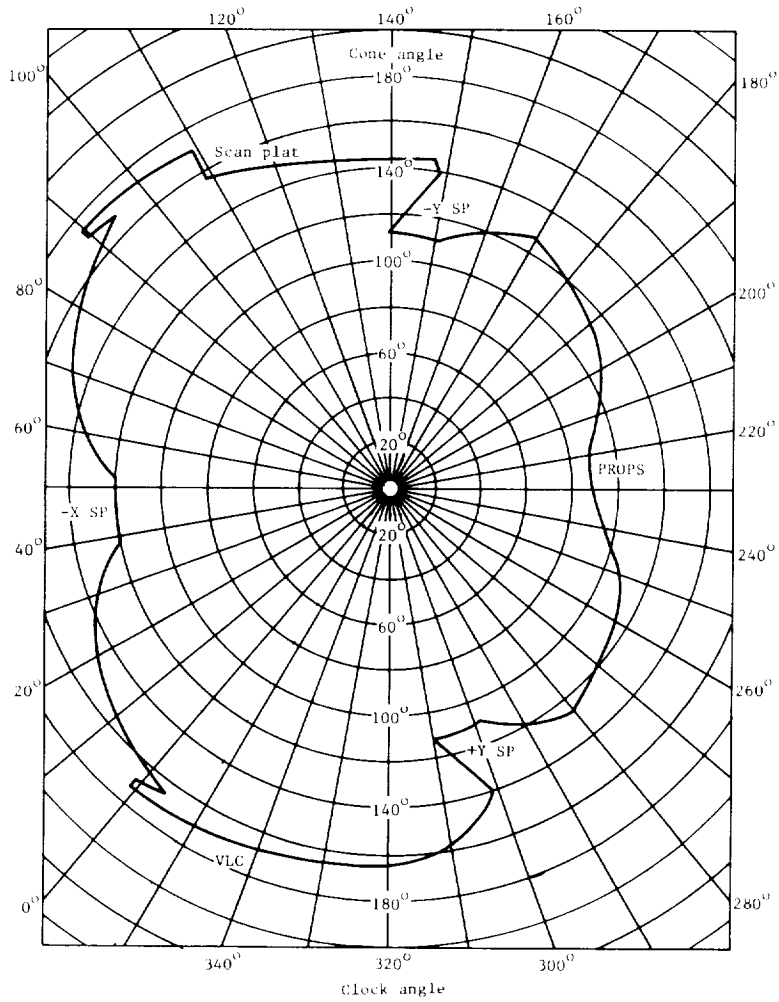

Figure 158.- Field of view of LGA.

TABLE 39.- L/A PERFORMANCE SUMMARY

Parameter	Specified performance
2115 MHz	
Gain	7.20 dB
Axial ratio (on axis)	2.30 dB
VSWR	1.30:1
3-dB beamwidth	90.0°
6-dB beamwidth	115.0°
10-dB beamwidth	136.0°
2295 MHz	
Gain	7.80 dB
Axial ratio (on axis)	2.30 dB
VSWR	1.30:1
3-dB beamwidth	84.0°
6-dB beamwidth	108.0°
10-dB beamwidth	134.0°

Figure 159 shows the X-band radiation pattern of the HGA. The figure shows three different curves as follows: the curve, labeled "ID3703111," which represents the pattern used for the VO/DSN interface mission planning before launch; the curve, labeled "measured postenvironmental," which is a typical measured pattern averaged over all roll angles; and the curve, labeled "$G/G_0 = \cos^{3.6}(a\theta)$," which is the approximation for the measured pattern used

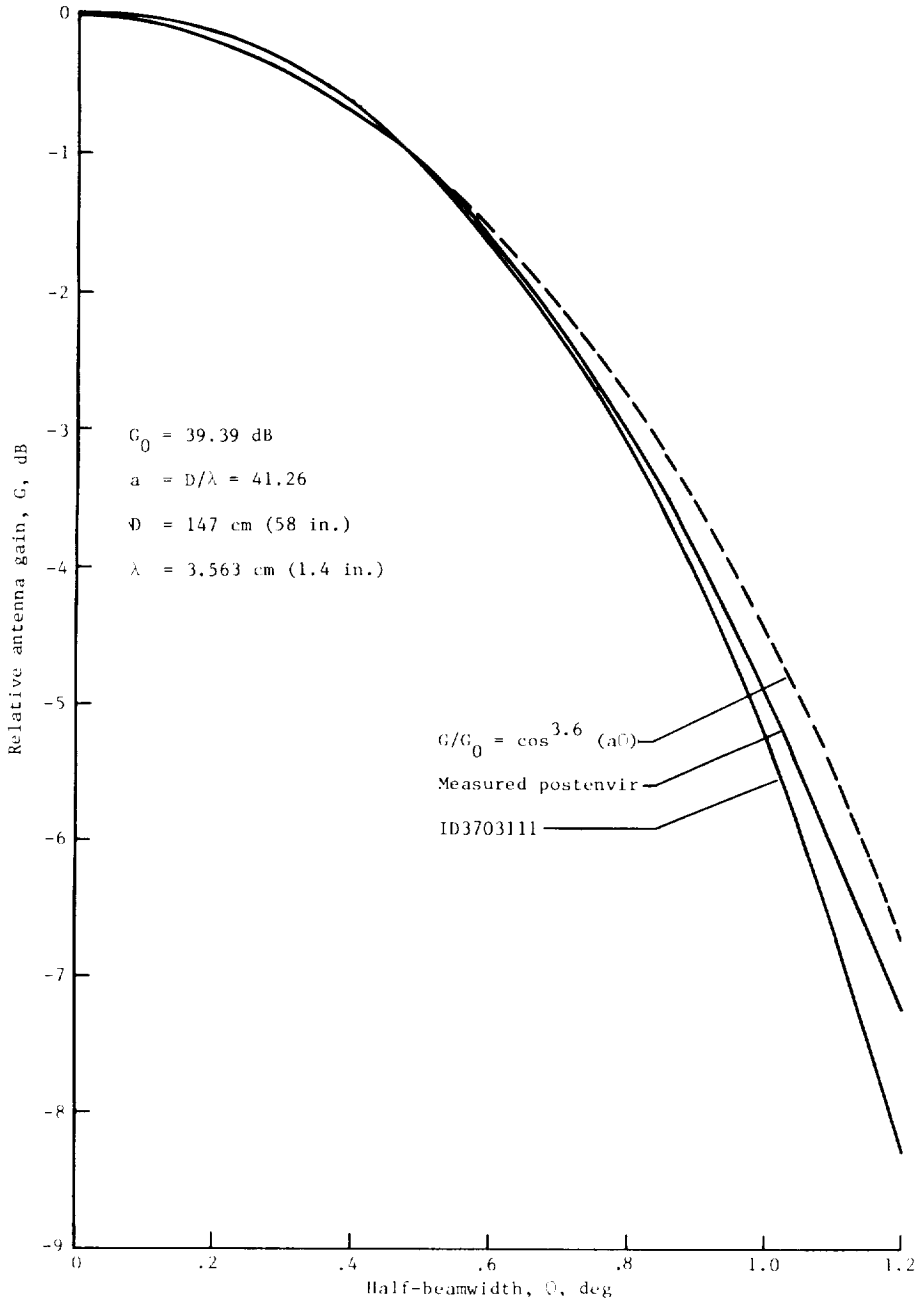

Figure 159.- X-band radiation pattern of HGA.

in the antenna pointing software program. Figure 160 shows the roll symmetry of the HGA X-band pattern; the antenna pointing assumed perfect roll symmetry,

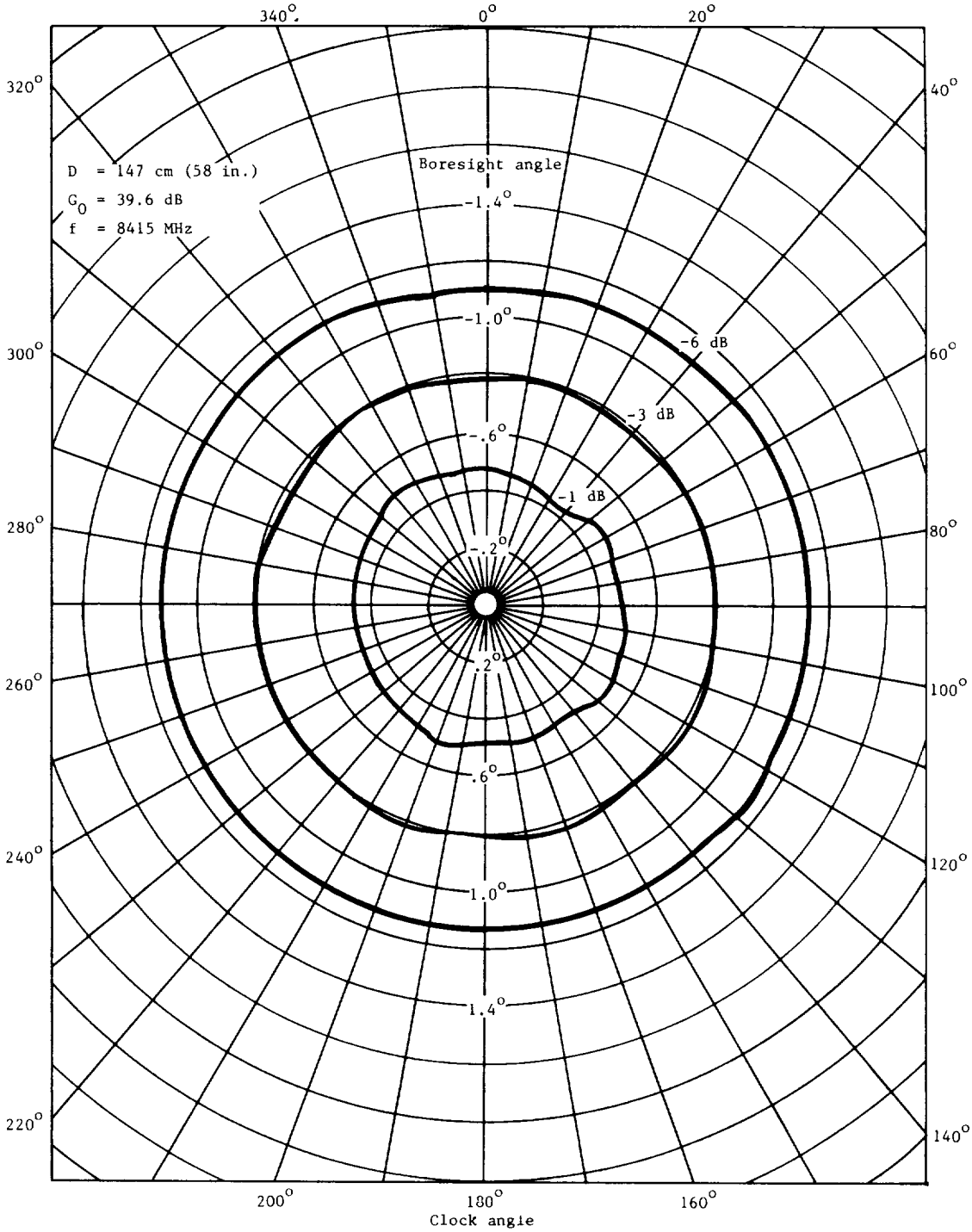

Figure 160.- X-band radiation pattern for roll symmetry of HGA.

and it turned out to be a valid assumption. Figure 161 is a typical radiation pattern at a receive frequency of 2115 MHz, and figure 162 is a typical radiation pattern at a transmit frequency of 2295 MHz (with the same three curves as

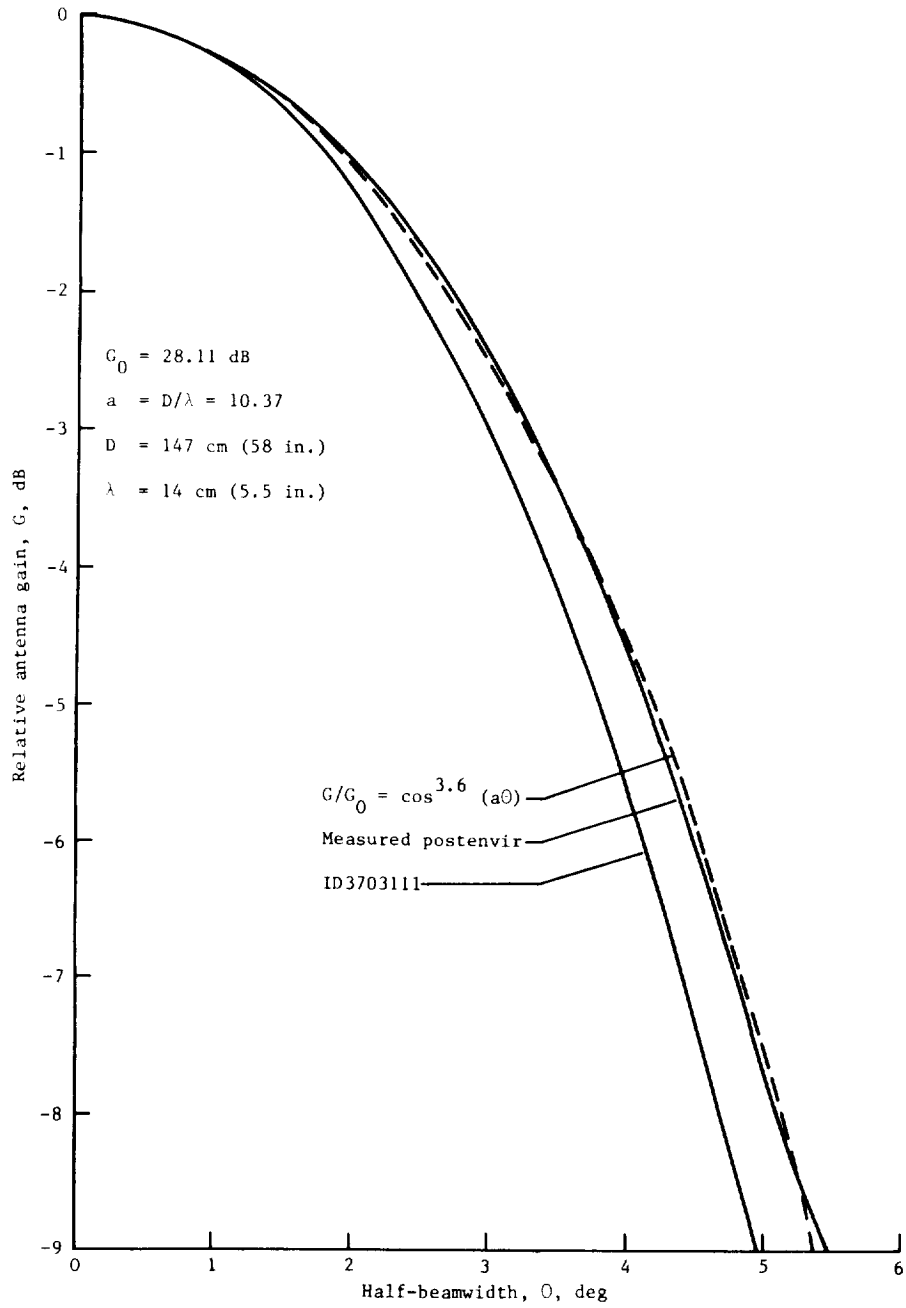

Figure 161.- S-band radiation pattern of HGA at receive frequency of 2115 MHz.

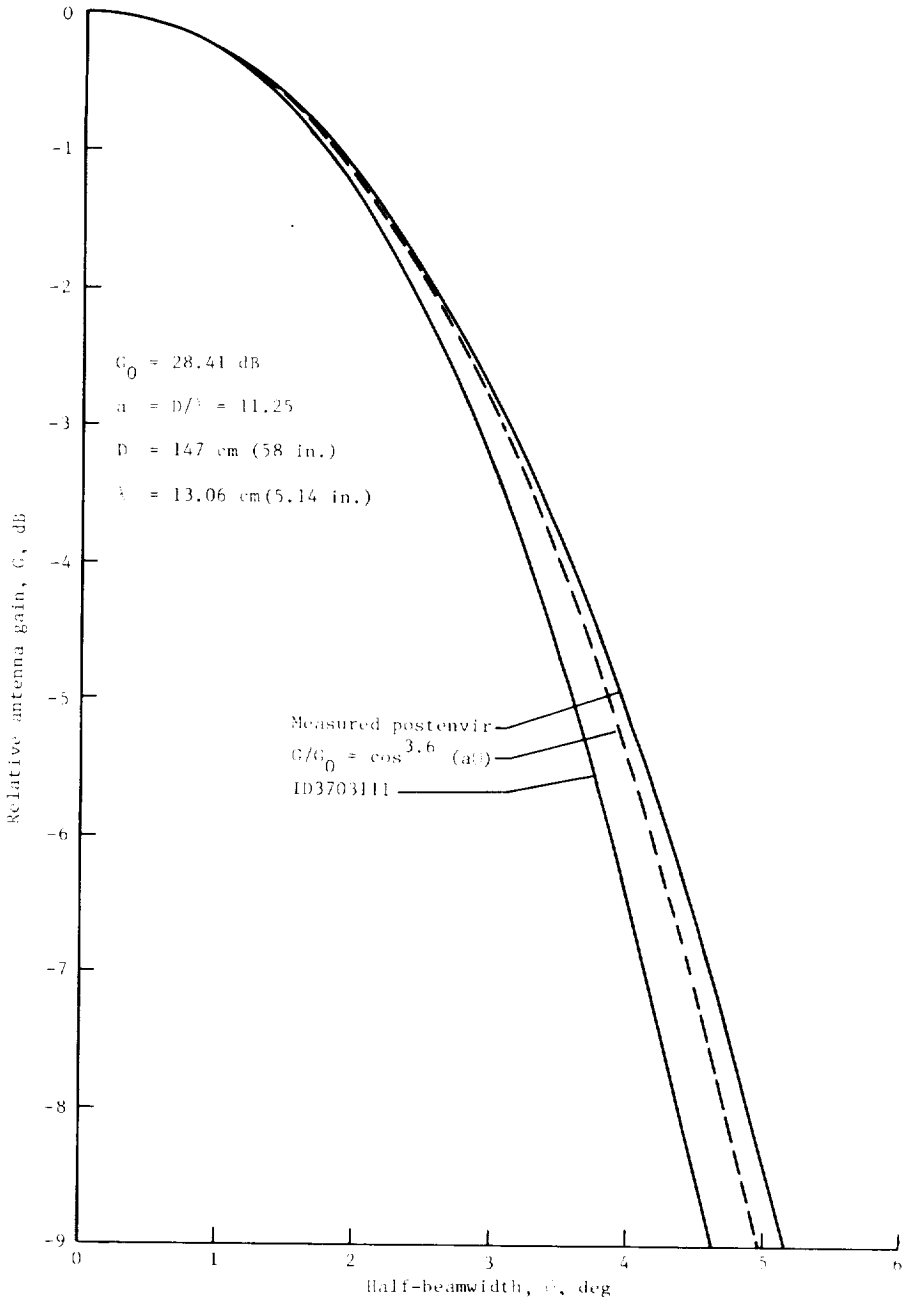

Figure 162.- S-band radiation pattern of HGA at transmit frequency of 2295 MHz.

designated in fig. 159). Figure 163 illustrates the field of view of the HGA, and tables 40, 41, and 42 indicate the performance characteristics of the HGA.

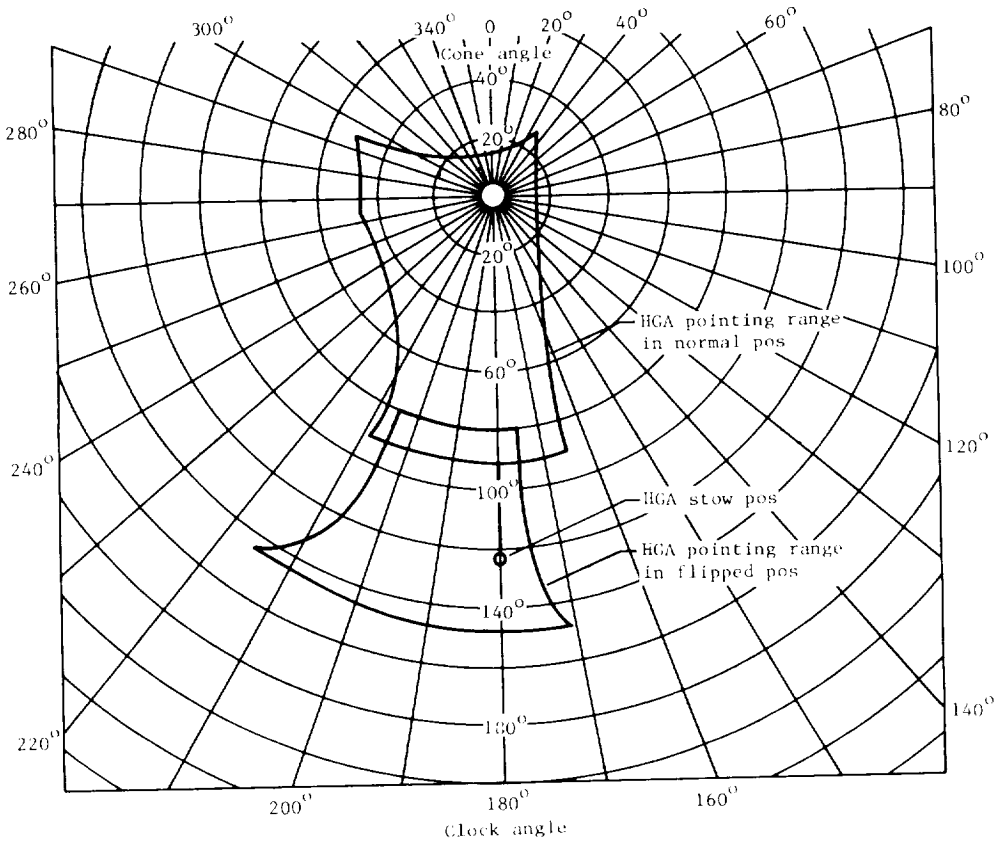

Figure 163.- FOV of HGA.

TABLE 40.- HGA GAIN SUMMARY

Freq, MHz	Specified gain accuracy, dB	Calculated gain accuracy, dB	Specified gain, dB	Typ preenvir gain, dB	Typ postenvir gain, dB
2115	±0.4	±0.319	27.5	28.02	27.63
2295	±.4	±.319	28.5	28.54	28.59
8415	±.4	±.330	39.0	39.29	39.28

TABLE 41.- S-BAND PERFORMANCE SUMMARY OF HGA

Item	Specified performance
2295 MHz	
Gain	>28.5 dB
Axial ratio (boresight)	<1.5 dB
VSWR (at back of dish)	<1.2:1
Beam alignment	$<0^{\circ}6'0"$
3-dB beamwidth	$5.7^{\circ} \pm 0.5^{\circ}$
6-dB beamwidth	$7.6^{\circ} \pm 0.5^{\circ}$
10-dB beamwidth	$9.5^{\circ} \pm 0.5^{\circ}$
2115 MHz	
Gain	>27.5 dB
Axial ratio (boresight)	<2.0 dB
VSWR (at back of dish)	<1.4:1
3-dB beamwidth	$6^{\circ} \pm 0.5^{\circ}$
6-dB beamwidth	$8.2^{\circ} \pm 0.5^{\circ}$
10-dB beamwidth	$10.2^{\circ} \pm 0.5^{\circ}$

TABLE 42.- X-BAND PERFORMANCE SUMMARY OF HGA AT 8415 MHz

Item	Specified performance
Gain	>39.0 dB
Axial ratio	<1.5 dB
VSWR (at back of dish)	<1.2:1
Beam alignment	$<0^{\circ}6'0"$
3-dB beamwidth	$1.6^{\circ} \pm 0.5^{\circ}$
6-dB beamwidth	$2.4^{\circ} \pm 0.5^{\circ}$
10-dB beamwidth	$2.6^{\circ} \pm 0.5^{\circ}$

DFRJ.- DFRJ's were provided to transfer the S-band and X-band rf signals across the AZ and EL axes of the HGA as shown in figures 156 and 31. The DFRJ's were connected to the S-band semirigid coaxial cable and the X-band waveguide to form part of the transmission lines from the RFS to the HGA and from the XTXS to the HGA. Table 43 gives the performance characteristics of the DFRJ's.

TABLE 43.- DFRJ PERFORMANCE SUMMARY

Item	S-band	X-band
Freq, MHz	2115 ± 5 2295 ± 5	8415 ± 20
VSWR	<1.2:1 ± 2%	<1.2:1 ± 2%
VSWR rotation variation	<0.02	<0.04
Ins loss, dB	<0.2 ± 0.05	<0.3 ± 0.05
Ins loss variation with rotation, dB	<0.05	<0.05
rf pwr capability, W	60 cont wave	1 cont wave
Ch iso	>30 dB between S-band and X-band	
Starting torque, N-cm (oz-in.)	<14 (20)	
Angle of rotation, deg	No less than 360	
Speed of rotation, deg/sec	0 to 2.0	

Transmission lines.- The transmission-line assemblies are shown in figure 156 and consisted of appropriate lengths of coaxial cable and waveguide with associated connectors and adapters to transfer the rf signals between the RFS and XTXS and the LGA and HGA via the DFRJ's in the lines to the HGA. The S-band (2115 ± 5 MHz and 2295 ± 5 MHz) transmission line was a semirigid, high-temperature type coaxial cable with a characteristic impedance of 50 Ω and a nominal diameter of 1.27 cm (0.50 in.). The cable connectors used were a special JPL design (JPL 4-channel track sexless connector) and were specially vented to prevent any excessive pressure build-up inside the transmission lines. The coaxial cables and the assembled transmission lines were designed to operate satisfactorily with 60 W continuous wave of S-band rf energy throughout all phases of the mission. In addition, the completed assembly of all the required transmission lines and the DFRJ's to the HGA or an equivalent load had a VSWR of less than 1.40:1 and a total insertion loss of 1.25 ± 0.35 dB. The LGA cable assembly connected to a load with a VSWR of 1.3:1 had a VSWR itself of less than 1.4:1.

The X-band (8415 ± 20 MHz) waveguide was EIA WR90 rectangular type designed to propagate the TE_{10} mode and attenuate other modes of transmission. The waveguide was vented through the HGA feed and used flanges with eight holes (all threaded holes had inserts). Several flexible waveguide sections approximately 5 to 7 cm (2 to 3 in.) long of gold-plated beryllium copper were used in the transmission line (at the rear of the dish, between the DFRJ's, and at each end of the outrigger section of waveguide) for potential minor misalignments. The bus waveguide assembly served as an adapter and matching section to which the flexible cable from the XTXS was connected. The coaxial connector on the

waveguide assembly was a TNC type, and the matching (tuning) section was approximately 3 cm (1.25 in.) long with six adjustable screws at the transmitter end of the section for matching the input impedance of the X-band transmission line. The final section of the X-band transmission line was a length of flexible coaxial cable with an impedance of 50 Ω and with an SMA connector at the XTXS and the TNC connector at the waveguide. The complete X-band transmission line assembly (including the DFRJ's) connected to the HGA or an equivalent load had a VSWR of less than 1.4:1 and a total insertion loss of 2.42 ± 0.35 dB. The assembly was also rated to handle at least 1 W continuous wave of X-band rf power.

Visual Imaging Subsystem

Purpose

The purposes of the VO imaging investigation were to aid in the selection of landing sites for the VLS and future landing sites, to monitor the region surrounding the VLS, and to provide additional spatial and temporal coverage of Mars in order to increase the knowledge of the planet. Pictures of star fields were also provided to improve the precision of approach navigation.

Description

The VIS had two identical camera systems, each consisting of a telescope and camera head which were mounted on the scan platform of the VO and an electronics assembly which was part of the spacecraft bus (fig. 164). The pointing of the two telescopes was offset and the timing of the camera frame starts was offset by one-half frame time so that the cameras covered differing fields of view and shuttered alternately at 4.48-sec intervals. The combined effect was to produce a contiguous swath of pictures as the motion of the spacecraft carried it across the surface of Mars. The camera sensors were 4-cm (1.5-in.), magnetically focused, slow-scan vidicons. A continuous VIS data stream was generated by reading out one camera while the second camera's sensor was being erased and exposed. VIS intensity data were converted to digital form and transferred to the FDS where they were multiplexed with appropriate identification, synchronization, engineering data, and other science data to form a composite data stream. This composite data stream was then transferred to the DSS and stored on magnetic tape for subsequent playback at a rate commensurate with communications link performance. The cameras operated in response to digital control words from the FDS which were set by ground command and specified the exposure duration, the stepping of the filter wheel, the light flood, the amplifier gain state, and the dc video offset. An exposure duration of 0 was specified when no picture was to be recorded, and it could also be used for the determination of sensor dark current and to prepare the sensor for low residual image.

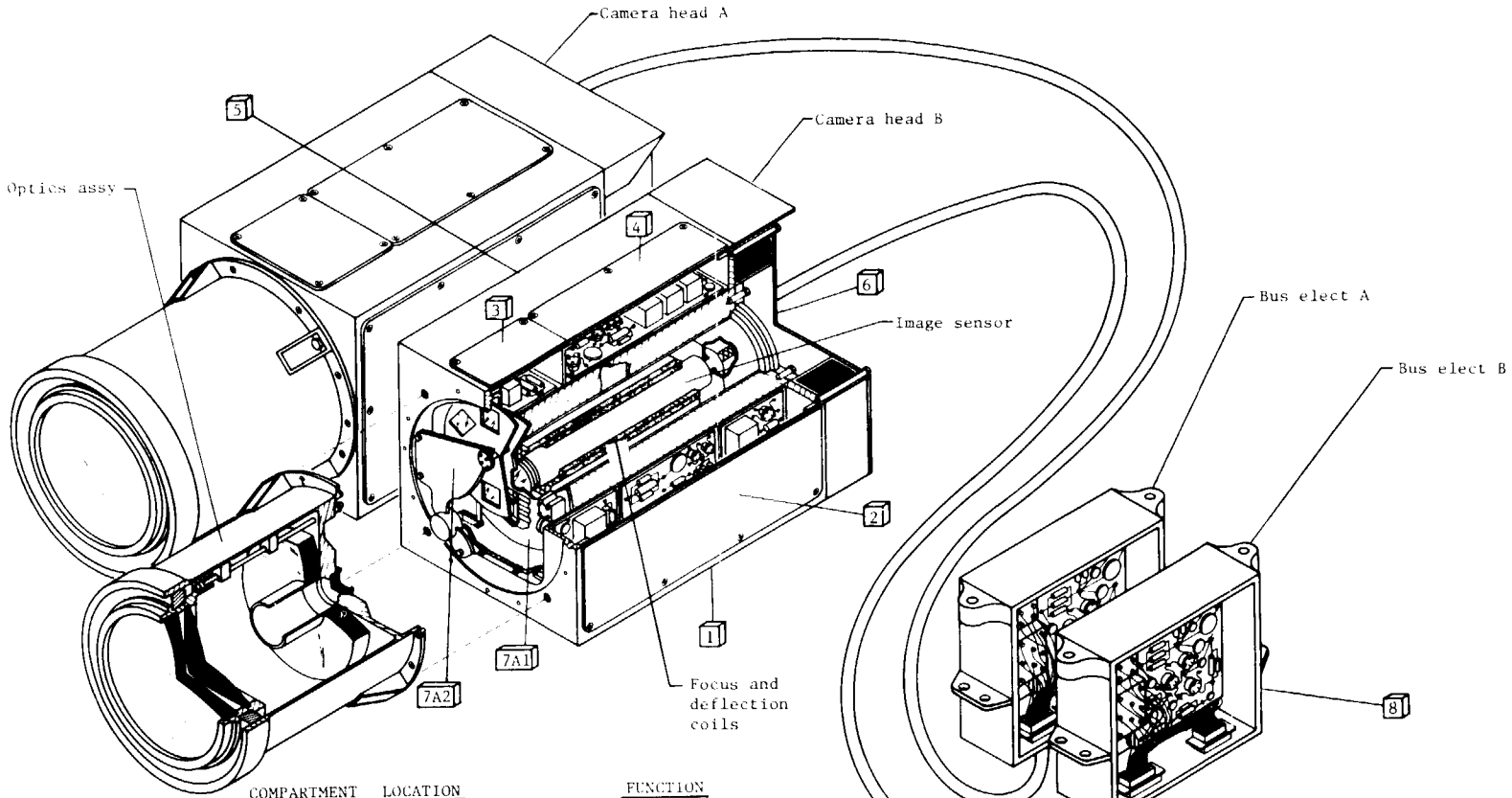

COMPARTMENT	LOCATION	FUNCTION
1	Bottom	Shutter & Fl wheel output elect
2	Left side	Digital sequencing logic
3	Top front	Video amp chain
4	Top rear	ADC
5	Right side	Vidicon analog controls
6	Rear	Vidicon P/S
7A1	Front	Shutter assy
7A2	Front	Fl wheel assy
8	Bus elect	Low-voltage P/S

Figure 164.- VIS configuration.

A simplified block diagram showing a single camera (one-half VIS) is given in figure 165. The bus electronics assembly functioned as a power conditioner for the VIS. It accepted 2.4-kHz square-wave spacecraft power and converted it to various voltages and currents needed throughout the VIS. It also limited input current to protect other subsystems if the VIS malfunctioned. Each camera had its own bus electronics assembly. The logic accepted timing signals and control words from the FDS and sequenced the various VIS circuits accordingly. It also stored and transmitted the VIS digital status word (including filter position and camera S/N) to the FDS. The vidicon was a selenium photosurface with four grids and a 4.48-sec readout time, continuous (unchopped) beam. Appropriate precision ramp currents were generated in the sweep circuits to drive the frame and line deflection coils. The sweep circuits accepted timing and control signals from the logic. Current through the focus coil was regulated in the focus regulator so as to produce a focused electron beam at the vidicon target. The alignment coil provided a means to minimize beam landing error in the vidicon tube and accepted regulated currents from the alignment regulator in the bus electronics assembly. The vidicon power supply generated

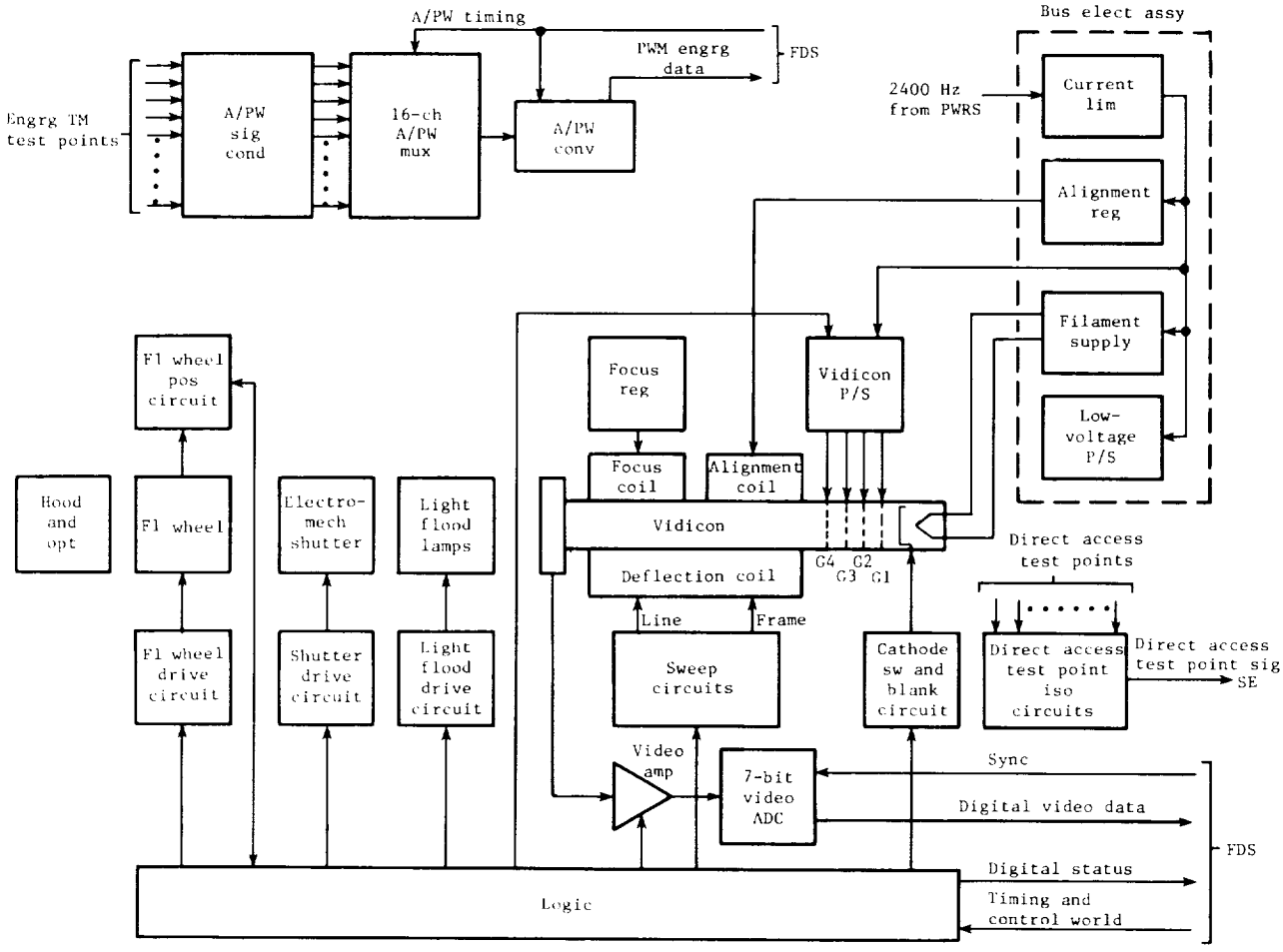

Figure 165.- Simplified block diagram of VIS.

the four grid voltages necessary to accelerate and focus the vidicon electron beam. The voltages were G1, -70 to -10 V; G2, 300 V; G3, 1050 V; and G4, 1250 V. The cathode switch and blanking circuit accepted timing and controls from the logic and set the cathode to either blank, read, or erase voltages. The video amplifier accepted vidicon target current and converted it to an analog video voltage; output was 6 V full-scale, 150-kHz 3-dB bandwidth. The dc offset and gain were commandable by control signals generated in the logic from the control word. The 7-bit video ADC converted analog video from the video amplifier to digital data and transmitted them to the FDS at 2.112×10^6 bits/sec and 3.01×10^5 samples/sec. Six spectral filters were used: blue, minus blue, violet, clear, green, and red. The violet filter also served as protection from direct Sunlight within the field of view during spacecraft maneuvers. Position was read out by a set of LED's and photosensors aligned with coded holes in the filter wheel. The filter wheel position circuit transmitted position code to logic circuitry, where it was subsequently transmitted to the FDS as part of the digital status word. The filter wheel drive circuit stepped the filter wheel upon command from the FDS (through the control word and the logic); maximum step rate was 1 step/8.96-sec frame. Resetting two-blade focal plane type shutters (speeds from 3 msec to 2.66 sec) provided the only means of varying exposure to the vidicon in any given filter position. Shutter drive circuit operated on timing generated in the logic from the control word. Eight incandescent lamps were mounted just behind the shutter to reduce residual image and to flood the photosurface to saturation just prior to erasure (commandable from control word). Sixteen engineering telemetry channels per camera were multiplexed to the input of a single A/PW converter. The multiplexer accepted timing from the FDS and stepped through all 16 channels in 4.48 sec. A/PW converter accepted timing from the FDS and converted the analog voltage at its input to a pulse with a width that was proportional to the input voltage level. The output pulse was transmitted to the FDS for conversion to digital engineering data.

Performance Characteristics

The performance characteristics of the VIS are given as follows:

Angular resolution, μrad/pixel	25.8
Single camera FOV	
Line dimension, mrad	29.52
Frame dimension, mrad	26.37
Dynamic range	100:1
Phase angle capability at 1500-km altitude and 12-msec exposure, deg	75
Geometric distortion, center to edge, pixels	<3
Residual image for high-contrast image followed by black flat field, DN	<2
Spectral response	
Peak, nm	525 ± 25
Greater than 5% (relative to peak), nm	380 and 630
Exposure time range, msec	3.182 to 2660 with increments in multiples of 1, 4/3, 2, 8/3, 4, 16/3, . . ., 2^n, $2^n/3$

Star imagery capability for SNR = 1	+7.5 magnitude
Data format	
Line format	
Line blanking, pixels	76
Total line, pixels	1280
Frame format, lines	1056
Data	
Video, pixels/frame	1 271 424
Blanking, pixels/frame	80 256
Total, pixels/frame	1 351 680
Encoding, bits/pixel	7
Total data, bits/frame	9 461 760
Data rate, bps	2.112×10^6
Frame time, sec	4.480

Subsystem Timing

The relationship between the various components which comprised VIS timing is illustrated in figure 166. Specific VIS rates and timing intervals are as follows:

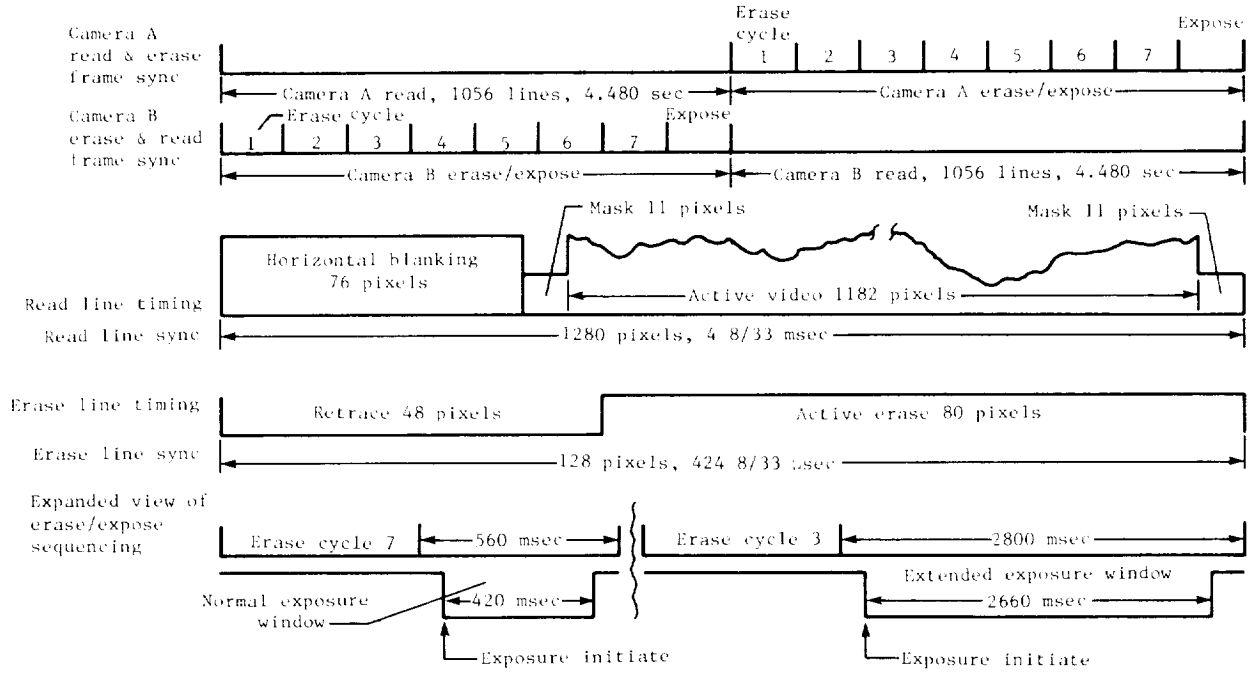

For exposure intervals between 420 msec and 2660 msec. Erase cycles 4, 5, 6, and 7 are inhibited by VIS. Light flooding when commanded occured during the first erase frame.

Figure 166.- VIS timing diagram.

ADC bit rate, bps	2.112×10^6
Pixel rate, pixels/sec (pixel time = 3 83/264 μsec)	$301\ 5/7 \times 10^3$
Line blanking time, μsec	251 59/66
Total read line time, msec	4 8/33
Read lines per read frame, lines	1056
Read frame time, sec	4.480
Erase line time, sec	424 8/33
Erase lines per erase cycle interval, lines	1320
Erase cycle time, msec	560
Erase cycles per normal erase frame, cycles	7
Normal exposure window, msec	420
Erase cycles per reduced erase frame, cycles	3
Extended exposure window, msec	2660

Control Word

During the first erase cycle of each erase frame, an 11-bit control word was transferred from the FDS to the VIS. The control words for camera A were sent over a separate interface from those for camera B.

Optical Design

The VIS optical system shown in figure 167 was an all-spherical catadioptric Cassegrain telescope consisting of six elements: two aperture correctors, two small field correctors near the image plane, and the primary and secondary

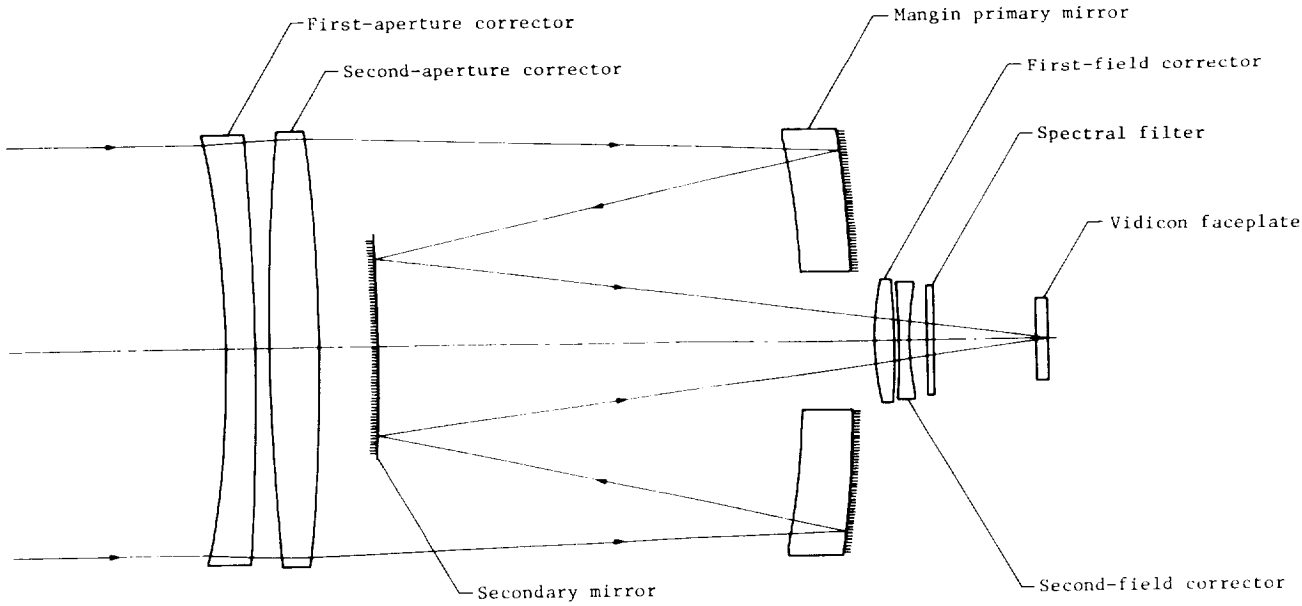

Figure 167.- Schematic diagram of VIS optical system.

mirrors. All elements were fabricated from ultra-pure fused silica, an extremely stable optical material. The telescope had a modulation transfer function that provided no less than 70 percent modulation at 42 l_p/mm, which was essentially a diffraction-limited performance. Optical parameters are summarized as follows:

Telescope	All-spherical catadioptric Cassegrain with Mangin primary mirror
Focal length, mm	475
Focal ratio	f/3.5
Effective focal ratio	T/5.6
Frame diagonal angular coverage, deg	2.3

Filter Characteristics

The spectral transmission characteristics of the optical filters are illustrated in figure 168. The VIS response characteristics with spectral filters are described in the following table:

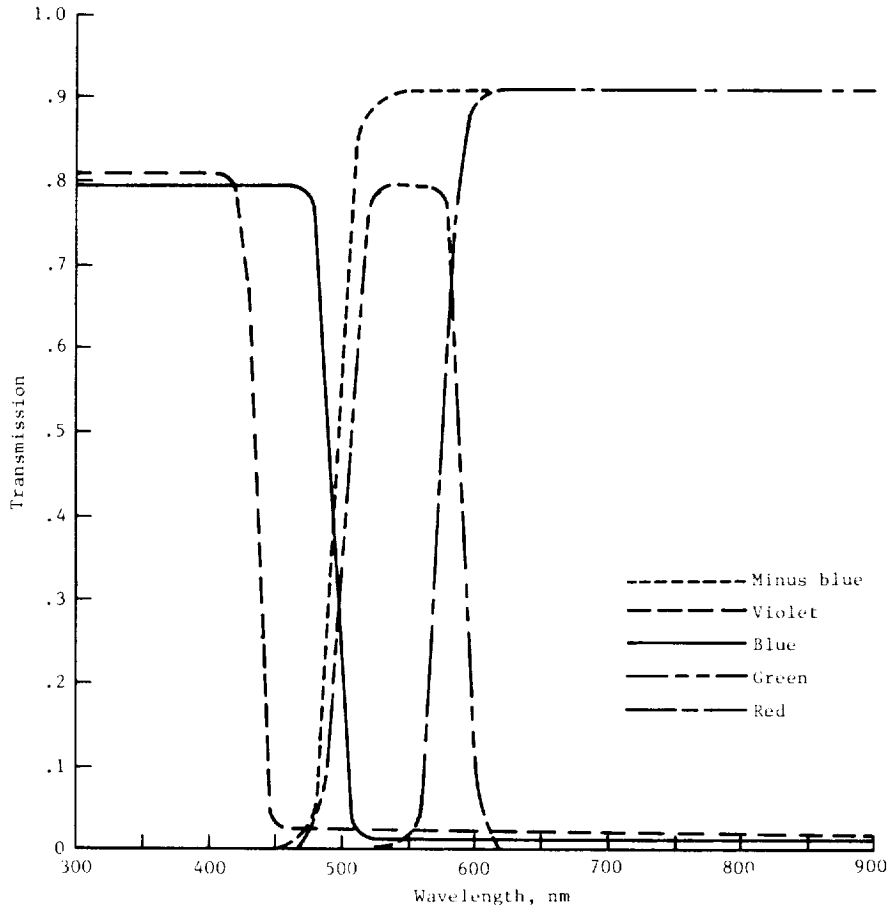

Figure 168.- Spectral transmission of optical filters.

Filter	Peak wavelength, nm	Passband, nm	Filter factor[a]
Blue	460	350 to 510	3.8
Minus blue	550	480 to 700	1.6
Violet	430	350 to 450	14.0
Clear	520	350 to 700	1.0
Green	540	480 to 600	2.4
Red	600	560 to 700	5.4

[a]Based on Mars spectral radiance.

Resolution and Field of View

The focal length of the VIS optics was 475 mm. Based on a vidicon scan density of 84.30 pixels/mm, the projected pixel dimension at a range of 1500 km was 37.5 m. The fields of view are illustrated in figure 169.

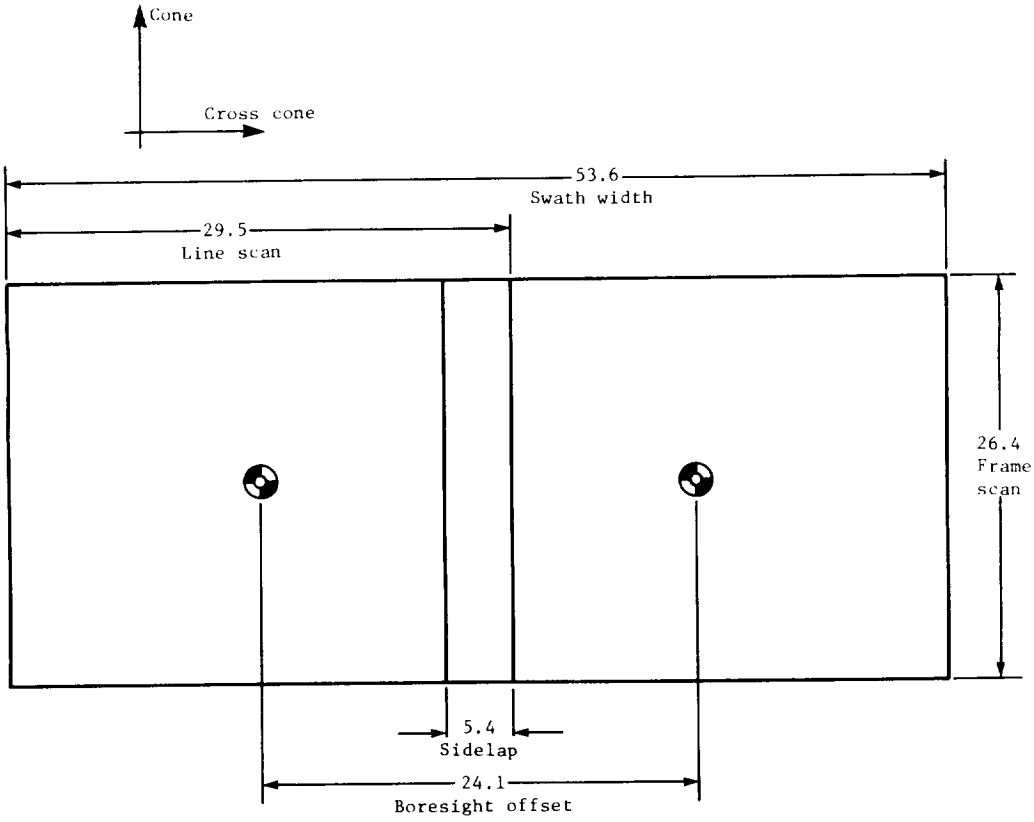

Figure 169.- Field of view of VIS. All dimensions are given in mrad.

Data Interface

Three types of data originated in the VIS: engineering telemetry, housekeeping telemetry, and imaging science data. These data were received on the ground as parts of various data formats and at rates determined by FDS mode selection. The VIS engineering telemetry data comprised of six temperature measurements of the VIS cameras and were available whenever the FDS was powered. FDS format selection determined which of the measurements would be included in the transmitted data and their locations within the format. In order to provide detailed visibility into VIS operation, 16 housekeeping telemetry parameters from each camera were monitored and telemetered to the ground whenever the VIS was powered. Each measurement was sampled once every VIS read frame (4.48 sec), such that measurements (A and B) repeat every 8.96 sec. The imaging science data originated within the VIS as a 150.5-kHz baseband analog signal. This signal was converted to a 7-bit serial digital signal at 2 112 000 bps and transferred to the FDS wherein a commutator selected VIS A or VIS B data and performed a serial-to-parallel conversion. Prior to this last conversion, the output of the IRS mux and the 1000-bps engineering mux were inserted in the line flyback time. Engineering data were also included as 8 1/3 or 33 1/3 bps data submultiplexed into the IRS stream. The 76 flyback bits were arranged as follows:

VO ID	2 bits
Sync word	29 bits
DTR track ID	3 bits
Engrg data	5 bits
Picture ID	19 bits
Line count	11 bits
FDS mode	1 bit
HR data ID	1 bit
IRS	5 bits

The parallel converted data were rate buffered from 2 112 000 bps to 301 714 2/7 bps and sent to both DTR's in the DSS via seven lines to each recorder. Buffering was accomplished by clocking out the 7 bits of a pixel at the serial pixel rate. The result was that output line 1 contained pixel one, 8, 15 . . .; line 2 contained pixels 2, 9, 16 . . .; . . . through line 7. These lines were routed to channels (tracks) 1 through 7, respectively, of the DTR's. When an operational sequence was commanded, the imaging data were recorded on DTR A or B.

Infrared Thermal Mapper Subsystem

Purpose

The thermal mapping investigation subsystem aided in the selection of landing sites for the VL's, monitored the regions surrounding the VL's, provided additional information on spatial and temporal distribution of surface and upper atmospheric temperatures and thermal balance, contributed to knowledge of Mars, and assisted in the selection of future landing sites. The IRTMS also

provided temperature measurements at the same time and over the same region covered by the VIS and provided independent observations at appropriate times and places. The IRTMS was designed to make measurements of Mars from any portion of orbit unless limited by spacecraft constraints. In order to provide optimum information about the surface, measurements were made of the dark side as long after local sunset as possible, including observations during solar occultation.

After the VLC had separated, the surface temperature was measured to an accuracy of ±1 K at 200 K and the measurement range was 130 K to 330 K; these measurements were taken within the spectral bands of 6.1 to 8.35 μm, 8.35 to 9.8 μm, 9.8 to 12.7 μm, and 18.0 to 24.0 μm. The atmosphere brightness temperature was measured in the spectral band of 14.56 to 15.41 μm to an accuracy of at least ±3 K at 170 K. The brightness of reflected solar radiation from the surface and atmosphere of the planet was measured in a spectral band of 0.24 to 3.0 μm. The angular resolution of each measurement was 5.2 mrad. Prior to VLC separation, some loss of absolute temperature accuracy could have occurred because of VLC interference.

Description

Scan mirror.- The IRTMS was a 28-channel radiometer and consisted of the major elements shown in the functional block diagram (fig. 170). Infrared radiation from Mars, from deep space, or from the IRTMS internal reference surface was selected by positioning the scan mirror to one of its three discrete positions. The scan mirror assembly consisted of a stepping motor, a position encoder, and the scan mirror. The mirror was mounted on the motor shaft at a 45° angle. Figure 171 shows the mirror in the position which would receive deep space radiation. The mirror selected the planet position if rotated 90° CW or selected the internal reference position if rotated 90° CCW. Direction was dependent on whether the mirror was viewed from the detector (telescope) side or from the motor side. The directions given corresponded to viewing from the telescope side. The mirror was rotated by a stepping motor which moved in 1.8° increments at a rate of 25 steps/sec; therefore, the mirror stepped 90° in 2 sec and 180° in 4 sec.

The stepping motor encoder provided a feedback signal to indicate the scan mirror positions - planet, space, or reference - or transit (between positions). The encoder indicated planet, space, or reference when the motor shaft was within $\pm 0.15^{\circ}$ of the discrete position.

Optics.- Infrared radiation was reflected from the selected source by the mirror into the cluster of four Cassegrain reflecting telescopes. Three were f/4, 5.6-cm-diameter (2.3 in.) telescopes and the fourth was a f/5.3, 3.8-cm-diameter (1.5 in.) telescope. Figure 172 shows the telescope configuration. The spectral bands were selected by the optical elements within each of the telescopes. Table 44 lists the materials used to select the spectral bands.

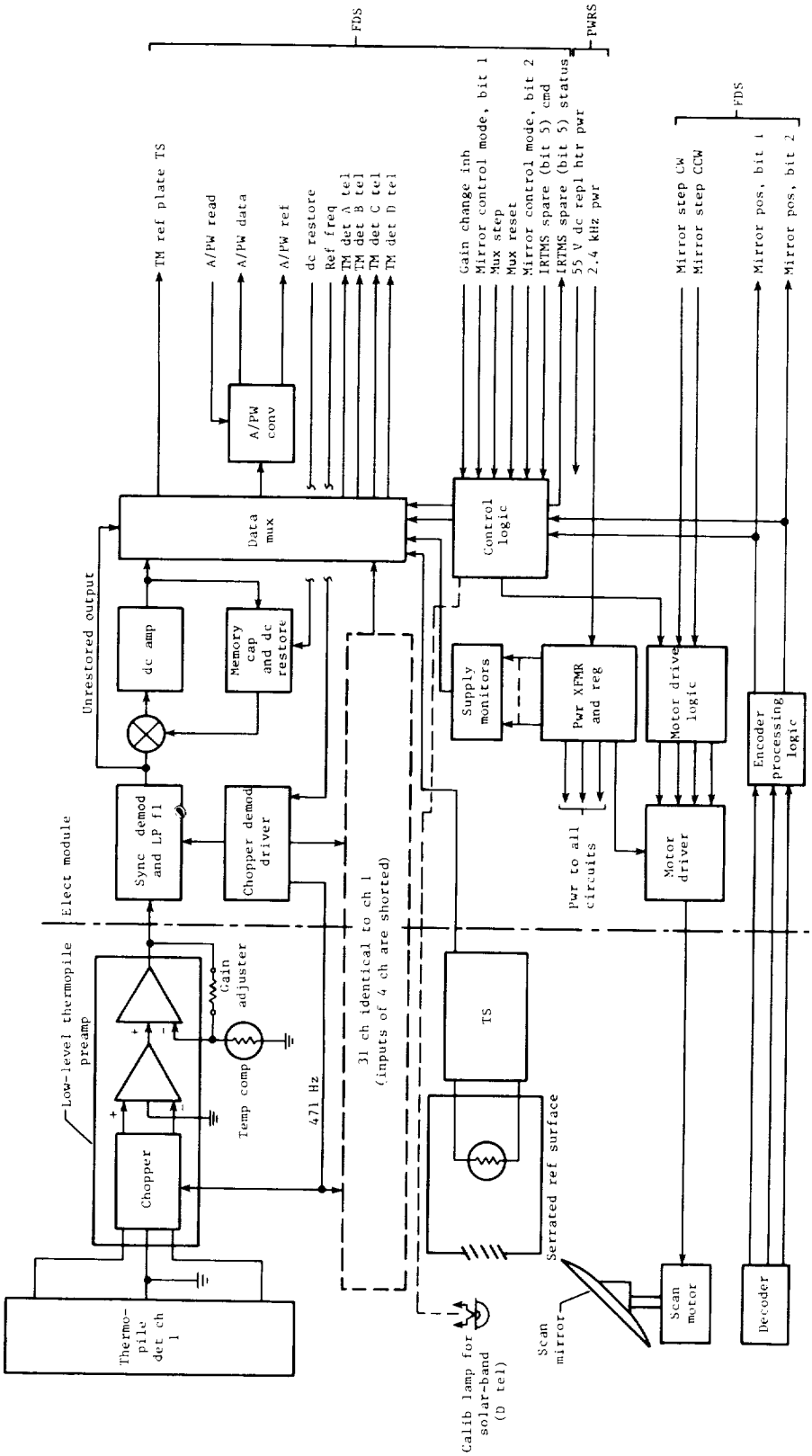

Figure 170.- Functional block diagram of IRTMS.

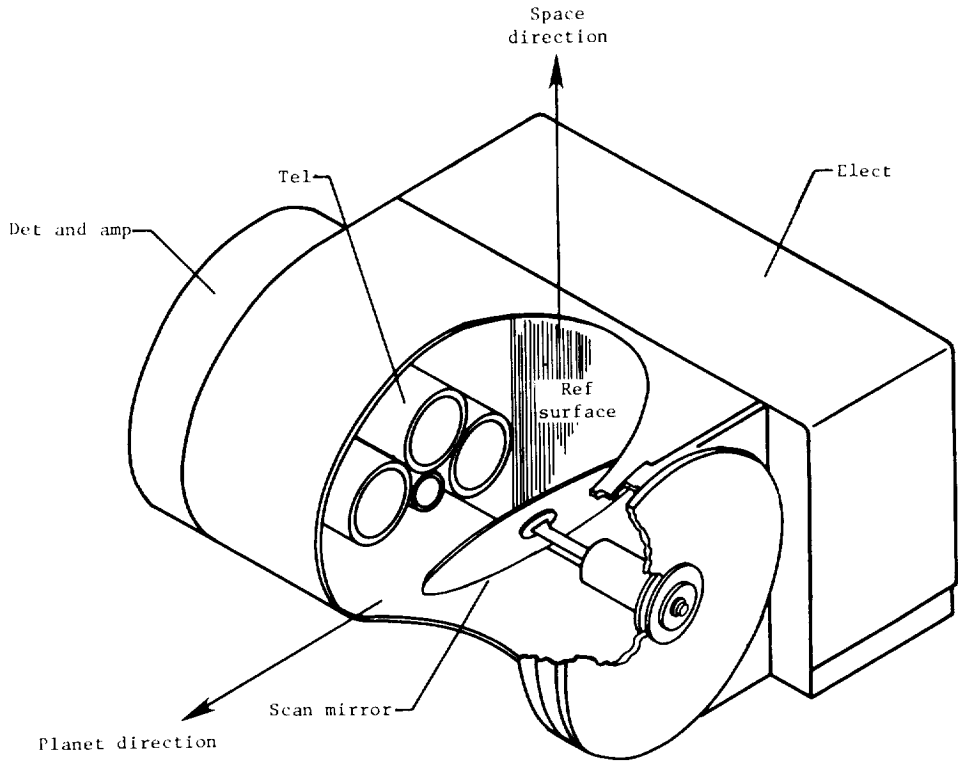

Figure 171.- IRTMS configuration.

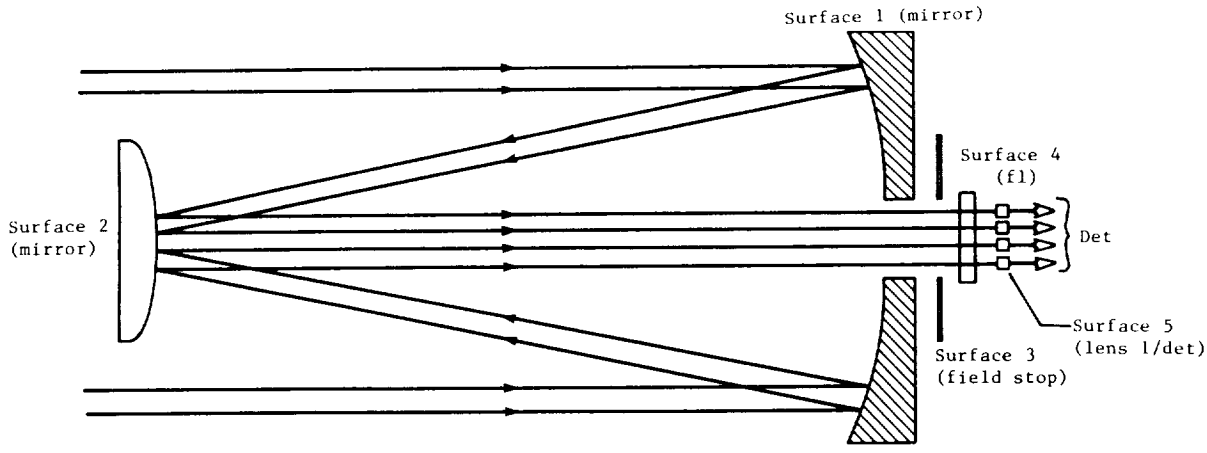

Figure 172.- Schematic diagram of IRTMS telescope configuration.

TABLE 44.- SELECTING ELEMENTS FOR SPECTRAL BANDS

Telescope	Materials (mirrors 1 and 2)	Coatings (mirrors 1 and 2)	Spectral range, μm	Filter substrate	Field lens
A	Zinc oxide		18.0 to 24	No filter (Restrahlen/ mirrors 1 and 2)	Irtran 6
B	Glass	Aluminum	9.8 to 12.7	Germanium	Germanium
C	Glass	Aluminum	6.1 to 8.35	Germanium + Irtran 3	Germanium
			8.35 to 9.8	Germanium + Irtran 3	Germanium
			14.56 to 15.41	Germanium + Irtran 4	Germanium
D	Glass	Aluminum	0.24 to 3.0	UV-22	Glass

Detectors.- Seven detectors were positioned behind each telescope in a chevron array as shown in figure 173. All 28 detectors were identical center-tapped antimony bismuth thermopiles composed of 6 junctions with a sensitive area of approximately 0.0005 cm^2. The individual field lenses focused the incoming radiation on the sensitive area. After being focused by the individual

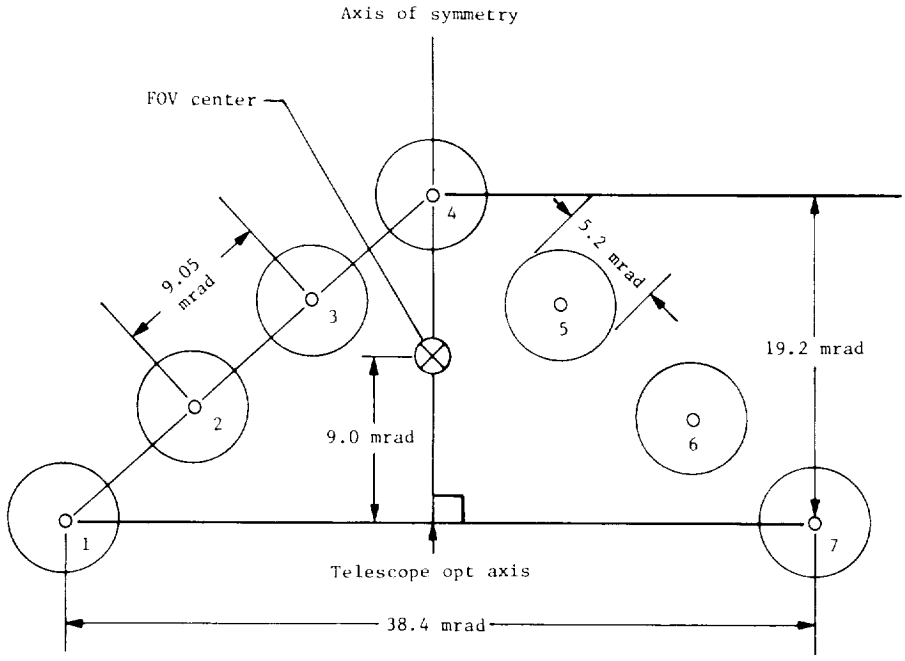

Figure 173.- IRTMS detector position in each telescope.

field lenses, the IR was converted to a voltage which was proportional to the radiation intensity. For each of the four telescopes, the ray passing through the FOV center is offset 9.0 mrad from the telescope optic axis. The FOV of telescope C is arranged with three detectors on the left of the axis of symmetry being designated C_1, a single detector on the extreme right being designated C_3, and the other three detectors being designated C_2.

Preamplifiers.- The output of each thermopile detector, 0 to 20 μV, was directly connected to the low-level preamplifier, a compact hybrid integrated circuit. The input of the preamplifier was a full wave chopper, which interrupted the thermopile signal at a rate of 471 3/7 Hz. The ac gain of the preamplifier was adjustable from 4000 to 50 000 by selecting an external feedback resistor and temperature compensating thermistor network. The thermistor corrected for a decrease in responsivity of the thermopile detector by about 0.5 percent per ^{o}C with increasing temperature.

Analog processing.- Each preamplifier output was connected to the analog processing circuitry, which demodulated, integrated, and buffered each channel. Each of the 28 infrared channels operated in an identical manner. In addition, there were four spare channels that were complete except for detectors. The preamplifier inputs were shorted and these channels would always produce their dc restore level. Thus, 32 identical infrared data channels were connected in parallel to the multiplexer.

Multiplexer.- There were 32 channels of engineering data also available for multiplexing: 8 temperature measurements from thermistors located throughout the IRTMS, 3 power supply voltage monitors, and 21 dc monitors. Because of the limitation of monitoring 32 engineering channels, the dc restore levels of only the 7 active channels from telescopes A, B, and C were monitored; the dc restore levels of the 4 spare channels (8, 16, 24, and 32) and the active channels from telescope D were not monitored. The 32 channels of engineering or science data were combined in each IRTMS data frame with 8 IRTMS status words; thus, 40 10-bit IRTMS words were yielded every 1.12 sec.

Multiplexer output buffers.- The multiplexer output was connected in parallel to two buffer amplifiers. One amplifier drove the A/PW converter; the other amplifier supplied the IRTMS multiplexer output signal to the instrument test connector, which was not used during flight.

Analog to pulse width converter.- The A/PW converter was essentially one-half a DAC. The A/PW converter accepted an input signal from within a -6 to 6 V range. A negative going linear ramp was generated within the A/PW converter. A reference pulse was always generated when the ramp crossed the 0-V level. The analog signal to be measured was continually compared with the ramp; when the ramp and analog signal levels were equal, the A/PW converter generated a data pulse. When the data pulse occurred prior to the reference pulse, the data sample was assigned positive polarity; when the reference pulse occurred first, the data sample was assigned negative polarity. The rest of the ADC was accomplished in the FDS where the time between the two pulses was measured and converted to a 9-bit digital word with an additional sign bit.

Telemetry Stream

The IRTMS telemetry stream operated in either an engineering or IRS mode. Both modes consisted of a 1.12-sec frame of 40 words; during a frame, the IRTMS generated either a complete engineering frame or a complete IRS frame. The majority of IRTMS data was IRS except for periods when the IRTMS was operating in the fixed reference mode.

Operating Modes and Commands

The IRTMS had five operating modes which were controlled by the FDS. The first two were precisely defined automatic sequences of the three mirror positions, whereas the remaining three corresponded to the three possible mirror positions. These five operating modes were normal mode, modified normal mode, fixed space mode, fixed planet mode, and fixed reference mode. In addition, each of these modes were modified (through the FDS) to incorporate one of two special functions or modifiers; these modifiers were gain change inhibit and dc restore.

Mars Atmospheric Water Detector Subsystem

Purpose and Function

Two major objectives of the atmospheric water vapor experiment were carried out during the Viking missions. The first of these was to map, during the far encounter and preliminary orbital phases, the distribution of water vapor over the planet, and in this way perform the initial function of certifying the landing site with respect to this particular characteristic. The second objective was to determine the nature of the water vapor cycle and the relationship between the Martian atmospheric and surface or subsurface water; to this end the observations were to provide latitudinal, diurnal, and seasonal variations of the water vapor but were not confined solely to the regions in the proximity of the landing sites.

The MAWDS measured the radiation at 5 wavelengths in the 1.38-μm water vapor absorption band. Figure 174 shows computed spectra for water vapor in this band and the spectral location of the five PbS detectors which were used in the water vapor measurement. The energy incident upon the detectors was predominantly reflected solar radiation received after two passes through the Mars atmosphere; the contribution to the received radiation from the thermal energy emitted by the Mars surface was negligible at this wavelength. In essence, the radiances measured at the three positions corresponding to water vapor absorption lines, taken as ratios to the radiances of the remaining two (continuum) wavelengths, enabled the absorption of the water vapor and its abundance to be determined.

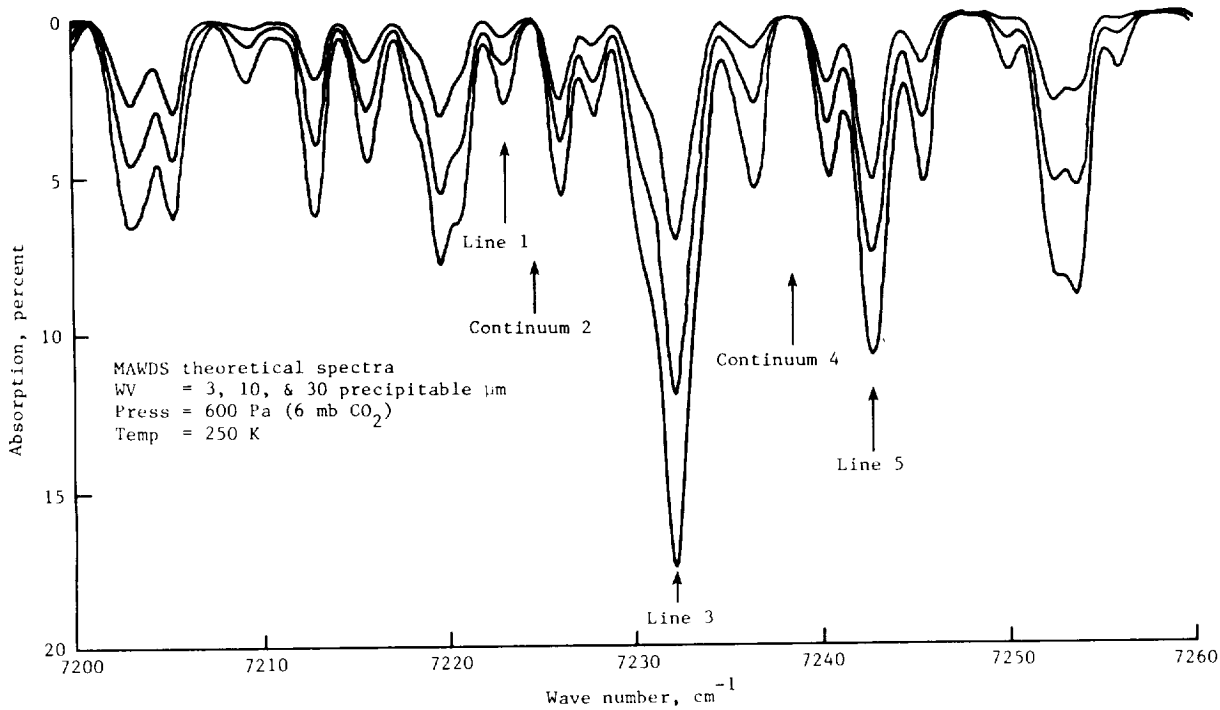

Figure 174.- MAWDS computed spectra.

Description

MAWDS was a fixed grating monochromator, designed using Pfund and Littrow principles, with a five-element radiation cooled PbS detector. Radiation from the planet was focused through a tuning fork chopper onto the input slit of the monochromator by a 25-mm, f/5 telescope which viewed the surface via an external scanning mirror. The IFOV of the instrument was 0.92° by 0.12° which, at a periapsis altitude of 1500 km, gave a projected area of 24 by 3 km on the surface. Figure 175 is a cutaway perspective of the MAWDS optical assembly. Figure 176 is the MAWDS optical layout schematic. Radiation entered the foreoptics section and was reflected from the scanning raster mirror, through the order isolation filter, and onto the first telescope mirror. It was focused onto the entrance slit and entered the monochromator section. The section was collimated by a 550-mm focal length paraboloid and then fell on a 1200-line/mm grating. The dispersed energy was reimaged by the collimating mirror onto the detectors which were in the same plane as the entrance slit. The signals from the detectors were individually and simultaneously amplified, synchronously demodulated, and integrated for approximately 260 msec. After integration was complete, the channels were sampled by the spacecraft data system and converted to serial digital words for transmission to Earth. The raster mirror was stepped every 280 msec through 15 positions to provide a scan of the planet surface. The scan direction could be reversed to provide the mirror image of

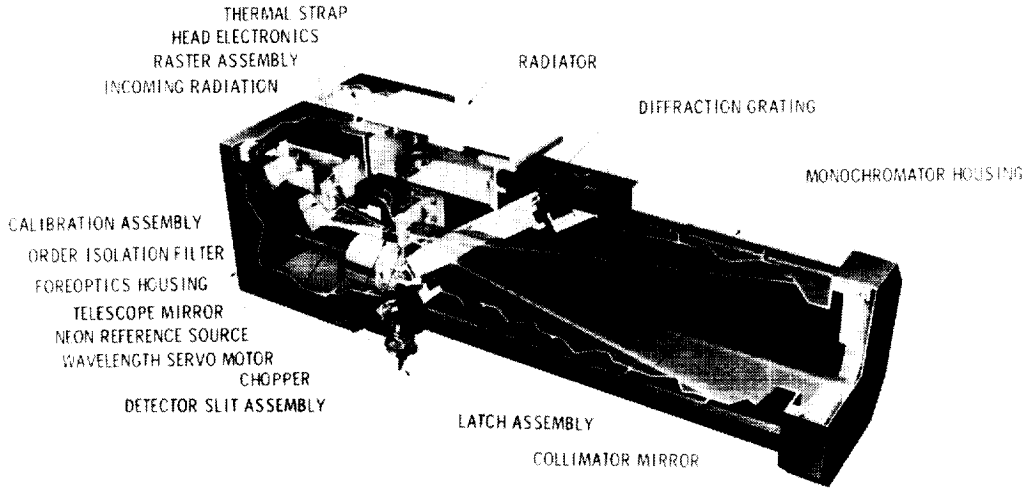

Figure 175.- MAWDS.

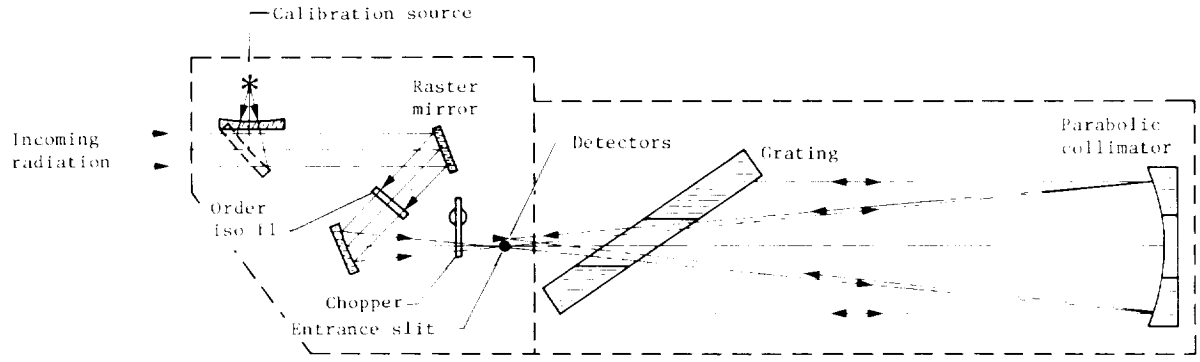

Figure 176.- Schematic diagram of MAWDS optical layout.

the track illustrated. Return to the initial position also took 280 msec so that each raster was 4.48 sec. During each flyback of the raster mirror (or every 16th frame) the wavelength servo system was actuated. This included turning on neon lamps which were located beyond the order filter and chopper. Silicon detectors were radiated by the neon line at 0.6931 μm, two detectors were used to fix the spectrum by means of a servo loop controlling the grating position, and two detectors monitored the beam position normal to the dispersion plane for the purpose of FOV correction. The responsivity of each PbS detector was measured every 64 rasters (4.78 min) by inserting radiation from an intensity source into the telescope FOV and blocking radiation normally viewed by the telescope. In order to monitor the purity of the spectra, the wavelength scan mode provided a look at the total spectra. This mode provided calibration of channel gains, continuum levels, spectral resolution, and total absorption

characteristics. To scan, the wavelength lock was bypassed and the grating was stepped through 20 percent of a resolution element (0.2 cm^{-1}) each time the raster was reset. After 160 such steps, which took the grating from its mean position to one end of its travel back through its full travel and to its original position, the wavelength servo loop lock was reestablished. This technique provided continuous and overlapping spectral coverage over the total wavelength range of the instrument (16 wave numbers per detector). Both the water vapor (PbS) and the neon (Si) detectors were monitored during the wavelength scan.

Performance Characteristics

The MAWDS performance characteristics are given as follows:

Detector	Wave number, cm^{-1}	Wavelength, μm
1	7223.13	1.3844
2	7224.50	1.3842
3	7232.20	1.5827
4	7238.50	1.3815
5	7242.74	1.3807

Resolution, cm^{-1}	0.25
Wave-number scan range, wave numbers/detector	±8
Intensity calibration, rasters of internal source	1
Spatial resolution, deg	0.12 by 0.92
Wavelength spectral knowledge, wave numbers	±0.05
Wavelength spectral accuracy, wave numbers (cm^{-1})	±0.25
Radiometric absolute accuracy, percent absolute	±10
Radiometric relative accuracy (ch to ch), percent	±1.0
PbS detectivity, D*, $cm\text{-}Hz^{1/2}\text{-}W^{-1}$	2.6×10^{11}
SNR at spectral radiance of 3.5×10^{-7} $W\text{-}(cm^{-1})^{-1}\text{-}cm^{-2}\text{-}sr^{-1}$	50
Wavelength of servo neon line, μm	0.6931
Data rate, bps	280

Optics

A schematic diagram of the optical layout is shown in figure 176. Individual assemblies are described in detail as follows.

Calibration source: The calibration source consisted of an integrating sphere coated with beryllium sulfate (BeS), four tungsten lamps, and a polished aluminum parabolic mirror. The mirror was rotated in or out of the input beam of the telescope by a rotary solenoid. The calibrator furnished a zero/intensity calibration of the PbS detectors every 64 rasters, and when commanded, it provided offsets and both absolute and relative radiometric knowledge.

Raster mirror: The raster mirror was a gold-coated flat mirror on a CER-VIT blank. It allowed the IFOV of the instrument to be stepped through 15 consecutive positions. Figure 177 shows a theoretical surface track of the instrument for a 1500-km periapsis with the mirror scanning. The mirror was mounted on flexural pivots which allow rotation through a limited angle.

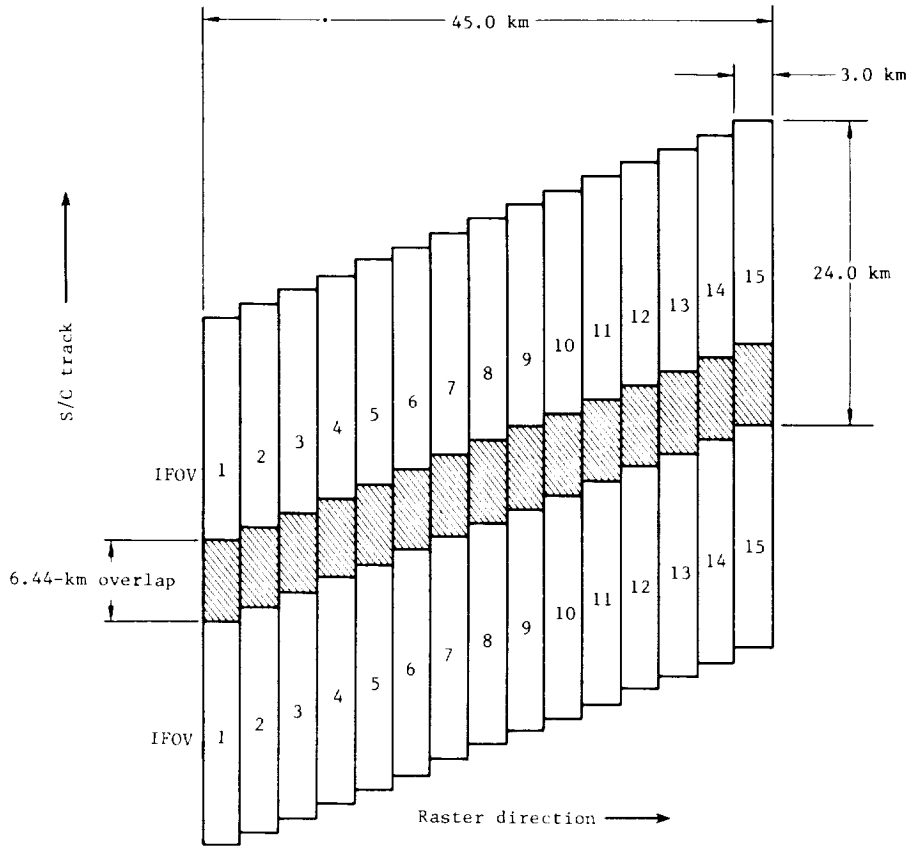

Figure 177.- MAWDS surface track.

Order isolation filter: The order isolation filter blocked radiance of higher order spectra from entering the monochromator and thus forming an interfering spectrum on the detectors. The filter was a silicon window 45.5 by 31.5 by 1.5 mm. The silicon transmission band extended from 1.2 to 15 μm. The window was coated for 96 percent transmission from 1.3 to 1.5 μm and for less than 0.1 percent transmission from 0.67 to 0.7 μm (second-order spectra).

Telescope mirror: The telescope primary mirror was a 45° off-axis 125-mm focal length paraboloid, gold coated on a CER-VIT blank. Its dimensions were 43 mm by 38 mm.

Chopper: Chopper blades attached to a tuning fork provided modulation of the beam. When resting, the blades were separated by approximately one-half the input beam diameter and when the blades close they overlap to completely block the input beam. The peak-to-peak motion of each blade was 4.0 mm.

Collimating mirror: The collimating mirror was an on-axis 169-mm-diameter paraboloid, gold coated on a CER-VIT blank. Its focal length was 500 mm. The entrance slit was located at the primary focus of the collimating mirror, which projected a parallel bundle of light onto the surface of the grating. The collimator focused the dispersed beam from the grating onto the array of detectors located on the image plane.

Grating: The grating was a 1200-line/mm gold-coated replicate plane grating mounted on a CER-VIT blank. It was blazed for the first-order spectrum (1.38 μm).

Detectors

As previously mentioned, two detector types were used in the instrument: PbS photoconductors for the 1.38 μm infrared water absorption band and Si for the neon line. The detector arrays are shown in figure 178, both lead sulfide (PbS) and silicon (Si).

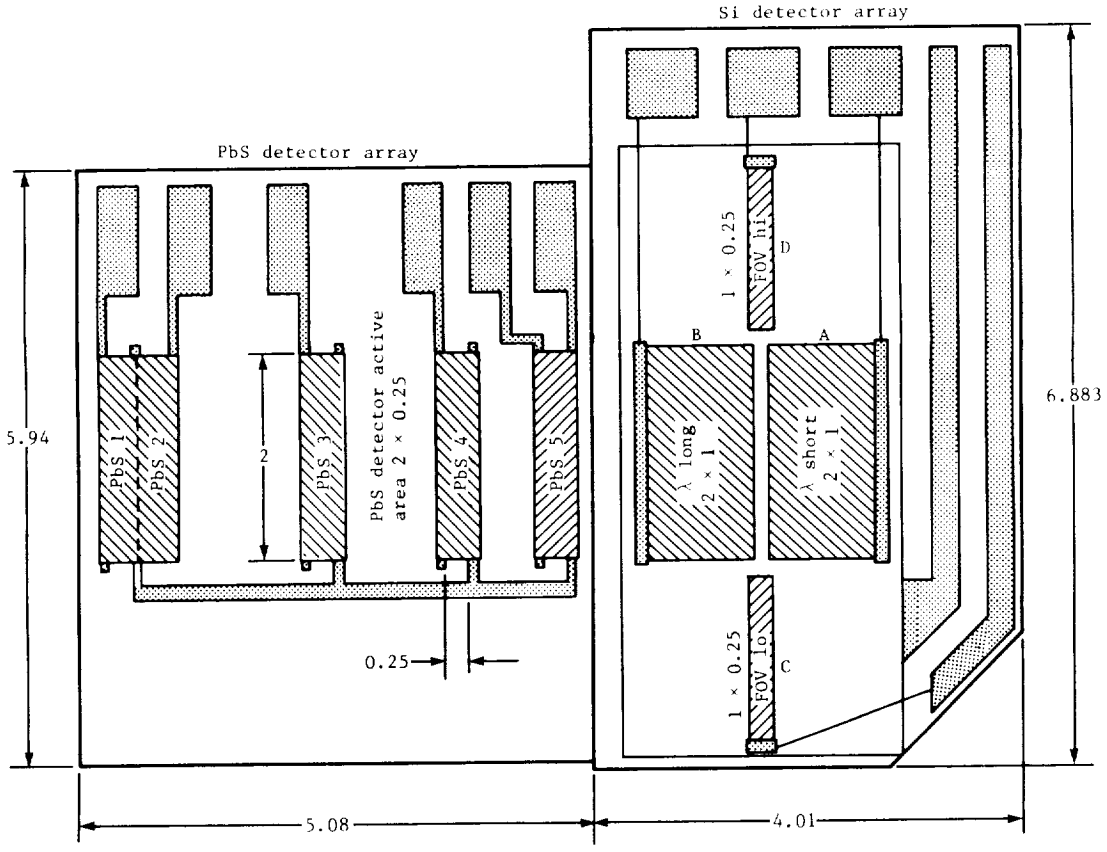

Figure 178.- MAWDS detector arrays. All dimensions are in mm.

The five PbS detectors had connected return electrodes and individual output electrodes. The electrodes determined the detector width or active area. Detectors 1 and 2 were only separated by their return electrode which was equivalent to 1.37 cm^{-1}. The detector header was radiation cooled to a nominal operating temperature of 203 K. At the nominal operating temperature, the detector proportional temperature controller limited the temperature drift to less than 0.02^{o} C/min. A drift of 0.02^{o} C/min translated into a responsivity change of 0.25 percent between intensity calibrations. The PbS detector NEP specification was 3×10^{-13} W-$Hz^{1/2}$ ($D^{*} = 2.6 \times 10^{11}$ cm-$Hz^{1/2}$-W^{-1}). The signal-to-noise ratio was 50 at a spectral radiance of $3.5 \times 10^{-7} \cdot W\text{-}(cm^{-1})^{-1}\text{-}cm^{-2}\text{-}sr^{-1}$.

The silicon detectors were of a common substrate. This arrangement produced detectors with the same characteristics over temperature and time. The wavelength error detectors (λ long and λ short) were the same height as the PbS and 4 times as wide (2 by 1 mm). The FOV detectors were the same width as the PbS and 1/2 as high (1 by 0.25 mm). As previously discussed, the Si detector received radiation from the neon line at 0.6931 μm. The Si detectors were operated in the photo voltaic mode for simplicity of operation. The FOV detectors had an NEP of 1×10^{-13} W and the wavelength error detectors had an NEP of 2×10^{-13} W.

Electronics

The MAWDS electronics were located in the MAWDS optical assembly and the VO bay. Located in the optical assembly of 5 single-sided boards were the detector preamplifiers (boards 1, 2, and 3); detector temperature control and servo preamplifiers (board 4); and monochromator heater control, neon lamp drivers, and bias regulator (board 5). Located in bay 8 were three double-sided trays that contained the remaining electronics. The detector electronics were on one tray, the servo electronics on a second tray, and the logic and power supplies on a third tray. Figure 179 is a functional block diagram of the MAWDS electronics.

Electromechanical

Signal processing circuits.- All five channels of the PbS amplifiers were identical. The preamplifier was a noninverting amplifier with a gain of 40. The gain of the gain select stage was varied through 8 discrete states from 1 to 128 to adapt to scenes of varying brightness. Manual gain selection could be made by ground command through the FDS-MAWDS control word, or automatic gain control could also be instituted through FDS. The measured PbS detector amplifier performance parameters were as follows:

Input noise voltage, μV-$Hz^{-1/2}$	≤ 0.09
Gain stability, percent/5 min	≤ 0.1
Phase stability, deg/5 min	≤ 0.9
Gain range of gain select	1 to 8

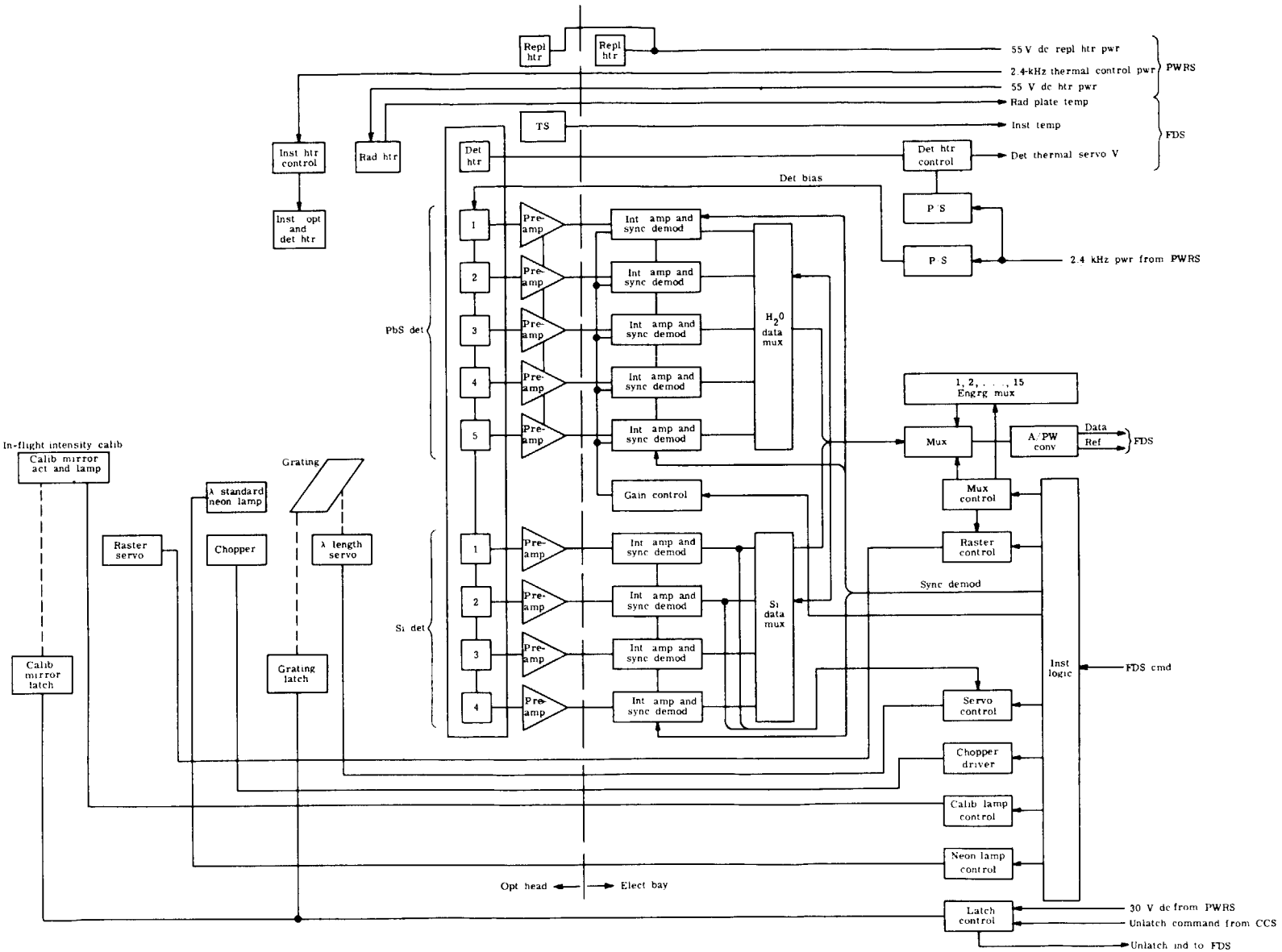

Figure 179.- Functional block diagram of MAWDS.

Wavelength servo.- The wavelength servo corrected for any optical misalignment resulting from thermal gradients of the instrument and maintained the wavelength accuracy to 0.25 wave number. A shift of the spectral line from the neon lamps along the line of the PbS detectors was measured by the two wavelength error detectors (Si), and the error voltage generated by their differential illumination was used to rotate the grating to compensate for the shift. The error voltage was generated by differentially illuminating the two error detectors with a spectral line provided by a neon lamp. When the error voltage exceeded a positive or negative threshold, a stepping motor was driven in the appropriate direction to reposition the grating during the raster mirror flyback period.

Raster servo.- Digital signals from the FDS were counted and converted to analog form. This signal was then compared to the output of an LVDT position sensor which monitored the position of the mirror. The difference, or position error, was then used to drive the raster mirror to the selected position. An increment of one count stepped the mirror one position (1.05 mrad). After 15 steps the digital-to-analog converter was reset by FDS, producing mirror flyback to position 1. The LVDT output was telemetered to indicate raster position for data reduction. The raster direction could be reversed to yield a mirror image track on the planet surface by causing the counter to count down instead of up.

Temperature control.- Due to the long folded path from slit to detectors, a small misalignment of the instrument due to either total or differential thermal expansion could produce wavelength errors as well as amplitude errors. The wavelength servo, wavelength scan, and FOV detector systems compensated for small thermal and mechanical errors. Detector heaters, controlled by a proportional circuit, were used to balance the thermal outflow from the detectors to the radiator plate such that the temperature of the detectors was maintained at -70° C. The detector thermal stability was such that the temperature change of the detectors between calibrations (4.78 min) was less than 0.1° C.

Silicon detector electronics.- The basic functions of the silicon detector electronics were to provide analog outputs of the two FOV monitors and grating position signals to the wavelength servo system.

A/PW calibration source.- The A/PW calibration source was a two-level reference signal that was stable to within ± 0.5 DN between instrument calibration periods of 4.78 min (64 rasters).

PbS detector bias supply.- Each of the 5 PbS detectors was furnished a bias supply between 10 and 50 V in order that each detector would operate at an optimum bias current corresponding to its minimum NEP. The bias supply had excellent short term stability and low noise. Bias noise must be ≤ 100 mV-Hz$^{-1/2}$.

Operating Modes and Sequencing

MAWDS had four operating modes, as follows:

(1) Planet scan - wavelength lock and raster mirror forward, reverse, or stationary

(2) Wavelength scan during planet scan - raster mirror forward, reverse, or stationary

(3) Intensity calibrate - raster IFOV 8 (fixed), with or without wavelength scan

(4) Diffuser - instrument viewing Sunlight from diffuse reflector on orbiter

MAWDS sequencing was governed by the MAWDS control word, which was transmitted by FDS once every raster period and controlled the instrument state and gain.

X-Band Transmitter Subsystem

The XTXS was a functional part of the VO telecommunications subsystems as shown in figure 180. The XTXS was used to provide an X-band downlink ranging signal which was both carrier and ranging modulation phase coherent with the S-band ranging signal from the RFS. The XTXS multiplied (×440) the oscillator frequency received from the active RFS exciter to an X-band frequency, coherently modulated the RFS detected uplink ranging code onto the XTXS carrier, and provided to the HGA the X-band signal which was at a frequency of 8415 ± 20 MHz and an rf level of approximately 200 mW. A simplified block diagram of XTXS is shown in figure 181, which also identifies the various interfaces with the XTXS. All major specifications are given in table 45. The XTXS remained off during the early portion of interplanetary cruise until the orbiter HGA could be pointed toward Earth and the deep space stations were configured for X-band reception. Upon HGA availability, the XTXS on each orbiter was turned on once to check XTXS functioning. A few weeks later, with 64-m DSN X-band availability, both XTXS's were turned on permanently. Continuous operation resulted in a more stable XTXS environment and operation for radio science purposes. This imposed a negligible penalty on spacecraft power management because of the low current drain of the XTXS.

Relay Radio Subsystem

The function of the RRS in the telecommunications area is shown in figure 182. As shown, it received the FSK Manchester-coded, UHF rf signal from the VL transmitter via the RAS, and with separate 4000 bps and 16 000 bps demodulators, it routed the data to the RTS corresponding bit synchronizers.

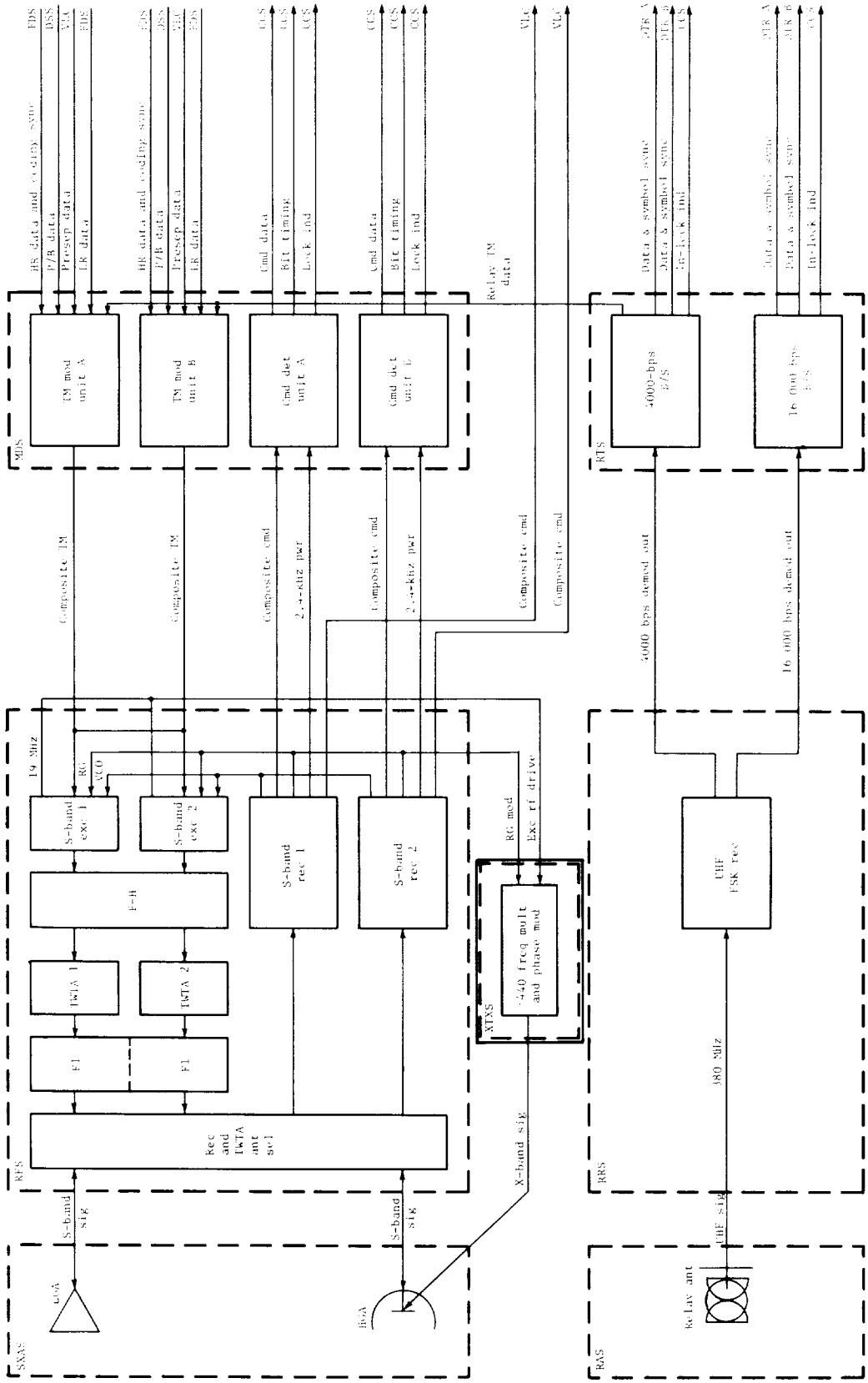

Figure 180.- Functional block diagram of telecommunications showing XTXS.

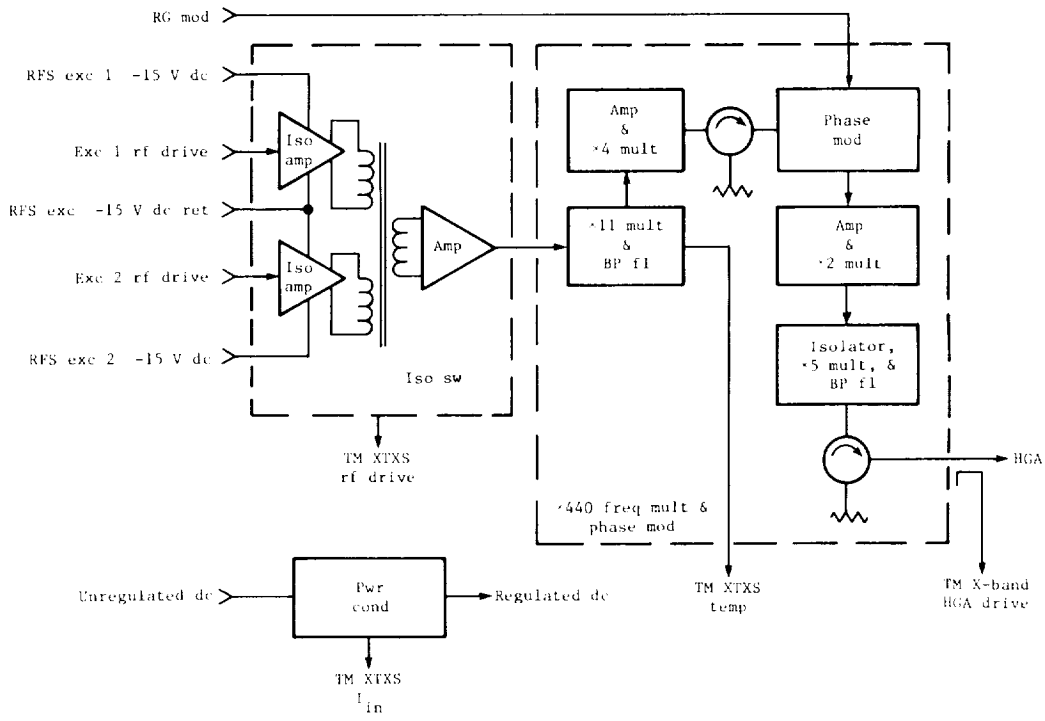

Figure 181.- Simplified block diagram of XTXS.

TABLE 45.- MAJOR SPECIFICATIONS OF XTXS

Parameter	Specified performance	Typical data
Frequency		
Input, MHz	19 ± 0.045	
Output, MHz	8415 ± 19.8	
dc input power		
Nom, W	11.5	11.0
Max, W	12.7	12.0
rf input pwr, dBm	0 ± 2	
rf output pwr at -		
PA temp (0° to 55° C), dBm	23	24 ± 1
TA temp (-20° to 75° C), dBm	23 ± 3	24 (+1 or -2)
Carrier phase stability		
(0° to 55° C), deg	1300	500
Harmonics (related to 19-MHz input)		
2041 to 2166 MHz, dBm	-80 (max)	-93
All others (includes -30 dB 1st 19 MHz sidebands), dB		-35
Modulation		
Max input level, V	Not specified	2 (peak)
Impedance, Ω	50 (± 5 ±j5)	49 (+j0)
Sensitivity, rad/V	1	1.4 (capability)
Sensitivity stability at -		
PA temp (0° to 55° C), percent	±5	8
TA temp (-20° to 75° C), percent	±7	±15
Linearity, percent of BSL	2 (up to 1.5 rad)	2 (up to 3 rad)
Amplitude modulation		
No modulation, percent	1	0.5
With modulation, percent	2	1.0
Group delay stability at 25° C (+ 30° or - 25°), nsec	±1	±2.5

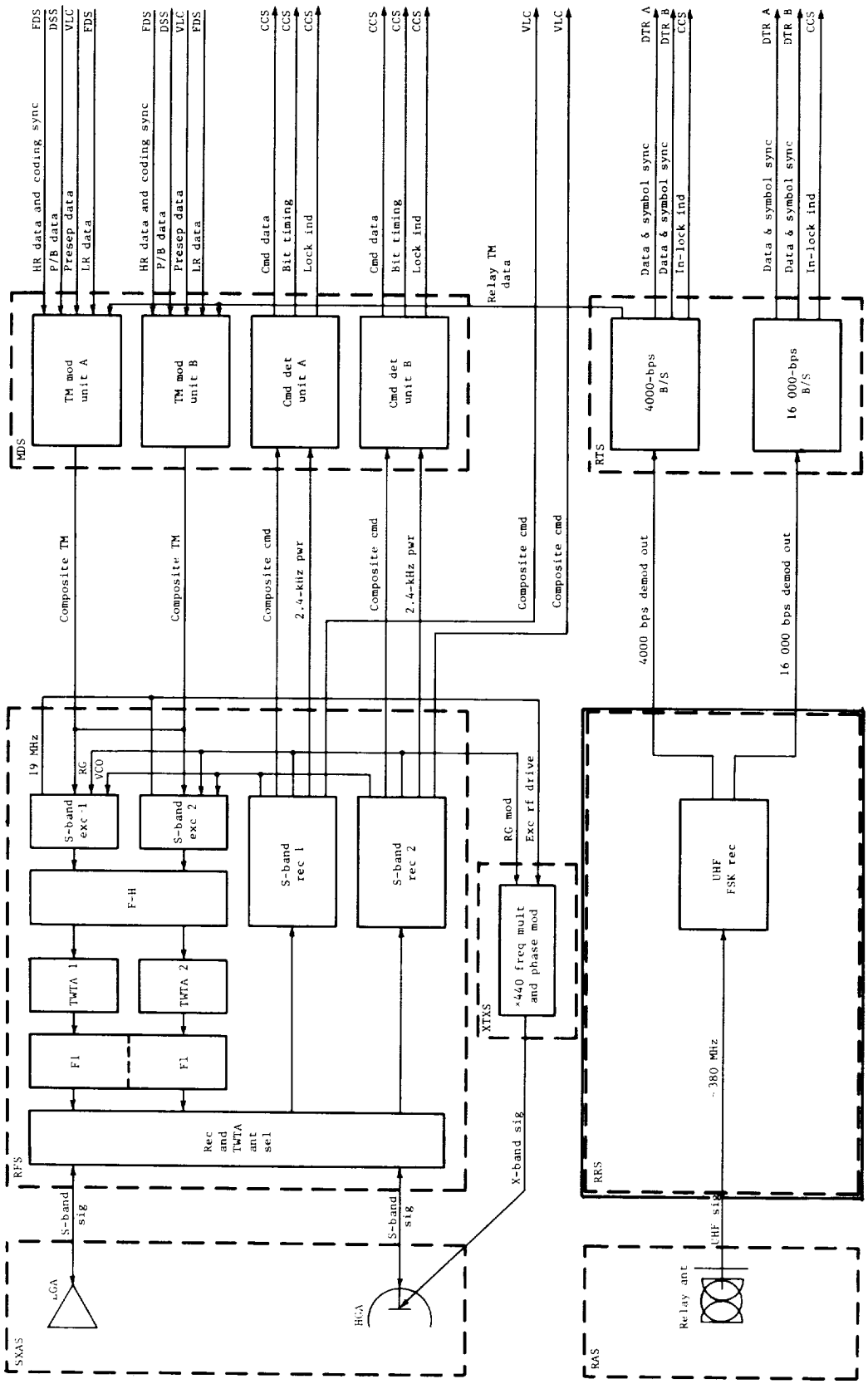

Figure 182.- Functional block diagram of telecommunications showing RRS.

In addition, as shown in figure 183, various parameters such as the received signal strength, LO drive, input current, and RRS temperature were provided to the FDS for engineering performance monitoring purposes. A simplified block diagram of the receiver is shown in figure 184.

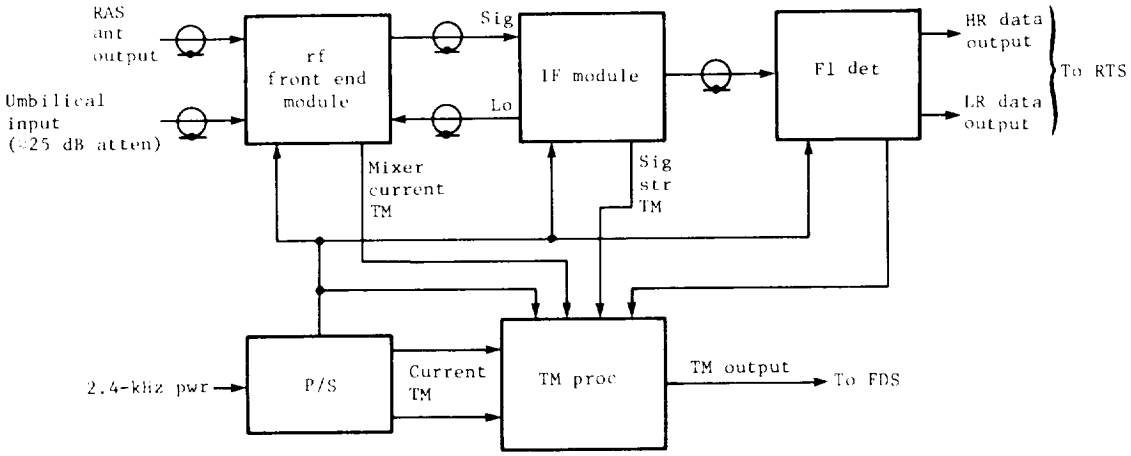

Figure 183.- Functional block diagram of RRS.

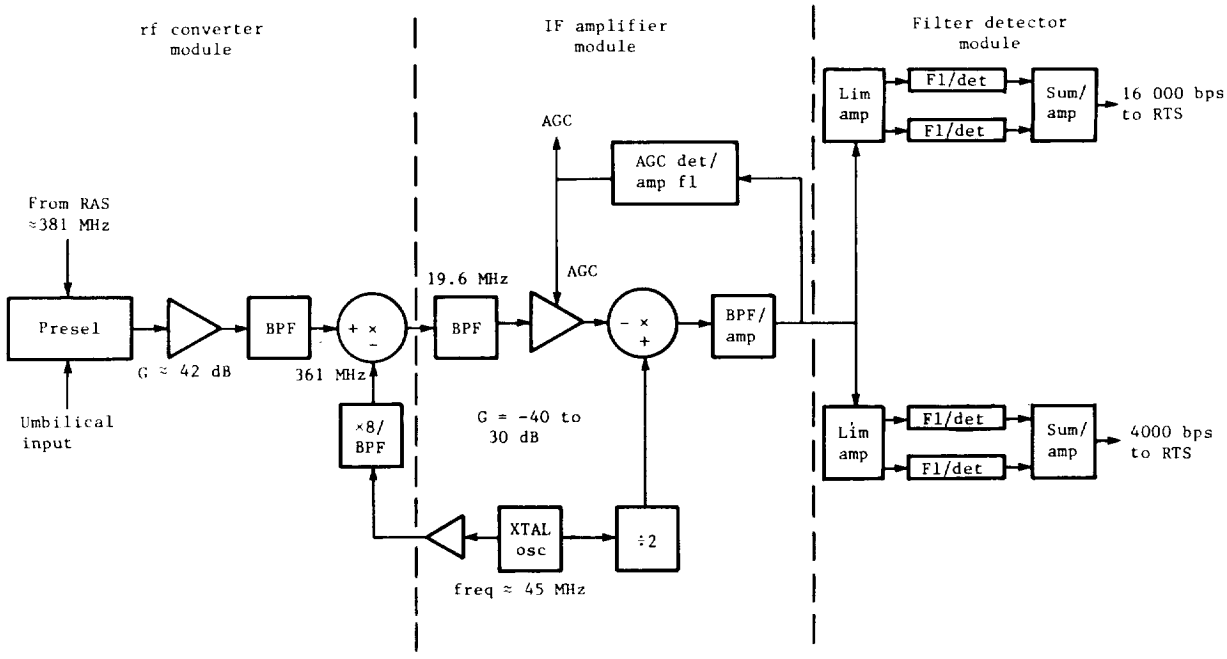

Figure 184.- Simplified block diagram of RRS.

The major characteristics of the RRS are given in table 46. Spurious signal rejection would not respond to or be degraded by interfering signals

TABLE 46.- RELAY RADIO ELECTRICAL CHARACTERISTICS

Parameter	Requirement	Typical values
Received sig freq, MHz	380.963303	
1st LO freq, MHz	361.376	
XTAL osc freq, MHz	45.172	
1st IF freq, MHz	19.5773	
2nd IF freq, MHz	3.000	
XTAL osc stability at -		
25 ±5° C, ppm	±3	±0.2
FA temp (0° to 55° C), ppm	±5	±1
Output sig		
Hi data rate	16 000 bps Manchester coded	
Lo data rate	4000 bps Manchester coded	
Number of output lines	2	
Threshold		
Hi data rate,[a] dBm	-111.9 (max)	-115
Lo data rate,[a] dBm	-117.3 (max)	-119
Output levels at -		
Threshold, mV rms	260 ± 50	270
Strong signal for		
Hi data rate ch, V rms	<4.5 times threshold	0.6
Lo data rate ch, V rms	<4.5 times threshold	1.1
Output polarity	Mark freq = +Voltage Space freq = -Voltage	
Ant (source) VSWR	<1.5:1 (over input ±1 MHz)	1.4:1
rf input VSWR	---	2:1
Noise figure at		
25° C, dB	4.5 (max)	4.3
FA temp, dB	5 (max)	4.8
Input level-survival operate, dBm	0 -70 to threshold (-120)	No damage to 0 0 to threshold
IF BW, kHz	323 ± 10%	
Demod freq sep, kHz	200	200
Space freq, kHz	-100	
Mark freq, kHz	100	
Demod equiv noise BW		
4000 bps, kHz	64 ± 15%	
16 000 bps, kHz	105 ± 15%	
Weight, kg (lb)	<3.516 (<7.75)	
Power, W	<2.7	
Volume, cm^3 (in^3)	2966 (181)	

[a]Defined as output ST/N_0 = 5.8 dB, based on BER of 3×10^{-3}.

at power levels equal to or less than those specified in the following table:

Freq, MHz	Maximum level into RRS ant terminal, dBm
[a]0 to 500	-70
500 to 2000	-50
Except 1425 ± 8	-55
1464 ± 8	-55
Above 2000	-30
Except 2295 ± 5	-20
2549 ± 4	-60
2600 ± 4	-40

[a]Excepting receiver rf BP frequencies 380 ± 10 MHz (allowable interference, 150 dBm).

The RRS was not turned on at launch and remained off through most of the cruise period. It was only turned on once for a VLC UHF equipment checkout prior to the major VLC preseparation checkout. After the preseparation checkout of the VLC, the RRS was left on continuously.

Relay Telemetry Subsystem

Purpose and Function

The RTS was the final S/S in the UHF chain of the Viking orbiter as is shown in figure 185. The RTS received the noisy split-phase PCM waveform from the RRS and provided recovered PCM data, synchronization, lock detector status, and telemetry to the appropriate VO subsystem. A simplified block diagram is shown in figure 186, and the primary performance characteristics are shown in table 47. The RTS consisted of two independent, functionally identical, bit synchronizers and their associated power supplies. The synchronizers were powered simultaneously with one synchronizer operating at 4000 bps and the other at 16 000 bps. A functional block diagram of one synchronizer is shown in figure 187. The RTS performed the following functions:

Established synchronization with respect to either a 4000-bps or a 16 000-bps split-phase coded data waveform provided by the RRS

Detected and restored the incoming data from the RRS to an NRZ-L format

Routed the recovered 4000-bps data to the MDS for immediate transmission back to Earth or routed the recovered 4000-bps and the 16 000-bps data along with symbol sync (Symbol rate = 2 × Bit rate) to the DSS

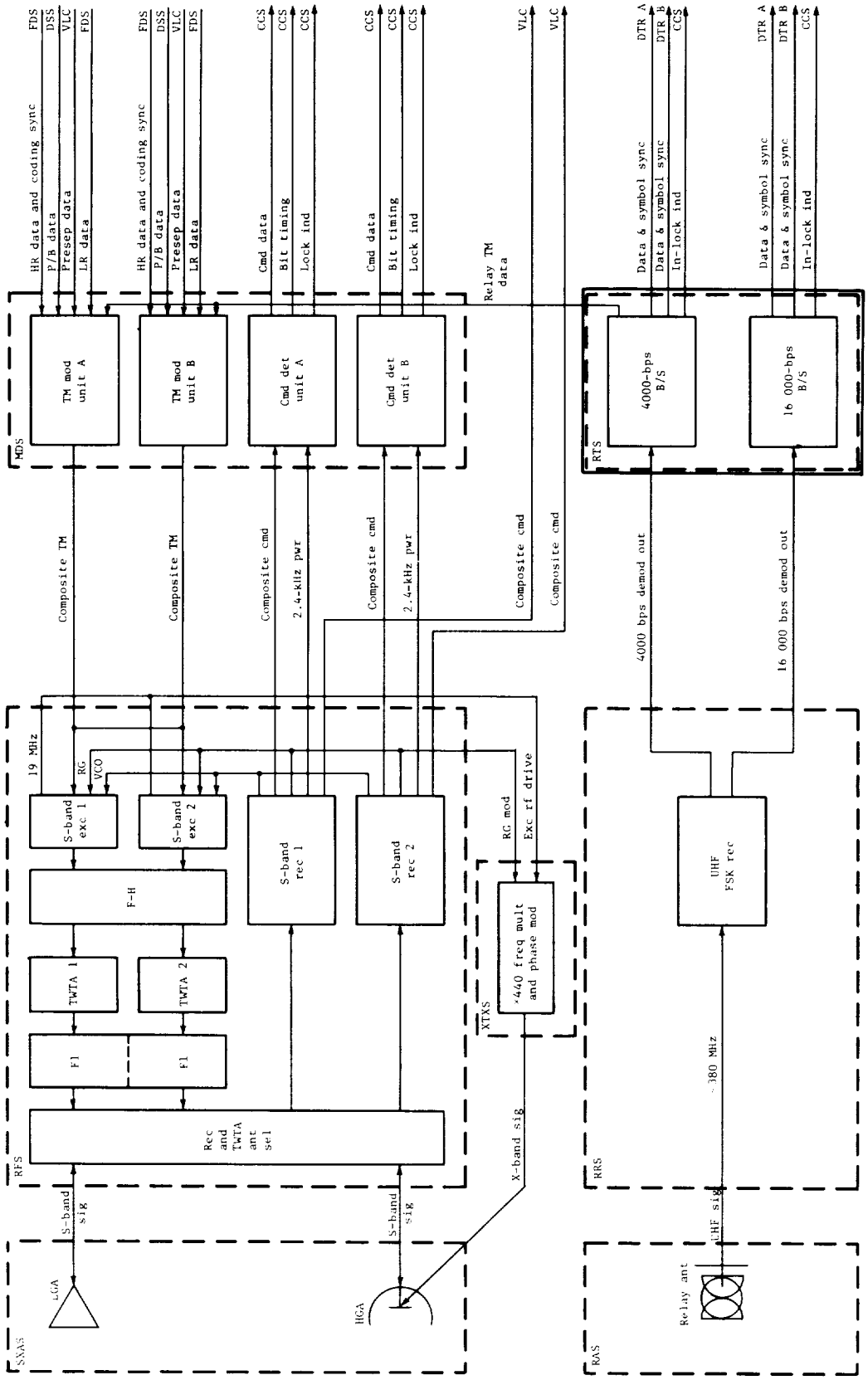

Figure 185.- Functional block diagram of telecommunications showing RTS.

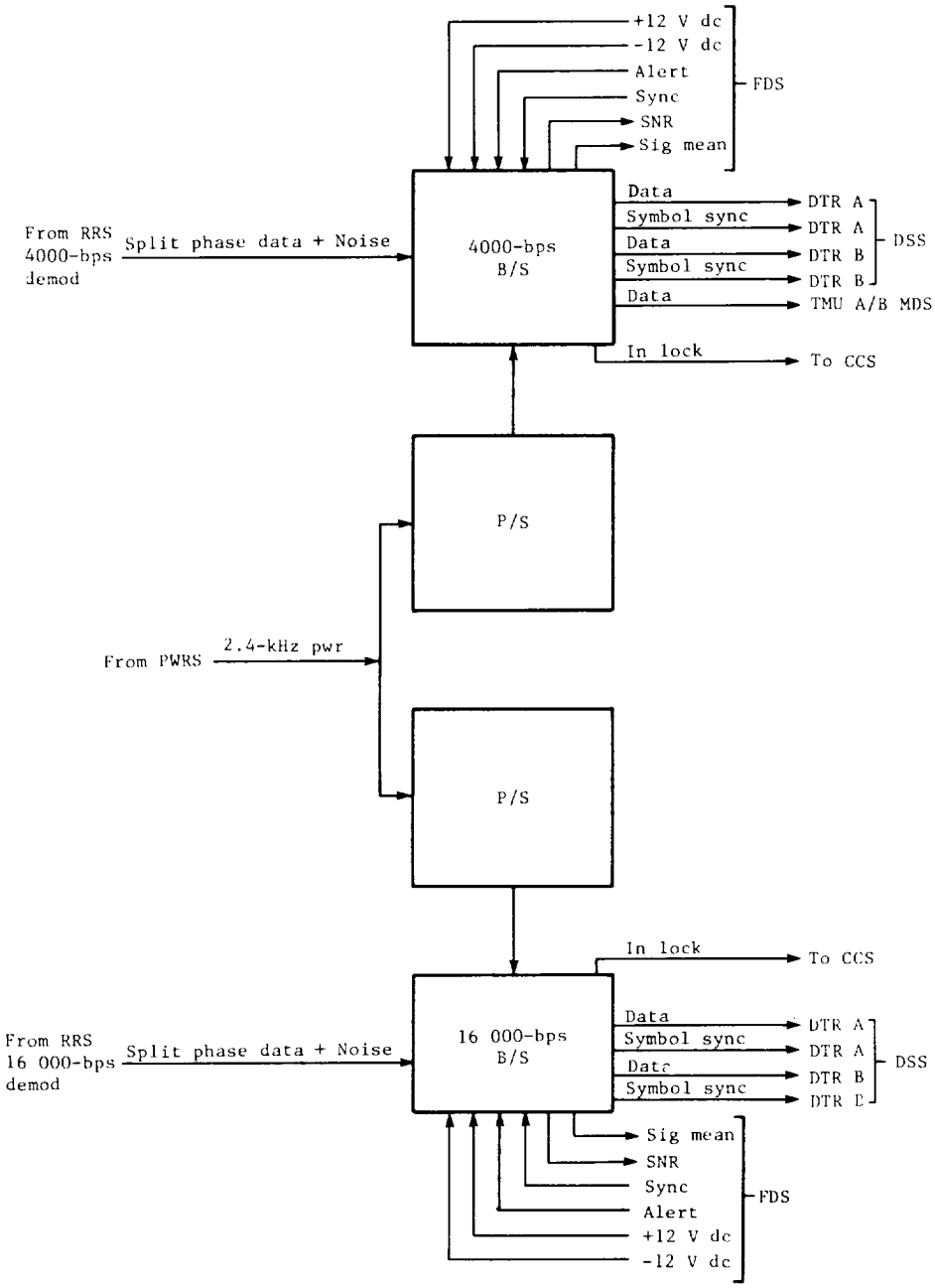

Figure 186.- Simplified block diagram of RTS.

TABLE 47.- RTS PERFORMANCE CHARACTERISTICS

Parameter	Design value	Tolerance
Threshold ST/N_o (at RTS input), dB	6.4	(+0.7 or -0.1)
Threshold BER	3×10^{-3}	
B/S timing jitter at threshold, deg (rms)	≤ 7	
B/S timing in absence of signal for -		
4000-bps synchronizer, kHz	4	±0.25%
16 000-bps synchronizer, kHz	16	±0.25%
Acq time (at ST/N_o = 2.8 dB at RTS input), bit times	≤ 4000	
Lock det decision level ST/N_o (at RTS input), dB	4	

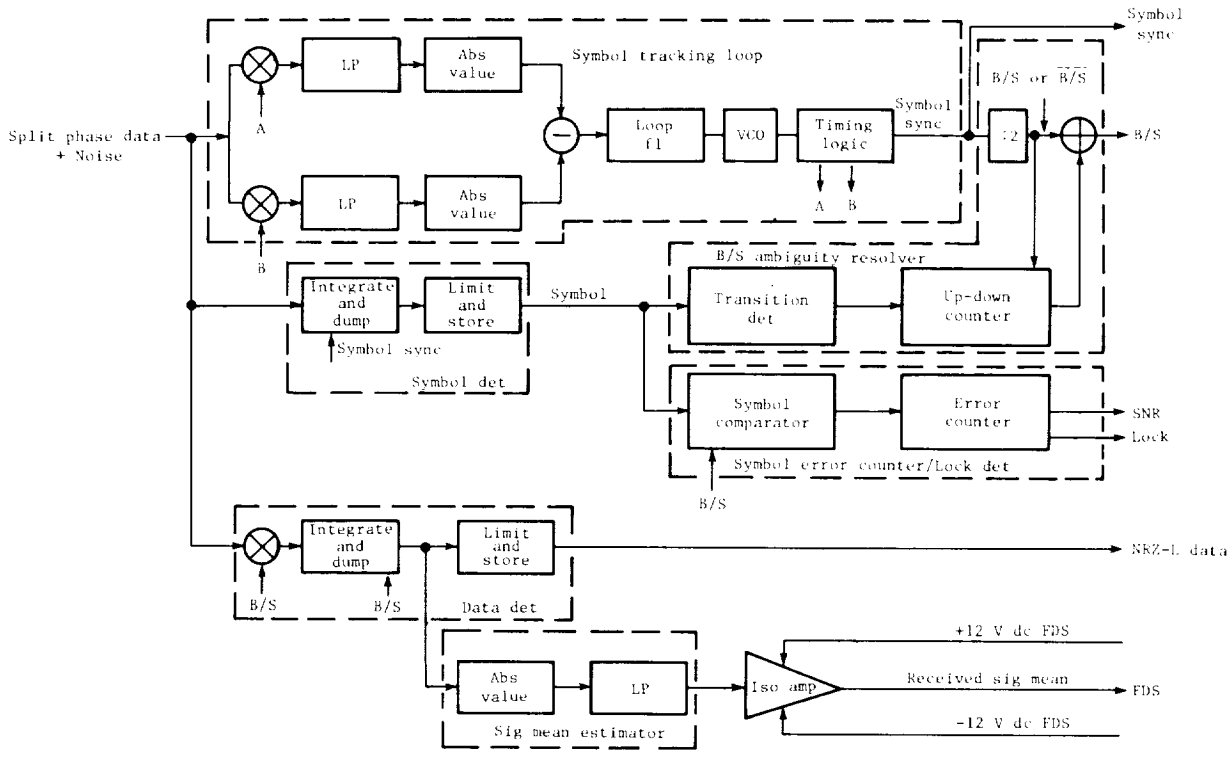

Figure 187.- Block diagram of RTS bit synchronizer.

Estimated the SNR and the SME of the data waveform from the RRS and provided this information in the form of telemetry measurements to the FDS

Provided an in-lock indication to the CCS when the incoming data was above a preselected threshold (BER of 3×10^{-3})

Description

Power to the RTS was supplied by the PWRS and controlled by the CCS. The RRS and both RTS synchronizers were turned on and off together by the same commands. The proper synchronizer automatically acquired sync when the signal from the RRS met the minimum preselected threshold requirement which was equivalent to or better than an input ST/N_O = 6.4 (+ 0.7 or - 0.1) dB. The in-lock signal to the CCS was derived from the symbol error measurement. In-lock was indicated whenever the symbol error rate was 63/1024 or less, and an out-of-lock indication was made when the symbol error rate was 64/1024 or greater. When the signal to the RRS was approximately 1 dB below threshold or higher, the RTS provided an in-lock indication to the CCS. All other data and sync signals to other S/S's were present whether the RTS was locked up or not. In the absence of a signal, output sync signals were at the rate of the internal free running oscillator, and random data appeared on the output data lines.

RTS SNR was a 7-bit telemetry word which was a direct measurement of the symbol error rate at the RTS. Since in split-phase coding each data bit consisted of a 1-0 or 0-1 pair, agreements between the recovered symbols in each bit represented symbol errors. The RTS counted symbol errors for a period of 2 to the 14th bit times, which was 1 sec at 16 000 bps and 4 sec at 4000 bps. The result was scaled so as to represent the number of symbol errors per 1024 symbols. The result of each count was averaged with the previous count prior to being supplied to the FDS. This produced a slight lag in the measurement whenever the link signal strength changed rapidly. The maximum count was a DN of 127 which represented a symbol error rate of 127/1024. The SNR measurement limited at 127 if the symbol error rate was above 127/1024. The relation between the symbol error rate and the data bit error rate is illustrated in figure 188 where both are plotted against ST/N_O at the RTS input. Figure 189 shows telemetered SNR plotted against BER and symbol error rate.

RTS signal mean was an analog signal provided to the FDS which was directly proportional to the signal from the RRS to the RTS. The signal from the RRS varied very rapidly as a function of the UHF signal in the vicinity of threshold. Figure 190 indicates the relationships of the RRS receiver input, RRS AGC, RTS SNR, and RTS SME in the 4000-bps and 16 000-bps operating modes.

Relay Antenna Subsystem

The RAS consisted of the UHF relay antenna and its associated transmission lines. The RAS was deployed after launch immediately after the solar panels were deployed. The RAS antenna was mounted on the back side of the +X outboard solar panel and provided almost hemispherical coverage behind the S/C in that

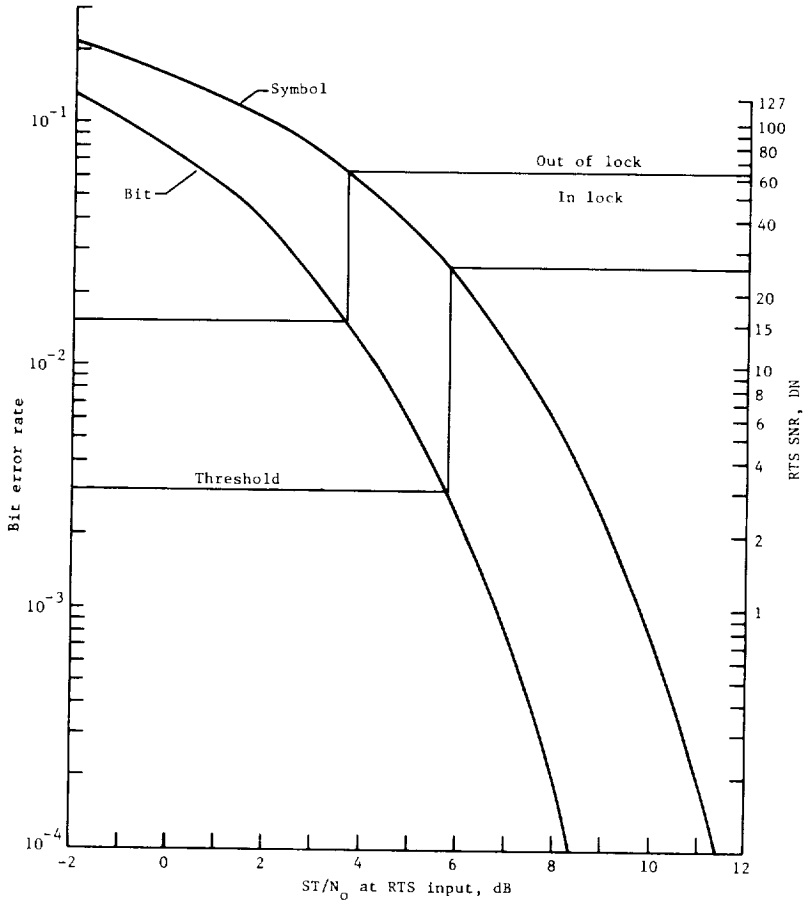

Figure 188.- RTS symbol and bit error curve.

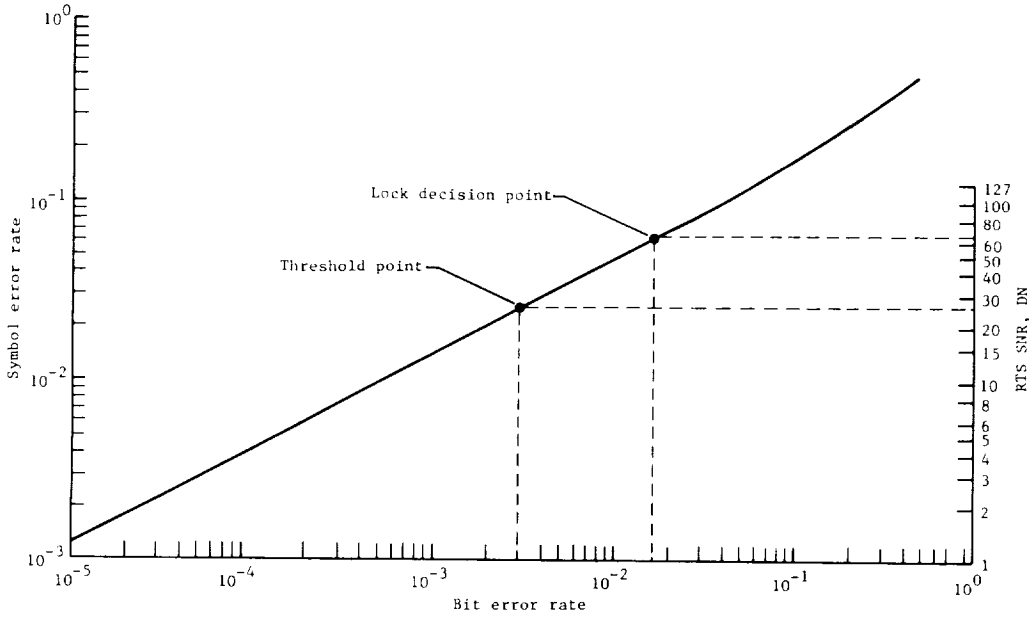

Figure 189.- RTS bit error rate versus symbol error rate and SNR.

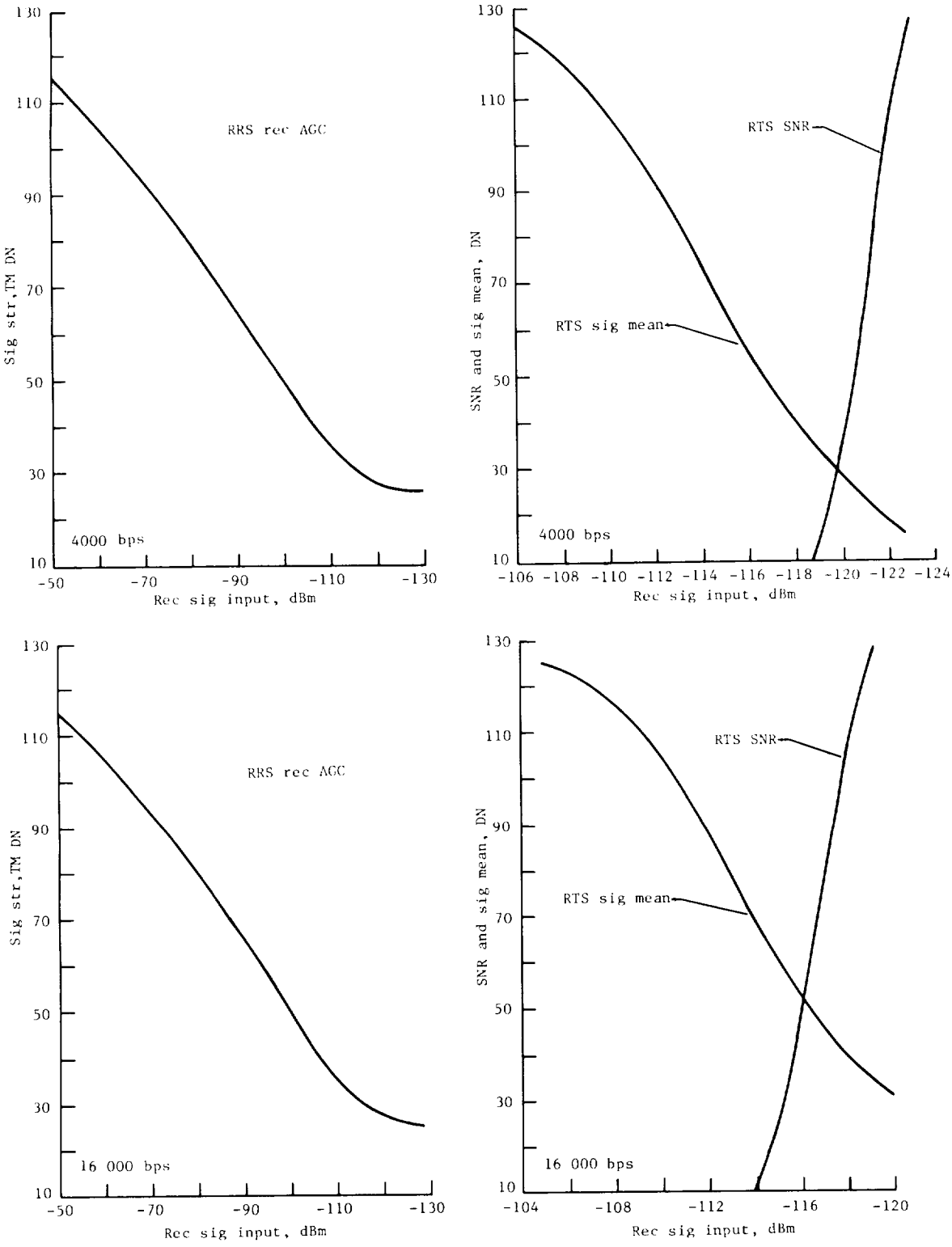

Figure 190.- RTS typical performance curves.

position (blockage caused by the S/C between 30° and 65° clock angle prevented total hemispherical coverage), as shown in figure 191. The RAS was designed to receive right-hand circular polarized rf energy in the UHF range of 380.963 ± 10 MHz. As shown in figure 192, the RAS antenna was known as a resonant quadrifilar helix consisting of a center post with four formed helices mounted above a ground plane. The ground plane also served as the mounting

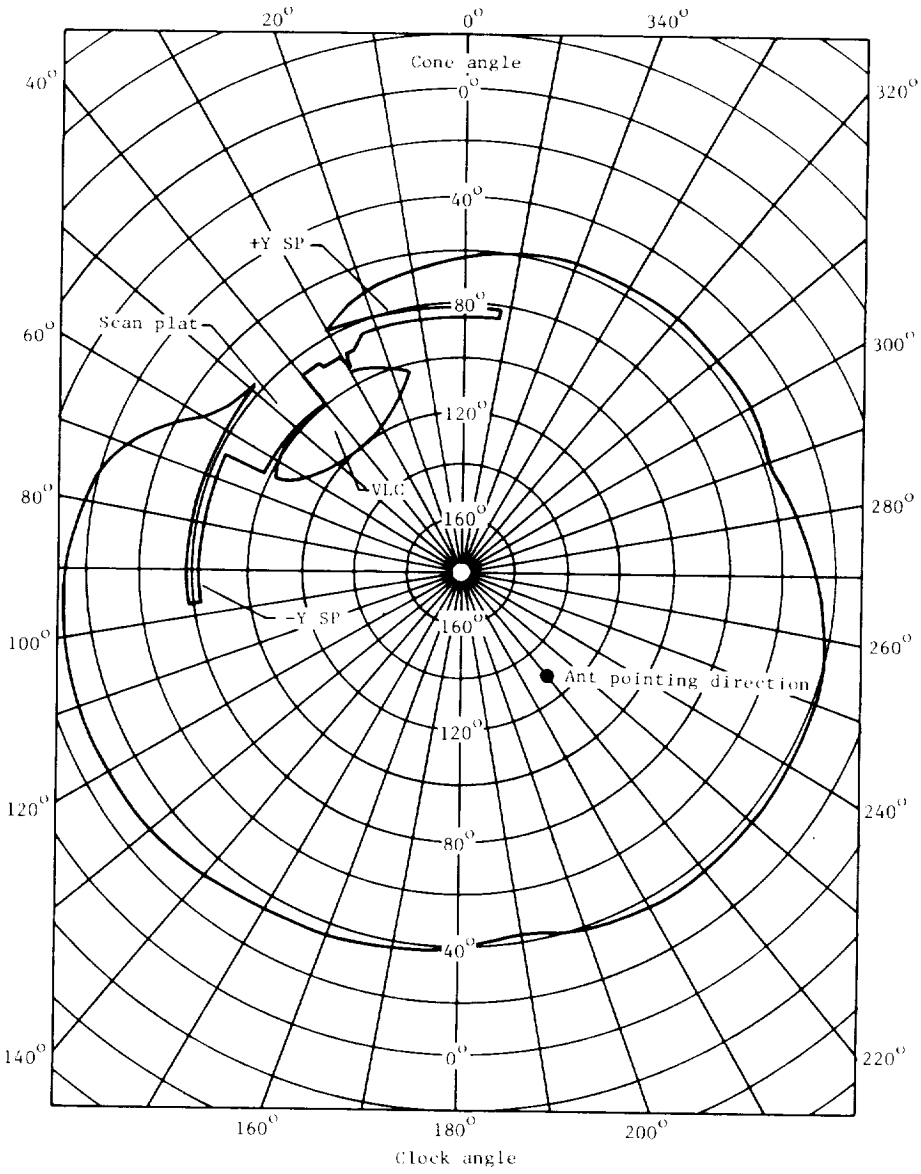

Figure 191.- FOV of relay antenna. Origin is at center of relay antenna ground plane.

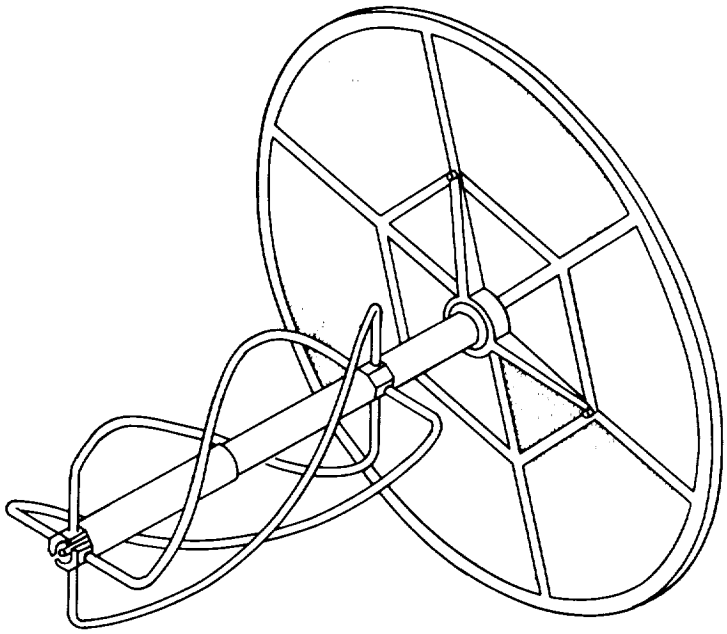

Figure 192.- Relay antenna.

surface for the antenna. Figure 193 is a block diagram of the RAS. The RAS was not required during launch and through the cruise phases of the mission. It was used for the VLC checkout tests, from VLC separation through descent, and for all relay communications after the VL touchdown. Figure 194 shows typical gain and axial ratio curves for the RAS, and tables 48 and 49 give the cable VSWR and insertion loss data.

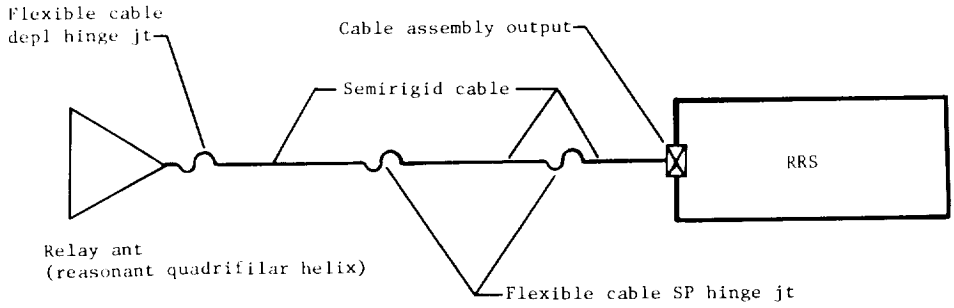

Figure 193.- Block diagram of RAS.

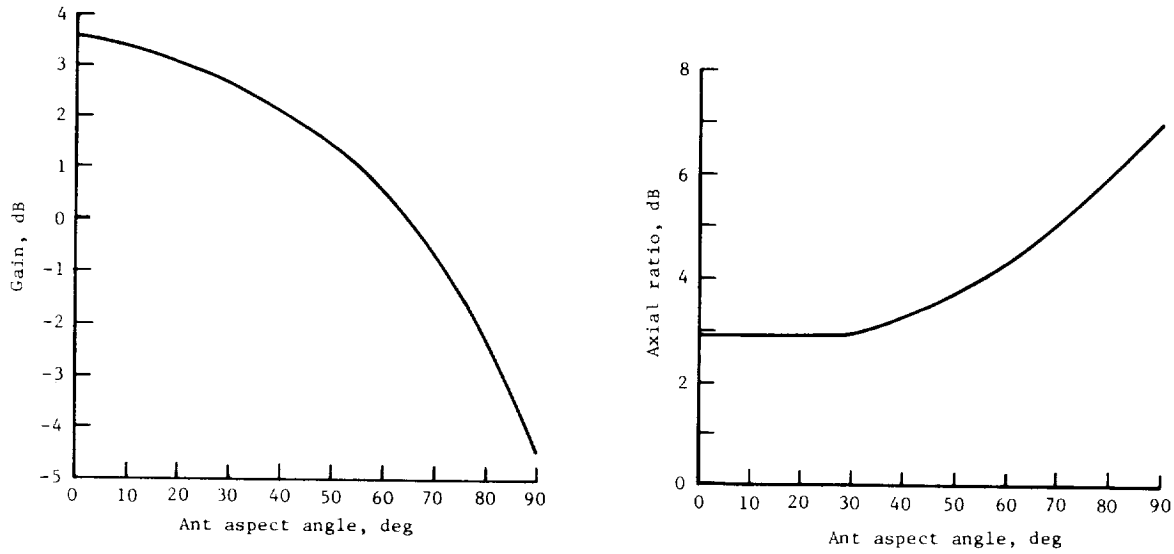

Figure 194.- Characteristics of orbiter UHF relay antenna.

TABLE 48.- RAS VSWR MEASUREMENTS

Freq, MHz	VSWR for -							
	Depl hinge cable	Outer SP cable	Outer hinge cable	Inner SP cable	Inner hinge cable	Bus cable	Relay ant	S/S cables
381.963	1.10:1.0	1.10:1.0	1.04:1.0	1.01:1.0	1.04:1.0	1.09:1.0	1.2:1.0	1.3:1.0
379.963	1.12:1.0	1.10:1.0	1.04:1.0	1.01:1.0	1.03:1.0	1.10:1.0	1.2:1.0	1.2:1.0
390.963	1.11:1.0	1.10:1.0	1.03:1.0	1.03:1.0	1.02:1.0	1.09:1.0	1.7:1.0	1.6:1.0
370.963	1.10:1.0	1.10:1.0	1.04:1.0	1.04:1.0	1.02:1.0	1.09:1.0	1.4:1.0	1.4:1.0
380.963	1.11:1.0	1.10:1.0	1.03:1.0	1.01:1.0	1.02:1.0	1.10:1.0	1.2:1.0	1.3:1.0
Required	1.20:1.0	1.10:1.0	1.20:1.0	1.10:1.0	1.20:1.0	1.10:1.0	[a]1.2:1.0 to [b]2.0:1.0	[a]1.4:1.0 to [b]2.2:1.0

[a]379.963 to 381.963 MHz.
[b]379.963 - 9 to 381.963 + 9 MHz.

TABLE 49.- RAS CABLE INSERTION LOSS

Freq, MHz	Insertion loss, dB, for -						
	Depl hinge cable	Outer SP cable	Outer hinge cable	Inner SP cable	Inner hinge cable	Bus cable	S/S cables
370.96	0.29	0.21	0.11	0.20	0.10	0.23	1.09
380.96	.29	.21	.11	.21	.10	.23	1.08
390.96	.30	.115	.11	.22	.10	.23	1.13
Required	≤.33	≤.29	≤.15	≤.27	≤.25	≤.26	≥1.20

APPENDIX

ABBREVIATIONS AND SYMBOLS

AAI	all axes inertial
ACE	attitude control electronics
AC&IU	antenna control and interface unit
ACQ SS	acquisition Sun sensor
ACS	attitude control subsystem
ADC	analog-to-digital converter
AGC	automatic gain control
AO	auxiliary oscillator
APC	automatic phase control
A/PW	analog to pulse width
ARTCS	articulation control subsystem
ASOC	automatic Sun occultation control
AZ	azimuth
abs	absolute
ac	alternating current
accel	accelerometer
acq	acquisition
act	actuator
amp	amplifier
ant	antenna
approx	approximately
assy	assembly

atten	attenuator
auto	automatic
avg	average
BC	block coder
B.C.	bolt circle
BER	bit error rate
BO	biorthogonal
BOT	beginning of tape
BP	band pass
B/P	bypass
BPA	bioshield power assembly (VL)
BPF	band-pass filter
BR	band reject
B/R	booster regulator
BRF	band-reject filter
BS	bioshield
B/S	bit synchronizer
BSC	bioshield cap
BSL	best straight line
B/U	backup
BW	bandwidth
bal	balance
bat	battery
biprop	bipropellant
bps	bits per second
CABLS	cabling subsystem

CC	coded command
CCS	computer command subsystem
CCW	counterclockwise
CDU	command detector unit
CLS	control level sensor
CM	center of mass
CO	changeover
CP	central processor
CR SS	cruise Sun sensor
CS	circulator switch (RFS)
CT	Canopus tracker
CTA	Centaur truss adapter
CU	control unit
CW	clockwise
calib	calibration
cap	capacitor
c.g.	center of gravity
ch	channel
chgr	charger
ck	check
ckt	circuit
cmd	command
comp	compensator
cond	conditioner
config	configuration
conn	connector

cont	continuous
conv	converter
cr	cruise
D*	detectivity
DAC	digital-to-analog converter
DBW	dual bridge wire
DC	discrete command
DCS	direct communications system (VL)
DEVS	mechanical devices subsystem
DFRJ	dual frequency rotary joint
DN	data number
DOD	depth of discharge
DR	derived rate
DRVID	differenced ranging versus integrated Doppler
DSE	data storage electronics (tape recorder electronics)
DSN	deep space network
DSS	data storage subsystem
DST	data storage transport
DTR	digital tape recorder
d	days
dc	direct current
depl	deployment
det	detector
dev	devices
diam	diameter
dist	distribution

E	error voltage
EA	electronic assembly
EL	elevation
EMI	electromagnetic interference
EOM	end of mission
EOT	end of tape
ETR	Air Force Eastern Test Range
EV	engine valve
elect	electronics
en	enable
eng	engine
engrg	engineering
envir	environmental
equiv	equivalent
exc	exciter
FA	flight acceptance
FB	flyback
F/B	feedback
FB&S	flyback and sweep
FBV	fuel bypass valve
FDS	flight data subsystem
F/F	flip flop
F-H	filter-hybrid
FOV	field of view
FSK	frequency shift keyed
FV	fuel valve

f, freq	frequency
f_o	oscillator frequency
fl	filter
G	gain
GA	gimbal actuator
GC	gain control
G&C	guidance and control
GCMS	gas chromatograph mass spectrometer
GCSC	guidance, control, and sequencing computer (VL)
GSA	gas share assembly
gen	generator
HGA	high-gain antenna
HPM	high-pressure module
HR	high rate
HRT	high-rate telemetry
hi	high
htr	heater
I	current
I_c	closing current
I_{in}	input current
I_o	opening current
I_{out}	output current
I_{sc}	short-circuit current
$I_{sc,r}$	radiation short-circuit current
ID	identification
IES	inertial electronics subassembly

IF	intermediate frequency
IFOV	instantaneous field of view
I/O	input/output
IR	infrared
IRP	interrupt processor
IRS	infrared science
IRTMS	infrared thermal mapper subsystem
IRU	inertial reference unit
ISS	inertial sensors subassembly
ITC	interplanetary trajectory correction
IU	input unit
inbd	inboard
ind	indication
inh	inhibit
ins	insertion
inst	instrument
int	intermediate
inv	inverter
iso	isolation
JPL	Jet Propulsion Laboratory
jt	joint
LC	inductance-capacitance
LCE	launch complex equipment
LED	light emitting diode
LF	light flood
LGA	low-gain antenna

LO	local oscillator
LP	low pass
LPAG	lander performance and analysis group
LPF	low-pass filter
LPM	low-pressure module
LR	low rate
LSB	least significant bit
LV	launch vehicle
LVDT	linear variable differential transformer
LVS	launch vehicle system
l_p	line pairs
lim	limiter
lo	low
MAWDS	Mars atmospheric water detector subsystem
MCCC	Mission Control and Computing Center
MDS	modulation/demodulation subsystem
M/O	master oscillator
MOI	Mars orbit insertion (time of start of engine)
MOT	Mars orbit trim
MR	medium rate
MRSD	mission requirements on system design
MSB	most significant bit
M71 S/C	Mariner 1971 spacecraft
mag	magnetic
max	maximum
meas	measurement

mech	mechanism
med	medium
min	minimum
mod	modulator
mult	multiplier
mux	multiplexer
N/A	not applicable
NC	normally closed
NEP	noise equivalent power
NO	normally opened
NRZ	nonreturn to zero
NRZ-L	nonreturn to zero level
nom	nominal
norm	normal
OPAG	orbiter performance and analysis group
OP code	operation code
OU	output unit
OV	overvoltage
Ox	oxidizer
OxBV	oxidizer bypass valve
OxV	oxidizer valve
o.d.	outside diameter
opt	optical or optics
osc	oscillator
outbd	outboard
PAS	pyrotechnic arming switch

PAU	propulsion actuation unit
P/B	playback
PC	processor command
PCA	pressurant control assembly
PCDA	power conditioning and distribution assembly
PCE	power conditioning equipment
PCM	pulse-code modulation
PIA	propellant isolation assembly
PLL	phase locked loop
PM	propulsion module
PMD	propellant management devices
PN	pseudonoise
POR	power on reset
PP	planet port
P-P	peak to peak
PPH	pulses per hour
PPS	pulses per second
PROPS	propulsion subsystem
PS	pressure sensor
P/S	power supply
PSE	PWRS support equipment
PSU	pyrotechnic switching unit
PTA	propellant or pressurant tank assembly
PTM	proof test model
PV	pressure valve

PWM	pulse width modulator
PWRS	power subsystem
PYROS	pyrotechnic subsystem
P_{BER}	probability of bit error rate
perf	performance
pert	perturbation
pk	peak
plat	platform
pos	position
pot	potentiometer
ppm	parts per million
prec	precision
press	pressure
proc	processor
prog	program
prop	propellant
pwr	power
pyro	pyrotechnic
R	radius or reset
RAS	relay antenna subsystem
RCA	reaction control assembly
RE	roll error
R/E	rate estimator
REA	rocket engine assembly
RFS	radio frequency subsystem

RG	ranging
RI	roll inertial
R/O	readout
RRS	relay radio subsystem
RSIN	roll reacquisition sequence inertial
RT	real time
RTG	radioisotope thermoelectric generator (VL)
RTS	relay telemetry subsystem
rad	radiator
rec	receiver
red	redundant
ref	reference
reg	regulator
repl	replacement
req	required
res	resistance
ret	return
rf	radio frequency
S	set
S - time	time relative to separation
SA	solar array
SAF	spacecraft assembly facility
SBW	single bridge wire
SC	subcarrier
S/C	spacecraft

SE	support equipment
SEC	solar energy controller
SG	Sun gate
SGL	Sun-gate logic
SLCO	Sun loss changeover
SME	signal mean component level estimate
S/N	serial number
SNORE	signal-to-noise-ratio estimate
SNR	signal-to-noise ratio
SO	switchover
SP	solar panel
S/P	subpanel
SPE	static phase error
SpP	space port
SS	Sun sensor
S/S	subsystem
STCE	system test complex equipment
ST/N_O	rate of signal energy to noise power spectral density
STRUS	structure subsystem
SXAS	S-band and X-band antenna subsystem (written as S/X band antenna subsystem)
sci	science
sel	selector
sep	separation
seq	sequence
sig	signal

sol	solenoid
std	standard
stdby	standby
str	strength
stru	structure
subcom	subcommutator
sum	summing
sw	switch
TA	type approval
TD	tolerance detector
TM	telemetry
TMEM	transport-mounted electronics module
TMI	trans-Mars injection
TMU	telemetry modulation unit
TS	temperature sensor
TV	television
TVC	thrust vector control
TWT	traveling wave tube
TWTA	traveling wave tube amplifier (TWT + P/S)
tach	tachometer
tel	telescope
temp	temperature
tran	transient
trk	tracking
typ	typical

UHF	ultrahigh frequency
UV	undervoltage
V	voltage
VCO	voltage controlled oscillator
VFT	Viking flight team
VIS	visual imaging subsystem
VL	Viking lander
VLC	Viking lander capsule
VLCA	Viking lander capsule adapter
VLS	Viking lander system
VMCCC	Viking Mission Control and Computing Center
VO	Viking orbiter
VOS	Viking orbiter system
V S/C	Viking spacecraft
V S/C A	Viking spacecraft adapter
VSWR	voltage standing-wave ratio
VTA	Viking transition adapter
V_{in}	input voltage
V_{oc}	open-circuit voltage
V_{out}	output voltage
WL, λ	wavelength
WV	water vapor
w/o	without
XFER	transfer
XFMR	transformer

XMTR	transmitter
XTAL	crystal
XTXS	X-band transmitter subsystem
YIG	yttrium-iron-garnet
α	cone angle
α_c	celestial cone angle
β	clock angle
β_c	celestial clock angle
ΔV	change in velocity
λ	wavelength
φ	SEC opening angle

1. Report No.	2. Government Accession No.	3. Recipient's Catalog No.
NASA RP-1027		

4. Title and Subtitle	5. Report Date
VIKING '75 SPACECRAFT DESIGN AND TEST SUMMARY VOLUME II - ORBITER DESIGN	November 1980
	6. Performing Organization Code
7. Author(s) Neil A. Holmberg, Robert P. Faust, and H. Milton Holt	8. Performing Organization Report No. L-12087
9. Performing Organization Name and Address NASA Langley Research Center Hampton, VA 23665	10. Work Unit No. 815-00-00-00
	11. Contract or Grant No.
12. Sponsoring Agency Name and Address National Aeronautics and Space Administration Washington, DC 20546	13. Type of Report and Period Covered Reference Publication
	14. Sponsoring Agency Code

15. Supplementary Notes

16. Abstract

This publication, in three volumes, discusses the design of the Viking lander and orbiter as well as the engineering test program that was developed to achieve confidence that the design was adequate to survive the expected mission environments and to accomplish the mission objective. Volume I includes a summary of the Viking Mission and the design of the Viking lander. Volume II consists of the design of the Viking orbiter and Volume III comprises the engineering test program for the lander and the orbiter.

17. Key Words (Suggested by Author(s))	18. Distribution Statement
Viking Project Viking orbiter design	Unclassified - Unlimited Subject Category 18

19. Security Classif. (of this report)	20. Security Classif. (of this page)	21. No. of Pages	22. Price
Unclassified	Unclassified	316	A14

For sale by the National Technical Information Service, Springfield, Virginia 22161

NASA-Langley, 1980